Invariant Ruelle Distributions for Open Hyperbolic Systems

—

An Analytical and Numerical Investigation

Von

Philipp Schütte

Eingereicht zur Erlangung des akademischen Grades

Doctor Rerum Naturalium

Betreut von

Prof. Dr. Tobias Weich

am

Institut für Mathematik der Universität Paderborn

Zusammenfassung: In der vorliegenden Dissertation wurden sowohl analytische als auch numerische Aspekte sogenannter invarianter Ruelle Distributionen behandelt. In einem ersten Schritt wurde eine gewichtete Zeta Funktion für offene hyperbolische Systeme meromorph fortgesetzt, um anschließend eine Formel für deren Residuen abzuleiten. Diese Residuenformel erlaubte es, invariante Ruelle Distributionen mittels gewichteter Zeta Funktionen konkret auszurechnen.
Eine Anwendung dieser analytischen Ergebnisse erfolgte dann im Rahmen der Streuung an konvexen Hindernissen und ermöglichte damit eine rigorose Behandlung gewisser semiklassischer Formeln, welche in der theoretischen Physik bereits früher mittels heuristischer Argumente abgeleitet worden waren.
Als zweiter Schritt wurde die Residuenformel für Ruelle Distributionen genutzt, um Letztere konkret numerisch für konvex-kokompakte hyperbolische Flächen zu berechnen und zu visualisieren. Neben der rigorosen Herleitung geeigneter numerischer Techniken, wurde weiterhin ein `PyZeta` getauftes Open Source Projekt implementiert, um eine Reihe von Aspekten sowohl der Pollicott-Ruelle Resonanzen als auch (dynamischer) Zeta Funktionen abzubilden.

Summary: The dissertation at hand encompasses a treatment of both analytical as well as numerical aspects of so-called invariant Ruelle distributions. As a first step a weighted zeta function for open hyperbolic systems was defined and meromorphically continued which allowed the subsequent derivation of a residue formula for the weighted zeta. This in turn enabled the concrete calculation of invariant Ruelle distributions via weighted zeta functions.
These analytical results were applied in the context of convex obstacle scattering which enabled a new rigorous approach to semiclassical formulae that had previously been considered in theoretical physics in a more heuristic manner.
As a second step the residue formula for Ruelle distributions was used to concretely numerically calculate and visualize the latter for convex-cocompact hyperbolic surfaces. Besides the rigorous justification of the concrete numerical approach the development of an open source project called `PyZeta` was an integral part of this thesis. The project incorporates a number of aspects concerning Pollicott-Ruelle resonances and (dynamical) zeta functions.

Introduction

This thesis is the culmination of the work that I did during my four years as a PhD student at Paderborn University. The techniques used cover rather diverse areas such as abstract analytical theorems, practical numerical investigations, and questions of concrete implementation all under a single unifying theme: *invariant Ruelle distributions*.

An invariant Ruelle distribution $\mathcal{T}_{\lambda_0}$ is a generalized density

$$\mathcal{T}_{\lambda_0} : \ \mathrm{C}^\infty(\mathcal{M}) \ni f \longrightarrow \mathcal{T}_{\lambda_0}(f) \in \mathbb{C}$$

on the finite-dimensional phase space manifold $\mathcal{M}$ of a *smooth continuous chaotic dynamical system*

$$\varphi_t : \ \mathcal{M} \longrightarrow \mathcal{M} \ , \qquad t \in \mathbb{R} \ ,$$

which is invariant under this dynamics. It is associated to one specific *Pollicott-Ruelle resonance* $\lambda_0 \in \mathbb{C}$ from a discrete subset of the complex plane called the *resonance spectrum*. These invariants of the given chaotic dynamics have found many applications since their inception due to Ruelle [Rue76] and Pollicott [Pol85], for example in convergence to equilibrium, decay of correlations, mixing, asymptotic distribution of periodic orbits, and linear response [Nau05, BL07, FS11, NZ15]. Furthermore they have been linked to certain invariants of the underlying phase space [DZ17, KW20, CDDP22].

The distributions $\mathcal{T}_{\lambda_0}$ now encode information about certain eigendistributions of λ_0 called *resonant states* and in some special cases they are even known to coincide with well-known objects like *Sinai-Ruelle-Bowen* (SRB) measures in the Anosov or *Bowen-Margulis measures* in the convex-cocompact setting [Rob03, BL07, BGW23].

If the chaotic dynamical system is more concretely given by a geodesic flow then it is naturally considered the classical counterpart of a quantum mechanical system described by the Laplace-Beltrami operator Δ. For the case of the underlying configuration space being a compact hyperbolic surface an additional reason for the importance of Pollicott-Ruelle resonances is provided by a *quantum-classical correspondence* [DFG15]: An explicit bijection between the quantum mechanical spectrum

$$0 = \lambda_0 \leq \lambda_1 \leq \ldots \leq \lambda_i \to \infty$$

of the Laplace-Beltrami operator, i.e.

$$\Delta\psi_i = \lambda_i\psi_i \ ,$$

and the classical resonance spectrum of the geodesic flow exists. It is based on a relationship between the eigenfunctions ψ_i and Pollicott-Ruelle resonant states, more precisely a linear isomorphism between certain finite-dimensional function spaces attached to respective spectral values, and the invariant Ruelle distributions coincide with well-known phase space quantities called *Patterson-Sullivan distributions* [AZ07].

This implies that quantum properties of the chaotic dynamics can be described using *purely classical* quantities and the implication extends to the case of some non-compact (namely convex-cocompact) hyperbolic surfaces as well, where the discrete quantum mechanical spectrum must be replaced by the quantum resonances of the Laplace-Beltrami operator [GHW18]. This setting will become of particular importance in our numerical applications later on.

It is therefore reasonable to expect that investigations of invariant Ruelle distributions should be able to provide interesting new insights. The notion of *weighted zeta function* introduced in this thesis was designed to explore precisely this idea: These complex-valued

functions Z_f encode closed orbit information of the classical dynamics on very general *open hyperbolic systems* with an additional weight function f on phase space. As is often the case for zeta functions Z_f is a priori defined as an infinite sum that converges locally uniformly only on a halfplane $\{\mathrm{Re}(\lambda) \gg 0\}$ but the potentially interesting information should somehow be encoded in an extension beyond this domain. It was therefore the first step of this thesis to prove the *meromorphic continuation* of the weighted zeta function

$$Z_f : \mathbb{C} \longrightarrow \mathbb{C} \ ,$$

subsequently identify the resulting poles as a subset of the Pollicott-Ruelle resonances, and finally establish a *residue formula*:

$$\operatorname*{Res}_{\lambda=\lambda_0} [Z_f(\lambda)] = \mathcal{T}_{\lambda_0}(f) \ .$$

These results build on previous work by [DG16] on the mermorphic continuation of the resolvent on open hyperbolic systems by expressing Z_f as a trace over the resolvent. With these steps completed weighted zeta functions do indeed allow one to investigate the rather abstractly defined invariant Ruelle distributions via a very concretely (up to meromorphic continuation) given complex function.

From there several applications were identified and carried out to demonstrate the usefulness of weighted zeta functions: The residue formula above made the proof of a classical trace formula for certain *quantum phase space distributions* called *Patterson-Sullivan distributions* possible. This proof worked in the very general setting of compact, locally symmetric spaces of rank one thereby extending and strengthening previous results of [AZ07].

Furthermore the definition and meromorphic extension of weighted zeta functions was successfully transferred to the setting of *convex obstacle scattering* which required significant additional technical effort in dealing with the discontinuous reflections at obstacle boundaries. And finally a numerical algorithm was developed to calculate and visualize invariant Ruelle distributions via weighted zeta functions. In practice this algorithm works well both on convex-cocompact hyperbolic surfaces and a particular instance of convex obstacle scattering namely scattering at round discs in the Euclidean plane. The former are compelling model systems due to their rich symmetry group and had previously been the main examples used in numerical investigations of (quantum) resonances [Bor14]. The latter model has the advantage of being physically realizable in a laboratory which makes them especially popular in the theoretical physics community [GR89a, GR89b, GR89c].

This further motivates the theoretical treatment of the obstacle scattering setting: Using this work as a basis made it possible to develop a rigorous approach [BSW22] to some semiclassical formulae which had previously been considered in the theoretical physics community but in a mathematically more heuristic fashion. This article relies heavily on the technical results obtained during other projects making up this thesis.

Naturally these practical investigations made it necessary to develop, extend, maintain, test, and document a constantly growing body of source code. To achieve code quality beyond a loose collection of scripts I decided to include two numerical open source projects of substantial extend into the scope of this thesis: `PyZeta` collects both functionality specific to the domain of (weighted) zeta functions and Pollicott-Ruelle resonances in general as well as more generic functionality for e.g. performance optimization and orchestration of numerical experiments. `PyZEAL` focuses on the root finding problem for holomorphic and meromorphic functions as a numerical task that is important independently of our particular application to zeta functions but surprisingly poorly covered by existing open source solutions.

The nature of the present thesis is **cumulative** – the bulk of the rigorous mathematical work is distributed over a total of **three research papers**:

- *Meromorphic Continuation of Weighted Zeta Functions on Open Hyperbolic Systems*, Schütte, P. and Weich, T. (with an appendix by Barkhofen, S. and Schütte, P. and Weich, T.), *Commun. Math. Phys.* (398), 2023 [SWB23],
- *Resonances and Weighted Zeta Functions for Obstacle Scattering via Smooth Models*, Delarue, B. and Schütte, P. and Weich, T., initially made available as the preprint *arXiv:2109.05907* (2021) [DSW21] and currently under revision at *Annales Henri Poincaré*,
- *Invariant Ruelle Distributions on Convex-Cocompact Hyperbolic Surfaces – A Numerical Algorithm via Weighted Zeta Functions*, Schütte, P. and Weich, T., currently available as the preprint *arXiv:2308.13463* (2023) [SW23] with additional numerical experiments being prepared for a journal submission.

For ease of reference these articles are contained in their respective latest (at the time of writing this thesis) versions as appendices. The body of the thesis text contains additional background information that was judged to be unsuited for inclusion into a journal submission. This includes more extensive motivations for decisions like why certain objects were considered or how given questions were approached but also summaries of failed approaches that provided valuable insights and straightforward generalizations with the downside of requiring additional technical overhead.

The applications of weighted zeta functions and smooth models for obstacle scattering developed in the paper [BSW22] mentioned above were deliberately not included in the appendices due to mostly targeting a physics instead of a mathematics audience. Instead the main text of this dissertation contains a short summary emphasizing the usefulness of weighted zeta functions as demonstrated by this article.

Furthermore detailed descriptions of `PyZeta` and `PyZEAL` are included with discussions of the central technical decisions and design tradeoffs. Overview papers are being prepared for both projects but at the moment of writing this thesis the code bases are still evolving in a manner that they are changing too frequently to make even a preprint publication possible in a meaningful way. The presentation deliberately focuses both on technical as well as design aspects to put the reader into a position where they can not only use but also contribute to either of these projects in a manner that is consistent with their overall philosophies.

Outline

The thesis at hand is partitioned into three distinct parts which build on top of each other to facilitate a coherent picture of the topics studied by the author during his PhD. Part I starts by introducing in Chapter 1 the central object which enables the many connections and numerical computations established later on: the *weighted zeta functions* $Z_f(\lambda)$. Their analytical properties and in particular their meromorphic continuation together with a residue formula were dealt with in detail in [SWB23] and Chapter 1 presents some additional details which had to be omitted from the paper due to space constraints. Here the notion of *invariant Ruelle distribution* gets introduced which will turn out to be a unifying theme between the three parts.

The subsequent chapters of Part I deal with applications of this analytical theory: Chapter 2 contains a brief overview of the paper [DSW21] which develops technical tools

that let one apply the theory of (weighted) zeta functions to scattering by convex obstacles. The final Chapter 3 summarizes the article [BSW22] which presents an application of weighted zetas to certain trace formulae for quantum mechanical matrix coefficients which had been published in the physics literature before but were lacking a rigorous mathematical justification. This relies both on [SWB23] as well as [DSW21]. In a numerical study the paper also presents some evidence how these results might be generalized to dynamical systems with less inherent symmetry.

Part II transitions from the purely theoretical realm treated in the first part to the practical numerical study of invariant Ruelle distributions via weighted zeta functions. The tools for this study together with a rigorous justification of their convergence in the context of convex cocompact hyperbolic surfaces is introduced in Chapter 4 by building on [SW23]. With this machinery at hand Chapter 5 can then present numerical experiments involving Ruelle distributions on a small number of fixed surfaces and Chapter 6 complements these with fundamentally different experiments where a large number of underlying geometries gets sampled from the moduli space of funneled tori to investigate random variables related to resonances and zeta functions.

The final Part III is of a more technical nature and describes high- and low-level programming details: Here the concrete implementation of the various resonance and Ruelle distribution related tools is discussed. Our use cases can roughly be subdivided into *finding resonances* and *calculating invariant Ruelle distributions*. This part of the thesis is correspondingly subdivided into a zeta function related project called `PyZeta` and described in Chapter 7 as well as a package dealing with the numerical calculation of zeros of holomorphic functions named `PyZEAL`, see Chapter 8.

Finally, as mentioned above, the three appendices contain the original publications which make up the backbone of this thesis in terms of rigorous mathematical proofs and theorems.

Acknowledgments

The writing of this thesis would have been impossible without the support and encouragement of several people.

I would like to begin by thanking my supervisor Prof. Tobias Weich for the opportunity to conduct the research which ultimately lead to the work at hand. I profited immensely not only from his mathematical guidance but also his willingness to let me pursue my own scientific interests independently. The open and motivational atmosphere he created in the research group Spektralanalysis at Paderborn University greatly benefited my scientific development during the past years and I appreciate the support by the members of the research group as a whole. In particular this includes Dr. Benjamin Delarue whose collaboration on the project making up Chapter 2 of this thesis was very instructive.

Special thanks go to Semyon Dyatlov for hosting me as a visiting PhD student at MIT in early 2020. Although cut short by the Covid19 pandemic the stay in Boston greatly enhanced the start of this project.

The financial support provided by a PhD scholarship from the *Studienstiftung des Deutschen Volkes* and the *DFG* funded Emmy Noether group *Microlocal Methods for Hyperbolic Dynamics* (Grant No. WE 6173/1–1) is also greatly appreciated.

Additional thanks go to William Hide for several helpful discussions regarding moduli and Teichmüller space as well as interesting questions to consider for numerical investigation. Without his initial interest the project that resulted in Chapter 6 would not have

been started in the first place.

Finally I am deeply indebted to my family and friends for everything they have done for me up until this point. Without you none of this would have been possible.

Philipp Schütte
Paderborn, September 2023

Contents

Part I.

Analytical Study of Open Hyperbolic Systems

Outline of Part I

The first part of this thesis will present an analytical study of *invariant Ruelle distributions* for a number of different dynamical systems, the most general of which are *open hyperbolic systems*. The results obtained here will find their practical numerical application in the subsequent Part II.

The analytical investigation starts with the very general class of open hyperbolic systems whose main characteristic is a compact trapped set on which the dynamics exhibits a hyperbolic splitting into neutral, expanding, and contracting directions. Resonances on these systems were defined and studied by Dyatlov and Guillarmou in [DG16]. In [SWB23] this work was used to obtain the meromorphic continuation of a certain *weighted zeta function* Z_f. This new zeta function has an added benefit over the well-known Ruelle zeta function that gets meromorphically continued in [DG16]: The residues of Z_f coincide with so-called invariant Ruelle distributions making the weighted zeta functions a prime tool for the study of these generalized densities. The details of these connections can be found in the paper [SWB23] which was included in Appendix A as it contains the central definitions, theorems, and proofs. A concise summary together with additional details form the contents of Chapter 1.

The dynamical assumptions made in [SWB23] are quite abstract. The collaborative work [DSW21] provides a detailed description of an application to a concrete dynamical system, namely *convex obstacle scattering*. The main feature of this system is its lack of smoothness at the obstacle boundaries. This required the development of the notion of *smooth model* for a scattering system. Again a summary and additional details, in particular motivations for certain rather technical constructions, are provided in Chapter 2 as part of the main text while the original publication is contained in Appendix B. It shall be reiterated that this article should be considered as the main source for definitions and results together with their proofs.

Part I is concluded by Chapter 3 which contains a short summary of the more physical review paper [BSW22]. While the contribution made by the author of this thesis to this particular article is less significant compared to the two previously mentioned ones[1] it is nevertheless interesting due to it offering an application of the theory developed in both [SWB23] and [DSW21] to questions heavily studied in the mathematical and theoretical physics communities.

[1] The contribution concretely encompasses proof reading, mathematical discussions, and the numerical experiments involving 3-disc systems (based on previous code by Barkhofen/Weich).

1. Meromorphic Continuation of Weighted Zeta Functions

The bulk of the analytical foundation built during this thesis is presented in the published article [SWB23]. The present chapter describes the results obtained there and supplements the presented proofs with further details which have been omitted from the paper due to space constraints. Appendix A contains the paper itself to make this thesis more self-contained.

1.1. The Geometric Setup

Before presenting the results together with additional details regarding their proofs in the following section an overview will be given of the geometric setup in which these results were obtained. This section adds value over [SWB23, Section 2.1] by choosing a more intuitive approach that emphasizes the meaning and the implications of the various assumptions.

The meromorphic continuation of weighted zeta functions follows the *microlocal* approach to Pollicott-Ruelle resonances as developed by Faure and Sjöstrand [FS11]. It is therefore natural to start with some smooth manifold $\overline{\mathcal{U}}$ of finite dimension. Furthermore the whole procedure relies heavily on the progress achieved in [DG16] regarding *open hyperbolic systems*. $\overline{\mathcal{U}}$ is therefore required to be *compact* but may possess non-empty smooth boundary $\partial\overline{\mathcal{U}}$.

Now the dynamical system under study is a flow $\varphi_t = \exp(tX)$ with a non-vanishing smooth generating vector field X. This setup encodes the notion of an *open* system because φ_t will generally not be complete if $\partial\overline{\mathcal{U}} \neq \emptyset$ because trajectories $\varphi_t(x_0)$ for $x_0 \in \overline{\mathcal{U}}$ may cease their existence at the boundary after some finite positive or negative (or both) escape time(s). Such trajectories should be interpreted as escaping to infinity.

For technical reasons one now wants to embed $\overline{\mathcal{U}}$ into an ambient *closed* manifold and extend X suitably. The flow associated with this construction then becomes complete, i.e. trajectories are defined for arbitrary times, which makes it much more amenable for further analysis. For this strategy to make sense it is vital that the extended flow preserves the interpretation of escaping to infinity introduced above. In other words the extension must be build in such a way that any trajectory of the extended flow which leaves the interior $\mathcal{U}$ of the original manifold with boundary does not re-enter $\mathcal{U}$ at some time larger[1] than the original escape time.

To formalize this discussion the embedding $\overline{\mathcal{U}} \subset \mathcal{M}$ into a compact manifold $\mathcal{M}$ *without* boundary should satisfy the following condition for every $T > 0$:

$$x, \varphi_T(x) \in \mathcal{U} \Longrightarrow \varphi_t(x) \in \mathcal{U} \ , \quad \forall\, 0 \leq t \leq T \ .$$

Here and in the following the extended flow as well as its generator will be denoted by the same symbols as the original flow and generator.

[1] Or smaller, in case of a negative escape time.

Now such an extension can indeed always be constructed under a condition that the authors of [DG16] term *strict convexity*. Stating a formal definition requires the introduction of an additional auxiliary object called a *boundary defining function*:

Definition 1.1.1: Boundary defining function

Let $\mathbf{M}$ be a smooth manifold with boundary $\partial\mathbf{M}$ and interior $\mathrm{int}(\mathbf{M})$. A *boundary defining function* is a smooth map $\rho : \mathbf{M} \to [0, \infty[$ with $\rho\big|_{\mathrm{int}(\mathbf{M})} > 0$, $\rho\big|_{\partial\mathbf{M}} = 0$ and $\mathrm{d}\rho\big|_{\partial\mathbf{M}} \neq 0$.

Any smooth manifold with boundary possesses a boundary defining function ([Lee12, p. 118f]). The standard proof constructs a boundary defining function by combining constant, non-zero functions on interior charts and the n-th coordinate function $x \mapsto x_n$ on boundary charts via a partition of unity. For a straightforward yet illuminating consequence of this definition consider a boundary chart $\varphi = (x^1, ..., x^n) : \mathbf{M} \supseteq U \to V \subseteq \mathbb{H}^n$ around some $p \in \partial\mathbf{M}$.[2] Then one computes for the differential of ρ

$$\begin{aligned} \mathrm{d}\rho_p &= \frac{\partial(\rho \circ \varphi^{-1})}{\partial x^i}\bigg|_{\varphi(p)} \mathrm{d}x^i\big|_p \\ &= \frac{\partial(\rho \circ \varphi^{-1})}{\partial x^n}\bigg|_{\varphi(p)} \mathrm{d}x^n\big|_p \neq 0 \ , \end{aligned}$$

where the summation convention is in effect in the first row. One immediately concludes that $\partial(\rho \circ \varphi^{-1})/\partial x^n > 0$ must hold on the boundary.

One calls those vectors $v = v^i \partial/\partial x^i \in T_p\mathbf{M}$ *inward pointing, outward pointing,* or *tangent to the boundary* that satisfy $v^n > 0$, $v^n < 0$, or $v^n = 0$ in some (and therefore any) chart (x^i). Using the previous property, inward/outward pointing and tangent can be characterized equivalently by the conditions $v(\rho) = \mathrm{d}\rho(v) > 0$, $v(\rho) < 0$, or $v(\rho) = 0$.

The dynamical condition mentioned above can now be expressed as follows: One calls the boundary $\partial\mathcal{U}$ *strictly convex* (w.r.t. X) if every boundary defining function ρ satisfies

$$(X\rho)(x_0) = 0 \implies X(X\rho)(x_0) < 0 \tag{1.1.1}$$

for any $x_0 \in \partial\mathcal{U}$. Before developing an intuition for this definition it will be shown that it suffices to verify Equation (1.1.1) on an arbitrary boundary defining function making the notion of *strict convexity* a meaningful property of the geometry of $\partial\mathcal{U}$.[3]

To prove this one calculates in coordinates (x^i) in which X has components (X^i)

$$\begin{aligned} X(X\rho)(x_0) &= X^i \frac{\partial}{\partial x^i}\left(X^j \frac{\partial \rho}{\partial x^j}\right)\bigg|_{x=x_0} \\ &= X^i X^j \frac{\partial^2}{\partial x^i \partial x^j}\rho\bigg|_{x=x_0} + X^i \frac{\partial \rho}{\partial x^j}\frac{\partial X^j}{\partial x^i}\bigg|_{x=x_0} \\ &= (X^n)^2 \frac{\partial^2}{\partial (x^n)^2}\rho\bigg|_{x=x_0} + \frac{\partial \rho}{\partial x^n} X^i \frac{\partial X^n}{\partial x^i}\bigg|_{x=x_0} \\ &= \frac{\partial \rho}{\partial x^n} X^i \frac{\partial X^n}{\partial x^i}\bigg|_{x=x_0} . \end{aligned}$$

[2] Recall that n-dimensional (smooth) manifolds with boundary are locally modeled on the upper half-spaces $\mathbb{H}^n := \{(x_1, \ldots, x_n) \in \mathbb{R}^n \,|\, x_n \geq 0\}$.

[3] Note that already the set of points where the premise $(X\rho)(p) = 0$ holds true is independent of ρ by the previously made statements.

The independence of the sign from any particular choice of ρ now follows from the fact that $\partial\rho/\partial x^n > 0$ holds for every boundary defining function.

With this out of the way a remark regarding the interpretation of strict convexity is in order. First of all $(X\rho)(x_0) = X_{x_0}(\rho) = 0$ means that X_{x_0} is tangent to the boundary. Now at any such point x_0 it is required that[4]

$$\sum_{i\neq n} X^i \frac{\partial X^n}{\partial x^i}\bigg|_{x=x_0} = \frac{\mathrm{d}}{\mathrm{d}t} X^n\left(\varphi_t(x_0)\right)\bigg|_{t=0} < 0 \ .$$

From the perspective of the flow this means that trajectories which intersect the boundary in a tangent manner can neither propagate within the boundary for any small but finite interval of time nor can they return to the interior $\mathcal{U}$ at a later time. It must cross the boundary and exit immediately where exit has to be understood as either ceasing existence or entering the ambient $\mathcal{M}$ depending on whether or not the latter was already constructed.

The rigorous statement assuring that strict convexity indeed yields the correct class of manifolds is [DG16, Lemma 1.1] where correctness is understood in the sense of the previous discussion. For this class of manifolds [DG16, Lemma 1.2] assures that the so-called *trapped set* K is contained in the interior $\mathcal{U}$:

$$\Gamma_\pm \coloneqq \bigcap_{\pm t\geq 0} \varphi_t(\overline{\mathcal{U}}) \ , \qquad K \coloneqq \Gamma_+ \cap \Gamma_- \subset \mathcal{U} \ .$$

This is required as the interesting dynamics happens on K alone thus making it necessary to be able to define K independently from an ambient $\mathcal{M}$. In fact it can be argued that $K \subseteq \mathcal{U}$ is the whole point of making the auxiliary technical assumption of strict convexity. This viewpoint is supported by the construction in [SWB23, Section 2.2] where strict convexity was removed in favor of assuming $K \subset \mathcal{U}$ from the outset.

The necessity of having this alternative formulation was made very clear during the work that resulted in Chapter 2: The practical application of meromorphically continued weighted zeta functions to obstacle scattering would have been quite a bit harder otherwise as a suitable candidate boundary defining function for verifying strict convexity does not seem obvious there.

The remaining dynamical assumptions as listed in [SWB23, Section 2.1] are basically twofold: On the one hand one has *hyperbolicity* of φ_t on K. This is the standard assumption under which ones proves existence of Pollicott-Ruelle resonances and its geometric interpretation is that of chaotic behavior with a (local) splitting into neutral, expanding and contracting directions:

$$T_x\mathcal{U} = \mathbb{R}\cdot X(x) \oplus E_s(x) \oplus E_u(x) \ , \qquad \forall\, x \in K \ , \tag{1.1.2}$$

where the splitting is continuous in $x \in K$, invariant under φ_t and the differential $\mathrm{d}\varphi_t(x)$ is exponentially contracting in either positive or negative time on $E_s(x)$ or $E_u(x)$, respectively.

On the other hand the setup gains significantly in generality without imposing further technical difficulties if the transition to the vector valued setting is made. Assuming a smooth $\mathbb{C}$-vector bundle $\mathcal{E} \to \overline{\mathcal{U}}$ and a first-order differential operator $\mathbf{X}$ on $\mathcal{E}$ one requires as the final condition a Leibniz rule to hold with respect to X:

$$\mathbf{X}(f\mathbf{u}) = (Xf)\mathbf{u} + f(\mathbf{X}\mathbf{u}) \ , \qquad f \in \mathrm{C}^\infty(\overline{\mathcal{U}}) \ , \ \mathbf{u} \in \mathrm{C}^\infty(\overline{\mathcal{U}}, \mathcal{E}) \ .$$

[4]The n-component does not appear as $X^n(x_0) = 0$ and it was excluded to emphasize this point.

Under these assumptions the triple $(\overline{\mathcal{U}}, \varphi_t, \mathbf{X})$ is called an *open hyperbolic system*.

The bundle data can again be extended to the ambient manifold $\mathcal{M}$ and a construction of resonances is possible not only for φ_t but also the transfer operator

$$\exp(-t\mathbf{X}) : \mathrm{L}^2(\mathcal{M}, \mathcal{E}) \longrightarrow \mathrm{L}^2(\mathcal{M}, \mathcal{E})$$

defined by the condition $(\mathrm{d}/\mathrm{d}t)\exp(-t\mathbf{X})u = -\mathbf{X}(\exp(-t\mathbf{X})u)$. In the following subsection a short overview over what this means and how it is achieved will be given.

1.2. Pollicott-Ruelle Resonances for Open Systems

Let an open hyperbolic system $(\overline{\mathcal{U}}, \varphi_t, \mathbf{X})$ as defined in the previous section be given. Spectral analysis as a general paradigm is concerned with the investigation of spectral invariants of this system and in particular the possibility of defining a suitable analog of the eigenvalue spectrum of linear operators on finite dimensional spaces. Even though the generalization of eigenvalues to infinite dimensional settings is quite straightforward it is not sufficient for many applications like eigenvalue counting, decay of correlations, or the expansion into eigenfunctions.

To substantiate this claim assume for simplicity a bounded linear operator $T : \mathcal{H} \to \mathcal{H}$ on a (complex) Hilbert space $\mathcal{H}$. If one takes as definition of eigenvalues of T the obvious candidate

$$\sigma_{\mathcal{H}}(T) \coloneqq \{\lambda \in \mathbb{C} \,|\, T - \lambda \text{ not invertible}\} \ ,$$

then this *spectrum* will generally neither be a discrete subset of $\mathbb{C}$ nor will it consist exclusively of eigenvalues. Similar statements hold for the case of unbounded operators where special care must be taken when dealing with their domains. Both phenomena are well-known from basic functional analysis. Without going into further detail recall the example $-\mathrm{i}\frac{\mathrm{d}}{\mathrm{d}x}$ on the Sobolev space $\mathrm{H}^1(\mathbb{R}) \subseteq \mathrm{L}^2(\mathbb{R})$ which has spectrum equal to the real line $\mathbb{R}$ but no eigenvalues as the generalized eigenfunctions $x \mapsto \exp(i\lambda x)$, $\lambda \in \mathbb{R}$, are not square integrable.

The theory of Pollicott-Ruelle resonances remedies this situation as follows: Starting with the (restricted) resolvent

$$\mathbf{R}(\lambda) \coloneqq \mathbf{1}_{\mathcal{U}} \, (\mathbf{X} + \lambda)^{-1} \, \mathbf{1}_{\mathcal{U}} : \mathrm{C}_{\mathrm{c}}^{\infty}(\mathcal{U}, \mathcal{E}) \longrightarrow \mathrm{L}^2(\mathcal{U}, \mathcal{E})$$

one extends the codomain to distributions $\mathcal{D}'(\mathcal{U}, \mathcal{E})$ and proves its *meromorphic continuation* to all of $\mathbb{C}$. This is highly non-trivial and constitutes a significant portion of [DG16]. Continuing to denote the meromorphic continuation by $\mathbf{R}(\lambda)$ one makes the following definition:

Definition 1.2.1: Pollicott-Ruelle resonances

The poles of $\mathbf{R}(\lambda)$ are called *Pollicott-Ruelle resonances* and collectively they are called the resonance spectrum of $\mathbf{X}$. The residue of $\mathbf{R}(\lambda)$ at a resonance $\lambda_0 \in \mathbb{C}$ is an operator

$$\Pi_{\lambda_0} : \mathrm{C}_{\mathrm{c}}^{\infty}(\mathcal{U}, \mathcal{E}) \longrightarrow \mathcal{D}'(\mathcal{U}, \mathcal{E})$$

called the spectral projector.

The operator Π_{λ_0} has finite rank by [DG16, Theorem 1]. Describing those of its additional properties that will become important for the proof presented in Section 1.3 requires the introduction of some additional technical machinery namely wavefront sets

and flat traces of (vector-valued) distributions. The precise definitions were not included in [SWB23] so they will be recalled here together with the related theorems which are used in the upcoming proof.

The foundational technical object gets introduced in the following definition:

Definition 1.2.2: Wavefront set [Hör13, Chapter 8.1]

Let $U \subseteq \mathbb{R}^n$ be an open set and $u \in \mathcal{D}'(U)$ a distribution on U. Then the *wavefront set* $\mathrm{WF}(u) \subseteq U \times \mathbb{R}^n \setminus \{0\}$ of u is defined by

$$(x,\xi) \notin \mathrm{WF}(u) \Longleftrightarrow \exists \chi \in \mathrm{C}_\mathrm{c}^\infty(U),\, \chi(x) = 1\, \exists \text{ conic neighborhood } V \ni \xi : \\ |\widehat{\chi \cdot u}(\zeta)| \leq C_N \frac{1}{(1+|\zeta|)^N} \forall N \in \mathbb{N},\, \forall \zeta \in V \ ,$$

where conic means invariant under multiplication with positive scalars and $\widehat{v}$ denotes the Fourier transform of a distribution v on $\mathbb{R}^n$.

Due to the presence of the cutoff functions χ in the definition above the notion of wavefront set is local in nature and can be extended to smooth manifolds.[5] Considering careful the role of the dual variable ξ one notices that an invariant definition is best given in terms of the cotangent bundle: Given a manifold $\mathbf{M}$ and a distribution $u \in \mathcal{D}'(\mathbf{M})$ its wavefront set is a subset $\mathrm{WF}(u) \subseteq T^*\mathbf{M} \setminus \mathrm{o}$, where o is the zero section. The concrete definition requires pullback of the distribution to coordinate patches. This can be done via the second theorem stated below but no details will be given here.[6]

The properties of the Fourier transform on distributions already suggest that $\mathrm{WF}(u)$ describes directions in which the distribution u fails to be smooth. A first straightforward corollary relates the wavefront set with the *singular support*, i.e. the set of all points where u fails to be smooth: Letting $\pi_{\mathbf{M}}$ be the projection onto the base manifold one has

$$\pi_{\mathbf{M}}(\mathrm{WF}(u)) = \mathrm{singsupp}(u) \ ,$$

and in particular u is smooth iff $\mathrm{WF}(u) = \emptyset$. The wavefront set therefore incorporates the spatial positions of singularities of u but combines these with additional information in phase space. The usefulness of this additional data is proven by the following two theorems which are essential building blocks for the upcoming proof of meromorphic continuation:

Theorem 1.2.3: [Hör13, Thm. 8.2.12]

Let X, Y be smooth manifolds, $A : \mathrm{C}_\mathrm{c}^\infty(X) \to \mathcal{D}'(Y)$ and $K_A \in \mathcal{D}'(Y \times X)$ the corresponding kernel. Then for $f \in \mathrm{C}_\mathrm{c}^\infty(X)$

$$\mathrm{WF}(Af) \subset \{(y,\eta) \,|\, (y,x,\eta,0) \in \mathrm{WF}(K_A) \text{ for some } x \in \mathrm{supp}(f)\} \ .$$

Proof. Only a short sketch of the idea of proof will be given here. For details refer to [Hör13, Chapter 8.2]. One proceeds by considering $K_1 \coloneqq (\chi \otimes f)K_A$ with an additional cutoff $\chi \in \mathrm{C}_\mathrm{c}^\infty(Y)$. Locally the Fourier transform of $\chi(Af)$ coincides with $\widehat{K_1}(\xi, 0)$ which suffices to estimate the cone where the Fourier transform of $\chi(Af)$ does not decay

[5] There are actually definitions of the wavefront set whose invariance is easier to see, e.g. via pseudodifferential operators.

[6] Recall that the notion of distribution on a manifold is itself defined in terms of local coordinate expressions satisfying an appropriate compatibility condition, c.f. [Hör13, Chapter 6.3].

rapidly. The theorem then follows by shrinking the support of χ to a single (arbitrary) point. □

The statement of the second theorem involves certain subspaces of distributions defined as follows for some closed cone $\Gamma \subseteq T^*\mathbf{M} \setminus \mathrm{o}$:

$$\mathcal{D}'_\Gamma(\mathbf{M}) \coloneqq \left\{ u \in \mathcal{D}'(\mathbf{M}) \,\middle|\, \mathrm{WF}(u) \subseteq \Gamma \right\} .$$

These spaces can be given a notion of sequential convergence[7] and the following theorem gives a sufficient condition that describes when the pullback on functions extends to a sequentially continuous operation on these subspaces of distributions:

Theorem 1.2.4: [Hör13, Thm 8.2.4]

Let X, Y be smooth manifolds, $f \in \mathrm{C}^\infty(X, Y)$, and $\Gamma \subset T^*Y \setminus \mathrm{o}$ conic. There exists a well-defined sequentially continuous extension of the pullback

$$\mathrm{C}^\infty(Y) \ni u \mapsto f^*(u) = u \circ f \in \mathrm{C}^\infty(X)$$

to an operator $\mathcal{D}'_\Gamma(Y) \to \mathcal{D}'_{f^*\Gamma}(X)$ if the wavefront condition

$$\Gamma \cap \left\{ (f(x), \xi) \in T^*Y \,\middle|\, \mathrm{d}f_x^t(\xi) = 0 \right\} = \emptyset$$

holds. Here

$$f^*\Gamma \coloneqq \left\{ (x, \mathrm{d}f_x^t(\xi)) \,\middle|\, (f(x), \xi) \in \Gamma \right\} .$$

Proof. Again only a sketch will be provided, [Hör13, Chapter 8.2] contains the details. To define f^*u for $u \in \mathcal{D}'(Y)$ one chooses a sequence $\mathrm{C}^\infty(Y) \ni u_j \to u$ and considers the sequence $\langle f^*u_j, \chi \rangle$ for some given testfunction $\chi \in \mathrm{C}^\infty_\mathrm{c}(X)$. The question of convergence of this sequence can now be reduced to a local argument involving the Fourier transforms $\widehat{\chi}$ and $\widehat{\phi u_j}$ introduced via the inversion formula. Here $\phi \in \mathrm{C}^\infty_\mathrm{c}(Y)$ is another suitable additional cutoff. The growth behavior of the former Fourier integral may now be controlled in a neighborhood of $\{\mathrm{d}f_x^t(\xi) \neq 0\}$ while the latter is controllable outside the wavefront set. The wavefront condition in the theorem now guarantees existence of the limit and its independence from the chosen sequence u_j.

The argument for sequential continuity proceeds quite similarly but requires additional care in the definition of χ due to the concrete choice of sequential convergence in $\mathcal{D}'_\Gamma(Y)$ and $\mathcal{D}'_{f^*\Gamma}(X)$. □

With these theorems at hand the precise definition of the central object under investigation and recurring theme of this thesis is now possible. Before stating this definition recall that any continuous operator $L : \mathrm{C}^\infty_\mathrm{c}(\mathbb{R}^n) \to \mathcal{D}'(\mathbb{R}^m)$ has a so-called *Schwartz kernel* $K_L \in \mathcal{D}'(\mathbb{R}^m \times \mathbb{R}^n)$ that satisfies

$$\langle L(f), g \rangle = \langle K_L, g \otimes f \rangle \ , \qquad \forall f \in \mathrm{C}^\infty_\mathrm{c}(\mathbb{R}^n),\, g \in \mathrm{C}^\infty_\mathrm{c}(\mathbb{R}^m) \ ,$$

where $g \otimes f(y, x) \coloneqq g(y)f(x)$, and an analogous statement holds for smooth manifolds. For details see e.g. [Tre07, Chapter 51] or [Tay11, Chapter 4.6] for the case of manifolds.

[7] It is actually a subtle problem to define a topology on these spaces such that one recovers the same notion of sequential convergence and simultaneously turns the desired operations on distributions into (fully) continuous functions [BDH14].

The kernel K_A of an operator $K : \mathrm{C}_\mathrm{c}^\infty \to \mathcal{D}'$ also allow a straightforward extension of the notion of wavefront set to operators:

$$\mathrm{WF}'(A) \coloneqq \{(x, y, \xi, \eta) \,|\, (x, y, \xi, -\eta) \in \mathrm{WF}(K_A)\} \ .$$

One could also consider a non-primed version $\mathrm{WF}(A)$ of operator wavefront sets. In some sense WF' is more natural, though, especially coming from microlocal analysis as $\mathrm{WF}'(A)$ for a pseudodifferential operator A has a direct connection to the symbol of A, see [GS94, Chap. 7].

Definition 1.2.5: Flat trace

Let $\mathbf{M}$ be a smooth manifold and $A : \mathrm{C}_\mathrm{c}^\infty(\mathbf{M}) \to \mathcal{D}'(\mathbf{M})$ a continuous linear operator with compactly supported Schwartz kernel $K_A \in \mathcal{D}'(\mathbf{M} \times \mathbf{M})$. Suppose further that the wavefront set of A does not intersect the diagonal $\Delta(T^*\mathbf{M})$ of $T^*\mathbf{M}$:

$$\mathrm{WF}'(A) \cap \Delta(T^*\mathbf{M}) = \emptyset$$

Then the *flat trace* of A is defined as the evaluation on the constant function $\mathbf{1}_\mathbf{M}$ of the pullback of K_A under the embedding $\iota : \mathbf{M} \to \mathbf{M} \times \mathbf{M}$, $\iota(x) \coloneqq (x, x)$:

$$\mathrm{tr}^\flat\,(A) \coloneqq \int_\mathbf{M} K_A(x, x)\,\mathrm{d}x = \langle (\iota^* K_A)\,, \mathbf{1}_\mathbf{M} \rangle \ .$$

Remark 1.2.6. To be applicable to the general setting of open hyperbolic systems the notions introduced so far obviously have to be extended to the vector valued setting. This is done by first defining spaces of vector valued distributions $\mathcal{D}'(\mathbf{M}, \mathcal{E})$ as the dual spaces of smooth compactly supported sections of a given vector bundle $\mathcal{E} \to \mathbf{M}$ with smooth inner product defined on its fibres. Here and in the following it is assumed that there exists an invariant density on the base manifold such that the distinction between generalized functions and generalized densities becomes insignificant. In particular this applies to the name invariant Ruelle *distribution* as the object defined below formally is a generalized density. The upcoming discussions are independent of the concrete choice of density as long as a consistent choice is used throughout.

The notion of wavefront set may then be defined component-wise because its initial definition was local to begin with. Schwartz kernels now take values in $\mathcal{D}'(\mathbf{M}_1 \times \mathbf{M}_2, \mathcal{E}_1 \boxtimes \mathcal{E}_2)$ where given bundles $\mathcal{E}_i \to M_i$ the bundle $\mathcal{E}_1 \boxtimes \mathcal{E}_2$ denotes the tensor product of the pullbacks of the $\mathcal{E}_i$ onto $M_1 \times M_2$. Note that [DZ16] uses the notation $\mathrm{End}(\mathcal{E})$ for the bundle $\mathcal{E} \boxtimes \mathcal{E}^*$ over $\mathcal{M} \times \mathcal{M}$. Finally the flat trace is easily generalized by taking the sum over flat traces of the diagonal components of the operator's kernel.

For additional details regarding vector valued distributions and generalized densities on manifolds refer to the extensive monograph [GKOS01, Chapter 3].

Definition 1.2.7: Ruelle distribution

Let $\lambda_0 \in \mathbb{C}$ be a resonance of the open hyperbolic system $(\overline{\mathcal{U}}, \varphi_t, \mathbf{X})$. Then the *invariant Ruelle distribution* $\mathcal{T}_{\lambda_0} \in \mathcal{D}'(\mathcal{U})$ associated with λ_0 is given by

$$\mathcal{T}_{\lambda_0}(f) \coloneqq \mathrm{tr}^\flat\,(\Pi_{\lambda_0} \mathrm{M}_f) \ , \qquad f \in \mathrm{C}^\infty(\mathcal{U}) \ .$$

Here Π_{λ_0} denotes the residue of the resolvent at λ_0 as defined above and M_f is the operator of multiplication by f.

A discussion of the aspects well-definedness and invariance of $\mathcal{T}_{\lambda_0}$ can be found in [SWB23]. Note also that invariant Ruelle distributions are compactly supported within the trapped set K.

1.3. Expanded Proof of Meromorphic Continuation

As announced above this section contains an extended proof of the meromorphic continuation of the most general weighted zeta functions $Z_f^{\mathbf{X}}(\lambda)$ for open hyperbolic systems. These are formally defined in terms of closed trajectories γ of an open hyperbolic system $(\mathcal{U}, \varphi_t, \mathbf{X})$ and a weight $f \in \mathrm{C}^\infty(\mathcal{U})$:

$$Z_f^{\mathbf{X}}(\lambda) \coloneqq \sum_\gamma \left(\frac{\exp\left(-\lambda T_\gamma\right) \operatorname{tr}(\alpha_\gamma)}{|\det(\mathrm{id} - \mathcal{P}_\gamma)|} \int_{\gamma^\#} f \right), \qquad \lambda \in \mathbb{C} \,. \tag{1.3.3}$$

Here $\mathcal{P}_\gamma$ denotes the linearized Poincaré map on γ which is the differential $\mathrm{d}\varphi_{-T_\gamma}(x)$ evaluated on some $x \in \gamma$. The determinant itself is independent of this base point so it can be omitted from the notation. Similarly α_γ is parallel transport along γ, i.e. $u \mapsto \exp(-T_\gamma \mathbf{X})\mathbf{u}(\varphi_{T_\gamma}(x))$ for $u \in \mathcal{E}_x$ and any smooth section $\mathbf{u}$ with $\mathbf{u}(x) = u$. This definition is independent of the choice of $\mathbf{u}$ and the trace is also independent of the concrete base point x. More details may be found in [SWB23, Section 2.1].

The general strategy to prove meromorphic continuation is to identify $Z_f^{\mathbf{X}}(\lambda)$ with a flat trace over the restricted resolvent $\mathbf{R}(\lambda)$. This connection is established via a weighted trace formula derived in Section 1.3.1 which is used by the subsequent Section 1.3.2 to represent $Z_f^{\mathbf{X}}(\lambda)$ as a trace and derive meromorphic extension as well as a formula for the residues from this representation.

1.3.1. A Weighted Trace Formula

The main tool for connecting the restricted resolvent with the weighted zeta function is a weighted version of the Atiyah-Bott-Guillemin trace formula which will be presented in this section. The proof is subdivided into three steps: First it is shown that the left-hand side of the trace formula is well-defined by estimating its wavefront set (Section 1.3.1). Next comes the proof a local version of the trace formula which amounts to choosing suitable coordinates and manipulating the resulting distributions on $\mathbb{R}^n$ (Section 1.3.1). Finally the local trace formula gets combined with a partition of unity argument to obtain the global version (Section 1.3.1). An unweighted formulation for open systems can be found in [DG16, Eq. (4.6)] and an analogous result for the compact case is presented in [DZ16, Eq. (2.4)].

Statement and Wavefront Estimate

The overall goal in the following sections is to prove the weighted Atiyah-Bott-Guillemin trace formula:

Lemma 1.3.1: Weighted Atiyah-Bott-Guillemin Trace Formula

For any cut-offs $\chi \in \mathrm{C}_\mathrm{c}^\infty(\mathbb{R}\backslash\{0\})$ and $\widetilde{\chi} \in \mathrm{C}_\mathrm{c}^\infty(\mathcal{U})$, with $\widetilde{\chi} \equiv 1$ near the trapped set K, the following holds:

$$\operatorname{tr}^\flat\left(\int_{\mathbb{R}} \chi(t) \widetilde{\chi} \mathrm{e}^{-t\mathbf{X}} f \widetilde{\chi} \mathrm{d}t \right) = \sum_\gamma \frac{\chi(T_\gamma)\operatorname{tr}(\alpha_\gamma)}{|\det(\mathrm{id} - \mathcal{P}_\gamma)|} \int_{\gamma^\#} f \,, \tag{1.3.4}$$

where the sum is over all closed orbits γ of φ_t.

Proof. The proof is directly adapted from [DG16, Sec. 4.1] and [DZ16, App. B] but the main points can already be found in [Gui77, §2 of Lecture 2]. The presentation proceeds in three steps spread out over the present and the following two subsections:

(1.) Show that the flat trace on the left-hand side is well-defined.

(2.) Prove a local version of the theorem.

(3.) Combine the local version with a partition of unity argument to prove the global theorem.

First of all, let $\chi \in \mathrm{C}_{\mathrm{c}}^{\infty}(\mathbb{R}\backslash\{0\})$ be given. Then $\mathbf{A}_{f,\chi} \coloneqq \int_{\mathbb{R}} \chi(t)\widetilde{\chi}\mathrm{e}^{-t\mathbf{X}}f\widetilde{\chi}\mathrm{d}t$ is an operator

$$\mathbf{A}_{f,\chi} : \mathrm{C}^{\infty}(\mathcal{M},\mathcal{E}) \longrightarrow \mathrm{C}^{\infty}(\mathcal{M},\mathcal{E}) \subseteq \mathcal{D}'(\mathcal{M},\mathcal{E}) \ ,$$

and via the Schwartz kernel theorem one can consider the integrand $\widetilde{\chi}\mathrm{e}^{-t\mathbf{X}}f\widetilde{\chi}$ as an operator

$$\mathrm{C}_{\mathrm{c}}^{\infty}(\mathbb{R}\backslash\{0\}) \to \mathcal{D}'(\mathcal{M}\times\mathcal{M}, \mathcal{E}\boxtimes\mathcal{E}^*) \ .$$

Applying the Schwartz kernel theorem once more therefore yields as its kernel a distribution $\mathbf{K}_f(x,y,t) \in \mathcal{D}'(\mathcal{M}\times\mathcal{M}\times\mathbb{R}\backslash\{0\}, \mathcal{E}\boxtimes\mathcal{E}^*)$:

$$\mathbf{A}_{f,\chi}\big(\mathbf{u}\big)(x) = \int_{\mathcal{M}\times\mathbb{R}} \mathbf{K}_f(x,y,t)\mathbf{u}(y)\chi(t)\mathrm{d}y\mathrm{d}t \ ,$$

where $\mathrm{d}y$ is the same (fixed but arbitrary) density on $\mathcal{M}$ used to define the kernel of $\mathbf{A}_{f,\chi}$ and $\mathbf{u} \in \mathrm{C}^{\infty}(\mathcal{M},\mathcal{E})$ is any smooth section of the bundle $\mathcal{E}$.

At this point Theorem 1.2.3 immediately shows that

$$\mathrm{WF}(\mathbf{K}_{f,\chi}) \subseteq \{(x,y,\xi,\eta) \,|\, \exists t \in \mathrm{supp}(\chi) \,\text{with}\, (x,y,t,\xi,\eta,0) \in \mathrm{WF}(\mathbf{K}_f)\} \ , \tag{1.3.5}$$

where $\mathbf{K}_{f,\chi} \in \mathcal{D}'(\mathcal{M}\times\mathcal{M}, \mathcal{E}\boxtimes\mathcal{E}^*)$ denotes the kernel of $\mathbf{A}_{f,\chi}$. As $\mathbf{K}_{f,\chi}$ is compactly supported by virtue of $\widetilde{\chi}$ one is left with the task of estimating the wavefront set of the kernel $\mathbf{K}_f$.

To do so, first of all note that the Leibniz rule (1.1.2) implies that $\mathrm{e}^{t\mathbf{X}}(f\mathbf{u}) = (f\circ\varphi_t)\left(\mathrm{e}^{t\mathbf{X}}\mathbf{u}\right)$ holds by differentiating both sides with respect to t and using uniqueness. Now suppose that $\chi\otimes\mathbf{u}\otimes\mathbf{v} \in \mathrm{C}_{\mathrm{c}}^{\infty}(I)\otimes\mathrm{C}^{\infty}(\mathcal{M},\mathcal{E})\otimes\mathrm{C}^{\infty}(\mathcal{M},\mathcal{E})$ is supported in a small coordinate patch $U\times U' \subseteq \mathcal{M}\times\mathcal{M}$ and an open $I \subseteq \mathbb{R}\backslash\{0\}$. Then one may assume $\mathbf{u} = u^i\mathbf{e}_i$, $\mathbf{v} = v^i\mathbf{e}'_i$ for local (orthonormal) frames $\{\mathbf{e}_i\}$ on U and $\{\mathbf{e}'_j\}$ on U', which allows

the following calculation[8]

$$\begin{aligned}
&\langle \mathbf{K}_f, \chi \otimes \mathbf{v} \otimes \mathbf{u} \rangle \\
&= \int_{\mathcal{M}} \langle (\mathbf{A}_{f,\chi}\mathbf{u})(x), \mathbf{v}(x) \rangle_{\mathcal{E}} \, \mathrm{d}x \\
&= \int_{\mathcal{M}} \left\langle \int_{\mathbb{R}} \chi(t)\widetilde{\chi}(x) \mathrm{e}^{-t\mathbf{X}} (f\widetilde{\chi}\mathbf{u})(x) \mathrm{d}t, \mathbf{v}(x) \right\rangle_{\mathcal{E}} \mathrm{d}x \\
&= \int_{\mathcal{M}\times\mathbb{R}} \chi(t)\widetilde{\chi}(x) \left\langle \mathrm{e}^{-t\mathbf{X}} (f\widetilde{\chi}\mathbf{u})(x), \mathbf{v}(x) \right\rangle_{\mathcal{E}} \mathrm{d}t\mathrm{d}x \\
&= \sum_{ij} \int_{\mathcal{M}\times\mathbb{R}} \chi(t) \left(f\widetilde{\chi}u^i\right)(\varphi_{-t}(x)) \left(\widetilde{\chi}v^j\right)(x) \left\langle \mathrm{e}^{-t\mathbf{X}} (\mathbf{e}_i), \mathbf{e}'_j \right\rangle_{\mathcal{E}} (x) \, \mathrm{d}t\mathrm{d}x \ .
\end{aligned}$$

These calculations already deduce that the Schwartz kernel $\mathbf{K}_f$ is supported on the graph $\Gamma_\varphi \coloneqq \{(x, \varphi_{-t}(x), t) \,|\, x \in \mathcal{M},\, t \in \mathbb{R}\}$ of φ_{-t}. To explicitly identify it as a smooth function multiplied with the delta function on Γ_φ one proceeds as follows:[9] Let $\widetilde{U} \subseteq U$ be a smaller coordinate neighborhood and fix a cutoff function $\rho \in \mathrm{C}^\infty_{\mathrm{c}}(U)$ with $\rho\big|_{\widetilde{U}} \equiv 1$. Then define the local component functions $a_{ij} \in \mathrm{C}^\infty(\widetilde{U} \times I)$ of the transfer operator via

$$\left(\mathrm{e}^{-t\mathbf{X}}\rho\mathbf{e}_j\right)(x) = \sum_i a_{ij}(x,t)\mathbf{e}_i(x) \ , \qquad x \in U,\, t \in I \ . \tag{1.3.6}$$

The above suppresses the dependency of the components a_{ij} on the charts for the sake of simplicity. Now choosing two additional cutoff functions $\phi \in \mathrm{C}^\infty_{\mathrm{c}}(\widetilde{U})$ and $\psi \in \mathrm{C}^\infty_{\mathrm{c}}(U')$ (note that $\phi = \rho\phi$) allows one to calculate the local components of the Schwartz kernel $\mathbf{K}_f$ w.r.t. the local frames $\{\mathbf{e}_i\}$ and $\{\mathbf{e}'_j\}$:

$$\begin{aligned}
&(\mathbf{K}_f)_{ij} \\
&\coloneqq \langle \mathbf{K}_f, \chi \otimes \left(\psi\mathbf{e}'_j\right) \otimes (\phi\mathbf{e}_i) \rangle \\
&= \sum_k \int_{U'} \int_I \chi(t) \left(f\widetilde{\chi}\phi\right)(\varphi_{-t}(x)) \left(\widetilde{\chi}\psi\right)(x) a_{ki}(x,t) \left\langle \mathbf{e}_k, \mathbf{e}'_j \right\rangle_{\mathcal{E}} (x) \, \mathrm{d}t\mathrm{d}x \ .
\end{aligned}$$

Now note that the wavefront set of $\mathbf{K}_f$ was defined above locally as the union of the wavefront sets of its component functions $(\mathbf{K}_f)_{ij}$. But the calculation above shows that these components are delta distributions on the graph of φ_{-t}, i.e. the submanifold Γ_φ, multiplied by some smooth functions. The final wavefront set is therefore contained in the conormal bundle $N^*\Gamma_\varphi$ given by [Hör13, Example 8.2.5]:

$$N^*\Gamma_\varphi \coloneqq \left\{ (x, y, t, \xi, \eta, \tau) \in T^*(\mathcal{M} \times \mathcal{M} \times \mathbb{R}) \,\middle|\, y = \varphi_{-t}(x),\, (\xi, \eta, \tau)\big|_{T(\Gamma_\varphi)} = 0 \right\} \ .$$

It is well-known that the tangent space to a graph is the image of the differential of the function defining the graph. Thus,

$$T_{(x,\varphi_{-t}(x),t)}(\Gamma_\varphi) = \left\{ (v, (\mathrm{d}\varphi_{-t}(x))v - \theta X_{\varphi_{-t}(x)}, \theta) \,\middle|\, v \in T_x\mathcal{M},\, \theta \in T_t\mathbb{R} = \mathbb{R} \right\} \ ,$$

[8] These formulae employ the Bochner integral for families of linear operators T_t which is defined via $\left(\int T_t \mathrm{d}t\right) v \coloneqq \int (T_t v)\mathrm{d}t$ and such that pointwise evaluation is linear and continuous.

[9] This is very similar to directly computing that the Schwartz kernel of φ^*_{-t} as a distribution in $\mathbb{R}\backslash\{0\} \times \mathcal{M} \times \mathcal{M}$ is a delta distribution on $\{y = \varphi_{-t}(x)\}$: In the scalar case, $\varphi^*_{-t} : \chi(t) \otimes f \otimes g \mapsto \int_{\mathcal{M}\times\mathbb{R}} \chi(t)(f \circ \varphi_{-t})(x)g(x)\mathrm{d}x\mathrm{d}t$ yields the kernel $\psi(t,x,y) \mapsto \int_{\mathcal{M}\times\mathbb{R}} \psi(t, x, \varphi_{-t}(x))\mathrm{d}x\mathrm{d}t$ for φ^*_{-t}.

and this immediately yields that $\mathrm{WF}(\mathbf{K}_f)$ is contained in

$$\big\{(x,y,t,\xi,\eta,\tau)\in T^*(\mathcal{M}\times\mathcal{M}\times\mathbb{R})\,\big|\,y=\varphi_{-t}(x),\,\eta\neq 0,\,\xi=-(\mathrm{d}\varphi_{-t}(x))^T\eta,\\ \tau=\langle\eta,X_y\rangle,\,x,y\in\mathrm{supp}(\widetilde{\chi})\big\}\ .$$

At this point it is possible to substitute into (1.3.5) to estimate the wavefront set of the right-hand side of the trace formula as follows:

$$\mathrm{WF}(\mathbf{K}_{f,\chi})\subseteq\big\{(x,y,\xi,\eta)\in T^*(\mathcal{M}\times\mathcal{M})\,\big|\,\exists t\in\mathrm{supp}(\chi)\,x,y\in\mathrm{supp}(\widetilde{\chi}):\\ y=\varphi_{-t}(x),\,\eta\neq 0,\,\xi=-(\mathrm{d}\varphi_{-t}(x))^T\eta,\,\langle\eta,X_y\rangle=0\big\}\ . \tag{1.3.7}$$

This set does not intersect the set $\{(x,x,\xi,-\xi)\,|\,\xi\in T^*_x\mathcal{M}\}$: Any $(x,x,\xi,-\xi)$ contained in the right-hand side of (1.3.7) would satisfy $\varphi_T(x)=x$, for some $T\neq 0$, and $\langle\xi,X_x\rangle=0$ together with $(\mathrm{id}-\mathrm{d}\varphi_{-T}(x)^T)\xi=0$. But $\mathrm{id}-\mathrm{d}\varphi_{-T}(x)$ is invertible on $E_u(x)\oplus E_s(x)$ and $T_x\mathcal{M}=E_u(x)\oplus E_s(x)\oplus X_x$ for any x on a closed geodesic. This therefore lets one conclude $\xi=0$ which does not belong to $\mathrm{WF}(\mathbf{K}_{f,\chi})$. Thus the flat trace on the left-hand side is well defined.

Local Trace Formula

Denoting by

$$i:\ \mathcal{M}\times(\mathbb{R}\backslash\{0\})\to\mathcal{M}\times\mathcal{M}\times(\mathbb{R}\backslash\{0\})$$

the inclusion $(x,t)\mapsto(x,x,t)$ one readily observes that the by Section 1.3.1 well-defined distribution $i^*\mathbf{K}_f$ is supported within

$$i^{-1}(\mathrm{supp}(\mathbf{K}_f))\subseteq\{(x_0,T)\,|\,\varphi_T(x_0)=x_0,\,T\neq 0\}\ .$$

As in [DZ16, Lemma B.1] it therefore makes sense to prove the following local lemma which will be the key ingredient for the final trace formula:

Lemma 1.3.2: Local Weighted Trace Formula

Suppose $x_0\in\mathcal{U}$ and $T\neq 0$ is such that $\varphi_T(x_0)=x_0$. Then there exist $\varepsilon>0$ and an open neighbourhood $x_0\in U\subseteq\mathcal{U}$ with $\varphi_s(x_0)\in U$ for any $|s|<\varepsilon$ and such that for any $\rho(x,t)=\sigma(x)\chi(t)\in\mathrm{C}^\infty_\mathrm{c}(U\times]T-\varepsilon,T+\varepsilon[)$ the following holds:

$$\begin{aligned}\mathrm{tr}^\flat\left(\int_{\mathbb{R}}\rho(x,t)\mathbf{K}_f(x,y,t)\mathrm{d}t\right)&=\int_{\mathbb{R}\times\mathcal{M}}\rho(x,t)\mathbf{K}_f(x,x,t)\mathrm{d}t\mathrm{d}x\\&=\frac{\mathrm{tr}(\alpha_\gamma)}{|\det(\mathrm{id}-\mathcal{P}_\gamma)|}\int_{-\varepsilon}^{\varepsilon}\rho(\varphi_s(x_0),T)f(\varphi_s(x_0))\mathrm{d}s\end{aligned} \tag{1.3.8}$$

Proof. First of all according to [Lee12, Thm. 9.22] there exists a chart $\kappa:U_1\subseteq\mathcal{M}\to\mathrm{B}^n_{\varepsilon_1}(0)$, $\kappa(x)=w$ around x_0 such that

$$\kappa(x_0)=0,\qquad\kappa_*(X)=\partial_{w_1}\ .$$

By composing κ with a suitable linear map one may also assume that

$$\mathrm{d}\kappa(x_0)\,(E_s(x_0)\oplus E_u(x_0))=\{\mathrm{d}w_1=0\}\ .$$

By the joint continuity of the flow φ in the variables (x,t) it is possible to find some $\varepsilon > 0$ such that $U \coloneqq \kappa^{-1}(\mathrm{B}^n_\varepsilon(0))$ satisfies $\varphi_{-t}(U) \subseteq U_1$ for any $|T-t| < \varepsilon$.

Next define two functions $A : \mathrm{B}^{n-1}_\varepsilon(0) \to \mathrm{B}^{n-1}_{\varepsilon_1}(0)$ and $F : \mathrm{B}^{n-1}_\varepsilon(0) \to]-\varepsilon_1, \varepsilon_1[$ by the relation

$$\kappa \circ \varphi_{-T}\left(\kappa^{-1}(0,w')\right) = \big(F(w'), A(w')\big)\,, \qquad \text{for } w' \in \mathbb{R}^{n-1},\ |w'| < \varepsilon\ .$$

Obviously $F(0) = 0$ and $A(0) = 0$. By the assumption $\kappa_*(X) = \partial_{w_1}$ one gets that $\varphi_{-T}\left(\kappa^{-1}(w_1,w')\right) = \kappa^{-1}\left(w_1 + F(w'), A(w')\right)$ for any $(w_1,w') \in \mathrm{B}^n_\varepsilon(0)$. Similarly it holds for $|T-t| < \varepsilon$ that

$$\varphi_{-t}\left(\kappa^{-1}\left(w_1,w'\right)\right) = \kappa^{-1}\left(T - t + w_1 + F(w'), A(w')\right)\ .$$

Within this local setup the flat trace may be calculated explicitly. First assume that the density $\mathrm{d}x$ used to define $\mathbf{K}_f$ is translated into the standard density on $\mathbb{R}^n$ under κ.[10] The tricky part of calculating the pullback of $\sigma\mathbf{K}_{f,\chi}$ along the inclusion $\iota : \mathcal{M} \ni x \mapsto (x,x) \in \mathcal{M}\times\mathcal{M}$ is given by the singular portion of $\mathbf{K}_{f,\chi}$. One therefore starts by calculating the pullback of $\delta_{y=\varphi_{-t}(x)}$ along $\widetilde{\kappa}^{-1} : (w,t) \mapsto (\kappa^{-1}(w), \kappa^{-1}(w), t)$.

To this end let $\psi \in \mathrm{C}^\infty_\mathrm{c}(\mathrm{B}^n_\varepsilon(0) \times \mathrm{B}^n_\varepsilon(0) \times]-\varepsilon,\varepsilon[)$ be an arbitrary test function and observe:

$$\begin{aligned}
&\left\langle \left(\widetilde{\kappa}^{-1}\right)^* \rho\delta_{y=\varphi_{-t}(x)}, \psi \right\rangle \\
&= \int_{\mathrm{B}^n_\varepsilon(0)} \int_{\mathbb{R}} \rho(\kappa^{-1}(w),t)\psi(w, \kappa\circ\varphi_{-t}\circ\kappa^{-1}(w), t)\mathrm{d}w\mathrm{d}t \\
&= \int_{\mathrm{B}^n_\varepsilon(0)} \int_{\mathbb{R}} \rho(\kappa^{-1}(w_1,w'),t)\psi((w_1,w'),(T-t+w_1+F(w'),A(w')),t)\mathrm{d}w_1\mathrm{d}w'\mathrm{d}t\ .
\end{aligned} \tag{1.3.9}$$

In summary Equation (1.3.9) implies that in coordinates $\rho\delta_{y=\varphi_{-t}(x)}$ equals $\rho(\kappa^{-1}(w),t)\delta(z_1 - T + t - w_1 - F(w'))\delta(z' - A(w'))$, with $z = (z_1, z')$. Distributions of this form are well known:

Let $U, V \subseteq \mathbb{R}^n$ be open and $f : U \to V$ a smooth function and define $b : U \times U \to \mathbb{R}^n$ by $b(x,y) \coloneqq y - f(x)$. Now observe

$$\delta(y - f(x)) \coloneqq \delta(y = f(x)) = b^*\delta_0\ ,$$

where δ_0 is the delta distribution at $x_0 = 0$: $\langle\delta_0,\varphi\rangle = \varphi(0)$. The pullback is well-defined because b is a submersion ([Hör13, Thm. 6.1.2]) and standard techniques can calculate it concretely: Let $\rho \in \mathrm{C}^\infty_\mathrm{c}(\mathbb{R}^n)$ be such that $\mathrm{supp}(\rho) \subseteq \mathrm{B}^n_1(0)$ and $\int \rho(x)\mathrm{d}x = 1$. Setting $\rho_\varepsilon(x) \coloneqq \varepsilon^{-n}\rho(x/\varepsilon)$ one has $\rho_\varepsilon \to \delta_0$ for $\varepsilon \to 0$ in $\mathcal{D}'$. For any $\varphi \in \mathrm{C}^\infty_c(U\times U)$ it holds that

$$\begin{aligned}
\langle\delta(y-f(x)),\varphi\rangle &= \lim_{\varepsilon\to 0} \int\int \rho_\varepsilon(y-f(x))\varphi(x,y)\mathrm{d}y\mathrm{d}x \\
&= \lim_{\varepsilon\to 0} \varepsilon^{-n} \int\int \rho_\varepsilon(y-f(x))\mathrm{d}y\,\varphi(x, y_{f(x),\varepsilon})\mathrm{d}x \\
&= \int \varphi(x,f(x))\mathrm{d}x\ ,
\end{aligned} \tag{1.3.10}$$

where $y_{f(x),\varepsilon}$ is a sequence of points with $|y_{f(x),\varepsilon} - f(x)| < \varepsilon$ and therefore $y_{f(x),\varepsilon} \to f(x)$ for $\varepsilon \to 0$.

[10] One may do this as the flat trace is independent of the choice of density (c.f. [DZ16, Section 2.4]).

Next let $g : U \to V$ be a smooth submersion (i.e. a local diffeomorphism, as domain and codomain have the same dimension). Let $(a_i)_{i\in I}$ be the zeros of g: $g(x) = 0 \Leftrightarrow x = a_i$ for some $i \in I$. Then one calculates the action of $g^*\delta_0$ on some $\varphi \in \mathrm{C}_\mathrm{c}^\infty(U)$ as follows by regarding δ_0 as an element of $\mathcal{D}'(V)$:

$$\begin{aligned}\langle g^*\delta_0, \varphi\rangle &= \lim_{\varepsilon\to 0}\int_V \rho_\varepsilon(g(x))\varphi(x)\mathrm{d}x \\ &= \lim_{\varepsilon\to 0}\int_D \rho_\varepsilon(g(x))\varphi(x)\mathrm{d}x\ ,\end{aligned} \tag{1.3.11}$$

where $D \coloneqq \mathrm{supp}(\varphi) \cap g^{-1}(\overline{\mathrm{B}}_\varepsilon^n(0))$. Now D is compact and contains, as g is a local diffeomorphism, only finitely many of the a_i, say $(a_i)_{i\in I'}$. Thus there exists $\delta > 0$ such that $g\big|_{\mathrm{B}_\delta^n(a_i)}$ is invertible for all $i \in I'$. Furthermore, $D\backslash\bigcup_{i\in I'}\mathrm{B}_\delta^n(a_i)$ is still compact and g restricted to this set is strictly positive. It is therefore possible to assume, by choosing ε small enough, that $D \subseteq \bigcup_{i\in I'}\mathrm{B}_\delta^n(a_i)$ and this implies

$$\begin{aligned}\langle g^*\delta_0, \varphi\rangle &= \lim_{\varepsilon\to 0}\sum_{i\in I'}\int_{\mathrm{B}_\delta^n(a_i)}\rho_\varepsilon(g(x))\varphi(x)\mathrm{d}x \\ &= \sum_{i\in I'}\lim_{\varepsilon\to 0}\int_{g\left(\mathrm{B}_\delta^n(a_i)\right)}\rho_\varepsilon(y)\varphi(g^{-1}(y))|\det\left((g^{-1})'(y)\right)|\mathrm{d}y \\ &= \sum_{i\in I'}\frac{\varphi(a_i)}{|\det(g'(a_i))|} = \sum_{i\in I}\frac{\varphi(a_i)}{|\det(g'(a_i))|}\ ,\end{aligned} \tag{1.3.12}$$

where the second equality follows by the transformation formula for diffeomorphisms. Noting again that any compact subset of U can only contain finitely many a_i the distribution finally reduces to the expression

$$g^*\delta_0 = \sum_{a\in g^{-1}(0)}\frac{\delta(x-a)}{|\det(g'(a))|}\ . \tag{1.3.13}$$

An application of this knowledge to our original distribution leads to $\iota^*\delta(y - f(x)) = \delta(x - f(x)) = |\det(\mathrm{id} - f'(0))|^{-1}\delta_0$ if $f(x) = x$ holds only for $x = 0$ and $f'(0)$ has no eigenvalue equal to one.

To calculate further consider the solutions to the equation $A(w') = w'$. The formula

$$\varphi_{-(T+F(w'))}\left(\kappa^{-1}(0,w')\right) = \kappa^{-1}\left(T - T - F(w') + F(w'), A(w')\right) = \kappa^{-1}(0, A(w'))\ ,$$

shows that $A(w') = w'$ entails that $\kappa^{-1}(0, w')$ lies on a closed trajectory with period $T + F(w')$. But ε can be chosen small enough that U does not intersect any closed trajectory with period in $[T - \varepsilon, T + \varepsilon]$ apart from $\varphi_t(x_0)$. Then $A(w') = w'$ implies $(0, w') = \kappa(x_0) = (0, 0)$ and indeed $w' = 0$. Combining these results and writing $\delta(x, y) = \int\chi(t)\delta_{y=\varphi_{-t}(x)}\mathrm{d}t$ results in

$$\begin{aligned}\langle\iota^*\left(\sigma(x)\delta(x,y)\right), \mathbf{1}\rangle &= \int_{\mathrm{B}_\varepsilon^n(0)}\rho(\kappa^{-1}(w_1,w'), T + F(w'))\delta(w' - A(w'))\mathrm{d}w_1\mathrm{d}w' \\ &= \frac{1}{|\det(\mathrm{id} - A'(0))|}\int_{-\varepsilon}^{\varepsilon}\rho(\kappa^{-1}(w_1, 0), T)\mathrm{d}w_1 \\ &= \frac{1}{|\det(\mathrm{id} - \mathcal{P}_\gamma)|}\int_{-\varepsilon}^{\varepsilon}\rho(\varphi_s(x_0), T)\mathrm{d}s\ ,\end{aligned} \tag{1.3.14}$$

where the last equality comes from the fact that $A'(0)$ is conjugated to $\mathcal{P}_\gamma$, where γ is the closed geodesic with period T containing x_0, via the map $\mathrm{d}\kappa(x_0)$ and $\varphi_{s-T}(x_0) = \kappa^{-1}(s,0)$. Note that one can integrate over $[0, T_\gamma^\#]$ instead of $[-\varepsilon, \varepsilon]$ as $\rho = 0$ outside the arc $\{\varphi_s(x_0) \,|\, s \in [-\varepsilon,\varepsilon]\} = \left\{\varphi_s(x_0) \,\middle|\, s \in [0,\varepsilon] \cup [T_\gamma^\# - \varepsilon, T_\gamma^\#]\right\}$.

The final step needs to combine this result with the additional smooth factors appearing in the actual kernel $\mathbf{K}_{f,\chi}$: First there are additional cut-off functions $\widetilde{\chi}$ and the weight function f but these can be taken care of by substituting $\widetilde{\chi}\rho\widetilde{\chi}f$ instead of ρ everywhere. The final integral will then contain ρf instead of ρ as $\widetilde{\chi} = 1$ on the trapped set K.

Finally, the flat trace of the $\mathcal{E} \boxtimes \mathcal{E}^*$-valued kernel $\mathbf{K}_f$ contains the trace over the local matrix coefficients defined in (1.3.6), i.e. the smooth function $\sum_i a_{ii}(\varphi_s(x_0), T)$ inside the integral. But given a local frame $\{\mathbf{e}_i\}$ one immediately calculates that

$$\alpha_{x,t} : \mathbf{e}_i(x) \longmapsto \left(\mathrm{e}^{-t\mathbf{X}}\mathbf{e}_i\right)(\varphi_t(x)) = \sum_j a_{ji}(\varphi_t(x), t)\mathbf{e}_j(\varphi_t(x)) \ ,$$

i.e. the matrix representing $\alpha_{x_0,T}$ in the basis $\{\mathbf{e}_i(x_0)\}$ is $(a_{ij}(\varphi_T(x_0), T))$. One therefore has

$$\sum_i a_{ii}(x_0, T) = \mathrm{tr}(\alpha_\gamma) = \sum_i a_{ii}(\varphi_s(x_0), T)$$

for all s, because the $\alpha_{\gamma(s),T}$ are conjugated to each other. Plugging this last ingredient into (1.3.14) yields the local trace formula. □

Completing the Proof

Now a *partition of unity* argument finishes the proof of Lemma 1.3.1: Let $\chi \in \mathrm{C}_\mathrm{c}^\infty(\mathbb{R}\backslash\{0\})$ and denote by $\mathcal{L}(\chi)$ the (finite) set of all closed trajectories γ of φ_t with periods T_γ contained in $\mathrm{supp}(\chi)$.

By compactness of γ any $\gamma \times \{T_\gamma\}$, $\gamma \in \mathcal{L}(\chi)$, can be covered by finitely many $U_{i,\gamma} \times]T_\gamma - \varepsilon_{i,\gamma}, T_\gamma + \varepsilon_{i,\gamma}[$ according to Lemma 1.3.2. Given a partition of unity $\chi_{i,\gamma}(x)$ subordinate to $\{U_{i,\gamma}\}$ one calculates

$$\begin{aligned}\mathrm{tr}^\flat\left(\mathbf{K}_{f,\chi}\right) &= \sum_{\gamma\in\mathcal{L}(\chi)} \sum_i \int_{\mathbb{R}\times\mathcal{M}} \chi(t)\chi_{i,\gamma}(x)\mathbf{K}_f(x,x,t)\mathrm{d}t\mathrm{d}x \\ &= \sum_\gamma \frac{\mathrm{tr}(\alpha_\gamma)\chi(T_\gamma)}{|\det(\mathrm{id} - \mathcal{P}_\gamma)|} \sum_i \int_{-\varepsilon_{i,\gamma}}^{\varepsilon_{i,\gamma}} \chi_{i,\gamma}(\varphi_s(x_{i,\gamma}))f(\varphi_s(x_{i,\gamma}))\mathrm{d}s\end{aligned}$$

Finally looking only at a fixed geodesic γ lets one drop the second subscript and write, by using the semi-group property of the flow,

$$\begin{aligned}\sum_i \int_{-\varepsilon_i}^{\varepsilon_i} \chi_i(\varphi_s(x_i))f(\varphi_s(x_i))\mathrm{d}s &= \sum_i \int_0^{T_\gamma^\#} \chi_i(\varphi_s(x_0))f(\varphi_s(x_0))\mathrm{d}s \\ &= \int_0^{T_\gamma^\#} f(\varphi_s(x_0))\mathrm{d}s = \int_{\gamma^\#} f \ ,\end{aligned}$$

which follows from the fact that the U_i cover $\gamma^\#$, $\varphi_\cdot(x_0)$ is a diffeomorphism from the torus of circumference $T_\gamma^\#$ onto $\gamma^\#$, and the χ_i are compactly supported on an arc of γ. □

1.3.2. Proof of the Main Theorem

This section finally proves the main theorem namely *meromorphic continuation* of the weighted zeta function $Z_f^{\mathbf{X}}(\lambda)$ of an open hyperbolic system $(\mathcal{U}, \varphi_t, \mathbf{X})$ and weight $f \in \mathrm{C}^\infty(\mathcal{U})$ as defined in Equation (1.3.3). In particular meromorphic continuation together with an explicit formula for the Laurent coefficients of $Z_f^{\mathbf{X}}$ are shown by using the trace formula of the previous Section 1.3.1:

Theorem 1.3.3: Meromorphic Continuation of Weighted Zetas

The weighted zeta function $Z_f^{\mathbf{X}}$ for open hyperbolic systems converges absolutely in $\{\mathrm{Re}(\lambda) \gg 0\}$ and continues meromorphically to $\{\lambda \in \mathbb{C}\}$.
Any pole λ_0 of Z_f is a Pollicott-Ruelle resonance of $\mathbf{X}$ and if λ_0 has order $J(\lambda_0)$ then for $k \leq J(\lambda_0)$ the following residue formula holds:

$$\mathrm{Res}_{\lambda=\lambda_0}\left[Z_f^{\mathbf{X}}(\lambda)(\lambda-\lambda_0)^k\right] = \mathrm{tr}^\flat\left((\mathbf{X}-\lambda_0)^k \Pi_{\lambda_0} f\right).$$

Proof. Proving that the formal expression (1.3.3) defines a holomorphic function on $\{\mathrm{Re}(\lambda) \gg 0\}$ is rather straightforward by showing uniform convergence on compact sets. To this end consider every term separately and then combine the results for a final estimate:

(1.) $\mathrm{N}(T) \coloneqq |\{\gamma \,|\, T_\gamma \leq T\}| \leq C_0 \mathrm{e}^{C_1 T}$ for constants $C_0, C_1 > 0$ according to [DZ16, Lemma 1.17].

(2.) $|\det(\mathrm{id} - \mathcal{P}_\gamma)|$ is bounded below by a constant $C_2 > 0$ as the converse would contradict the existence of a uniform contraction/expansion constant $\gamma > 0$.

(3.) $|\mathrm{tr}(\alpha_\gamma)| \leq C_4 \mathrm{e}^{C_3 T_\gamma}$ by the operator norm estimate on $\mathrm{e}^{-t\mathbf{X}}$.

Combining (1.), (2.) and (3.) results in

$$\begin{aligned}
\sum_\gamma \left| \frac{\mathrm{e}^{-\lambda T_\gamma}\mathrm{tr}(\alpha_\gamma)}{|\det(\mathrm{id}-\mathcal{P}_\gamma)|} \int_{\gamma^\#} f \right| &\leq \sum_{n\in\mathbb{N}} \sum_{T_\gamma \in]n-1,n]} \left| \frac{\mathrm{e}^{-\lambda T_\gamma}\mathrm{tr}(\alpha_\gamma)}{|\det(\mathrm{id}-\mathcal{P}_\gamma)|} \int_{\gamma^\#} f \right| \\
&\leq \sum_{n\in\mathbb{N}} C_0 \mathrm{e}^{C_1 n} |\mathrm{e}^{-(n-1)\lambda}| C_4 \mathrm{e}^{C_3 n} C_2^{-1} n |f|_K \\
&\leq C \sum_{n\in\mathbb{N}} n \cdot \left(\mathrm{e}^{C-\mathrm{Re}(\lambda)}\right)^n
\end{aligned}$$

$Z_f(\lambda)$ thus converges uniformly if λ varies in a compact subset of $\mathrm{Re}(\lambda) > C$. In conclusion, the function $Z_f(\lambda)$ is holomorphic on some right halfplane.

The proof proceeds by expressing the weighted zeta function as the flat trace of an expression involving the *restricted resolvent* and using the trace formula presented in Section 1.3.1 as the main tool. The presentation closely follows [DZ16, §4]. It begins by choosing $0 < t_0 < T_\gamma \,\forall\gamma$, $\chi_T \in \mathrm{C}_\mathrm{c}^\infty(]t_0/2, T+1[)$ and $\chi_T \equiv 1$ on $[t_0, T]$. Furthermore assume t_0 small enough such that $\varphi_{-t_0}(\mathrm{supp}(\widetilde{\chi})) \subseteq \mathcal{U}$. Then define the family of operators

$$B_T \coloneqq \int_0^\infty \chi_T(t) \mathrm{e}^{-\lambda t} \left(\widetilde{\chi} \mathrm{e}^{-t\mathbf{X}} \widetilde{\chi} f\right) \mathrm{d}t \,,$$

and Lemma 1.3.1 shows that for $\mathrm{Re}(\lambda) \gg 0$

$$\begin{aligned}\lim_{T\to\infty} \mathrm{tr}^\flat\left(B_T\right) &= \lim_{T\to\infty} \sum_\gamma \frac{\chi_T(T_\gamma)\mathrm{e}^{-\lambda T_\gamma}\mathrm{tr}(\alpha_\gamma)}{|\det(\mathrm{id}-\mathcal{P}_\gamma)|}\int_{\gamma^\#} f \\ &= \sum_\gamma \frac{\mathrm{e}^{-\lambda T_\gamma}\mathrm{tr}(\alpha_\gamma)}{|\det(\mathrm{id}-\mathcal{P}_\gamma)|}\int_{\gamma^\#} f \ ,\end{aligned}$$

because the right-hand side series converges uniformly for $\mathrm{Re}(\lambda) \gg 0$ by virtue of the exponential growth of the number of closed trajectories $\mathrm{N}(T)$.

Now by [DZ16, Lemma 2.8] there exists a family of smoothing operators[11] $E_\varepsilon \in \Psi^{-\infty}(\mathcal{M}, \mathrm{End}(\mathcal{E}))$, $\varepsilon > 0$, such that

$$\mathrm{tr}^\flat\left(B_T\right) = \lim_{\varepsilon\to 0} \mathrm{tr}\left(E_\varepsilon B_T E_\varepsilon\right) \ ,$$

and the kernels $E_\varepsilon(x,y)$ are supported in $\{(x,y)\in\mathcal{M}\times\mathcal{M}\,|\,\mathrm{d}(x,y)<\varepsilon\}$ for some fixed $c_1 > 0$ and some smooth distance function $\mathrm{d}(\cdot,\cdot)$. Here the right-hand side trace is taken in $\mathrm{L}^2(\mathcal{M},\mathcal{E})$. It exists as $E_\varepsilon B_T E_\varepsilon$ is smoothing and thus trace class by the compactness of $\mathcal{M}$. Now consider the following splitting of the integral over the t-variable (note that the L^2-trace is a bounded linear operator and therefore commutes with $\int \mathrm{d}t$):

$$\begin{aligned}\mathrm{tr}(E_\varepsilon B_T E_\varepsilon) = &\int_{t_0/2}^{t_0} \chi_T(t)\mathrm{e}^{-\lambda t}\mathrm{tr}\left(E_\varepsilon\widetilde{\chi}\mathrm{e}^{-t\mathbf{X}}\widetilde{\chi}fE_\varepsilon\right)\mathrm{d}t \\ &+ \int_{t_0}^{\infty} \chi_T(t)\mathrm{e}^{-\lambda t}\mathrm{tr}\left(E_\varepsilon\widetilde{\chi}\mathrm{e}^{-t\mathbf{X}}\widetilde{\chi}fE_\varepsilon\right)\mathrm{d}t \ .\end{aligned}$$

As in [DZ16, §4] the first summand vanishes for ε small enough because

$$\begin{aligned}&\mathrm{tr}\left(E_\varepsilon\widetilde{\chi}\mathrm{e}^{-t\mathbf{X}}\widetilde{\chi}fE_\varepsilon\right) \\ &= \int_{\mathcal{M}\times\mathcal{M}} E_\varepsilon(x,y)\widetilde{\chi}(y)\left(\sum_i a_{ii}(y,t)\right) f(\varphi_{-t}(y))\widetilde{\chi}(\varphi_{-t}(y))E_\varepsilon(\varphi_{-t}(y),x)\mathrm{d}y\mathrm{d}x \ ,\end{aligned}$$

and $E_\varepsilon(x,y) = 0$ if $\mathrm{d}(x,y) \geq c_1\varepsilon$ by the support property of the kernel $E_\varepsilon(x,y)$. By $t_0 < T_\gamma$ for all closed γ the minimum c_2 of $\mathrm{d}(\varphi_{-t}(x),x)$ for $t\in[t_0/2,t_0]$ and $x\in\mathcal{M}$ is strictly positive; if one chooses $\varepsilon < c_2/(2c_1)$ then

$$E_\varepsilon(x,y)E_\varepsilon(\varphi_{-t}(y),x) \neq 0$$

would imply $\mathrm{d}(x,y) < c_1\varepsilon$ *and* $\mathrm{d}(\varphi_{-t}(y),x) < c_1\varepsilon$, i.e. $\mathrm{d}(y,\varphi_{-t}(y)) < 2c_1\varepsilon < c_2$, a contradiction. The integrand and therefore the trace vanishes for $t\in[t_0/2,t_0]$.

Next one can interchange the limits in T and ε, again for $\mathrm{Re}(\lambda)$ sufficiently large,

$$\lim_{T\to\infty} \mathrm{tr}^\flat\left(B_T\right) = \lim_{T\to\infty}\lim_{\varepsilon\to 0} \mathrm{tr}\left(E_\varepsilon B_T E_\varepsilon\right) = \lim_{\varepsilon\to 0}\lim_{T\to\infty} \mathrm{tr}\left(E_\varepsilon B_T E_\varepsilon\right) \ ,$$

as the limit $\varepsilon\to 0$ exists for any finite T and the limit $T\to\infty$ is uniform in $\varepsilon > 0$. To see the latter, simply observe that the same calculation as in [DZ16, Lemma 4.1] shows

$$\int_T^{T+1} \left|\mathrm{tr}\left(\mathrm{e}^{-\lambda t}E_\varepsilon\widetilde{\chi}\mathrm{e}^{-t\mathbf{X}}\widetilde{\chi}fE_\varepsilon\right)\right|\mathrm{d}t \leq C\mathrm{e}^{-\mathrm{Re}(\lambda)T}\mathrm{e}^{CT} \ , \tag{1.3.15}$$

[11] One can directly apply the scalar-valued version of [DZ16] by choosing the mollifiers E_ε to be diagonal in the fiber variable.

where the constant C especially contains the supremum of f on the compact support of $\widetilde{\chi}$ and the supremum of the local fiber traces $\sum_i a_{ii}(x,t)$ which in the t-variable can be estimates by $C\mathrm{e}^{C'T}$ due to [DZ16, Eq. (0.9)]. Now (1.3.15) implies

$$\begin{aligned}
&\left|\int_{t_0}^{\infty} \mathrm{e}^{-\lambda t}\mathrm{tr}\left(E_\varepsilon\widetilde{\chi}\mathrm{e}^{-t\mathbf{X}}\widetilde{\chi}fE_\varepsilon\right)\mathrm{d}t - \int_{t_0}^{\infty}\chi_T(t)\mathrm{e}^{-\lambda t}\mathrm{tr}\left(E_\varepsilon\widetilde{\chi}\mathrm{e}^{-t\mathbf{X}}\widetilde{\chi}fE_\varepsilon\right)\mathrm{d}t\right| \\
&\quad\leq \sum_{n=0}^{\infty}\int_{T+n}^{T+n+1}\mathrm{e}^{-\lambda t}\left|\mathrm{tr}\left(E_\varepsilon\widetilde{\chi}\mathrm{e}^{-t\mathbf{X}}\widetilde{\chi}fE_\varepsilon\right)\right|\mathrm{d}t \\
&\quad\leq C\mathrm{e}^{(-\mathrm{Re}(\lambda)+C)T}\sum_{n=0}^{\infty}\mathrm{e}^{(-\mathrm{Re}(\lambda)+C)n} \leq \widetilde{C}\mathrm{e}^{(-\mathrm{Re}(\lambda)+C)T}\ ,
\end{aligned}$$

which indeed converges for $T\to\infty$ and uniformly in $\varepsilon>0$ (an immediate adaptation of the first equation in [DZ16, Lemma 4.1] shows that the integral which is the limit as $T\to\infty$ converges absolutely for every $\varepsilon>0$).

Using the commutativity of the two limits and the absolute convergence of the integral in the t-variable one finally arrives at the expression

$$\lim_{T\to\infty}\mathrm{tr}^\flat\left(B_T\right) = \lim_{\varepsilon\to 0}\int_{t_0}^{\infty}\mathrm{e}^{-\lambda t}\mathrm{tr}\left(E_\varepsilon\widetilde{\chi}\mathrm{e}^{-t\mathbf{X}}\widetilde{\chi}fE_\varepsilon\right)\mathrm{d}t\ ,$$

where $\mathrm{Re}(\lambda)\gg 0$. One therefore has

$$\begin{aligned}
Z_f^{\mathbf{X}}(\lambda) &\coloneqq \sum_\gamma \frac{\mathrm{e}^{-\lambda T_\gamma}\mathrm{tr}(\alpha_\gamma)}{|\det(\mathrm{id}-\mathcal{P}_\gamma)|}\int_{\gamma^\#} f = \lim_{T\to\infty}\mathrm{tr}^\flat(B_T) \\
&= \lim_{\varepsilon\to 0}\int_0^{\infty}\mathrm{e}^{-\lambda(t+t_0)}\mathrm{tr}\left(E_\varepsilon\widetilde{\chi}\mathrm{e}^{-(t+t_0)\mathbf{X}}\widetilde{\chi}fE_\varepsilon\right)\mathrm{d}t \\
&= \mathrm{e}^{-\lambda t_0}\lim_{\varepsilon\to 0}\mathrm{tr}\left(E_\varepsilon\widetilde{\chi}\mathrm{e}^{-t_0\mathbf{X}}\left(\int_0^{\infty}\mathrm{e}^{-\lambda t}\mathrm{e}^{-t\mathbf{X}}\mathrm{d}t\right)\widetilde{\chi}fE_\varepsilon\right) \\
&= \mathrm{e}^{-\lambda t_0}\lim_{\varepsilon\to 0}\mathrm{tr}\left(E_\varepsilon\widetilde{\chi}\mathrm{e}^{-t_0\mathbf{X}}(\mathbf{X}+\lambda)^{-1}\widetilde{\chi}fE_\varepsilon\right)\ ,
\end{aligned} \tag{1.3.16}$$

which at first only holds for $\mathrm{Re}(\lambda)\gg 0$. At this point one would of course want to apply the meromorphic continuation of the *restricted resolvent* $\mathbf{R}(\lambda)=\mathbf{1}_{\mathcal{U}}(\mathbf{X}+\lambda)^{-1}\mathbf{1}_{\mathcal{U}}:\Gamma_{\mathrm{c}}^\infty(\mathcal{U},\mathcal{E})\to\mathcal{D}'(\mathcal{U},\mathcal{E})$ as achieved in [DZ16]. To do so first observe that $(\mathbf{X}+\lambda)^{-1}\widetilde{\chi}=(\mathbf{X}+\lambda)^{-1}\mathbf{1}_{\mathcal{U}}\widetilde{\chi}$ by $\mathrm{supp}(\widetilde{\chi})\subseteq\mathcal{U}$. Now even demanding t_0 to be small enough that $\varphi_{-t_0}(\mathrm{supp}(\widetilde{\chi}))\subseteq\mathcal{U}$ holds allows the rewrite $\widetilde{\chi}\mathrm{e}^{-t_0\mathbf{X}}(\mathbf{X}+\lambda)^{-1}\mathbf{1}_{\mathcal{U}}\widetilde{\chi}=\widetilde{\chi}\mathrm{e}^{-t_0\mathbf{X}}\mathbf{1}_{\mathcal{U}}(\mathbf{X}+\lambda)^{-1}\mathbf{1}_{\mathcal{U}}\widetilde{\chi}$ by the support property of $\mathrm{e}^{-t_0\mathbf{X}}$.

Now if $\lambda\in\mathbb{C}$ is not a resonance then the general wavefront estimates [Hör13, Example 8.2.5] and [Hör13, Thm. 8.2.14] together with the estimate of $\mathrm{WF}'(\mathbf{R}(\lambda))$ in [DZ16, Equation (3.43)] and the fact that multiplication with smooth functions does not enlarge the wavefront set yield

$$\begin{aligned}
&\mathrm{WF}'\left(\widetilde{\chi}\mathrm{e}^{-t_0(\lambda+\mathbf{X})}\mathbf{R}(\lambda)\widetilde{\chi}f\right) \\
&\subseteq\left\{\left(\mathrm{e}^{t_0H_p}(x,\xi),x,\xi\right)\ \middle|\ (x,\xi)\in T^*\mathcal{U}\backslash 0\right\}\cup(E_+^*\times E_-^*) \\
&\quad\cup\left\{\left(\mathrm{e}^{(t_0+t)H_p}(x,\xi),x,\xi\right)\ \middle|\ (x,\xi)\in T^*\mathcal{U}\backslash 0,\ t\geq 0,\ p(x,\xi)=0\right\}\ ,
\end{aligned} \tag{1.3.17}$$

where $p(x,\xi)\coloneqq\xi(X_x)$, $\mathrm{e}^{t_0H_p}(x,\xi)=(\varphi_t(x),(\mathrm{d}\varphi_t(x))^{-T}\xi)$ and the wavefront set of $\mathrm{e}^{-t_0\mathbf{X}}$ is contained in the graph of $\mathrm{e}^{t_0H_p}$. Now the wavefront set (1.3.17) *does not intersect* the diagonal: For the first component this immediately follows from $t_0<T_\gamma$ for all closed

orbits γ and for the second component it is implied by the directness of the dual hyperbolic splitting, i.e. $E^*_+(x) \cap E^*_-(x) = \{0\}$ for every $x \in K$. Finally, any vector in the intersection of the third component and the diagonal would satisfy $(\mathrm{d}\varphi_t(x))^{-T}\xi = \xi$ for some $t \geq t_0$ as well as $\xi(X_x) = 0$. This is impossible for any $\xi \neq 0$ as $\mathrm{id} - \mathrm{d}\varphi_t(x)$ is invertible on $E_s(x) \oplus E_u(x)$ and $T_x\mathcal{U} = X_x \oplus E_s(x) \oplus E_u(x)$ for $x \in K$.

Now if λ *is* a resonance, then the analogous argument using [DZ16, Lemma 3.5] and linearity of $\mathrm{tr}^\flat$ shows that the right-hand side of (1.3.16) admits a Laurent expansion around λ whose finitely many coefficients of negative order are the flat traces of the coefficients of $\mathbf{R}(\lambda)$. This produces a meromorphic continuation for $Z_f^{\mathbf{X}}(\lambda)$ onto $\{\lambda \in \mathbb{C}\}$ with its poles contained in the set of Pollicott-Ruelle resonances of $\mathbf{X}$ and for λ not a resonance the identity

$$Z_f^{\mathbf{X}}(\lambda) = \mathrm{e}^{-\lambda t_0}\mathrm{tr}^\flat\left(\widetilde{\chi}\mathrm{e}^{-t_0\mathbf{X}}\mathbf{R}(\lambda)\widetilde{\chi}f\right) \ . \tag{1.3.18}$$

holds.

To complete the proof an explicit formula for the Laurent coefficients at a resonance λ_0 will be shown. The starting point is (1.3.18) combined with Equation (0.13) in [DZ16, Thm. 2]. Upon substituting the expansion in the second equation into the first one gets

$$Z_f^{\mathbf{X}}(\lambda) = Z_{f,H}^{\mathbf{X}}(\lambda) + \sum_{j=1}^{J(\lambda_0)} \mathrm{tr}^\flat\left(\widetilde{\chi}\frac{\mathrm{e}^{-t_0(\lambda+\mathbf{X})}(-\mathbf{X}-\lambda)^{j-1}\Pi_{\lambda_0}}{(\lambda-\lambda_0)^j}\widetilde{\chi}f\right) \ ,$$

where $Z_{f,H}^{\mathbf{X}}(\lambda)$ is holomorphic near λ_0.

For $0 \leq k < J(\lambda_0)$ one can use the Taylor expansion of the exponential around λ_0, i.e. $\exp(-\lambda t_0) = \sum_{n=0}^\infty (-t_0)^n \exp(-\lambda_0 t_0)(\lambda-\lambda_0)^n/n!$, to obtain the weighted zeta function's Laurent coefficient of order k at λ_0:

$$\begin{aligned}\operatorname*{Res}_{\lambda=\lambda_0}\left[Z_f^{\mathbf{X}}(\lambda)(\lambda-\lambda_0)^k\right] &= \operatorname*{Res}_{\lambda=\lambda_0}\left[\sum_{j=k+1}^{J(\lambda_0)}\sum_{n=0}^{\infty}\mathrm{tr}^\flat\left(\widetilde{\chi}\frac{(-t_0)^n\mathrm{e}^{-t_0(\lambda_0+\mathbf{X})}(-\mathbf{X}-\lambda_0)^{j-1}\Pi_{\lambda_0}}{n!(\lambda-\lambda_0)^{j-k-n}}\widetilde{\chi}f\right)\right] \\ &= \sum_{n=0}^{J(\lambda_0)-k-1}\frac{(-1)^n t_0^n}{n!}\mathrm{tr}^\flat\left(\widetilde{\chi}\mathrm{e}^{-t_0(\lambda_0+\mathbf{X})}(-\mathbf{X}-\lambda_0)^{k+n}\Pi_{\lambda_0}\widetilde{\chi}f\right)\end{aligned} \tag{1.3.19}$$

The operator $\mathbf{X}+\lambda$ is nilpotent on the image $\mathrm{im}(\Pi_{\lambda_0})$ by Equations (0.12) and (0.15) in [DZ16]. This simplifies the propagator $\mathrm{e}^{-t_0(\mathbf{X}+\lambda_0)}$ drastically:

$$\mathrm{e}^{-t_0(\mathbf{X}+\lambda_0)}\Big|_{\mathrm{Im}(\Pi_{\lambda_0})} = \sum_{m=0}^{J(\lambda_0)-1}\frac{t_0^m(-\mathbf{X}-\lambda_0)^m}{m!}\Big|_{\mathrm{Im}(\Pi_{\lambda_0})} \ . \tag{1.3.20}$$

Substitution into Equation (1.3.19) and usage of the abbreviation $N \coloneqq J(\lambda_0) - k - 1$ yields:

$$\begin{aligned}\operatorname*{Res}_{\lambda=\lambda_0}\left[Z_f^{\mathbf{X}}(\lambda)(\lambda-\lambda_0)^k\right] &= \sum_{n=0}^{N}\sum_{m=0}^{N-n}(-1)^n\frac{t_0^{n+m}}{n!m!}\mathrm{tr}^\flat\left(\widetilde{\chi}(-\mathbf{X}-\lambda_0)^{n+m+k}\Pi_{\lambda_0}\widetilde{\chi}f\right) \\ &= \sum_{s=0}^{N}\sum_{n=0}^{s}(-1)^n\frac{t_0^s}{n!(s-n)!}\mathrm{tr}^\flat\left(\widetilde{\chi}(-\mathbf{X}-\lambda_0)^{s+k}\Pi_{\lambda_0}\widetilde{\chi}f\right) \ ,\end{aligned} \tag{1.3.21}$$

where the second line is obtained by using the variable $s := n + m$ as a reparametrization of the double sum. A close examination of Equation (1.3.21) reveals that the binomial theorem can be applied to show for $s > 0$

$$\sum_{n=0}^{s} \frac{(-1)^n}{n!(s-n)!} \frac{s!}{s!} = \frac{1}{s!} \sum_{n=0}^{s} (-1)^n (1)^{s-n} \binom{s}{n} = 0 \ .$$

From this the following formula for the k-th Laurent coefficient follows:

$$\operatorname*{Res}_{\lambda=\lambda_0} \left[Z_f^{\mathbf{X}}(\lambda)(\lambda - \lambda_0)^k \right] = \operatorname{tr}^\flat \left(\widetilde{\chi}(-\mathbf{X} - \lambda_0)^k \Pi_{\lambda_0} \widetilde{\chi} f \right) \ ,$$

which completes the proof because the restriction of the kernel of Π_{λ_0} to the diagonal is supported in $\Gamma_+ \cap \Gamma_- = K$ and $\widetilde{\chi} \equiv 1$ on K, i.e. the cutoff functions can be dropped. □

1.4. Remarks on Patterson-Sullivan Distributions

As previously mentioned the meromorphic continuation together with the trace formula just described provide the basis for all applications in the upcoming chapters. One major applications was already presented in the article [SWB23] itself and a short summary of this will conclude the chapter at hand. Precise definitions, theorems, and references can be found in [SWB23, Section 4].

On the one hand invariant Ruelle distributions are interesting objects to consider due to their connection to (generalized) resonant states, i.e. elements in the image of Π_{λ_0}. On the other hand they derive much of their significance from their connection to certain *quantum mechanical* phase space distributions called *Patterson-Sullivan distributions* $\widehat{\mathrm{PS}}_{\psi_i}$. The precise theorem can be stated as general as for Riemannian compact locally symmetry spaces $\mathbf{M}$ of rank one. On such spaces the well-known Laplace-Beltrami operator $\Delta_{\mathbf{M}}$ has purely discrete spectrum λ_i with smooth, real-valued eigenfunctions ψ_i:

$$\Delta_{\mathbf{M}} \psi_i = \lambda_i \psi_i \ , \quad \psi_i \in \mathrm{C}^\infty(\mathbf{M}, \mathbb{R}) \ .$$

To any such eigenfunction ψ_i a distribution $\widehat{\mathrm{PS}}_{\psi_i}$ on the unit sphere bundle $S\mathbf{M}$ may be attached and the following trace formula holds [SWB23, Thm. 4.1]:

$$\operatorname*{Res}_{\lambda=-\rho+\mathrm{i}r} [Z_g(\lambda)] = \sum_{i=1}^{m} \widehat{\mathrm{PS}}_{\psi_i}(g) \ ,$$

for any $g \in \mathrm{C}^\infty(S\mathbf{M})$ and $r > 0$ such that $\rho^2 + r^2$ is an eigenvalue of $\Delta_{\mathbf{M}}$. Here ρ denotes the halfsum of restricted roots which in constant curvature -1 equals $1/2$ and the righthand side sum extends over an orthonormal basis of the $(\rho^2 + r^2)$-eigenspace of $\Delta_{\mathbf{M}}$.

The Patterson-Sullivan distributions can in turn be identified with so-called *Wigner distributions* which are given by matrix coefficients of quantizations of test functions on the eigenstates ψ_i. Even though this statement only holds in the high frequency limit $r \to \infty$ it is an important bridge between the theory of Pollicott-Ruelle resonances and quantum ergodicity.

Unfortunately to the author's knowledge there does not exist a similar correspondence in the convex cocompact case yet: On the level of resonances [GHW18] did manage to generalized the correspondence. Here the role of the discrete Laplace-Beltrami spectrum is played by *quantum resonances* which are obtained by meromorphic continuation of the

resolvent for the Laplace-Beltrami operator. The resulting discrete subset of $\mathbb{C}$ has an exact and well-understood relationship with the spectrum of Pollicott-Ruelle resonances of the geodesic flow, see [GHW18, Theorem 1.2].[12] The missing ingredient is a theory of Patterson-Sullivan distributions connecting invariant Ruelle and Wigner distributions on phase space.

This in turn means that a rigorous mathematical basis for the interpretation of the experiments performed in Part II as experiments on Wigner distributions is still an open question which should be pursued in the future. Some experimental evidence for why this connection might be expected to exist was provided in [BSW22] and will be summarized in Chapter 3. The following Diagram 1.1 summarizes the connections established so far as well as outstanding conjectures.[13]

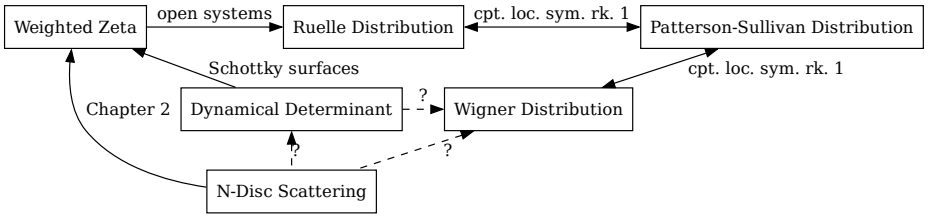

Figure 1.1.: Established and conjectured connections between invariant Ruelle and Wigner distributions.

Note that some of the edges in the figure have not been presented yet but will be the contents of upcoming chapters.

[12] The quantum resonances can also be calculated numerically using so-called *Selberg zeta functions.* For details on these see Chapter 6 and for the concrete relationship between classical and quantum resonances on convex-cocompact hyperbolic surfaces see Chapter 5.

[13] The diagram was created using the *dot* graph description language and the *graphviz* package.

2. Weighted Zetas for Convex Obstacle Scattering

The rather abstract theory of Chapter 1 finds its first application in the setting of *convex obstacle scattering*. The upcoming chapter describes this application as developed in [DSW21]. The original article itself is again included as Appendix B for reference.

2.1. Geodesic Billiard Dynamics

The initial motivation for the project described in this chapter was the extensive analytical, experimental, and numerical investigation of so-called *3-disc scattering* in the theoretical and experimental physics communities. With the theory of weighted zeta functions as described in Chapter 1 it seemed possible to develop a rigorous underpinning for the numerical investigation of phase space distributions on these systems with the precise definition of resonances and weighted zeta functions as a first step. For additional background information refer to the introduction in [DSW21, Section 1].

The actual setting as considered in [DSW21] is a rather straightforward abstraction of the idea of scattering at compact, convex obstacles in the plane: The ambient phase space of the *billiard dynamics* is given by the unit tangent bundle

$$M \coloneqq S\big(\Sigma \setminus \mathring{\Omega}\big)$$

over a complete connected smooth Riemannian manifold Σ with the interior of a smooth submanifold with boundary Ω and full dimension removed. The connected components of Ω are then interpreted as *obstacles*. Intuitively the dynamics φ_t is just given by trajectories of the geodesic flow between obstacles and instantaneous reflections on the obstacle boundaries for boundary intersections with either inward or outward pointing velocity vectors.

A trajectory which is neither inward nor outward pinting, i.e. which intersects an obstacle boundary in a tangent manner, is called *grazing*. To obtain a consistent definition without having to require e.g. convexity of the obstacles the dynamics φ_t simply stops when the geodesic flow hits an obstacle in a grazing manner. In the main example case of convex obstacles one could continue along grazing trajectories to obtain a strictly larger domain of definition. This is excluded from the outset, though, not only to preserve as much generality as possible but even more so because the smooth model construction in Chapter 2.2 below cannot incorporate grazing boundary directions anyways.

In summary the *non-grazing billiard flow* φ_t is thus given by an *incomplete* flow[1] on

$$M \setminus \partial_{\mathrm{g}} M \ ,$$

where $\partial_{\mathrm{g}} M \coloneqq \partial M \cap T(\partial\Omega)$ denotes the grazing boundary component just mentioned.

[1] Note that the billiard dynamics does in fact *not* define a flow in the classical sense of a one-parameter group of diffeomorphisms because the group property fails on the boundary. But this is a minor technical inconvenience easily solved by transitioning to the smooth model flow introduced below.

A precise version of this rather short and simplified discussion together with basic properties of the resulting objects are the contents of [DSW21, Section 2] but see also the motivating special case of Euclidean obstacle scattering considered in the introductory [DSW21, Section 1]. In particular the former section defines the notions of *trapped set* K and *hyperbolicity* for φ_t. For the main application of scattering of a hard point particle in Euclidean space K coincides with the intuitive notion of trapped trajectories if the Euclidean flow is *non-grazing*, i.e. no grazing trajectories are trapped in both forward and backward time. This is termed the *non-grazing trapped set condition*. Furthermore hyperbolicity holds if the Euclidean obstacles are strictly convex.

Now the main difficulty with φ_t is the fact that it does not define even a continuous, let alone smooth, mapping: Smoothness only holds on the preimage $\varphi^{-1}(\mathring{M})$ of the interior of phase space and breaks down when φ_t undergoes boundary reflections. To be able to apply the theory developed in Chapter 1 it is thus necessary to construct a smooth substitute which preserves the dynamical properties of the original flow. In particular this should include a length preserving bijection between the closed trajectories of the original dynamics and its smooth variant.

Before the approach presented in the next section was developed the author of this thesis made a rather naive first attempt to derive a smooth model flow from φ_t. A summary of this attempt will conclude this introductory section and motivate the necessity for a refined approach. For simplicity and guided by the numerical work presented in [BSW22] the setting of finitely many discs in Euclidean space was chosen for first explorations. Furthermore the restriction to scattering of the geodesic flow on the Euclidean line $\mathbb{R}$ with finitely many holes seemed a suitable reduction in complexity compared to the more interesting but also geometrically more complicated case of scattering at finitely many discs in the Euclidean plane $\mathbb{R}^2$. The former can easily be visualized due to its low dimensionality – the three-dimensional phase space of the latter requires significantly more effort in this respect.

The toy model setting is as follows: Let the configuration space be

$$\mathcal{C} \coloneqq \{x \in \mathbb{R} \mid |x| \geq a\} ,$$

the Euclidean real line with the one-dimensional "disc" $\{|x| < a\}$ of radius $a > 0$ removed as an obstacle. The associated phase space is then a manifold with boundary given by the sphere bundle

$$S\mathcal{C} = \mathcal{C} \times \{1, -1\} = \mathcal{C} \times \mathrm{S}^0$$

and the *billiard dynamics* φ_t on this phase space is defined piece-wise for $(x, v) \in S\mathcal{C}$ as a straightforward formalization of the scattering of a particle traveling at unit speed and experiencing hard-ball reflections at the obstacle boundary. Concretely for $x \geq a$ put

$$\varphi_t(x, 1) \coloneqq \begin{cases} (x + t, 1) & \text{if } x + t \geq a, \\ (a - (t + x - a), -1) & \text{if } x + t < a, \end{cases} ,$$

together with $\varphi_t(x, -1) \coloneqq (x', -v')$ if $\varphi_{-t}(x, 1) = (x', v')$ and $\varphi_t(x, v) \coloneqq (-x'', -v'')$ for $x \leq -a$ such that $\varphi_t(-x, -v) = (x'', v'')$. For a graphical illustration of these definitions see Figure 2.1. Note that this functional prescription violates the flow property on the boundary $\{|x| = a\} \times \{-1, 1\}$ because $\varphi_{-t}(\varphi_t(a, -1)) = (a, 1) \neq (a, -1)$ for times $t > 0$. Furthermore it is not even continuous due to the presence of the boundary reflection $v \mapsto -v$.

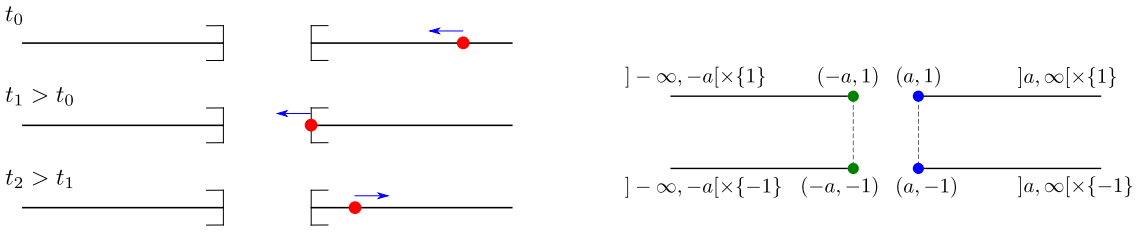

(a) Geometric setup of obstacle scattering at a single disc in one dimension.

(b) Illustration of the gluing procedure employed to obtain a smooth model flow.

Figure 2.1.: Illustration of one-dimensional scattering of a free particle at a single disc centered at the origin together with the construction of a smooth model flow on a quotient of phase space.

Implementing the philosophy of constructing a smooth model of this dynamics which preserves the important characteristics of φ_t is quite straightforward in this simple example: Defining the quotient space by boundary reflection yields the set

$$\mathcal{M} \coloneqq \{(x,v) \in S\mathcal{C} \mid |x| > a\} \cup \{[(a,1)],[(-a,1)]\} \ , \tag{2.1.1}$$

where $[(\pm a,1)] = \{(\pm a,1),(\pm a,-1)\}$ and equivalence classes $\{(x,v)\}$ with a single element are identified with their member (x,v). A smooth structure on $\mathcal{M}$ which is obviously compatible with the standard smooth structure on the first term of the disjoint union (2.1.1) is given by the chart $\widetilde{x} : \mathcal{O} \to \mathbb{R}$ defined as

$$\begin{aligned} \mathcal{O} \coloneqq]a,\infty[\times\{-1,1\} \cup \{[(a,1)]\} &\longrightarrow]-\infty,\infty[\\ [(a,1)] &\longmapsto 0 \\ (x,1) &\longmapsto x-a \\ (x,-1) &\longmapsto a-x \ , \end{aligned}$$

combined with an analogous definition on the domain $]-\infty,a[\times\{-1,1\} \cup \{[(-a,1)]\}$. Geometrically these charts correspond to a straightforward gluing of the directions in the sphere bundle over the boundary of configuration space. Note that $\mathcal{M}$ is no longer a manifold with boundary but genuinely smooth.

There is now an obvious definition for a *smooth model flow* ϕ_t on $\mathcal{M}$ namely the translation flow in the chart $\widetilde{x}$ just given. In $\widetilde{x}$-coordinates its generator coincides with $\partial_{\widetilde{x}}$ and it models the original φ_t in the sense that on the interior

$$S\mathring{\mathcal{C}} = \{|x| > a\} \times \{1,-1\}$$

of phase space both are related by pushforward along the diffeomorphism $\pi|_{S\mathring{\mathcal{C}}}$ obtained from the projection

$$\pi : S\mathcal{C} \longrightarrow \mathcal{M}$$

via restriction to $S\mathring{\mathcal{C}}$.

It is straightforward to generalize this construction to $\mathbb{R}$ with $N+1$, $N>0$, intervals removed. This setup yields a non-trivial, albeit simple, associated weighted zeta function. The interesting characteristic of this system is not the interval sizes but rather the mutual distances $a_1,\ldots,a_N$ of neighboring intervals. The construction just discussed now yields a smooth flow which exhibits a length spectrum of closed trajectories in bijection to the length spectrum of the original billiard flow. One may therefore immediately apply the theory of Chapter 1 to obtain the existence of Pollicott-Ruelle resonances and the meromorphic continuation of weighted zeta functions.

Remark 2.1.1. In this particularly simple example it is of course rather trivial to obtain e.g. meromorphic continuation of weighted zeta functions with constant weight by hand:

$$\begin{aligned} Z(\lambda) &\coloneqq \sum_{\gamma} \frac{\mathrm{e}^{-\lambda T_\gamma} T_\gamma^{\#}}{|\det(1-\mathcal{P}_\gamma)|} \\ &= \sum_{n\geq 1} \sum_{i=1}^{N} 2a_i \mathrm{e}^{-2a_i\lambda n} \\ &= \sum_{i=1}^{N} \frac{2a_i}{\mathrm{e}^{2a_i\lambda}-1} \ , \end{aligned}$$

and one may take the poles $\bigcup_{i=1}^{N} \frac{\mathrm{i}\pi}{a_i}\mathbb{Z}$ of this zeta function as the definition of resonances for the scattering system. Note that in the spirit of Chapter 4 one could also consider resonances as defined by the zeros of the dynamical determinant

$$\mathrm{d}(\lambda) \coloneqq \prod_{i=1}^{N} \left(1-\mathrm{e}^{-2a_i\lambda}\right)$$

that satisfies $\mathrm{d}'(\lambda)/\mathrm{d}(\lambda) = Z(\lambda)$.

At first glance the generalization of this construction to higher dimensions seems straightforward. Before describing this generalization in a more abstract setting in Section 2.2 a short description of some subtleties already appearing in the two-dimensional case of discs will round out this motivational excursion. The following material should provide the reader with enough of a background to understand the necessity for the technical depth required and care taken in [DSW21].

The two-dimensional setup itself is an immediate generalization of the one-dimensional situation presented above: Configuration space is a manifold with boundary given by the exterior of a disc of radius $a > 0$ centered at the origin

$$\mathcal{C} \coloneqq \{x \in \mathbb{R}^2 \mid \|x\| \geq a\}$$

and representing particle positions such that phase space is simply the unit sphere bundle

$$S\mathcal{C} = \mathcal{C} \times \mathrm{S}^1$$

where the fiber coordinate varies on the unit circle S^1 representing particle velocity vectors of unit length. The billiard dynamics on $S\mathcal{C}$ is again given by straight lines in the interior of phase space. Upon intersection with the boundary a trajectory experiences a reflection at the tangent line to the circle and through the point of intersection. Note that the additional dimension produces a new phenomenon: A trajectory may hit the boundary $\{\|x\| = a\}$ in a tangential manner corresponding to points within the grazing boundary component $\partial_{\mathrm{g}}(S\mathcal{C}) = T(\partial\mathcal{C}) \cap S\mathcal{C}$ of phase space. These trajectories pass the disc obstacle unaltered and are termed *grazing*. Removing these directions from the boundary of phase space produces a splitting into disjoint open subsets $\partial(S\mathcal{C}) \setminus \partial_{\mathrm{g}}(S\mathcal{C}) = \partial_{\mathrm{in}}(S\mathcal{C}) \cup \partial_{\mathrm{out}}(S\mathcal{C})$ called the *inward* and *outward* boundaries. They are defined as those directions whose scalar product with the tangent line is either strictly positive or strictly negative and they should be interpreted as the flow directions pointing into or away from the disc obstacle boundary. A graphical illustration of this setup can be found in Figure 2.2.

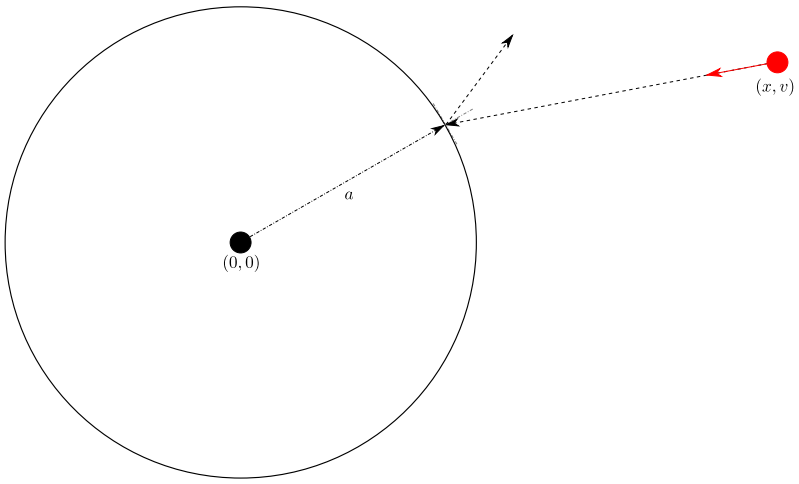

Figure 2.2.: Illustration of two-dimensional scattering of a free particle at position $x \in \mathbb{R}^2$ with velocity vector $v \in S\mathbb{R}^2$ about a single disc of radius $a > 0$ centered at the origin.

The one-dimensional example now suggests the following procedure: By introducing polar coordinates outside the disc obstacle together with angle coordinates in the fiber phase space can be parameterized via the map

$$\begin{aligned} \mathbb{R}_{\geq 0} \times \mathrm{S}^1 \times \mathrm{S}^1 &\longrightarrow S\mathcal{C} \setminus \partial_{\mathrm{g}}(S\mathcal{C}) \\ (r, \theta, \alpha) &\longmapsto ((r+a)\cos(\theta), (r+a)\sin(\theta), \cos(\alpha), \sin(\alpha)) \end{aligned}$$

and the billiard dynamics φ_t is defined completely analogously as before.

Recalling the gluing procedure from above it is unclear how to deal with the grazing boundary $\partial_{\mathrm{g}}(S\mathcal{C})$. It is therefore natural to exclude the grazing boundary points from $S\mathcal{C}$ before proceeding with the gluing – due to $\partial_{\mathrm{g}}(S\mathcal{C})$ being a smooth closed submanifold the resulting space $S\mathcal{C} \setminus \partial_{\mathrm{g}}(S\mathcal{C})$ is still a well-defined smooth manifold with boundary. If the billiard dynamics intersects $\partial_{\mathrm{g}}(S\mathcal{C})$ then it shall be redefined to stop right at the point of intersection thereby resulting in an incomplete flow.[2] Now the idea of gluing along the radial direction suggests itself quite naturally: Take as the underlying set for the smooth model manifold

$$\mathcal{M} \coloneqq \{\|x\| > a\} \times \mathrm{S}^1 \cup \{[(x,v)] \mid (x,v) \in \partial(S\mathcal{C}) \setminus \partial_{\mathrm{g}}(S\mathcal{C})\}$$

where the equivalence classes are taken with respect to reflection at the tangent line through x denoted by $(x,v) \mapsto (x,v')$, i.e. $[(x,v)] \coloneqq \{(x,v),(x,v')\}$, and define a smooth structure for $\mathcal{M}$ via the following coordinates on the open subset of phase space that contains all points which at some point in the past or future intersect the obstacle boundary:

$$\begin{aligned} [(x,v)] &\longmapsto (0, \theta(x), v) && \text{if } (x,v) \in \partial_{\mathrm{in}}(S\mathcal{C}) \\ (x,v) &\longmapsto \begin{cases} (r(x), \theta(x), v_0) & \exists (x_0,v_0) \in \partial_{\mathrm{in}}(S\mathcal{C}), t < 0 : \varphi_t(x_0,v_0) = (x,v) \\ (-r(x), \theta(x), v_0) & \exists (x_0,v_0) \in \partial_{\mathrm{in}}(S\mathcal{C}), t > 0 : \varphi_t(x_0,v_0) = (x,v) \end{cases} \end{aligned} \tag{2.1.2}$$

Intuitively this means that we consider trajectories which intersect the obstacle and glue the halves before and after the boundary intersection together. By definition this gluing happens in a manner that makes the radial coordinate on Euclidean space smooth.

[2] Note that the same remark regarding failure of the flow property on the boundary made in the one-dimensional example continues to hold here.

Unfortunately this definition does *not* lead to a smooth model for the billiard dynamics. Again φ_t is readily transferred to a flow ϕ_t on $\pi(S\mathcal{C}\setminus\partial(S\mathcal{C}))$ because outside the boundary the quotient map π is in fact a diffeomorphism. But expressing ϕ_t in the coordinates (2.1.2) reveals that a continuation to $\pi(\partial(S\mathcal{C}))$ can be achieved as a continuous but *not a smooth flow*. More concretely the generating vector field exhibits a discontinuity at $r = 0$ in the ∂_θ-coordinate. The concrete calculations are elementary but rather tedious so the details are omitted here.

The conclusion from these observations goes as follows: While the procedure of gluing over the boundary still seems rather promising additional care should be taken in how to define a smooth structure on the resulting quotient space. One immediate observation is the need to take account of the billiard dynamics within the smooth structure itself. This is quite in line with the one-dimensional example where the flow direction simply coincided with the standard coordinate chart. It turns out that the correct analogue of the coordinate chosen there was not the radial one but instead the t-parameter of the dynamics itself. Unfortunately both coincide in the one-dimensional case. This approach does in fact lead to a complete solution of the goals outlined above and even in the far more general setting of billiards on Riemannian manifolds which abstract the Euclidean examples just discussed nicely. A recollection of the central points of this construction forms the contents of the two upcoming sections.

2.2. Smooth Models

The overall goal as introduced in the previous chapter was the definition of resonances and meromorphic continuation of weighted zeta functions for Riemannian obstacle scattering via an application of the theory presented in Chapter 1. To account for the lack of smoothness of the non-grazing billiard flow φ_t on the boundary of phase space an everywhere smooth substitute ϕ_t called a *smooth model flow* was constructed. Here the central observation is the fact that the lack of smoothness of φ_t is an immediate consequence of the boundary reflections which were successfully removed in the one-dimensional example above: Identification of those velocity vectors over the boundary of configuration space that are related through reflection gave a well-defined smooth manifold with not only a canonical choice of smooth structure but also an immediate pendant for the billiard flow satisfying the requirement of identical length spectrum. The two-dimensional example then revealed the need for suitable coordinates on the quotient.

In the general setting of Riemannian obstacle scattering one has the advantage of a very clear set of geometrical tools to try and approach the subject matter of such suitable coordinates. From the failed attempt above it becomes rather clear that the smooth structure on the quotient should somehow be derived from the flow itself. Now the central lemma in this direction is [DSW21, Lemma 2.4]: It turns out by a rather straightforward application of the inverse function theorem that the map $\varphi(t, x, v) \coloneqq \varphi_t(x, v)$ itself can be used as a coordinate map when restricted to a suitable subset $N_{\mathrm{in}} \subset \mathbb{R} \times \partial_{\mathrm{in}} M$. Here $\partial_{\mathrm{in}} M \subset \partial M$ denotes the set of all *inward pointing* directions over the boundary.[3]

The construction of the smooth model $\mathcal{M}$ now follows the idea outlined above: First one defines

$$\mathcal{M} \coloneqq (M \setminus \partial_{\mathrm{g}} M)/\sim$$

[3]The choice of inward pointing directions is completely arbitrary and the whole upcoming argument could also be made with the outward pointing directions requiring only trivial modifications of the notation.

as a topological quotient space where the equivalence relation $\sim$ is given by one-element equivalence classes for points $(x, v) \in \mathring{M}$ and two-element classes $[(x, v)] \coloneqq \{(x, v), (x, v')\}$ for boundary points. Here $v \mapsto v'$ denotes the boundary reflection map in the fiber coordinate. The smooth structure for $\mathcal{M}$ is now defined by the requirement that both $\pi|_{\mathring{M}}$ for the projection $\pi : M \setminus \partial_{\mathrm{g}} M \to \mathcal{M}$ as well as

$$\begin{aligned} N_{\mathrm{in}} &\longrightarrow \mathcal{M} \\ (t, x, v) &\longmapsto [\varphi_t(x, v)] \end{aligned}$$

be diffeomorphisms. Note that this is a natural requirement if there is to be any hope that the obvious candidate (disregarding again the technical issue of precise domains)

$$\phi_t([x, v]) \coloneqq [\varphi_t(x, v)]$$

is indeed a smooth flow with the same dynamical properties as the original φ_t. The well-definedness and properties of these definitions forms the main content of [DSW21, Section 4] and the heart of this paper. One of the most important dynamical properties is the fact that the flow ϕ_t is a *contact flow*.

The preceding [DSW21, Chapter 3] formalizes this construction into the abstract definition of a *smooth model* for the billiard flow φ_t but this is actually only a matter of procedural preference: The abstraction admits basically only a single realization, namely the one just outlined, up to a very rigid class of isomorphisms. This being said the author is of the opinion that the choice of presenting the abstract formalism has the distinct advantage that statements like [DSW21, Proposition 3.6 and Proposition 3.7] on the trapped set and hyperbolicity, respectively, can be formulated and proven without the burden of relying on an explicit realization of the smooth model as a quotient of the original phase space. This makes them even more useful as black box theorems in the context of resonances and zeta functions.

2.3. Meromorphic Continuation

The construction of smooth models itself can already be regarded as a first main result of [DSW21]. The second major result concerns the meromorphic continuation of the same formal *weighted zeta function* as considered in Chapter 1:

$$Z_f(\lambda) \coloneqq \sum_{\gamma} \frac{\exp(-\lambda T_\gamma)}{|\det(\mathrm{id} - \mathcal{P}_\gamma)|} \int_{\gamma^\#} f \ ,$$

where the sum now extends over the closed trajectories of the non-grazing billiard flow φ_t. With smooth models as a foundation this meromorphic continuation now follows in a straightforward manner from the general theory of weighted zeta functions by observing that $Z_f(\lambda)$ coincides with the weighted zeta function for the smooth model flow ϕ_t. But the latter fits into the general framework due to its smoothness and under the assumption that the original flow φ_t had *compact trapped set* K and exhibited a *hyperbolic splitting* over K. This allows for the definition of *Pollicott-Ruelle resonances* of φ_t as the poles of the weighted zeta function $Z_1(\lambda)$ with constant weight.

The actual results presented in [DSW21] are somewhat more detailed, though: The initial goal was to also define and then meromorphically continue a resolvent for φ_t. Let the reader be reminded that this was the central ingredient for the meromorphic continuation of $Z_f(\lambda)$! Because of the lack of smoothness this resolvent cannot simply

be taken as the inverse of a generating vector field but a closely related substitute exists called the *billiard generator*

$$\begin{aligned} \mathbf{P} : \mathrm{C}^\infty_{\mathrm{Bill}}(O) &\longrightarrow \mathrm{C}^\infty_{\mathrm{Bill}}(O) \\ \mathbf{P}f(x,v) &:= \left.\frac{\mathrm{d}}{\mathrm{d}t}\right|_{t=0} f \circ \varphi_t(x,v) \ . \end{aligned}$$

Here $O \subset M \setminus \partial_{\mathrm{g}} M$ is any open set such that $O \cap (\partial M \setminus \partial_{\mathrm{g}} M)$ is reflection symmetric and the elements of $\mathrm{C}^\infty_{\mathrm{Bill}}(O) := \{f \in \mathrm{C}^\infty(O) \mid f \circ \varphi \in \mathrm{C}^\infty(\varphi^{-1}(O))\}$ are called *billiard functions*. The operator $\mathbf{P}$ is thus a formal generator of φ_t on an adapted function space with a non-local constraint on function values in a neighborhood of the boundary.

Now it is indeed possible to define for compact, reflection-symmetric $U \supset K$ a resolvent $\mathbf{R}_U(\lambda) : \mathrm{C}^\infty_{\mathrm{Bill,c}}(\mathring{U}) \to \mathrm{C}_{\mathrm{Bill,c}}(\mathring{U})$ by an explicit formal integral formula.[4] This resolvent satisfies the obviously desirable relation [DSW21, Corollary 5.5]

$$(\mathbf{P} + \lambda)\mathbf{R}_U(\lambda) = \mathrm{id} \qquad \mathrm{Re}(\lambda) \gg 0 \ ,$$

and the matrix coefficients with respect to the Riemannian volume

$$\langle \mathbf{R}_U(\lambda) f, g \rangle_{\mathrm{L}^2} \ , \qquad f, g \in \mathrm{C}^\infty_{\mathrm{Bill,c}}(\mathring{U}) \ ,$$

continue meromorphically from $\mathrm{Re}(\lambda) \gg 0$ to the whole complex plane $\mathbb{C}$. Furthermore their possible poles are independent of f, g in the sense that only the Pollicott-Ruelle resonances of φ_t can appear. Again these statements are directly related to analogous statements for the smooth model flow ϕ_t which in turn follow from the general smooth theory of [DG16] as recalled in Chapter 1.

It was chosen to formulate the result in terms of meromorphic matrix coefficients instead of a meromorphic operator family because the latter would have required the development of a theory of billiard distributions without any obvious significant gain in generality or usefulness.

Remark 2.3.1. The construction of smooth models can be generalized even further without requiring too much additional effort: Let a smooth complex vector bundle $\widetilde{\mathcal{E}} \to M \setminus \partial_{\mathrm{g}} M$ together with a first order differential operator $\widetilde{\mathbb{X}}$ on smooth sections of $\widetilde{\mathcal{E}}$ satisfying the Leibniz rule

$$\widetilde{\mathbb{X}}(\widetilde{f}\widetilde{\sigma}) = (\mathbf{P}\widetilde{f})\widetilde{\sigma} + \widetilde{f}(\widetilde{\mathbb{X}}\widetilde{\sigma})$$

for any billiard function $\widetilde{f}$ and smooth section $\widetilde{\sigma}$ be given. Then a very similar gluing procedure yields a smooth model bundle $\mathcal{E}$ and a smooth model operator $\mathbb{X}$ on smooth sections of $\mathcal{E}$. This point shall not be elaborated on further in this thesis and the reader is referred to [DSW21, Appendix B] for details. It should be strongly emphasized, though, that the same idea of using the flow (together with a closely related parallel transfer map in the fiber) as a coordinate chart still underpins the whole construction.

[4] The function spaces appearing in this formula are given by the obvious adaptations of the definition of $\mathrm{C}^\infty_{\mathrm{Bill}}$.

3. Weighted Zetas for Wigner Distributions

The upcoming chapter contains a short overview over the article [BSW22]. While it does not contain new results in the strict sense and addresses as its main audience theoretical physicists rather than mathematicians it does present interesting connections of and new perspectives on the material developed in the mathematically more rigorous works [SWB23] and [DSW21].

Besides his expertise regarding weighted zeta functions the author of this thesis concretely contributed the presentation and numerical study of 3–disc systems in Section 5 by extending and applying prior numerical `Python` code by Tobias Weich and Sonja Barkhofen.

3.1. Semiclassical and Faure-Tsujii Zeta Functions

The overall goal of [BSW22] was the mathematically rigorous reconstruction of certain trace formulae relating zeta functions defined in terms of classical data with quantum mechanical matrix coefficients. To this end Section 2 begins by describing the general mathematical setting of uniformly hyperbolic flows $\exp(tX)$ on compact manifolds $\mathcal{M}$. This simplifies significantly the subsequent description of the meromorphic continuation to $\lambda \in \mathbb{C}$ of the resolvent $\mathbf{R}(\lambda)$ as an operator

$$\mathbf{R}(\lambda) \coloneqq (-X - \lambda)^{-1} : \ \mathrm{C}^\infty(\mathcal{M}) \longrightarrow \mathcal{D}'(\mathcal{M}) \ ,$$

and the corresponding definition of Pollicott-Ruelle resonances as the poles of $\mathbf{R}(\lambda)$ compared to the most general open systems setting as outlined in Chapter 1 of this thesis. The section is concluded by an introduction of invariant Ruelle distributions $\mathcal{T}_{\lambda_0}$ and their residue formula interpretation via weighted zeta functions. The former are motivated as products of test functions f with resonant states u and co-resonant[1] states v

$$\mathcal{T}(f) = \langle v \,|\, f \,|\, u \rangle$$

while the latter simply serve as convenient means enabling the concrete calculation of $\mathcal{T}_{\lambda_0}$. This choice of presentation emphasizes the (at this point heuristic) analogy with matrix coefficients of quantum mechanical observables which are exceedingly common objects in physics.

The actual application of this material then follows in [BSW22, Section 3]: Inspired by certain zeta functions considered in the physics literature the authors introduce the following *semiclassical zeta function* for the geodesic flow on an oriented, closed, negatively curved surface N and a test function $f \in \mathrm{C}^\infty(T^*N)$ on phase space

$$Z_f^{\mathrm{sc}}(E) \coloneqq -\mathrm{i} \sum_{\gamma \subseteq \Sigma_E} \frac{\exp(\mathrm{i}\sqrt{E} L_\gamma)}{|\det(1 - \mathcal{P}_\gamma)|^{1/2}} \int_{\gamma^\#} f \ .$$

[1] These are the elements in the image of the spectral projector as well as its conjugate, respectively. The simple product representation holds in the case of a rank one projector, i.e. $\Pi_{\lambda_0} = |u\rangle\langle v|$.

Here the variable E is interpreted as energy, Σ_E denotes the sphere bundle of radius E, i.e. the energy shell of energy E, the sum extends over closed trajectories of the geodesic flow contained in Σ_E, L_γ is the length of γ, and $\mathcal{P}_\gamma$ again denotes the linearized Poincaré map of γ.

To make the connection with the theory of weighted zeta functions a second variant called the *Faure-Tsujii* zeta function is introduced next

$$Z_f^{\mathrm{FT}}(\lambda) := \sum_\gamma \frac{\exp(-\lambda L_\gamma)|\Lambda_\gamma|^{1/2}}{|\det(1-\mathcal{P}_\gamma)|} \int_{\gamma^\#} f \ ,$$

where Λ_γ denotes the expanding eigenvalue of the differential of the geodesic flow on the closed geodesic γ. Here is where weighted zeta functions come into play: Z_f^{FT} turns out to be a weighted zeta obtained by lifting the geodesic flow to a certain density bundle. Meromorphic continuation of Z_f^{FT} therefore follows from the general theory regarding weighted zetas.

By expanding the terms involving the determinant

$$\det(1-\mathcal{P}_\gamma) = (1-\Lambda_\gamma)(1-\Lambda_\gamma^{-1})$$

in the respective denominators of Z_f^{sc} and Z_f^{FT} one obtains respective terms of order zero which may now be compared directly in a certain right halfplane

$$\{\mathrm{Re}(\lambda) \geq h_{\mathrm{top}} - \frac{3}{2}\beta_{\min}\} \ . \tag{3.1.1}$$

The fact that the less easily comparable higher order terms do not contribute poles within this halfplane is a direct consequence of the uniform hyperbolicity of the geodesic flow on T^*N which in turn follows from the curvature assumption.

Now the comparison yields that any pole λ_n of $Z_f^{\mathrm{sc}}(-\lambda^2)$ in the halfplane (3.1.1) is a resonance of the geodesic flow lifted to a certain vector bundle and the residue coincides with the associated invariant Ruelle distribution. Semiclassical results in the physics literature now suggest a correspondence between the Ruelle distribution and quantum matrix coefficients which should appear as the residues of the semiclassical zeta function in the semiclassical limit. The mathematically rigorous version of this correspondence has so far only been established in the setting of *constant* negative curvature a recollection of which is contained in [BSW22, Section 4], see also the results presented as Chapter 1.4 of the present thesis.

3.2. Numerical Study of 3-Disc Scattering Systems

The concluding Section 5 of [BSW22] presents some compelling evidence towards profound extensions of the rigorous results discussed above. The setup of the numerical experiments conducted there is that of so-called n–disc systems: An arrangement of $n \geq 3$ discs in the plane $\mathbb{R}^2$ which may be considered as scattering either free classical particles or quantum mechanical wave functions by imposing Dirichlet boundary conditions in the latter case. It therefore allows the direct comparison of classical and quantum dynamics similar to the situation on Riemannian manifolds.

Both the classical (see Chapter 2) as well as the quantum mechanical setting admit notions of resonances, compare the quantum resonances on Schottky surfaces obtained from meromorphic continuation of the resolvent of the Laplace-Beltrami operator as outlined e.g in Chapter 6. To a classical resonance one can again associate a Ruelle distribution

which is the residue of a weighted zeta function. A natural counterpart on the quantum side is the *Wigner distribution* which may be obtained as matrix coefficients of quantizations of test functions f on phase space with respect to energy eigenstates $\Delta\psi = \lambda\psi$:

$$W_\psi(f) \coloneqq \langle \mathrm{Op}(f)\psi, \psi \rangle \ .$$

Note that the ambiguity in the choice of quantization Op has not much of an impact because the following discussion revolves around the high frequency limit anyways. The phase space distributions calculated numerically actually were variants particularly well suited for numerical purposes called *Poicaré-Husimi distributions*.

The first noteworthy result which had already been observed previously was a remarkable coincidence between the classical and quantum mechanical spectra beyond the first couple of resonances. As a new avenue the authors of [BSW22] considered the Ruelle and Poincaré-Husimi distributions at corresponding spectral parameters. While the results were not directly comparable on a quantitative level they showed a remarkable resemblence on a qualitative level. This was even more apparent while moving the considered resonance in the complex plane and observing the corresponding oscillations in both types of distributions.

These observations suggest a quantum-classical correspondence for a dynamical system far beyond the exceptionally symmetrical class of compact constant curvature surfaces to which the rigorous results are restricted so far. The concluding remarks of [BSW22] state some conjectures why there might indeed be or not be actual mathematical correspondences to be proven as future rigorous theorems.

With regards to this thesis the discussion shall be concluded with the observation that [BSW22] used weighted zeta functions, their residue formula, and a related circle of numerical ideas and techniques to connect older approaches from the physics literature with more recent mathematical developments and provided some intriguing evidence for future mathematical research. Especially the second point should be motivation enough to dive deeper into the numerical-practical aspect of weighted zeta functions in the upcoming Part II of this thesis.

Part II.

Numerical Study of Convex-Cocompact Hyperbolic Surfaces

Outline of Part II

The second part builds on the theoretical framework developed in Part I by applying it to the concrete dynamics of geodesic flows on *convex-cocompact* hyperbolic surfaces also known as *Schottky* surfaces. Compared to the application to obstacle (and in particular 3-disc) scattering presented in Part I these dynamical systems not only enable an immediate numerical study of both their resonances as well as their invariant Ruelle distributions – their particularly simple structure also allows for a technically straightforward proof of the convergence properties of our numerical algorithms.

While the former has been consider in various papers starting with [Bor14] (but see also [BW16, BPSW20]) the latter is a new contribution by the author of this thesis.

Before any experiments could be conducted the numerical machinery and its convergence properties had to be developed in a mathematically sound manner. This was done in the paper [SW23] which is included in Appendix C. A summary of the main results and algorithms developed there as well as additional details regarding a generalization to certain systems of holomorphic functions termed *hyperbolic map systems* was included as Chapter 4.

With this machinery at hand it becomes possible to numerically investigate invariant Ruelle distributions on Schottky surfaces. Chapter 5 presents such experiments complementing the simpler proof-of-concept calculations contained in [SW23].

The final Chapter 6 of this part presents another numerical study, this time using the Selberg zeta function to calculate quantum mechanical resonances. While the numerical techniques are basically the same as in [Bor14] the application is new: Instead of considering shared properties of subsets of resonances for a fixed surface such as those belonging to the same resonance chain now statistical properties of randomly sampled surfaces are investigated. Chapter 6 gives a brief description of the Weil-Petersson measure on Teichmüller space of funneled tori from which the surfaces were sampled to then proceed with a more detailed description of how the sampling was realized practically and the actual results obtained. From these a few hypotheses are extracted but their proofs are beyond the scope of this thesis.

This concluding chapter should be viewed as additional support for the claim that numerical experiments are a valuable asset in rigorous mathematics in general and the field of Pollicott-Ruelle or quantum resonances in particular.

4. Numerical Machinery

This chapter provides an overview over the numerical machinery developed in the paper [SW23] for the calculation of invariant Ruelle distributions on convex cocompact hyperbolic surfaces. Instead of simply summarizing the contents a generalization that abstracts the concrete setting of Schottky surfaces will be developed and the adaptions necessary to prove counterparts of the theorems in [SW23] are sketched. This generalization was already announced in the paper itself and the reasoning behind this procedure becomes clear in the following Chapter 5: The generalized setting carries over seamlessly to the numerical implementation and provides firm grounds for a full symmetry reduction of surfaces with n_f funnels.

The original paper itself was included as Appendix C because it contains the bulk of the algorithmic as well as numerical work and to make this thesis more self contained. In particular the article contains the foundational definitions for the following sections like that of Schottky groups and surfaces as well as the surrounding terminology.

4.1. Hyperbolic Map Systems and Dynamical Determinants

The fundamental definition of this chapter embodies the dynamics of a hyperbolic system of analytic maps as follows, see also [Rug92]:

Definition 4.1.1: Hyperbolic map system

Let pairwise disjoint, bounded domains $\{D_i\}_{i=1,\dots,N} \subset \mathbb{C}$ and an adjacency matrix $A_{(i,j),(k,l)} \in \{0,1\}^{N^2 \times N^2}$ be given. A family of maps

$$\phi_{(i,j),(k,l)} = \left(\phi^{(1)}_{i,k}, \phi^{(2)}_{j,l}\right)$$

for every $(i,j),(k,l)$ such that $A_{(i,j),(k,l)} = 1$ is called a *hyperbolic map system* if every $\phi_{(i,j),(k,l)}$ is analytic on a neighborhood of $\overline{D_i} \times \overline{D_j}$ and

$$\begin{aligned} \phi^{(1)}_{i,k} &: D_i \longrightarrow \phi^{(1)}_{i,k}(D_i) \supset \overline{D_k} \\ \phi^{(2)}_{j,l} &: D_j \longrightarrow \phi^{(2)}_{j,l}(\overline{D_j}) \subset D_l \ . \end{aligned}$$

This generalizes the setup in [SW23] via the following translation prescription: Suppose $g_1, \dots, g_r$ generate a Schottky group of rank r and denote by $D_1, \dots, D_{2r}$ corresponding fundamental discs, i.e. g_i maps the interior of D_i to the exterior of D_{i+r}. Furthermore the convention $g_{i+r} \coloneqq g_i^{-1}$ together with $g_{i+2r} = g_i$ for $i = 1, \dots, r$ will be used. For a more detailed introduction see [SW23, Section 1.2]. Now $N = 2r$ and the adjacency matrix is given by

$$A_{(i,j),(k,l)} = 1 \iff i \neq j,\ k \neq l,\ \text{and } l = i + r \ ,$$

and the family of hyperbolic maps is defined in terms of the generators as

$$\phi_{(i,j),(k,i+r)}(z_1, z_2) = (g_i z_1, g_i z_2) \in (\mathbb{C} \setminus D_{i+r}) \times D_{i+r} \ , \quad (z_1, z_2) \in D_i \times D_j,\ i \neq j,\ k \neq i+r \ .$$

Example 4.1.2. From the numerical standpoint the most important hyperbolic map system which does not come from generators of a Schottky surface is the *flow adapted n_f-funnel surface* as first described in [BW16]. Instead of repeating the definitions made there concrete formulae for the case of a *flow adapted hyperbolic cylinder* will be presented. While requiring less notation to set up the cylinder already exhibits the central ideas of flow adaptation very clearly. Furthermore the formulae become much more explicit and therefore provide an ideal example for the verification of numerical procedures later on. Lastly the paper [BW16] only considered the case of $n_f \geq 3$ funnels to begin with making the statement of concrete formulae for the cylinder case a worthwhile addition to the literature.[1]

The *hyperbolic cylinder* X_ℓ is the rank-1 Schottky surface associated to the Schottky group generated by the single hyperbolic element

$$\begin{pmatrix} e^{\ell/2} & 0 \\ 0 & e^{-\ell/2} \end{pmatrix} . \tag{4.1.1}$$

It depends on the positive real parameter $\ell > 0$ whose geometric interpretation is that of the hyperbolic length of the single simple closed geodesic on X_ℓ. Figure 4.1 shows an illustration of the canonical fundamental domain.

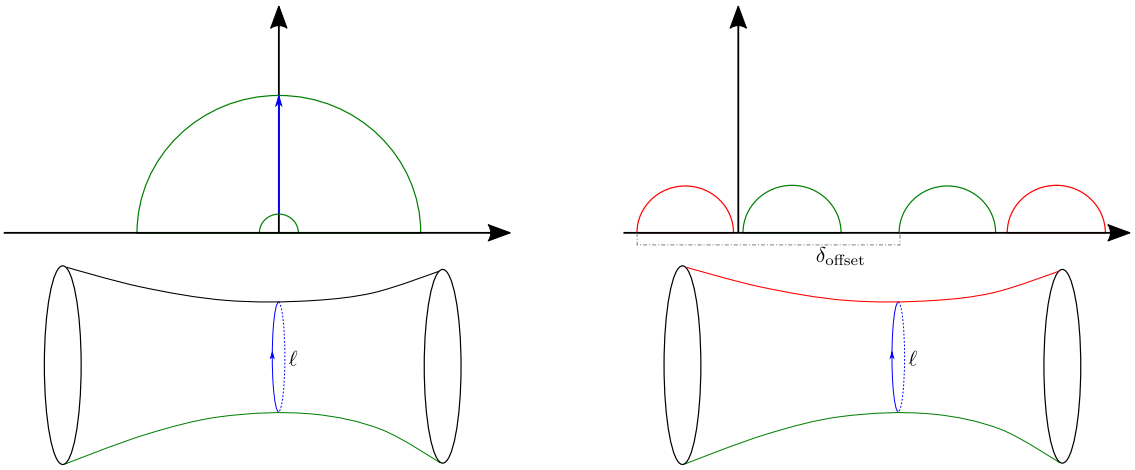

(a) Fundamental circles of the hyperbolic cylinder X_ℓ as a Schottky surface together with a (non-isometric) embedding into $\mathbb{R}^3$.

(b) Fundamental circles of the flow adapted representation of the hyperbolic cylinder X_ℓ together with a (non-isometric) embedding into $\mathbb{R}^3$.

Figure 4.1.: Illustration of both the Schottky group (Bowen-Series) and flow-adapted representations of the hyperbolic cylinder X_ℓ.

Geometrically this representation as a Schottky surface corresponds to a cutting of the cylinder along a single line perpendicular to the closed geodesic around the waist. In the light of symmetry reduction as described in [BW16] one would expect that this does not lead to a maximally symmetric representation: Cutting along two lines perpendicular to the waist geodesic and with a hyperbolic distance of $\ell/2$ should introduce as an additional symmetry reflection about the hyperplane containing both cuts. The lower part of Figure 4.1(b) illustrates this geometric idea.

Mathematically this heuristic corresponds to replacing the Schottky group above with an iterated function system defined by four reflections. The notion of iterated function

[1] The flow adapted cylinder is particularly interesting as a means of practically checking the correctness of implementations of the numerical algorithms presented later on due to the explicit knowledge of its resonance spectrum.

system is closely related to the definition of hyperbolic map systems above but only incorporates the expanding direction.[2] For details see e.g. [BW16]. The presentation here starts with such a function system because the general flow adapted n_f-funnel surfaces are such systems. The translation from function to hyperbolic map systems is very similar to the translation procedure for Schottky surfaces and will be described shortly.

The first two reflections along one should glue the two portions of the cylinder can basically be read off directly from the upper part of Figure 4.1(b) as

$$\widetilde{R}_1 \coloneqq \begin{pmatrix} 0 & \mathrm{e}^{\ell/4} \\ \mathrm{e}^{-\ell/4} & 0 \end{pmatrix} , \qquad \widetilde{R}_2 \coloneqq \begin{pmatrix} 0 & \mathrm{e}^{-\ell/4} \\ \mathrm{e}^{\ell/4} & 0 \end{pmatrix} ,$$

but this definition is slightly inconvenient because the reflection circles of $\widetilde{R_1}$ and $\widetilde{R_2}$ overlap. Fortunately a very explicit rotation by $\pi/4$ yields the more practical reflections

$$R_1 \coloneqq \begin{pmatrix} \cosh(\ell/4) & -\sinh(\ell/4) \\ \sinh(\ell/4) & -\cosh(\ell/4) \end{pmatrix} , \qquad R_2 \coloneqq \begin{pmatrix} \cosh(\ell/4) & \sinh(\ell/4) \\ -\sinh(\ell/4) & -\cosh(\ell/4) \end{pmatrix} , \tag{4.1.2}$$

through circles centered at $m_\pm = \pm\cosh(\ell/4)/\sinh(\ell/4)$ and radius $r = 1/\sinh(\ell/4)$. Using these reflections the (iterated) function system can now be defined by the adjacency matrix

$$A = \begin{pmatrix} 0 & 0 & 0 & 1 \\ 0 & 0 & 1 & 0 \\ 0 & 1 & 0 & 0 \\ 1 & 0 & 0 & 0 \end{pmatrix} ,$$

together with the maps

$$\begin{aligned} \phi_{1,4}(u) &\coloneqq R_1(u) + \delta_{\text{offset}} , & \phi_{2,3}(u) &\coloneqq R_2(u) + \delta_{\text{offset}} \\ \phi_{3,2}(u) &\coloneqq R_1(u - \delta_{\text{offset}}) , & \phi_{4,1}(u) &\coloneqq R_2(u - \delta_{\text{offset}}) . \end{aligned}$$

Here $\delta_{\text{offset}} \coloneqq 2(\cosh(\ell/4) + 1)/\sinh(\ell/4) + 1$ is the distance between the left-most and right-most points of the reflection circles incremented by one to make sure that the intervals of definition for these maps

$$\begin{aligned} &I_1 \coloneqq [m_- - r, m_- + r] , I_2 \coloneqq [m_+ - r, m_+ + r] , \\ &I_3 \coloneqq I_1 + \delta_{\text{offset}} , I_4 \coloneqq I_2 + \delta_{\text{offset}} , \end{aligned}$$

do not intersect. Figure 4.1(b) shows clearly how these maps correspond to the symmetric cutting procedure outlined above: The left and right pairs of circles correspond to the upper and lower half of the cylinder and both halves are glued along the reflection maps.

From here it is straightforward to identify the flow-adapted hyperbolic cylinder as a hyperbolic map system by setting

$$A_{(i,j),(k,l)} = 1 \iff A_{j,l} = 1,\ k \neq l, \text{ and } (\{i,j\} = \{1,2\} \text{ or } \{i,j\} = \{3,4\}) ,$$

combined with the analytic maps

$$\phi_{(i,j),(k,l)}(z_1, z_2) \coloneqq (\phi_{j,l}(z_1), \phi_{j,l}(z_2)) \in (\mathbb{R} \setminus I_l) \times I_l \quad (z_1, z_2) \in I_i \times I_j,\ A_{(i,j),(k,l)} = 1 .$$

After defining the dynamical determinant below it will be justified precisely how this flow adapted map system is related to its plain, non-adapted Schottky counterpart.

The general case of flow-adapted n_f-funneled surfaces works quite similarly but requires a pair of circles for every funnel. This makes the notation more involved but does not pose any substantial conceptual difficulties.

[2] Note that iterated function systems form one of the central abstractions for the implementations presented in Chapter 7.

With this example at hand it is time to return to the general setting of hyperbolic map systems. Using the prescription for translation from and to the Schottky setting as a blueprint makes it rather straightforward to reformulate the theorems given in [SW23] in terms of hyperbolic map systems. The first step is the definition of the transfer operator associated with a hyperbolic map system. Then once again one wants to prove the trace class property for this operator to be able to consider its Fredholm determinant as a holomorphic function. This is achieved by a straightforward generalization of the transfer operator as defined in [SW23, Thm. 2.2]. Recall that $\mathcal{H}^2(\mathcal{D})$ denotes the Bergman space of square integrable, holomorphic functions in a complex domain $\mathcal{D}$ and $\mathcal{H}^{-2}(\mathcal{D})$ denotes its dual space. The dual is again identified with $\mathcal{H}^2(\mathbb{C}\setminus\mathcal{D})$ via integration over the boundary.

Theorem 4.1.3: Transfer operator for hyperbolic map systems

Let $\phi_{(i,j),(k,l)}$ be a hyperbolic map system on domains $D_1,\dots,D_N$ with adjacency matrix A and V a potential which is analytic in a neighborhood of $\bigcup_{i\neq j} D_i \times D_j$. The associated *transfer operator* defined by the formula

$$\begin{aligned}
&\mathrm{L}_V : \bigoplus_{i,j} \mathcal{H}^{-2}(D_i)\otimes\mathcal{H}^2(D_j) \longrightarrow \bigoplus_{i,j} \mathcal{H}^{-2}(D_i)\otimes\mathcal{H}^2(D_j)\ ,\\
&\qquad \langle \mathrm{L}_V u(z_1,z_2), v(z_1)\rangle\Big|_{\substack{v\in\mathcal{H}^2(D_i)\\ z_2\in D_j}}\\
&:= \sum_{\substack{(k,l):\\ A_{(i,j),(k,l)}=1}} \int_{\partial D_i} V(z_1,z_2)v(z_1)u(\phi_{(i,j),(k,l)}(z_1,z_2))\frac{\mathrm{d}z_1}{2\pi\mathrm{i}}\ ,
\end{aligned}$$

is a well-defined trace-class operator and its Fredholm determinant is an analytic function that satisfies the following identity for sufficiently small $|z|$:

$$\det\left(\mathrm{id}-z\mathrm{L}_V\right) = \exp\left(-\sum_{n=1}^{\infty}\frac{z^n}{n}\sum_{w\in\mathcal{W}_n}\frac{V_w}{|\det\left(\mathrm{id}-\phi_w'\right)|}\right)\ .$$

The notation was chosen in direct adaptation of [SW23]: $\mathcal{W}_n$ represents the set of admissible words of length n over the alphabet $\mathcal{A} := \{1,\dots,N\}$, i.e.

$$\mathcal{W}_n := \left\{((i_1,j_1),\dots,(i_n,j_n)) \,\middle|\, A_{(i_m,j_m),(i_{m+1},j_{m+1})}=1\ \forall\, 1\le m<n \text{ and } A_{(i_n,j_n),(i_1,j_1)}=1\right\}$$

and the iterations along a closed orbit represented by $w\in\mathcal{W}_n$ are given by

$$\begin{aligned}
V_w &:= V(z_w)\prod_{m=2}^{n} V\left(\phi_{(i_{m-1},j_{m-1}),(i_m,j_m)}\circ\ldots\circ\phi_{(i_1,j_1),(i_2,j_2)}\right)(z_w)\ ,\\
\phi_w &:= \phi_{(i_n,j_n),(i_1,j_1)}\phi_{(i_{n-1},j_{n-1}),(i_n,j_n)}\circ\ldots\circ\phi_{(i_1,j_1),(i_2,j_2)}\ ,
\end{aligned}$$

where finally $z_w\in D_{i_1}\times D_{j_1}$, $i_1\neq j_1$, is the unique fixed point of ϕ_w. Note how these definitions recover those in [SW23, Section 1.2 and Section 2.1] for the concrete case of a hyperbolic map system derived from a Schottky surface. The proof is a straightforward adaptation of the one given in [SW23].

Remark 4.1.4. From here it is rather obvious how to define Pollicott-Ruelle resonances for hyperbolic map systems, namely as the zeros of the holomorphic Fredholm determinant

$$d(\lambda) := \det\left(\mathrm{id}-\mathrm{L}_{V_\lambda}\right)$$

associated to the transfer operator for the map system with potential $V_\lambda(z_1, z_2) \coloneqq [\phi'_{(i,j),(k,l)}(z_2)]^{-\lambda}$ for $(z_1, z_2) \in D_i \times D_j$. This recovers the usual notion of Pollicott-Ruelle resonances on Schottky surfaces if the hyperbolic map system was initially derived from a Schottky group as explained above.

Now the main point of introducing hyperbolic map systems at all becomes clear: If one chooses either one of the potentials [SW23, Eq. (20) or Eq. (22)] for the flow-adapted hyperbolic cylinder then the resulting dynamical determinant possesses the exact same zeros as the dynamical determinant for the (Schottky) hyperbolic cylinder, i.e. at the Pollicott-Ruelle resonances. This is quite immediate to see from the fact that closed words for the flow-adapted map system must be of even length and every possible neighboring pair of generators coincides with a genuine Schottky generator:

$$\begin{pmatrix} 0 & \mathrm{e}^{\pm\ell/4} \\ \mathrm{e}^{\mp\ell/4} & 0 \end{pmatrix} \begin{pmatrix} 0 & \mathrm{e}^{\mp\ell/4} \\ \mathrm{e}^{\pm\ell/4} & 0 \end{pmatrix} = \begin{pmatrix} \mathrm{e}^{\pm\ell/2} & 0 \\ 0 & \mathrm{e}^{\mp\ell/2} \end{pmatrix} .$$

A similar observations holds for the push-forward of Ruelle distributions, i.e. the logarithmic derivative of the dynamical determinant, onto the fundamental domain: The test functions calculated according to [SW23, Eq. (20)] for the Schottky representation coincide with the flow-adapted variant if one uses the evaluation points $x_j + \mathrm{i}y_j \coloneqq g_0 g_{i_{2j}} \cdots g_{i_1} g \cdot \mathrm{i}$ in the latter case.

Concerning the restriction of Ruelle distributions to a Poincaré section flow-adaptation must obviously yield a different approximation if one uses the natural choice of symmetric section instead of the one naturally employed in the Bowen-Series case: They are not easily comparable now as they yield functions on $\bigcup_{i,j} I_i \times I_j$ with I_i their respective (different) fundamental intervals. But this difference between the two approaches can simply be attributed to the usage of more symmetric test functions on a geometrically more natural hypersurface. It seems very reasonable to expect the central qualitative features of Ruelle distributions to be visible in both of these two-dimensional distributions.

Analogous statements hold true for the general flow-adapted n_f-funneled surfaces by a direct adaptation of [BW16, Proposition 5.4].

Remark 4.1.5. Note that the dimensional reduction procedures presented in [SW23] were chosen by considering objects which are directly derived from $\mathcal{T}_{\lambda_0}$ in the sense that they can be calculated via dynamical determinants by use of the theory of weighted zeta functions and at the same time satisfy the following (competing) guidelines:

(i) one must be able to evaluate the period integrals necessary for the computation of the object via dynamical determinants efficiently;

(ii) the object must retain a significant fraction of the information contained in the full original distribution $\mathcal{T}_{\lambda_0}$;

(iii) the object should be motivated geometrically to allow an interpretation in the context of both Bowen-Series and flow-adapted systems.

The discussion in [SW23, Section 4] could without complications and in a modular fashion be replaced by any other object satisfying these constraints. In principle one could e.g. numerically calculate full Ruelle distributions if one comes up with a parametrization of $S\mathbf{X}_\Gamma$ that makes period integrals efficient to calculate and allows the human eye to distinguish the relevant features in the resulting three-dimensional plots. The usage of a better symmetry adapted Poincaré section fits perfectly with this philosophy.

4.2. Full Symmetry Reduction of Flow-Adapted Systems

At this point the introduction of hyperbolic map systems remains a generalization without practical impact – the flow-adapted surfaces introduced as the main examples above are basically reformulations of their Schottky counterparts. The true usefulness of flow-adaptation only reveals itself through the following definition which is a straightforward adaptation of [SW23, Definition 5.2]:

Theorem 4.2.1: Symmetry group of hyperbolic map systems

Let $\phi_{(i,j),(k,l)}$ be a hyperbolic map system on domains $D_1, \dots, D_N$ and adjacency matrix A, and $\mathbf{G}$ a finite group acting on $\bigcup_i D_i$ by holomorphic functions extending continuously to the boundary and defining a $\mathbf{G}$-action on $\{1, \dots, N\}$ by the relation $\mathbf{g}(D_i) = D_{\mathbf{g}\cdot i}$.
Then $\mathbf{G}$ is called a *symmetry group of the hyperbolic map system* if for any $\mathbf{g} \in \mathbf{G}$ and $(i,j),(k,l)$ with $A_{(i,j),(k,l)} = 1$ there exist $(i',j'),(k',l')$ with $A_{(i',j'),(k',l')} = 1$ and

$$\mathbf{g} \cdot (\phi_{(i,j),(k,l)}(z_1, z_2)) = \phi_{(i',j'),(k',l')}(\mathbf{g} \cdot z_1, \mathbf{g} \cdot z_2) \ , \qquad \forall (z_1, z_2) \in D_i \times D_j \ .$$

With this definition at hand the same symmetry reduction methodology of [SW23, Section 5] can be generalized to the setting of hyperbolic map systems: The Hilbert spaces $\bigoplus \mathcal{H}^{-2}(D_i) \otimes \mathcal{H}^2(D_j)$ decompose as finite sums of Hilbert spaces indexed by (equivalence classes of) irreducible unitary representations of $\mathbf{G}$. This decomposition in turn induces a finite product representation of $\det(\mathrm{id} - z\mathrm{L}_V)$ which finally results in a symmetry reduced analogue of [SW23, Proposition 5.4].

This finally justifies the effort of discussing the abstract formulation of hyperbolic map systems: Considering the flow-adapted hyperbolic cylinder provides an alternative route of calculating invariant Ruelle distributions but with *strictly larger* symmetry group. The Schottky representation has as its symmetries the two-element group generated by the map $z \mapsto 1/z$ which is obvious by the calculation

$$\begin{pmatrix} 0 & 1 \\ 1 & 0 \end{pmatrix} \begin{pmatrix} \mathrm{e}^{\ell/2} & 0 \\ 0 & \mathrm{e}^{-\ell/2} \end{pmatrix} \begin{pmatrix} 0 & 1 \\ 1 & 0 \end{pmatrix} = \begin{pmatrix} \mathrm{e}^{-\ell/2} & 0 \\ 0 & \mathrm{e}^{\ell/2} \end{pmatrix} \ .$$

Keeping in mind the additional rotation introduced above this translates to the following symmetry of the flow-adapted representation:

$$g_1 \coloneqq \begin{cases} z & \longmapsto -z \ , & z \in D_1 \cup D_2 \\ z & \longmapsto -z + 2\delta_{\text{offset}} \ , & z \in D_3 \cup D_4 \end{cases}$$

Verifying that this is indeed a symmetry is as straightforward as calculating e.g. $g_1 \circ \phi_{2,3} \circ g_1 = \phi_{1,4}$. But the flow-adaptation reveals an additional symmetry not present in the original Schottky representation namely

$$g_2 \coloneqq \begin{cases} z & \longmapsto z + \delta_{\text{offset}} \ , & z \in D_1 \cup D_2 \\ z & \longmapsto z - \delta_{\text{offset}} \ , & z \in D_3 \cup D_4 \end{cases}$$

Again the defining properties of symmetries are easily verified, e.g. $g_2 \circ \phi_{2,3} \circ g_2 = \phi_{4,1}$. Compare again Figure 4.1 both both these symmetries. The action of the resulting four-element symmetry group on the letters $\{1,2,3,4\}$ immediately follows to be

$$\begin{aligned} g_1 &: \ 1 \mapsto 2, \ 2 \mapsto 1, \ 3 \mapsto 4, \ 4 \mapsto 3, \\ g_2 &: \ 1 \mapsto 3, \ 2 \mapsto 4, \ 3 \mapsto 1, \ 4 \mapsto 2. \end{aligned}$$

A similar observation holds for n_f-funnel surfaces: Flow adaptation reveals symmetry groups which are strictly larger than those of the more classical Schottky group representations. For the details refer to the presentation in [BW16, Section 5.1]. The practical observation that larger symmetry groups lead to significantly better numerical convergence properties, see [SW23, Section 6], justifies the effort of introducing hyperbolic map systems in the first place.

4.3. Dynamical Determinants beyond Hyperbolic Map Systems

While Bergman spaces of holomorphic functions offer a convenient and powerful tool for the treatment of dynamical determinants their usage is restricted to holomorphic dynamics which exhibit the simple and convenient splitting into stable/unstable directions heavily exploited in [SW23]. It is for this reason that this work refrained from treating Schottky surfaces and n–disc systems on the same footing. The latter seem to require more sophisticated Banach spaces and a generalization of the Fredholm determinant like the ones used in [Bal18]. Note, though, that the remainder of [SW23] remains valid for n-disc systems (and potentiall even more generally smooth weight functions) once one has proven the analogue of [SW23, Thm. 2.2] for them.

This concluding section sketches a promising approach for the extension of the results for Schottky surfaces (or the slightly more general hyperbolic map systems) to a setting which does not require analyticity and an explicit splitting into stable and unstable directions. The upcoming discussion is based on [Bal18, Chapter 6]. First, recall some required definitions and central results:

Let $\mathbf{M}$ be a *compact, connected Riemannian manifold without boundary*, $V \subseteq \mathbf{M}$ an *open* subset and $T : V \to \mathbf{M}$ a C^r-*diffeomorphism* with $r > 1$. Let the following data be given:

- A *compact, T-invariant, locally maximal* and *hyperbolic* $\emptyset \neq \Lambda \subseteq V$;
- Existence of a *dense orbit* of T as a function $\Lambda \to \Lambda$;
- A C^{r-1} weight $g : \mathbf{M} \to \mathbb{C}$ with $\mathrm{supp}(g) \subseteq V$.

Then [Bal18, p. 184] defines the dynamical determinant for (T, g) as the formal power series

$$d_{T,g}(z) \coloneqq \exp\left(-\sum_{m=1}^{\infty} \frac{z^m}{m} \sum_{\substack{x \in \Lambda \\ T^m(x)=x}} \frac{g^{(m)}(x)}{|\det(\mathrm{id} - \mathrm{D}T^m(x))|} \right), \tag{4.3.3}$$

where $z \in \mathbb{C}$, $g^{(m)}(x) \coloneqq g(x)g(T(x)) \cdots g(T^{(m-1)}(x))$ is the iteration of g over the closed orbit of T through x and $\mathrm{D}T^m(x)$ denotes the differential at x of the map T^m (which by $T^m(x) = x$ is an endomorphism of $T_x\mathbf{M}$). With this data at hand the following two statements hold:

Lemma 4.3.1: Absolute Convergence of $d_{T,g}$ ([Bal18, Lemma 6.1])

The infinite sum over m in (4.3.3) converges for $|z| < 1/Q^{0,0}(T, g)$ such that in this disc $d_{T,g}$ is a nowhere vanishing holomorphic function. If additionally $g \geq 0$ on Λ then $d_{T,g}$ has a zero at $z = Q^{0,0}(T, g)$.

Theorem 4.3.2: Holomorphic Extension of $d_{T,g}$ ([Bal18, Thm. 6.2])

$d_{T,g}$ has a holomorphic extension onto the disc with radius $1/Q_{r-1}(T,g)$.

The constants $Q^{0,0}(T,G)$ and $Q_{r-1}(T,g)$ will be defined and discussed in Subsection 4.3.3.

One may apply these results to the cycle expansion of weighted zeta functions on Schottky surfaces $\Gamma\backslash\mathbb{H}$ as follows: First the appropriate dynamical system is identified with ambient phase space $\mathbf{M} \coloneqq \partial\mathbb{D} \times \partial\mathbb{D}$, domain $V \coloneqq Q \coloneqq \bigcup_{k\neq l} I_k \times I_l$ and time evolution

$$T : V \longrightarrow \mathbf{M} ,$$
$$I_k \times I_l \ni (x_-, x_+) \longmapsto (g_l(x_-), g_l(x_+)) \ .$$

First note that $\mathbf{M}$ is indeed compact without boundary and Riemannian (viewing $\partial\mathbb{D}$ as a submanifold of $\mathbb{C}$), $V \subseteq \mathbf{M}$ is open and $T \in \mathrm{C}^\infty(V)$ because the generators g_l are smooth on the components $\bigcup_k I_k \times I_l$.

Second choose $\Lambda \coloneqq (\Lambda(\Gamma) \times \Lambda(\Gamma)) \cap V = (\Lambda(\Gamma) \times \Lambda(\Gamma)) \cap \overline{V}$.[3] Then $\emptyset \neq \Lambda \subseteq V$ is compact in $\mathbf{M}$, as $\Lambda(\Gamma)$ is a closed subset of the compact manifold $\partial\mathbb{D}$, and T-invariant. To see the latter take $(x_-, x_+) \in \Lambda \cap I_k \times I_l$. Then $T(x_-, x_+) = (g_l(x_-), g_l(x_+)) \in \Lambda(\Gamma) \times \Lambda(\Gamma)$ because the limit set is Γ-invariant and $(g_l(x_-), g_l(x_+)) \in I_{l+r} \times (\partial\mathbb{D}\backslash I_{k+r})$. Thus, $T(x_-, x_+) \in \Lambda(\Gamma)\times\Lambda(\Gamma)\cap I_{l+r}\times(\partial\mathbb{D}\backslash I_{k+r}) \subseteq \Lambda(\Gamma)\times\Lambda(\Gamma)\cap I_{l+r}\times(\bigcup_{m\neq l+r} I_m) \subseteq \Lambda$. Finally, Λ is a hyperbolic set for T because the second coordinate of T coincides with the Bowen-Series map B making it expanding while its first coordinate coincides with the inverse of B making it contracting, see [Bor16, Chap. 15.2].[4]

To verify local maximality and existence of a closed orbit some additional effort is required in the following two subsections.

4.3.1. Local Maximality

This sections shows that any open $\Lambda \subseteq U \subsetneq \Lambda$ is separating for Λ. A particular one is constructed by observing that the limit set is properly separated from the boundary points of fundamental intervals. After denoting the minimal distance between $\Lambda(\Gamma)$ and $\bigcup_k I_k$ as ε define $U \coloneqq \bigcup_{(x_-,x_+)\in\Lambda} B_{\frac{\varepsilon}{2}}(x_-) \times B_{\frac{\varepsilon}{2}}(x_+)$ where $B_\delta(y)$ denotes the open δ-interval around y.

Suppose now that $T^m(x_-, x_+) \in \overline{U}$ for all $m \in \mathbb{Z}$. This supposition implies $\mathrm{B}^n(x_+) \in \bigcup_k I_k$ for all $n \in \mathbb{N}$, i.e. there exists a sequence of generators $(g_{i_n}) \subseteq \Gamma$ such that $g_{i_n} \cdots g_{i_1}(x_+) \in I_{i_{n+1}}$. Thus,

$$x_+ \in \bigcap_{n\geq 1} g_{i_1}^{-1} \cdots g_{i_n}^{-1} I_{i_{n+1}} \subseteq I_{i_1} \ .$$

Intersections of this kind converge to elements of the limit set by [Dal11, Prop. 1.10 and 1.11] so one concludes $x_+ \in \Lambda(\Gamma)$. The same reasoning applied to T^{-1} and x_- shows $x_- \in \Lambda(\Gamma)$. In summary it follows that

$$\bigcap T^m(\overline{U}) = \Lambda \ .$$

[3] Here $\Lambda(\Gamma)$ denotes the *limit set* of the Schottky group Γ. It is properly separated from the boundaries of the I_k so the intersection with V really equals the one with $\overline{V}$. The latter is advantageous for seeing that Λ is indeed compact, though. For details see [Dal11, II.1].

[4] Suppose $(x_-, x_+) \in I_k \times I_l$, $k \neq l$. Then one immediately calculates that $(g_k(x_-), g_k(x_+)) \in (\partial\mathbb{D}\backslash I_{k+r})\times I_{k+r}$ is the inverse of T.

4.3.2. Existence of Dense Orbits

To prove existence of a dense orbit this section constructs a suitable symbolic dynamic for the topological dynamical system $T : \Lambda \to \Lambda$ following [Dal11, p. 98ff]. The goal is to find a shift system that is topologically conjugate to T and for which standard theorems guarantee existence of dense orbits. As usual denote the alphabet of Γ by $\mathcal{A} \coloneqq \{g_1, \dots, g_r, g_{r+1} = g_1^{-1}, \dots, g_{2r} = g_r^{-1}\}$ and define the corresponding one-sided shift space as $\Sigma^+ \coloneqq \{(s_i)_{i\geq 1} \mid s_i \in \mathcal{A},\ s_{i+1} \neq s_i^{-1}\}$.

Next denote by $o \in \mathbb{D}$ a point outside all fundamental circles. Then the map

$$\begin{aligned} f : \Sigma^+ &\longrightarrow \Lambda(\Gamma) \\ (s_i) &\longmapsto \lim_{n\to\infty} s_1 \cdots s_n(o) \end{aligned}$$

is a homeomorphism after endowing Σ^+ with the metric $\delta((s_i),(t_i)) \coloneqq 1/\min\{i \mid s_i \neq t_i\}$ if $(s_i) \neq (t_i)$ and $\delta((s_i),(s_i)) \coloneqq 0$ ([Dal11, Lemma IV.1.2]). More important for the present purposes is the two-sided shift space

$$\Sigma \coloneqq \{(S_i)_{i\in\mathbb{Z}} \mid S^+ \coloneqq (S_i)_{i\geq 1} \in \Sigma^+,\ S^- \coloneqq (S_{-i+1}^{-1})_{i\geq 1} \in \Sigma^+,\ S_0^{-1} \neq S_1\}$$

with the product metric $\Delta((S_i),(T_i)) \coloneqq \left(\delta(S^+,T^+)^2 + \delta(S^-,T^-)^2\right)^{\frac{1}{2}}$. As a final ingredient let the shift operator be denoted by $\widetilde{T}$:

$$\begin{aligned} \widetilde{T} : \Sigma &\longrightarrow \Sigma \\ (S_i)_{i\in\mathbb{Z}} &\longmapsto (S_{i+1})_{i\in\mathbb{Z}} \end{aligned}$$

From the proof of [Dal11, Lemma 1.5] it follows that $F = (f,f) : \Sigma \to \Lambda$ is again a homeomorphism. Injectivity and continuity follows from the corresponding properties of f; surjectivity holds because those elements of $\Lambda(\Gamma) \times \Lambda(\Gamma)$ not contained in the image of F necessarily belong to some diagonal square $I_k \times I_k$. But exactly those squares are excluded in Λ. Finally, F^{-1} is necessarily continuous because F is continuous and Σ is compact.

In order to carry out the strategy outlined above it remains to show that T and $\widetilde{T}$ are indeed conjugate to each other. But taking $(S_i) \in \Sigma$ one readily calculates

$$\begin{aligned} F^{-1} \circ T \circ F((S_i)) &= F^{-1} \circ T(f(S^+), f(S^-)) \\ &= F^{-1}(g_{l+r}(f(S^+)), g_{l+r}(f(S^-))) \\ &= F^{-1}(\lim S_0 S_1 S_2 \cdots S_n(o), \lim S_0 S_0^{-1} S_{-1}^{-1} \cdots S_{-n+1}^{-1}(o)) \\ &= F^{-1}(f(S_0, S_1, ...), f(S_{-1}^{-1}, S_{-1}^{-2}, ...)) \\ &= (S_{i+1}) = \widetilde{T}((S_i)) \ , \end{aligned}$$

because if $S_1 = g_k$ and $S_0^{-1} = g_l$ then $f(S^+) \in I_{k+r}$ and $f(S^-) \in I_{l+r}$. It therefore follows that indeed $F \circ \widetilde{T} \circ F^{-1} = T$.

At this point a final pair of definitions enables the employment of standard machinery for shift systems. Let M be a non-nilpotent matrix indexed by an alphabet $\mathcal{A}$ of $N \geq 2$ letters and with entries in $\{0,1\}$. Then the corresponding two-sided *Markov shift* is defined as

$$\Sigma_M \coloneqq \{(x_i)_{i\in\mathbb{Z}} \in \mathcal{A}^{\mathbb{Z}} \mid M_{x_i,x_{i+1}} = 1\ \forall i \in \mathbb{Z}\} \ .$$

Now according to [ES14, Satz 1.32] *if M is irreducible then the shift operator on Σ_M is topologically transitive*, i.e. possesses a dense orbit. Irreducibility for a matrix M means that for any pair of indices a, b there exists $n \in \mathbb{N}$ such that $(M^n)_{a,b} > 0$.

The concrete shift space Σ on the Schottky group's alphabet $\mathcal{A}$ is indeed a Markov shift. The defining conditions for Σ, namely $S_i \neq S_{i+1}^{-1}$, can be rephrased as $S_{i+1} \in \mathcal{A}\backslash\{g_{k+r}\}$ if $S_i = g_k$. Thus $\Sigma = \Sigma_M$ with a matrix whose second power already exclusively consists of positive entries and is therefore irreducible. The dynamics $\widetilde{T} : \Sigma \to \Sigma$ therefore has a dense orbit. But this property is obviously hereditary under conjugation resulting in the desired existence of a dense orbit for $T : \Lambda \to \Lambda$.

4.3.3. Domain of Holomorphic Extension

This final subsection derives explicit expressions for the quantity $Q^{0,0}(T, g)$ which bounds the disc of absolute convergence of $d_{T,g}$ as well as the quantity $Q_{r-1}(T, g)$ whose inverse bounds the disc of holomorphic continuation.
Again start by recalling some required definitions from [Bal18, Chap. 5]:

$$\begin{aligned} Q^{t,s}(T,g) &\coloneqq \exp\left(\sup_{\mu\in\mathrm{Erg}(\Lambda,T)}\left\{h_\mu(T)+\chi_\mu\left(\frac{g}{\det(\mathrm{D}T\big|_{E^u})}\right)\right.\right. \\ &\qquad\left.\left.+\max\left\{t\chi_\mu(\mathrm{D}T\big|_{E^s}),|s|\chi_\mu(\mathrm{D}T^{-1}\big|_{E^u})\right\}\right\}\right) \qquad (4.3.4) \\ Q_{r-1}(T,g) &\coloneqq \inf_{t-(r-1)<s<0<t} Q^{t,s}(T,g)\ , \end{aligned}$$

where $\mathrm{Erg}(\Lambda, T)$ denotes the set of T-invariant, ergodic Borel probability measures on Λ, $h_\mu(T)$ is the metric entropy of (μ, T) for $\mu \in \mathrm{Erg}(\Lambda, T)$, $\chi_\mu(A) \in \{-\infty\} \cup \mathbb{R}$ stands for the largest Lyapunov exponent of a linear cocycle A over $T\big|_\Lambda$, and E^u, E^s denotes the stable and unstable subspaces of $\mathrm{D}T$ on Λ. Details on these objects can be found in [Bal18, App. B] and references therein.

Now [Bal18, p. 158] shows that

$$Q^{t,s}(T,g) \leq \lambda^{\min(t,|s|)} \cdot Q^{0,0}(T,g)\ , \qquad (4.3.5)$$

where $\lambda < 1$ is the constant which appears in the hyperbolicity condition for $T\big|_\Lambda$. This statement suffices to prove holomorphic extension onto the entire complex plane $\mathbb{C}$ if one chooses the same potential as in [SW23, Corollary 2.4] derived from a *smooth* weight $f \in \mathrm{C}^\infty(S(\Gamma\backslash\mathbb{H}))$: The potential used as g yields arbitrarily high regularity r resulting in arbitrarily small $Q_{r-1}(T, g)$. Furthermore this choice of potential yields[5]

$$\begin{aligned} d_{T,g}(z) &= \exp\left(-\sum_{m=1}^{\infty}\frac{z^m}{m}\sum_{\substack{x\in\Lambda\\ T^m(x)=x}}\frac{g^{(m)}}{|\det(\mathrm{id}-\mathrm{D}T^m(x))|}\right) \\ &= \exp\left(-\sum_{m=1}^{\infty}\frac{z^m}{m}\sum_{g\in\mathcal{W}_m}\frac{\mathrm{e}^{-\lambda\ell(g)-\beta\int_{\gamma(g)}f}}{|(1-\mathrm{e}^{\ell(g)})(1-\mathrm{e}^{-\ell(g)})|}\right) \\ &= d_f(\lambda,z,\beta)\ , \end{aligned}$$

thus recovering the holomorphic extension of the dynamical determinant d_f [SW23, Def. 2.1]. But recovering the whole strength of [SW23, Corollary 2.4] requires a deeper investigation of the dependence on the parameters (λ, β). While this should be possible using wavefront estimates to control the flat traces appearing in the holomorphic extension of $d_{T,g}$ it is beyond the scope of this thesis.

[5] To be precise an additional cutoff $\chi : \mathbf{M} \to \mathbb{R}$ is required with $\chi|_\Lambda = 1$ and $\mathrm{supp}(\chi) \subset Q$ to make sure that $\mathrm{supp}(g) \subset Q$.

The exemplary presentation above used Schottky surfaces but the same reasoning should apply to a much broader class of hyperbolic dynamics including n-disc systems. This approach should therefore provide an angle to prove holomorphic continuation of dynamical determinants and thus convergence of cycle expansions for disc scattering thereby justifying the numerical calculations presented in [BSW22, Section 5].

5. Numerical Investigation of Invariant Ruelle Distributions

The present chapter serves to purposes: On the one hand it contains in Section 5.1 a short overview over the different kinds of visualizations of invariant Ruelle distributions developed in the article [SW23] together with some related conjectures for future numerical investigations in the fashion of a review. In particular the focus here is more on the runtime requirements of the different kinds of experiments as a basis for potential optimizations of the code itself as well as estimations of the runtime of upcoming explorations.[1]

One the other hand this chapter presents in Section 5.2 visualizations of invariant Ruelle distributions on the fundamental domain of convex-cocompact hyperbolic surfaces. The mathematical foundations for this were already presented in [SW23] but this article does not contain actual numerical results for these quantities. The presentation is restricted to a proof-of-principle and indepth investigations will be left for future extensions of [SW23].

5.1. How to Visualize Invariant Ruelle Distributions

A necessary requirement for any experiments on invariant Ruelle distributions is knowledge about an interesting set of Pollicott-Ruelle resonances for some convex-cocompact surface under investigation. In [SW23] the funneled torus $Y(10, 10, \pi/2)$ as well as the three-funneled surface $X(12, 12, 12)$ were chosen. This choice is motivated by two properties: First the two surfaces constitute maximally symmetry representatives for the two possible topologies of rank two Schottky surfaces. Here restricting to rank two is not fundamentally necessary in terms of the developed algorithm but when it comes to practical computations going beyond rank two is only feasible for highly symmetric n_f-funneled surfaces due to computation times.[2] The choice of symmetric surfaces enables the demonstration of quite impressive perfomance gains due to symmetry reduction.

Second the quantum resonances of these concrete surfaces were previously investigated in the literature, see [Bor14]. If one wants to solely investigate invariant Ruelle distribution such previous calculations could be taken as a starting point due to the quantum-classical correspondence on convex-cocompact hyperbolic surfaces [GHW18]: The quantum resonances as calculated using Selberg's zeta function coincide with the classical Pollicott-Ruelle resonances up to a shift

$$s \longmapsto \lambda = s - 1 \ ,$$

where s denotes the quantum and λ the classical spectral parameter. In the article [SW23] another perspective was chosen namely to calculate directly the classical resonances and use the comparison with their quantum counterparts both as a sanity check for the algorithm implemented for dynamical determinants as well as a practical demonstration of the quantum-classical correspondence.

[1] The calculations presented in the article [SW23] were run on a machine with Intel(R) Xeon(R) W-2125 processor (8 cores @ 4.00 GHz) and 128 GB of DDR4 RAM so the runtime estimates below are given with respect to these hardware specifications.

[2] The number of closed geodesics always grows exponentially with their lengths but the exponential rate increases with the number of generators of the surface!

The results are presented in [SW23, Figures 7 and 14] and have been reproduced as a reference side-by-side in Figure 5.1. Both plots show high qualitative agreement with resonance plots from the literature and a re-implementation of Selberg's zeta function did indeed prove this to be a highly accurate quantitative agreement as well.

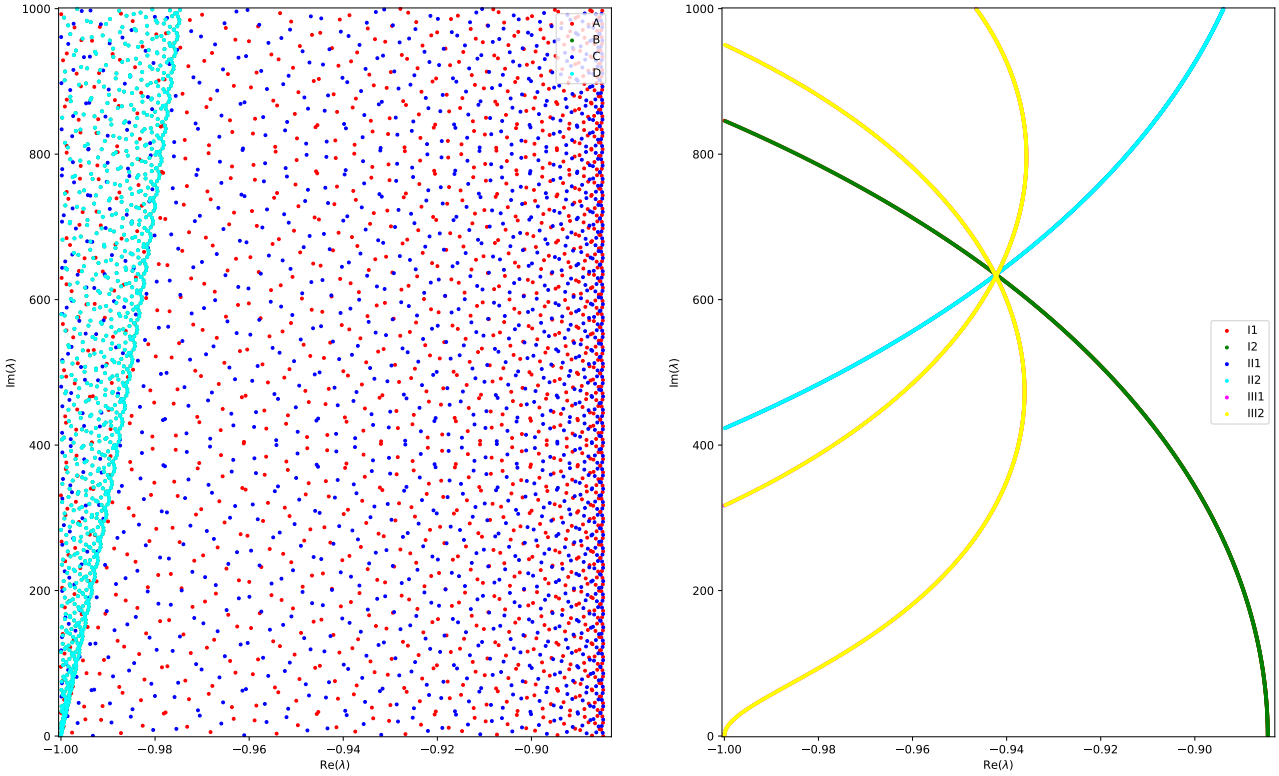

Figure 5.1.: Pollicott-Ruelle resonances for the funneled torus $Y(10, 10, \pi/2)$ (left) and the three-funneled surface $X(12, 12, 12)$ (right) calculated using weighted dynamical determinants of constant weight in full symmetry reduction.

With a sample set of resonances at hand one may now start calculating approximations to invariant Ruelle distributions. For the proof-of-principle showcase in [SW23] the restriction $t^{\Sigma}_{\lambda_0,\sigma}$ to the canonical Poincaré section was chosen as the preferred mode of presentation due to its straightforward interpretation and favorable convergence properties.

This being said one is still faced with a problem in terms of dimensionality: The domain of the restriction $t^{\Sigma}_{\lambda_0,\sigma}$ to the Poincaré section as defined in [SW23, Section 4] is two-dimensional but the codomain is still $\mathbb{C}$ thus requiring four dimensions for visualization of all contained information. The following figures illustrate various possibilities to do so:[3] The simplest approach is certainly to plot real and imaginary parts of $t^{\Sigma}_{\lambda_0,\sigma}$ for given values of resonance λ_0 and Gaussian width σ side-by-side. This is shown in Figure 5.2 for the funneled torus and Figure 5.3 for the three-funneled surface chosen above. These plots show nicely first features such as the fact that the distributions associated with the respective first resonances $\lambda_0 \approx -0.8847$ and $\lambda_0 \approx -0.8845$ are real-valued and positive.

[3] For comprehensive descriptions of details regarding the upcoming figures refer to [SW23, Section 6] in Appendix C.

This is expected because the first invariant Ruelle distribution is known to always coincide with a measure called the *Bowen-Margulis measure*.

Remark 5.1.1. While the coordinates for the canonical Poincaré section as described in [SW23, Section 4] vary within the product

$$\bigcup_{i \neq j} I_i \times I_j$$

with I_i the fundamental intervals of the underlying surface the upcoming plots are actually not parameterized exactly like this. Instead the effective resolution of the plots was increased by first restricting the number of intervals used and second zooming into the left over intervals. The former makes sense because plots over the full coordinate domain still contain quite some redundancies due to internal symmetries of the distributions. The latter is motivated by the fact that with the concretely used Gaussian widths σ the distributions are supported quite far away from the interval boundaries so that plotting the whole fundamental intervals produces a significant amount of whitespace. For details on these matters refer to [SW23, Section 6].

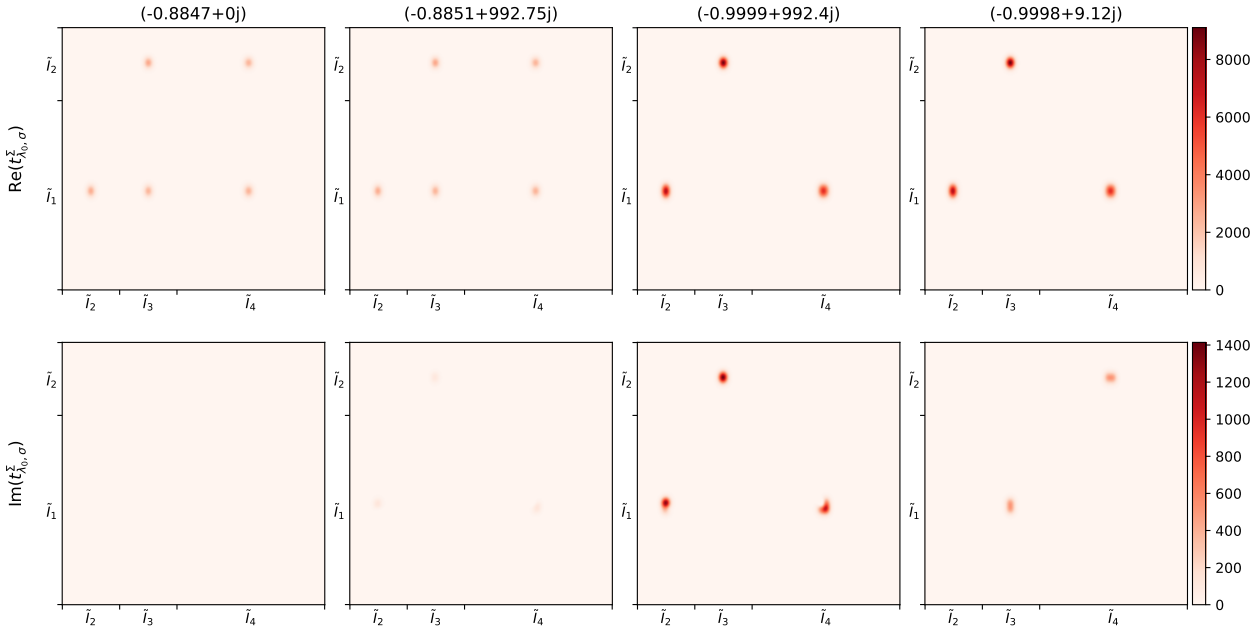

Figure 5.2.: Real (upper half) and imaginary (lower half) parts of the approximation $t^{\Sigma}_{\lambda_0,\sigma}$ to the invariant Ruelle distribution on the canonical Poincaré section of the funneled torus $Y(10, 10, \pi/2)$. The columns depict different resonances but all plots use the same width $\sigma = 10^{-3}$ for the Gaussian test functions used in the approximations. Instead of on the whole coordinate domain the distributions were plotted on representative sub-intervals $\widetilde{I}_i \subset I_i$ of the fundamental intervals I_i.

While certainly comprehensive these plots make it hard to comprehend all of the available information – the reader is required to go back and forth between real and imaginary plots. Furthermore any correlation between real and imaginary parts is hard or even impossible to see with the bare eye. Finally for larger suites of experiments this representation doubles the number of generated plots thereby running the risk of obscuring the relevant information by sheer quantity of the output.

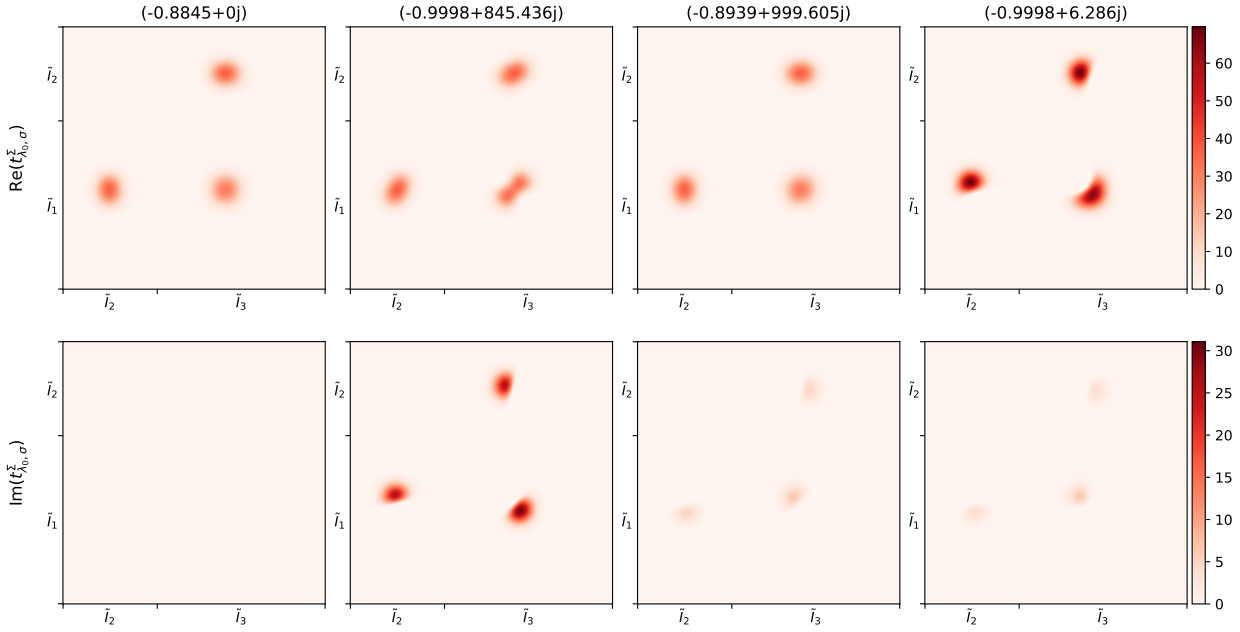

Figure 5.3.: An analogous illustration of $t^{\Sigma}_{\lambda_0,\sigma}$ as in Figure 5.2 but now for a collection of resonances of the (flow-adapted) three-funneled surface $X(12, 12, 12)$ and a Gaussian width of $\sigma = 10^{-2}$. The choice of refined sub-intervals $\widetilde{I}_i$ was also adapted to the symmetry group of this surface.

The visualizations in Figures 5.4 and 5.5 address these issues: The first rows illustrate the absolute values of the distributions. This provides a very compact way of visualizing the general qualitative behavior and the interpretation of the plots is still straightforward. But it also loses information as most distinctly shown by the four plots in Figure 5.4: All plots seem to indicate roughly the same qualitative behavior up to overall scale which would make them less interesting than expected.

That this homogeneity is actually not present was already clear from the plots of real and imaginary parts but can also be seen from the second rows in Figures 5.4 and 5.5: These encode the complex argument, i.e. the angle between real and imaginary parts, as colors on the color wheel while the absolute value gets shown as the lightness of the particular color. Here an angle of 0 corresponds to light blue, an angle of π to red, and particularly light/white colors indicate small absolute value. For a graphical illustration of this encoding see [SW23, Figure 8].

These phase-color/absolute-value-lightness plots show nicely that there are significant differences between the invariant Ruelle distributions associated with different resonances especially for the funneled torus. One can also very clearly identify the similarities between the first two columns in Figure 5.4. This observation is rather straightforward to link to the recurrence to the global spectral gap [Nau05] and is one of the most interesting candidates that will be investigated in future experiments.

A qualitative feature which is not as prominently expressed by these phase plots is the overall support of the distributions. This aspect is quite important, though, especially when considering the convergence of the support towards the limit set of the surface as $\sigma \to 0$. This is most clearly visible in the pure absolute value plots. To reflect both the phase information as well as the support information yet another kind of visualization was developed namely a three-dimensional one, see Figure 5.7: The horizontal plane contains

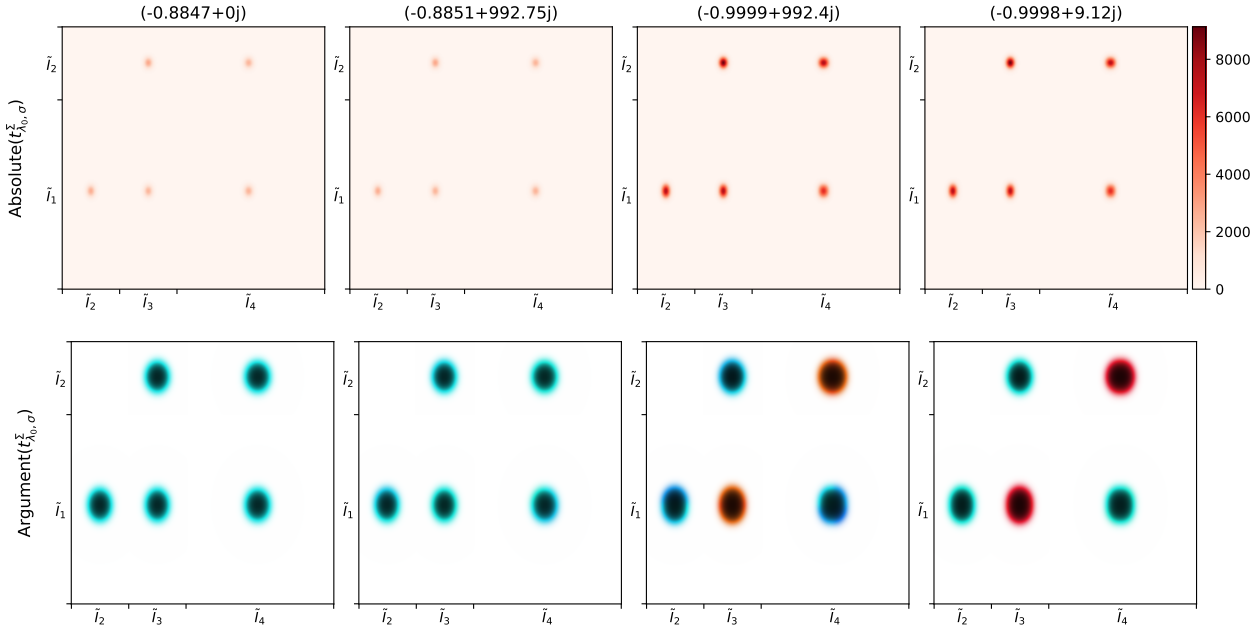

Figure 5.4.: Visualization of the same data as in Figure 5.2. Here the first row shows the absolute value of the invariant Ruelle distribution and the second row uses color and lightness to indicate the complex argument and absolute value of this complex valued quantity.

(again a subset of) the two-dimensional coordinate domain of the Poincaré section whereas the third (vertical) coordinate axis depicts the absolute value of the distribution. The same phase information as in the previously discussed plots is encoded as the color of the resulting surface.

For the summarizing purposes of this section two such three-dimensional plots are shown in Figures 5.6 and 5.7. Both contain the first invariant Ruelle distribution of the funneled torus $Y(10, 10, \pi/2)$ and the three-funneled surface $X(12, 12, 12)$, respectively. Both plots illustrate nicely the support of these distributions, the relative intensity of the peaks, and the globally constant complex phase which is here directly related to the distribution being real-valued and positive.

Runtime Considerations

All of the plots presented here as well as the extended versions in [SW23] were plotted on a grid of support points with sizes about 960×960 pixels. This achieves a compromise between sufficient resolution of the final plots and manageable runtime requirements. Given these grid sizes the calculations for funneled tori at $n_{\max} = 5$ and in full symmetry reduction required roughly 5 min to complete. While this is already quite long for first interactive explorations the experiments in [SW23] showed that $n_{\max} = 3$ is more than sufficient in a wide range of parameters especially for real parts near the global spectral gap. The corresponding calculation times with this cutoff ranged more around 30 sec which allows almost real-time interactivity and unlocks the possibility of running large suites of experiments as batches.

For the fully reduced three-funneled surface the situation is quite similar: While the maximal considered cutoff $n_{\max} = 7$ took about 10 min to compute on a given resonance the more than sufficient value of $n_{\max} = 5$ brought this down to the practically very

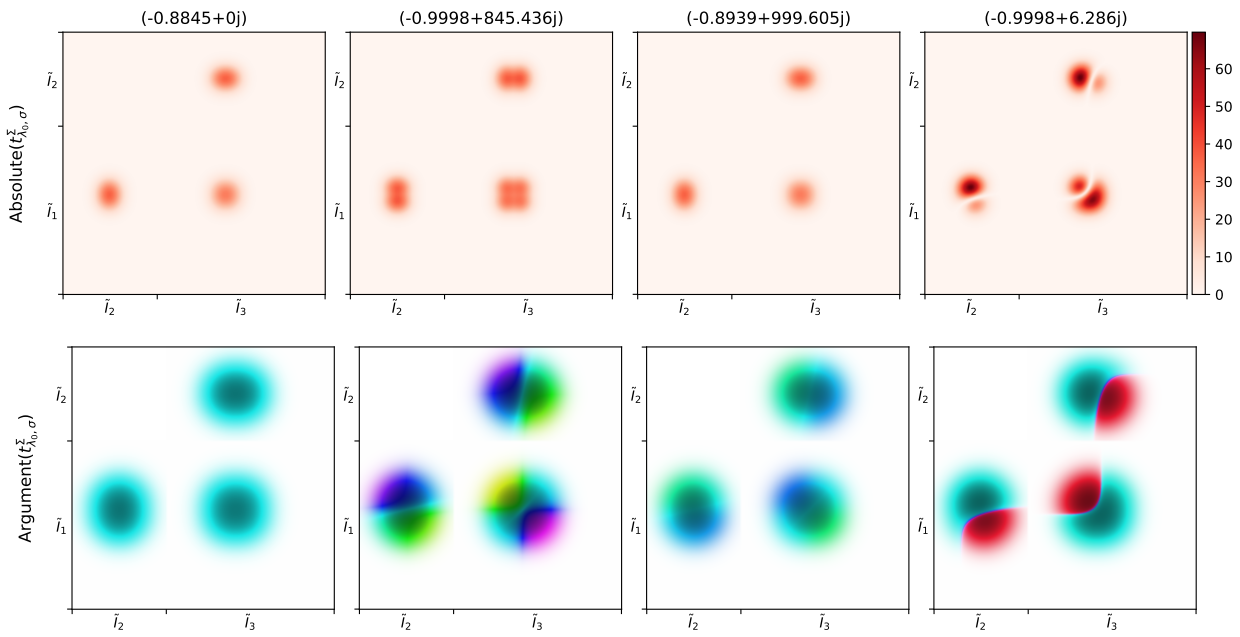

Figure 5.5.: Illustration of the same kind as in the previous Figure 5.4 but for the same data as in Figure 5.3, i.e. for a funneled torus $X(12, 12, 12)$ and Gaussian width $\sigma = 10^{-2}$.

acceptable duration of roughly 30 sec to 1 min.

Symmetry reduction shows its strengths prominently when comparing these values with their non-reduced counterparts: The funneled torus required $n_{\max} = 7$ to converge decently well and for the three-funneled surface one even had to go as high as $n_{\max} = 12$. The computational times associated with these cutoffs ranged at about 20 min and 30 min, respectively. Especially far from the global spectral gap where these high cutoffs were genuinely necessary the symmetry reduction technique is a must to make numerical experiments on invariant Ruelle distributions practically feasible.

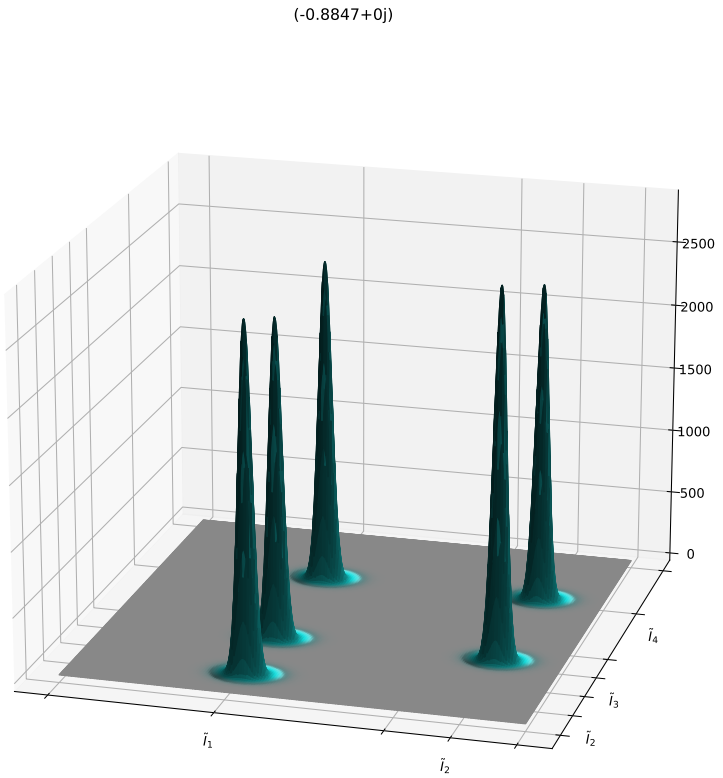

Figure 5.6.: Three-dimensional plot of the first invariant Ruelle distribution for the funneled torus $Y(10, 10, \pi/2)$ on (a subset of) the canonical Poincaré with Gaussian width $\sigma = 10^{-3}$. The height of the surface corresponds to the absolute value of the distribution while the color encodes the complex argument similar to the second row in Figure 5.4.

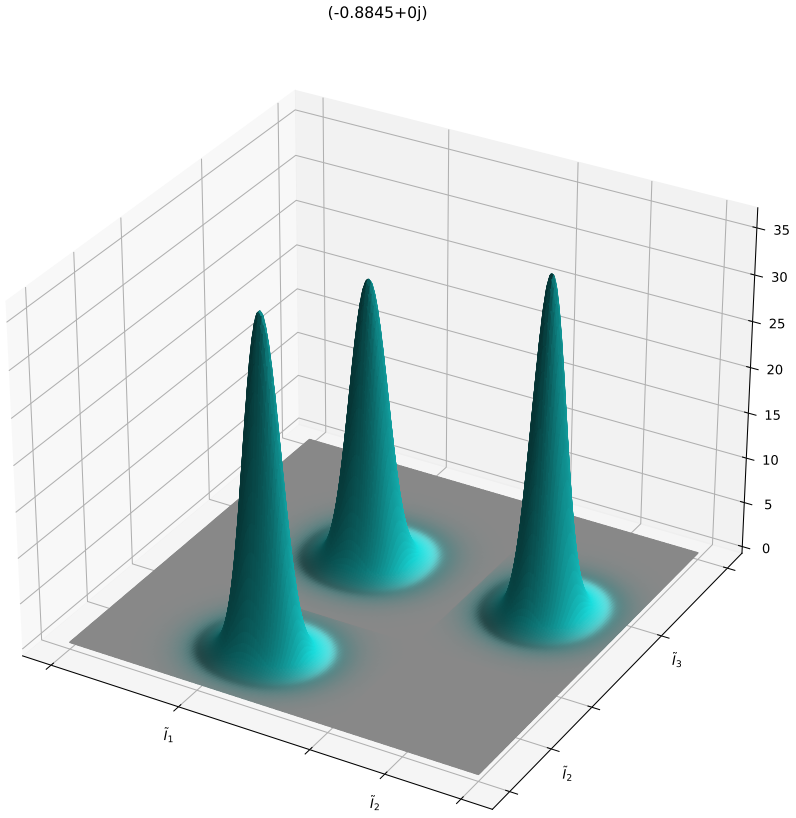

Figure 5.7.: Three-dimensional plot of the first invariant Ruelle distribution similar to Figure 5.6 but for the three-funneled surface $X(12, 12, 12)$ and with Gaussian width $\sigma = 10^{-2}$.

5.2. Invariant Ruelle Distributions on the Fundamental Domain

This section complements the summary presented above with a new kind of plot not considered in the preprint [SW23]: The pushforward of an invariant Ruelle distribution to the fundamental domain of the underlying surface, see Figure 5.8.

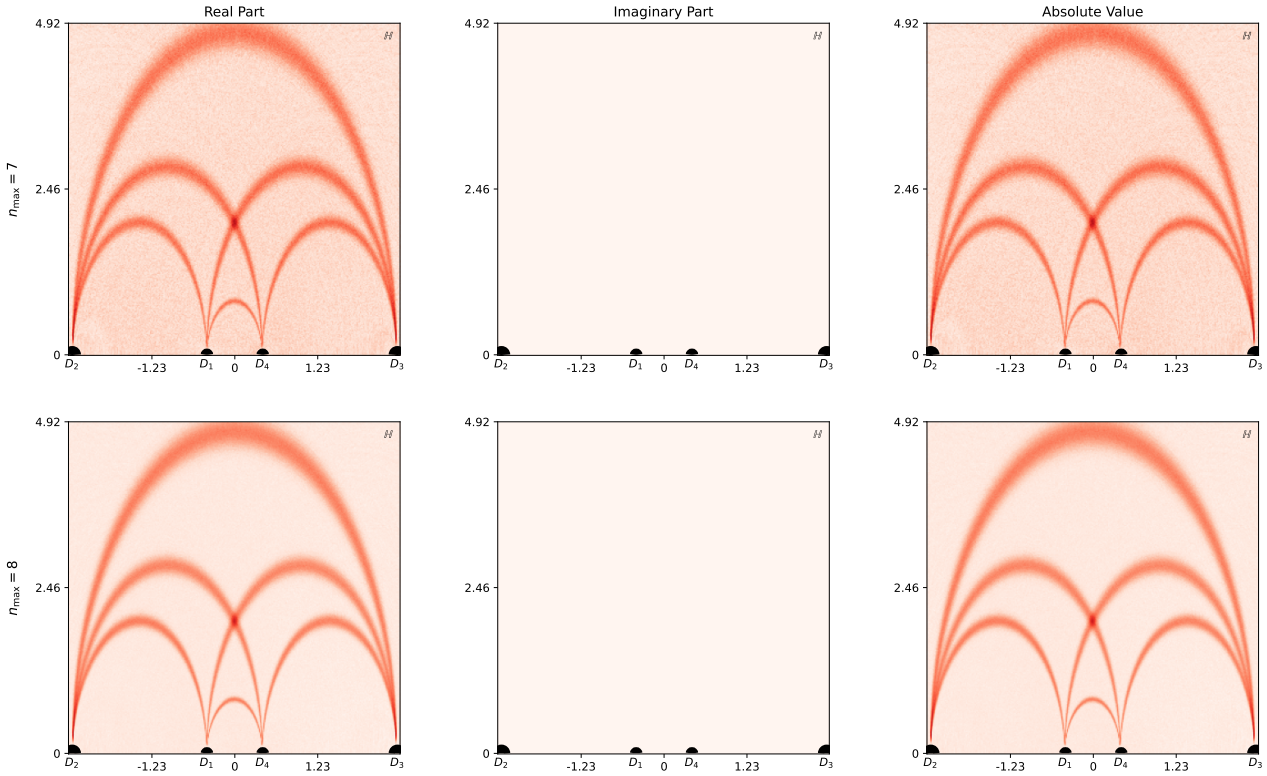

Figure 5.8.: Plot of the pushforward to $\mathbb{H}$ of the invariant Ruelle distribution associated with the first resonance $\lambda_0 \approx -0.8847$ of the funneled torus $Y(10, 10, \pi/2)$. The Gaussian width $\sigma = 5 \cdot 10^{-2}$ was chosen and the fundamental (semi-)circles are indicated in black. For the distributions themselves the same colormap as in the plots on the Poincaré section was used. Here the rows show successive values for the maximal number of summands $n_{\max} \in \{7, 8\}$ in the cycle expansion to illustrate convergence. The columns contain (from left to right) the real part, imaginary part, and absolute value of the distribution clearly proving that it is real-valued and positive.

While this remains a proof-of-principle calculation some basic features of invariant Ruelle distributions on the fundamental domain of the underlying Schottky surface $\mathbf{X}_\Gamma$ are already clearly visible: The support concentrates around the images of closed geodesics under the projection

$$S\mathbf{X}_\Gamma \longrightarrow \mathbf{X}_\Gamma$$

and the distribution exhibits the same symmetries as $\mathbf{X}_\Gamma$, i.e. invariance under the anti-holomorphic functions[4]

$$z \longmapsto -\overline{z}\ , \qquad z \longmapsto 1/\overline{z}\ .$$

Finally the plots show distinctly that this first distribution is real-valued and positive as expected due to it actually being a measure.

[4]Remember that the symmetries of the generating set were described as holomorphic maps but here the anti-holomorphic versions are easier to visualize as they are functions $\mathbb{H} \to \mathbb{H}$.

Remark 5.2.1. These calculations on the fundamental domain were conducted without symmetry reduction to obtain a baseline in terms of computational effort required (they took about 6 min at $n_{\max} = 8$). Symmetry reduced as well as more extensive calculations are planned for future versions of the preprint [SW23].

6. Resonance Sampling on Moduli Space

So far the resonance experiments conducted as part of this thesis followed a common theme: Before calculating resonances in some interesting region of the complex plane some accessible geometry was chosen and held fixed during the calculations. In cases where the underlying geometry was varied the variation was quite limited and deterministic like small perturbations of boundary lengths to observe the presence or absence of chains depending on parameter choices. The same comments apply to resonance experiments performed in previous articles like [Bor14, BPSW20] and the new types of experiments involving Ruelle distributions performed in [SW23].

The present chapter explores a new approach which views the variation of the underlying geometric object as the phenomenon of interest. More concretely a topological class of geometries will be fixed by considering Teichmüller or moduli space of *funneled tori*. On these spaces there exists a probability measure called *Weil-Peterson measure* which is a natural object to study in Teichmüller theory. This chapter contributes to this study by presenting an algorithm which samples from moduli space and produces different kinds of resonance data for these samples. One can then calculate various statistics which in turn allow the formulation of conjectures regarding random variables that involve resonances on hyperbolic surfaces. After presenting the general procedure in Section 6.1 these techniques are applied to conduct a first numerical study in Section 6.2.

6.1. Introduction to Teichmüller and Moduli Space

To start this section the sample set from which funneled tori will be drawn must be defined. As anything resembling a comprehensive introduction to Teichmüller theory is far beyond the scope of this thesis the following description is restricted to the bare minimum necessary for our concrete application. A classical reference for the following material is [Bus10] and the presentation proceeds in similar fashion as [Bor16, Chapter 2.7.2].

In the following a *funneled torus* is any hyperbolic surface of genus g = 1 with one attached funnel. The *Teichmüller space* $\mathcal{T}$ of funneled tori is the space of equivalence classes of complete hyperbolic, i.e. curvature equal to negative one, metrics on these tori. Two metrics belong to the same equivalence class if they are related via pullback by some diffeomorphism which is homotopic to the identity. For an illustration see Figure 6.1.

An important construction in this context is the so-called *pants decomposition*. A *hyperbolic pair of pants* is a hyperbolic surface which is diffeomorphic to the Poincaré disc with three points removed. Each of these points has a neighborhood which is either a cusp or a geodesic boundary. Here we do not consider the case of cusps and it can be shown that for any triple (ℓ_1, ℓ_2, ℓ_3) there exists a unique pair of pants whose three boundary lengths coincide with this triple. Now any geometrically finite, non-elementary[1] hyperbolic surface without cusps and n_f funnels may be obtained by gluing a number of pairs of

[1] Here geometrically finite means that the surface decomposes as the union of a compact core and a finite number of cusps and funnels. The surface being non-elementary makes sure that the group Γ of isometries that realizes the surface as $\Gamma \backslash \mathbb{H}$ is neither trivial nor a cylic group of hyperbolic or parabolic elements [Bor16, Chapter 2].

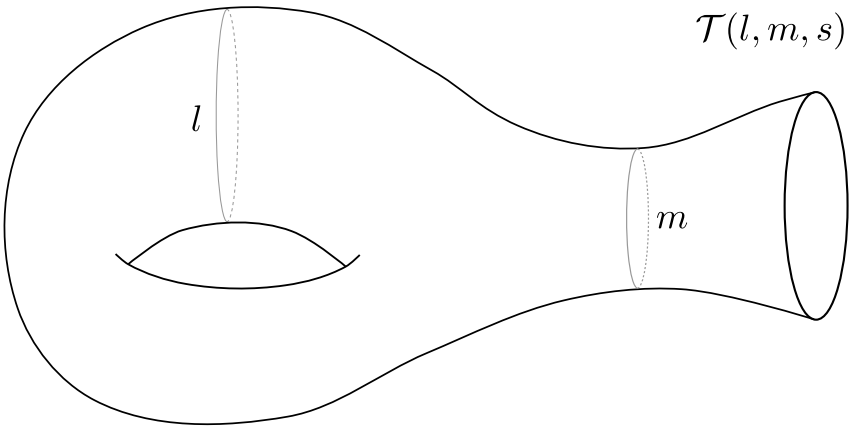

Figure 6.1.: Non-isometric embedding of a funneled torus $\mathcal{T}(l,m,s)$ into three-dimensional Euclidean space. The twist parameter s was omitted from the figure because it is hard to visualize once the pair of pants has been glued.

pants at geodesic boundaries of equal lengths and attaching n_f funnels at the remaining geodesic boundaries. For any pair of glued pants boundaries there exists an additional degree of freedom that can be interpreted as a twist angle and these twists together with the boundary lengths provide smooth coordinates on Teichmüller space. Specifying this discussion to the case of funneled tori this yields

$$\mathcal{T} \cong \mathbb{R}_{>0} \times \mathbb{R}_{>0} \times \mathbb{R} \ ,$$

because the funneled torus is the result of taking a pair of pants with boundary lengths (l,l,m), gluing the boundaries of equal lengths l together with twist $s \in \mathbb{R}$ and attaching a funnel at the third boundary geodesic of length m. To be able to do numerics in the next section a concrete expression for the generators g_1 and g_2 of a torus $\mathcal{T}(l,m,s)$ with parameters (l,m,s) is required. Fortunately such an expression is readily found in the literature [NN98, Section 4.2]:

$$g_1 \coloneqq \begin{pmatrix} \exp(l/2) & 0 \\ 0 & \exp(-l/2) \end{pmatrix} \ , \qquad g_2 \coloneqq \begin{pmatrix} \mathrm{e}^{s/2}a & \mathrm{e}^{s/2}b \\ \mathrm{e}^{-s/2}b & \mathrm{e}^{-s/2}a \end{pmatrix} \ ,$$

where $a = \sqrt{1+b^2}$, $b = \sqrt{1+k}/\sinh(l/2)$, and k is determined by the boundary length m via $1+2k = \cosh(m/2)$. Unfortunately these generators contain in their fundamental intervals the points $\{0,\infty\} \subset \overline{\mathbb{R}}$ so they are not suited for the algorithm that calculates invariant Ruelle distributions. This situation is easily remedied, though: A simple conjugation by the rotation about $\pi/4$ produces an isometric surface with the alternative generators

$$\widetilde{g}_1 \coloneqq \begin{pmatrix} \cosh(l/2) & \sinh(l/2) \\ \sinh(l/2) & \cosh(l/2) \end{pmatrix} \ , \qquad \widetilde{g}_2 \coloneqq \begin{pmatrix} (a-b)\cosh(s/2) & (a+b)\sinh(s/2) \\ (a-b)\sinh(s/2) & (a+b)\cosh(s/2) \end{pmatrix} \ .$$

For later reference let it be noted that $\mathcal{T}$ may also be expressed in the following alternative coordinates [NN98, Section 4.3]:

$$\mathcal{T} \cong \left\{ x,y,z \,\middle|\, x^2+y^2+z^2-xyz = -4k,\ x,y,z > 2 \right\} \ ,$$

where the transition map between the two coordinate systems is simply $x \coloneqq \mathrm{tr}(g_1)$, $y \coloneqq \mathrm{tr}(g_2)$ and $z \coloneqq \mathrm{tr}(g_1 g_2)$.

For an application to spectral problems like the ones discussed in this thesis it is more natural to identify those complete hyperbolic metrics on the funneled torus which are isometric. The resulting *moduli space* $\mathcal{M}$ contains only points with distinct length spectra, i.e. sets of lengths of closed geodesics, by a result of [BS88]. This makes $\mathcal{M}$ an ideal candidate to sample resonance related quantities using zeta functions. The measure from which funneled tori are sampled is a natural choice called the *Weil-Petersson measure* and given on $\{m = \text{const.}\} \subset \mathcal{T}$ by

$$\mathrm{d}l \otimes \mathrm{d}s \ . \tag{6.1.1}$$

This descends to a measure μ_{WP}^m on $\mathcal{M}$ because $\mathcal{M}$ is in fact the quotient of $\mathcal{T}$ by the so-called *mapping class group* which in turn is the quotient of orientation preserving isometries by isometries isotopic to the identity. But the measure in (6.1.1) is invariant under the action of this group making it well-defined on the quotient $\mathcal{M}$ [NN98, Section. 4.4].

For practical purposes it would be optimal to have an explicit expression for a fundamental domain of $\{m = \text{const.}\} \subset \mathcal{M}$ in (l, s)-coordinates on $\mathcal{T}$. While this seems to be quite hard to obtain a good substitute is given by [NN98, Lemma 4.6]: Let $C \coloneqq C_u \cup C_l$ be the union of

$$C_u \coloneqq \left\{ 2 < x < 2\sqrt{1+\sqrt{1+k}},\ 2a < y < x \cdot a \right\} \cup \left\{ 2\sqrt{1+\sqrt{1+k}} < x < y < x \cdot a \right\}$$

with its image $C_l \coloneqq \rho(C_u)$ under the reflection at $x = y$. Then the closure of C contains a point of every mapping class orbit and the stabilizer of C is a cyclic subgroup of order three. In particular this concrete expression lets one calculate the total area vol_m of $\{m = \text{const.}\} \subset \mathcal{M}$ to be $\mathrm{vol}_m = \frac{m^2}{24} + \frac{\pi^2}{6}$ [NN98]. Even the result that the total area is finite is quite astounding already.

Besides giving the volume the concrete expression for C also suggests the following sampling method that produces coordinate pairs (l, s) according to the measure μ_{WP}^m:

(i) Sample (l, s) uniformly from $]0, l_{\max}] \times]0, s_{\max}]$ for some cutoffs $l_{\max}, s_{\max} > 0$.

(ii) Transform the sample (l, s) into $(x(l, s), y(l, s))$-coordinates according to the transition map.

(iii) Accept the sample if $(x(l, s), y(l, s)) \in C$ and discard it otherwise.

The cutoffs are necessary because uniform sampling from $]0, \infty]$ is impossible numerically. They should be chosen in such a fashion that the resulting compact subset $\widetilde{C} \subset C$ has sufficiently large ratio $\mu_{\mathrm{WP}}^m(\widetilde{C})/\mathrm{vol}_m$. Then the results approximate uniform sampling from μ_{WP}^m in a close manner.

In practice the value of this ratio can be computed on the fly in the spirit of a Monte-Carlo simulation. As soon as its current value becomes stable one can decide to adjust the cutoffs if required. It is then necessary to re-sample but this should be fine as sampling is quite cheap numerically as long as the cutoffs remain reasonably sized.

This concludes the necessarily short and incomplete introduction to Teichmüller and moduli space of funneled tori. The next section presents some numerical results obtained by combining the sampling procedure just described with resonance and zeta function related techniques.

6.2. Numerical Sampling of Moduli Space

Resonance Sampling

Before discussing numerical sampling experiments involving resonance data the sampling procedure itself is illustrated in Figure 6.2. In the spirit of a Monte-Carlo experiment several thousand samples from the upper half of the pseudo-fundamental domain C_u were drawn according to μ_{WP}^m for fixed $m = 5$. In the x-y-coordinates one clearly recognizes the shape of C as illustrated in [NN98, Fig. 4.3]. Furthermore it is very plausible on a qualitative level that the density of points follows the law derived via transformation formula in [NN98, Section 4.4]. The analogous sanity check in l-s-coordinates yields a good qualitative agreement with the theoretically demanded uniform distribution.

Remark 6.2.1. This section actually considers the *quantum* resonances of funneled tori but this is a minor issue as they differ from the classical Pollicott-Ruelle resonances of the geodesic flow only by a shift $\lambda \mapsto \lambda + 1$. The quantum variant was chosen here as it is the somewhat more popular scaling one sees in numerical investigations of resonances as initiated by Borthwick [Bor14]. Additional remarks on this matter can be found in the next subsection and Chapter 5.

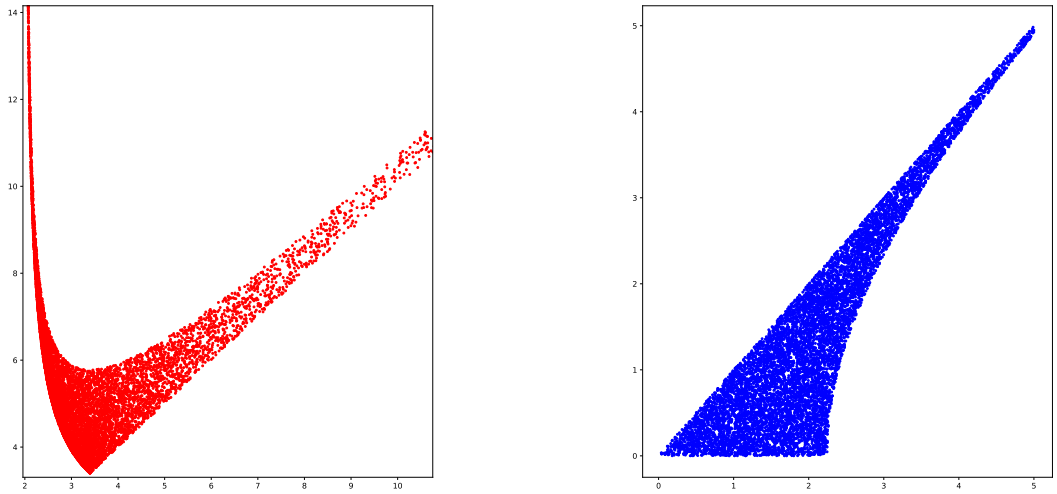

(a) Samples of funneled tori parameters from the upper half C_u of the pseudo-fundamental domain C expressed in x-y-coordinates for $m = 5$.

(b) Samples of funneled tori parameters from the upper half C_u of the pseudo-fundamental domain C expressed in l-s-coordinates for $m = 5$.

Figure 6.2.: Parameter samples from moduli space of funneled tori in different coordinates.

As a first numerical experiment the behavior of the first (quantum) resonance δ depending on the surface parameters was investigated. Recall that δ coincides with the Hausdorff dimension of the limit set of the surface. The exact dependency $\delta(l, m, s)$ should be expected to be quite complex. One reasonable approach to reduce this complexity is to average out the variables (l, s) and consider the quantity

$$\widehat{\delta}(m) := \frac{1}{\mathrm{vol}_m} \int \delta(l, m, s) \, \mathrm{d}\mu_{\mathrm{WP}}^m(l, s) \ .$$

From a geometrical standpoint it now makes sense to ask for the limit behavior of $\widehat{\delta}(m)$ as $m \to \infty$ which corresponds to increasingly open dynamics of the geodesic flow. Thus

one would expect $\widehat{\delta}(m) \to 0$ as $m \to \infty$ but to the author's knowledge the speed of convergence has not been investigated rigorously before making numerical experiments a worthwhile endeavor.

The concrete procedure is straightforward given the preliminaries above: For a given value of the boundary length m a number of samples $\{(l_i, s_i)\}$ must be generated. From these an ensemble average is calculated as an approximation to $\widehat{\delta}(m)$. Figure 6.3 shows the results for several values of m in the interval $[15, 110]$. These bounds were chosen as mutually exclusive compromises: If m is too small then the dynamics of the surface samples tend to be quite closed making the calculation of the first resonance rather expensive with the cycle expansion technique. If on the contrary m becomes very large then the generators of the surface samples tend to involve very large matrix entries approaching and eventually exceeding double floating point precision.

The errors for a particular average of δ were simply taken to be the standard deviations σ of the ensemble mean. The ensemble sizes were initially chosen somewhere around 100 samples but had to be adapted for some data points to correct for statistical outliers causing particularly high values of σ.

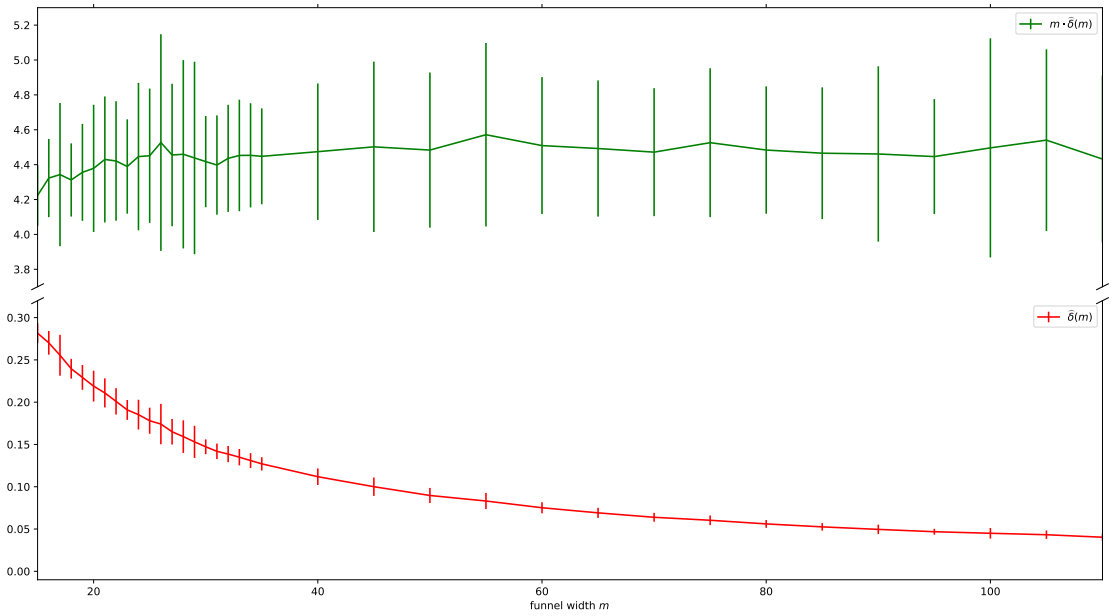

Figure 6.3.: Expectation values of first resonances for funneled tori. The tori were sampled from Weil-Petersson measure μ_{WP}^m for several fixed values of the funnel width m.

Several features of Figure 6.3 warrant attention: The plot in the upper half already qualitatively suggests the behavior $\widehat{\delta}(m) \sim C/m$ as $m \to \infty$. The lower plot supports this hypothesis because the rescaled quantity $\widehat{\delta}(m) \cdot m$ strongly resembles the constant function starting already at rather small values of roughly $m \approx 30$. Furthermore the constant can be read off to be $C \approx 4.5$ with an error of about ± 0.5, i.e. $\pm 11.1\%$.

The next series of experiments goes beyond the first resonance δ by considering all resonances in the rectangular region $[0, \delta] + \mathrm{i}[0, 100]$ of the complex plane. The first try at this setup is contained in Figure 6.4: For a funnel width of $m = 80$ the resonances for said rectangle were calculated with $m = 100$ samples and drawn into a shared scatter plot. The general shape already suggests an increase in resonance density as the complex

parameter s decreases from $s = \widehat{\delta}(80)$ towards $s = 0$ but the large number of points makes it rather hard to distinguish finer features.

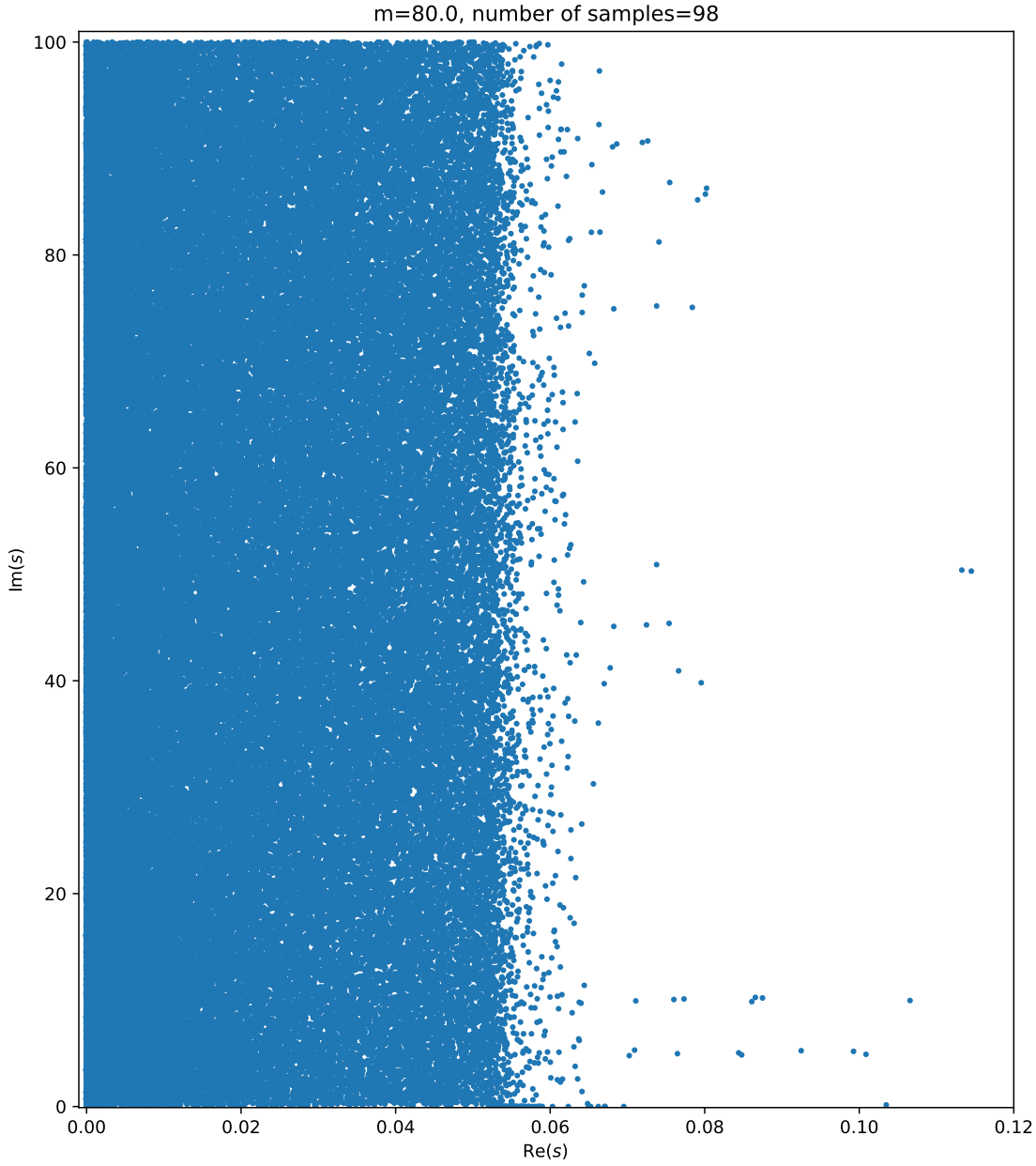

Figure 6.4.: Resonances in the rectangle $[0, \delta] + \mathrm{i}[0, 100]$ for funneled tori sampled from moduli space for fixed $m = 80$.

To increase visibility of any left-to-right patterns in the resonance density plot the individual resonances were first projected to the real axis and subsequently collected into bins of equal sizes. Finally the total numbers of resonances in every bin were divided by the bin width and the overall number of resonances to obtain the probability p of

a particular resonance to fall into a particular bin. The resulting histogram is shown in Figure 6.4 where $\mathrm{Re}(s)$ on the horizontal axis was rescaled by m to increase comparability with the upcoming histograms for other choices of m.

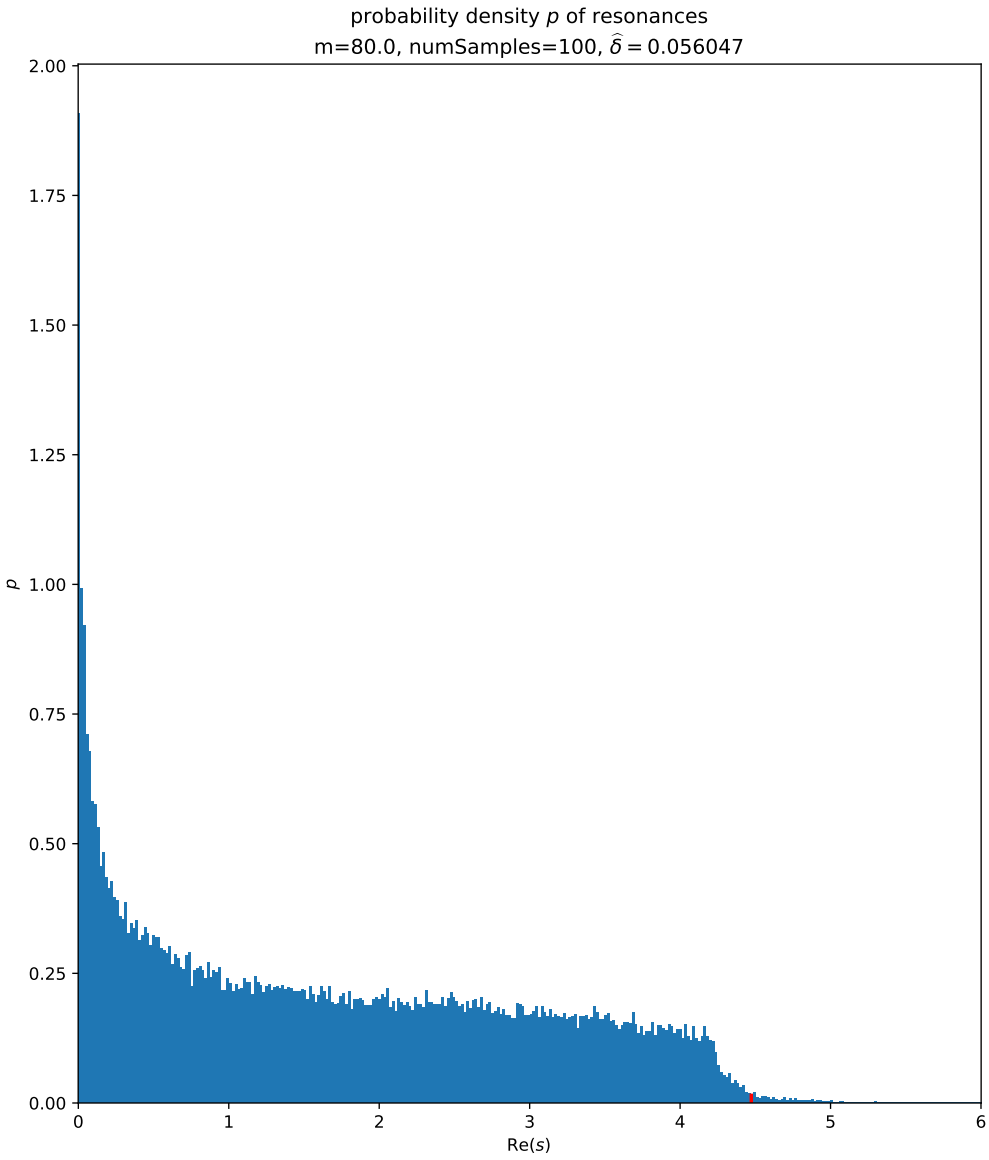

Figure 6.5.: Histogram of projections $s \mapsto \mathrm{Re}(s)$ of resonances of funneled tori to the real axis and plotted against the real part of s rescaled via multiplication by m. The 120 tori were sampled from moduli space for fixed $m = 80$. p denotes the probability of a resonances to belong to a given bin of the histogram, i.e. the absolute number of occurrences of some real part divided by the bin size and the total number of resonances. The red bin contains the first resonance $\widehat{\delta} \approx 0.056047$.

Figure 6.4 exhibits a number of noteworthy features: Going from right to left the histogram shows a residual tail that seems to pick up in intensity roughly at the first resonance (here and in the following histograms the bin corresponding to $m \cdot \widehat{\delta}(m)$ was marked in red). Shortly after the first resonance comes a steep edge which transitions into a more

or less constant section until around $m \cdot \mathrm{Re}(s) \approx 0.5$ where a final steep increase ends in the global maximum located at $m \cdot \mathrm{Re}(s) = 0$.

Both the edge and the increase towards $m \cdot \mathrm{Re}(s) = 0$ would be interesting features to investigate rigorously if they were in fact present in the exact theoretical distribution of resonances projected to the real line. To support the hypothesis that this is indeed the case in the limit $m \to \infty$ further resonance density histograms were computed for additional values of $m \in \{30, 50, 60, 90\}$.

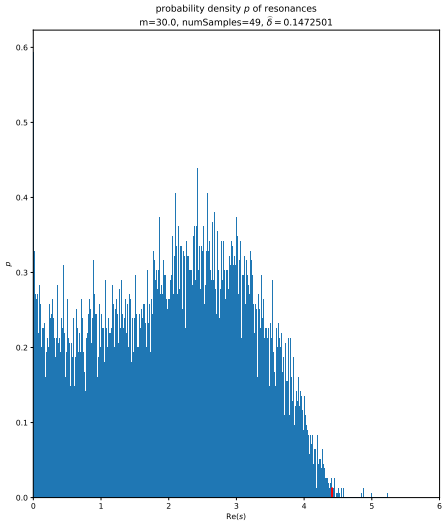

(a) Resonance histogram for funneled tori samples with $m = 30$ plotted against the rescaled real part of s.

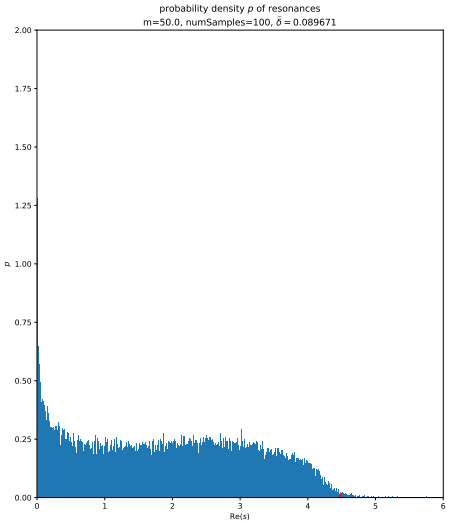

(b) Resonance histogram for funneled tori samples with $m = 50$ plotted against the rescaled real part of s.

Figure 6.6.: Similar results to Figure 6.5 for the additional values $m \in \{30, 50\}$.

The left plot in Figure 6.6a contains the results for $m = 30$. This histogram exhibits a very rough structure as compared to the very smooth enveloping curve visible for $m = 80$. Even though the steep edge shortly before the expected first resonance still seems to be there although less pronounced. Increasing the boundary width to $m = 50$ in the right-hand side of Figure 6.6a smooths out the enveloping curve significantly and both the edge before the first resonance as well as the rapid increase in probability around $m \cdot \mathrm{Re}(s) = 0$ are clearly distinguishable. The same observations persist when increasing the boundary length to $m = 60$ and $m = 90$ in Figures 6.7 and 6.8.

For the maximal value $m = 90$ considered in the present series of experiments it appears as if the edge around $90 \cdot \widehat{\delta}(90)$ is even sharper than for smaller widths. A possible conjecture could be that in the limit $m \to \infty$ the histogram would show the behavior of a step function with jump at $\lim_{m\to\infty} m \cdot \widehat{\delta}(m)$. A conjecture for the enveloping curve in a neighborhood of $\mathrm{Re}(s) = 0$ is less immediate to come up with but the plots suggest some smooth limiting envelope to exist.

Average Zeta Function

The concluding numerical results in this chapter involve not some sort of average over individual or ensembles of resonances but averages over the zeta function itself: Let the *average zeta function* $\widehat{\zeta}$ for funnel width $m > 0$ be defined as

$$\widehat{\zeta}_m(s_0) \coloneqq \frac{1}{\mathrm{vol}_m} \int \zeta_{(l,m,s)}(s_0)\ \mathrm{d}\mu_{\mathrm{WP}}^m(l,s)\ , \qquad s_0 \in \mathbb{C}\ ,$$

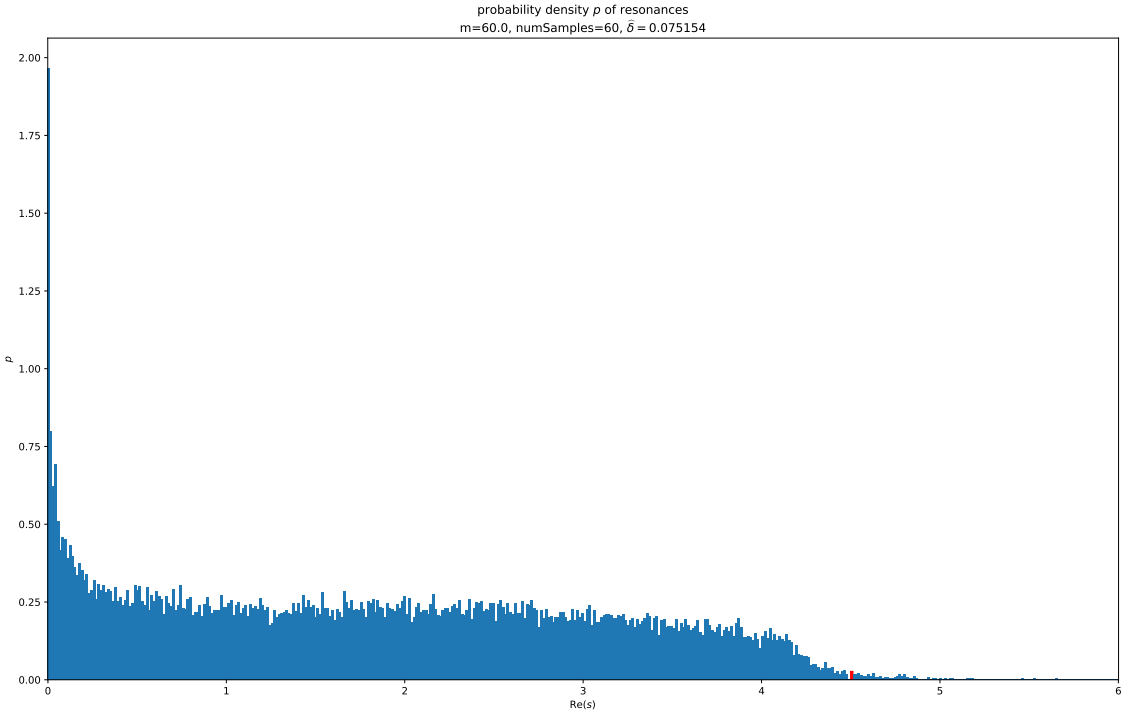

Figure 6.7.: Resonance histogram for funneled tori samples with $m = 60$ and plotted against the rescaled real part $m \cdot \mathrm{Re}(s)$. The number of samples was 60 and the first resonance $\widehat{\delta} \approx 0.075154$ lies in the red bin.

where $\zeta_{(l,m,s)}$ denotes the Selberg zeta function for the funneled torus with parameters (l, s, m). For $\mathrm{Re}(s_0) \geq 1$ this holomorphic function is given by the infinite product

$$\zeta_{(l,m,s)}(s_0) \coloneqq \prod_{\gamma} \prod_{k=0}^{\infty} \left(1 - \mathrm{e}^{(s_0+k)T_\gamma}\right) \ ,$$

where the first product ranges over all *primitive* closed geodesics γ of $\mathcal{T}(l, m, s)$ and T_γ again denotes the length of γ. This function continues to $\mathbb{C}$ as a holomorphic function and its zeros coincide with the *quantum resonances* of the torus. An alternative approach to defining these quantum resonances is as the poles of the meromorphic continuation of the resolvent of the Laplace-Beltrami operator $\Delta_{(l,m,s)}$ of the torus

$$\mathbf{R}_{(l,m,s)}(s_0) \coloneqq \left(\Delta_{(l,m,s)} - s_0(1-s_0)\right)^{-1} : \ \mathrm{L}^2_{\mathrm{c}} \longrightarrow \mathrm{L}^2_{\mathrm{loc}} \ ,$$

acting on the space $\mathrm{L}^2_{\mathrm{c}}$ of compactly supported square-integrable functions and codomain the space $\mathrm{L}^2_{\mathrm{loc}}$ of locally square-integrable functions, both with domain $\mathcal{T}(l, m, s)$. The discrete set obtained by this procedure naturally generalizes the discrete spectrum of the Laplace-Beltrami operator in the setting of compact manifolds and is very analogous to the way in which Pollicott-Ruelle resonances of a flow are obtained by meromorphic continuation of the resolvent of the generating vector field. They do in fact satisfy an exact correspondence with the classical Pollicott-Ruelle resonances of the geodesic flow as mentioned in Chapter 1.4 and techniques for their numerical calculation exist due to Borthwick [Bor14] very similar to those presented in Chapter 4.[2]

Remark 6.2.2. Compare Selberg's zeta function $\zeta_{(l,m,s)}(s_0)$ as defined above with *Ruelle's zeta function* given by

$$\zeta_{\mathrm{Ruelle}}(\lambda) \coloneqq \prod_{\gamma^\#} \left(1 - \mathrm{e}^{-\lambda T_{\gamma^\#}}\right) \ ,$$

[2]The initial idea to study this average zeta function was proposed by William Hide.

where the product ranges over *primitive* closed geodesics. This zeta function continues meromorphically from $\{\mathrm{Re}(\lambda) \gg 0\}$ to $\mathbb{C}$ but its poles coincide with the Pollicott-Ruelle resonances of the geodesic flow lifted to certain vector bundles containing differential forms [DG16, Theorem 3] instead of the resonances of the geodesic flow itself. This makes Selberg's zeta function (or alternatively the dynamical determinant introduced in [SW23], see also Chapter 4.1) the better suited candidate for numerical investigations.

Again the sampling procedure developed above lends itself very well to a numerical study of $\widehat{\zeta}$. One simply generates parameter samples $\{(l_i, s_i)\}$, calculates the corresponding zeta functions, and finally averages over the results. An evaluation of these averages is numerically quite expensive with the technique of cycle expansion if one chooses large arrays of support points in $\mathbb{C}$ on which to evaluate.

A question that comes to mind immediately in this context concerns the relationship between the zeros of $\widehat{\zeta}_m$ of averages over zeros of individual zeta functions, i.e. resonances. While a precise answer to this question exceeds the scope of the thesis at hand a final pair of plots in Figure 6.9 provides some first insights: There both the absolute values as well as the complex argument of an ensemble average of Selberg's zeta function over 50 random funneled tori for $m = 80$ is shown. The average was evaluated on a discretized rectangular region of the complex plane and the region contains the numerically calculated value $\widehat{\delta}(80)$ in its center. From both plots it is clear that this approximation to $\widehat{\zeta}$ has a simple zero that coincides with $\widehat{\delta}(80)$ very well within the numerically calculated standard deviation for the latter (it is even the case that σ is significantly larger than the actual difference between the two – this could be taken as evidence that the calculated $\widehat{\delta}(80)$ in reality is much more accurate than suggested by σ). This suggests the conjecture that in the limit $m \to \infty$ the (first) zero of $\widehat{\zeta}_m$ is simple and equals the average first resonance $\widehat{\delta}(m)$.

Some concluding remarks are in order to end this chapter: First of all the presented numerical experiments should be taken as a first step towards the development of conjectures regarding the random variables $\widehat{\delta}$ and $\widehat{\zeta}$. If one decides to undertake rigorous mathematical proofs regarding their properties it naturally suggests itself to complement these with additional and more focused numerics. This holds especially true because the `PyZeta` project presented in Chapter 7 offers a broad range of capabilities to reproduce and extend the plots of this chapter with minimal overhead in terms of effort. At the same time there are probably several additional random variables amenable to the methods employed here that are of interest from an analytical perspective.

Finally the general philosophy of sampling from moduli space exploited here is certainly not limited to funneled tori. As soon as Teichmüller space coordinates are given which admit explicit generators combined with a sampling procedure that produces coordinates from a fundamental domain of moduli space according to Weil-Petersson measure one can start calculating averages of observables like Hausdorff dimension or average zeta functions.

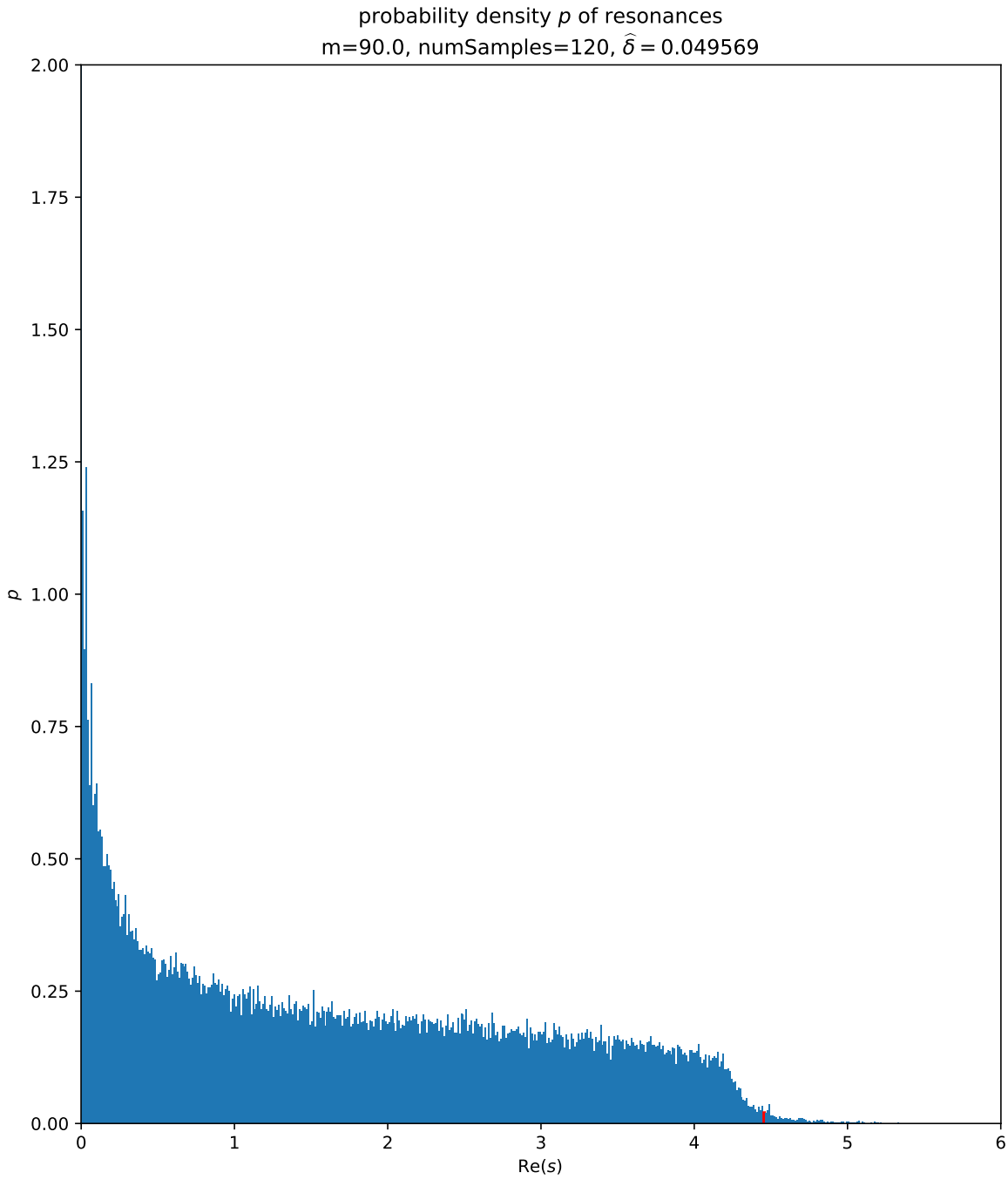

Figure 6.8.: Resonance histogram for funneled tori samples with $m = 90$ and plotted against the rescaled real part $m \cdot \mathrm{Re}(s)$. The number of samples was 120 and the first resonance $\widehat{\delta} \approx 0.049569$ lies in the red bin.

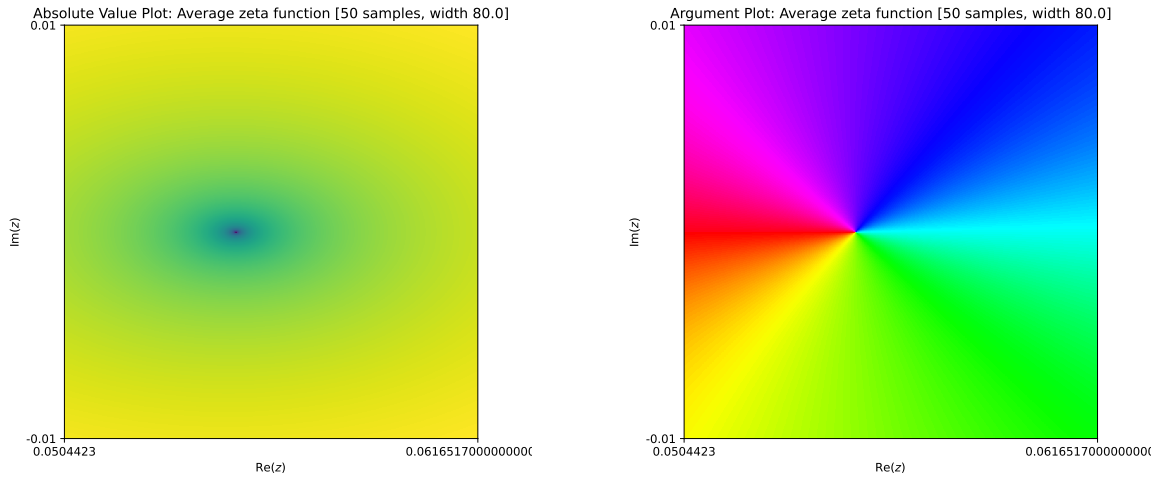

(a) Absolute value plot of Selberg zeta functions averaged over 50 samples for boundary length $m = 80$ in a small region around the expected first resonance at $\widehat{\delta} \approx 0.056047$.

(b) Argument plot of Selberg zeta functions averaged over 50 samples for boundary length $m = 80$ in a small region around the expected first resonance at $\widehat{\delta} \approx 0.056047$.

Figure 6.9.: Absolute value and argument plots of averaged zeta functions on the complex plane.

Part III.

Technical Implementation

Outline of Part III

The third and final part of this thesis contains a description of the two major programming projects conducted during the course of the author's PhD. Chapter 7 deals with the `PyZeta` package which encompasses all implementations related to zeta functions, dynamical determinants and hyperbolic map systems. At the time of writing this thesis the setting for these capabilities is restricted to Schottky surfaces but all interfaces are designed in a generic manner such that additional dynamical systems like 3-disc scattering dynamics should be rather straightforward to incorporate in the future.

While this directly resonance related functionality forms the core of the package it furthermore provides a wide range of additional capabilities aimed at reducing the effort necessary when conducting numerical experiments. At the same time the project aspires to build a foundation for becoming the seed of a larger and ongoing open source project targeted towards supporting research in the area of classical Pollicott-Ruelle, semiclassical, and quantum mechanical resonances and mathematical chaos with a number of available model systems and numerical techniques.

The second project forming the contents of Chapter 8 is called `PyZEAL` and was initially a part of `PyZeta` before growing into an independent endeavor: It provides facilities for the calculation of roots of holomorphic functions. Despite the complexity and richness of techniques present in the literature the author could not find readily available, actively maintained, and validated software addressing this problem. It was therefore decided to separate the very rudimentary root finding capabilities from the main `PyZeta` development branch and both improve as well as extend them independently. Again great care was taken to create an open source project that is as extensible and usable as possible with the aim of supporting the use case of someone wanting a straightforward API for root calculations but also with the orthogonal use case of someone wanting to investigate new root finding algorithms in mind.

Both chapters in this part contain a mix of abstract mathematical and architectural descriptions with concrete explanations of implementation details. Due to the size of the code bases it is far beyond this thesis to comment on every line of code. Fortunately the open source nature of the projects gives easy access to the code and additional, though necessarily constantly changing and evolving, documentation is available online. As a consequence of the very dynamic nature of programming projects in general the following two chapters will almost certainly become outdated at some point in the future. Please refer to the chapter introductions for the specific versions to which they apply and ways of obtaining the most up to date versions of the software and its respective documentation.

The early development of the immediate predecessor of `PyZeta` was partly supported by Sebastian Albrecht as a student assistant. Not only his work on documentation and tests but specifically his involvement in prototypes regarding resonance selection and resonance handling tools are greatly appreciated. Without his help significant additional amounts of resources would have had to be deducted away from the core algorithms and data structures related to resonances.

The development of `PyZEAL` was partly supported by Luca Wasmuth as a student assistant. His work on documentation, tests, and examples is greatly appreciated.

7. The PyZeta Project

The `PyZeta` project embodies the cumulation of resonance related implementations created during the PhD leading to this dissertation. The author's work began by using and extending a legacy implementation by Tobias Weich developed mostly in 2014 during his own PhD. This legacy code contained the Selberg zeta function both with and without symmetry reduction, implementations of various iterated function systems including in particular Schottky surfaces, and a simple root finder for holomorphic functions.[1] The author added additional dynamics and implemented first versions of (weighted) dynamical determinants during his Master's thesis with the aim of further extending the code base and conducting numerical experiments using the code during his PhD. Soon after the start of the latter two major obstacles emerged:

(i) The current state of the source code made it very cumbersome to introduce some basic software engineering tools and principles like *continuous integration, a build pipeline, automated unit testing, automated deployment of documentation, and continuous deployment of build artifacts.*

(ii) The legacy code was written in `Python2` and heavily dependent on `Sage`[2] making the source significantly less portable and harder to get up and running on a new machine. In addition new features of `Python3` like type hints could not be taken advantage of easily.

(iii) The original code had not been designed to be an extensible project for several generations of programmers to work on and to accommodate a changing and evolving set of requirements and use cases.

(iv) With the existing internal and external dependencies it was either very difficult or even impossible to use tools like `Numba` or `Cython` to overcome some of the performance limitations inherent with `Python` and detrimental to the performance requirements of a numerical project.

The author of this thesis therefore undertook a complete re-write of the original code base as an open source project[3]. During this endeavor the existing functionality was significantly enhanced in terms of algorithms to enable new numerical experiments with the hope of gaining insights into mechanisms related to resonances and resonance states. In addition a whole new framework together with an extensible and flexible architecture were created with the perspective of building the foundation for a project that continues to evolve beyond this thesis. As useful references regarding the design and implementation of larger software products the monographs [FR03, McC04] were consulted during several different phases of design and implementation of the presented projects. Another important and extensively used resource was the original monograph [GHJV03] on *design patterns*. These semi-formalized templates provide a unifying language and toolkit

[1] The latter will be discussed in more detail in the following Chapter 8.
[2] `https://www.sagemath.org/index.html`.
[3] `https://github.com/Spectral-Analysis-UPB/PyZeta`.

for common programming and design tasks. In the following descriptions many of the patterns distilled there will be explicitly mentioned to convey the design decisions within `PyZeta` as succinctly as possible.

With the current state of the code base the `PyZeta` project should now provide anyone interested in the numerical investigation of Pollicott-Ruelle resonances an easily accessible means to achieve just that. Possible applications range from the simple generation of illustrations for a conference talk or paper to complex numerical experiments that serve as a basis for new conjectures or the guide to proving new theorems.

The theoretical foundations for `PyZeta` have been presented in great detail in the previous Parts I and II. After a concise and rather generic discussion of different foundational technological aspects in Chapter 7.1 the then following Section 7.2 will therefore dive right into the heart of the architecture that supports the various mathematical objects discussed up to this point. After that details regarding specific choices of how mathematical entities were mapped to the implementation will be summarized. The concluding Section 7.3 provides an outlook on future directions.

The following sections refer to `PyZeta` version `v0.1.1`.

7.1. General Remarks on Technologies

In this section some technologies are discussed which were used in the practical implementation of `PyZeta`. A top-down approach is taken: Beginning with the programming language used and some hints regarding the general development environment the presentation proceeds with more detailed tools used for testing, speed measurements, optimizing code, and more.

7.1.1. Programming Language and Development Environment

For the practical implementation of this project the general purpose, multi-paradigm programming language `Python`[4] was used. `Python` is a high-level interpreted language that is very widely used especially in a scientific context due to its easy to learn syntax, flexibility, and large, welcoming community. Furthermore it compiles to an intermediate bytecode representation which is then executed on the `Python` virtual machine making it mostly platform independent. Finally `Python` ships with an extensive standard library, has developed a huge ecosystem of open source modules, and possesses a native interface to the compiled languages `C/C++` for e.g. performance critical subroutines. For all these reasons `Python` was chosen as the primary implementation language of both the `PyZeta` as well as `PyZEAL` projects.

Besides the possibility of writing and integrating native `C`-code there exists a project called `numba` which provides *just-in-time* (JIT) compilation facilities backed by the `LLVM` toolchain. JIT contrasts the maybe more traditional concept of *ahead-of-time* (AOT) compilation customary for languages like `C/C++` or `Rust`: Blocks of code like functions are only compiled when first needed. This incurs an overhead at first encounter but provides tremendous speedups at subsequent calls. This technique therefore lends itself especially for functions that get called multiple times e.g. inside a loop. The concrete technical realization via `Python` decorators often allows easy performance wins without significant additional effort as long as some basic rules are followed.[5] `numba` is used throughout both

[4] `https://www.python.org/`.

[5] The best gains are achieved in strict no-python mode which avoids the Python interpreter completely. This means that some language features are not accessible in this mode and their usage must be avoided for successful compilation.

PyZeta as well as PyZEAL. A detailed description is well outside the scope of this thesis but the numba documentation[6] is a great starting point.

Due to being such a dynamical and flexible scripting language the author strongly believes that Python requires additional tooling and setup when it comes to the structured development of larger software projects. Fortunately the community agrees up to the point where a continuously improving repertoire of utilities exists either as part of the core language development effort or as external tooling. For the projects at hand a set of such tools was chosen as *mandatory* requirements to safeguard long-term code quality:

- Type hints as introduced in PEP484 as part of Python3.5 are fully embraced in both presented projects. Not only do they allow increased safety by leveraging static code analysis but they also constitute a means for the code to self-document things like function and method interfaces. This static typing is optional and ignored by the interpreter making it necessary to use external tools like mypy for verification.
- Code style guidelines are enforced by the tools black and isort to guarantee a homogeneous appearance through the code base.
- A whole collection of static code analysis tools helps to improve overall code quality. The projects pylint and pylama serve as frontends to these utilities.
- A command line tool like Wily (written in Python) provides a more sophisticated means of recording and tracking various code complexity measures. This can be especially useful for identifying promising candidates at the beginning of the *debug cycles* regularly interspersed in the overall development methodology.

Remark 7.1.1. Setting up a suitable development environment is crucial for efficient software development in general and to get the most out of the tools just introduced in particular. As a general recommendation this should include a text editor like vim or VSCode with syntax highlighting and direct integration of the above tooling. Things like tests could then be run either directly from the editor or from a terminal. Alternatively one could use a Python-specific full fledged itegrated development environment (IDE) like PyCharm or Spyder.

Besides manual runs during development on a local machine the main project repository will also have an automated continuous integration/continuous deployment (CI/CD) pipeline which ensures the build status upon every commit or pull request. More details on this repository infrastructure can be found in the following Section 7.1.2.

7.1.2. Software Documentation and Version Control

An aspect that is central to the success and longevity of a software project such as PyZeta is the ability of both developers as well as users to obtain explanations and descriptions of the different components making up the code base. It is central to have this *documentation* available for several levels of detail ranging from comments for particular lines or blocks of code to an API documentation of the internal functionality to the external application programming interface (API) meant for end user purposes.

To compile such a documentation for PyZeta a tool called sphinx was chosen:[7] This application takes a bundle of markup files in .rst format and converts them into a number of output formats. For the purposes of this project the most important ones are interactive

[6] https://numba.pydata.org/.

[7] https://www.sphinx-doc.org/en/master/.

`html` documents for display in a browers and static `pdf` files for easy distribution. A core feature heavily used in `PyZeta` is the ability of `sphinx` to extract *docstrings* from `Python` source files and turn them into an API documentation for the particular annotated class, method, etc. Combining this facility with auxiliary markup files containing things like background information, motivations for certain design decisions, and extended examples yields a comprehensive overview of `PyZeta`. Many of the examples are provided as `jupyter` notebooks in the repository and compiled to the output format upon documentation build. This gives the user the option to choose a suitable notebook as a starting point for their custom applications.

To make this documentation available to any (potential) users without requiring them to build the documentation themselves the `html` version is hosted on `https://pyzeta.readthedocs.io/en/latest/`. The mentioned `pdf` version can also be downloaded from there. Please refer to these documents for extended information on many topics covered in the upcoming sections.

Another critical component of software development is controlling the complexity that comes from having many different documents including source code, documentation, tests, requirements, configuration, specifications, and more. The matter becomes even more complex when all these documents run through several iterations producing a graph of more or less valid versions. An invaluable tool to manage all this is *version control software*. The discussed projects will be using a particular such system called `git` which is very widespread and builds on the concept of *repository* containing all documents associated with a particular project together with the history of their revisions. The handbook [Sil13] provides a compact introduction to technical background information and offers its reader a quick way to get started. A more comprehensive overview can be found in the reference [CS14] which is also freely available online.

While `git` could very well just be run locally, it is even more useful to have one's repositories hosted remotely to enable e.g. collaborative work. The present projects will do this via a provider called `GitHub`[8] which besides hosting repositories can also be used to manage various other aspects of the software development lifecycle. In particular `GitHub` provides a framework for continuous integration/continuous deployment through their concept of `actions`. On certain events like uploading new content to the repository (called a push) or trying to combine divergent so-called branches of work (called a pull request) corresponding scripts are envoked on computing infrastructure provided by `GitHub` themselves. For the purposes of this thesis these scripts contain in particular invocations of static code analysis tools, docstring coverage checks with `docstr-coverage`, automatic rebuilds of the documentation, and the publishing of a soure distribution to the `Python` package index (PyPI) in case the specific event was related to an incremented project version. Any potential user may therefore install the newest (stable) version of `PyZeta` locally and automatically using the package manager `pip` over the internet:

```
$ pip install "pyzeta[all]"
```

to install `PyZeta` with all optional dependencies. For a detailed description of the possible options refer to the full documentation.

Remark 7.1.2. Unfortunately the description of even the basic feature set of `git` is outside the scope of this thesis even though it constitutes a core technology in terms of practical contribution to the code base. The following short summary of the prototypical `git` workflow for `PyZeta` or `PyZEAL` therefore contains some terms which will not be discussed

[8] `https://github.com/`.

in detail. For a user that is new to `git` and wants to contribute to these projects the consultation of further documentation can thus not be circumvented:

(i) Clone the mainline repository locally. This step can be skipped if the repo already exists on the local file system.

(ii) Create a new branch with a name indicating the current work item (like `/dev/feature/my-new-feature`).

(iii) Work on the new branch until the work item has reached a stable state. Create several small commits with descriptive commit messages. These descriptions should be formulated in imperative style.

(iv) Create a pull request on the `main` branch together with a comprehensive description of the completed work item(s).

(v) If the pull request passes the automatic checks and at least one positive review by a core developer it can be (squash-)merged into `main`. The new work item is now part of the mainline project!

Remark 7.1.3. For some types of documents used during development `git` does not yield the most useful outputs when using functionality like `git diff` or `git merge`. In particular this is true for `jupyter` notebooks which are a great tool for prototyping and algorithmic experimentation. This can be alleviated by integrating additional functionality as e.g. provided by the `Python` project `nbdime` directly into `git`. Similar tools exist e.g. for `LaTeX` documents.

7.1.3. Testing Framework

The CI/CD pipeline as described in the previous Section 7.1.2 contains a step in which a suite of automated tests gets executed upon pull request. The status of the most recent test run is indicated on the repository front page and the pipeline is considered failed if any of the tests did not pass. This security measure is meant to block the inclusion of faulty code within the code base. Furthermore the test suite can and should also be executed locally on a regular basis during development both as regression tests during e.g. refactoring and to verify the functioning of newly implemented features. From this it follows immediately that the writing of tests is an integral part of the software development process. For `PyZeta` it is explicitly recommended to follow a *test-driven* development methodology: Before a new feature gets implemented it should be specified to a point where some set of tests for this feature can be written. Feature implementation then aims at making these tests pass. In a final step the code is refactored while maintaining a successful test status.

As a framework for the automated testing of modules `PyZeta` uses a `Python` package called `pytest`[9]. Using this framework one can write tests in several ordinary `Python` modules. The runner `pytest` then collects all such tests, runs them, and reports back their status.

Besides this very basic usage `pytest` includes its own functions and classes that simplify testing considerably. Among those commonly used within `PyZeta` are the so-called `fixtures` which allow the user to define objects required for several tests once in a single place and have them injected into tests dynamically by the testing framework.

`pytest` also generates *test coverage reports* which illustrate the overall and line-by-line test coverage of the code base. The CI/CD pipeline generates these reports automatically

[9] `https://docs.pytest.org/en/7.1.x/`.

and shares them with a third-party service provider called `codecov.io`. Their web frontend displays a host of useful information like coverage percentage over time data. Again a badge on the project repository homepage redirects to this service.

7.1.4. Measuring and Documenting Performance

For this project measuring the performance of software applications in first approximation reduces to two aspects: How much memory (RAM) and how many computing (CPU) resources does the application consume? A wide range of tools exists to answer these questions, from general command line utilities to very `Python` specific modules. One should always be guided by the specific problem at hand when selecting one or several of these; in most cases a tiered approach where one starts with a general purpose tool to identify the largest possible gain and proceeds to something like a detailed line-by-line analysis using a specialized tool is practical.[10] A (necessarily incomplete) listing can be found in Table 7.1.4:

Table 7.1.: Profiling tools and their application areas

tool	purpose	usage

`time.time()`
`time.perf_counter()`
	part of the standard library; coarse measurement of e.g. time differences between two points of a `Python` script	`import time`
		`t1 = time.time()`
		`do_work()`
		`t2 = time.time()`
		`duration = t2 - t1`

module `timeit`	part of the standard library; coarse measurement of execution times of e.g. simple expressions, short snippets, or single functions	`$ python -m timeit \`
		`> <options> "<code>"`
		--- 	
		`In [1]: %timeit do_work()`

`/usr/bin/time`	standard utility on Unix-like operating systems; measurement of total program runtime without taking internal structure into account	`$ /usr/bin/time -p python` `> <script.py>`

`cProfile`, `pstats`	part of the standard library; measurement of execution time of every function encountered during a run of the `Python` virtual machine; useful for first identification of problem areas and verification/falsification of hypothesis	`$ python -m cProfile -s`
		`> cumulative <script.py>`
		--- 	
		`$ python -m cProfile -o`
		`> prof.stats <script.py>`
		⟶ analyze with `pstats`

`snakeviz`	third-party module; visualization of `.stats` files generated using `cProfile`	

Continued on next page

[10] Note that accumulating more detailed profiling information often comes with a trade-off in terms of increased computational overhead incurred by the profiling tool!

Table 7.1 – continued from previous page

tool	purpose	usage
`line_profiler`	third-party module; records, displays and saves (`.lprof`) a line-by-line CPU usage statistics of a function chosen via decoration with `@profile`	`$ kernprof -l -v` `> <script.py>`

`memory_profiler`	third-party module; records and displays a line-by-line memory (RAM) usage statistics of a function chosen via decoration with `@profile`; statistics can also be collected and plotted over time using the `mprof` utility	`$ python -m`
		`> memory_profiler`
		`> <script.py>`
		--- 	
		`$ mprof run <script.py>`
		`$ mprof plot`

`PySpy`	third-party module; online display of resource usage of a running `Python` process	`$ sudo env "PATH=$PATH` `> py-spy --pid <pid>`
`perf` (`top`, `ps`)	command line utility available for Linux[11] operating systems; provide detailed measurements of CPU utilization efficiency in terms of parameters like e.g. cache misses, page faults, and context switches[12]	`$ perf stat -e [OPTIONS]` `> python <script.py>`

A key component sometimes overlooked is the *systematic* documentation of past performance and in particular runtime measurements as an integral part of configuration management. `PyZeta` proposes to use an open-source tool written in `Python` called `asv`.[13] It runs a suite of performance tests similar to `pytest` but additionally records the timing results together with the hardware used and saves this data in a `.json` format enabling later reference, comparison, and visualization of the state of the project at specific points in time.

7.1.5. Optimizing Code

The literature on performance optimization and highly performant computing is vast. As an introductory text which specifically emphasizes best practices and tools in `Python` the author suggests [GO20]. First of all recall a fundamental principle of code optimization:

[11] Tools with similar functionality are available for MacOS and Windows.

[12] Available options include *cycles, instructions, cache-references, cache-misses, branches, branch-misses, task-clock, faults, minor-faults, cs, migrations*. For details refer to the documentation of either **perf** or **perf-stat**.

[13] `https://github.com/airspeed-velocity/asv`.

> "Premature optimization is the root of all evil!"
>
> – Donald Knuth ([Knu74])

For the purposes of `PyZeta` this should be interpreted as saying to avoid optimizing code which has not been measured for performance. Before starting optimization activities beyond obvious inefficiencies with quick fixes one should have some hard facts at hand to justify the particular portion of program one is attempting to improve. Note that this implies that optimization activities only ever apply to code which actually runs and satisfies all applicable functional requirements. It should be stressed again that modifying such code is only admissible if an automated test suite exists and can be used to verify that any modifications leave the functional behavior invariant.

After measuring code performance and identifying a specific area of code as the bottleneck of highest priority one has several options to improve performance significantly and overcome the intrinsically slow nature of `Python`. The following non-exhaustive selection of tools is heavily influenced by the technologies actually used within `PyZeta`:

- `numpy` provides very fast array computations and a variety of algorithms from linear algebra by using a `C` and `Fortran` backend. It is safe to say that without this package `Python` could not have reached its current popularity within numerical and scientific computing.
- `numba` is a just-in-time (JIT) compiler that produces optimized machine code from `Python` functions through a simple decorator interface. While limited in the number of `Python` features it can compile it offers sufficient flexibility to achieve great performance gains in many numerical applications.
- `multiprocessing` is a standard library module which enables the usage of multiple cores in parallel to decrease runtime for CPU-bound problems. This is in contrast to the `multithreading` module which does not allow for true concurrency due to `Pythons` *GIL*.[14]
- `Cython` is an ahead-of-time (AOT) compiler that generates `C`-code from either pure or `C`-like annotated `Python` code and often achieves near to native `C` speed. Compared to `numba` this tool necessitates some knowledge of its mix between `C` and `Python` syntax to get the most out of it.

Besides these technical tools that help overcome the intrinsically slow nature of `Python` one should always keep an eye out for *algorithm or programmatic improvements*. These often offer easy and fast speed gains especially at the stage of a first working proof-of-principle implementation.

[14] The *global interpreter lock* prevents the virtual machine from running more than one thread at a time. While this avoids an abundance of issues related to data corruption, especially related to reference counting, it also forces programmers to go beyond the core language if true concurrency is required in their calculations.

7.2. Architecture and Internals of PyZeta

This section gives an overview over general architectural aspects which were considered upon first design of `PyZeta` or came up during implementation. For an initial overview refer to Figure 7.1.

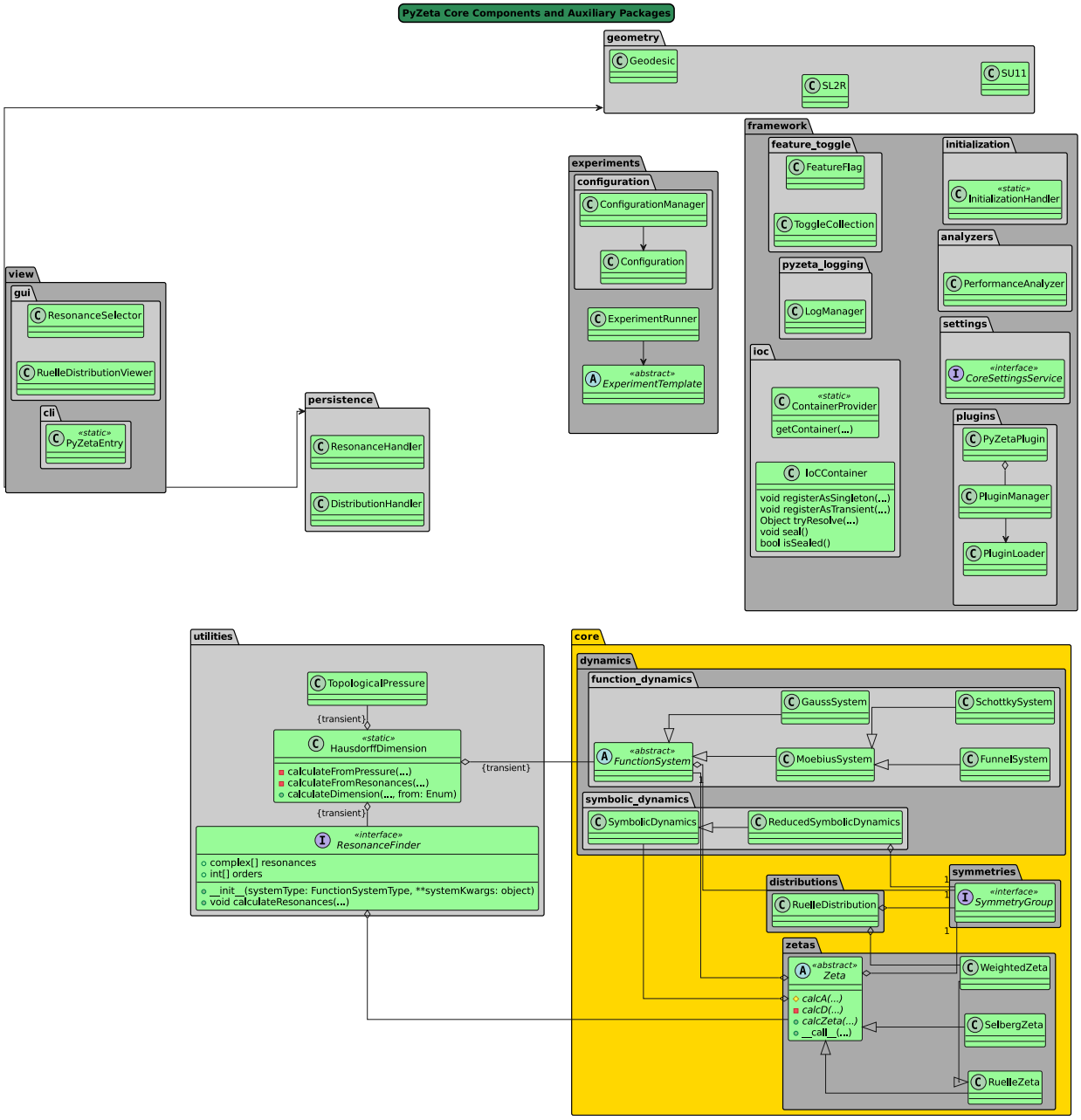

Figure 7.1.: UML diagram of project components and their interactions.

7.2.1. PyZeta Framework Elements

The framework elements included in `PyZeta` abstract as many architectural decisions as possible from the concrete topic of zeta functions and Pollicott-Ruelle resonances.

Dependency Injection and Initialization

One of the overarching themes of the `PyZeta` architecture is its usage of the concept of *inversion of control* or more specifically *dependency injection*. This pattern aims to separate the construction of objects from their usage as part of a general *separation of concerns* design philosophy. According to this philosophy objects should be abstracted as much as (reasonably) possible and object interactions should always be governed by their respective interfaces not their concrete implementations. An exhaustive discussion of this circle of ideas goes well beyond the scope of this thesis. Refer to the monograph [Sv19] for an in-depth treatment. There are many mature projects that contain very similar facilities compared to the implementation discussed next, e.g. the `Java` framework `Spring`. For `PyZeta` a custom implementation is preferable, though: On the one hand there seem to be no mature and actively maintained implementations targeting `Python` in particular, probably due to its highly dynamic nature and predominant usage as a scripting language. On the other hand mature implementations usually provide significantly more powerful and general capabilities exceeding the requirements of `PyZeta` by far.

Now in the custom `PyZeta` realization of dependency injection the central authority that controls which concrete instances get injected into dependent objects is the `pyzeta.framework.ioc.container.Container`. This class serves as a container for configurations which describe how to obtain instances of types. This works as follows:

(i) To make a service of type `T` accessible from the container it must be registered using either one of the methods `registerAsSingleton(serviceType, instance)` to save a singleton [GHJV03, p. 127] configuration or its companion `registerAsTransient(serviceType, factory)` to deposit a transient configuration. The former must be supplied with the concrete service instance while the latter requires a factory method returning instances of `T`.

(ii) Once some service `A` needs to make use of services provided by `B` it simply calls `tryResolve(B, **kwargs)` on the container instance. The container then checks if a valid configuration for `B` exists and returns either the singleton instance or invokes the factory with keyword arguments `**kwargs`. Usually this dictionary of keyword arguments is either empty or rather small because the container tries to provide as many of the factory method arguments as possible by recursively examining and resolving their types. This is an instance of a technique called *(runtime) reflection*.

The substantial benefit of the container concept comes from the fact that services are no longer required to take care of the creation of their dependent services. This is taken care of in an automatic and recursive manner as long as correct and complete configurations were supplied initially. It should be remarked that the dependencies of a service remain very explicit with this approach as they can be read off directly from the constructor signature.

The missing ingredient in the explanations so far is the question of how a service obtains a reference to the container. This could be resolved by e.g. *constructor injection*: The constructor of any service that requires services from the container receives the container as an additional parameter. But the service itself should be resolved from the container in the first place making it possible for the container to inject itself when creating the service instance. Alternative approaches include `Python` specific solutions via decorators or the injection via special instance properties.

To keep the system as simple as possible `PyZeta` chose to supply a project-global container instance via a static class called `ContainerProvider`. This class exposes

static methods to set and retrieve a container instance. Now the actual runtime container instance gets constructed and set during project initialization by the class `PyZetaInitializationHandler`. This class exposes several different startup modes which mostly differ in the kind of service configurations they register. For additional details regarding the container and initialization refer to either the full documentation of the source code.

Logging

The logging of different events during program runtime is an important and powerful mechanism to gain insights into the often complicated runtime dependencies and interactions of object oriented software systems. In `PyZeta` this facility is provided by a `pyzeta_logging` framework package. Its main API is a `mixin` called `Loggable`. Due to the multiple inheritance possible in `Python` any class needing to log information can simply include `Loggable` into its list of superclasses. After doing so it automatically possesses a property of interface type `PyZetaLogger` offering a method to log events at several different levels of severity. This facade [GHJV03, p. 185] effectively abstracts the concrete logger implementation used at any given moment thus making it possible to use different implementations e.g. during and after initialization. At the time of writing this thesis a straightforward implementation based on the standard library `logging` module and managed by a static `LogManager` is available.

Plugins

One typical use case of `PyZeta` is the need to calculate e.g. Pollicott-Ruelle resonances for some function system or Schottky surface which had not previously been implemented as part of the core project. The plugin mechanism is designed as a lightweight alternative that injects custom code into a running instance of the main project without having to implement a genuine module or package within the main repository infrastructure.

The general procedure to achieve this is quite simple and straightforward: Plugins generally provide a means of extending `PyZeta` by instances of some type `T`. In most circumstances `T` will be a subtype of some other type already built into `PyZeta`. The custom plugin must now be realized as a class that derives from `PyZetaPlugin[T]`. This generic abstract base class contains abstract properties returning the type `T` provided by the plugin, a plugin version, and a plugin name for unique identification of plugins. The main functionality must be implemented as a static method `initialize()` which has to return a callable that in turn provides instances for the type `T`, acting as a factory method [GHJV03, p. 107]. Lastly plugins are always implemented as singletons so they require a static `getInstance()` method.

As an example consider the following code contained in a file called `custom_group.py`. It implements a custom (albeit non-functional) version of the trivial symmetry group `TrivialGroup` as an instance of the abstract service `SymmetryGroup` which corresponds to the general type `T` in the discussion above.

```
class TestGroup(TrivialGroup):
    "Custom (trivial) group implementation to supply as a plugin."

    def __init__(self) -> None:
        "Just inherit the super constructor."
        super().__init__()
```

```
        def getElements(self) -> Tuple[tGroupElement, ...]:
            "Override this 'new' functionality in the custom group."
            raise NotImplementedError("test group not implemented!")

    class GroupPlugin(PyZetaPlugin[SymmetryGroup]):
        "Test plugin providing a simple custom symmetry group to PyZeta."

        _instance: Optional[PyZetaPlugin[SymmetryGroup]] = None

        @staticmethod
        def initialize() -> Callable[..., SymmetryGroup]:
            "This is the hook of plugins into `PyZeta`."
            return lambda: TestGroup()

        @staticmethod
        def getInstance() -> PyZetaPlugin[SymmetryGroup]:
            "Plugins should be realized as singletons."
            if GroupPlugin._instance is None:
                GroupPlugin._instance = GroupPlugin()
            return GroupPlugin._instance

        @property
        def pluginType(self) -> Type[SymmetryGroup]:
            "The type provided by the plugin."
            return SymmetryGroup

        @property
        def pluginName(self) -> str:
            "The name of the plugin."
            return "TestGroupPlugin"

        @property
        def pluginVersion(self) -> Tuple[int, int, int]:
            """
            The plugin version (combination of version and name should
            be unique). The semantics are (`major`, `minor`, `patch`).
            """
            return (22, 1, 0)
```

A plugin such as this custom symmetry group can then be installed from the command line using

```
pyzeta plugin --install custom_group.py
```

Afterwards an automatic discovery of installed plugins happens during initialization so that the plugin is available for use during runtime. Obtaining instances of the type `T` provided by the custom plugin again happens through the inversion of control container as described above. An extended example which also demonstrates how to inject custom (constructor) data into the plugin is available as a `jupyter` notebook in the documentation.

Feature Toggles

A feature toggle in the context of `PyZeta` is basically a boolean flag with additional functionality. The motivation to introduce this capability comes from batch processing of numerical experiments. In practice one often has a script or `jupyter` notebook with several distinct experiments or parts of experiments that combine to an overall workflow in several different ways. A straightforward way to distinguish between these experiments or combinations is to wrap them into functions and control their execution with boolean flags. Unfortunately this approach does not scale very well. Large collections of simple boolean variables soon become confusing in terms of e.g. which variable is associated with which function and which variables were active on a particular run of the script or notebook.

Feature toggles alleviate this situation by wrapping the following data:

- The boolean flag itself as the toggle's main functionality,
- A name for identification within a set of toggles,
- A description of the purpose that the toggle serves,
- An optional integer number of times the toggle may be accessed before becoming invalid (i.e. `False`),
- A `PyZetaLogger` that logs usages of the toggle.

When it comes to usage in a script or notebook toggles should not be declared on their own but rather through subclasses of `ToggleCollection` like so:

```
class MyToggles(ToggleCollection):
    "Collection of feature toggles for my script."
    toggle1: bool
    toggle2: bool
```

Using the two toggles in the collection is now as easy as instantiating `toggles = MyToggles(my_toggles.json)` and calling something like `if toggles.toggle1:` at the appropriate points within the program. The configuration of the wrapped data happens within the configuration file `my_toggles.json`:

```
{
    "toggle1": {
        "name": "...",
        "value": true,
        "description": "...",
        "timesAccessible": 1
    },
    "toggle2": {
        "name": "...",
        "value": false,
        "description": "...",
        "timesAccessible": -1
    }
}
```

Note that the key `timesAccessible` may be either omitted or set to a negative value to indicate a toggle with unlimited lifetime. Note also that the wrapped logger does not need to be supplied manually. It is again provided by the `Loggable` mixin and injected automatically.

Remark 7.2.1. The `pyzeta.framework.feature_toggle` package contains a `json` schema against which toggle configuration files can (and should) be verified to make sure that their formatting does not cause runtime exceptions.

Settings

A larger application like `PyZeta` contains a lot of configurable variables and settings. To make their handling as easy and straightforward as possible the framework contains a `SettingsService` interface which exposes read-write properties for application wide configuration of miscellaneous default values. Different possible implementations of this interface could be imagined and the current implementation offers a `json`-backed and a memory-backed (i.e. non-persistent) solution. The former is usually instantiated during project initialization and may be accessed for programmatic manipulation of settings through the container. Alternatively one may also change settings from the command line interface which is also the preferred way to inspect the current state of the possible default values. The latter is mostly used to substitute the former during unit testing. It offers the advantage of consistent and isolated testing environments that are neither influenced by nor change the user's defaults.

Remark 7.2.2. The specific settings available are one of the areas of the code subject to more frequent changes. It therefore makes little sense to go into too much detail here. To get a first overview over available settings simply type

```
$ pyzeta settings -h
```

in the terminal with `PyZeta` installed and follow the instructions given there. Alternatively a look into the source code or the online documentation provides more in-depth and up-to-date details.

Analyzers

This section discusses the emergence of and solution to a concrete instance of a class of problems often called *cross-cutting concerns* in the context of `PyZeta`. In general the term cross-cutting concern applies to functionality or behavior that both violates the component boundaries defined for a system during the functional decomposition step of design and cannot be encapsulated in a straightforward and consistent manner into its own abstraction on which other components might depend. As a consequence an implementation of this functionality would require the scattered duplication of code throughout the system effectively leading to poor overall design quality.

One approach to solving this problem is provided by *aspect-oriented programming (AOP)*. Since the foundational publication [KLM+97] this programming paradigm has received much attention and mature implementations exist like `AspectJ` for the `Java` programming language. The fundamental idea of AOP is to deal with cross-cutting concerns by encapsulating a given functionality (*advice*) together with points during program execution where it should be executed (*point-cuts*) into a new object called an *aspect*. The programmer defines these aspects in a single place and completely separate from their

later point(s) of execution. An additional program called an *aspect weaver* controls the insertion of the correct advice and corresponding point-cuts thus solving the problem of manual maintenance of scattered code.

A common criticism with this approach is the increased complexity when reasoning about the runtime behavior of an application: With complicated advice and point-cuts one requires detailed knowledge of the whole system to be able to determine dynamic properties. To keep this increased complexity at bay the implementation within `PyZeta` described below takes special care to implement practically useful but at the same time not overly powerful aspect-oriented facilities.

One of the framework elements of `PyZeta` discussed above already exhibited the central traits of a cross-cutting concern, namely *logging*. Many different objects within the system participate in logging with a large overlap in requirements in overall behavior. It was decided to achieve logging through the mixin solution presented above for a simple reason: While logging is not a primary concern of any single object it is simply most straightforward to force every system component to participate in the logging effort at statically determined points. While this does lead to code duplication the points at which messages are created should not be subject to frequent change and the corresponding code is almost always as short as a single method invocation. Instead of a complicated runtime allocation of logging responsibility the user may assume that any object alive during system runtime also emits log messages. An application of AOP would thus have been an example of definitive over-engineering.

A different case shall be made for the concern of memory and runtime *profiling*. While it also cross-cuts almost all core components of `PyZeta` one usually wants to very specifically profile a small number of continuously changing objects. Aside from that during production (which means concrete numerical experiments) profiling should be disabled completely due to the significant performance penalty incurred.

As the result of these considerations a basic AOP framework together with concrete profiling extensions were created as part of the framework portion within `PyZeta`. The former is meant to support future requirements and application areas that could benefit from an AOP approach while the latter addresses existing requirements in terms of profiling resonance experiments. Again due to the dynamic nature of `Python` and its less common appearance as the main language in large industrial software projects no suitable prior implementations were found and the combination of `Python` with AOP was deemed an interesting endeavor in its own right.

The generic AOP facilities of `PyZeta` are represented by the following classes:

- `Advice`: This class stores callbacks for an application before and/or after a wrapped method. In addition it contains the logic for wrapping a given method in its `__call__` magic method.
- `PointCut`: This class stores a name pattern and provides logic for matching a method name with this pattern via its `match` method.
- `Rule`: A simple container for pairs of corresponding `Advice` and `PointCut` instances.
- `Aspect`: The central class that contains a list of rules and the logic to apply `Advice` from a rule to a given method iff its corresponding `PointCut` matches the method name. It does so for all methods belonging to a given (concrete) class.

The practical usage of these classes is now straightforward: First create an `Advice` together with a `PointCut`

```
advice = Advice(preCallback, postCallback)
pointCut = PointCut("calculate.*")
```

from two callbacks `preCallback`, `postCallback` and a pattern matching any method that starts with `calculate`. The first callback must accept any arguments valid for the wrapped method while the second callback must additionally accept the return value of the wrapped method as its first argument. For most applications the signatures

```
preCallback(*args, **kwargs)
postCallback(returnArg, *args, **kwargs)
```

are most suitable with as little assumptions on `*args, **kwargs` as feasible. For simple use cases such as injecting additional custom logging statements it might suffice to provide lambda expressions. For more involved logic it is recommended to create a custom subclass of `Advice` with the callbacks given by (private) instance methods.

The two objects just created can now wrap the matching methods of a given class `MyClass` by simply calling

```
aspect = Aspect(rules=[Rule(pointCut, advice)])
aspect(MyClass)
```

A working example is provided as the notebook `aop_example.ipynb` contained in the documentation of `PyZeta`. This notebook also details the usage of `ProfilingAdvice`, a subclass of `Advice` which contains predefined callbacks that wrap functionality from the standard library `cProfile` module. To enable profiling for `MyClass` one thus follows the same pattern as above but replacing the instantiation of generic `Advice` with the line

```
advice = ProfilingAdvice(fileName)
```

where `fileName` is a string indicating the file in which the resulting profile should be stored.[15] `ProfilingAdvice` and additional convenience classes for the reading of profile files are part of the package `pyzeta.framework.aop.analyzers`.

Remark 7.2.3. A typical user of the scripting API of `PyZeta` should actually not need to interact this concretely with the `Advice` API. During design it was expected that the standard use case looks more like the following: A user obtained an `Advice` instance `advice` either by subclassing or by reusing builtin subclasses. The logic within this instance would typically be supposed to be applied to all types implementing some interface, i.e sharing a common set of methods. To achieve this the call to `advice(classType)` should be replace with the simple function call

```
registerAspectGlobally(aspect, interfaceType)
```

which internally calls `registerAspect(aspect, interfaceType)` on the global container instance. The container can now intercept object creation via `tryResolve(interfaceType)` and adorn the class of the concrete resolved object with the given aspect. An example of this pattern is again provided as part of `aop_example.ipynb`!

[15] Filenames are expected without an extension – the default *.cprofile* gets appended automatically.

7.2.2. PyZeta Core Components

The core package frames the fundamental abstractions making up all zeta function related functionality together with their respective implementations. This section summarizes the relevant classes in the order imposed by a further organizational subdivision into smaller packages.

The central package `pyzeta.core.zetas` exposes both an abstract zeta and an abstract weighted zeta function. These callable classes implement the step d_n of the Bell iteration described in [Bor14] for Selberg's zeta function and in [SW23] for (weighted) dynamical determinants, respectively, while leaving the initial term a_k abstract. Different concrete implementations like symmetry or non-symmetry reduced variants therefore only need to implement this remaining initial term. This introduces additional flexibility that should prove useful when implementing further zeta functions like the semiclassical variants discussed in Chapter 3. The list of concrete implementations covers the areas Selberg zeta function and (weighted) dynamical determinant for the calculation of quantum mechanical and classical resonances, respectively. Both are available in symmetry reduced and non-reduced versions. Concretely there are

```
AbstractZeta
AbstractWeightedZeta
SelbergZeta
WeightedZeta
ReducedSelbergZeta
ReducedWeightedZeta
```

All concrete implementations available at the moment require two dependent services namely a *symbolic dynamics* to provide the symbolic words satisfying certain constraints and up to some maximal word length together with either an *iterated function system* or a *hyperbolic map system* to convert symbolic words into periodic orbit data like instabilities or period integrals. The abstractions and implementations of these are contained within the sub-packages `symbolic_dynamics` and `function_systems` of `pyzeta.core.dynamics`. Again a hierarchy abstracts the fundamental aspects of these services:

```
AbstractSymbolicDynamics
SymbolicDynamics
ReducedSymbolicDynamics
```

provide a `wordGenerator` method for the generation of parallel arrays of symbolic words and closing elements from some given finite symmetry group. Attributes like `prime`, `permFree`, or `cyclRed` may be provided to specify subsets of words suited to the particular application. For example zeta functions without symmetry reduction require only `cyclRed` because their function or map systems expect cyclically reduced words for stability generation.

This functionality gets complemented by the much larger hierarchy below the abstract bases

```
FunctionSystem
HyperbolicMapSystem
```

The former exposes `getStabilities` which requires an array of cyclically reduced symbolic words generated from an underlying property `adjacencyMatrix` and produces a

parallel array of stabilities of the orbit represented by each of the words. The latter also provides `getStabilities` which differs in that it yields two parallel arrays of stabilities and instabilities.[16] Additionally `HyperbolicMapSystem` also has a property `fundamentalIntervals` as well as a method `getPeriodicPoints` which from an array of symbolic words calculates two parallel arrays of repelling and attracting fixed points of the orbits associated with each individual word.

The respective functionality of both abstractions is made concrete in a variety of subclasses including

```
MoebiusFunctionSystem
MoebiusMapSystem
```

for systems whose functions or maps are given by Moebius transformations on the upper halfplane,

```
SchottkyFunctionSystem
SchottkyMapSystem
```

for systems that represent geodesic flow dynamics on convex cocompact hyperbolic surfaces, and the non-exhaustive collection

```
HyperbolicCylinder
HyperbolicCylinderMap
FlowAdaptedCylinder
FlowAdaptedCylinderMap
FunnelTorus
FunnelTorusMap
GeometricFunnelTorus
GeometricFunnelTorusMap
...
```

The latter are now concrete classes that constitute the bottom of the hierarchy. Again instances need not be created by the user. Instead the `Container` decides dynamically the correct system to construct based on the user supplied data. If as an example the user wants to construct a Selberg zeta function for a hyperbolic cylinder it suffices to call

```
initArgs: HyperbolicCylinderArgs = {"funnelWidth": 5.0, "rotate": True}
zeta = SelbergZeta(
    functionSystem=FunctionSystemType.HYPERBOLIC_CYLINDER,
    systemInitArgs=initArgs,
)
```

The responsibility of knowing that `SelbergZeta` requires a `FunctionSystem` not a `HyperbolicMapSystem` instance as well as how to construct such an instance in the cylinder case is handled by appropriate components automatically.

The `WeightedZetaFunction` depends on a third service called `IntegralProvider`. As suggested by its name this component supplies orbit integrals via a `getOrbitIntegrals` method taking an array of symbolic words as input. The concrete implementations

```
FundamentalDomainIntegrals
PoincareSectionIntegrals
```

[16] For Hamiltonian dynamics like geodesic flows on Schottky surfaces a pair of stabilities and instabilities must multiply together to one.

represent the two approximations to invariant Ruelle distributions discussed in [SW23, Section 4] namely pushforward to the Dirichlet fundamental domain and restriction to the canonical Poincaré section.

This functionality gets complemented by sub-packages of `pyzeta.core` called `symmetries` for symmetry groups used with symmetry reduction and `distributions` for invariant Ruelle distributions. Again the general principle of supplying central abstractions like a `SymmetryGroup` together with concrete implementations like `TrivialGroup` was followed. It should be emphasized again that any service should only ever address its dependent services through their abstract interface and never through their concrete implementation! Together with carefully chosen abstractions this guarantees the largest possible degree of flexibility and extensibility.

Remark 7.2.4. `PyZeta` version `v0.1.1` does not yet contain a complete implementation of symmetry reduction. This functionality exists as part of the non-open source legacy code created by the author of this thesis during preparation of the article [SW23] but still requires (straightforward) porting to the open source domain.

7.2.3. Additional Layers and Components

The design of `PyZeta` incorporates a couple of additional layers which exist independently from the core business logic described above to enforce decoupling and coherence of the different components. These layers could roughly be categorized as providing more generic *auxiliary capabilities* beyond the specific resonance and zeta function core. Their design and functional requirements are naturally dictated by the necessities of the core logic, though. The following list contains an overview of these layers and components with general descriptions of their exposed API. Many of them are still evolving and the most up-to-date presentation is available as part of the inline documentation in the GitHub repository. For an overview over the interplay of some of the components mentioned in this section refer to Figure 7.2.

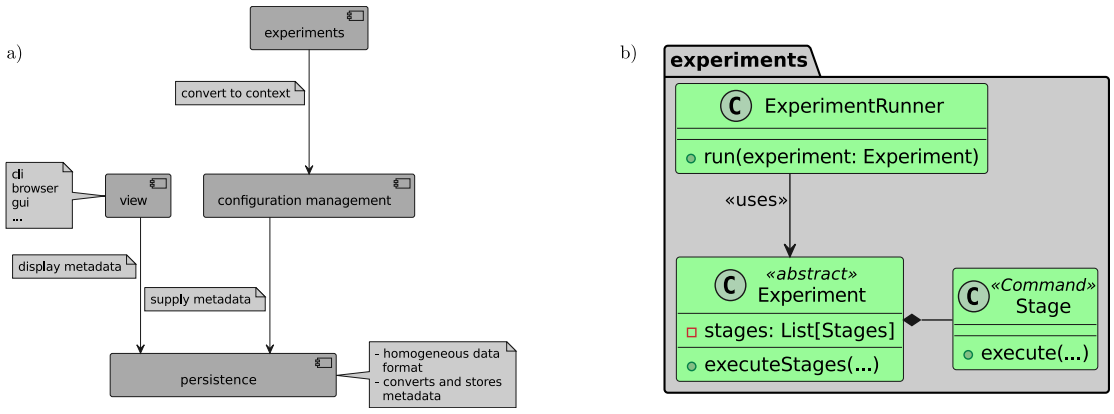

Figure 7.2.: Illustration of a) component and b) partial class diagrams for the *view, experiments, configuration management* and *persistence* packages.

- `pyzeta.view`: The view layer groups all components related to the graphical representation or manipulation of data generated by or to be processed by the `PyZeta` core components. In particular this includes a tool called `ResonanceSelector` which is built on top of the package `bokeh` and allows its users to pick individual resonances from larger collections. This is exceedingly useful to e.g. extract resonances along a chain for further investigation. Furthermore this layer groups the *command line*

interface which exposes functionality like manipulation of settings, test execution, and plugin management.

- `pyzeta.persistence`: The persistence layer incorporates all classes that handle the storage and retrieval of data like resonances or Ruelle distributions. Its primary goal is to make the whole process of saving data for later reference as transparent to the user as possible while preserving all necessary information required to reconstruct the context in which the respective data was initially gathered, i.e. *metadata*.

- `pyzeta.geometry`: The geometry package contains everything related to the geometry of hyperbolic space, Schottky surfaces, and more. It provides a backend to the view layer whenever data is to be displayed in the context of hyperbolic geometry like Ruelle distributions on their fundamental domain.

- `pyzeta.experiments`: The experiments package is envisioned to provide a generic, extensible and flexible framework for the configuration and management of numerical experiments in the context of Pollicott-Ruelle resonances and zeta functions. Important aspects of this endeavour are the possibility of configuring experiment scripts with as little code as possible, i.e. shifting work into configuration files, and tracking such configurations over multiple runs or batches. Concrete examples of configurations in this context are things like which Schottky surfaces together with which parameters were used or which series cutoff was chosen for dynamical determinants.

- `pyzeta.utils`: The utilities package collects functions and classes which do not fit into any of the aforementioned packages. The package is not designed to host larger collections of related functionality, though: Due to the generality of the term *utility* anything that may sensibly be grouped into a coherent set of components should at some point be refactored into a more specific package!

7.3. Conclusion and Outlook

Due to its large scope the `PyZeta` project is still under active development at the time of writing this thesis. There are open tasks[17] in several directions:

- Some parts of the core functionality still require porting from the legacy to the new open source project. In particular this includes work on documentation and testing making it a non-trivial task in terms of time and effort required but the programming itself should be rather straightforward because the algorithms have already been thoroughly investigated and extensively used during the preparation of the article [SW23].

- Supplementary details regarding the infrastructure come up frequently during implementation of core capabilities like additional settings to include. Also the documentation could be improved especially in terms of description of the theory. Apart from such minor details the architecture elements are complete and should be straightforward to adapt to future requirements.

[17] Many of these are listed under the *Issues* tab on GitHub. It is common practice for open source projects to use this mechanism both for enhancement proposals as well as bug fixes.

- The implementations regarding the `pyzeta.persistence` package mostly have the status of prototypes at the time of writing this thesis. In particular this applies to a `ResonanceHandler` class which bundles capabilities for loading and saving resonance data. This existing code needs to be ported to the open source project after proper refactoring because the class accumulated too many different data and metadata formats over its lifetime and offers quite a bit of potential in terms of coherency. Additionally the loading and saving capabilities need to be extended to also cover use cases involving invariant Ruelle distributions.
- At the time of writing this thesis the `pyzeta.view` package consists mainly of command line functionality regarding plugins, settings, and local installation tests, as well as of a prototype of the `ResonanceSelector` tool. The latter requires heavy refactoring and adaption to the planned new data format before it integrates seamlessly into the open source branch.
- The `pyzeta.experiments` package is the newest of the different `PyZeta` components. This is primarily due to the circumstance that the concrete requirements and use cases addressed by this package came up during the experiments conducted as part of [SW23]. The basic structure as indicated in Figure 7.2 is in place but concrete experiments and runners must still be implemented. This should happen in conjunction with the implementation of the planned *configuration management* whose design in turn heavily depends on the data and metadata formats.

In summary it can be stated that the core functionality is in place as demonstrated in [SW23] apart from conceptually minor points like documentation. The user-facing convenience infrastructure is more of a work in progress with a number of supporting documents like use case diagrams, requirement descriptions, and class diagrams created but also some concrete implementations left to be done. The guiding principle here is to reduce the boilerplate code required to run concrete resonance or Ruelle distribution experiments to a minimum. Instead potential future users should interact with the currently existing code only through a short driver script which gets configured without actually writing any `Python` code. This should minimize the entry barrier to the project because the typical user is probably more experienced with but also more interested in the underlying mathematics as compared to the implementation and programming details.

Besides these points there exist a number of exciting new research directions which would lend themselves perfectly for inclusion within `PyZeta`. On the one hand there are additional techniques for convex-cocompact hyperbolic surfaces like the ones developed in [BPSW20] which approximate the function spaces that the transfer operators act on resulting in an approximation of the Fredholm determinants by ordinary (finite-dimensional) determinants. This complements well the cycle expansion approach and could unlock a larger region of resonances that invariant Ruelle distributions can be investigated for.

Another aspect would be facilities to calculate and visualize quantum resonant states on Schottky surfaces, c.f. [Str17, LS21]. This would make it possible to consider directly quantum matrix coefficients and investigate further the high frequency limit where invariant Ruelle and Wigner distributions coincide. Also it could offer a way of independently verifying numerical results such as those presented in [SW23] whose validity can at the moment only be made plausible on a qualitative level.

On the other hand there exist practically well-established techniques for classical, semiclassical, and quantum resonances as well as certain phase space distributions on n-disc systems. An inclusion as part of `PyZeta` would be very worthwhile because these objects have so far been investigated only in highly symmetric 3-disc arrangements. The

possibility of running direct comparisons of these model systems within the same numerical project might also uncover new differences between resonances for locally symmetric spaces and general hyperbolic systems for which there is no algebraic structure theory that allows the derivation of a rigorous quantum-classical correspondence.

8. The PyZEAL Project

This chapter illustrates the numerical `PyZEAL` package which constitutes the second major programming project conducted during the course of this thesis. The style of the presentation is very similar to the previous Chapter 7 but more room will be dedicated to the comparison between the approaches to and implementations of `PyZEAL` and `PyZeta` as well as the mathematical foundations which are mostly disjoint from the theoretical chapters in Parts I and II.

8.1. Origins of the Project and Requirements

Based on the mathematical machinery developed in Chapter 4 it was possible to implement an efficient numerical procedure for calculating various kinds of zeta functions in Chapter 7. Even with these pieces in place practical experiments show that it is still highly desirable to minimize the number of zeta function evaluations required for the resonance and Ruelle distribution experiments in question.

The first such experiments conducted for this thesis were simple calculations of resonances in compact regions of $\mathbb{C}$. To this end a legacy implementation of a root finding algorithm by Tobias Weich was used. This algorithm implemented immediately the simple *divide-and-conquer* scheme suggested by the well-known argument principle from complex analysis[1]. A more detailed description of this theorem and its consequences will be given below.

While quite straightforward and easy to use the practical usage of the aforementioned implementation revealed several shortcomings such as

- high number of required function evaluations,
- large unused potential for parallel execution, i.e. an instance of what the literature on parallel programming often calls an *embarrassingly parallel problem*,
- ad-hoc solution to problems some of which are inherent to the algorithm used and some of which are not,
- unused implicit knowledge of root orders kept as data internal to the algorithm.

These problems and their (partial) solution will be described in greater detail in the upcoming sections.

Even a short look into the applied mathematics literature reveals that an abundance of algorithms have been developed for the root finding problem in the holomorphic category. For some reason, though, these theoretical developments do not seem to have made the transition from research papers and private proof-of-concept implementations to well tested and well documented open source packages that are easily accessible and possess a gentle learning curve for their users. A web search prior to starting the endeavor constituting the contents of this chapter uncovered the following projects with accessible code related to zeros of holomorphic functions:

[1] See also the remarks in [Bor14, Section 4.1].

- `https://github.com/rparini/cxroots` which is written in `Python`. Judging from its commit history this project is semi-actively maintained but has not been under active development since 2018.
- `https://github.com/nennigb/polze` is also written in `Python` and claims to calculate zeros *and* poles. The implementation follows [Che22] but the repository seems to be neither actively maintained nor currently under development and has an overall low number of commits.

A much older implementation is a package called `ZEAL` written in `Fortran90` [KVR+00]. It implements the algorithm as described in [KV00] and serves as namesake for the subject of this chapter. While apparently planned as an end user solution by its original authors it appears to be practically unavailable and moreover technologically inaccessible nowadays. Due to its excellent documentation in the form of the textbook just mentioned `ZEAL` serves as a major source of inspiration for the new code base in terms of mathematical algorithms and overall functionality.

With these points in mind the `PyZEAL` project was conceived. It aims to tackle these problems and provide a solution to the following set of requirements:

(i) Build well tested, thoroughly documented software that is easy to use and extend – in particular, this implies a widely popular language for implementation.

(ii) Make the end product cross-platform and easy to install even with little to no prior technological experience.

(iii) Provide an abstraction of the root finding problem that applies to various kinds of holomorphic data independent of the zeta function setting.

(iv) Create a sandbox for experimentation with new root finding methods and comparison of different approaches. This aspect should be considered on equal footing with the point of view purely focused on the user wanting to solve a holomorphic root finding problem with some black-box algorithm.

It is therefore not only the aim of this project to support one of the main use cases of `PyZeta`, namely the calculation of resonances as zeros of zeta functions, but also to establish a foundational implementation for anyone interested in holomorphic root finding to use and extend as part of their own research interests. As such `PyZEAL` is necessarily incomplete in terms of algorithms included but substantial progress was made compared to the situation prior to the establishment of the project, both in terms of an improvement of the existing methodology as well as the implementation of new methods.[2]

To mark the completion of the general framework and working implementations of first algorithms a stable version `v1.0.0` of `PyZEAL` was published as open source on May 1st, 2023.[3] This is also the reference version for this thesis.

The remaining sections of this chapter will proceed as follows: Section 8.2 describes the preliminaries necessary for the concrete algorithms. This description remains rather concise as the material is standard complex analysis. In Section 8.3 an overview over the applied mathematics literature regarding the holomorphic root finding setting is given. While also being far from comprehensive all methods currently implemented within `PyZEAL` are covered as well as some promising future directions. With these prerequisites out of the

[2] Additionally it should be clear that even including implementations of a significant fraction of methods to be found in the literature is far beyond the scope of any single thesis.

[3] `https://github.com/Spectral-Analysis-UPB/PyZEAL`.

way both the general architecture can be described in Section 8.4 as well as some noteworthy internal details regarding framework elements and algorithms in Section 8.5. The concluding Section 8.6 presents an outlook and future directions for `PyZEAL`.

8.2. Mathematical Preliminaries

The mathematical domain that `PyZEAL` deals with is that of complex analysis and in particular *holomorphic* and *meromorphic functions*. This section summarizes some basic facts regarding these classes of functions for the reader's convenience. The material is completely standard and can be found in any textbook dealing with complex analysis such as [RS02].

A function $f : U \to \mathbb{C}$ on an open subset $U \subseteq \mathbb{C}$ is called holomorphic if it satisfies both

(i) differentiability as a function $U \to \mathbb{R}^2$, where any subset of $\mathbb{C}$ is viewed as a subset of $\mathbb{R}^2$ via the standard identification $z \mapsto (\mathrm{Re}(z), \mathrm{Im}(z))$, and

(ii) $\mathbb{C}$-linearity of its differential at every point of U or, equivalently, its $\mathbb{R}$-linear differential can be identified with a complex number.

It is standard that provided condition (i) holds the requirement in (ii) is equivalent to the so-called Cauchy-Riemann equations on the partial derivatives of the real and imaginary parts of f. Furthermore one commonly denotes the complex numbers whose existence is demanded in (ii) by $f'(z)$, $z \in U$, and calls them the *complex derivative* of f. In practice this derivative can be calculated as the limit in $\mathbb{C}$ of a difference quotient analogous to the single-variable real case.

Now holomorphic functions possess a number of very rigid properties much stronger than those of differentiable functions $\mathbb{R}^2 \to \mathbb{R}^2$:

- holomorphic functions can be developed into locally compactly convergent *power series* around any point of their domain,
- holomorphic functions are already *infinitely often complex differentiable*,
- the values of a holomorphic function on the boundary of a disc determine its values (as well as values of its derivatives) completely as expressed by *Cauchy's integral formula*,
- path integrals of holomorphic functions on simply connected domains are path independent as expressed by *Cauchy's integral theorem*.

The strong properties of holomorphic functions already suggest that more specific methods tailored to their holomorphic nature should yield better algorithms than the more generic ones that exist for (k-times) differentiable functions on $\mathbb{R}^2$. A common starting point for many of the algorithms present in the literature is the following theorem often called the *argument principle*:

Let a holomorphic function $f : U \to \mathbb{C}$ on a simply connected domain $U \subseteq \mathbb{C}$ and a simple, closed, piece-wise differentiable curve $\gamma \subseteq U$ be given. If no zeros of f lie on γ then

$$\mathrm{N}_f(\gamma) = \frac{1}{2\pi \mathrm{i}} \int_\gamma \frac{f'(z)}{f(z)} \mathrm{d}z \ , \tag{8.2.1}$$

where $\mathrm{N}_f(\gamma)$ denotes the number of zeros of f inside the region bounded by γ and counted according to their multiplicity. The proof for (8.2.1) is rather straight forward using the power series expansion of f around its zeros together with the *residue theorem*. A proof of a more general formulation will be given shortly.

For the cases of interest here the quotient f'/f appearing in the argument principle (8.2.1) is in fact not holomorphic as expressed by the fact that the integral does not vanish if $\mathrm{N}_f(\gamma) \neq 0$. At every zero of f the denominator diverges but f'/f still represents what is called a *meromorphic function*!

A function g is called meromorphic on the domain $U \subseteq \mathbb{C}$ if there exists a set without accumulation points $S \subseteq U$ such that $g : U \setminus S \to \mathbb{C}$ is holomorphic and the elements of S are *poles* of g. In generalization of power series expansions one can expand a meromorphic function g into its Laurent series around a pole z_0, i.e.

$$g(z) = \sum_{k=-n}^{\infty} a_k (z - z_0)^k \ , \qquad \text{for } z \text{ near } z_0 \ ,$$

and the coefficient a_{-1} is called the *residue of g at z_0*, denoted by $\mathrm{Res}(g, z_0) \coloneqq a_{-1}$.

The residue of a meromorphic function is of particular importance because it figures prominently in the residue theorem: Given a meromorphic function $g : U \to \mathbb{C}$ on a simply connected domain $U \subset \mathbb{C}$ together with a simple, closed, piece-wise differentiable curve $\gamma \subseteq U$ that does not contain any poles of g one has

$$\frac{1}{2\pi \mathrm{i}} \int_\gamma g(z) \mathrm{d}z = \sum_{i=1}^{m} \mathrm{Res}(g, a_i) \ ,$$

where $\{a_1, ..., a_k\}$ is the list of poles of g contained in the interior of γ. The residue theorem is useful in applications of both theoretical (calculating definite integrals) as well as practical (signal processing, control theory, or electrodynamics) nature.

The upcoming sections will refer to the following *generalized argument principle* which is straightforward to prove using the residue theorem:

Theorem 8.2.1: Generalized argument principle

Let a holomorphic function $f : U \to \mathbb{C}$ on a simply connected domain $U \subseteq \mathbb{C}$ and a simple, closed, piece-wise differentiable curve $\gamma \subseteq U$ be given. If no zeros of f lie on γ then

$$\frac{1}{2\pi \mathrm{i}} \int_\gamma \frac{f'(z)}{f(z)} z^N \mathrm{d}z = \sum_{i=1}^{n} z_i^N \ , \qquad N \in \mathbb{N} \ ,$$

where $z_1, ..., z_n$ are the zeros of f contained in the interior of γ and repeated according to their multiplicity.

Proof. By the residue theorem it suffices to calculate the residues of $z^N f'(z)/f(z)$ at the zeros of f. Letting z_i by an arbitrary such zero one observes that there exists $\varepsilon > 0$ such that in any ball $\mathrm{B}_r(z_i)$ of radius $r < \varepsilon$ around z_i one can write

$$f(z) = (z - z_i)^k g(z) \ , \qquad \forall\, z \in \mathrm{B}_r(z_i) \ ,$$

with some non-vanishing holomorphic $g : \mathrm{B}_r(z_i) \to \mathbb{C}$. This is obvious from the power series expansion of f around z_i and g is obtained by factoring from it the highest possible

power of $(z - z_i)$. Now a simple calculation yields the residue:

$$\frac{f'(z)}{f(z)} z^N = \frac{k}{z - z_i} z^N + \frac{g'(z)}{g(z)} z^N \ , \qquad z \in \mathrm{B}_r(z_i) \ .$$

The second term has vanishing residue due to being holomorphic while the first term's residue is easily identified as being kz_i^N. □

8.3. Root Finding Algorithms

This section reviews some algorithms regarding holomorphic root finding to be found in the literature. Aiming at anything close to completeness would greatly exceeding the constraints of this thesis. The following presentation is therefore restricted to those algorithms which have either already been implemented as part of `PyZEAL` or have been chosen as promising candidates for future inclusion. That being said it should be reiterated that `PyZEAL` aims to provide a framework within which any sort of root finding algorithms for holomorphic functions can be implemented efficiently.

The presentation begins with [KV00] as it seems to be the major reference textbook on this subject matter. While being quite short and concise it contains a good overview over algorithms using

- higher moments of f'/f to construct polynomials whose zeros coincide with the zeros of f (see Section 8.3.1);
- subdivision schemes and careful tracking of complex logarithms of f to avoid usage of f' (see Section 8.3.2);
- formal orthogonal polynomials to construct generalized eigenvalue problems related to the zeros of f and more generally the zeros and poles of meromorphic functions (see Section 8.3.3);

It also contains a description of the `Fortran90` package `ZEAL` which serves as the namesake of the present project as described in the previous Section 8.1.

Much of the material can also be found in the paper [KV99] by the same authors. Not only does it contain a wealth of references but it also summarizes several approaches in a readable and concise manner. The authors have several other papers in this subject area including [KVH99] which more generally deals with meromorphic functions.

8.3.1. Higher Moment Construction

The pioneering paper [DL67] seems to be the first rigorous investigation into how the argument principle could be used for calculating roots of holomorphic functions. As such it is often cited in later works on the subject and provides a great starting point before diving into more recent works.

Mathematically it uses the generalized argument principle Theorem 8.2.1 to identify the *higher moments*

$$s_N \coloneqq \int_\gamma \frac{f'(z)}{f(z)} z^N \mathrm{d}z$$

with the sums over N-th powers of the roots of f within γ. Having obtained $s_1, \ldots, s_n$ for $n = s_0 = \mathrm{N}_f(\gamma)$ one can use Newton's identities to iteratively construct the coefficients of

the polynomial p of degree n whose zeros coincide with the zeros $z_1, \ldots, z_n$ of f within γ:

$$p(z) \coloneqq \prod_{i=1}^{n} (z - z_i) \ .$$

This reduces the root finding problem for f to one for the polynomial p which in general is far easier and for which sophisticated methods are readily available (e.g. as part of `numpy.polynomial`[4]).

One disadvantage of this approach is the fact that the mapping from the s_N to the coefficients of p is generally ill-conditioned and the zeros of p dependent on its coefficients in a very sensitive manner. Many papers in the literature try to remedy this shortcoming by requiring some global information on f or its derivatives to be able to bound the error incurred from errors in calculating s_N via some quadrature scheme.

In the companion paper [LD67] to [DL67] further details on contour integration are provided. This is especially helpful for practical implementation purposes.

8.3.2. Derivative-free Algorithms

The algorithms in this category generally make use of the fact that the argument principle can be reformulated as

$$\mathrm{N}_f(\gamma) = \frac{1}{2\pi \mathrm{i}} \int_{f \circ \gamma} \frac{1}{z} \mathrm{d}z \ ,$$

where the expression on the right-hand side can be recognized as the winding number of the curve $f \circ \gamma$ around $0 \in \mathbb{C}$. This winding number can in principle be calculated as the change in argument of f along the curve γ divided by 2π. After subdividing γ into finitely many arcs $[\gamma_i, \gamma_{i+1}]$, $i = 1, \ldots, M$, one gets the numerically feasible expression

$$\mathrm{N}_f(\gamma) = \frac{1}{2\pi} \sum_{i=1}^{M} \arg\left(\frac{f(\gamma_{i+1})}{f(\gamma_i)} \right) \ . \tag{8.3.2}$$

where $\gamma_{M+1} \coloneqq \gamma_1$. As a reference refer to [Hen88, p. 233].

In practice one is faced with the problem that (8.3.2) only holds true if the absolute value of the change in argument within any segment $[\gamma_i, \gamma_{i+1}]$ does not exceed π. In general this cannot be verified without further information on f [KV00, Theorem 1.1.2] and many authors have contributed theorems and algorithms in this direction. An example of such a contribution is [YNK88].

8.3.3. Formal Orthogonal Polynomials

To remedy some of the shortcomings of the procedure sketched in Section 8.3.1 one can treat the zeros $z_1, \ldots, z_n$ of f counted *without multiplicities* and their multiplicities $\nu_1, \ldots, \nu_n$ on equal footing. Concretely this means considering the following pairing which generalizes the construction of higher moments s_N above:

$$\langle \cdot, \cdot \rangle_f : \quad \mathbb{C}[z] \times \mathbb{C}[z] \longrightarrow \mathbb{C} \ ,$$
$$\langle \varphi, \psi \rangle_f \coloneqq \frac{1}{2\pi \mathrm{i}} \int_\gamma \frac{f'(z)}{f(z)} \varphi(z)\psi(z)\mathrm{d}z = \sum_{i=1}^{n} \nu_i \varphi(z_i)\psi(z_i) \ ,$$

where $\mathbb{C}[z]$ denotes the vector space of polynomials in the variable z.

[4] See `https://numpy.org/doc/stable/index.html`.

From $\langle \cdot, \cdot \rangle_f$ one constructs generalized eigenvalue problems whose solutions yield both the zeros $z_1, \ldots, z_n$ as well as the multiplicities $\nu_1, \ldots, \nu_n$. This is done via Hankel matrices constructed from the higher moments $s_N = \langle 1, z^N \rangle$ and using the theory of formal orthogonal polynomials, i.e. monic $p \in \mathbb{C}[z]$ satisfying

$$\left\langle p(z), z^k \right\rangle = 0 \ , \qquad \forall\, k = 0, 1, \ldots, \deg(p) - 1 \ .$$

While the first two approaches presented above have already been implemented as part of the `PyZEAL` code base it is this approach via formal orthogonal polynomials which seems to be a particularly promising next candidate for implementation.

8.4. Architecture of PyZEAL

The underlying philosophy and architecture of `PyZEAL` is very similar to the ideas discussed in the previous Chapter 7. Most of the concepts mentioned there were actually first implemented for and improved in the context of `PyZEAL`. Note in particular the many similarities of Figure 8.1 with Figure 7.1 in terms of framework elements. The architectural description can therefore be shortened to focus on the actual business logic in the following Section 8.5.

Remark 8.4.1. One of the main architectural differences between `PyZeta` and `PyZEAL` is the fact that the latter uses a static container to facilitate dependency injection called `ServiceLocator`. While this locator still gets configured during initialization and follows the same principles as the dynamic container of `PyZeta` it offers significantly less flexibility due to its static project-wide visibility. This is particularly pronounced during testing where special care must be taken to initialize the locator in a manner suitable for all test cases and to guard unit tests for the business logic from changes made during tests of the locator itself.

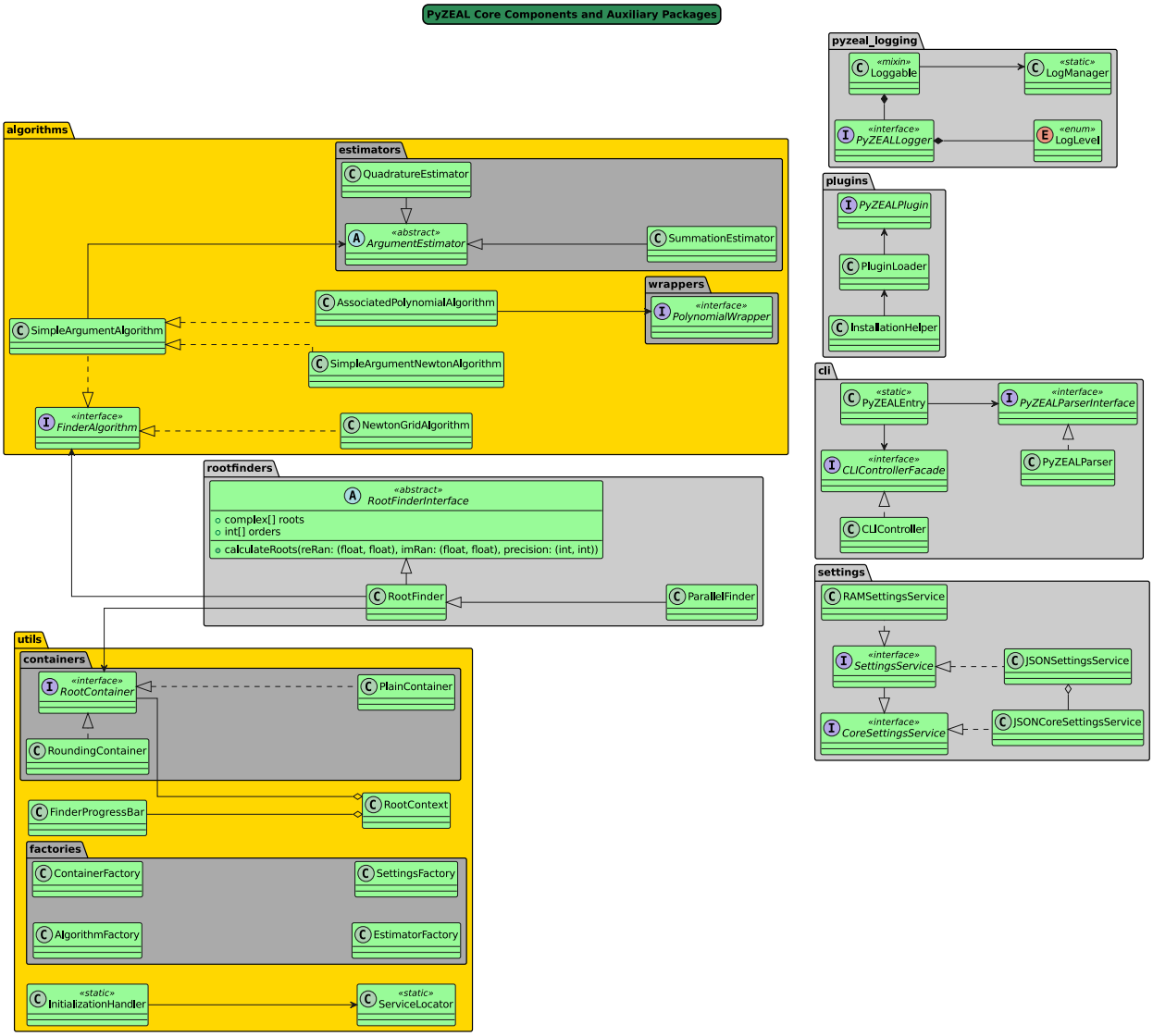

Figure 8.1.: UML diagram of project components and their interactions.

8.5. PyZEAL Internals

The main user API for scripting purposes is provided by the abstract base

`RootFinderInterface`

The main API of this class consists of a single abstract method called

`calculateRoots(reRan, imRan, precision)`

that initiates a root search together with two abstract properties `roots` and `orders` which contain the found roots and their multiplicities, respectively. The parameters `reRan` and `imRan` are pairs of floats determining the boundaries in real and imaginary parts of a rectangle within which zeros are searched. The final integer parameter `precision` determines the accuracy of the root search in terms of considered decimal places.

This abstract base is implemented by a class `RootFinder` and a multiprocessing variant `ParallelFinder`. Both set up a context for the search and delegate the actual work to implementations of an abstract base

`FinderAlgorithm`

where the parallel variant has the added responsibility of distributing work amongst several such algorithm instances. The context includes geometric information on the search domain as well as auxiliary information like accuracy and optional progress bar objects all encoded in the data transfer object `RootContext`.

Progressing deeper into the chain of dependent services consider the `FinderAlgorithm` next. This service exposes an exceedingly simple interface consisting of a single abstract method `calcRoots(context)` taking a data transfer object `context` of type `RootContext` as the setting in which to execute the algorithm. This embodies a rather typical implementation of the classical *strategy pattern* [GHJV03, p. 315]. The advantage of this modular approach comes from its increase in flexibility as compared to approaches which e.g. hard-code different algorithmic variants into subclasses of the `RootFinderInterface`. It keeps the inheritance hierarchy flat while simultaneously reducing the task of creating new algorithms to a new implementation of `FinderAlgorithm`. Combining this with the plug-in mechanism mentioned in Chapter 7 significantly reduces the required overhead when prototyping a new root finding algorithm for holomorphic functions.

The following list contains a short summary of the currently implemented algorithms from `pyzeal.algorithms`. Note how a variety of different algorithmic approaches fit neatly into the structure just outlined:

- `NewtonGridAlgorithm`: Straightforward implementation creating a grid of support points to use as starting points for a classical Newton algorithm. This algorithm suffers from the drawback that the zeros of many practically important functions like those of `PyZeta` vary heavily in the degree in which they attract the Newton iteration. Such cases require very fine grid spacing and often the optimal spacing is not known a priori.

- `SimpleArgumentAlgorithm`: Adaptation of the argument principle based on successive refinements of search rectangles. A specific rectangle can be dropped if the total estimated argument falls below a certain threshold. This is quite stable due to the fact that theoretical values are integer multiples of 2π.

- `SimpleArgumentNewtonAlgorithm`: Refined version of the previous simple variant combining the argument estimation and refinement procedure with the classical Newton algorithm which is started upon finding a single simple root within a search rectangle. From the total argument the expected number of roots is known so the algorithm can correct itself if the Newton iteration does not converge properly.

- `AssociatedPolynomialAlgorithm`: Second refinement of the simple argument procedure following the ideas in Section 8.3.1: After estimating the higher moments of the logarithmic derivative the associated polynomial is constructed from these estimates. Afterwards one of the implementations of the interface `PolynomialWrapper` that wraps classical methods for roots of polynomials can be used to recover the original zeros.

Apart from the first one all of these algorithms heavily depend on a reliable backend for argument estimation. In `PyZEAL` this facility gets provided by implementations of the abstract base class

`ArgumentEstimator`

This abstract base itself exposes `calcMoment(order, reRan, imRan, context)` as the API used by algorithm objects. The bulk of the work gets delegated to a template method [GHJV03, p. 325] handling argument estimation along a line segment in $\mathbb{C}$ called `calcMomentAlongLine(order, zStart, zEnd, context)`. Concrete estimator implementations like `SummationEstimator` and `QuadratureEstimator` must provide their own realizations of this abstract member. The former solves this by summing changes in complex arguments of function values compared to the numerical quadrature of the logarithmic derivative as used in the latter.

Another important abstraction used in `PyZEAL` is that of

`RootContainer`

Instances of its implementations offer methods for the storage and retrieval of roots and their orders while implementing different approaches to the problem of roots that should be considered equal with respect to the given precision. This abstraction therefore cleanly separates the concern of *how to find roots* from the concern of *how to store roots*. The main implementation available at the moment is the `RoundingContainer` which rounds roots upon insertion and stores them in a *set* to eliminate duplicates. A purely internally used implementation called `PlainContainer` supports the multiprocessing implementation of `RootFinderInterface` by wrapping a shared concurrent queue used for inter-process communication.

8.6. Conclusion and Outlook

As of version `v1.0.0` the `PyZEAL` project offers a stable API for the calculation of zeros of holomorphic functions together with several different algorithms ready for use and a platform for straightforward insertion of new algorithms into the existing infrastructure. With this being said there are multiple angles for improvements and extensions which could not be addressed during the present thesis due to time constraints.

On the one hand smaller open issues like an enhancement of the `SummationEstimator` to cover higher moments, improved documentation and test coverage, or smaller algorithmic adjustments of the existing algorithms remain. Another open challenge is the detailed profiling and targeted optimization of the code using the techniques and tooling presented in Chapter 7. The most recent non-comprehensive list of work items may again be found under the *Issues* tab of the `PyZEAL` GitHub repository.

As an example one very interesting of these items is the possibility of solving the root finding problem for polynomials (e.g. resulting from a reduction via associated polynomials) by training a neural network. If such an approach could estimate zeros of polynomials with high accuracy even for high degrees then the existing algorithms would receive a significant boost as they could stop subdividing the search array after fewer steps.

On the other hand many interesting algorithmic approaches to be found in the literature remain to be implemented. One such candidate should certainly be the method of formal orthogonal polynomials as outlined in Section 8.3.3 above. Due to the infrastructure currently in place the implementation of a first prototype should become significantly easier. The full implementation with a cleanly refactored solution, appropriate unit test coverage, and documentation will naturally still take some effort, though.

Part IV.

Appendices

A. Meromorphic Continuation of Weighted Zeta Functions on Open Hyperbolic Systems

This appendix contains the research paper *Meromorphic Continuation of Weighted Zeta Functions on Open Hyperbolic Systems* [SWB23] which was published with the co-authors Tobias Weich and Sonja Barkhofen during the author's PhD.

P.S. and T.W. contributed to the development of the research question and proof strategy. P.S. worked out the proofs and wrote the manuscript. This was accompanied by regular blackboard discussions with T.W. and all three co-authors contributed to the proof reading of the manuscript.

The numerical experiments in the appendix were based on mutual planning by all three co-authors. They were conducted by P.S. based on code previously written by S.B. and T.W.

MEROMORPHIC CONTINUATION OF WEIGHTED ZETA FUNCTIONS ON OPEN HYPERBOLIC SYSTEMS

PHILIPP SCHÜTTE AND TOBIAS WEICH
WITH AN APPENDIX BY SONJA BARKHOFEN, PHILIPP SCHÜTTE AND TOBIAS WEICH

Abstract. In this article we prove meromorphic continuation of weighted zeta functions Z_f in the framework of open hyperbolic systems by using the meromorphically continued restricted resolvent of Dyatlov and Guillarmou [DG16]. We obtain a residue formula proving equality between residues of Z_f and invariant Ruelle distributions. We combine this equality with results of Guillarmou, Hilgert and Weich [GHW21] in order to relate the residues to Patterson-Sullivan distributions. Finally we provide proof-of-principle results concerning the numerical calculation of invariant Ruelle distributions for 3-disc scattering systems.

Mathematical Subject Classification. 37D05, 37C30 (Primary), 58J50 (Secondary).

1. Introduction

1.1. **Motivation.** A closed hyperbolic surface $(\mathbf{M}, g)$, i.e. a closed two-dimensional Riemannian manifold of constant negative curvature, can be considered as a paradigmatic mathematical model that allows the study of classically chaotic dynamics on the one hand and the investigation of spectral properties of the associated quantized system on the other hand: From the perspective of classical mechanics, the free motion of a particle on the curved configuration space $\mathbf{M}$ is described by the geodesic flow on the unit cosphere bundle $S\mathbf{M} \coloneqq \{\xi \in T^*\mathbf{M}; |\xi|_g = 1\}$, which is the unit energy shell in the classical phase space $T^*\mathbf{M}$. On the quantum mechanical side, the Hamiltonian operator is given by the positive Laplace-Beltrami operator Δ acting as an unbounded self adjoint operator on $L^2(\mathbf{M})$. It has discrete spectrum $0 = \lambda_0 < \lambda_1 \leq \lambda_2 \leq \ldots$, where we repeat the eigenvalues according to multiplicity, and we denote by $\psi_i \in L^2(\mathbf{M})$ the associated eigenfunctions. On hyperbolic surfaces, it is convenient to parametrize the spectrum by $\lambda_i = 1/4 + r_i^2$ (where r_i is real valued for eigenvalues $\geq 1/4$ and imaginary for those $< 1/4$). If we fix a semi-classical Weyl quantization $\mathrm{Op}_h, h > 0$, sending test functions in $\mathrm{C}_\mathrm{c}^\infty(T^*\mathbf{M})$ to bounded operators on $L^2(\mathbf{M})$ (see e.g. [Zwo12]) then we can associate to any Laplace eigenfunction ψ_i its Wigner distribution $W_{\psi_i} : \mathrm{C}_\mathrm{c}^\infty(T^*\mathbf{M}) \ni g \mapsto \langle \mathrm{Op}_{1/r_i}(g)\psi_i, \psi_i\rangle_{L^2(\mathbf{M})}$. This generalized function should be interpreted as a representation of the quantum state ψ_i on the classical phase space $T^*\mathbf{M}$.

In this setting, Anantharaman and Zelditch [AZ07] proved the remarkable result that one can define zeta functions that are given purely in terms of the classical geodesics but nevertheless allow one to express the quantum phase space distributions by means of residue formulae. More precisely, for any $f \in \mathrm{C}^\infty(S\mathbf{M})$ they consider the following weighted zeta function

$$\mathcal{Z}_f^{AZ}(s) \coloneqq \sum_\gamma \frac{\mathrm{e}^{-sT_\gamma}}{1 - \mathrm{e}^{-T_\gamma}} \int_{\gamma^\#} f \ , \tag{1.1}$$

where the sum runs over all closed oriented geodesics $\gamma \subset S\mathbf{M}$, T_γ is the period length of the closed geodesic and $\gamma^\#$ is the corresponding primitive geodesic. By an elementary

Key words and phrases. Ruelle resonances, invariant Ruelle distributions, zeta functions, hyperbolic dynamics, numerical zeta functions.

estimate on the number of periodic geodesics with period length $\leq T$ one directly obtains that $\mathcal{Z}_f^{AZ}(s)$ defines a holomorphic function for $\mathrm{Re}(s) > 1$. Anantharaman and Zelditch now show the following:

Theorem 1.1: [Anantharaman-Zelditch 2007]

If $g \in \mathrm{C}_c^\infty(T^*\mathbf{M})$ such that $g|_{S\mathbf{M}}$ is real analytic then $\mathcal{Z}_{g|_{S\mathbf{M}}}^{AZ}(s)$ admits a meromorphic continuation to $\mathbb{C}$.
Furthermore for any $r > 0$, if $1/2+\mathrm{i}r$ is a pole of $\mathcal{Z}_{g|_{S\mathbf{M}}}^{AZ}(s)$ then $1/4+r^2$ is a Laplace eigenvalue and one has the following spectral interpretation of the residue:

$$\operatorname*{Res}_{s=\frac{1}{2}+\mathrm{i}r}\left[\mathcal{Z}_{g|_{S\mathbf{M}}}^{AZ}(s)\right] = \sum_{\lambda_i=\frac{1}{4}+r^2} W_{\psi_i}(g) + \mathcal{O}(1/r),$$

For their proof, Anantharaman and Zelditch develop the notion of Patterson-Sullivan distribution and their techniques for meromorphic continuation and the residue formula heavily rely on the Lie-theoretic description of hyperbolic surfaces.

The aim of this article is to show that microlocal analysis allows the meromorphic continuation of weighted zeta functions very similar to (1.1) but in the considerably more general setting of open hyperbolic dynamical systems as studied in [DG16]. We also obtain a spectral interpretation of poles and residues of these weighted zeta functions in terms of Ruelle resonances and resonant states. Combining these results with previously obtained results on the quantum classical correspondence we recover the above mentioned theorem of Anantharaman and Zelditch in the special case of geodesic flows on closed hyperbolic surfaces.

1.2. **Statement of Results.** To formulate our main results let $\mathcal{M}$ be a smooth manifold with smooth (possibly empty) boundary, X a smooth, nowhere vanishing vector field on $\mathcal{M}$, and φ_t its flow. In addition, denote by $\mathcal{E}$ a smooth, complex vector bundle over $\mathcal{M}$ and by $\mathbf{X}$ a first-order differential operator acting on sections of $\mathcal{E}$ which is related to X via the Leibniz rule

$$\mathbf{X}(f\mathbf{u}) = (Xf)\mathbf{u} + f(\mathbf{X}\mathbf{u}), \qquad f \in \mathrm{C}^\infty(\mathcal{M}),\ \mathbf{u} \in \mathrm{C}^\infty(\mathcal{M},\mathcal{E})\ .$$

The dynamics of interest from the point of view of our application happen on the *trapped set* K of φ_t, i.e. on the set

$$K := \{x \in \mathcal{M} \,|\, \varphi_t(x) \text{ defined } \forall t \in \mathbb{R} \text{ and } \exists \text{ cpt. } A \subseteq \mathcal{M} \text{ with } \varphi_t(x) \in A\ \forall t \in \mathbb{R}\}\,. \quad (1.2)$$

Finally, we make the following *dynamical assumptions*:

(1) K is compact,
(2) $K \subseteq \mathring{\mathcal{M}}$, with $\mathring{\mathcal{M}}$ the manifold interior of $\mathcal{M}$,
(3) φ_t is hyperbolic on K.

For the formal definition of hyperbolicity see Section 2. Note that there are rich classes of dynamical systems that satisfy the above assumptions, e.g. Anosov flows on closed manifolds (in particular geodesic flows on closed manifolds with negative sectional curvature), Axiom A flows near a basic set (e.g. geodesic flows on asymptotically hyperbolic manifolds in the sense of Mazzeo-Melrose and more concretely geodesic flows on convex co-compact hyperbolic manifolds, see [DG16, Section 5.3]), or billiard flows obtained by non-grazing convex obstacles scattering (see [KSW21]).

In the setting just described one can define a discrete subset of the complex plane $\mathbb{C}$ called *Pollicott-Ruelle resonances* of $\mathbf{X}$, directly based on the work of Dyatlov and Guillarmou [DG16]. They arise as the poles of the meromorphic continuation of the resolvent $(\mathbf{X}+\lambda)^{-1}$ and any such resonance λ_0 is associated with a finite rank residue operator Π_{λ_0}. It is possible to obtain a precise wavefront set estimate for Π_{λ_0} which in particular guarantees the existence of the flat trace $\mathrm{tr}^\flat$ and therefore the well-definedness of the *invariant Ruelle*

distributions $\mathrm{C}_c^\infty(\mathcal{M}) \ni f \mapsto \mathrm{tr}^\flat(\Pi_{\lambda_0} f)$. Here the flat trace is defined by restriction of the distributional kernel to the diagonal and subsequent integration.

With these ingredients we can formally define our object of main interest, namely the *weighted zeta function* with weight $f \in \mathrm{C}^\infty(\mathcal{M})$ at $\lambda \in \mathbb{C}$:

$$Z_f^{\mathbf{X}}(\lambda) \coloneqq \sum_\gamma \left(\frac{\exp(-\lambda T_\gamma)\,\mathrm{tr}(\alpha_\gamma)}{|\det(\mathrm{id} - \mathcal{P}_\gamma)|} \int_{\gamma^\#} f \right), \tag{1.3}$$

where the sum is over all closed trajectories γ of φ_t, T_γ is its period, $\gamma^\#$ denotes the corresponding primitive closed trajectory, $\mathcal{P}_\gamma$ its linearized Poincaré map and α_γ the parallel transport map in $\mathcal{E}$ associated with $\mathbf{X}$. For formal definitions of these objects we again refer the reader to Section 2. Our main result now reads as follows:

Theorem 1.2: Meromorphic Continuation of Weighted Zetas I

$Z_f^{\mathbf{X}}$ converges absolutely in $\{\mathrm{Re}(\lambda) \gg 1\}$ and continues meromorphically to $\mathbb{C}$. Any pole λ_0 of Z_f is a Pollicott-Ruelle resonance of $\mathbf{X}$ and if the resolvent has a pole of order $J(\lambda_0)$ at λ_0 then for $k \leq J(\lambda_0)$ we have

$$\mathrm{Res}_{\lambda=\lambda_0}\left[Z_f^{\mathbf{X}}(\lambda)(\lambda - \lambda_0)^k \right] = \mathrm{tr}^\flat\left((\mathbf{X} - \lambda_0)^k \Pi_{\lambda_0} f \right). \tag{1.4}$$

Remark 1.3. Note that in the particularly simple situation of a trivial, one-dimensional bundle $\mathcal{E} = \mathcal{M} \times \mathbb{C}$ and $\mathbf{X} = X$ our weighted zeta simplifies and is given by the following expression:

$$Z_f(\lambda) \coloneqq Z_f^{\mathbf{X}}(\lambda) = \sum_\gamma \left(\frac{\exp(-\lambda T_\gamma)}{|\det(\mathrm{id} - \mathcal{P}_\gamma)|} \int_{\gamma^\#} f \right).$$

If G is a semisimple Lie group with finite center and real rank 1, $K \subset G$ a maximally compact subgroup and $\Gamma \subset G$ a discrete, cocompact and torsion free subgroup, then the rank one locally symmetric space $\mathbf{M} = \Gamma\backslash G/K$ is a closed manifold of strictly negative curvature[1]. Thus the results of Theorem 1.2 apply to this setting. Furthermore recent results on quantum classical correspondences [GHW21] building on ideas developed in [DFG15] show that the invariant Ruelle distribution $\mathrm{C}^\infty(S\mathbf{M}) \ni f \mapsto \mathrm{tr}^\flat(\Pi_{\lambda_0} f)$ is related to quantum phase space distributions in the semiclassical limit. Using these results we recover[2] the result of Anantharaman and Zelditch for hyperbolic surfaces and generalize it to arbitrary rank one locally symmetric spaces (see Theorem 4.1 for a slightly more detailed version).

Theorem 1.4: Quantum Phase Space Distributions as Residues

Let $\mathbf{M} = \Gamma\backslash G/K$ be a compact Riemannian locally symmetric space of rank one, $\Delta_{\mathbf{M}}$ its Laplacian and φ_t the geodesic flow on $S\mathbf{M}$. Let $\rho > 0$ denote the half-sum of the restricted roots of G. Then the following holds:
Given $r > 0$ such that $-\rho + ir$ is a Ruelle resonance of φ_t then $\rho^2 + r^2$ is an eigenvalue of $\Delta_{\mathbf{M}}$ and for any $g \in \mathrm{C}_c^\infty(T^*\mathbf{M})$

$$\operatorname*{Res}_{\lambda=-\rho+ir}\left[Z_{g|_{S\mathbf{M}}}(\lambda) \right] = \sum_{l=1}^m W_{\psi_l}(g) + \mathcal{O}(1/r),$$

where the sum on the right-hand side extends over an orthonormal L^2-basis of the $\Delta_{\mathbf{M}}$-eigenspace with eigenvalue $\rho^2 + r^2$.

[1] Important special cases of such rank one locally symmetric spaces are d-dimensional manifolds of constant negative curvature (corresponding to $G = PSO(1,d), K = PSO(d)$) and even more particularly hyperbolic surfaces ($G = PSO(1,2) \cong PSL(2,\mathbb{R}), K = PSO(2)$). The latter coincides with the setting of Theorem 1.1.

[2] Actually we even slightly improve it, by allowing the much more permissive class of smooth instead of real analytic test functions.

1.3. **Applications.** Let us mention two applications of our main Theorem 1.2: For certain dynamical systems that allow for a simple combinatorial coding of the closed orbits it has been observed that Ruelle resonances can be calculated numerically in a very efficient manner by finding zeros of a dynamical determinant [Bor14, BW16, BPSW21]. These dynamical determinants are closely related to our weighted zeta functions. In fact, the logarithmic derivative of the dynamical determinant yields the weighted zeta function for the constant weight $f \equiv 1$. For the same reasons that the dynamical determinant can be efficiently calculated from the periodic orbits, we can also calculate the poles and residues of our weighted zeta functions with adapted numerical algorithms. This allows not only to perform numerical experiments on how resonances are distributed in the complex plane, but also to study the behavior of the invariant Ruelle distributions for the first time. In the appendix we show some first numerical results for the obstacle scattering on three hard discs and already observe an interesting common localization pattern of the invariant Ruelle distributions of resonances that are very close to the spectral gap (see Figure 4). Besides the 3-disc system there exists another practically feasible dynamical system where the numerical algorithms work very well, namely geodesic flows on convex co-compact hyperbolic surfaces. We conjecture that an analogous statement to Theorem 1.4 also holds for convex co-compact hyperbolic manifolds. This would then provide an efficient algorithm for the numerical calculation of localization properties of Laplace resonances on Schottky surfaces.

A second application of our main theorem is presented in [BSW22]: Three decades ago Eckhardt et al. [EFMW92] used semiclassical trace formulae to derive (in a mathematically non-rigorous way) weighted zeta functions and to predict that their residues are given by quantum phase space distributions in a semiclassical limit. In [BSW22] we explain how Theorem 1.4 can be interpreted as a rigorous version of these theoretical predictions on rank-one locally symmetric spaces. Furthermore we detail how for more general physical systems (such as convex obstacle scattering) Theorem 1.2 allows us to reinterpret the residue formulae of [EFMW92] in terms of rigorously defined twisted invariant Ruelle distributions which we investigate numerically. For symmetric 3-disc systems we find a surprisingly good agreement between the twisted invariant Ruelle distributions and quantum phase space distributions. This had been predicted by theoretical physics but does – to our best knowledge – still lack any mathematically rigorous justification until today.

1.4. **Paper organization.** We begin with a detailed introduction to our geometric setting in Section 2. This entails first the notion of open hyperbolic systems as used in [DG16] (Section 2.1) and second a setup quite similar to open hyperbolic systems but without the requirement of strict convexity (Section 2.2). In particular we define the restricted resolvent, Pollicott-Ruelle resonances and invariant Ruelle distributions. For our numerics it turns out to be useful to be able to restrict the invariant Ruelle distributions to certain hypersurfaces transversal to the flow (Section 2.3).

The following Section 3 introduces weighted zeta functions formally and proves their meromorphic continuation using a weighted trace formula (Section 3.1) and wavefront estimates for the restricted resolvent (Section 3.2 – 3.3). The proofs mostly follow the approaches of [DZ16] and [DG16] and in many parts we only outline how the arguments in these references must be adapted to fit our present situation. For full details we refer to the first author's PhD thesis [Sch23].

In Sections 2 – 3 we worked with the setting of general hyperbolic flows with compact trapped set. In Section 4 we restrict to the special case of geodesic flows on compact locally symmetric spaces of rank one. For these systems our residue formula (1.4) can be interpreted as a classical description of quantum mechanical phase space distributions known as *Patterson-Sullivan distributions*. This allows us to extend results of Anantharaman and

Zelditch [AZ07] as well as Emonds [Emo14] to general rank one, compact, locally symmetric spaces and arbitrary smooth weight functions f on their unit tangent bundle.

One of our main motivations for proving Theorem 1.2 is the fact that dynamical zeta functions can often be calculated numerically and in a very efficient manner. Our theorem then immediately allows us to calculate the invariant Ruelle distributions numerically. So far these distributions have not been studied in depth and we hope that they encode certain aspects of the spectrum similar to the Laplace eigenfunctions in quantum chaos. As a first proof-of-principle we show in Appendix A some exemplary numerical calculations of invariant Ruelle distributions for the 3-disc scattering systems. Even in the few plots provided here one can already observe some interesting behavior which could serve as a starting point for more in depth numerical investigations.

Acknowledgments. We dedicate this article to the memory of Steve Zelditch and thank him for very encourraging E-Mail discussions that we had after the appearance of this article as a preprint not long before his tragic death.

This work has received funding from the Deutsche Forschungsgemeinschaft (DFG) (Grant No. WE 6173/1-1 Emmy Noether group "Microlocal Methods for Hyperbolic Dynamics") and by an individual grant of P.S. from the Studienstiftung des Deutschen Volkes. We acknowledge helpful discussions concerning the relation to the theory of Patterson-Sullivan distributions with Joachim Hilgert. P.S. acknowledges numerous fruitful discussions with Semyon Dyatlov during a research stay at MIT in spring 2020.

Data Availability Statements. The datasets generated during and/or analysed during the current study are available from the corresponding author on reasonable request.

2. Geometric Setup

First, we introduce the notion of *open hyperbolic system* as it was used in [DG16] in Section 2.1. This setting will allow us to employ the meromorphically continued restricted resolvent which makes the upcoming proof of our main theorem in Section 3.2 rather straightforward later on. Afterwards in Section 2.2 we extend these results slightly by removing the requirement of strict convexity following ideas developed in [GMT21]. This will allow us to give a more practically feasible formulation of our main result in Section 3.3. The underlying idea was already used by the authors in their paper [KSW21] together with Benjamin Küster in the slightly more concrete setting of convex obstacle scattering. We finish this section with the proof of a dimensional reduction technique for invariant Ruelle distributions which is essential for the numerical calculations in Appendix A.

2.1. Open Hyperbolic Systems.

Let $\overline{\mathcal{U}}$ be a compact, n-dimensional smooth manifold with interior $\mathcal{U}$ and smooth boundary $\partial\mathcal{U}$. We may have $\partial\mathcal{U} = \emptyset$, i.e. the case of a closed manifold. The dynamical object of main interest is a non-vanishing C^∞-vector field X on $\overline{\mathcal{U}}$. We denote by $\varphi_t = \varphi_t^X = \mathrm{e}^{tX}$ the corresponding flow on $\overline{\mathcal{U}}$, which for $\partial\mathcal{U} \neq \emptyset$ will generally not be complete.

Before stating the dynamical requirements for X we have to introduce some auxiliary objects. Concretely, let $\rho \in \mathrm{C}^\infty(\overline{\mathcal{U}}, [0,\infty[)$ be a boundary defining function, that is $\rho^{-1}(0) = \partial\mathcal{U}$ and $\mathrm{d}\rho(x) \neq 0$ for any $x \in \partial\mathcal{U}$. Boundary defining functions always exist ([Lee12, p. 118]). Furthermore, let $\mathcal{M} \supseteq \overline{\mathcal{U}}$ be an embedding into a *compact manifold without boundary*, such that X extends onto $\mathcal{M}$ in a manner making $\mathcal{U}$ *convex*[3]:

$$x,\ \varphi_T(x) \in \mathcal{U} \text{ for some } T > 0 \quad \Longrightarrow \quad \varphi_t(x) \in \mathcal{U}\ \forall t \in [0,T]\ .$$

[3]We keep the notation X and φ_t for the continuations of our vector field and its flow; note that the continued flow is now complete by compactness of $\mathcal{M}$ so the upcoming definitions make sense.

Such an ambient manifold $\mathcal{M}$ and continuation of X always exist by [DG16, Lemma 1.1], given that (A1) below holds. Then [DG16, Lemma 1.2] asserts that the trapped set K is contained in the interior $\mathcal{U}$, i.e.

$$\Gamma_\pm \coloneqq \bigcap_{\pm t \geq 0} \varphi_t(\overline{\mathcal{U}}), \quad K \coloneqq \Gamma_+ \cap \Gamma_- \subseteq \mathcal{U} \ .$$

The set K, called the *trapped set* of X, is independent of $\mathcal{M}$ and the extension of X. Finally, let $\mathcal{E}$ be a complex C^∞-vector bundle over $\overline{\mathcal{U}}$ and $\mathbf{X} : \mathrm{C}^\infty(\overline{\mathcal{U}}, \mathcal{E}) \to \mathrm{C}^\infty(\overline{\mathcal{U}}, \mathcal{E})$ a first order differential operator.

With these preliminaries given we call the triple $(\mathcal{U}, \varphi_t, \mathbf{X})$ an open hyperbolic system if it satisfies the following dynamical requirements:

(A1) The boundary $\partial\mathcal{U}$ is *strictly convex*, i.e.:

$$x \in \partial\mathcal{U}, \ (X\rho)(x) = 0 \quad \Longrightarrow \quad X(X\rho)(x) < 0 \ .$$

This condition is independent of the choice of ρ.

(A2) The flow φ_t is *hyperbolic on* K, i.e. for any $x \in K$ the tangent space splits as

$$T_x\mathcal{M} = \mathbb{R} \cdot X(x) \oplus E_s(x) \oplus E_u(x) \ ,$$

where E_s and E_u are continuous in $x \in K$, invariant under φ_t and there exist constants $C_0, C_1 > 0$ with

$$\begin{aligned} \|\mathrm{d}\varphi_t(x)v\|_{T_{\varphi_t(x)}\mathcal{M}} &\leq C_0 \exp(-C_1 t)\|v\|_{T_x\mathcal{M}}, \qquad t \geq 0, \ v \in E_s(x) \\ \|\mathrm{d}\varphi_t(x)v\|_{T_{\varphi_t(x)}\mathcal{M}} &\geq C_0^{-1} \exp(C_1 t)\|v\|_{T_x\mathcal{M}}, \qquad t \geq 0, \ v \in E_u(x) \ . \end{aligned} \tag{2.5}$$

$\|\cdot\|$ denotes any continuous norm on the tangent bundle.[4]

(A3) $\mathbf{X}$ satisfies

$$\mathbf{X}(f\mathbf{u}) = (Xf)\mathbf{u} + f(\mathbf{X}\mathbf{u}), \qquad f \in \mathrm{C}^\infty(\overline{\mathcal{U}}), \ \mathbf{u} \in \mathrm{C}^\infty(\overline{\mathcal{U}}, \mathcal{E}) \ . \tag{2.6}$$

We also denote by $\mathbf{X}$ an arbitrary extension onto $\mathcal{M}$ that still satisfies (2.6).

Within the setting just described we will need some additional dynamical objects derived from the flow φ_t and the operator $\mathbf{X}$. We start by fixing a smooth density on $\mathcal{M}$ and a smooth scalar product on $\mathcal{E}$. That lets us consider the *transfer operator* $\exp(-t\mathbf{X}) : \mathrm{L}^2(\mathcal{M}, \mathcal{E}) \to \mathrm{L}^2(\mathcal{M}, \mathcal{E})$ associated with $\mathbf{X}$, i.e. the solution semigroup of

$$\frac{\partial}{\partial t}\mathbf{v}(t,x) = (-\mathbf{X}\mathbf{v})(t,x), \qquad \mathbf{v}(0,\cdot) = \mathbf{u} \ .$$

This allows us to define the linear *parallel transport* map at $x \in \mathcal{U}$ and $t > 0$ such that $\varphi_t(x) \in \mathcal{U}$:

$$\begin{aligned} \alpha_{x,t} : \mathcal{E}_x &\longrightarrow \mathcal{E}_{\varphi_t(x)} \\ u &\longmapsto \left(\mathrm{e}^{-t\mathbf{X}}\mathbf{u}\right)(\varphi_t(x)) \ , \end{aligned}$$

where $\mathbf{u}$ is some smooth section of $\mathcal{E}$ with $\mathbf{u}(x) = u$. The definition does not depend on the choice of $\mathbf{u}$ because $\mathbf{u}(x) = 0$ implies $\left(\mathrm{e}^{-t\mathbf{X}}\mathbf{u}\right)(\varphi_t(x)) = 0$ by [DG16, Eq. (0.8)] and an expansion in terms of a local frame for $\mathcal{E}$. In particular, if $\gamma(t) = \varphi_t(x_0)$ is a closed orbit with period T_γ then $\alpha_{x_0,T_\gamma} = \alpha_{x_0,t}^{-1} \circ \alpha_{\gamma(t),T_\gamma} \circ \alpha_{x_0,t}$ and the trace

$$\mathrm{tr}(\alpha_\gamma) \coloneqq \mathrm{tr}(\alpha_{\gamma(t),T_\gamma})$$

is well-defined independent of t.

Next we define the so-called *linearized Poincaré map* which at $x \in \mathcal{U}$ and $t > 0$ satisfying $\varphi_t(x) \in \mathcal{U}$ is defined as the linear map

$$\mathcal{P}_{x,t} \coloneqq \mathrm{d}\varphi_{-t}(x)\big|_{E_s(x)\oplus E_u(x)} \ .$$

[4]The definition does not depend on the specific norm as K is compact. The same holds for upcoming arbitrary choices of densities, etc.

Again we will use this map if x is located on a closed trajectory γ. In this case $\mathcal{P}_{x,T_\gamma}$ is an endomorphism and $\det(\mathrm{id}-\mathcal{P}_\gamma) \coloneqq \det(\mathrm{id}-\mathcal{P}_{x,T_\gamma})$ is independent of x because similarly as for the parallel transport one finds that $\mathcal{P}_{x,T_\gamma}$ is conjugate to any $\mathcal{P}_{y,T_\gamma}$ provided y also belongs to γ.

We finish this section by recasting the definition of *invariant Ruelle distributions* from [GHW21] into our setting: Let $(\overline{\mathcal{U}},\varphi_t,\mathbf{X})$ be an open hyperbolic system, then we denote by $\mathbf{R}(\lambda) \coloneqq \mathbf{1}_{\mathcal{U}}(\mathbf{X}+\lambda)^{-1}\mathbf{1}_{\mathcal{U}} : \mathrm{C}_{\mathrm{c}}^\infty(\mathcal{U},\mathcal{E}) \to \mathcal{D}'(\mathcal{U},\mathcal{E})$ λ_0 its *restricted resolvent*. In [DG16] it was proven that $\mathbf{R}(\lambda)$ continues meromorphically onto $\mathbb{C}$ and its poles are called *Ruelle resonances*. Furthermore, the residue of $\mathbf{R}(\lambda)$ at a resonance λ_0 is a finite rank operator $\Pi_{\lambda_0} : \mathrm{C}_{\mathrm{c}}^\infty(\mathcal{U},\mathcal{E}) \to \mathcal{D}'(\mathcal{U},\mathcal{E})$ that satisfies [DG16, Thm. 2]

$$\mathbf{X}\Pi_{\lambda_0} = \Pi_{\lambda_0}\mathbf{X}, \quad \operatorname{supp}\left(K_{\Pi_{\lambda_0}}\right) \subseteq \Gamma_+ \times \Gamma_-, \quad \mathrm{WF}'\left(\Pi_{\lambda_0}\right) \subseteq E_+^* \times E_-^*, \tag{2.7}$$

where $K_{\Pi_{\lambda_0}}$ is the Schwartz kernel of Π_{λ_0}, WF' denotes the wavefront set, and $E_\pm^*$ are subbundles of $T^*\mathcal{U}$ over $\Gamma_\mp$ constructed in [DG16, Lemma 1.10]. In particular, the support property in (2.7) shows that the restriction $K_{\Pi_{\lambda_0}}\big|_\Delta$ to the diagonal $\Delta \subseteq \mathcal{U}\times\mathcal{U}$ is supported in $\Gamma_+ \cap \Gamma_- = K$ and therefore yields an element of $\mathcal{E}'(\mathcal{U})$. Now combining this with the wavefront estimate [DG16, Eq. (0.14)] of $K_{\Pi_{\lambda_0}}$ guarantees that the following map is well-defined:

$$\mathcal{T}_{\lambda_0} : \begin{cases} \mathrm{C}^\infty(\mathcal{U}) & \longrightarrow \quad \mathbb{C} \\ f & \longmapsto \ \mathrm{tr}^\flat\left(\Pi_{\lambda_0} f\right) \end{cases}. \tag{2.8}$$

The generalized density $\mathcal{T}_{\lambda_0}$ is called the *invariant Ruelle distribution* associated with λ_0. Note that we can re-write $\mathcal{T}_{\lambda_0}(f) = \mathrm{tr}^\flat(\Pi_{\lambda_0} f) = \mathrm{tr}^\flat(f\Pi_{\lambda_0})$ as the trace is cyclic.

The adjective *invariant* is justified because $\mathcal{T}_{\lambda_0}$ is indeed invariant under the flow: The Leibniz rule (2.6) implies $\Pi_{\lambda_0}(Xf) = \Pi_{\lambda_0}\mathbf{X}f - \Pi_{\lambda_0} f\mathbf{X}$ which together with the vanishing of the commutator (2.7) and the cyclic property yields

$$\begin{aligned} \mathcal{T}_{\lambda_0}(Xf) &= \mathrm{tr}^\flat\left(\Pi_{\lambda_0}\mathbf{X}f - \Pi_{\lambda_0} f\mathbf{X}\right) \\ &= \mathrm{tr}^\flat\left(\mathbf{X}\Pi_{\lambda_0} f - \mathbf{X}\Pi_{\lambda_0} f\right) = 0. \end{aligned}$$

2.2. **Removing Strict Convexity for Resolvents.** In practical applications it often turns out to be difficult to verify the strict convexity condition. To circumvent this difficulty we recast the meromorphic continuation achieved in [DG16] into a simpler setting by constructing a perturbation of the generator X of φ_t and of the operator $\mathbf{X}$. Our proof mostly follows [GMT21] which uses techniques developed in [CE71] and [Rob80]. For a very similar application but without the extension to the vector valued case see [DG18].

Let $\mathcal{M}$ be a smooth manifold with manifold interior $\mathring{\mathcal{M}}$ and smooth, possibly empty boundary, X a smooth, nowhere vanishing vector field on $\mathcal{M}$, and φ_t the flow associated with X. Furthermore, let a smooth, complex vector bundle $\mathcal{E}$ over $\mathcal{M}$ together with a first-order differential operator $\mathbf{X} : \mathrm{C}^\infty(\mathcal{M},\mathcal{E}) \to \mathrm{C}^\infty(\mathcal{M},\mathcal{E})$ be given. We assume that $\mathbf{X}$ satisfies the Leibniz rule (2.6), that the trapped set K of φ_t defined in (1.2) is compact and satisfies $K \subseteq \mathring{\mathcal{M}}$, and finally that φ_t is hyperbolic on K as defined in (2.5).

First we observe that we may assume $\mathcal{M}$ to be compact with smooth, non-empty boundary: If it is not then there exists a compact submanifold with smooth boundary of $\mathcal{M}$ which still contains K in its manifold interior. This follows by standard tools in smooth manifold theory, namely via a smooth exhaustion function ([Lee12, Prop. 2.28]) combined with Sard's theorem. If necessary, we may replace $\mathcal{M}$ with this submanifold.

Now [GMT21, Prop. 2.2 and Lemma 2.3] immediately yields the existence of a compact $\overline{\mathcal{U}}_0 \subseteq \mathcal{M}$ with manifold interior $\mathcal{U}_0$ and smooth boundary $\partial\mathcal{U}_0$ such that $K \subseteq \mathcal{U}_0$, and the existence of a smooth vector field X_0 on $\mathcal{M}$ such that $\partial\mathcal{U}_0$ is strictly convex w.r.t. X_0 in the above sense and $X - X_0$ is supported in an arbitrarily small neighbourhood of $\partial\mathcal{U}_0$. In addition, the trapped set of X_0 coincides with K. Finally, we may assume both the flow

φ_t as well as the flow φ_t^0 of X_0 to be complete by embedding $\mathcal{M}$ into an ambient closed manifold and extending X, X_0 arbitrarily. In this setting we define the *escape times* from some compact set $A \subseteq \mathcal{M}$ to be

$$\tau_A^{\pm}(x) \coloneqq \pm \sup\left\{t \geq 0 \,\middle|\, \varphi_{\pm s}(x) \in A \,\forall s \in [0,t]\right\},$$
$$\tau_A^{0,\pm}(x) \coloneqq \pm \sup\left\{t \geq 0 \,\middle|\, \varphi_{\pm s}^0(x) \in A \,\forall s \in [0,t]\right\}, \qquad x \in A.$$

The respective *forward and backward trapped sets* are then given by

$$\Gamma_{\pm}(A) \coloneqq \left\{x \in A \,\middle|\, \tau_A^{\mp}(x) = \mp\infty\right\}, \quad \Gamma_{\pm}^0(A) \coloneqq \left\{x \in A \,\middle|\, \tau_A^{0,\mp}(x) = \mp\infty\right\},$$

such that in particular we have $K = \Gamma_+(\overline{\mathcal{U}}_0) \cap \Gamma_-(\overline{\mathcal{U}}_0)$.

Next we require an appropriate perturbation of $\mathbf{X}$ which satisfies the Leibniz rule (2.6) with respect to X_0 instead of X. But this is straightforward: Given any section $\mathbf{u} \in \mathrm{C}^\infty(\overline{\mathcal{U}}, \mathcal{E})$ and $x \in \overline{\mathcal{U}}$ we consider a local frame $\mathbf{e}_i$ in a neighbourhood of x. Then $\mathbf{u}$ expands as $\mathbf{u} = \sum_i u^i \mathbf{e}_i$ in this neighbourhood and we define

$$\mathbf{X}_0\mathbf{u} \coloneqq \mathbf{X}\mathbf{u} + \sum_i \left((X_0 - X)\, u^i\right) \cdot \mathbf{e}_i.$$

The second term on the right-hand side obviously yields a well-defined first-order differential operator and $\mathbf{X} - \mathbf{X}_0$ is supported near $\partial\mathcal{U}_0$. Given $f \in \mathrm{C}^\infty(\overline{\mathcal{U}})$ we can verify the Leibniz rule via the following calculation in a neighbourhood of x:

$$\begin{aligned}
\mathbf{X}_0(f \cdot \mathbf{u}) &= \mathbf{X}(f \cdot \mathbf{u}) + \sum_i \left((X_0 - X)\, f u^i\right) \cdot \mathbf{e}_i \\
&= (Xf) \cdot \mathbf{u} + f \cdot (\mathbf{X}\mathbf{u}) + (X_0 f - Xf) \cdot \mathbf{u} + f \cdot \sum_i \left((X_0 - X)\, u^i\right) \cdot \mathbf{e}_i \\
&= f \cdot (\mathbf{X}_0\mathbf{u}) + (X_0 f)\, \mathbf{u}.
\end{aligned}$$

We are now in a position to state and prove the main result of this section. For some open set $\mathcal{O} \subseteq \mathcal{M}$, a section $\mathbf{u} \in \mathrm{C}_{\mathrm{c}}^\infty(\mathcal{O}, \mathcal{E})$, and a spectral parameter $\lambda \in \mathbb{C}$ consider the *resolvent* given by the following formal integral:

$$\mathbf{R}_{\mathcal{O}}(\lambda)\mathbf{u}(x) \coloneqq \int_0^{-\tau_{\overline{\mathcal{O}}}^-(x)} \mathrm{e}^{-(\mathbf{X}+\lambda)t} \mathbf{u}(x) \mathrm{d}t, \tag{2.9}$$

where $\exp(-\mathbf{X}t)$ denotes the transfer operator associated with $\mathbf{X}$ as defined in the previous section. At this point, the expression in (2.9) remains formal because on the one hand τ^- may be of low regularity and on the other hand the integral may not converge for $\tau^-(x) = -\infty$. By choosing an appropriate $\mathcal{O}$ we can get around these issues and obtain the following theorem:

Theorem 2.1: Meromorphic Resolvent Without Strict Convexity

Let $\mathcal{M}$ be a smooth manifold with smooth boundary, X a smooth, nowhere vanishing vector field on $\mathcal{M}$, and K the trapped set of the flow φ_t of X. Also, let $\mathcal{E}$ be a smooth, complex vector bundle over $\mathcal{M}$ and $\mathbf{X}$ a first-order differential operator on $\mathcal{E}$.
Assume that $\mathbf{X}$ satisfies the Leibniz rule (2.6), K is compact, $K \subseteq \mathring{\mathcal{M}}$, and φ_t is hyperbolic on K. Then there exists an arbitrarily small compact $\overline{\mathcal{U}} \subseteq \mathcal{M}$ which contains K in its interior $\mathcal{U}$ such that

(1) $\mathbf{R}_{\mathcal{U}}(\lambda)$ is well-defined for $\mathrm{Re}(\lambda) \gg 0$ as an operator on $\mathrm{L}^2(\mathcal{M}, \mathcal{E})$ and satisfies $(\mathbf{X} + \lambda)\mathbf{R}_{\mathcal{U}}(\lambda) = \mathrm{id}_{\mathrm{C}_{\mathrm{c}}^\infty(\mathcal{U},\mathcal{E})}$,
(2) $\mathbf{R}_{\mathcal{U}}(\lambda)$ continues meromorphically to $\mathbb{C}$ as a family of operators $\mathrm{C}_{\mathrm{c}}^\infty(\mathcal{U}, \mathcal{E}) \to \mathcal{D}'(\mathcal{U}, \mathcal{E})$ with poles of finite rank,
(3) the residue Π_{λ_0} of $\mathbf{R}_{\mathcal{U}}(\lambda)$ satisfies (2.7).

Proof. For this proof we assume the setting and notation introduced in this section. Observe that both $X = X_0$ and $\mathbf{X} = \mathbf{X}_0$ on any compact $\overline{\mathcal{U}}$ with $\overline{\mathcal{U}} \subseteq \mathcal{U}_0$. If we additionally had for all $t \geq 0$ the property

$$x, \varphi_t^0(x) \in \overline{\mathcal{U}} \quad \Longrightarrow \quad \varphi_s^0(x) \in \overline{\mathcal{U}} \, \forall s \in [0,t], \tag{2.10}$$

then it would immediately follow for any $x \in \mathcal{U}$, $\mathbf{u} \in \mathrm{C}_{\mathrm{c}}^\infty(\mathcal{U}, \mathcal{E})$ and $\mathrm{Re}(\lambda) \gg 0$ that

$$\begin{aligned}\mathbf{R}_{\mathcal{U}}(\lambda)\mathbf{u}(x) &= \int_0^{-\tau_{\overline{\mathcal{U}}}^-(x)} \mathrm{e}^{-(\mathbf{X}+\lambda)t}\mathbf{u}(x)\mathrm{d}t \\ &= \int_0^\infty \mathrm{e}^{-(\mathbf{X}_0+\lambda)t}\mathbf{u}(x)\mathrm{d}t = \mathbf{1}_{\mathcal{U}} \left(\mathbf{X}_0 + \lambda\right)^{-1} \mathbf{1}_{\mathcal{U}}\mathbf{u}(x),\end{aligned}$$

and the claims (1) - (3) would be shown by a straightforward application of the material from [DG16] recalled in Section 2.1.

It therefore remains to construct an arbitrarily small $\overline{\mathcal{U}}$ satisfying (2.10). First note that we may assume (2.10) to hold on $\overline{\mathcal{U}}_0$ by choosing the extension of X_0 appropriately, see [DG16, Eq. (0.2)]. Given any open $\mathcal{O}$ with $K \subseteq \mathcal{O} \subseteq \overline{\mathcal{O}} \subseteq \mathcal{U}_0$ we can then set

$$\overline{\mathcal{U}} := \varphi_{-T}^0(\overline{\mathcal{U}}_0) \cap \overline{\mathcal{U}}_0 \cap \varphi_T^0(\overline{\mathcal{U}}_0),$$

where choosing $T > 0$ large enough guarantees $\overline{\mathcal{U}} \subseteq \mathcal{O}$ by [DG16, Lemma 1.4]. It is now easily verified that $\overline{\mathcal{U}}$ satisfies (2.10). □

In Section 3 we will show that the poles of $\mathbf{R}_{\mathcal{U}}(\lambda)$ are independent of the choice of a set $\overline{\mathcal{U}}$ (and also independent of $\overline{\mathcal{U}}_0$). They are called the *Pollicott-Ruelle resonances* of φ_t and will figure prominently below as the poles of our weighted zeta function. Furthermore we can define invariant Ruelle distributions $\mathcal{T}_{\lambda_0}$ in the setting of Theorem 2.1 by the same formula (2.8) presented in the previous Section 2.1.

Remark 2.2. The residue Π_{λ_0} at a resonance λ_0 is also independent of the set $\overline{\mathcal{U}}$ in the sense that

$$\Pi_{\lambda_0}\big|_{\mathrm{C}_{\mathrm{c}}^\infty(\mathcal{U}',\mathcal{E})} = \Pi'_{\lambda_0},$$

where $\overline{\mathcal{U}}' \subseteq \mathcal{U}$ denotes a second set on which the resolvent can be continued meromorphically and Π'_{λ_0} denotes the residue of this continuation $\mathbf{R}_{\mathcal{U}'}(\lambda)$. This follows immediately by uniqueness of meromorphic continuation and the fact that the restriction of $\mathbf{R}_{\mathcal{U}}(\lambda)$ to $\mathrm{C}_{\mathrm{c}}^\infty(\mathcal{U}', \mathcal{E})$ coincides with $\mathbf{R}_{\mathcal{U}'}(\lambda)$ for $\mathrm{Re}(\lambda) \gg 0$. In particular, note that this implies the independence of $\mathcal{T}_{\lambda_0}$ from $\mathcal{U}$. An analogous independence statement holds for $\overline{\mathcal{U}}_0$.

2.3. **Restricting Ruelle Distributions.** One of the main applications of our weighted zeta functions Z_f is the concrete numerical calculation of invariant Ruelle distributions $\mathcal{T}_{\lambda_0}$ for certain 3-dimensional dynamical systems. For ease of calculation as well as plotting we would like to reduce this to a reasonable distribution on a 2-dimensional space. In this section we present a general theorem which allows just this.

For the general setup let $\mathcal{T}_{\lambda_0} \in \mathcal{D}'(\mathcal{M})$ be an invariant Ruelle distribution in the setting of Theorem 2.1. We will call a smooth submanifold $\Sigma \subseteq \mathcal{M}$ a *Poincaré section for* φ_t if Σ has codimension one and is transversal to φ_t on the trapped set K, i.e. for each $x \in K$ we have

$$T_x\mathcal{M} = \mathbb{R} \cdot X(x) \oplus T_x\Sigma,$$

where as above X denotes the generator of φ_t.

Lemma 2.3: Restriction of Ruelle Distributions

Let $\mathcal{T}_{\lambda_0}$ be an invariant Ruelle distribution for a dynamical system $(\mathcal{M}, \varphi_t, \mathbf{X})$ as in Theorem 2.1 and $\Sigma \subseteq \mathcal{M}$ a Poincaré section for φ_t. Then the pullback of $\mathcal{T}_{\lambda_0}$ along $\iota_\Sigma : \Sigma \hookrightarrow \mathcal{U}$ is well-defined and will be called the *restriction to* Σ:

$$\mathcal{T}_{\lambda_0}\big|_\Sigma := (\iota_\Sigma)^* \, \mathcal{T}_{\lambda_0} \in \mathcal{D}'(\Sigma). \tag{2.11}$$

Proof. For the existence of the pullback we use the classical Hörmander condition [Hör13, Theorem 8.2.4] similar to the proof of Theorem 1.2, i.e. what we need to show is

$$\mathrm{WF}\left(\mathcal{T}_{\lambda_0}\right) \cap N^*\Gamma_{\iota_\Sigma} = \{0\},$$

with $N^*\Gamma_{\iota_\Sigma}$ the conormal bundle to the graph of ι_Σ. Now the invariance property $X\mathcal{T}_{\lambda_0} = 0 \in \mathrm{C}^\infty(\mathcal{M})$ proven above immediately implies the following estimate on $\mathrm{WF}\left(\mathcal{T}_{\lambda_0}\right)$:

$$\mathrm{WF}\left(\mathcal{T}_{\lambda_0}\right) \subseteq E_s^* \oplus E_u^* \subseteq T^*\mathcal{M}.$$

Now the conormal bundle is explicitly given by

$$N^*\Gamma_{\iota_\Sigma} = \left\{ (x,\xi) \,\middle|\, x \in \Sigma,\, \xi\big|_{T_x\Sigma} = 0 \right\} \subseteq T^*\mathcal{M},$$

and an element $(x,\xi) \in \mathrm{WF}(\mathcal{T}_{\lambda_0}) \cap N^*\Gamma_{\iota_\Sigma}$ therefore satisfies $x \in K \cap \Sigma$, $\xi(T_x\Sigma) = 0$ and $\xi(X_x) = 0$ by the definition of E_s^* and E_u^*. Now the transversality condition $T_x\mathcal{M} = \mathbb{R}\cdot X(x) \oplus T_x\Sigma$ yields $\xi = 0$. □

3. Proof of the Main Theorem

In this section we prove our main theorem, namely the *meromorphic continuation* of the following weighted zeta function defined in terms of closed trajectories γ of an open hyperbolic system $(\mathcal{U}, \varphi_t, \mathbf{X})$ and a weight $f \in \mathrm{C}^\infty(\mathcal{U})$:

$$Z_f^{\mathbf{X}}(\lambda) \coloneqq \sum_\gamma \left(\frac{\exp\left(-\lambda T_\gamma\right) \mathrm{tr}(\alpha_\gamma)}{|\det(\mathrm{id} - \mathcal{P}_\gamma)|} \int_{\gamma^\#} f \right), \qquad \lambda \in \mathbb{C}.$$

In Section 3.2 we state and prove this meromorphic continuation result using a trace formula presented in Section 3.1. In practice the defining properties of open hyperbolic systems are rather cumbersome to handle. We therefore remove these requirements in Section 3.3 to obtain the result cited in the introduction.

Full details can be found either in an earlier arXiv version of this paper or in the first author's PhD thesis [Sch23]. At several points where rather technical passages would only require straightforward modifications of existing results we leave out the details and point to the corresponding literature instead.

3.1. A Weighted Trace Formula.

Our main tool for connecting the restricted resolvent with our weighted zeta function is a weighted version of the Atiyah-Bott-Guillemin trace formula. In this section we present the statement together with a short sketch of the proof. A formulation for open systems but without weight function can be found in [DG16, Eq. (4.6)] and an analogous result for the compact case is presented in [DZ16, Eq. (2.4)].

Lemma 3.1: Weighted Atiyah-Bott-Guillemin Trace Formula

For any cut-offs $\chi \in \mathrm{C}_\mathrm{c}^\infty(\mathbb{R}\backslash\{0\})$ and $\widetilde{\chi} \in \mathrm{C}_\mathrm{c}^\infty(\mathcal{U})$, with $\widetilde{\chi} \equiv 1$ near the trapped set K, the following holds:

$$\mathrm{tr}^\flat\left(\int_{\mathbb{R}} \chi(t) \widetilde{\chi} \mathrm{e}^{-t\mathbf{X}} f \widetilde{\chi} \mathrm{d}t \right) = \sum_\gamma \frac{\chi(T_\gamma)\mathrm{tr}(\alpha_\gamma)}{|\det(\mathrm{id} - \mathcal{P}_\gamma)|} \int_{\gamma^\#} f \,, \tag{3.12}$$

where the sum is over all closed orbits γ of φ_t.

Proof. The proof is directly adapted from [DG16, Sec. 4.1] and [DZ16, App. B] but the main points can already be found in [Gui77, §2 of Lecture 2].

For a given $\chi \in \mathrm{C}_\mathrm{c}^\infty(\mathbb{R}\backslash\{0\})$ one defines $\mathbf{A}_{f,\chi} \coloneqq \int_{\mathbb{R}} \chi(t)\widetilde{\chi}\mathrm{e}^{-t\mathbf{X}} f \widetilde{\chi} \mathrm{d}t$ as an operator

$$\mathbf{A}_{f,\chi} : \mathrm{C}^\infty(\mathcal{M},\mathcal{E}) \longrightarrow \mathrm{C}^\infty(\mathcal{M},\mathcal{E}) \subseteq \mathcal{D}'(\mathcal{M},\mathcal{E}) \,,$$

and via the Schwartz kernel theorem we can consider the integrand $\widetilde{\chi}\mathrm{e}^{-t\mathbf{X}}f\widetilde{\chi}$ as an operator[5]

$$\mathrm{C}_{\mathrm{c}}^{\infty}(\mathbb{R}\backslash\{0\}) \to \mathcal{D}'(\mathcal{M}\times\mathcal{M}, \mathcal{E}\boxtimes\mathcal{E}^*) \ .$$

Applying the Schwartz kernel theorem once more we therefore obtain as its kernel a distribution $\mathbf{K}_f(x,y,t) \in \mathcal{D}'(\mathcal{M}\times\mathcal{M}\times\mathbb{R}\backslash\{0\}, \mathcal{E}\boxtimes\mathcal{E}^*)$:

$$\mathbf{A}_{f,\chi}(\mathbf{u})(x) = \int_{\mathcal{M}\times\mathbb{R}} \mathbf{K}_f(x,y,t)\mathbf{u}(y)\chi(t)\mathrm{d}y\mathrm{d}t \ ,$$

where $\mathrm{d}y$ is the same (fixed but arbitrary) density on $\mathcal{M}$ used to define the kernel of $\mathbf{A}_{f,\chi}$ and $\mathbf{u} \in \mathrm{C}^{\infty}(\mathcal{M},\mathcal{E})$ is any smooth section of the bundle $\mathcal{E}$. At this point the classical [Hör13, Thm. 8.2.12] immediately shows that

$$\mathrm{WF}(\mathbf{K}_{f,\chi}) \subseteq \{(x,y,\xi,\eta) \,|\, \exists t \in \mathrm{supp}(\chi) \text{ with } (x,y,t,\xi,\eta,0) \in \mathrm{WF}(\mathbf{K}_f)\} \ , \tag{3.13}$$

where $\mathbf{K}_{f,\chi} \in \mathcal{D}'(\mathcal{M}\times\mathcal{M}, \mathcal{E}\boxtimes\mathcal{E}^*)$ denotes the kernel of $\mathbf{A}_{f,\chi}$. As $\mathbf{K}_{f,\chi}$ is compactly supported by virtue of $\widetilde{\chi}$, we are left with the task of estimating the wavefront set of the kernel $\mathbf{K}_f$.

As in the references cited above we can calculate a local coordinate expression for $\mathbf{K}_f$ to verify that this kernel is a delta distribution on the graph $\Gamma_\varphi := \{(x,\varphi_{-t}(x),t) \,|\, x \in \mathcal{M},\, t\in\mathbb{R}\}$ of φ_{-t}, multiplied by smooth functions. The latter include suitable cutoffs, the coordinate expressions of the transfer operator $\exp(-t\mathbf{X})$ and the weight f.

The final wavefront set is therefore contained in the conormal bundle $N^*\Gamma_\varphi$ given by ([Hör13, Example 8.2.5]):

$$N^*\Gamma_\varphi := \left\{(x,y,t,\xi,\eta,\tau) \in T^*(\mathcal{M}\times\mathcal{M}\times\mathbb{R}) \,\middle|\, y=\varphi_{-t}(x),\ (\xi,\eta,\tau)\big|_{T(\Gamma_\varphi)} = 0\right\} \ ,$$

and substituting into (3.13) we may estimate the wavefront set of the right-hand side of the trace formula as follows:

$$\begin{aligned}\mathrm{WF}(\mathbf{K}_{f,\chi}) \subseteq \big\{(x,y,\xi,\eta) \in T^*(\mathcal{M}\times\mathcal{M}) \,\big|\, &\exists t\in\mathrm{supp}(\chi)\, x,y\in\mathrm{supp}(\widetilde{\chi}) : \\ &y=\varphi_{-t}(x),\ \eta\neq 0,\ \xi = -(\mathrm{d}\varphi_{-t}(x))^T\eta,\ \langle\eta, X_y\rangle = 0\big\} \ .\end{aligned} \tag{3.14}$$

This set does not intersect $\{(x,x,\xi,-\xi) \,|\, \xi\in T_x^*\mathcal{M}\}$ by the hyperbolicity of φ_t on closed trajectories. Thus, the flat trace on the left-hand side is well defined.

The pullback of $\mathbf{K}_f$ is supported on the closed trajectories of φ_t. As in [DZ16, Lemma B.1], it therefore makes sense to prove a local version of the final trace formula:

Lemma 3.2: Local Weighted Trace Formula

Suppose $x_0 \in \mathcal{U}$ and $T\neq 0$ is such that $\varphi_T(x_0) = x_0$. Then there are $\varepsilon>0$ and an open neighbourhood $x_0\in U\subseteq\mathcal{U}$ with $\varphi_s(x_0)\in U$ for any $|s|<\varepsilon$ and such that for any $\rho(x,t) = \sigma(x)\chi(t) \in \mathrm{C}_{\mathrm{c}}^{\infty}(U\times]T-\varepsilon, T+\varepsilon[)$ the following holds:

$$\begin{aligned}\mathrm{tr}^\flat\left(\int_{\mathbb{R}}\rho(x,t)\mathbf{K}_f(x,y,t)\mathrm{d}t\right) &= \int_{\mathbb{R}\times\mathcal{M}}\rho(x,t)\mathbf{K}_f(x,x,t)\mathrm{d}t\mathrm{d}x \\ &= \frac{\mathrm{tr}(\alpha_\gamma)}{|\det(\mathrm{id}-\mathcal{P}_\gamma)|}\int_{-\varepsilon}^{\varepsilon}\rho(\varphi_s(x_0),T)f(\varphi_s(x_0))\mathrm{d}s\end{aligned} \tag{3.15}$$

Proof. Using adapted coordinates similar to the proof of [DZ16, Lemma B.1] one may reduce the flat trace to an integral of delta distributions of the general form $\delta(x-g(x))$. Formula (3.15) then follows from a straightforward calculation.

Note that additional care must be taken to account for the weight function f, but this basically amounts to the fact that the cutoffs present in [DZ16, Lemma B.1] are no longer constant on closed trajectories and therefore do not cancel. □

[5]Given bundles $\mathcal{E}_i \to M_i$ then $\mathcal{E}_1\boxtimes\mathcal{E}_2$ denotes the tensor product of the pullbacks of the $\mathcal{E}_i$ onto $M_1\times M_2$. Note that [DG16] uses the notation $\mathrm{End}(\mathcal{E})$ for the bundle $\mathcal{E}\boxtimes\mathcal{E}^*$ over $\mathcal{M}\times\mathcal{M}$.

Now a *partition of unity* argument combining the compactness of closed trajectories with the semi-group property of the flow finishes the proof of Lemma 3.1. □

3.2. **Continuation on Open Hyperbolic Systems.** We prove meromorphic continuation together with an explicit formula for the Laurent coefficients of Z_f:

Theorem 3.3: Meromorphic Continuation of Weighted Zetas I

The weighted zeta function $Z_f^{\mathbf{X}}$ defined in (1.3) for open hyperbolic systems converges absolutely in $\{\mathrm{Re}(\lambda) \gg 1\}$ and continues meromorphically to $\{\lambda \in \mathbb{C}\}$. Any pole λ_0 of Z_f is a Pollicott-Ruelle resonance of $\mathbf{X}$ and if the pole λ_0 has order $J(\lambda_0)$ then for $k \leq J(\lambda_0)$ we have

$$\mathrm{Res}_{\lambda=\lambda_0}\left[Z_f^{\mathbf{X}}(\lambda)(\lambda-\lambda_0)^k\right] = \mathrm{tr}^\flat\left((\mathbf{X}-\lambda_0)^k \Pi_{\lambda_0} f\right).$$

Proof. First, we prove that the formal expression (1.3) defines a holomorphic function in $\{\mathrm{Re}(\lambda) \gg 0\}$ by showing uniform convergence on compact sets. To this end, we treat every term separately and then combine the results for a final estimate:

(1.) $\mathrm{N}(T) \coloneqq |\{\gamma \,|\, T_\gamma \leq T\}| \leq C_0 \mathrm{e}^{C_1 T}$ for constants $C_0, C_1 > 0$ by [DG16, Lemma 1.17].
(2.) $|\det(\mathrm{id} - \mathcal{P}_\gamma)| \geq C_2 > 0$ by uniform contraction and expansion.
(3.) $|\mathrm{tr}(\alpha_\gamma)| \leq C_4 \mathrm{e}^{C_3 T_\gamma}$ by the operator norm estimate on the transfer operator $\mathrm{e}^{-t\mathbf{X}}$.

Combining (1.), (2.) and (3.) we get

$$\sum_\gamma \left| \frac{\mathrm{e}^{-\lambda T_\gamma}\mathrm{tr}(\alpha_\gamma)}{|\det(\mathrm{id}-\mathcal{P}_\gamma)|} \int_{\gamma\#} f \right| \leq \sum_{n\in\mathbb{N}} \frac{nC_0C_4}{C_2} \mathrm{e}^{(C_1+C_3)n} |\mathrm{e}^{-(n-1)\lambda}| |f|_K \leq C \sum_{n\in\mathbb{N}} n \left(\mathrm{e}^{C-\mathrm{Re}(\lambda)}\right)^n$$

$Z_f(\lambda)$ thus converges uniformly if λ varies in a compact subset of $\mathrm{Re}(\lambda) > C$. In conclusion, the function $Z_f(\lambda)$ is holomorphic on some right halfplane.

The proof proceeds by expressing the weighted zeta function as the flat trace of an expression involving the *restricted resolvent* and using the trace formula presented in Section 3.1 as the main tool. The procedure closely follows [DZ16, §4]: We begin by choosing $0 < t_0 < T_\gamma \, \forall \gamma$, $\chi_T \in \mathrm{C}_\mathrm{c}^\infty(]t_0/2, T+1[)$ and $\chi_T \equiv 1$ on $[t_0, T]$. Furthermore, we assume t_0 small enough such that $\varphi_{-t_0}(\mathrm{supp}(\widetilde{\chi})) \subseteq \mathcal{U}$. Then we can define the family of operators

$$B_T \coloneqq \int_0^\infty \chi_T(t) \mathrm{e}^{-\lambda t} \left(\widetilde{\chi} \mathrm{e}^{-t\mathbf{X}} \widetilde{\chi} f\right) \mathrm{d}t \,,$$

and Lemma 3.1 shows that, for $\mathrm{Re}(\lambda) \gg 1$,

$$\lim_{T\to\infty} \mathrm{tr}^\flat(B_T) = \lim_{T\to\infty} \sum_\gamma \frac{\chi_T(T_\gamma)\mathrm{e}^{-\lambda T_\gamma}\mathrm{tr}(\alpha_\gamma)}{|\det(\mathrm{id}-\mathcal{P}_\gamma)|} \int_{\gamma\#} f = \sum_\gamma \frac{\mathrm{e}^{-\lambda T_\gamma}\mathrm{tr}(\alpha_\gamma)}{|\det(\mathrm{id}-\mathcal{P}_\gamma)|} \int_{\gamma\#} f \,.$$

By [DZ16, Lemma 2.8] we may re-express $\mathrm{tr}^\flat(B_T)$ using a family of smoothing operators E_ε and the limit $\varepsilon \to 0$. The scalar-valued version of [DZ16] is directly applicable by choosing our E_ε to be diagonal in the fiber variable.

As in [DZ16, §4] we split the resulting integrals in a vanishing part and a part strictly separated from $t = 0$. These calculations require no significant modifications as the weight f can simply be carried along together with the cutoffs necessary to account for the open dynamics.

A simple calculation combined with an adaptation of [DZ16, Lemma 4.1] shows that the limits in $T \to \infty$ and $\varepsilon \to 0$ may be exchanged, and doing so yields

$$\begin{aligned} Z_f^{\mathbf{X}}(\lambda) &= \lim_{T\to\infty} \mathrm{tr}^\flat(B_T) = \lim_{\varepsilon\to 0} \int_0^\infty \mathrm{e}^{-\lambda(t+t_0)} \mathrm{tr}\left(E_\varepsilon \widetilde{\chi} \mathrm{e}^{-(t+t_0)\mathbf{X}} \widetilde{\chi} f E_\varepsilon\right) \mathrm{d}t \\ &= \mathrm{e}^{-\lambda t_0} \lim_{\varepsilon\to 0} \mathrm{tr}\left(E_\varepsilon \widetilde{\chi} \mathrm{e}^{-t_0\mathbf{X}} (\mathbf{X}+\lambda)^{-1} \widetilde{\chi} f E_\varepsilon\right) \,, \end{aligned} \tag{3.16}$$

which at first only holds for $\mathrm{Re}(\lambda) \gg 1$. Next we apply the meromorphic continuation of the *restricted resolvent* $\mathbf{R}(\lambda) := \mathbf{1}_{\mathcal{U}}(\mathbf{X}+\lambda)^{-1}\mathbf{1}_{\mathcal{U}} : \Gamma_c^\infty(\mathcal{U},\mathcal{E}) \to \mathcal{D}'(\mathcal{U},\mathcal{E})$ achieved in [DG16]. To do so we first observe that $(\mathbf{X}+\lambda)^{-1}\widetilde{\chi} = (\mathbf{X}+\lambda)^{-1}\mathbf{1}_{\mathcal{U}}\widetilde{\chi}$ by $\mathrm{supp}(\widetilde{\chi}) \subseteq \mathcal{U}$. But we even demanded t_0 to be small enough that $\varphi_{-t_0}(\mathrm{supp}(\widetilde{\chi})) \subseteq \mathcal{U}$ holds, which by the support property of $\mathrm{e}^{-t_0\mathbf{X}}$ lets us rewrite $\widetilde{\chi}\mathrm{e}^{-t_0\mathbf{X}}(\mathbf{X}+\lambda)^{-1}\mathbf{1}_{\mathcal{U}}\widetilde{\chi} = \widetilde{\chi}\mathrm{e}^{-t_0\mathbf{X}}\mathbf{1}_{\mathcal{U}}(\mathbf{X}+\lambda)^{-1}\mathbf{1}_{\mathcal{U}}\widetilde{\chi}$.

Now if $\lambda \in \mathbb{C}$ is not a resonance then the general wavefront estimates [Hör13, Example 8.2.5] and [Hör13, Thm. 8.2.14] together with the estimate of $\mathrm{WF}'(\mathbf{R}(\lambda))$ in [DG16, Equation (3.43)] yield

$$\begin{aligned}&\mathrm{WF}'\left(\widetilde{\chi}\mathrm{e}^{-t_0(\lambda+\mathbf{X})}\mathbf{R}(\lambda)\widetilde{\chi}f\right)\\ &\subseteq \left\{\left(\mathrm{e}^{t_0H_p}(x,\xi),x,\xi\right) \,\middle|\, (x,\xi)\in T^*\mathcal{U}\backslash 0\right\} \cup (E_+^* \times E_-^*)\\ &\quad\cup \left\{\left(\mathrm{e}^{(t_0+t)H_p}(x,\xi),x,\xi\right) \,\middle|\, (x,\xi)\in T^*\mathcal{U}\backslash 0,\, t\geq 0,\, p(x,\xi)=0\right\}\ ,\end{aligned} \tag{3.17}$$

where $p(x,\xi) := \xi(X_x)$, $\mathrm{e}^{t_0H_p}(x,\xi) = (\varphi_t(x),(\mathrm{d}\varphi_t(x))^{-T}\xi)$ and the wavefront set of $\mathrm{e}^{-t_0\mathbf{X}}$ is contained in the graph of $\mathrm{e}^{t_0H_p}$. The wavefront set (3.17) *does not intersect* the diagonal by $t_0 < T_\gamma$, the directness of the hyperbolic splitting and bijectivity of $\mathrm{id} - \mathrm{d}\varphi_t(x)$ on $E_s(x)\oplus E_u(x)$.

Now if λ_0 *is* a resonance, then the same argument using [DG16, Lemma 3.5] (and linearity of $\mathrm{tr}^\flat$) shows that the right-hand side of (3.16) admits a Laurent expansion around λ_0 whose finitely many coefficients of negative order are the flat traces of the Laurent coefficients of $\mathbf{R}(\lambda)$. We therefore have a meromorphic continuation for $Z_f^{\mathbf{X}}(\lambda)$ onto $\{\lambda \in \mathbb{C}\}$, its poles are contained in the set of Pollicott-Ruelle resonances of $\mathbf{X}$ and for λ not a resonance we have

$$Z_f^{\mathbf{X}}(\lambda) = \mathrm{e}^{-\lambda t_0}\mathrm{tr}^\flat\left(\widetilde{\chi}\mathrm{e}^{-t_0\mathbf{X}}\mathbf{R}(\lambda)\widetilde{\chi}f\right)\ . \tag{3.18}$$

To complete our proof we show an explicit formula for the Laurent coefficients at a resonance λ_0. The starting point is (3.18) combined with (0.13) in [DG16, Thm. 2]. If we substitute the expansion in the second equation into the first we get

$$Z_f^{\mathbf{X}}(\lambda) = Z_{f,H}^{\mathbf{X}}(\lambda) + \sum_{j=1}^{J(\lambda_0)} \mathrm{tr}^\flat\left(\widetilde{\chi}\frac{\mathrm{e}^{-t_0(\lambda+\mathbf{X})}(-\mathbf{X}-\lambda)^{j-1}\Pi_{\lambda_0}}{(\lambda-\lambda_0)^j}\widetilde{\chi}f\right)\ ,$$

where $Z_{f,H}^{\mathbf{X}}(\lambda)$ is holomorphic near λ_0.

For $0 \leq k < J(\lambda_0)$, one can use the Taylor expansion of the exponential around λ_0, i.e. $\exp(-\lambda t_0) = \sum_{n=0}^\infty (-t_0)^n \exp(-\lambda_0 t_0)(\lambda-\lambda_0)^n/n!$, to obtain the weighted zeta function's Laurent coefficient of order k at λ_0:

$$\begin{aligned}\operatorname*{Res}_{\lambda=\lambda_0}\left[Z_f^{\mathbf{X}}(\lambda)(\lambda-\lambda_0)^k\right] &= \operatorname*{Res}_{\lambda=\lambda_0}\left[\sum_{j=k+1}^{J(\lambda_0)}\sum_{n=0}^{\infty}\mathrm{tr}^\flat\left(\widetilde{\chi}\frac{(-t_0)^n\mathrm{e}^{-t_0(\lambda_0+\mathbf{X})}(-\mathbf{X}-\lambda_0)^{j-1}\Pi_{\lambda_0}}{n!(\lambda-\lambda_0)^{j-k-n}}\widetilde{\chi}f\right)\right]\\ &= \sum_{n=0}^{J(\lambda_0)-k-1}\frac{(-1)^n t_0^n}{n!}\mathrm{tr}^\flat\left(\widetilde{\chi}\mathrm{e}^{-t_0(\lambda_0+\mathbf{X})}(-\mathbf{X}-\lambda_0)^{k+n}\Pi_{\lambda_0}\widetilde{\chi}f\right)\end{aligned} \tag{3.19}$$

The operator $\mathbf{X}+\lambda$ is nilpotent on the image $\mathrm{im}(\Pi_{\lambda_0})$ by Equations (0.12) and (0.15) in [DG16]. This simplifies the transfer operator $\mathrm{e}^{-t_0(\mathbf{X}+\lambda_0)}$ drastically, and substituting this simplification into Equation (3.19) together with the abbreviation $N := J(\lambda_0)-k-1$

yields:

$$\begin{aligned}\operatorname*{Res}_{\lambda=\lambda_0}\left[Z_f^{\mathbf{X}}(\lambda)(\lambda-\lambda_0)^k\right] &= \sum_{n=0}^{N}\sum_{m=0}^{N-n}(-1)^n\frac{t_0^{n+m}}{n!m!}\mathrm{tr}^\flat\left(\widetilde{\chi}(-\mathbf{X}-\lambda_0)^{n+m+k}\Pi_{\lambda_0}\widetilde{\chi}f\right)\\ &= \sum_{s=0}^{N}\sum_{n=0}^{s}(-1)^n\frac{t_0^{s}}{n!(s-n)!}\mathrm{tr}^\flat\left(\widetilde{\chi}(-\mathbf{X}-\lambda_0)^{s+k}\Pi_{\lambda_0}\widetilde{\chi}f\right)\ ,\end{aligned} \tag{3.20}$$

where the second line is obtained by using the variable $s := n+m$ as a reparametrization of the double sum. A close examination of Equation (3.20) reveals that the binomial theorem can be applied to show the vanishing of all coefficients with $s > 0$. We therefore have the following formula for the k-th Laurent coefficient:

$$\operatorname*{Res}_{\lambda=\lambda_0}\left[Z_f^{\mathbf{X}}(\lambda)(\lambda-\lambda_0)^k\right] = \mathrm{tr}^\flat\left(\widetilde{\chi}(-\mathbf{X}-\lambda_0)^{k}\Pi_{\lambda_0}\widetilde{\chi}f\right)\ ,$$

which finishes our proof because the restriction of the kernel of Π_{λ_0} to the diagonal is supported in $\Gamma_+ \cap \Gamma_- = K$ and $\widetilde{\chi} \equiv 1$ on K, i.e. we can drop the cutoff functions. □

Remark 3.4. Note that by [DG16, Eq. (4.8)] we have $\operatorname*{Res}_{\lambda=\lambda_0}\left[Z_f^{\mathbf{X}}(\lambda)\right] = \mathrm{rank}(\Pi_{\lambda_0})$ if $f \equiv \mathbf{1}$, the constant function on $\mathcal{U}$. All Laurent coefficients of higher (negative) order vanish for this particular choice of test function.

Remark 3.5. For a slightly different formulation of the final formula for the Laurent coefficients, one could replace the flat trace by an ordinary trace in an appropriate anisotropic Sobolev space ([DZ16, Lemma 4.2] and the proof of [DG16, Thm. 4]).

3.3. **Removing Strict Convexity for Zetas.** The geometric setup of open hyperbolic systems and the requirement of strict convexity in particular are quite cumbersome to state and difficult to verify in practice. Given an arbitrary flow φ_t with compact trapped set K which is hyperbolic on K we therefore remove this requirement via the perturbations of X and $\mathbf{X}$ constructed in Section 2.2. This will complete the proof of the claims made in the introduction.

Theorem 3.6: Meromorphic Continuation of Weighted Zetas II

Let the setting of Theorem 2.1 and a weight $f \in \mathrm{C}^\infty(\mathcal{M})$ be given. Then the weighted zeta function $Z_f^{\mathbf{X}}$ defined in (1.3) continues meromorphically onto $\mathbb{C}$ and its Laurent coefficients are given by (1.4).

Proof. Recall the discussion in Section 2.2 where we constructed a vector field X_0 and an operator $\mathbf{X}_0$ which satisfy the requirements of open hyperbolic systems and coincide with X and $\mathbf{X}$ on a neighborhood of the trapped set. It is now clear that the weighted zeta function associated with X_0 and $\mathbf{X}_0$ coincides with the weighted zeta function for X and $\mathbf{X}$ as both functions depend only on the dynamics near the trapped set. This yields the claim by an immediate application of Theorem 1.2. □

Remark 3.7. Theorem 3.6 implies the independence of the set of resonances from the open sets $\mathcal{U}$ and $\mathcal{U}_0$ promised in Section 2.2: Choosing as our weight the constant function $f \equiv \mathbf{1}$ we obtain $\mathrm{Res}_{\lambda=\lambda_0}[Z_{\mathbf{1}}(\lambda)] = \mathrm{tr}^\flat(\Pi_{\lambda_0}) = \mathrm{rank}(\Pi_{\lambda_0})$, where the second equality was proven in [DG16, proof of Thm. 4]. Now this implies that the resonances coincide exactly with the poles of the weighted zeta function with constant weight, but the definition of the latter only involves the dynamics on the trapped set.

4. Residue Formula for Patterson-Sullivan Distributions

In this section we relate the residues of $Z_f^{\mathbf{X}}$, defined in purely classical terms such as closed trajectories, with certain quantum mechanical phase space distributions called

Patterson-Sullivan distributions. For the general setup suppose $\mathbf{M}$ is a Riemannian manifold, φ_t its geodesic flow on the unit tangent bundle $S\mathbf{M}$, X the geodesic vector field, and $\Delta_{\mathbf{M}}$ its Laplacian.

If $\mathbf{M}$ is a *compact hyperbolic surface*, i.e. a compact surface of constant negative curvature equal to -1, the spectrum of $\Delta_{\mathbf{M}}$ is purely discrete and consists only of eigenvalues: $\sigma(\Delta_{\mathbf{M}}) = \{\lambda_i\}$, $0 = \lambda_0 < \lambda_1 \leq ...$ and $\Delta_{\mathbf{M}}\psi_i = \lambda_i\psi_i$ for an orthonormal basis of real-valued eigenfunctions $\{\psi_i\} \subseteq \mathrm{C}^\infty(\mathbf{M})$. It is convenient to parameterize the eigenvalues as $\lambda_i = 1/4 + r_i^2$. In this setting [AZ07] associated to any ψ_i a Patterson-Sullivan distribution $\mathrm{PS}_{\psi_i} \in \mathcal{D}'(S\mathbf{M})$ that are invariant under the geodesic flow $(\varphi_t)_* (\mathrm{PS}_{\psi_i}) = \mathrm{PS}_{\psi_i}$ and which, in the high frequency limit $r_i \to \infty$, fulfill [AZ07, Eq. (1.4) and Thm. 1.1]:

$$\forall a \in \mathrm{C}^\infty(T^*\mathbf{M}): \quad \widehat{\mathrm{PS}}_{\psi_i}(a|_{S\mathbf{M}}) = \langle \mathrm{Op}_{1/r_i}(a)\psi_i, \psi_i\rangle_{\mathrm{L}^2(\mathbf{M})} + \mathcal{O}(1/r_i) \ . \tag{4.21}$$

Here Op_h denotes some fixed semiclassical Weyl quantization procedure (see e.g. [Zwo12])on the classical phasespace $T^*\mathbf{M}$ and $\widehat{\mathrm{PS}}_{\psi_i}$ denotes the Patterson-Sullivan distribution normalized to $\widehat{\mathrm{PS}}_{\psi_i}(\mathbf{1}_{S\mathbf{M}}) = 1$. The expression $\mathrm{W}_{\psi_i}(a) \coloneqq \langle \mathrm{Op}_{1/r_i}(a)\psi_i, \psi_i\rangle$ is known under the name *Wigner distribution* and the second equation in (4.21) should be interpreted as the equivalence of Patterson-Sullivan and Wigner distributions in the high-frequency limit. [HHS12, Def. 4.8, Prop. 4.10] generalizes the construction of Patterson-Sullivan distributions to arbitrary compact locally symmetric spaces. These distributions still retain (generalizations of) the properties (4.21) [HHS12, Remark 4.11, Thm. 7.4]. Our results concerning the residues of weighted zeta functions provide a new view on these phasespace distributions. Concretely, we can use our main Theorem 1.2 and the results obtained by [GHW21] to prove the following residue formula for Patterson-Sullivan distributions in the closed case:

Theorem 4.1: Patterson-Sullivan Distributions as Residues

Let $\mathbf{M} = \Gamma\backslash G/K$ be a compact Riemannian locally symmetric space of rank one, $\Delta_{\mathbf{M}}$ its Laplacian and φ_t the geodesic flow on $S\mathbf{M}$. Let $\rho > 0$ denote the half-sum of the restricted roots of G. Then the following holds:
Given $r > 0$ such that $-\rho + \mathrm{i}r$ is a Ruelle resonance of φ_t then $\rho^2 + r^2$ is an eigenvalue of $\Delta_{\mathbf{M}}$ and for any $g \in \mathrm{C}^\infty(T^*\mathbf{M})$

$$\operatorname*{Res}_{\lambda=-\rho+\mathrm{i}r} \left[Z_{g|_{S\mathbf{M}}}(\lambda)\right] = \sum_{l=1}^{m} \widehat{\mathrm{PS}}_{\psi_l}(g|_{S\mathbf{M}}) = \sum_{l=1}^{m} W_{\psi_l}(g) + \mathcal{O}(1/r) \ ,$$

where the sum is over an orthonormal L^2-basis of the $\Delta_{\mathbf{M}}$-eigenspace with eigenvalue $\rho^2 + r^2$.

Proof. By Theorem 1.2 we have $\mathrm{Res}_{\lambda=-\rho+\mathrm{i}r}\left[Z_f(\lambda)\right] = \mathcal{T}_{-\rho+\mathrm{i}r}(f)$ and by [GHW21, Corollary 6.1] we have $\mathcal{T}_{-\rho+\mathrm{i}r}(f) = \sum_{l=1}^{m} \langle \widehat{\mathrm{PS}}_{\psi_l}, f\rangle$. Note that the constants $c(\mathrm{i}r)$ appearing in [GHW21, Corollary 6.1] and defined in [GHW21, Eq. (6.1)] are the normalization factors for PS_{ψ_l}; the additional factor of m^{-1} appearing in [GHW21, Corollary 6.1] are due to their slightly different definition of $\mathcal{T}_{\lambda_0}$ in [GHW21, Eq. (2.1)]. Combining these two results proves our claim. □

We would like to compare our result with previously known results obtained with different techniques. In their paper [AZ07], Anantharaman and Zelditch proved a similar close connection between slightly different weighted zeta functions and Patterson-Sullivan distributions: For $f \in \mathrm{C}^\infty(S\mathbf{M})$ they define a weighted zeta function via [AZ07, Eq. (1.9)]

$$\mathcal{Z}_f^{AZ}(\lambda) \coloneqq \sum_{\gamma} \left(\frac{\exp(-\lambda T_\gamma)}{1 - \exp(-T_\gamma)} \int_{\gamma^\#} f \right), \tag{4.22}$$

where one sums over all closed geodesics γ. In [AZ07, Thm. 1.3] they state that, provided f is *real analytic*, $\mathcal{Z}_f^{AZ}$ continues meromorphically onto $\mathbb{C}$, its poles in $\{0 < \mathrm{Re}(\lambda) < 1\}$ are of the form $\lambda = 1/2 + \mathrm{i}r$ where $1/4 + r^2$ is an eigenvalue of $\Delta_{\mathbf{M}}$ and the following residue formula holds:

$$\operatorname*{Res}_{\lambda=1/2+\mathrm{i}r} \left[\mathcal{Z}_f^{AZ}(\lambda)\right] = \sum_{\psi_i:\, \lambda_i = 1/4+r^2} \langle \widehat{\mathrm{PS}}_{\psi_i}, f \rangle.$$

They give two different proofs with the first relying on the thermodynamic formalism and the second on representation theory and a version of Selberg's trace formula. See also the later work [AZ12] for a generalization of the intertwining between Wigner and Patterson-Sullivan distributions to the non-diagonal case.

Note that for hyperbolic surfaces $\det(\mathrm{id} - \mathcal{P}_\gamma) = (1 - \exp(-T_\gamma))(1 - \exp(T_\gamma))$, i.e. a simple calculation yields the following relation between $\mathcal{Z}_f^{AZ}$ and our weighted zeta:

$$Z_f(\lambda) = \sum_{n=1}^{\infty} \mathcal{Z}_f^{AZ}(\lambda + n).$$

We can therefore conclude that given an eigenvalue $1/4 + r^2$ of $\Delta_{\mathbf{M}}$ the value $-1/2 + \mathrm{i}r$ is a Ruelle resonance of the geodesic flow on $S\mathbf{M}$ and

$$\mathrm{Res}_{\lambda=-1/2+\mathrm{i}r} \left[Z_f(\lambda)\right] = \sum_{\psi_i:\, \lambda_i = 1/4+r^2} \langle \widehat{\mathrm{PS}}_{\psi_i}, f \rangle.$$

In his thesis [Emo14], Emonds extended the residue formula of [AZ07] to the case of hyperbolic manifolds of arbitrary dimension. But this result again imposes a significant restriction on the space of test functions, namely that f be K-finite, and the proof heavily relies on techniques from representation theory. It appears that the methods of microlocal analysis are better suited for the meromorphic continuation of (weighted) zeta functions.

Let us finally note that our main result also holds for open systems, so we immediately obtain residue formulae for weighted zeta functions of geodesic flows on convex cocompact hyperbolic manifolds in terms of invariant Ruelle distributions. While there exists so far no theory of Patterson-Sullivan distributions for these systems, a quantum classical correspondence has been established on the level of resonances and resonant states [GHW18]. We thus conjecture that also in this setting the invariant Ruelle distributions are, in the high frequency limit, asymptotically equivalent to phase space distributions of quantum resonant states. Given the fact that the residues of Z_f can be numerically calculated quite efficiently, this would provide a method to study phase space distributions of quantum resonant states on Schottky surfaces numerically.

Appendix A. Numerical Calculation of Invariant Ruelle Distributions (with Sonja Barkhofen)

In this appendix we provide a short outlook on a major application of the weighted zeta function developed in the main text, namely the numerical calculation of invariant Ruelle distributions $\mathcal{T}_{\lambda_0}$. While these distributions are interesting in their own right, they also provide a new perspective on quantum mechanical matrix coefficients, c.f. (4.21). This circumstance makes efficient tools for their calculation even more desirable. For a physics-oriented discussion of the connection between weighted zeta functions and quantum mechanical phase space distributions we refer to the companion article [BSW22].

Now in principle one wants to exploit Theorem 3.6 and more concretely the relation

$$\langle \mathcal{T}_{\lambda_0}, f \rangle = \mathrm{Res}_{\lambda=\lambda_0} Z_f(\lambda).$$

To use this numerically we require an efficient method for calculating (the residues of) the weighted zeta function Z_f. While this endeavor is hopeless in the abstract setting of Theorem 2.1 there are concrete dynamical systems where this calculation is possible due

to the availability of a symbolic encoding of the dynamics. Two such system which are well-known in the literature are *convex obstacle scattering* and *geodesic flows on convex cocompact hyperbolic surfaces*. For the sake of brevity we will focus on a particular instance of the former class of systems, namely so-called *symmetric 3-disc systems*.

This appendix is organized as follows: We begin by giving a short introduction to 3-disc systems in Section A.1. With this setup at hand we then provide some first numerical results in Section A.2.

A.1. **Introducing 3-Disc Systems.** The 3-disc system is a paradigmatic example of a convex obstacle scattering dynamics [Ika88, GR89]. It is given by three discs $\mathrm{D}(x_i, r_i) \subseteq \mathbb{R}^2$, $i \in \{1,2,3\}$, with radii $r_i > 0$, centers $x_i \in \mathbb{R}^2$ and disjoint closures. The dynamics takes place on the unit sphere bundle $S\left(\mathbb{R}^2 \setminus \bigcup_{i=1}^3 \mathring{\mathrm{D}}(x_i, r_i)\right)$: In the interior $S\left(\mathbb{R}^2 \setminus \bigcup_{i=1}^3 \mathring{\mathrm{D}}(x_i, r_i)\right)$ its trajectories coincide with the Euclidean geodesic flow, and upon boundary intersection the trajectories experience specular reflections. We will only consider fully *symmetric* 3-disc systems here, and for our purposes these are uniquely described by the quotient d/r of the common radius $r = r_1 = r_2 = r_3$ and the side length $d > 0$ of the equilateral triangle on which the centers of the discs are positioned. For a graphical illustration of this setup see Figure 1.

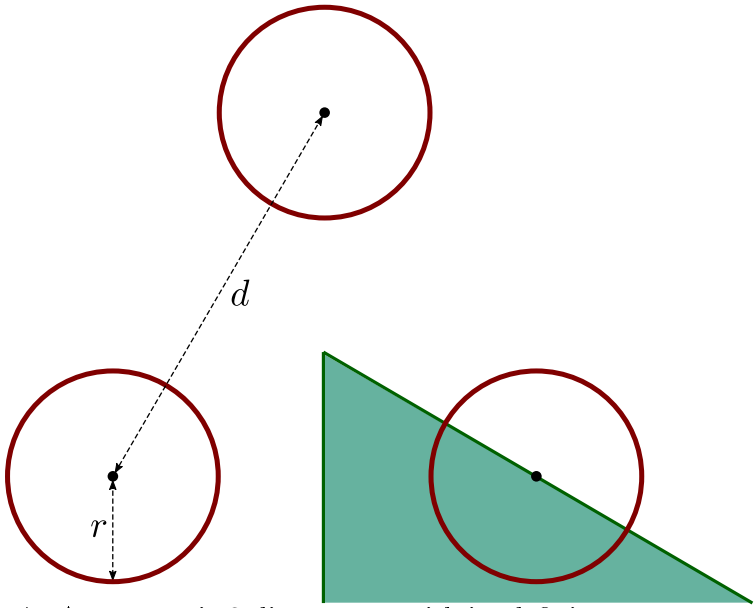

FIGURE 1. A symmetric 3-disc system with its defining paramters r and d. The fundamental domain is given by the green region.

Now the dynamics just described is obviously not smooth because of the instantaneous boundary reflections. If we assume that d/r is sufficiently large then this lack of smoothness is properly separated from the trapped set, though. In this case it can be dealt with via smooth models. To keep our presentation short we refer the reader to [KSW21] where the construction of smooth models as well as the meromorphic continuation of weighted zeta functions was carried out in detail and in a more general setting.

What we will actually investigate numerically is not quite the 3-disc dynamics just described, but rather a symmetry reduced variant. A fundamental domain of this symmetry reduction is shown in green in Figure 1. The reduced dynamics still admits a symbolic coding and is well understood on the classical as well as on the quantum side. It is used

here as it provides the model of choice for experimental realizations [PWB$^+$12, BWP$^+$13]. For more details and references see [WBK$^+$14].

Our numerical algorithm itself resembles the algorithm developed by Cvitanovic and Eckhardt [CE89, CE91] in physics and Jenkinson and Pollicott [JP02] or Borthwick [Bor14] in mathematics: One can derive a cycle expansion for the weighted zeta function Z_f associated with a given 3-disc system. To calculate concrete summands in this expansion we make use of the symbolic encoding of closed trajectories available for sufficiently large d/r. A detailed description of the algorithm will be presented elsewhere [BSW22]. We just want to mention the following two central simplifications:

(1) To be able to plot the distributions $\mathcal{T}_{\lambda_0}$ we calculate their convolution with Gaussians with variance $\sigma > 0$. In the limit $\sigma \to 0$ this convolution converges to $\mathcal{T}_{\lambda_0}$ in $\mathcal{D}'$ and it is reasonable to expect the numerical results for small but positive σ to reveal interesting properties of $\mathcal{T}_{\lambda_0}$ itself.
(2) While the convolutions discussed in (1) are smooth they still live on the 3-dimensional state space of the 3-disc system. To obtain 2-dimensional plots we restrict $\mathcal{T}_{\lambda_0}$ to a Poincaré section Σ via Lemma 2.3.

For the numerics presented below we used a specific Poincaré section $\Sigma \subseteq S\mathbb{R}^2$ defined by so-called *Birkhoff coordinates* as follows: First, fix one of the discs and an origin on the boundary of this disc. Then a point $(q, p) \in [-\pi, \pi] \times [-1, 1]$ corresponds to the point $(x, v) \in S\mathbb{R}^2$ such that the boundary arc connecting the origin and x has length $q \cdot r$ and such that the projection $\langle v, t(x)\rangle$ of v onto the tangent $t(x)$ to the disc at x equals p. For an illustration of these coordinates see Figure 2. Now the transversality condition of Lemma 2.3 is obviously satisfied, making the restriction $\mathcal{T}_{\lambda_0}\big|_\Sigma$ a well-defined distribution. It is this object which will be plotted numerically in the following section.

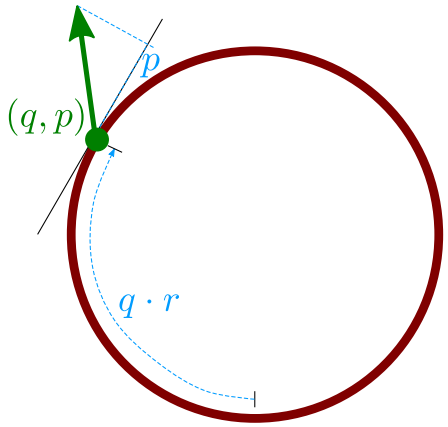

FIGURE 2. The Birkhoff coordinates for the Poincaré section $\Sigma \subseteq S\mathbb{R}^2$ of a symmetric 3-disc system used in the numerics below.

A.2. **Proof-of-Principle Results.** In this section we present first numerical calculations of invariant Ruelle distributions. As already mentioned we restrict the distributions to the Poincaré section Σ and then approximate by convolution with Gaussians of width σ. As the trapped set K itself is fractal and therefore hard to visualize, we chose the following alternative: Denote by $K_1 \supseteq K$ those points of phase space which experience at least one disc reflection either in forward or backward time. We included the intersection $\Sigma_1 := K_1 \cap \Sigma$ in the figures below to give an idea of where the invariant Ruelle distributions are supposed to be supported in theory.

We begin the first series of illustrations by plotting four example resonances and associated distributions along the first clearly distinguishable resonance chain. In particular,

we begin with the point closest to the spectral gap and continue towards the intersection with the second distinct chain. Our choices are marked in red in the first row of Figure 3.

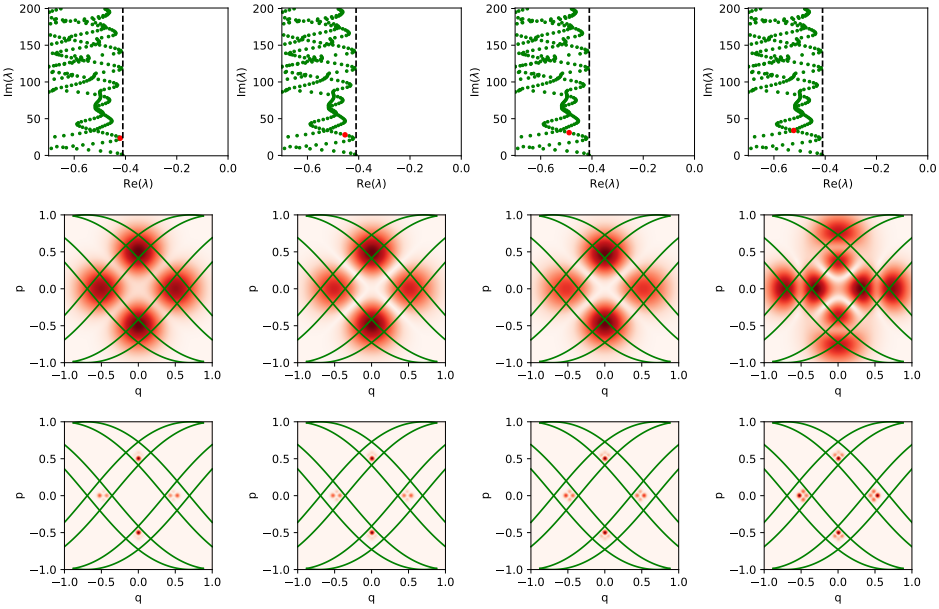

FIGURE 3. Comparison of invariant Ruelle distributions along a resonance chain for $d/r = 6$. The first row highlights in red the resonance at which the distributions in the second and third rows was evaluated. The second row was computed with $\sigma = 0.1$ and the third row with $\sigma = 0.001$. One clearly recognizes dynamical changes in $\mathcal{T}_{\lambda_0}$ as λ_0 varies along the chain. In addition, the reduction of σ seems to further localize the distribution on the trapped set, which theoretically contains the support of any $\mathcal{T}_{\lambda_0}$.

In the second and third rows of Figure 3 we plotted the distribution associated with the marked resonance and the two choices $\sigma = 0.1$ and $\sigma = 0.001$, respectively. Going from left to right in either the first or the second row shows that the invariant Ruelle distributions clear encode some kind of information regarding the location of their associated resonances. Especially the distribution at the point of intersection of the first two chains (fourth column in Figure 3) differs significantly from the first three, which only exhibit a gradual reduction of intensity in the left and right component of Σ_1.

Going from top to bottom in Figure 3 we see how the reduction of σ by two orders of magnitude significantly increases the localization of the distributions on the trapped set. This behavior is expected by the theory developed above and could allow a detailed numerical investigation of invariant Ruelle distributions on successively finer scales of the fractal trapped set.

Our second series of invariant Ruelle distributions is meant to give a first impression of a curious phenomenon which has not been understood theoretically yet: Calculating numerically resonances with imaginary part up to about 750 it would appear that the maximal real part which occurs becomes progressively smaller the larger $\mathrm{Im}(\lambda)$ becomes. If we proceed to even larger imaginary parts this progression reverses and at about $\mathrm{Im}(\lambda) = 1500$ we observe several resonances with real parts close to the theoretical maximum of λ_1, where λ_1 denotes the first resonance on the real line. These observations are shown in the

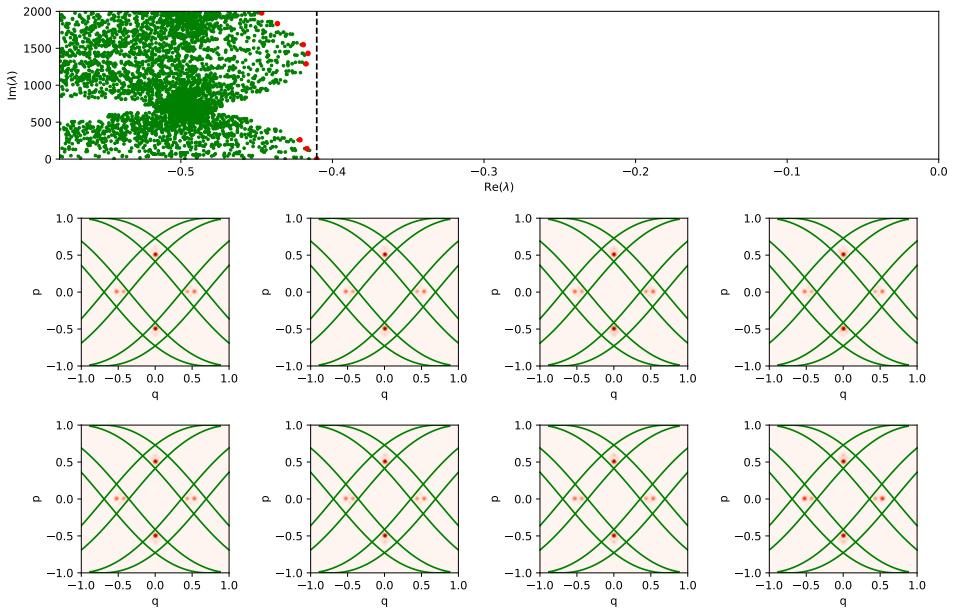

FIGURE 4. Comparison of invariant Ruelle distributions for several different resonances near the line $\mathrm{Re}(\lambda) = \lambda_1$, where λ_1 denotes the resonances with maximal real part. The resonances marked in red (from bottom to top) correspond to the plotted distributions (from top left to bottom right). Throughout we have $\sigma = 0.001$. Note how the distributions all appear very similar, even on this second level of the fractal trapped set.

first row of Figure 4. The same effect has been observed in even more pronounced fashion for resonances on Schottky surfaces [BW16].

As the question of asymptotic spectral gaps for such open systems is an important unsolved problem, it is interesting to understand such a recurrence of resonances to a neighborhood of the critical line. We therefore calculated the invariant Ruelle distributions for those resonances close to the critical line in the second and third rows of Figure 4: The distribution plots from top left to bottom right belong to the resonances marked in red and ordered from small to large imaginary part. We immediately notice that all eight distributions while associated with different resonances appear exceedingly similar, even though we already calculated them with the rather small value of $\sigma = 0.001$. We have to admit that we cannot explain this observation so far but find it quite remarkable.

https://go.upb.de/ruelle

Additional and more detailed illustrations can be found on the supplementary website `https://go.upb.de/ruelle`. In particular, it contains several additional distributions along the first chain discussed above, illustrations of further resonances near the spectral gap, and plots along a second resonance chain.

References

[AZ07] Nalini Anantharaman and Steve Zelditch, *Patterson–Sullivan Distributions and Quantum Ergodicity*, Annales Henri Poincaré (2007), no. 8(2007), 361–426.

[AZ12] ———, *Intertwining the geodesic flow and the schrödinger group on hyperbolic surfaces*, Mathematische Annalen **353** (2012), no. 4, 1103–1156.

[Bor14] David Borthwick, *Distribution of Resonances for Hyperbolic Surfaces*, Experimental Mathematics **1** (2014), no. 23, 25–45.

[BPSW21] Oscar F Bandtlow, Anke Pohl, Torben Schick, and Alexander Weiße, *Numerical resonances for schottky surfaces via lagrange–chebyshev approximation*, Stochastics and Dynamics **21** (2021), no. 03, 2140005.

[BSW22] Sonja Barkhofen, Philipp Schütte, and Tobias Weich, *Semiclassical formulae for wigner distributions*, arXiv:2201.04892 (2022).

[BW16] David Borthwick and Tobias Weich, *Symmetry reduction of holomorphic iterated function schemes and factorization of selberg zeta functions*, Journal of Spectral Theory **6** (2016), no. 2, 267–329.

[BWP+13] S. Barkhofen, T. Weich, A. Potzuweit, H.-J. Stöckmann, U. Kuhl, and M. Zworski, *Experimental observation of the spectral gap in microwave n-disk systems*, Phys. Rev. Lett. **110** (2013), 164102.

[CE71] Charles Conley and Robert Easton, *Isolated invariant sets and isolating blocks*, Transactions of the American Mathematical Society **158** (1971), no. 1, 35–61.

[CE89] Predrag Cvitanovic and Bruno Eckhardt, *Periodic-orbit Quantization of Chaotic Systems*, Physical Review Letters **823** (1989), no. 63.

[CE91] ———, *Periodic orbit expansions for classical smooth flows*, Journal of Physics A: Mathematical and General **24** (1991), no. 5, L237.

[DFG15] Semyon Dyatlov, Frédéric Faure, and Colin Guillarmou, *Power spectrum of the geodesic flow on hyperbolic manifolds*, Anal. PDE **8** (2015), no. 4, 923–1000 (English).

[DG16] Semyon Dyatlov and Colin Guillarmou, *Pollicott–Ruelle Resonances for Open Systems*, Annales Henri Poincaré **17** (2016), no. 11, 3089–3146.

[DG18] ———, *Afterword: Dynamical zeta functions for axiom a flows*, Bull. Amer. Math. Soc. (2018), no. 55, 337–342.

[DZ16] Semyon Dyatlov and Maciej Zworski, *Dynamical Zeta Functions for Anosov Flows via Microlocal Analysis*, Annales Scientifiques de L'Ecole Normale Superieure **4** (2016), no. 49, 543–577.

[EFMW92] B Eckhardt, S Fishman, K Müller, and D Wintgen, *Semiclassical matrix elements from periodic orbits*, Physical Review A **45** (1992), no. 6, 3531.

[Emo14] Jan Emonds, *A dynamical interpretation of patterson-sullivan distributions*, Ph.D. thesis, Paderborn University, 2014.

[GHW18] Colin Guillarmou, Joachim Hilgert, and Tobias Weich, *Classical and quantum resonances for hyperbolic surfaces*, Mathematische Annalen **370** (2018), 1231–1275.

[GHW21] Colin Guillarmou, Joachim Hilgert, and Tobias Weich, *High frequency limits for invariant ruelle densities*, Annales Henri Lebesgue **4** (2021), 81–119.

[GMT21] Colin Guillarmou, Marco Mazzucchelli, and Leo Tzou, *Boundary and lens rigidity for non-convex manifolds*, 2021, pp. 533–575.

[GR89] Pierre Gaspard and Stuart A Rice, *Scattering from a classically chaotic repellor*, The Journal of chemical physics **90** (1989), no. 4, 2225–2241.

[Gui77] Victor Guillemin, *Lectures on spectral theory of elliptic operators*, Duke Math. J. **44** (1977), no. 3, 485–517.

[HHS12] Sönke Hansen, Joachim Hilgert, and Michael Schröder, *Patterson-Sullivan distributions in higher rank*, Mathematische Zeitschrift (2012), no. 272(2012), 607–643.

[Hör13] Lars Hörmander, *The Analysis of Linear Partial Differential Operators I: Distribution Theory and Fourier Analysis*, 2nd ed., Classics in Mathematics, Springer, Berlin, Heidelberg, 2013.

[Ika88] Mitsuru Ikawa, *Decay of solutions of the wave equation in the exterior of several convex bodies*, Annales de l'Institut Fourier **38** (1988), no. 2, 113–146.

[JP02] Oliver Jenkinson and Mark Pollicott, *Calculating hausdorff dimension of julia sets and kleinian limit sets*, American Journal of Mathematics **124** (2002), no. 3, 495–545.

[KSW21] Benjamin Küster, Philipp Schütte, and Tobias Weich, *Resonances and weighted zeta functions for obstacle scattering via smooth models*, arXiv:2109.05907 (2021).

[Lee12] John M. Lee, *Introduction to Smooth Manifolds*, 2nd ed., Graduate Texts in Mathematics, vol. 218, Springer New York, New York, NY, 2012.

[PWB+12] A. Potzuweit, T. Weich, S. Barkhofen, U. Kuhl, H.-J. Stöckmann, and M. Zworski, *Weyl asymptotics: From closed to open systems*, Phys. Rev. E **86** (2012), 066205.

[Rob80] Clark Robinson, *Structural stability on manifolds with boundary*, Journal of Differential Equations **37** (1980), no. 1, 1–11.

[Sch23] Philipp Schütte, *Analytics and Numerics of Weighted Zeta Functions on Open, Chaotic Systems*, PhD thesis, Paderborn University (in progress, 2023).

[WBK+14] Tobias Weich, Sonja Barkhofen, Ulrich Kuhl, Charles Poli, and Henning Schomerus, *Formation and interaction of resonance chains in the open three-disk system*, New Journal of Physics **16** (2014), 033029.

[Zwo12] Maciej Zworski, *Semiclassical analysis*, Grad. Stud. Math., vol. 138, Providence, RI: American Mathematical Society (AMS), 2012 (English).

Paderborn University, Institute of Mathematics, Warburger Str. 100, 33098 Paderborn, Germany

Email address, Philipp Schütte: pschuet2@math.uni-paderborn.de

Email address, Tobias Weich: weich@math.uni-paderborn.de

Paderborn University, Department of Physics, Warburger Str. 100, 33098 Paderborn, Germany

Email address, Sonja Barkhofen: sonja.barkhofen@uni-paderborn.de

B. Resonances and Weighted Zeta Functions for Obstacle Scattering via Smooth Models

This appendix contains the research paper *Resonances and Weighted Zeta Functions for Obstacle Scattering via Smooth Models* which was written with the co-authors Benjamin Delarue (formerly Küster) and Tobias Weich during the author's PhD. The article is under revision at *Annales Henri Poincaré* at the time of writing this thesis and was included here in its revised version which differs in some details from the version [DSW21].

The three co-authors contributed equally to the development of the research question and the proof strategy. B.D. and P.S. worked out the details of the proofs and wrote the manuscript in equal parts. This process was accompanied by regular discussions between all three co-authors.

The proof reading was done by all three co-authors. B.D. and P.S. conducted the revision after submission to the journal.

RESONANCES AND WEIGHTED ZETA FUNCTIONS FOR OBSTACLE SCATTERING VIA SMOOTH MODELS

BENJAMIN DELARUE, PHILIPP SCHÜTTE, AND TOBIAS WEICH

Abstract. We consider a geodesic billiard system consisting of a complete Riemannian manifold and an obstacle submanifold with boundary at which the trajectories of the geodesic flow experience specular reflections. We show that if the geodesic billiard system is hyperbolic on its trapped set and the latter is compact and non-grazing the techniques for open hyperbolic systems developed by Dyatlov and Guillarmou [DG16] can be applied to a smooth model for the discontinuous flow defined by the non-grazing billiard trajectories. This allows us to obtain a meromorphic resolvent for the generator of the billiard flow. As an application we prove a meromorphic continuation of weighted zeta functions together with explicit residue formulae. In particular, our results apply to scattering by convex obstacles in the Euclidean plane.

1. Introduction

Open hyperbolic flows combine two interesting dynamical phenomena: chaotic behavior on the one hand and escape towards infinity on the other hand. In the mathematical physics literature there are two paradigmatic example classes of such flows: geodesic flows on Schottky surfaces and convex obstacle scattering.

The geodesic flows on (convex co-compact) Schottky surfaces are mathematically much easier to handle (see e.g. [Dal10] for an introduction). They are complete smooth flows on Riemannian locally symmetric spaces whose algebraic structure allows for an application of powerful techniques from harmonic analysis and structure theory. One has e.g. meromorphic continuations of zeta functions [Fri86, Gui92], precise estimates on the counting of periodic trajectories [Gui86, Lal89], or exact correspondences with the quantum counterpart of the geodesic flow [GHW18] given by the Laplace-Beltrami operator.

The example of obstacle scattering, in contrast, has the advantage that it is much less abstract and can be seen as a concrete model of a physical particle in a two-dimensional plane performing specular reflections at a finite number of hard obstacles. It has therefore been intensively studied in the physics literature in the context of classical [GR89b], semiclassical [GR89c], or quantum-mechanical [GR89a] dynamical systems and allows for numerical [CE89, Wir99, LSZ03, BFW14, WBK$^+$14] as well as physical experiments [PLS00, BWP$^+$13, PWB$^+$12]. Obstacle scattering has however been also in the focus of mathematical literature, see e.g. [Ika88, Gé88], where the focus lies on quantum resonances. It features similarities with the scattering theory of Schrödinger-type operators involving a potential rather than a family of obstacles, see e.g. [NZ09].

In this article we focus on the theory of Ruelle-Pollicott resonances. These resonances were introduced by Ruelle [Rue76] and Pollicott [Pol85] to describe the convergence to equilibrium of hyperbolic flows. Since then, several technical approaches to the definition and the study of these resonances have been developed on various levels of generality. While early results such as [Dol98] were achieved using Markov partitions and symbolic dynamics, in most modern formulations the resonances occur as a discrete spectrum of the generating vector field X of the flow – regarded as a differential operator of order one – in an anisotropic function space and as poles of a meromorphic resolvent of X. The existence of such a discrete resonance spectrum has been established since Liverani's result [Liv04] on contact Anosov flows in many different settings such as Anosov flows

on compact manifolds [BL07, FS11, DZ16], Morse-Smale flows [DR19, DR20b], geodesic flows on manifolds with cusps [GBW21], basic sets of Axiom-A flows [DG16], general Axiom-A flows [Med21], higher rank Anosov actions [GBGHW20], or finite horizon Sinai billiards [BDL18]. The respective meromorphic resolvents are not only useful to define the Ruelle resonances but also have many additional applications such as meromorphic continuation of zeta functions [GLP13, DZ16] or Poincaré series [DR20a] and to geometric inverse problems [GL19, GBL23]. The geodesic flow on Schottky surfaces provides concrete examples of basic sets of an Axiom-A flow and it neatly fits into the setting of open hyperbolic systems treated in [DG16]. In contrast, for obstacle scattering this is not directly the case: As is typical for billiard flows, there are technical difficulties such as the only piecewise smoothness of the flow and singularities caused by grazing trajectories. The aim of this paper is to provide a rigorous framework to define the Ruelle-Pollicott resonances for obstacle scattering by establishing the meromorphic continuation of the resolvents of the generators of appropriate flows and their matrix coefficients.

We first state a simplified version of our main results in the classical case of Euclidean billiards before stating the results for more general obstacle setups.

1.1. **Results for Euclidean billiards.** Let $\Omega_i \subset \mathbb{R}^n$, $i = 1, \dots, N$ and $n \geq 2$, be a finite number of disjoint, compact, connected, strictly convex obstacle sets with smooth[1] boundaries and non-empty interiors. Let the *configuration space* be $\mathcal{C} := \mathbb{R}^n \setminus \mathring{\Omega}$, where we write $\Omega := \bigcup_{i=1}^N \Omega_i$ and $\mathring{\Omega}$ denotes the interior of Ω in $\mathbb{R}^n$. The *billiard trajectories* $\{x_t\}_{t\in\mathbb{R}} \subset \mathcal{C}$ are defined as straight lines parametrized at unit speed unless they intersect the boundary $\partial\Omega$, where at each intersection point $x \in \partial\Omega$ they undergo an *instantaneous reflection* at the tangent plane $T_x\partial\Omega$, i.e., they leave x at an outgoing angle with $T_x\partial\Omega$ identical to the incoming angle. The trajectories are oriented by the standard orientation of $\mathbb{R}$. If a trajectory intersects $\partial\Omega$ tangentially at some point we call it *grazing* and any trajectory remaining inside a bounded subset of $\mathbb{R}^n$ is called *trapped*. Note that a trajectory is trapped if and only if it undergoes infinitely many boundary reflections both in forward and backward time. We demand that the billiard satisfy the

non-grazing trapped set condition: No trapped trajectory is grazing.

A classical geometric condition which is sufficient but in general not necessary for the non-grazing trapped set condition to hold is the so-called *no-eclipse condition* [Ika88]: For any two obstacles Ω_i, Ω_j the convex hull of their union does not intersect any distinct third obstacle Ω_k.

While the billiard trajectories in the configuration space can be grasped intuitively, the boundary reflections make it ambiguous how to lift these trajectories to a flow on the *phase space*

$$M := S\mathcal{C} = S(\mathbb{R}^n \setminus \mathring{\Omega}),$$

the unit tangent bundle of the configuration space. To describe the situation in phase space first note that M is a submanifold with boundary $\partial M = (S\mathbb{R}^n)|_{\partial\Omega}$ of $S\mathbb{R}^n$. For $(x, v) \in \partial M$ the Euclidean inner product of v and the inward unit normal of $\partial\Omega$ at x can be strictly negative (v is *outward pointing*), vanish (v is tangent), or strictly positive (v is *inward pointing*). Denote by $\partial_{\mathrm{in}}M, \partial_{\mathrm{out}}M \subset \partial M$ the subsets of all inward and outward pointing vectors, respectively (for a graphical depiction see Figure 2 on page 6).

Given $(x, v) \in M$, the strict convexity of the obstacles ensures that there is a unique billiard trajectory $\{x_t\}_{t\in\mathbb{R}} \subset \mathcal{C}$ characterized as follows:

(1) If $(x, v) \in M \setminus (\partial_{\mathrm{in}}M \cup \partial_{\mathrm{out}}M)$, then $x_t = x + tv$ for all $t \in \mathbb{R}$ close enough to 0.
(2) If $(x, v) \in \partial_{\mathrm{out}}M$, then $x_t = x + tv$ for all $t \geq 0$ close enough to 0.
(3) If $(x, v) \in \partial_{\mathrm{in}}M$, then $x_t = x + tv$ for all $t \leq 0$ close enough to 0.

[1]Throughout this paper, *smooth* means C^∞, i.e., infinitely differentiable.

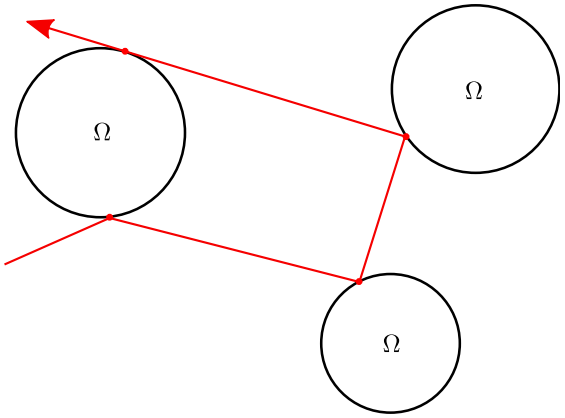

FIGURE 1. Grazing trajectory in a Euclidean billiard in $\mathbb{R}^2$ with obstacles given by three discs. Note that the above configuration of obstacles satisfies the no-eclipse condition – in particular, it satisfies the less restrictive non-grazing trapped set condition.

More generally, for any $t \in \mathbb{R}$, both one-sided limits $v_t^\pm := \lim_{s \to t^\mp} \dot{x}_t \in S_{x_t}\mathbb{R}^n$ exist (the dot indicating time derivatives) and if $x_t \in \partial\Omega$ then $v_t^\pm$ is the reflection of $v_t^\mp$ at the hyperplane $T_x\partial\Omega$. This implies that neither of the two maps

$$\varphi^{b\pm} : \mathbb{R} \times M \mapsto M, \qquad (t, x, v) \mapsto (x_t, v_t^\pm) =: \varphi_t^{b\pm}$$

defines a flow because $\varphi_0^{b\pm}$ is not the identity over $\partial_{\mathrm{in}}M \cup \partial_{\mathrm{out}}M$. However, since the violation of the flow property happens only at the boundary, it does not cause serious difficulties. To formalize the billiard dynamics we introduce a map

$$\varphi^b : \mathbb{R} \times M \to M$$

which we call the *billiard flow* in spite of it violating the flow property on the boundary. It is built from φ^{b+} and φ^{b-} by "symmetrization" so that neither outward nor inward vectors are preferred: Given $(t, x, v) \in \mathbb{R} \times M$ we define $\varphi_t^b(x, v) := (x, v)$ if $t = 0$. If $t \neq 0$ then $\varphi_t^{b+}(x, v) \in M \setminus (\partial_{\mathrm{in}}M \cup \partial_{\mathrm{out}}M)$ iff $\varphi_t^{b-}(x, v) \in M \setminus (\partial_{\mathrm{in}}M \cup \partial_{\mathrm{out}}M)$ and in this case $\varphi_t^{b+}(x, v) = \varphi_t^{b-}(x, v) =: \varphi_t^b(x, v)$. In the remaining cases we put $\varphi_t^b(x, v) := \varphi_t^{b\pm}(x, v)$ if $\pm t > 0$. Note that φ^b remains discontinuous.

Under the assumption of the non-grazing trapped set condition one deduces that the trapped set

$$K^b := \{(x, v) \in M \,|\, \varphi_t^b(x, v) \text{ stays in a compact set for all } t \in \mathbb{R}\} \tag{1}$$

contains no grazing trajectories.

In Section 2.4 we introduce for a class of open sets $U \subset M$ spaces of *smooth billiard functions* $\mathrm{C}^\infty_{\mathrm{Bill}}(U)$ and *billiard test functions* $\mathrm{C}^\infty_{\mathrm{Bill,c}}(U) = \mathrm{C}^\infty_{\mathrm{Bill}}(U) \cap \mathrm{C}^\infty_{\mathrm{c}}(U)$ whose main property to be noted here is that $\mathrm{C}^\infty_{\mathrm{c}}(U \setminus \partial M) \subset \mathrm{C}^\infty_{\mathrm{Bill,c}}(U) \subset \mathrm{C}^\infty_{\mathrm{c}}(U)$. Since M is a manifold with boundary such open U may intersect ∂M. We then prove the following theorem:

Theorem 1.1. *There is an open neighborhood U of K^b in M such that with the backward escape time $\tau_U^-(x, v) := \sup\{t < 0 \,|\, \varphi_t^b(x, v) \notin U\}$, $(x, v) \in U$, and for $\lambda \in \mathbb{C}, \mathrm{Re}(\lambda) \gg 0$,*

$$\mathbf{R}_U(\lambda)f(x, v) := \int_0^{-\tau_U^-(x,v)} \mathrm{e}^{-\lambda t} f\big(\varphi_{-t}^b(x, v)\big)\mathrm{d}t, \qquad f \in \mathrm{C}^\infty_{\mathrm{Bill,c}}(U),\ (x, v) \in U,$$

yields a well-defined family of linear maps $\mathbf{R}_U(\lambda) : \mathrm{C}^\infty_{\mathrm{Bill,c}}(U) \to \mathrm{C}(U)$ and its matrix coefficients

$$\langle \mathbf{R}_U(\lambda)f, g\rangle_{\mathrm{L}^2(M)}, \qquad f, g \in \mathrm{C}^\infty_{\mathrm{Bill,c}}(U)$$

extend from holomorphic functions on a half-plane where $\mathrm{Re}(\lambda)$ *is large enough to meromorphic functions on* $\mathbb{C}$ *with poles contained in a discrete set of complex numbers that is independent of* f *and* g*. Moreover, the discrete set of complex numbers is also independent of the choice of* U*.*

We will also see that on $\mathrm{C}^\infty_{\mathrm{Bill}}(U)$ we can define an infinitesimal generator $\mathbf{P}$ of the billiard flow and $\mathbf{R}_U(\lambda)$ can be seen as its resolvent in the sense that $(\mathbf{P}+\lambda)\mathbf{R}_U(\lambda) = \mathrm{id}$ on $\mathrm{C}^\infty_{\mathrm{Bill}}(U)$ if $\mathrm{Re}(\lambda)$ is large enough. The locations of the possible poles for the matrix coefficients are then defined to be the *Ruelle-Pollicott resonances of the billiard flow.*

1.2. **General Results.** The three essential features of the setup in Section 1.1 which allow us to prove Theorem 1.1 are

I) the trapped set K^b defined in (1) is compact;
II) K^b contains no grazing trajectories;
III) the billiard flow is hyperbolic on K^b (c.f. Def. 2.12).

Here I) follows from the compactness of the union Ω of the obstacles, II) from the non-grazing trapped set condition, and III) from the strict convexity of the obstacles, see Remark 5.10. Having identified I)–III) as the core assumptions allows us to work without additional further effort in the more general setting of billiards on Riemannian manifolds of arbitrary dimension (as considered previously by e.g. [BFK02]) under the assumption of a compact trapped set for the non-grazing dynamics and hyperbolicity on the trapped set. Theorem 1.1 is then deduced as a special case of the more general Corollary 5.5, see Remark 5.10. Let us briefly explain this general approach and compare it to Section 1.1:

We replace $\mathbb{R}^n$ by an arbitrary smooth complete connected Riemannian manifold (Σ, g) of dimension $n \geq 1$ without boundary and Ω by an arbitrary n-dimensional smooth submanifold with boundary of Σ whose connected components are the obstacles. Accordingly phase space is $M := S(\Sigma \setminus \mathring{\Omega})$. We emphasize that neither convexity nor compactness of Ω is assumed. Such "low-level" geometrical or topological assumptions are avoided in favor of the "high-level" assumptions I)–III). Concerning II) there is a major conceptual difference to the situation of Section 1.1: In the latter, the strict convexity of the obstacles allowed us to define the billiard flow points $\varphi^b_t(x,v)$ for all times $t \in \mathbb{R}$ at each point (x,v) in the phase space M, allowing for grazing collisions. We therefore needed the non-grazing trapped set condition to ensure that II) holds. In contrast the general situation restricts attention to the *non-grazing* billiard flow φ on the *non-grazing phase space* $M \setminus S\partial\Omega$ to begin with. More precisely, $(t,x,v) \mapsto \varphi_t(x,v)$ is a map $D \mapsto M \setminus S\partial\Omega$ defined on an open set $D \subset \mathbb{R} \times (M \setminus S\partial\Omega)$ containing $\{0\} \times (M \setminus S\partial\Omega)$ thus excluding grazing *a priori*. The trapped set K of φ is then defined analogously as in (1) and II) is trivially fulfilled for K. This leaves only the crucial conditions I) and III). In the situation of Section 1.1 we have $\varphi = \varphi^b|_D$ and the non-grazing trapped set condition ensures $K = K^b$ so we may work with either the complete billiard flow φ^b or its non-grazing restriction φ. This observation justifies the more abstract general approach lacking an analogue of φ^b.

We emphasize that neither construction nor study of smooth models for the non-grazing billiard flow, which represent cornerstones in our approach to resonances and zeta functions, require assumptions I)–III). They are used only from Section 5 onwards.

In Appendix B we explain how the results are transferred to a vector-valued situation where the billiard generator $\mathbf{P}$ is lifted to an operator acting on smooth sections of a possibly non-trivial vector bundle over M. Finally, Remark 5.13 mentions further possible (immediate) generalizations of our approach which e.g. allow treatment of billiards involving Hamiltonian dynamics with electric potentials or magnetic fields.

1.3. **Methods.** We obtain the meromorphic resolvent by constructing a smooth model of the billiard flow (Sections 3 and 4) and showing that this flow fits into the framework of [DG16] (Section 5). For the latter step we crucially use results of Conley-Easton [CE71]

and Robinson [Rob80] similarly as it was done in [GMT21, DG18]. The construction of the smooth model allows to work with the well-known notion of resolvent of a smooth vector field (Theorem 5.3) and by [DG16] we directly get the meromorphic continuation and precise wavefront estimates for this resolvent. Now this allows for a large variety of applications: A first such application is established in this article by the *meromorphic continuation to* $\mathbb{C}$ of weighted zeta functions, which in the simplest case of constant weight take the form

$$Z(\lambda) = \sum_{\gamma} \frac{T_\gamma^{\#} \exp\left(-\lambda T_\gamma\right)}{\left|\det\left(\mathrm{id} - \mathcal{P}_\gamma\right)\right|}, \qquad \mathrm{Re}(\lambda) \gg 0,$$

where the sum ranges over all closed trajectories γ of the billiard dynamics, $T_\gamma^{\#}$ denotes the primitive period of γ and $\mathcal{P}_\gamma$ its Poincaré map (for precise definitions and the general theorem we refer to Section 5.3). In the case of 3-disk systems these weighted zeta functions allow the efficient numerical calculation of invariant Ruelle densities (see [BSW22a, Appendix]). In addition, the meromorphic resolvent from Theorem 5.3 allows the rigorous study of semiclasscial zeta functions that are of great importance for understanding quantum resonances. Based on the present framework of smooth models Chaubet and Petkov proved that the semiclassical zeta functions associated with the Dirichlet and Neumann problems for finitely many strictly convex compact obstacles in Euclidean space satisfying the no-eclipse condition continue meromorphically to the whole complex plane and solved the modified Lax-Philipps conjecture in the case of analytic obstacle boundaries [CP22]. Furthermore in [BSW22b] the results regarding meromorphically continued zeta functions were used to provide, in the setting of compact hyperbolic surfaces, a rigorous interpretation of semiclassical zeta functions for Wigner distributions as introduced by Eckhardt et. al. [EFMW92] together with a numerical study of obstacle scattering with obstacles given by three discs in the plane. Another application is given by Yann Chaubet's work [Cha22] on counting asymptotics of periodic trajectories with a fixed reflection number at some fixed obstacle based on previous results in a non-billiard setting [Cha21].

Let us finally mention a recent related result on the definition of Ruelle-Pollicott resonances for billiard flows. In [BDL18] Baladi, Demers and Liverani perform a meromorphic continuation of the billiard resolvent for the Sinai billiard with finite horizon together with a spectral gap in order to establish exponential mixing of the billiard flow. This setting is technically much more challenging than ours because the grazing trajectories cannot be separated from the dynamically relevant region, which is possible in our case by the non-grazing trapped set condition.

1.4. **Acknowledgments.** This project was initiated during P.S.'s stay at MIT in spring 2020 and profited from numerous fruitful discussions with Semyon Dyatlov. We greatly acknowledge his input. We furthermore thank Colin Guillarmou for very helpful discussions concerning the ideas drawn from his work [GMT21] and Yann Chaubet for stimulating discussions and helpful suggestions on an earlier version of the manuscript. This work has received funding from the Deutsche Forschungsgemeinschaft (DFG) (Grant No. WE 6173/1-1 Emmy Noether group "Microlocal Methods for Hyperbolic Dynamics" as well as through the Priority Programme (SPP) 2026 "Geometry at Infinity"). P.S. gratefully acknowledges support from the Studienstiftung des deutschen Volkes. Finally we thank two anonymous referees for many helpful comments.

2. Geometric setup

In this section we will introduce the notation and define the billiard flow.

Let (Σ, g) be a smooth (meaning C^∞) complete connected Riemannian manifold of dimension $n \geq 1$ without boundary, $S\Sigma \coloneqq \{(x,v) \in T\Sigma \,|\, g_x(v,v) = 1\} \subset T\Sigma$ its unit

tangent bundle, and denote by $\mathrm{pr} : S\Sigma \to \Sigma$, $(x,v) \mapsto x$, the bundle projection as well as by $\varphi^g : \mathbb{R} \times S\Sigma \to S\Sigma$, $(t,x,v) \mapsto \varphi_t^g(x,v)$, the geodesic flow. Let $\Omega \subset \Sigma$ be an n-dimensional smooth submanifold with boundary of Σ. We do not assume Ω to be connected – in fact, we regard the connected components of Ω as *obstacles*. Denoting the manifold boundary and the manifold interior of Ω by $\partial\Omega$ and $\mathring{\Omega} := \Omega \setminus \partial\Omega$, respectively, we note that $\mathring{\Omega} \neq \emptyset$ and $\partial\Omega \neq \emptyset$ if $\Omega \neq \emptyset$ and define the *phase space* for our *geodesic billiard* to be

$$M := S(\Sigma \setminus \mathring{\Omega}) = \mathrm{pr}^{-1}(\Sigma \setminus \mathring{\Omega}),$$

the unit tangent bundle over $\Sigma \setminus \mathring{\Omega}$. The space M is a $(2n-1)$-dimensional submanifold with boundary of $S\Sigma$. Its boundary and manifold interior are given by

$$\partial M = (S\Sigma)|_{\partial\Omega}, \qquad \mathring{M} = S(\Sigma \setminus \Omega). \tag{2}$$

Each fiber $S_x\Sigma$, $x \in \partial\Omega$, of the $(n-1)$-sphere bundle ∂M intersects the tangent space $T_x(\partial\Omega)$ in the $(n-2)$-sphere $S_x(\partial\Omega)$. The latter divides $S_x\Sigma$ into two disjoint open hemispheres[2]: One of them is the *inward* hemisphere $(S_x\Sigma)_{\mathrm{in}}$ containing all vectors "pointing towards Ω", i.e., all $v \in S_x\Sigma$ satisfying $g_x(v, n_x) > 0$ with n_x the inward unit normal vector at $x \in \partial\Omega$. The other one is the *outward* hemisphere $(S_x\Sigma)_{\mathrm{out}}$ defined by $g_x(v, n_x) < 0$. This fiber-wise decomposition effects a decomposition of the $(2n-2)$-dimensional manifold ∂M into a disjoint union

$$\partial M = \partial_{\mathrm{g}} M \sqcup \partial_{\mathrm{in}} M \sqcup \partial_{\mathrm{out}} M \tag{3}$$

of the *grazing boundary*

$$\partial_{\mathrm{g}} M := \partial M \cap T(\partial\Omega),$$

a $(2n-3)$-dimensional submanifold of ∂M, as well as the *inward* and *outward boundaries*

$$\partial_{\mathrm{in/out}} M := \bigcup_{x \in \partial\Omega} (S_x\Sigma)_{\mathrm{in/out}},$$

which are open in ∂M. See Figure 2 for an illustration of the three boundary components.

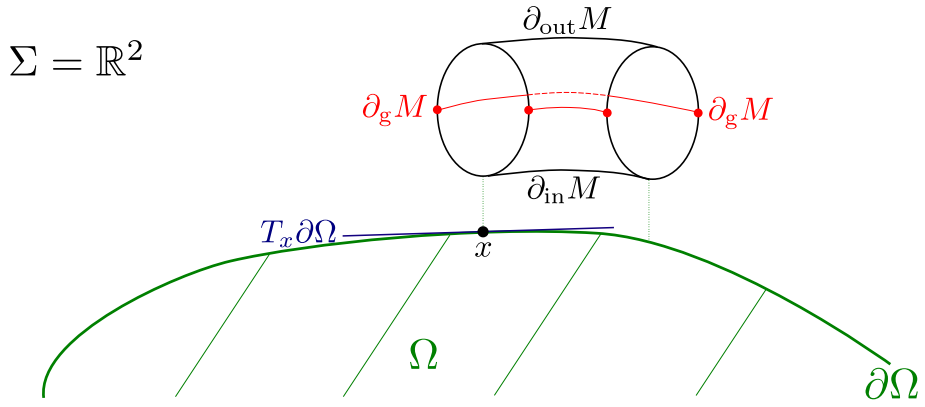

FIGURE 2. In this example with $\Sigma = \mathbb{R}^2$, the boundary $\partial M = S\Sigma|_{\partial\Omega}$ is a circle bundle and therefore looks locally like a cylinder. The red grazing boundary $\partial_{\mathrm{g}} M$ separates the open "half-cylinders" $\partial_{\mathrm{in}} M$ and $\partial_{\mathrm{out}} M$. The intersection of the tangent line $T_x\partial\Omega$ (which here is drawn through x) with ∂M is given by the two red points in the circle over the point $x \in \partial\Omega$.

[2]If $n = 1$, then $S_x(\partial\Omega)$ is empty; it remains true that the 0-sphere $S_x\Sigma$ is divided into two disjoint open "hemispheres" in this case, namely the two points of which it consists. Eq. (3) then holds with $\partial_{\mathrm{g}} M = \emptyset$.

Remark 2.1 (Topological conventions and notation). In this paper, "(smooth) manifold" means "second-countable Hausdorff C^∞-manifold without boundary". "(Smooth) manifold with boundary" means "second-countable Hausdorff C^∞-manifold with boundary". I.e., manifolds only possess a non-empty boundary when explicitly specified. Subsets of smooth manifolds (with or without boundary) are equipped with the induced subspace topology. Whenever we write "an open set $O \subset X$", we mean that O is open in X, i.e., relative to the topology of X. Note that this means, for example, that an open set $O \subset M \setminus \partial_{\mathrm{g}} M$ can intersect ∂M non-trivially.

Remark 2.2. The constructions carried out and the theorems proved in the subsequent sections could potentially be generalized to a setting where we replace the obstacle boundary $\partial\Omega$ by an arbitrary codimension-1 submanifold $B \subset \Sigma$ at which the specular reflections of φ^g occur and which is not necessarily the boundary of an n-dimensional submanifold Ω with boundary. This setting would be more general because not every codimension-1 submanifold occurs as the boundary of a codimension-0 submanifold. However, the example of the circle $\Sigma = S^1$ with $B = \{\mathrm{pt}\}$ a single point, for which our constructions do not work due to the lack of a distinction between "interior" and "exterior", shows that we would then have to impose some additional assumptions on B or to generalize our methods in a somewhat tedious way, so we stick to the case $B = \partial\Omega$ to simplify the presentation.

2.1. **Non-grazing billiard dynamics.** We focus on a *non-grazing* geodesic billiard dynamics. That is, we define trajectories in $M \setminus \partial_{\mathrm{g}} M$ by the rule that they are given by those of the geodesic flow φ^g until they hit ∂M. Then we distinguish two cases:

(1) If a trajectory hits ∂M in a non-grazing way, then the velocity vector is reflected at the tangent hyperplane of the obstacle.
(2) If a trajectory hits ∂M in a grazing way, then it ceases to exist.

Remark 2.3. Before we make the above rules precise, we emphasize that the obtained trajectories will not actually combine to a flow φ on $M \setminus \partial_{\mathrm{g}} M$ in the technical sense because the flow property $\varphi_t(\varphi_{t'}(p)) = \varphi_{t+t'}(p)$ is violated for some points p when $t + t' = 0$, as explained around (8). For simplicity of the terminology, we shall adopt the convention that we call the map φ formed by the billiard trajectories a *flow* regardless of the partial violation of the flow property. We will see that this does not cause any problems. This generalization of terminology applies exclusively to φ (and φ^b, which appears only in the introductory Section 1.1); all other maps called *flow* are honest flows in the usual sense.

For convex obstacles one could of course continue the flow at grazing reflections as in Section 1.1. However, in the following we would be forced to remove such grazing trajectories anyway as with our approach via a quotient construction they cause technical problems when identifying incoming and outgoing directions. It is therefore more convenient to start right away with a non-complete flow that stops at grazing reflections. As a side effect we do not need to make any further a priori assumptions on the nature of the boundary such as absence of inflection points (cf. [CM06, Assumption A3]). Instead, the necessary assumptions can be efficiently formulated as compactness of the trapped set of the non-grazing billiard flow and hyperbolicity of the flow on that set, see Section 2.2.1.

2.1.1. *Definition of the non-grazing billiard flow.* Before we enter the rather technical process of translating the above rules (1) and (2) into a formal definition, we point out that the various formulas are accompanied by two illustrations in Figures 3 and 4.

To begin, we define a tangential reflection $\partial M \to \partial M$, $(x, v) \mapsto (x, v')$, by letting $v' \in S_x\Sigma$ be the reflection of $v \in S_x\Sigma$ at the hyperplane $T_x(\partial\Omega) \subset T_x\Sigma$. In terms of the inward unit normal n_x this reflection is given by $v' = v - 2g_x(v, n_x)n_x$. The tangential reflection fixes $\partial_{\mathrm{g}} M$ and interchanges the two boundary components $\partial_{\mathrm{in}} M$ and $\partial_{\mathrm{out}} M$.

For each point $(x,v) \in M \setminus \partial_{\mathrm{g}} M$ we now define the following extended real numbers which correspond to the first boundary intersection in forward and backward time:

$$\begin{aligned} t_-(x,v) &:= \begin{cases} \sup\{t<0 \,|\, \varphi_t^g(x,v) \in S\Omega\}, & (x,v) \in \mathring{M} \cup \partial_{\mathrm{in}} M, \\ \sup\{t<0 \,|\, \varphi_t^g(x,v') \in S\Omega\}, & (x,v) \in \partial_{\mathrm{out}} M \end{cases} && \in [-\infty, 0), \\ t_+(x,v) &:= \begin{cases} \inf\{t>0 \,|\, \varphi_t^g(x,v) \in S\Omega\}, & (x,v) \in \mathring{M} \cup \partial_{\mathrm{out}} M, \\ \inf\{t>0 \,|\, \varphi_t^g(x,v') \in S\Omega\}, & (x,v) \in \partial_{\mathrm{in}} M \end{cases} && \in (0, \infty]. \end{aligned} \tag{4}$$

Here the inequalities $t_+(x,v) > 0$ and $t_-(x,v) < 0$ follow in the case $(x,v) \in \mathring{M}$ from the continuity of φ^g and the fact that $\mathring{M}$ is open in $S\Sigma$, and in the case $(x,v) \in \partial M \setminus \partial_{\mathrm{g}} M$ from the fact that the flow φ^g is transversal to $\partial M \setminus \partial_{\mathrm{g}} M$.

We begin with the local definition of the billiard trajectories near the boundary: First, let $(x,v) \in \mathring{M}$. Then the billiard flow simply equals the geodesic flow as long as it does not meet an obstacle boundary:

$$\varphi_t(x,v) := \varphi_t^g(x,v), \qquad t_-(x,v) < t < t_+(x,v). \tag{5}$$

If the geodesic flow meets an obstacle boundary in a non-grazing way, i.e., if $t_+(x,v) \in \mathbb{R}$ or $t_-(x,v) \in \mathbb{R}$, then we extend the trajectory via the following obvious definition:

$$\varphi_{t_\pm(x,v)}(x,v) := \varphi^g_{t_\pm(x,v)}(x,v). \tag{6}$$

Now let $(x,v) \in \partial M \setminus \partial_{\mathrm{g}} M$. Then we have to distinguish between inward and outward components:

$$\varphi_t(x,v) := \begin{cases} \varphi_t^g(x,v), & \big((x,v) \in \partial_{\mathrm{out}} M,\ 0 \le t < t_+(x,v)\big) \\ & \text{or } \big((x,v) \in \partial_{\mathrm{in}} M,\ t_-(x,v) < t \le 0\big), \\ \varphi_t^g(x,v'), & \big((x,v) \in \partial_{\mathrm{in}} M,\ 0 < t < t_+(x,v')\big) \\ & \text{or } \big((x,v) \in \partial_{\mathrm{out}} M,\ t_-(x,v') < t < 0\big). \end{cases} \tag{7}$$

The fact that φ^g is a flow implies that the trajectories of φ also have the flow property except for boundary points where the flow property only holds modulo reflection. More precisely, whenever $\varphi_{t'}(\varphi_t(x,v))$ and $\varphi_{t+t'}(x,v)$ are defined by (5), (6), or (7), one has

$$\varphi_{t'}(\varphi_t(x,v)) = \begin{cases} \varphi_{t+t'}(x,v), & t+t' \neq 0 \text{ or } \varphi_{t+t'}(x,v) \in \mathring{M} \text{ or} \\ & \big(t<0, (x,v) \in \partial_{\mathrm{in}} M\big) \text{ or } \big(t>0, (x,v) \in \partial_{\mathrm{out}} M\big), \\ (x,v'), & \big(t+t'=0, t>0, (x,v) \in \partial_{\mathrm{in}} M\big) \text{ or} \\ & \big(t+t'=0, t<0, (x,v) \in \partial_{\mathrm{out}} M\big), \end{cases} \tag{8}$$

while $\varphi_0(x,v) = (x,v)$ for all $(x,v) \in M \setminus \partial_{\mathrm{g}} M$. The additional boundary reflection causing the violation of the flow property does not pose any problems for the remaining paper, though, as points on the boundary related by reflection will be indistinguishable in our smooth models anyway.

Finally we extend the trajectories to their maximal lengths, which is formally somewhat cumbersome: We define for $(x,v) \in M \setminus \partial_{\mathrm{g}} M$ recursively

$$\begin{aligned} t_\pm^0(x,v) &:= t_\pm(x,v), \\ t_\pm^n(x,v) &:= \begin{cases} t_\pm^{n-1}(x,v) + t_\pm\big(\varphi^g_{t_\pm^{n-1}}(x,v)\big), & t_\pm^{n-1}(x,v) \in \mathbb{R} \text{ and } \varphi^g_{t_\pm^{n-1}}(x,v) \notin \partial_{\mathrm{g}} M, \\ t_\pm^{n-1}(x,v), & \text{else,} \end{cases} \end{aligned}$$

where $n \in \mathbb{N}$. Then the sequences $\{t_+^n(x,v)\}_{n\in\mathbb{N}_0} \subset (0,\infty]$ and $\{t_-^n(x,v)\}_{n\in\mathbb{N}_0} \subset [-\infty, 0)$ are non-decreasing and non-increasing, respectively, and we put

$$T_{\max}(x,v) := \limsup_{n\to\infty} t_+^n(x,v) \in (0,\infty], \qquad T_{\min}(x,v) := \liminf_{n\to\infty} t_-^n(x,v) \in [-\infty, 0).$$

These are the maximal times for which the non-grazing billiard flow can be defined: Given $t \in (T_{\min}(x,v), T_{\max}(x,v))$ we can find some $N \in \mathbb{N}_0$ and real numbers $t_0, \dots, t_N \in (T_{\min}(x,v), T_{\max}(x,v))$ with $\sum_{j=0}^{N} t_j = t$ and such that every term in the composition

$$\varphi_t(x,v) \coloneqq \varphi_{t_0}(\varphi_{t_1}(\cdots(\varphi_{t_N}(x,v))\cdots)) \tag{9}$$

is well-defined by either (5), (6), or (7). This definition of $\varphi_t(x,v)$ is then independent of the choice of the numbers $t_0, \dots, t_N$ by virtue of the flow property (8). The definition (9) extends the trajectory through (x,v) such that in summary using the extended terminology from Remark 2.3, we obtain a flow

$$\varphi : D \to M \setminus \partial_{\mathrm{g}} M, \qquad (t,x,v) \mapsto \varphi_t(x,v),$$

on the domain given by

$$D \coloneqq \{(t,x,v) \in \mathbb{R} \times (M \setminus \partial_{\mathrm{g}} M) \,|\, t \in (T_{\min}(x,v), T_{\max}(x,v))\}. \tag{10}$$

Some basic properties of this domain will be proved below in Lemma 2.7. In particular, we shall see that D is open in $\mathbb{R} \times (M \setminus \partial_{\mathrm{g}} M)$. In the following we will call the triple (Σ, g, M) a *geodesic billiard system* and φ its associated *non-grazing billiard flow*, keeping Remark 2.3 in mind.

2.2. **Properties of the non-grazing billiard flow.** By definition, the flow φ has discontinuities at $\varphi^{-1}(\partial M \setminus \partial_{\mathrm{g}} M)$, which makes the following constructions necessary in the first place. A further property of the flow φ that can be read off directly from its definition and which will become important below is its invariance under tangential reflections at the boundary:

$$\forall\ (t,x,v) \in D \cap ((\mathbb{R} \setminus \{0\}) \times \partial M) : \quad (t,x,v') \in D,\ \varphi(t,x,v) = \varphi(t,x,v'). \tag{11}$$

While φ itself is not continuous except in the trivial case $\partial M = \emptyset$, its composition with the projection $\mathrm{pr} : M \to \Sigma \setminus \mathring{\Omega}$ is continuous and describes the *spatial billiard dynamics*. For graphical illustrations of $\mathrm{pr} \circ \varphi$ and φ see Figures 3 and 4.

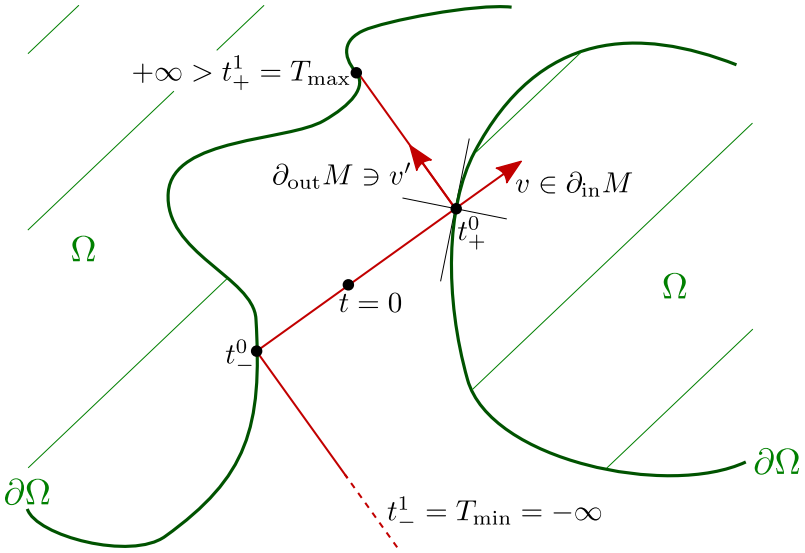

FIGURE 3. A trajectory of the spatial billiard dynamics described by the composition $\mathrm{pr} \circ \varphi : \mathbb{R} \times M \to \Sigma \setminus \mathring{\Omega}$ in an example where $\Sigma = \mathbb{R}^2$ is the Euclidean plane. The arrows indicate a point $(x,v) \in \partial_{\mathrm{in}} M$ as well as its tangential reflection $(x,v') \in \partial_{\mathrm{out}} M$. The reflection happens at the first "forward boundary intersection time" $t_+^0 = t_+^0(x_0,v_0)$ of the (not explicitly annotated) point $(x_0,v_0) \in \mathring{M}$ at $t = 0$. The non-convexity of Ω is not problematic – the trajectory simply ceases to exist at $T_{\max}$.

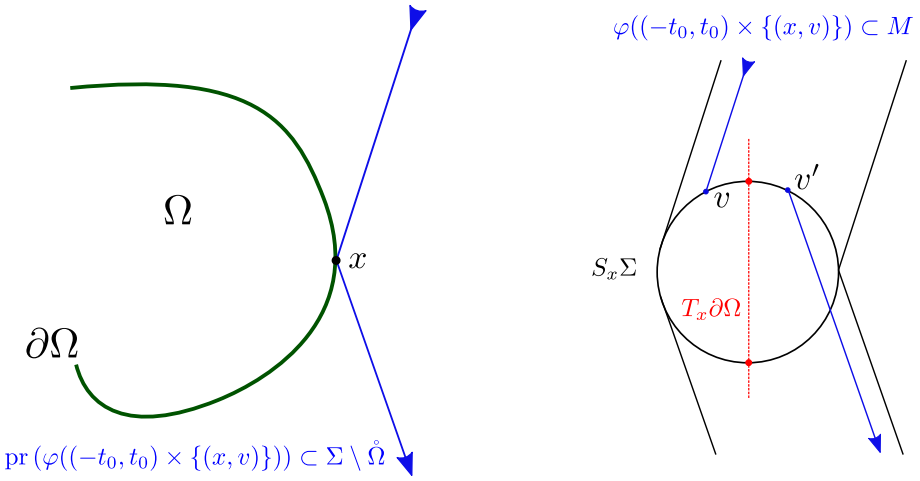

FIGURE 4. The partial flow trajectory $\varphi((-t_0,t_0)\times\{(x,v)\})\subset M$ of a point $(x,v)\in\partial_{\mathrm{in}}M$ and its spatial projection in an example where $\Sigma=\mathbb{R}^2$ is the Euclidean plane. The right-hand side depicts the sphere bundle over the spatial trajectory, which locally looks like a cylinder. Notice the discontinuity in the flow trajectory due to the tangential reflection $(x,v)\mapsto(x,v')$. Projecting the trajectory onto Σ removes this discontinuity.

In spite of its discontinuous nature, the non-grazing billiard flow φ possesses useful transversality properties at the non-grazing boundary $\partial M\setminus\partial_{\mathrm{g}}M$ which we collect in the technical Lemma 2.4 below. This lemma will allow us to prove, among other statements, that the domain D is open in $\mathbb{R}\times(M\setminus\partial_{\mathrm{g}}M)$ and we will later use Lemma 2.4 to consider the flow-time as a "coordinate" transverse to $\partial M\setminus\partial_{\mathrm{g}}M$.

Lemma 2.4. *There exists an open subset $N\subset\mathbb{R}\times(\partial M\setminus\partial_{\mathrm{g}}M)$ such that*

i) One has the inclusions $\{0\}\times(\partial M\setminus\partial_{\mathrm{g}}M)\subset N\subset D$.

ii) The set N is invariant under tangential reflection in the sense that for all $(t,x,v)\in\mathbb{R}\times(\partial M\setminus\partial_{\mathrm{g}}M)$ one has $(t,x,v)\in N$ iff $(t,x,v')\in N$.

iii) The restricted map $\varphi|_N:N\to M$ is open and its image is contained in $M\setminus\partial_{\mathrm{g}}M$.

iv) Decomposing N into the two disjoint open subsets

$$N_{\mathrm{in}}:=N\cap(\mathbb{R}\times\partial_{\mathrm{in}}M),\qquad N_{\mathrm{out}}:=N\cap(\mathbb{R}\times\partial_{\mathrm{out}}M),$$

the two maps $\varphi|_{N_{\mathrm{in/out}}}:N_{\mathrm{in/out}}\to M\setminus\partial_{\mathrm{g}}M$ are injective.

v) The two inverse maps $\varphi|^{-1}_{N_{\mathrm{in/out}}}:\varphi(N_{\mathrm{in/out}})\to N_{\mathrm{in/out}}$ are smooth.

vi) Decomposing N_{in} and N_{out} further into the subsets

$$N^{\pm}_{\mathrm{in/out}}:=N_{\mathrm{in/out}}\cap(\mathbb{R}_{\pm}\times\partial_{\mathrm{in/out}}M),\qquad\mathbb{R}_{\pm}:=\{t\in\mathbb{R}\,|\,\pm t\geq 0\},\tag{12}$$

one has

$$\varphi_t(x,v)=\begin{cases}\varphi^g_t(x,v), & (t,x,v)\in N^-_{\mathrm{in}}\cup N^+_{\mathrm{out}},\\ \varphi^g_t(x,v'), & (t,x,v)\in(N_{\mathrm{in}}\setminus N^-_{\mathrm{in}})\cup(N_{\mathrm{out}}\setminus N^+_{\mathrm{out}}).\end{cases}\tag{13}$$

The proof of Lemma 2.4 is given in Appendix A.1. See Figure 5 for an illustration of $N_{\mathrm{in/out}}$ and $\varphi(N_{\mathrm{in/out}})$ in a 2-dimensional example.

Remark 2.5. Note that by *i)* and *iii)* the images $\varphi(N_{\mathrm{in/out}})$ are open subsets of $M\setminus\partial_{\mathrm{g}}M$ which intersect the boundary $\partial M\setminus\partial_{\mathrm{g}}M$ non-trivially. In particular, the sets $\varphi(N_{\mathrm{in/out}})$ are themselves manifolds with non-empty boundaries (except in the trivial case $\partial M=\emptyset$). In contrast, the open sets $N_{\mathrm{in/out}}\subset\mathbb{R}\times\partial_{\mathrm{in/out}}M$ are manifolds without boundary.

The following definition is motivated by the subsequent important lemma.

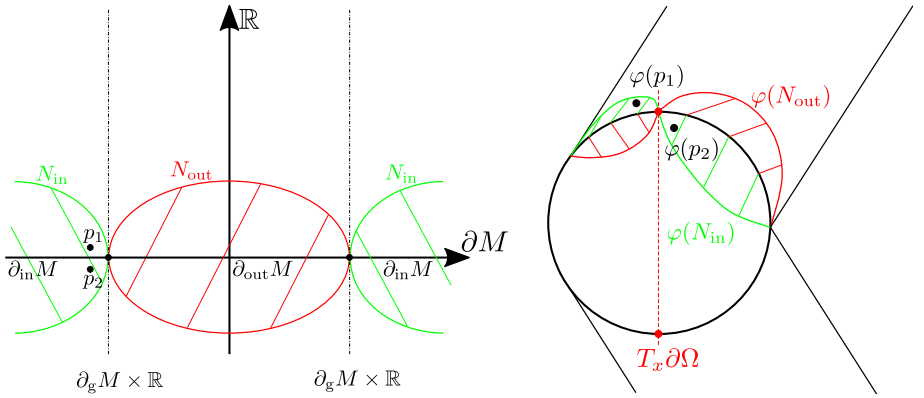

FIGURE 5. Schematic illustration of the sets $N_{\text{in/out}}$ from Lemma 2.4 and their images under φ in a Euclidean setting as in Figure 4. Note that $N_{\text{in/out}}$ and $\varphi(N_{\text{in/out}})$ are actually 3-dimensional. In the image on the left-hand side the dimension has been reduced by drawing the 2-dimensional manifold ∂M simply as a coordinate axis, whereas on the right-hand side the dimension has been reduced by focusing on the circle $S_x\Sigma \subset \partial M$ over some chosen point $x \in \partial\Omega$. Also shown is the action of φ on two points $p_1, p_2 \in N_{\text{in}}$ with strictly negative and strictly positive time coordinates, respectively.

Definition 2.6. *We call a set $A \subset \partial M \setminus \partial_{\text{g}}M$* reflection-symmetric *if for every point $(x,v) \in A$ its tangential reflection (x,v') also belongs to A.*

Using this terminology we can conveniently describe a crucial continuity property of the non-grazing billiard flow φ which puts the discontinuity of the latter into perspective:

Lemma 2.7. *Let $O \subset M \setminus \partial_{\text{g}}M$ be an open set such that $O \cap (\partial M \setminus \partial_{\text{g}}M)$ is reflection-symmetric. Then $\varphi^{-1}(O) \subset D$ is open in $\mathbb{R} \times (M \setminus \partial_{\text{g}}M)$ and invariant under tangential reflection in the sense that*

$$\forall\, (t,x,v) \in \mathbb{R} \times (\partial M \setminus \partial_{\text{g}}M) : (t,x,v) \in \varphi^{-1}(O) \iff (t,x,v') \in \varphi^{-1}(O). \tag{14}$$

In particular, the domain $D = \varphi^{-1}(M \setminus \partial_{\text{g}}M)$ is open in $\mathbb{R} \times (M \setminus \partial_{\text{g}}M)$ and satisfies (14).

The proof of Lemma 2.7 is given in Appendix A.2.

Having shown in Lemma 2.7 that D is open in $\mathbb{R} \times (\partial M \setminus \partial_{\text{g}}M)$ and recalling from (10) that for any $(x,v) \in M \setminus \partial_{\text{g}}M$ the set $\{t \in \mathbb{R} \,|\, (t,x,v) \in D\}$ is an open interval containing 0, these two properties together make D what is often called a *flow domain* for φ.

Finally, let us mention without detailing the proof that using similar arguments as in the proof of Lemma 2.7 one can show that the flow φ is smooth on the set $\varphi^{-1}(\mathring{M})$. The latter is open in $\mathbb{R} \times (M \setminus \partial_{\text{g}}M)$ by Lemma 2.7.

2.2.1. *Trapped set and hyperbolicity.* We define the *trapped set* of φ as those points for which the flow is globally defined and the trajectory remains within a compact region, i.e.:

$$\begin{aligned} K := \big\{ (x,v) \in M \setminus \partial_{\text{g}}M \,|\, & \mathbb{R} \times \{(x,v)\} \subset D, \\ & \exists \text{ compact } W \subset M \setminus \partial_{\text{g}}M \text{ with } \varphi(\mathbb{R} \times \{(x,v)\}) \subset W \big\}. \end{aligned} \tag{15}$$

An illustration of K in a 2-dimensional Euclidean setting can be found in Figure 6.

Lemma 2.8. *$K \cap (\partial M \setminus \partial_{\text{g}}M)$ is reflection-symmetric in the sense of Definition 2.6.*

Proof. This follows immediately from the fact that for every $(x,v) \in K \cap (\partial M \setminus \partial_{\text{g}}M)$ the trajectory $\varphi(\mathbb{R} \times \{(x,v')\})$ is well-defined and coincides with $\varphi(\mathbb{R} \times \{(x,v)\})$ except at $t = 0$, as follows from (11). □

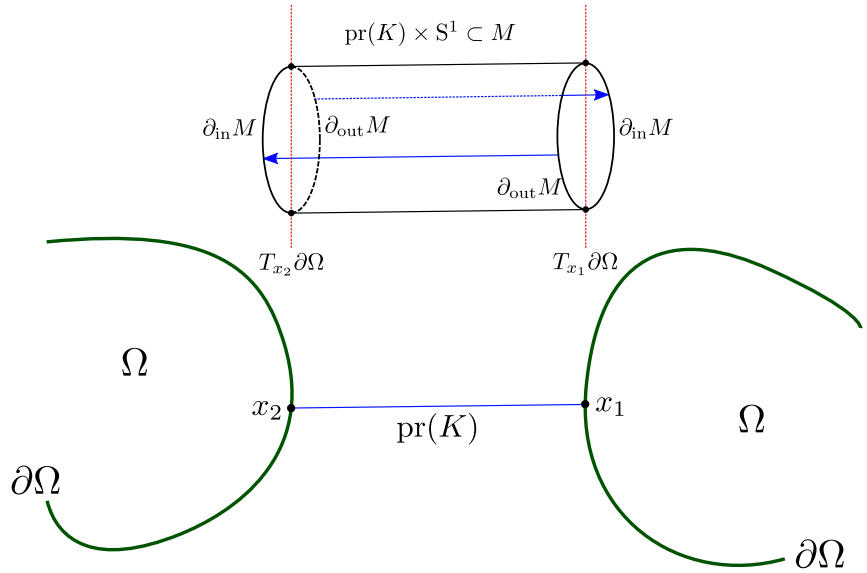

FIGURE 6. Illustration of the trapped set K in an example where $\Sigma = \mathbb{R}^2$ is the Euclidean plane and $\mathrm{pr}(K)$ consists of a single closed "bouncing" trajectory of the spatial billiard flow.

Remark 2.9. For the proof of our main results (Theorem 5.3, Corollary 5.5) we will assume that the trapped set K is compact. Note that this assumption is a non-trivial condition on the global geometry of the obstacles because we work with the non-grazing dynamics. The compactness of the trapped set implies that all trapped trajectories are located at a strictly positive distance from the grazing trajectories.

Lemma 2.10. *If in the n-dimensional Euclidean convex obstacle scattering setup considered in the introduction the obstacles $\Omega = \cup_{i=1}^N \Omega_i \subset \mathbb{R}^n$ fulfill the non-grazing trapped set condition (thus in particular if they fulfill the no-eclipse condition), then the trapped set K of the non-grazing billiard flow, defined in* (15)*, agrees with the trapped set K^b of the billiard flow defined in* (1)*. In particular, K is compact.*

Proof. As our non-grazing billiard flow φ is a restriction of the complete billiard flow φ^b up to the first grazing collision one clearly has $K \subset K^b$. Now the non-grazing trapped set condition implies that none of the trajectories in K^b experiences a grazing collision which lets us infer the reverse inclusion $K^b \subset K$. Finally, in view of the compactness of $\cup_{i=1}^N \Omega_i$, it is a well-known fact that K^b is compact, see [FL21, Section 1.3] and the references given therein. □

Remark 2.11. If the obstacles $\cup_{i=1}^N \Omega_i$ are not assumed to satisfy the non-grazing trapped set condition it is easy to construct examples that have a non-compact trapped set K (but nevertheless a compact trapped set K^b for the billiard flow φ^b), see Figure 7.

Finally we introduce a notion of *hyperbolicity* for the billiard dynamics.

Definition 2.12. *The non-grazing billiard flow φ is called* hyperbolic on its trapped set K *if the following holds: For any $(x,v) \in K \cap \mathring{M}$ the tangent bundle exhibits a continuous splitting*

$$T_{(x,v)}M = \mathbb{R} \cdot X(x,v) \oplus E_s(x,v) \oplus E_u(x,v), \tag{16}$$

where $X(x,v)$ denotes the flow direction at (x,v), $E_{s/u}(x,v)$ is mapped onto $E_{s/u}(\varphi_t(x,v))$ under the differential of φ_t whenever $\varphi_t(x,v) \in K \cap \mathring{M}$, and there exist constants $C_0, C_1 > 0$

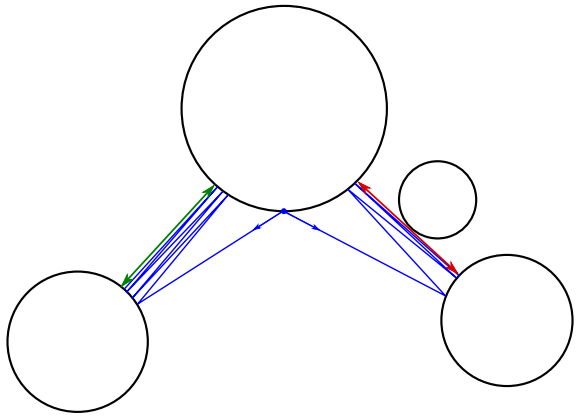

FIGURE 7. The red trajectory belongs to the spatial projection of the trapped set K^b of the billiard flow, but not to the spatial projection of K as it contains a grazing collision. The green and blue trajectories, however, belong to the spatial projections of K^b as well as K. Note that the red trajectory clearly lies in the closure of the blue trajectory in $\Sigma \setminus \mathring{\Omega}$ and the latter touches the former tangentially, thus K is not closed in $M \setminus \partial_{\mathrm{g}} M$ and hence not compact.

such that

$$\begin{aligned} \|\mathrm{d}\varphi_t(x,v)W\|_{\varphi_t(x,v)} &\leq C_0 \exp(-C_1 t)\|W\|_{(x,v)}, \quad t \geq 0,\ \varphi_t(x,v) \in K \cap \mathring{M},\ W \in E_s(x,v) \\ \|\mathrm{d}\varphi_t(x,v)W\|_{\varphi_t(x,v)} &\geq C_0^{-1} \exp(C_1 t)\|W\|_{(x,v)}, \quad t \geq 0,\ \varphi_t(x,v) \in K \cap \mathring{M},\ W \in E_u(x,v), \end{aligned} \tag{17}$$

where $\|\cdot\|$ *denotes any continuous norm on the tangent bundle* TM.

Remark 2.13. Let $\Omega \subset \mathbb{R}^n$ be the disjoint union of finitely many compact, connected, strictly convex sets with smooth boundaries and take on $\mathbb{R}^n$ the Euclidean metric. Then [CM06, Chapter 4.4] and [CP22, Appendix] show that the associated non-grazing billiard is hyperbolic on its trapped set. See also [Dya18, Section 5.2] for an introductory exposition of hyperbolicity of dispersing billiards.

2.3. **Reflection-invariance of the canonical contact structure.** The sphere bundle $S\Sigma$ carries a canonical contact form α corresponding to the Liouville form (the tautological 1-form) on the co-sphere bundle $S^*\Sigma$ under the diffeomorphism $S\Sigma \cong S^*\Sigma$ provided by the Riemannian metric g, i.e., $\alpha_{(x,v)}(w) := g_x(v, \mathrm{d}\pi_{(x,v)}w)$ for the projection $\pi(x,v) = x$ and a vector $w \in T_{(x,v)}(S\Sigma)$. The restriction of α to the submanifold $\partial M = (S\Sigma)|_{\partial\Omega} \subset S\Sigma$ can be pulled back along the tangential reflection map $R : \partial M \to \partial M$, $(x,v) \mapsto (x,v')$. It turns out that $\alpha|_{\partial M}$ is invariant under this pullback, a property we will need later on:

Lemma 2.14. *One has the equality of* 1*-forms* $R^*(\alpha|_{\partial M}) = \alpha|_{\partial M}$.

Proof. Let $\pi : \partial M = (S\Sigma)|_{\partial\Omega} \to \partial\Omega$ be the bundle projection $(x,v) \mapsto x$. Then we compute for $(x,v) \in \partial M$, $w \in T_{(x,v)}(\partial M)$ using the formula $v' = v - 2g_x(v,n_x)n_x$ featuring the inward normal vector $n_x \perp T_x(\partial\Omega)$:

$$\begin{aligned} \alpha_{(x,v)}(w) &= g_x(v, \mathrm{d}\pi_{(x,v)}(w)), \\ R^*(\alpha|_{\partial M})_{(x,v)}(w) &= g_x(v', \mathrm{d}(\pi \circ R)_{(x,v)}(w)) \\ &= g_x(v - 2g_x(v,n_x)n_x, \mathrm{d}\pi_{(x,v)}(w)) \\ &= \alpha_{(x,v)}(w) - 2g_x(v,n_x)\underbrace{g_x(n_x, \mathrm{d}\pi_{(x,v)}(w))}_{=0}. \end{aligned}$$

Here we used the facts that $\pi \circ R = \pi$ and $\mathrm{d}\pi_{(x,v)}(w) \in T_x(\partial\Omega)$. □

2.4. **Billiard functions and the billiard generator.** Although the non-grazing billiard flow $\varphi : D \to M \setminus \partial_{\mathrm{g}} M$ is not continuous and partially violates the flow property, and therefore does not possess a generating vector field, we can associate with φ natural function spaces as well as an operator providing a replacement for the generator of φ.

Indeed, recall from Lemma 2.7 that D is open in $\mathbb{R} \times (M \setminus \partial_{\mathrm{g}} M)$ and that more generally for every open set $O \subset M \setminus \partial_{\mathrm{g}} M$ such that $O \cap (\partial M \setminus \partial_{\mathrm{g}} M)$ is reflection-symmetric the inverse image $\varphi^{-1}(O) \subset D$ is open. Fix such a set O. Then we define the vector space of (compactly supported) *smooth billiard functions* on O by

$$\mathrm{C}^\infty_{\mathrm{Bill}}(O) \coloneqq \{f \in \mathrm{C}^\infty(O) \,|\, f \circ \varphi \in \mathrm{C}^\infty(\varphi^{-1}(O))\}, \quad \mathrm{C}^\infty_{\mathrm{Bill,c}}(O) \coloneqq \mathrm{C}^\infty_{\mathrm{Bill}}(O) \cap \mathrm{C}^\infty_{\mathrm{c}}(O). \tag{18}$$

Note how this definition requires smoothness up to the boundary $O \cap \partial M$ but also imposes additional constraints of a non-local nature between boundary points which are related via the boundary reflection map.

These spaces are non-trivial: The smoothness of φ on $\varphi^{-1}(\mathring{M})$ implies that there is an injection $\mathrm{C}^\infty_{\mathrm{c}}(O \cap \mathring{M}) \hookrightarrow \mathrm{C}^\infty_{\mathrm{Bill,c}}(O)$. We consider these spaces as interesting because they provide natural domains for the following differential operator

$$\begin{aligned} &\mathbf{P} : \mathrm{C}^\infty_{\mathrm{Bill}}(O) \longrightarrow \mathrm{C}^\infty_{\mathrm{Bill}}(O), \\ &(\mathbf{P}f)(x,v) \coloneqq \frac{\mathrm{d}}{\mathrm{d}t}\bigg|_{t=0} f \circ \varphi_t(x,v), \qquad (x,v) \in O. \end{aligned} \tag{19}$$

The operator $\mathbf{P}$ is well-defined, preserves $\mathrm{C}^\infty_{\mathrm{Bill,c}}(O)$ and will henceforth be called the *billiard generator*. This name is justified by (19) which makes $\mathbf{P}$ a formal generator of the flow φ, where the discontinuity and the partial violation of the flow property of the latter are dealt with by passing to the function space $\mathrm{C}^\infty_{\mathrm{Bill}}(O)$. On the subspace $\mathrm{C}^\infty_{\mathrm{c}}(O \cap \mathring{M}) \subset \mathrm{C}^\infty_{\mathrm{Bill,c}}(O)$ the operator $\mathbf{P}$ simply acts as the geodesic vector field which is smooth up to points in the manifold boundary ∂M. In fact, if $X^g : \mathrm{C}^\infty(O) \to \mathrm{C}^\infty(O)$ denotes the generator of the geodesic flow φ^g on the set O, then for every function $f \in \mathrm{C}^\infty_{\mathrm{Bill}}(O)$ the smooth function $\mathbf{P}f$ agrees with $X^g f$ on $O \cap \mathring{M}$ which is dense in O, so it follows that $\mathbf{P}f = X^g f$ on all of O. This shows that the billiard generator $\mathbf{P}$ is nothing but the restriction of X^g to the domain $\mathrm{C}^\infty_{\mathrm{Bill}}(O)$:

$$\mathbf{P} = X^g|_{\mathrm{C}^\infty_{\mathrm{Bill}}(O)}. \tag{20}$$

In particular, we see that X^g preserves $\mathrm{C}^\infty_{\mathrm{Bill}}(O)$ and $\mathrm{C}^\infty_{\mathrm{Bill,c}}(O)$.

Note that we can easily extend the construction (18) to define analogous spaces of continuous billiard functions $\mathrm{C}_{\mathrm{Bill}}(O)$ and billiard functions of limited regularity $\mathrm{C}^N_{\mathrm{Bill}}(O)$.

We refrain from introducing topologies on the spaces $\mathrm{C}^\infty_{\mathrm{Bill}}(O)$, e.g. the subspace topologies induced by $\mathrm{C}^\infty(O)$, and $\mathrm{C}^\infty_{\mathrm{Bill,c}}(O)$ to avoid further technicalities. Instead we will introduce *smooth models* for the billiard flow which will allow us to work with ordinary smooth functions and distributions on a smooth manifold as well as a smooth vector field $\mathbf{X}$ instead of the above defined operator $\mathbf{P}$.

3. Smooth models for the non-grazing billiard flow

The fact that the non-grazing billiard flow is discontinuous is highly inconvenient. However, we shall see that a smooth model for the non-grazing billiard flow φ exists and is unique in a strong sense, so that we can consider it as intrinsic to the geodesic billiard system (Σ, g, Ω). The literature on billiards often presupposes a smooth model or works on $\varphi^{-1}(\mathring{M})$ to begin with, see e.g. [CM06]. Here we give a definition of smooth models in a slightly more general geometric setting and perform an explicit construction to show the existence of such a model. While smooth models no longer carry the bundle structure of $S\Sigma$, the smooth model flows remain *contact flows*. This constitutes a very convenient technical feature which is often implicit in concrete coordinate calculations in the billiard

literature. We remind the reader that *smooth* refers to C^∞-regularity throughout this article and diffeomorphisms are always assumed to be C^∞ as well.

Definition 3.1. *A* smooth model *for the non-grazing billiard flow $\varphi : D \to M$ is a triple $(\mathcal{M}, \pi, \phi)$ consisting of a smooth manifold $\mathcal{M}$, a smooth surjection $\pi : M \setminus \partial_{\mathrm{g}} M \to \mathcal{M}$ such that $\mathcal{D} := (\mathrm{id}_{\mathbb{R}} \times \pi)(D) \subset \mathbb{R} \times \mathcal{M}$ is open, and a smooth flow $\phi : \mathcal{D} \to \mathcal{M}$ such that*

i) The restriction $\pi|_{\mathring{M}}$ is a diffeomorphism onto its image.

ii) The flows φ and ϕ are intertwined by π:

$$\phi \circ (\mathrm{id}_{\mathbb{R}} \times \pi)|_D = \pi \circ \varphi. \tag{21}$$

We emphasize that in the above definition ϕ must be a flow – the exceptional generalized terminology introduced in Remark 2.3 only applies to φ.

Definition 3.1 is motivated by the following existence and uniqueness results.

Theorem 3.2. *There exists a smooth model $(\mathcal{M}, \pi, \phi)$ for φ such that ϕ is a contact flow.*

Proof. In the subsequent Section 4 we give an explicit construction of a manifold $\mathcal{M}$, a map π, a flow ϕ, and a contact form $\alpha_{\mathcal{M}}$ with the required properties, culminating in the final Corollary 4.3. □

Proposition 3.3. *Suppose that $(\mathcal{M}, \pi, \phi)$ and $(\mathcal{M}', \pi', \phi')$ are two smooth models for φ. Then $(\mathcal{M}, \phi)$ and $(\mathcal{M}', \phi')$ are uniquely smoothly conjugate. More precisely, there is a unique diffeomorphism $F : \mathcal{M} \to \mathcal{M}'$ such that $F \circ \pi = \pi'$, $(\mathrm{id}_{\mathbb{R}} \times F)(\mathcal{D}) = \mathcal{D}'$, and $F \circ \phi = \phi' \circ (\mathrm{id}_{\mathbb{R}} \times F)|_{\mathcal{D}}$.*

The proof of Proposition 3.3 is given in Appendix A.3.

Corollary 3.4. *Let $(\mathcal{M}, \pi, \phi)$ be a smooth model for φ. Then ϕ is a contact flow, i.e., there exists a contact form $\alpha_{\mathcal{M}}$ on $\mathcal{M}$ whose Reeb vector field is the generator $\mathbf{X}$ of ϕ.*

Proof. A contact form with the desired property is provided by the pullback of the contact form whose existence is guaranteed by Theorem 3.2 along the unique diffeomorphism of Proposition 3.3. □

3.1. **Smooth models and the billiard generator.** Here we show that smooth models for the non-grazing billiard flow φ are naturally related to the spaces of billiard functions and the billiard generator $\mathbf{P}$ defined in Section 2.4. In the following, let $(\mathcal{M}, \pi, \phi)$ be a smooth model for φ as in Definition 3.1, let $\mathcal{O} \subset \mathcal{M}$ be an open set, and write $O := \pi^{-1}(\mathcal{O}) \subset M \setminus \partial_{\mathrm{g}} M$. Then $O \cap (\partial M \setminus \partial_{\mathrm{g}} M)$ is reflection-symmetric by Lemma A.1. Further, we denote by $\mathbf{X} : \mathrm{C}^\infty(\mathcal{O}) \to \mathrm{C}^\infty(\mathcal{O})$ the generator of the smooth flow ϕ on $\mathcal{O}$.

Proposition 3.5. *The pullback $\pi^* : \mathrm{C}^\infty(\mathcal{O}) \to \mathrm{C}^\infty(O)$ is injective and one has*

$$\pi^*(\mathrm{C}^\infty(\mathcal{O})) = \mathrm{C}^\infty_{\mathrm{Bill}}(O), \qquad \pi^*(\mathrm{C}^\infty_{\mathrm{c}}(\mathcal{O})) = \mathrm{C}^\infty_{\mathrm{Bill,c}}(O). \tag{22}$$

Moreover, we have the equality

$$\pi^* \circ \mathbf{X} \circ (\pi^*)^{-1} = \mathbf{P} \tag{23}$$

of linear operators $\mathrm{C}^\infty_{\mathrm{Bill}}(O) \to \mathrm{C}^\infty_{\mathrm{Bill}}(O)$ or $\mathrm{C}^\infty_{\mathrm{Bill,c}}(O) \to \mathrm{C}^\infty_{\mathrm{Bill,c}}(O)$.

Proof. The injectivity of π^* is due to the surjectivity of π. The inclusions $\pi^*(\mathrm{C}^\infty(\mathcal{O})) \subset \mathrm{C}^\infty_{\mathrm{Bill}}(O)$ and $\pi^*(\mathrm{C}^\infty_{\mathrm{c}}(\mathcal{O})) \subset \mathrm{C}^\infty_{\mathrm{Bill,c}}(O)$ follow from the fact that $\pi \circ \varphi : D \to \mathcal{M}$ is smooth by (21) and that π is proper by Lemma A.1.

To prove the reverse inclusions, let f be a function that belongs to one of the billiard function spaces appearing on the right-hand side of (22). Using Lemma (A.1) and the definition $\mathcal{G} := \pi(\partial_{\mathrm{in}} M)$ we define $g : \mathcal{O} \to \mathbb{C}$ by

$$g(p) := \begin{cases} f(\pi|_{\mathring{M}}^{-1}(p)), & p \in \mathcal{O} \cap \pi(\mathring{M}), \\ f(\pi|_{\partial_{\mathrm{in}} M}^{-1}(p)), & p \in \mathcal{O} \cap \pi(\partial_{\mathrm{in}} M) = \mathcal{O} \cap \mathcal{G}. \end{cases}$$

Then we have $g \circ \pi = f$, in particular, g has compact support if f has compact support because π is continuous. By the same argument as in the proof of Proposition 3.3 smoothness of g is only non-trivial around $\mathcal{G}$ and this boils down to showing smoothness of $f \circ \varphi$ in some neighborhood of $\{0\} \times \partial_{\mathrm{in}} M$ with respect to $\mathbb{R} \times \partial_{\mathrm{in}} M$. Proving that g is C^∞ thus reduces to showing that for an open set $V \subset (\mathbb{R} \times \mathcal{G}) \cap \mathcal{D}$ containing $\{0\} \times \mathcal{G}$ the composition $g \circ \phi|_W : W \to \mathbb{C}$ is C^∞, where $W := \phi^{-1}(\mathcal{O}) \cap V$.

To this end we use (21), by which $g \circ \phi \circ (\mathrm{id}_{\mathbb{R}} \times \pi)|_D = g \circ \pi \circ \varphi = f \circ \varphi$. Since $\pi|_{\partial_{\mathrm{in}} M} : \partial_{\mathrm{in}} M \to \mathcal{G}$ is a diffeomorphism by Lemma A.1, we see that $g \circ \phi|_W$ is smooth iff the restriction of $f \circ \varphi$ to the set $(\mathrm{id}_{\mathbb{R}} \times \pi|^{-1}_{\partial_{\mathrm{in}} M})(W) \subset \mathbb{R} \times \partial_{\mathrm{in}} M$ is smooth. The latter holds true since f is a smooth billiard function. Indeed, $(\mathrm{id}_{\mathbb{R}} \times \pi|^{-1}_{\partial_{\mathrm{in}} M})(W)$ is open in $\mathbb{R} \times \partial_{\mathrm{in}} M$ which is a boundary submanifold of $\mathbb{R} \times (M \setminus \partial_{\mathrm{g}} M)$ and the restriction of the smooth function $f \circ \varphi$ to that boundary submanifold is again smooth. We conclude that $f = g \circ \pi = \pi^* g$ as stated in the proposition above.

To finally prove (23), we first note that the generator $\mathbf{X}$ of ϕ acts on $f \in \mathrm{C}^\infty(\mathcal{O})$ via

$$\mathbf{X} f(p) = \frac{\mathrm{d}}{\mathrm{d}t}\bigg|_{t=0} f \circ \phi_t(p), \quad p \in \mathcal{O}.$$

Given $p \in O$ and $f \in \mathrm{C}^\infty(\mathcal{O})$ we therefore calculate using (21)

$$\mathbf{P}(f \circ \pi)(p) = \frac{\mathrm{d}}{\mathrm{d}t}\bigg|_{t=0} f \circ \pi \circ \varphi_t(p) = \frac{\mathrm{d}}{\mathrm{d}t}\bigg|_{t=0} f \circ \phi_t(\pi(p)) = \mathbf{X} f(\pi(p)),$$

finishing the proof. □

3.2. **Smooth trapped set, closed trajectories, and hyperbolicity.** We already defined the trapped set of the non-grazing billiard flow φ in Section 2.2.1. Given a smooth model $(\mathcal{M}, \pi, \phi)$ of φ as in Definition 3.1 we define the corresponding notion of trapped set for ϕ as

$$\mathcal{K} := \{p \in \mathcal{M} \,|\, \mathbb{R} \times \{p\} \subset \mathcal{D},\ \exists \text{ compact } \mathcal{W} \subset \mathcal{M} \text{ with } \phi(\mathbb{R} \times \{p\}) \subset \mathcal{W}\}. \tag{24}$$

We then get the following dynamical correspondence between the non-grazing billiard flow and its smooth model flow:

Proposition 3.6. *The equalities $\mathcal{K} = \pi(K)$, $\pi^{-1}(\mathcal{K}) = K$ hold, and there exists a natural period-preserving bijection between the closed trajectories of ϕ and the closed trajectories of φ. More precisely:*

- *i) Given $p \in \mathcal{M}$ with $\phi_T(p) = p$ for some $T > 0$ and $\phi_t(p) \neq p$ for all $t \in (0, T)$, there exists $(x, v) \in M \setminus \partial_{\mathrm{g}} M$ such that $\varphi_T(x, v) = (x, v)$, $\varphi_t(x, v) \neq (x, v)$ for all $t \in (0, T)$, and $\pi(x, v) = p$.*
- *ii) Conversely, given $(x, v) \in M \setminus \partial_{\mathrm{g}} M$ with $\varphi_T(x, v) = (x, v)$ for some $T > 0$ and $\varphi_t(x, v) \neq (x, v)$ for all $t \in (0, T)$, then $\pi(x, v) \in \mathcal{K}$, $\phi_T(\pi(x, v)) = \pi(x, v)$, and $\phi_t(\pi(x, v)) \neq \pi(x, v)$ for all $t \in (0, T)$.*

Proof. The equalities $\mathcal{K} = \pi(K)$, $\pi^{-1}(\mathcal{K}) = K$ follow from (21) and the facts that π is continuous and also proper by Lemma A.1.

Let $p = \pi(x, v) \in \mathcal{M}$ be as in *i)*. If $p \in \pi(\partial M \setminus \partial_{\mathrm{g}} M)$ we can make the choice $(x, v) \in \partial_{\mathrm{in}} M$ because by Lemma A.1 and $\mathcal{M} = \pi(\mathring{M}) \sqcup \mathcal{G}$ we must have $\pi^{-1}(p) = \{(x, v), (x, v')\}$. Then, regardless of whether $p \in \pi(\partial M \setminus \partial_{\mathrm{g}} M)$ or not, $\phi_T(p) = p$ implies $\varphi_T(x, v) = (x, v)$ and $\varphi_t(x, v) = (x, v)$ for $t \in (0, T)$ would imply the contradiction $\phi_t(p) = p$. Claim *ii)* can be checked directly by using the relation $\phi_t \circ \pi = \pi \circ \varphi_t$. □

Finally we discuss hyperbolicity of our smooth models: The model flow ϕ is called *hyperbolic on its trapped set* $\mathcal{K}$ if the following condition similar to Definition 2.12 holds:

For any $p \in \mathcal{K}$ the tangent bundle $T_p\mathcal{M}$ splits in a continuous and flow invariant fashion as

$$T_p\mathcal{M} = \mathbb{R} \cdot \mathbf{X}(p) \oplus \mathcal{E}_s(p) \oplus \mathcal{E}_u(p), \tag{25}$$

and there exist constants $C_0, C_1 > 0$ such that

$$\begin{aligned} \|\mathrm{d}\phi_t(p)W\|_{\phi_t(p)} &\leq C_0 \exp(-C_1 t)\|W\|_p, \quad t \geq 0,\ W \in \mathcal{E}_s(p) \\ \|\mathrm{d}\phi_t(p)W\|_{\phi_t(p)} &\geq C_0^{-1} \exp(C_1 t)\|W\|_p, \quad t \geq 0,\ W \in \mathcal{E}_u(p), \end{aligned} \tag{26}$$

where $\|\cdot\|$ denotes any continuous norm on $T\mathcal{M}$. The next proposition connects hyperbolicity of φ with hyperbolicity of its smooth model flows:

Proposition 3.7. *Let $\varphi : D \to M$ be a non-grazing billiard flow that is hyperbolic on its trapped set K. Then any smooth model $(\mathcal{M}, \pi, \phi)$ for φ is hyperbolic on its trapped set $\mathcal{K}$.*

Proof. We construct the hyperbolic splitting over $\mathcal{K}$ as follows: On $\mathring{M}$ the natural candidate is the one already given in (16) and transported via the differential of the diffeomorphism $\kappa := \pi|_{\mathring{M}}$, i.e., for $p = \pi(x, v) \in \mathcal{M} \setminus \mathcal{G}$ we have

$$T_p\mathcal{M} = \mathbb{R} \cdot \mathbf{X}(p) \oplus \mathcal{E}_s(p) \oplus \mathcal{E}_u(p), \tag{27}$$

where $\mathcal{E}_{s/u}(\pi(x, v)) := \mathrm{d}\kappa(x, v)E_{s/u}(x, v)$ and $\mathbf{X}(\pi(x, v)) = \mathrm{d}\kappa(x, v)X(x, v)$ is the generator of ϕ evaluated at $\pi(x, v)$. This splitting is again invariant under ϕ_t whenever $\phi_t(\pi(x, v)) \in \mathcal{K} \cap \pi(\mathring{M}) = \mathcal{K} \cap (\mathcal{M} \setminus \mathcal{G})$ by the relation $\phi_t \circ \pi = \pi \circ \varphi_t$ and the flow invariance of the original splitting.

We now extend this splitting to all of $\mathcal{K}$ as follows: For $p = \pi(x, v) \in \mathcal{K} \cap \mathcal{G}$ we define

$$\mathcal{E}_{s/u}(p) = \mathrm{d}\phi_{-t}\left(\mathcal{E}_{s/u}(\phi_t(p))\right)$$

for any $t \in \mathbb{R}$ such that $\phi_t(p) \notin \mathcal{G}$; in particular, any $t \neq 0$ close enough to 0 will do the job. By the flow property of ϕ and the flow invariance of the original splitting (16) this definition is independent of t, (27) holds for p as $\mathrm{d}\phi_{-t}$ is an isomorphism $T_{\phi_t(p)}\mathcal{M} \to T_p\mathcal{M}$, and the obtained splitting is continuous by continuity of ϕ.

It remains to show that the hyperbolicity estimates (17) hold. Given $W \in \mathcal{E}_s(p)$ and arbitrary $t' \geq 0$ we calculate

$$\|\mathrm{d}\phi_{t'}(p)W\|_{\phi_{t'}(p)} \leq C_0 \mathrm{e}^{-C_1(t'-t)}\|\mathrm{d}\phi_t(p)W\|_{\phi_t(p)},$$

where $t > 0$ is sufficiently small such that $\phi((0, t] \times \{p\}) \subset \mathcal{M} \setminus \mathcal{G}$. In the limit $t \to 0$ we obtain the desired estimate. □

Remark 3.8. Let φ be the non-grazing billiard flow constructed from the Euclidean metric on $\mathbb{R}^n$ and the disjoint union of finitely many compact, connected, strictly convex obstacles with smooth boundaries. Then Proposition 3.7 combined with Remark 2.13 shows that any smooth model for φ is hyperbolic on its trapped set.

4. Construction of a smooth model

This section is devoted to proving the existence Theorem 3.2 by explicitly constructing the required objects. In view of the strong uniqueness result Proposition 3.3 our construction method is essentially unique. We break up the proof into several lemmas and corollaries until we arrive at the final Corollary 4.3.

4.1. The topological space $\mathcal{M}$ and continuous flow ϕ.

We first define $\mathcal{M}$ as a topological space and ϕ as a continuous flow. In the subsequent Section 4.2 we proceed to proving that $\mathcal{M}$ can be equipped with a smooth structure such that ϕ is smooth.

We define our model space as

$$\mathcal{M} := (M \setminus \partial_{\mathrm{g}}M)/\sim,$$

where the equivalence relation $\sim$ on $M \setminus \partial_{\mathrm{g}} M$ is defined by the equivalence classes

$$[x,v] \coloneqq \begin{cases} \{(x,v)\}, & (x,v) \in \mathring{M}, \\ \{(x,v),(x,v')\}, & (x,v) \in \partial M. \end{cases}$$

We denote by

$$\pi : M \setminus \partial_{\mathrm{g}} M \to \mathcal{M}, \qquad (x,v) \mapsto [x,v], \tag{28}$$

the canonical projection and equip $\mathcal{M}$ with the quotient topology making π continuous. We call the set $\mathcal{G} \coloneqq \pi(\partial M \setminus \partial_{\mathrm{g}} M) \subset \mathcal{M}$ formed by all 2-element equivalence classes the *gluing region*. It is a closed subset of $\mathcal{M}$ since $\pi^{-1}(\mathcal{M} \setminus \mathcal{G}) = \mathring{M}$ is open in M. As suggested by Definition 3.1, we define the domain

$$\mathcal{D} \coloneqq (\mathrm{id}_{\mathbb{R}} \times \pi)(D) \subset \mathbb{R} \times \mathcal{M},$$

where D is the non-grazing flow domain of φ defined in (10). The symmetry (14) of D under tangential reflection implies that $(\mathrm{id}_{\mathbb{R}} \times \pi)^{-1}(\mathcal{D}) = D$, so Lemma 2.7 implies that $\mathcal{D}$ is open in $\mathbb{R} \times \mathcal{M}$ as required by Definition 3.1. The compatibility property (11) of φ with the tangential reflection now allows us to define a flow

$$\phi : \mathcal{D} \to \mathcal{M}, \qquad \phi(t,[x,v]) \coloneqq [\varphi(t,x,v)], \qquad (t,x,v) \in D,$$

which by construction satisfies the relation $\phi \circ (\mathrm{id}_{\mathbb{R}} \times \pi) = \pi \circ \varphi$ on D.

The main motivation for the definition of $\mathcal{M}$ using the equivalence relation $\sim$ is the *continuity* of the flow ϕ:

Lemma 4.1. *The flow $\phi : \mathcal{D} \to \mathcal{M}$ is continuous.*

Proof. Given an open set $\mathcal{O} \subset \mathcal{M}$ we first note that $O \coloneqq \pi^{-1}(\mathcal{O}) \subset M \setminus \partial_{\mathrm{g}} M$ is open by continuity of π. Since $O \cap (\partial M \setminus \partial_{\mathrm{g}} M)$ is reflection-symmetric in view of the definition of π, Lemma 2.7 tells us that $\varphi^{-1}(O)$ is open in D. Now we simply calculate

$$(\mathrm{id}_{\mathbb{R}} \times \pi)^{-1}(\phi^{-1}(\mathcal{O})) = (\pi \circ \varphi)^{-1}(\mathcal{O}) = \varphi^{-1}(O), \tag{29}$$

which by definition of the quotient topology shows that $\phi^{-1}(\mathcal{O})$ is open in $\mathcal{D}$. □

4.2. **Smooth structure.** The topological gluing process carried out in Section 4.1 to define $\mathcal{M}$ does not automatically equip $\mathcal{M}$ with any canonical smooth structure. However, since our goal is to make φ smooth, it suggests itself to use *flow charts* around the gluing region in $\mathcal{M}$ to define the smooth structure.

More precisely, to equip $\mathcal{M}$ with a smooth structure we choose an open set $N = N_{\mathrm{in}} \sqcup N_{\mathrm{out}} \subset \mathbb{R} \times (\partial M \setminus \partial_{\mathrm{g}} M)$ as in Lemma 2.4 and define the continuous map

$$\Phi : N_{\mathrm{in}} \to \mathcal{M}, \qquad \Phi(t,x,v) = [\varphi(t,x,v)] = \phi(t,[x,v]).$$

Note that choosing N_{in} over N_{out} is arbitrary; N_{out} defines an equivalent smooth structure in the arguments below since the involution $N_{\mathrm{in}} \to N_{\mathrm{out}}$, $(t,x,v) \mapsto (t,x,v')$, is a canonical diffeomorphism between the two. The key observation is that Φ is an embedding:

Corollary 4.2. *The map Φ is a homeomorphism onto its image which is an open neighborhood of the gluing region $\mathcal{G}$.*

Proof. The set $\Phi(N_{\mathrm{in}})$ contains $\mathcal{G}$ because N_{in} contains $\{0\} \times \partial_{\mathrm{in}} M$ and $\pi(\{0\} \times \partial_{\mathrm{in}} M) = \mathcal{G}$. Since we have $\Phi(N_{\mathrm{in}}) = \pi(\varphi(N_{\mathrm{in}}))$ and $\pi|_{\varphi(N_{\mathrm{in}})}$ is an open map, we only need to prove that $\varphi : N_{\mathrm{in}} \to M$ is an injective open map. This is true by Lemma 2.4. □

Corollary 4.3. *The model space $\mathcal{M}$ can be equipped with the structure of a smooth manifold such that the projection $\pi : M \setminus \partial_{\mathrm{g}} M \to \mathcal{M}$ is a smooth map and the flow $\phi : \mathcal{D} \to \mathcal{M}$ is smooth. Furthermore, there exists a contact form $\alpha_{\mathcal{M}}$ on $\mathcal{M}$ whose Reeb vector field is the generator $\mathbf{X}$ of ϕ.*

Proof. At this point we have at our disposal the two homeomorphism $\Phi : N_{\mathrm{in}} \to \Phi(N_{\mathrm{in}})$ and $\pi|_{\mathring{M}} : \mathring{M} \to \mathcal{M} \setminus \mathcal{G}$ whose codomains provide an open cover of $\mathcal{M}$. Since $\mathring{M}$ as well as N_{in} are smooth manifolds, we see that $\mathcal{M}$ is second-countable and Hausdorff. To equip $\mathcal{M}$ with an atlas we take on $\mathcal{M} \setminus \mathcal{G}$ the diffeomorphism $\pi|_{\mathring{M}}^{-1}$ as a chart and on $\Phi(N_{\mathrm{in}})$ we use Φ^{-1} as a chart. As φ is smooth on $\varphi^{-1}(\mathring{M})$, the so-defined charts are compatible on the overlap $\Phi(N_{\mathrm{in}}) \cap (\mathcal{M} \setminus \mathcal{G})$ and thus define a smooth structure on $\mathcal{M}$.

Now $\pi|_{\mathring{M}}$ is a diffeomorphism and in particular smooth. On the other hand $\pi|_{\varphi(N_{\mathrm{in}})}$ is smooth if $\Phi^{-1} \circ \pi|_{\varphi(N_{\mathrm{in}})} = (\varphi|_{N_{\mathrm{in}}})^{-1} : \varphi(N_{\mathrm{in}}) \to N_{\mathrm{in}}$ is smooth. The latter holds true by Lemma 2.4 *v)*.

Since ϕ is a continuous flow and $\{\Phi(N_{\mathrm{in}}), \mathcal{M} \setminus \mathcal{G}\}$ constitutes an open cover of $\mathcal{M}$, proving that ϕ is smooth reduces to showing that both $\phi : \mathcal{D} \cap (\mathbb{R} \times (\mathcal{M} \setminus \mathcal{G})) \to \mathcal{M}$ as well as $\phi : \mathcal{D} \cap (\mathbb{R} \times (\Phi(N_{\mathrm{in}}))) \to \mathcal{M}$ are smooth. Note that by the flow property one only needs to check smoothness around points $(0, [x, v])$, i.e., the problem reduces to checking smoothness in the cases $[x, v] \in \pi(\mathring{M})$ and $[x, v] \in \mathcal{G} \subset \Phi(N_{\mathrm{in}})$.

The former easily follows from the smoothness of φ on $\varphi^{-1}(\mathring{M})$. For the latter we take $(s, y, w) \in N_{\mathrm{in}}$ and calculate for sufficiently small $t \in \mathbb{R}$

$$\Phi^{-1} \circ \phi \circ (\mathrm{id}_{\mathbb{R}} \times \Phi)\,(t, s, y, w) = \Phi^{-1} \circ \phi_t(\phi_s(y, w)) = (t + s, y, w), \tag{30}$$

by virtue of the flow property $\phi(t, \phi(s, x, v)) = \phi(s + t, x, v)$. This is obviously smooth.

We begin the construction of $\alpha_{\mathcal{M}}$ by recalling that in the setting of Lemma 2.4 the non-grazing billiard flow φ restricted to N_{in} is a diffeomorphism onto its image and the map Φ provides a chart around $\mathcal{G}$ with respect to which the generator of ϕ is given by $(\Phi^{-1})_* \mathbf{X} = \partial_t$.

Now let $\alpha \in \Omega^1(S\Sigma)$ be the canonical contact form on $(S\Sigma, g)$ whose Reeb vector field is the geodesic vector field X^g (for details see [Pat99, Chap. 1]). Note that the equation $\phi \circ (\mathrm{id}_{\mathbb{R}} \times \pi) = \pi \circ \varphi$ on D immediately entails $\mathbf{X} = \pi_* X^g$ on $\pi(\mathring{M}) = \mathcal{M} \setminus \mathcal{G}$ and the 1-form defined via

$$\alpha_{\mathcal{M}} \coloneqq \left(\pi\big|_{\mathring{M}}^{-1}\right)^* \alpha \in \Omega^1(\pi(\mathring{M}))$$

thus still satisfies $\iota_{\mathbf{X}} \alpha_{\mathcal{M}} = 1$ and $\iota_{\mathbf{X}} \mathrm{d}\alpha_{\mathcal{M}} = 0$. We will now continue this definition smoothly to $\mathcal{G}$: First observe that α is φ_t^g-invariant and $(\varphi^g|_N)_* \partial_t = X^g$, ergo

$$\left(\varphi\big|_{N_{\mathrm{in}}}\right)^* \alpha(t, x, v) = \mathrm{d}t + \alpha|_{\partial M \setminus \partial_{\mathrm{g}} M}(x, v), \tag{31}$$

where we recall from the discussion before Lemma 2.14 that $\alpha|_{\partial M \setminus \partial_{\mathrm{g}} M}$ is really a 1-form on the submanifold $\partial M \setminus \partial_{\mathrm{g}} M$. Denote the restriction away from $\mathcal{G}$ of our above flow chart as $\Phi' \coloneqq \Phi\big|_{\{t \neq 0\}}$, where $\{t \neq 0\} = \Phi^{-1}(\mathcal{M} \setminus \mathcal{G}) = N \setminus (\{0\} \times \mathcal{G})$. We first observe that

$$(\Phi')^* \alpha_{\mathcal{M}} = \left(\pi\big|_{\mathring{M}}^{-1} \circ \Phi'\right)^* \alpha = \left(\varphi\big|_{N_{\mathrm{in}} \cap \{t \neq 0\}}\right)^* \alpha. \tag{32}$$

But $\varphi|_{N_{\mathrm{in}} \cap \{t < 0\}} = \varphi^g|_{N_{\mathrm{in}} \cap \{t < 0\}}$ and $\varphi|_{N_{\mathrm{in}} \cap \{t > 0\}} = \varphi^g \circ \widetilde{R}|_{N_{\mathrm{in}} \cap \{t > 0\}}$ where $\widetilde{R}(t, x, v) = R(t, x, v')$ denotes the obvious lift of the tangential reflection $R(x, v) = (x, v')$ to N. Combining this with (31) and (32) yields

$$\left(\Phi'\right)^* \alpha_{\mathcal{M}}(t, x, v) = \begin{cases} \mathrm{d}t + \alpha|_{\partial M \setminus \partial_{\mathrm{g}} M}(x, v), & t < 0 \\ \mathrm{d}t + R^*(\alpha|_{\partial M \setminus \partial_{\mathrm{g}} M})(x, v), & t > 0. \end{cases} \tag{33}$$

We have already seen in Lemma 2.14 that $R^*(\alpha|_{\partial M}) = \alpha|_{\partial M}$ which implies that we can interpret the right-hand side of (33) as defined on the whole coordinate domain N_{in} and the definition $\alpha_{\mathcal{M}} \coloneqq \left(\Phi^{-1}\right)^* (\mathrm{d}t + \alpha|_{\partial M \setminus \partial_{\mathrm{g}} M})$ extends $\alpha_{\mathcal{M}}$ to a well-defined 1-form on all of $\mathcal{M}$ which is still a contact form with $\mathbf{X}$ its Reeb vector field because (33) shows that $\iota_{\mathbf{X}} \alpha_{\mathcal{M}} = 1$ and $\iota_{\mathbf{X}} \mathrm{d}\alpha_{\mathcal{M}} = 0$ both due to $(\Phi^{-1})_* \mathbf{X} = \partial_t$. □

Remark 4.4 (Flow time vs. Riemannian distance as transversal coordinate). We emphasize the fact that the particularly simple coordinate expression of the flow in (30) is due to the usage of *flow coordinates* in the direction transversal to $\mathcal{G}$ or, equivalently, to $\partial M \setminus \partial_{\mathrm{g}} M$. Alternatively one could consider the Riemannian distance $\mathrm{dist}_g(x, \Omega)$ as the transversal coordinate of a point $(x, v) \in M \setminus \partial_{\mathrm{g}} M$ close to $\partial_{\mathrm{out}} M$ and $-\mathrm{dist}_g(x, \Omega)$ if (x, v) is close to $\partial_{\mathrm{in}} M$. With this choice of coordinates on $\mathcal{M}$ near $\mathcal{G}$ the model flow ϕ would in general be non-smooth, though, as can be directly verified for e.g. $\Sigma = \mathbb{R}^2$, $\Omega = \{x \in \mathbb{R}^2 \,|\, |x| \leq 1\}$, equipped with the Euclidean metric.

4.3. **Dependence of the model space on the Riemannian metric.** Suppose that g and g' are two complete Riemannian metrics on Σ. Then the unit tangent bundles with respect to g and g' are canonically diffeomorphic via the obvious rescaling diffeomorphism, so we can consider them as one and the same space $S\Sigma$ carrying the two geodesic flows φ^g and $\varphi^{g'}$. With this identification the inward, outward, and grazing boundaries of M are the same for the two metrics g and g'. However, the tangential reflections on $\partial M \setminus \partial_{\mathrm{g}} M$ with respect to g and g' will differ in general. Let us denote them by

$$(x, v) \mapsto (x, R_{g(x)} v), \qquad (x, v) \mapsto (x, R_{g'(x)} v),$$

respectively. Consider now the non-grazing billiard flows $\varphi_g : D_g \to M \setminus \partial_{\mathrm{g}} M$ and $\varphi_{g'} : D_{g'} \to M \setminus \partial_{\mathrm{g}} M$ of g and g' on their domains $D_g, D_{g'} \subset \mathbb{R} \times (M \setminus \partial_{\mathrm{g}} M)$. It is a natural question how the smooth models $(\mathcal{M}_g, \pi_g, \phi_g)$ and $(\mathcal{M}_{g'}, \pi_{g'}, \phi_{g'})$ for φ_g and $\varphi_{g'}$, as constructed above, are related. In particular, we would like to know when there is a diffeomorphism $\mathcal{M}_g \cong \mathcal{M}_{g'}$ making the diagram

$$\begin{array}{ccc} & M \setminus \partial_{\mathrm{g}} M & \\ {\scriptstyle \pi_g}\swarrow & & \searrow{\scriptstyle \pi_{g'}} \\ \mathcal{M}_g & \xrightarrow{\quad\cong\quad} & \mathcal{M}_{g'} \end{array} \tag{34}$$

commute. In this case, one can consider ϕ_g and $\phi_{g'}$ as flows on the same smooth manifold, which allows to compare them.

An answer to this question is given by the following result that describes a regularity condition on the geodesic flows φ^g, $\varphi^{g'}$ and the tangential reflections with respect to g and g' which is both necessary and sufficient for (34) to hold. In order to formulate the regularity condition we need to introduce some more terminology: Since the geodesic flows φ^g and $\varphi^{g'}$ are transversal to $\partial M \setminus \partial_{\mathrm{g}} M$ the inverse function theorem tells us that we can find an open neighborhood N of $\{0\} \times (\partial M \setminus \partial_{\mathrm{g}} M)$ in $\mathbb{R} \times (\partial M \setminus \partial_{\mathrm{g}} M)$ such that $\varphi^g|_N$ and $\varphi^{g'}|_N$ are diffeomorphisms onto their images in $S\Sigma$. For any such neighborhood we can define "geometric reflection maps" $\tilde{R}_g : \varphi^g(N) \to \varphi^g(N)$ and $\tilde{R}_{g'} : \varphi^{g'}(N) \to \varphi^{g'}(N)$ by putting

$$\tilde{R}_g(x, v) := \varphi^g(t, x_0, R_{g(x_0)} v_0), \qquad \varphi^g|_N^{-1}(x, v) = (t, x_0, v_0) \in N,$$

and analogously for g'. With these preparations we can state

Proposition 4.5. *The following two statements are equivalent:*

1. *There is a diffeomorphism $\mathcal{M}_g \cong \mathcal{M}_{g'}$ making the diagram* (34) *commute.*
2. *There is an open neighborhood N of $\{0\} \times (\partial M \setminus \partial_{\mathrm{g}} M)$ in $\mathbb{R} \times (\partial M \setminus \partial_{\mathrm{g}} M)$ such that the two maps $N \cap (\mathbb{R} \times \partial_{\mathrm{in}} M) \to S\Sigma$ given by*

$$(t, x, v) \mapsto \begin{cases} \varphi^g(t, x, v), & t \leq 0, \\ (\tilde{R}_{g'} \circ \varphi^g)(t, x, R_{g(x)} v), & t > 0, \end{cases}$$

$$(t, x, v) \mapsto \begin{cases} \varphi^{g'}(t, x, v), & t \leq 0, \\ (\tilde{R}_g \circ \varphi^{g'})(t, x, R_{g'(x)} v), & t > 0, \end{cases}$$

are well-defined and smooth.

If (1) or equivalently (2) holds, then the diffeomorphism in (34) *is unique.*

The proof of Proposition 4.5 is given in Appendix A.4.

Remark 4.6. An obvious case in which Proposition 4.5 can be applied is when g and g' differ only by a constant conformal factor in a neighborhood of $\partial\Omega$. In this case, the identification of the two unit tangent bundles directly eliminates that factor near ∂M and Proposition 4.5 becomes trivial since $\mathcal{M}_g$ and $\mathcal{M}_{g'}$ coincide near their gluing regions.

5. Meromorphic continuation of the resolvent and weighted zeta function

In this section we derive two meromorphic continuation results: After recalling the meromorphically continued resolvent of [DG16, Thm. 1] in Section 5.1 we continue meromorphically a restricted resolvent of the generator of a smooth model flow for a non-grazing, hyperbolic billiard in Section 5.2. This result immediately translates to the billiard operator $\mathbf{P}$ via the pullback π^*. Finally we derive the meromorphic continuation of weighted zeta functions for non-grazing billiard flows in Section 5.3. As a corollary we obtain meromorphic continuation of the weighted zeta function for Euclidean billiards in $\mathbb{R}^n$.

5.1. **Meromorphic continuation on open hyperbolic systems.** In the following we will invoke the meromorphic continuation result obtained in [DG16] in the setting of *open hyperbolic systems*. To make the paper more self-contained we recall their setting and results here: An open hyperbolic system is given by a flow ψ on a compact manifold $\mathcal{U}$ with boundary satisfying the following requirements:

(1) The manifold boundary $\partial\mathcal{U}$ of $\mathcal{U}$ is smooth and *strictly convex* w.r.t. the generator X of ψ, i.e., for any boundary defining function $\rho \in \mathrm{C}^\infty(\mathcal{U})$

$$p \in \partial\mathcal{U},\ (X\rho)(p) = 0 \quad \Longrightarrow \quad X(X\rho)(p) < 0. \tag{35}$$

(2) Let $K(\psi)$ denote the trapped set of ψ, i.e., the set of $p \in \mathcal{U}$ for which $\psi_t(p)$ exists $\forall t \in \mathbb{R}$. The flow ψ is *hyperbolic* on $K(\psi)$, i.e., for any $p \in K(\psi)$ the tangent bundle $T_p\mathcal{U}$ splits in a continuous and flow invariant fashion as

$$T_p\mathcal{U} = \mathbb{R}\cdot X(p) \oplus E_s(p) \oplus E_u(p), \tag{36}$$

and there exist constants $C_0, C_1 > 0$ such that

$$\begin{aligned} \|\mathrm{d}\psi_t(p)W\|_{\psi_t(p)} &\le C_0 \exp(-C_1 t)\|W\|_p, \quad t \ge 0,\ W \in E_s(p) \\ \|\mathrm{d}\psi_t(p)W\|_{\psi_t(p)} &\ge C_0^{-1} \exp(C_1 t)\|W\|_p, \quad t \ge 0,\ W \in E_u(p), \end{aligned} \tag{37}$$

where $\|\cdot\|$ denotes any continuous norm on $T\mathcal{U}$. Denote by $\mathring{\mathcal{U}}$ the manifold interior of $\mathcal{U}$.

Now in this setting the following holds [DG16, Thm. 1]: The family of operators

$$\mathbf{R}(\lambda) \coloneqq \mathbf{1}_{\mathring{\mathcal{U}}}(X+\lambda)^{-1}\mathbf{1}_{\mathring{\mathcal{U}}} : \mathrm{C}_\mathrm{c}^\infty(\mathring{\mathcal{U}}) \to \mathcal{D}'(\mathring{\mathcal{U}})$$

is analytic for $\mathrm{Re}(\lambda) \gg 0$ and continues meromorphically to $\mathbb{C}$. Its poles are called *Ruelle resonances* and the residue of $\mathbf{R}(\lambda)$ at a resonance λ_0 is given by a finite-rank operator

$$\Pi_{\lambda_0} : \mathrm{C}_\mathrm{c}^\infty(\mathring{\mathcal{U}}) \to \mathcal{D}'(\mathring{\mathcal{U}}). \tag{38}$$

In particular Dyatlov and Guillarmou showed in [DG16, Thm. 2] a very precise wavefront set estimate for the Schwartz kernel $K_{\Pi_{\lambda_0}}$ of Π_{λ_0} which allows one to calculate the *flat trace* $\mathrm{tr}^\flat$ of Π_{λ_0} defined as the integral over the restriction of the kernel to the diagonal [DG16, Section 4.1]:

$$\mathrm{supp}(K_{\Pi_{\lambda_0}}) \subset \Gamma_+ \times \Gamma_-, \quad \mathrm{WF}'(\Pi_{\lambda_0}) \subset E_+^* \times E_-^*,$$

where $\Gamma_\pm$ are the incoming/outgoing tails of ψ, i.e., those $p \in \mathcal{U}$ for which $\psi_{\mp t}(p)$ exists for all $t \ge 0$, and $E_\pm^* \subset T^*\mathcal{U}$ are extensions of the dual stable/unstable foliations $E_{u/s}^*$

onto $\Gamma_\pm$ constructed in [DG16, Lemma 1.10]. For the regular (holomorphic) part $\mathbf{R}_H(\lambda)$ in the neighborhood of some $\lambda_0 \in \mathbb{C}$ a similar estimate is known [DG16, Lemma 3.5]:

$$\mathrm{WF}'(\mathbf{R}_H(\lambda)) \subset \Delta(T^*\mathring{\mathcal{U}}) \cup (E_+^* \times E_-^*) \cup \mathcal{Y}_+, \tag{39}$$

where $\mathcal{Y}_+ \coloneqq \left\{ \left(\mathrm{e}^{tH_p}(y,\eta), y, \eta\right) \,\middle|\, t \geq 0,\, p(y,\eta) = 0,\, y \in \mathring{\mathcal{U}},\, \psi_t(\mathring{\mathcal{U}}) \right\}$ with $p(y,\eta) \coloneqq \langle X(y), \eta\rangle$ and e^{tH_p} the flow of the Hamiltonian vector field H_p associated with p, and $\Delta(T^*\mathring{\mathcal{U}}) \subset T^*\mathring{\mathcal{U}} \times T^*\mathring{\mathcal{U}}$ denotes the diagonal of the cotangent bundle over $\mathring{\mathcal{U}}$.

For the definition of the flat trace and the rather technical background on the related techniques we refer the reader to [DZ16, Section 2.4].

Remark 5.1. The setting of [DG16] covers the more general vector-valued case of a first order differential operator $\mathbf{X} : \mathrm{C}^\infty(\mathcal{U};\mathcal{E}) \to \mathrm{C}^\infty(\mathcal{U};\mathcal{E})$ acting on smooth sections of a vector bundle $\mathcal{E}$ over $\mathcal{U}$ which is a lift of X in the sense that

$$\mathbf{X}(fs) = X(f)s + f\mathbf{X}(s) \qquad \forall\, s \in \mathrm{C}^\infty(\mathcal{U};\mathcal{E}),\ f \in \mathrm{C}^\infty(\mathcal{U}).$$

Our considerations of the following section therefore go through in this more general case, but we postpone the explicit treatment to Appendix B to keep the notation as simple as possible and the theorems self-contained for the reader who is primarily interested in the scalar case.

5.2. **A meromorphic resolvent for billiard systems.** Let (Σ, g, Ω) be a geodesic billiard system such that the associated non-grazing billiard flow φ has compact trapped set K and is hyperbolic on K in the sense of Definition 2.12. Before we state and prove our main theorem we first establish the following lemma concerning the generator $\mathbf{X}$ of the smooth flow ϕ of a smooth model $(\mathcal{M}, \pi, \phi)$ for φ as in Definition 3.1 and the compact set $\mathcal{K} \subset \mathcal{M}$ defined in (24):

Lemma 5.2. *There exists a compact submanifold with boundary $\mathcal{U}_0$ of $\mathcal{M}$ with manifold interior $\mathring{\mathcal{U}}_0$ such that*

$$\mathcal{K} \subset \mathring{\mathcal{U}}_0 \tag{40}$$

and such that there exists a smooth vector field $\mathbf{X}_0$ on $\mathcal{U}_0$ with the following properties:

i) the manifold boundary $\partial\mathcal{U}_0$ of $\mathcal{U}_0$ is strictly convex w.r.t. $\mathbf{X}_0$ in the sense of (35)*;*
ii) $\mathbf{X} - \mathbf{X}_0$ is supported in an arbitrarily small neighborhood of $\partial\mathcal{U}_0$;
iii) the trapped set of the flow of $\mathbf{X}_0$ coincides with $\mathcal{K}$.

Proof. First we choose a compact submanifold with boundary $\mathcal{N}$ of $\mathcal{M}$ with manifold interior $\mathring{\mathcal{N}}$ such that $\mathcal{K} \subset \mathring{\mathcal{N}}$. The existence of such an $\mathcal{N}$ is standard in smooth manifold theory, but we provide a proof for convenience: There exists a smooth function $F : \mathcal{M} \to \mathbb{R}$ such that $F^{-1}((-\infty, c])$ is compact for each $c \in \mathbb{R}$ and the sets $F^{-1}((-\infty, n])$, $n \in \mathbb{N}$ exhaust $\mathcal{M}$ (see e.g. [Lee12, Prop. 2.28]). By compactness of $\mathcal{K}$ there exists some $c_0 \in \mathbb{R}$ such that $\mathcal{K} \subset F^{-1}((-\infty, c_0))$. Using Sard's theorem we find some $\varepsilon > 0$ such that $c_0 + \varepsilon$ is a regular value of F and taking $\mathcal{N} \coloneqq F^{-1}((-\infty, c_0 + \varepsilon])$ does the trick.

Now we can invoke [GMT21, Prop. 2.2], which in turn builds upon [CE71, Rob80], to obtain a submanifold with boundary $\mathcal{U}_0 \subset \mathring{\mathcal{N}}$ containing $\mathcal{K}$ in its manifold interior and [GMT21, Lemma 2.3] to obtain the vector field $\mathbf{X}_0$ with the claimed properties. □

This lemma immediately yields the meromorphic extension of the restricted resolvent $\mathbf{1}_{\mathring{\mathcal{U}}_0}(\mathbf{X}_0 + \lambda)^{-1}\mathbf{1}_{\mathring{\mathcal{U}}_0}$ to the complex plane $\mathbb{C}$ via an application of [DG16, Theorems 1, 2] to the open hyperbolic system $(\mathcal{U}_0, \mathbf{X}_0)$. Now our main theorem makes a statement about the generator $\mathbf{X}$ itself instead of the perturbation $\mathbf{X}_0$. To state and prove it we have to introduce some additional auxiliary objects and notations:

In the situation of (the proof of) Lemma 5.2 we may without loss of generality assume an embedding $\mathcal{N} \subset \mathcal{M}'$ into a closed manifold $\mathcal{M}'$ of the same dimension as $\mathcal{M}$. We thus

arrive at the following overall situation:

$$\mathcal{K} \subset \mathring{\mathcal{U}}_0 \subset \mathcal{U}_0 \subset \mathring{\mathcal{N}} \subset \mathcal{N} \subset \mathcal{M}'.$$

Furthermore we may extend the vector fields $\mathbf{X}$ and $\mathbf{X}_0$ to $\mathcal{M}'$ arbitrarily and continue to denote such an extension by $\mathbf{X}$ and $\mathbf{X}_0$, respectively. Their respective flows ϕ and ϕ^0 are therefore complete. While we choose the extension of $\mathbf{X}$ arbitrarily, we choose the extension of $\mathbf{X}_0$ such that for all $t \geq 0$: If $p, \phi_t^0(p) \in \mathcal{U}_0$ then $\phi_s^0(p) \in \mathcal{U}_0$ for all $s \in [0,t]$. This is possible by Lemma 5.2 and [DG16, Lemma 1.1]. Analogously to [GMT21] we can define the *escape times* from a compact set $\mathcal{U} \subset \mathcal{N}$ as

$$\begin{aligned}\tau_{\mathcal{U}}^{\pm}(p) &\coloneqq \pm \sup\left\{t \geq 0 \,\middle|\, \phi_{\pm s}(p) \in \mathcal{U}\, \forall s \in [0,t]\right\},\\ \tau_{\mathcal{U}}^{0,\pm}(p) &\coloneqq \pm \sup\left\{t \geq 0 \,\middle|\, \phi_{\pm s}^0(p) \in \mathcal{U}\, \forall s \in [0,t]\right\}, \quad p \in \mathcal{N},\end{aligned}$$

together with the forward and backward trapped sets

$$\Gamma_{\pm}(\mathcal{U}) \coloneqq \left\{p \in \mathcal{U} \,\middle|\, \tau_{\mathcal{U}}^{\mp}(p) = \mp\infty\right\}, \qquad \Gamma_{\pm}^0(\mathcal{U}) \coloneqq \left\{p \in \mathcal{U} \,\middle|\, \tau_{\mathcal{U}}^{0,\mp}(p) = \mp\infty\right\}.$$

Next, we define a natural candidate for the inverse of $(\mathbf{X}+\lambda)$ on any open set $\mathcal{O} \subset \mathcal{N}$: For any $f \in \mathrm{C}_{\mathrm{c}}^\infty(\mathcal{O})$ and $\lambda \in \mathbb{C}$ consider the function on $\mathcal{O}$ formally given by the following integral

$$\mathbf{R}_{\mathcal{O}}(\lambda) f(p) \coloneqq \int_0^{-\tau_{\overline{\mathcal{O}}}^-(p)} \mathrm{e}^{-\lambda t} f\left(\phi_{-t}(p)\right) \mathrm{d}t, \quad p \in \mathcal{O}\ .$$

This definition requires formal justification for two reasons: On the one hand the integral may not converge if $\tau_{\overline{\mathcal{O}}}^-(p) = -\infty$, and on the other hand the regularity properties of $\mathbf{R}_{\mathcal{O}}(\lambda) f$ are not obvious from the definition. We can overcome these problems if we assume that $\mathcal{O}$ is chosen such that:

(1) $\mathbf{X} = \mathbf{X}_0$ on $\overline{\mathcal{O}}$
(2) $\overline{\mathcal{O}}$ is *dynamically convex with respect to* ϕ^0, i.e., for any $t \geq 0$ we have

$$p,\, \phi_t^0(p) \in \overline{\mathcal{O}} \quad \Longrightarrow \quad \phi_s^0(p) \in \overline{\mathcal{O}}\ \forall s \in [0,t].$$

Then by the first assumption we get

$$\mathbf{R}_{\mathcal{O}}(\lambda) f(p) = \int_0^{-\tau_{\overline{\mathcal{O}}}^-(p)} \mathrm{e}^{-\lambda t} f\left(\phi_{-t}^0(p)\right) \mathrm{d}t, \quad p \in \mathcal{O}.$$

By the second assumption and the fact that f is supported in $\mathcal{O}$ we can replace the upper integration bound by ∞ and obtain for $\mathrm{Re}(\lambda) \gg 0$ that

$$\mathbf{R}_{\mathcal{O}}(\lambda) f = \int_0^\infty \mathrm{e}^{-\lambda t} \left(\phi_{-t}^0\right)^* f \,\mathrm{d}t = \left((\mathbf{X}_0 + \lambda)^{-1} \mathbf{1}_{\mathcal{O}}\right) f\ ,$$

which holds as an equality of e.g. continuous functions on $\mathcal{O}$ by the integral formula and in turn lets us conclude that

$$\mathbf{R}_{\mathcal{O}}(\lambda) = \mathbf{R}(\lambda)\big|_{\mathrm{C}_{\mathrm{c}}^\infty(\mathcal{O})} : \mathrm{C}_{\mathrm{c}}^\infty(\mathcal{O}) \to \mathcal{D}'(\mathring{\mathcal{U}}_0) \hookrightarrow \mathcal{D}'(\mathcal{O})\ . \tag{41}$$

In particular we have that $\mathbf{R}_{\mathcal{O}}(\lambda) : \mathrm{C}_{\mathrm{c}}^\infty(\mathcal{O}) \to \mathrm{C}(\mathcal{O})$ is a holomorphic family of continuous operators on $\{\mathrm{Re}(\lambda) \gg 0\}$ which satisfies $(\mathbf{X}+\lambda)\mathbf{R}_{\mathcal{O}}(\lambda) = \mathrm{id}_{\mathrm{C}_{\mathrm{c}}^\infty(\mathcal{O})}$. With these preliminaries at hand we can now show meromorphic continuation of $\mathbf{R}_{\mathcal{O}}(\lambda)$ to $\mathbb{C}$ by providing as a particular candidate for $\mathcal{O}$ a concrete dynamically convex neighborhood of the trapped set and applying the results of [DG16] to $\mathbf{X}_0$. Concretely we prove the following:

Theorem 5.3. *Let (Σ, g, Ω) be a geodesic billiard system with non-grazing billiard flow φ, $(\mathcal{M}, \pi, \phi)$ a smooth model for φ as in Definition 3.1, and $\mathbf{X}$ the generator of ϕ. If the trapped set K of φ is compact and φ is hyperbolic on K in the sense of Definition 2.12, then there exists an arbitrarily small compact $\mathcal{U} \subset \mathcal{M}$ with $\mathcal{K} \subset \mathring{\mathcal{U}}$ such that $\mathbf{R}_{\mathring{\mathcal{U}}}(\lambda)$ extends*

from $\mathrm{Re}(\lambda) \gg 0$ *to* $\mathbb{C}$ *as a meromorphic family of operators* $\mathrm{C}_{\mathrm{c}}^{\infty}(\mathring{\mathcal{U}}) \to \mathcal{D}'(\mathring{\mathcal{U}})$. *Its residue at a pole* λ_0 *is a finite-rank operator* $\Pi_{\lambda_0} : \mathrm{C}_{\mathrm{c}}^{\infty}(\mathring{\mathcal{U}}) \to \mathcal{D}'(\mathring{\mathcal{U}})$ *satisfying*

$$\mathrm{supp}(K_{\Pi_{\lambda_0}}) \subset \Gamma_+(\mathcal{U}) \times \Gamma_-(\mathcal{U}), \quad \mathrm{WF}'\left(\Pi_{\lambda_0}\right) \subset E_+^* \times E_-^*. \tag{42}$$

Furthermore, the holomorphic part $\mathbf{R}_{\mathring{\mathcal{U}}}^H(\lambda)$ *of* $\mathbf{R}_{\mathring{\mathcal{U}}}(\lambda)$ *with* λ *in a neighborhood of* λ_0 *satisfies the following wavefront estimate:*

$$\mathrm{WF}'\big(\mathbf{R}_{\mathring{\mathcal{U}}}^H(\lambda)\big) \subset \Delta(T^*\mathring{\mathcal{U}}) \cup (E_+^* \times E_-^*) \cup \mathcal{Y}_+, \tag{43}$$

with $\Delta(T^*\mathring{\mathcal{U}})$ *and* $\mathcal{Y}_+$ *defined after* (39). *Finally,* $\mathcal{U}$ *can be chosen to be an isolating block as defined in* [CE71, Section 1.C.] *and such that it satisfies the dynamical convexity condition (2) introduced above.*

Remark 5.4. In Theorem 5.3 *arbitrarily small* means that given any open neighborhood $\mathcal{O}$ of $\mathcal{K}$ in $\mathcal{M}$ we can choose $\mathcal{U}$ such that $\mathcal{U} \subset \mathcal{O}$.

Proof of Theorem 5.3. By (41) we only need to construct a dynamically convex neighborhood $\mathcal{U}$ of the trapped set $\mathcal{K}$ satisfying $\mathcal{U} \subset \mathring{\mathcal{U}}_0$. Then we can choose $\mathbf{X}_0$ in Lemma 5.2 in such a way that $\mathbf{X} - \mathbf{X}_0 = 0$ on $\mathcal{U}$ and the stated properties of the residue Π_{λ_0} transfer from the respective properties of the restricted resolvent $\mathbf{1}_{\mathring{\mathcal{U}}_0}(\mathbf{X}_0+\lambda)^{-1}\mathbf{1}_{\mathring{\mathcal{U}}_0}$. The wavefront estimate for $\mathbf{R}_H(\lambda)$ follows from [DG16, Lemma 3.5].

To construct $\mathcal{U}$ let $\mathcal{U}_0 \subset \mathcal{M}$ be the compact submanifold of Lemma 5.2 and $\mathcal{O}$ any open neighborhood of $\mathcal{K}$ satisfying $\overline{\mathcal{O}} \subset \mathring{\mathcal{U}}_0$. By [DG16, Lemma 1.4] there exists $T > 0$ such that

$$\mathcal{U} \coloneqq \phi^0_{-T}(\mathcal{U}_0) \cap \mathcal{U}_0 \cap \phi^0_T(\mathcal{U}_0) \subset \mathcal{O}.$$

But $\mathcal{U}$ is also dynamically convex with respect to ϕ^0, because if $p, \phi^0_t(p) \in \mathcal{U}$, $t > 0$, then $\phi^0_{-T}(p), \phi^0_{t+T}(p) \in \mathcal{U}$ by definition of $\mathcal{U}$. But $\mathcal{U}_0$ is already strictly convex with respect to ϕ^0 which implies $\phi^0_s(p) \in \mathcal{U}_0$ for all $s \in [-T, t+T]$ and therefore $\phi^0_{s'}(p) \in \mathcal{U}$ for all $s' \in [0,t]$. □

Finally, we would like to transfer the results about $\mathbf{X}$ to the geodesic billiard system. To this end we first introduce the escape time of φ from a compact set $U \subset M \setminus \partial_g M$ and the forward/backward trapped set of U as follows:

$$\tau_U^{\pm}(x,v) \coloneqq \pm \sup\left\{t \geq 0 \,\middle|\, (\pm[0,t]) \times \{(x,v)\} \subset D : \varphi_{\pm s}(x,v) \in U \,\forall s \in [0,t]\right\},$$
$$\Gamma_{\pm}(U) \coloneqq \left\{(x,v) \in U \,\middle|\, \tau_U^{\mp}(x,v) = \mp\infty\right\}.$$

Note that given $(x,v) \in U$ the compactness of U implies either $\mathbb{R} \times \{(x,v)\} \subset D$ and $\varphi(\mathbb{R} \times \{(x,v)\}) \subset U$ or the trajectory through (x,v) can be extended to a small neighborhood of $[\tau_U^-(x,v), \tau_U^+(x,v)]$.

We can now obtain the following meromorphic continuation result as a rather immediate corollary of Theorem 5.3 and the characterization of the billiard operator $\mathbf{P}$ in (23):

Corollary 5.5. *Let* (Σ, g, Ω) *be a geodesic billiard system with non-grazing billiard flow* φ *and* $\mathbf{P}$ *the differential operator of Section 2.4. If the trapped set* K *of* φ *is compact and* φ *is hyperbolic on* K, *then there exists an arbitrarily small compact set* $U \subset M \setminus \partial_{\mathrm{g}} M$ *with* $K \subset \mathring{U}$ *and* $U \cap (\partial M \setminus \partial_{\mathrm{g}} M)$ *reflection-symmetric such that the definition*

$$\mathbf{R}_U(\lambda) f(x,v) \coloneqq \int_0^{-\tau_U^-(x,v)} \mathrm{e}^{-\lambda t} f\left(\varphi_{-t}(x,v)\right) \mathrm{d}t, \qquad f \in \mathrm{C}_{\mathrm{Bill,c}}^{\infty}(\mathring{U}) \text{ and } (x,v) \in U,$$

yields a well-defined family of linear maps $\mathbf{R}_U(\lambda) : \mathrm{C}_{\mathrm{Bill,c}}^{\infty}(\mathring{U}) \to \mathrm{C}_{\mathrm{Bill}}(\mathring{U})$ *which satisfy* $(\mathbf{P}+\lambda)\mathbf{R}_U(\lambda) = \mathrm{id}$ *for* $\mathrm{Re}(\lambda) \gg 0$ *and whose matrix coefficients*

$$\langle \mathbf{R}_U(\lambda) f, g \rangle_{\mathrm{L}^2(\mathrm{dvol}_g)}, \qquad f, g \in \mathrm{C}_{\mathrm{Bill,c}}^{\infty}(\mathring{U}),$$

extend from holomorphic functions on $\mathrm{Re}(\lambda) \gg 0$ *to meromorphic functions on* $\mathbb{C}$ *with poles contained in a discrete set of complex numbers that is independent of* f *and* g*. Here* dvol_g *is the Riemannian volume density associated with the Sasaki metric on* $S\Sigma$*.*

Proof. Let $\mathcal{U}$ be chosen according to Theorem 5.3 and set $U \coloneqq \pi^{-1}(\mathcal{U})$. First we note that

$$\mathbf{R}_U(\lambda)f(x,v) = \int_0^{-\tau_{\mathcal{U}}^-(\pi(x,v))} \mathrm{e}^{-\lambda t}\left((\pi^*)^{-1}f\right)(\phi_{-t}(\pi(x,v)))\,\mathrm{d}t,$$

which yields $\mathbf{R}_U(\lambda) = \pi^* \circ \mathbf{R}_{\mathcal{U}}(\lambda) \circ (\pi^*)^{-1}$. The first claim then follows from Theorem 5.3 and Proposition 3.5 while the second claim follows from

$$\langle \mathbf{R}_U(\lambda)f, g\rangle_{\mathrm{L}^2(\mathrm{dvol}_g)} = \langle \mathbf{R}_{\mathcal{U}}(\lambda)\widetilde{f}, \widetilde{g}\rangle_{\mathrm{L}^2(\mu)},$$

where $\widetilde{f} \coloneqq (\pi^*)^{-1}f$, $\widetilde{g} \coloneqq (\pi^*)^{-1}g$, and $\mu \coloneqq \mathrm{dvol}_g \circ \pi^{-1}$ is the pushforward measure of the measure dvol_g along π, in combination with the meromorphic continuation result in Theorem 5.3. □

Remark 5.6. Corollary 5.5 could be extended to a formulation analogous to Theorem 5.3 if one developed a theory of "billiard distributions" with the compactly supported smooth billiard functions as test functions, see the discussion at the end of Section 2.4. We restrict our attention to the easier result above, though, as the functional analysis otherwise required would distract too much from the main theme of smooth models and their application.

Remark 5.7 (Continuation of Remark 5.1). Theorem 5.3 and Corollary 5.5 generalize immediately to the vector valued setting described in Appendix B: First we construct the smooth model bundle and the smooth substitute $\mathbb{X}$ for a given operator $\widetilde{\mathbb{X}}$. Then we can immediately replace $\widetilde{\mathbb{X}}$ by $\mathbb{X}$ in the proof of Theorem 5.3 and [BSW22a] provides a simple procedure to obtain a vector valued generalization of the auxiliary vector field $\mathbb{X}_0$. The transition from Theorem 5.3 to Corollary 5.5 happens analogously as above but now relies on Theorem B.4.

5.3. **Application: meromorphic continuation of Z_f.** In this section we derive our second main result, the meromorphic continuation of the following formal *weighted zeta function* associated with a *weight* $f : M \setminus \partial_{\mathrm{g}}M \to \mathbb{C}$ and a geodesic billiard system (Σ, g, Ω) whose non-grazing billiard flow φ is hyperbolic on its trapped set K in the sense of Definition 2.12:

$$Z_f(\lambda) \coloneqq \sum_{\gamma} \left(\frac{\exp(-\lambda T_\gamma)}{|\det(\mathrm{id} - \mathcal{P}_\gamma)|} \int_{\gamma^\#} f \right), \tag{44}$$

where $\lambda \in \mathbb{C}$, the sum runs over all closed trajectories of φ, T_γ is the period of the closed trajectory γ, $\gamma^\#$ is the corresponding primitive closed trajectory, and $\mathcal{P}_\gamma$ denotes the linearized Poincaré map associated with γ, i.e., given any $t \in [0, T_\gamma] \subset \mathbb{R}$ such that $\gamma(t) \in \mathring{M}$ one defines

$$\mathcal{P}_\gamma \coloneqq \mathrm{d}\varphi_{T_\gamma}(\gamma(t)) : E_s(\gamma(t)) \oplus E_u(\gamma(t)) \longrightarrow E_s(\gamma(t)) \oplus E_u(\gamma(t)),$$

where the determinant in (44) is independent of the chosen t and $E_{u/s}$ denotes the hyperbolic splitting as in Definition 2.12.

Theorem 5.8 (Meromorphic continuation of weighted zeta functions)**.** *Let* (Σ, g, Ω) *be a geodesic billiard system such that the trapped set* K *of the associated non-grazing billiard flow* φ *is compact. Assume also that* φ *is hyperbolic on* K *in the sense of Definition 2.12 and fix a weight* $f \in \mathrm{C}^\infty_{\mathrm{Bill}}(M \setminus \partial_{\mathrm{g}}M)$*. Then the following holds:*

i) The weighted zeta function Z_f *defined in* (44) *is a well-defined holomorphic function on* $\{\mathrm{Re}(\lambda) \gg 0\}$ *that extends meromorphically to* $\mathbb{C}$*.*

ii) Considering a smooth model $(\mathcal{M}, \pi, \phi)$ for φ as in Definition 3.1 and the setting of Theorem 5.3, every pole of Z_f is also a pole of the meromorphically extended resolvent $\mathbf{R}_{\mathring{\mathcal{U}}}(\lambda)$. For each pole λ_0 of $\mathbf{R}_{\mathring{\mathcal{U}}}(\lambda)$ and $k \in \mathbb{N}_0$ one has the following residue formula:

$$\operatorname{Res}_{\lambda=\lambda_0}\big(Z_f(\lambda)(\lambda-\lambda_0)^k\big) = \operatorname{tr}^\flat\left((\mathbf{X}-\lambda_0)^k \Pi_{\lambda_0} \widetilde{f}\right), \tag{45}$$

where $\widetilde{f} \coloneqq (\pi^*)^{-1} f$ and $\Pi_{\lambda_0} : \mathrm{C}_\mathrm{c}^\infty(\mathring{\mathcal{U}}) \to \mathcal{D}'(\mathring{\mathcal{U}})$ is the finite rank operator of Theorem 5.3.

iii) The poles of Z_f with $f \equiv 1$ coincide with the poles of the resolvent $\mathbf{R}_{\mathring{\mathcal{U}}}(\lambda)$ of ii).

Proof. We begin by observing that the weighted zeta function Z_f for φ coincides with the weighted zeta function $Z_{\tilde{f}}$ for the smooth model flow ϕ and $\widetilde{f} \coloneqq (\pi^*)^{-1} f$ by Proposition 3.6, where the latter zeta function is again defined by Formula (44). We can therefore employ [BSW22a] where meromorphic continuation of $Z_{\tilde{f}}$ to $\mathbb{C}$ gets proven by writing the weighted zeta function as the flat trace over the resolvent. The result applies if we can verify that ϕ is hyperbolic on $\mathcal{K}$ because $Z_{\widetilde{f}}$ coincides with the weighted zeta function for $\mathbf{X}_0$ of Lemma 5.2. But now Proposition 3.7 implies hyperbolicity therefore proving *i)*.

The claims of *ii)* also follow directly from an application of [BSW22a] to the zeta function associated with the flow of $\mathbf{X}_0$ and weight $\widetilde{f}$ combined with the observation that $\mathbf{X} = \mathbf{X}_0$ on $\operatorname{ran}(\Pi_{\lambda_0}) \subset \mathcal{D}'(\mathring{\mathcal{U}})$.

The final statement *iii)* follows from the observation that $\operatorname{Res}_{\lambda=\lambda_0}\big(Z_1(\lambda)\big) = \operatorname{tr}^\flat(\Pi_{\lambda_0}) = \operatorname{rk}(\Pi_{\lambda_0})$, where the second relation is shown in [DG16, proof of Thm. 4]. □

Corollary 5.9. *The set of poles of the meromorphically continued resolvent in Theorem 5.3 is independent of the choice of the set $\mathcal{U}$. Consequently, the set of poles of the matrix coefficients in Corollary 5.5 is independent of the choice of the set U.*

Proof. This follows immediately from *iii)* in Theorem 5.8 as Z_1 is independent of $\mathcal{U}$. □

Remark 5.10. For a billiard in Euclidean space $\mathbb{R}^n$ whose obstacles are strictly convex and fulfill the non-grazing trapped set condition (or even the stronger no-eclipse condition, see Section 1) Lemma 2.10 assures the compactness of K and Remark 2.13 the hyperbolicity of φ on K. As a special case of Corollaries 5.5 and 5.9 we thus obtain Theorem 1.1 announced in the introduction.

Remark 5.11. The *(ordinary) zeta function* associated with the (non-grazing or Euclidean) billiard flow φ is defined as

$$\zeta(\lambda) \coloneqq \prod_{\gamma^\#} \left(1 - \mathrm{e}^{-\lambda T_{\gamma^\#}}\right),$$

with the product running over all closed primitive trajectories of φ. Note that, under the assumption that the stable/unstable foliations $\mathcal{E}_{s/u}$ constructed in the proof of Theorem 5.8 are *orientable*, $\zeta(\lambda)$ also continues meromorphically to $\mathbb{C}$ (provided the non-grazing trapped set condition holds): We can employ the same proof as for Theorem 5.8 but instead of using the continuation result of [BSW22a] we directly invoke [DG16, Thm. 3]. The orientability condition can actually be dropped, see [BWS21]. This generalizes a result of Morita [Mor07] who proved meromorphic continuation to a right halfplane.

Remark 5.12 (Conclusion of Remarks 5.1 and 5.7). Using the vector-valued versions of Theorem 5.3 and Corollary 5.5 we obtain the meromorphic continuation to $\mathbb{C}$ of weighted zeta functions associated with vector-valued data as in [DG16, Thm. 4] and [BSW22a]:

$$Z_f^{\widetilde{\mathbb{X}},\kappa}(\lambda) \coloneqq \sum_\gamma \left(\frac{\exp(-\lambda T_\gamma)\operatorname{tr}(\widetilde{\alpha}_\gamma)}{|\det(\mathrm{id} - \mathcal{P}_\gamma)|} \int_{\gamma^\#} f\right),$$

where $\operatorname{tr}(\widetilde{\alpha}_\gamma) = \operatorname{tr}(\widetilde{\alpha}_{\gamma(t),T_\gamma})$ denotes the trace of the billiard parallel transport along a closed trajectory γ, which is independent of the chosen base point $\gamma(t)$. Note that $\widetilde{\alpha}$ depends crucially on both the operator $\widetilde{\mathbb{X}}$ as well as the boundary gluing map κ as indicated by the superscripts.

This proves very useful in practice, as for example using a line bundle whose restriction to $\mathring{M}$ is trivial and which possesses a twist at each obstacle boundary, one can treat dynamical zeta functions involving a sign depending on the number of reflections occurring in the closed trajectories. Similarly one can use the vector-valued setting to treat zeta functions with the modified denominator $\sqrt{\mathrm{id} - \mathcal{P}_\gamma}$. Such zeta functions are of particular interest as they exhibit connections with quantum resonances for obstacle scattering. They have been treated in the literature before, see e.g. [Pet08, CP22].

Remark 5.13. Finally, we would like to point out that in principle the constructions and results of this paper also apply (with the assumption of a compact trapped set on which the non-grazing billiard flow is hyperbolic) in a more general abstract situation where instead of the geodesic flow φ^g on the unit tangent bundle $S\Sigma \supset M$ and the Riemannian tangential reflection $R : \partial M \to \partial M$ one considers some arbitrary smooth flow φ^0 on an arbitrary smooth manifold M with boundary ∂M together with an abstract reflection map $R : \partial M \to \partial M$ that satisfies certain natural axioms such as compatibility with φ^0 which allow to define the non-grazing billiard flow φ associated with φ^0 and R in the same way as above. An example of such a setting is given by an electric potential or a magnetic field on the space Σ. This would still result in specular reflections at the boundary $\partial\Omega$ with unchanged reflection R but the Hamiltonian dynamics would no longer be those of a geodesic flow.

Appendix A. Technical proofs

Here we provide some rather technical proofs to avoid interruptions of the text flow.

A.1. **Proof of Lemma 2.4.** First, we introduce a smooth involution $\widetilde{R} : \mathbb{R}\times\partial M\setminus\partial_{\mathrm{g}}M \to \mathbb{R} \times \partial M \setminus \partial_{\mathrm{g}}M$ by putting $\widetilde{R}(t,x,v) \coloneqq (t,x,v')$. Due to the transversality between the vectors in $\partial M \setminus \partial_{\mathrm{g}}M$ and $T(\partial\Omega)$ the inverse function theorem implies that the geodesic flow

$$\varphi^g : \mathbb{R} \times (\partial M \setminus \partial_{\mathrm{g}}M) \to S\Sigma$$

restricts to a diffeomorphism from an open neighborhood N of $\{0\} \times (\partial M \setminus \partial_{\mathrm{g}}M)$ in $\mathbb{R}\times(\partial M\setminus\partial_{\mathrm{g}}M)$ onto an open neighborhood of $\partial M\setminus\partial_{\mathrm{g}}M$ in $S\Sigma$. By replacing N with its intersection with the open set $(\varphi^g)^{-1}(S\Sigma \setminus \partial_{\mathrm{g}}M)$ we achieve that $\varphi^g(N)$ is disjoint from $\partial_{\mathrm{g}}M$. By shrinking N further we achieve that N is $\widetilde{R}$-invariant and satisfies convexity w.r.t. the flow, i.e. a point $(t,x,v) \in \mathbb{R} \times (\partial M \setminus \partial_{\mathrm{g}}M)$ with $t \geq 0$ lies in N iff all points (s,x,v) and (s,x,v') with $s \in [0,t]$ lie in N, and similarly for $t < 0$.

Now for every $(x,v) \in \partial_{\mathrm{in}}M$ and small $t > 0$ we have that $\varphi^g_t(x,v) \notin M$, while for every $(x,v) \in \partial_{\mathrm{out}}M$ and small $t < 0$ we have that $\varphi^g_t(x,v) \notin M$. This shows that

$$\begin{aligned} \{(t,x,v) \in N \,|\, \varphi^g(t,x,v) \in M\} &= N^+_{\mathrm{out}} \cup N^-_{\mathrm{in}}, \\ \{(t,x,v) \in N \,|\, \varphi^g(t,x,v') \in M\} &= N^-_{\mathrm{out}} \cup N^+_{\mathrm{in}}. \end{aligned} \tag{46}$$

Recalling (4) and taking into account that $N \subset \mathbb{R}\times(\partial M\setminus\partial_{\mathrm{g}}M)$ is open and the projection $\mathbb{R} \times (\partial M \setminus \partial_{\mathrm{g}}M) \to \mathbb{R}$ is an open map, (46) shows that every point $(t,x,v) \in N$ satisfies $t_-(x,v) < t < t_+(x,v)$. This proves the inclusion $N \subset D$ and recalling (7) we get (13).

Let $(t_1,x_1,v_1),(t_2,x_2,v_2) \in N_{\mathrm{in}}$ satisfy $\varphi_{t_1}(x_1,v_1) = \varphi_{t_2}(x_2,v_2)$. Then by (46) the signs of t_1 and t_2 must coincide and by (13) we have

$$\begin{cases} \varphi^g_{t_1}(x_1,v_1) = \varphi^g_{t_2}(x_2,v_2), & t_1 \leq 0, t_2 \leq 0, \\ \varphi^g_{t_1}(x_1,v_1') = \varphi^g_{t_2}(x_2,v_2'), & t_1 > 0, t_2 > 0. \end{cases}$$

We conclude that $(x_1, v_1) = (x_2, v_2)$ because φ^g and $\varphi^g \circ \widetilde{R}$ are injective on N_{in}. This proves that φ is injective on N_{in}. We argue analogously for N_{out}.

That $\varphi : N \to M$ is open follows once we know that $\varphi(N_{\mathrm{in/out}})$ are open in M and $\varphi|^{-1}_{N_{\mathrm{in/out}}} : \varphi(N_{\mathrm{in/out}}) \to N_{\mathrm{in/out}}$ are smooth, because $N = N_{\mathrm{in}} \sqcup N_{\mathrm{out}}$. By (13), combined with the fact that $\widetilde{R}$ interchanges N_{in} with N_{out} as well as $N^{\pm}_{\mathrm{in}}$ with $N^{\pm}_{\mathrm{out}}$, one has

$$\begin{aligned} \varphi(N^-_{\mathrm{in}}) &= M \cap \varphi^g(N_{\mathrm{in}}), & \varphi(N^+_{\mathrm{out}}) &= M \cap \varphi^g(N_{\mathrm{out}}), \\ \varphi(N_{\mathrm{in}} \setminus N^-_{\mathrm{in}}) &= M \cap \varphi^g(N_{\mathrm{out}} \setminus N^-_{\mathrm{out}}), & \varphi(N_{\mathrm{out}} \setminus N^+_{\mathrm{out}}) &= M \cap \varphi^g(N_{\mathrm{in}} \setminus N^+_{\mathrm{in}}). \end{aligned} \tag{47}$$

This shows that the sets on the left-hand sides of the equalities are open in M because they are intersections with M of open subsets of $S\Sigma$, $\varphi^g : N \to S\Sigma$ being an open map. As we already know that φ is injective on $N_{\mathrm{in/out}}$, we now see that each of the sets $\varphi(N_{\mathrm{in/out}}) \subset M$ decomposes into a disjoint union of two open subsets of M as follows:

$$\varphi(N_{\mathrm{in}}) = \varphi(N^-_{\mathrm{in}}) \sqcup \varphi(N_{\mathrm{in}} \setminus N^-_{\mathrm{in}}), \qquad \varphi(N_{\mathrm{out}}) = \varphi(N^+_{\mathrm{out}}) \sqcup \varphi(N_{\mathrm{out}} \setminus N^+_{\mathrm{out}}).$$

To prove that $\varphi|^{-1}_{N_{\mathrm{in}}}$ is smooth we use that $(\varphi^g)^{-1} : \varphi^g(N) \to N$ and $(\varphi^g \circ \widetilde{R})^{-1} : \varphi^g(N) \to N$ are smooth: By (13) the map $\varphi|^{-1}_{N_{\mathrm{in}}}$ coincides with $(\varphi^g)^{-1}$ on $\varphi(N^-_{\mathrm{in}})$ and with $(\varphi^g \circ \widetilde{R})^{-1}$ on $\varphi(N_{\mathrm{in}} \setminus N^-_{\mathrm{in}})$. The latter two disjoint open sets cover $\varphi(N_{\mathrm{in}})$ proving that $\varphi|^{-1}_{N_{\mathrm{in}}}$ is smooth. We argue analogously for $\varphi|^{-1}_{N_{\mathrm{out}}}$.

Finally, we note that $\varphi(N)$ is disjoint from $\partial_{\mathrm{g}} M$ since $\varphi^g(N)$ is disjoint from $\partial_{\mathrm{g}} M$. □

A.2. **Proof of Lemma 2.7.** Given $(t, x, v) \in \varphi^{-1}(O)$ with $t \geq 0$, suppose first that the compact trajectory segment $\varphi([0, t] \times \{(x, v)\})$ lies in $\mathring{M}$, so that it agrees with a trajectory segment of the geodesic flow: $\varphi([0, t] \times \{(x, v)\}) = \varphi^g([0, t] \times \{(x, v)\}) \subset \mathring{M}$. Then it follows from the continuity of φ^g that there is an $\varepsilon > 0$ and an open set $U \subset \mathring{M}$ containing (x, v) such that $\varphi^g([t - 2\varepsilon, t + 2\varepsilon] \times U) \subset \mathring{M} \cap O$. Now $t_-(\tilde{x}, \tilde{v}) < t - \varepsilon$, $t_+(\tilde{x}, \tilde{v}) > t + \varepsilon$ for all $(\tilde{x}, \tilde{v}) \in U$. It follows that $(t - \varepsilon, t + \varepsilon) \times U \subset \varphi^{-1}(O)$, so that (t, x, v) is an interior point of $\varphi^{-1}(O)$.

As a second case, suppose that $t > 0$, $\varphi([0, t) \times \{(x, v)\}) \subset \mathring{M}$, and $(x_0, v_0) \coloneqq \varphi_t(x, v) \in (\partial M \setminus \partial_{\mathrm{g}} M) \cap O$. Then $\varphi_t(x, v) \in \partial_{\mathrm{in}} M \cap O$ because the trajectory is incoming. Recalling the definition of φ departing from (5), the half-open trajectory segment $\varphi([0, t) \times \{(x, v)\})$ agrees with a trajectory segment of the geodesic flow: $\varphi([0, t) \times \{(x, v)\}) = \varphi^g([0, t) \times \{(x, v)\}) \subset \mathring{M}$. Let $N_{\mathrm{in}} \subset \mathbb{R} \times \partial_{\mathrm{in}} M$ be an open set as in Lemma 2.4. Then, since N_{in} is a neighborhood of $\{0\} \times \partial_{\mathrm{in}} M$ in $\mathbb{R} \times \partial_{\mathrm{in}} M$ and by the continuity of φ^g we can choose a small open subset $S_{\mathrm{in}} \subset \partial_{\mathrm{in}} M$ and a small $\delta > 0$ such that S_{in} contains $(x_0, v_0) = \varphi_t(x, v)$, $\overline{S}_{\mathrm{in}} \subset \partial_{\mathrm{in}} M \cap O$ is compact, $(-\delta, \delta) \times \overline{S}_{\mathrm{in}} \subset N_{\mathrm{in}}$, and $\varphi^g((-\delta, 0] \times S_{\mathrm{in}}) \subset O$. Then (13) gives us $\varphi((-\delta, 0] \times S_{\mathrm{in}}) = \varphi^g((-\delta, 0] \times S_{\mathrm{in}}) \subset O$. In addition we introduce the open set $S_{\mathrm{out}} \coloneqq \{(x, v') \,|\, (x, v) \in S_{\mathrm{in}}\} \subset \partial_{\mathrm{out}} M$ which contains (x_0, v_0'). Then by the reflection-symmetry of $(\partial M \setminus \partial_{\mathrm{g}} M) \cap O$ we have $\overline{S}_{\mathrm{out}} \subset \partial_{\mathrm{out}} M \cap O$. Using again the continuity of φ^g and (13) we can achieve, shrinking δ if necessary, that $\varphi^g([0, \delta) \times S_{\mathrm{out}}) = \varphi([0, \delta) \times S_{\mathrm{out}}) \subset O$.

Now, the continuity of φ^g and the fact that $\varphi((-\delta, \delta) \times S_{\mathrm{in}}) \cap \mathring{M}$ is open in $S\Sigma$ by Lemma 2.4 *iii)* imply that there is a small $\varepsilon \in (0, t)$ and a small open set $U \subset \mathring{M}$ containing (x, v) such that $\varphi^g([0, t - \varepsilon] \times U) \subset \mathring{M}$ and $\varphi^g_{t-\varepsilon}(U) \subset \varphi((-\delta, 0) \times S_{\mathrm{in}}) \cap O$. Then by (5) we have $[0, t - \varepsilon] \times U \subset D$ and $\varphi([0, t - \varepsilon] \times U) = \varphi^g([0, t - \varepsilon] \times U)$. See Figure 8 for an illustration.

Lemma 2.4 *iv)* and the flow property $\varphi_s(\varphi_{s'}(\tilde{x}, \tilde{v})) = \varphi_{s+s'}(\tilde{x}, \tilde{v})$ now imply the inclusion $(t - \varepsilon, t + \varepsilon) \times U \subset \varphi^{-1}(O)$, so that (t, x, v) is an interior point of $\varphi^{-1}(O)$.

If the trajectory segment $\varphi([0, t] \times \{(x, v)\})$ does not lie entirely in $\mathring{M}$, we can cut it into finitely many segments each of which lies either entirely in $\mathring{M}$ or intersects $\partial M \setminus \partial_{\mathrm{g}} M$ precisely in one of its endpoints. It then suffices to repeat the arguments above inductively finitely many times to show that (t, x, v) is an interior point of $\varphi^{-1}(O)$. The case $t < 0$ is treated analogously, finishing the proof that $\varphi^{-1}(O)$ is open.

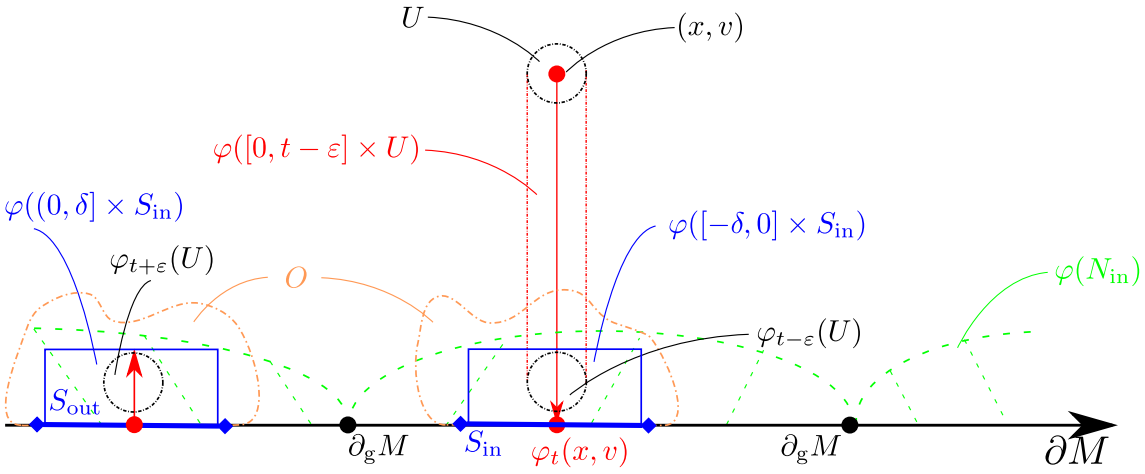

FIGURE 8. Illustration of the argument in the proof of Lemma 2.7. The transversality properties of φ established in Lemma 2.4 allow us to extend the trajectories of all points in U to the time interval $[0, t+\varepsilon)$.

Finally, (14) follows immediately from a combination of (11) with the presupposed reflection-symmetry of $O \cap (\partial M \setminus \partial_{\mathrm{g}} M)$. This completes the proof. □

A.3. **Proof of Proposition 3.3.** The proof of Proposition 3.3 relies on the following auxiliary result which describes some general technical properties of smooth models for the non-grazing billiard flow:

Lemma A.1. *Let $(\mathcal{M}, \pi, \phi)$ be a smooth model for φ. Then π is a proper map, one has*

$$\pi(\partial_{\mathrm{in}} M) = \pi(\partial_{\mathrm{out}} M) =: \mathcal{G}, \qquad \mathcal{M} = \pi(\mathring{M}) \sqcup \mathcal{G},$$

the set $\mathcal{G}$ is a codimension 1 submanifold of $\mathcal{M}$, and the maps $\pi|_{\partial_{\mathrm{in/out}} M} : \partial_{\mathrm{in/out}} M \to \mathcal{G}$ are diffeomorphisms. In particular, for every set $\mathcal{A} \subset \mathcal{M}$ the set $\pi^{-1}(\mathcal{A}) \cap (\partial M \setminus \partial_{\mathrm{g}} M)$ is reflection-symmetric. Furthermore, the flow ϕ is transversal to $\mathcal{G}$.

Proof. From (21), (7), and the continuity of π and ϕ it follows that

$$\pi(x,v) = \pi(x,v') \qquad \forall\, (x,v) \in \partial M \setminus \partial_{\mathrm{g}} M. \tag{48}$$

Since the tangential reflection $(x,v) \mapsto (x,v')$ interchanges $\partial_{\mathrm{in}} M$ and $\partial_{\mathrm{out}} M$, this shows that $\pi(\partial_{\mathrm{in}} M) = \pi(\partial_{\mathrm{out}} M)$. From the fact that $M \setminus \partial_{\mathrm{g}} M = \mathring{M} \sqcup \partial_{\mathrm{in}} M \sqcup \partial_{\mathrm{out}} M$ and the surjectivity of π it follows that $\mathcal{M} = \pi(\mathring{M}) \cup \mathcal{G}$. Suppose that there is a point $p \in \mathcal{G} \cap \pi(\mathring{M})$. Then there are points $\tilde{p} \in \mathring{M}$ and $\tilde{p}' \in \partial M \setminus \partial_{\mathrm{g}} M$ such that $\pi(\tilde{p}) = \pi(\tilde{p}') = p$. Since each trajectory of the non-grazing billiard flow φ intersects $\partial M \setminus \partial_{\mathrm{g}} M$ only at a discrete set of time parameters, we can find an $\varepsilon > 0$ such that $\varphi_\varepsilon(\tilde{p}), \varphi_\varepsilon(\tilde{p}') \in \mathring{M}$. Then (21) implies

$$\pi|_{\mathring{M}}(\varphi_\varepsilon(\tilde{p})) = \phi_\varepsilon(p) = \pi|_{\mathring{M}}(\varphi_\varepsilon(\tilde{p}')),$$

and the injectivity of $\pi|_{\mathring{M}}$ and φ_ε yields $\tilde{p} = \tilde{p}'$, contradicting the fact that $\mathring{M}$ and $\partial M \setminus \partial_{\mathrm{g}} M$ intersect trivially. This proves that $\mathcal{G} \cap \pi(\mathring{M}) = \emptyset$ hence $\mathcal{M} = \pi(\mathring{M}) \sqcup \mathcal{G}$.

To prove that $\mathcal{G}$ is a smooth submanifold of $\mathcal{M}$, let $N_{\mathrm{in}} \subset \mathbb{R} \times \partial_{\mathrm{in}} M$ be an open set as in Lemma 2.4 and put $\mathcal{N} := (\mathrm{id}_{\mathbb{R}} \times \pi)(N_{\mathrm{in}}) \subset \mathbb{R} \times \mathcal{G}$. Then $\{0\} \times \mathcal{G} \subset \mathcal{N} \subset \mathcal{D}$ by Lemma 2.4 *i)*. Let $(x,v) \in \partial_{\mathrm{in}} M$ and choose a small open set $S \subset \partial_{\mathrm{in}} M$ containing (x,v) and a small $\varepsilon > 0$ such that $(-\varepsilon, \varepsilon) \times S \subset N_{\mathrm{in}}$. This is possible because N_{in} is a neighborhood of $\{0\} \times \partial_{\mathrm{in}} M$ in $\mathbb{R} \times \partial_{\mathrm{in}} M$ by Lemma 2.4 *i)*. Consider the set N_{in}^- from (12) and recall from

(13) that $\varphi|_{N_{\mathrm{in}}^-} = \varphi^g|_{N_{\mathrm{in}}^-}$. Now, since $\pi|_{\mathring{M}}$ is a diffeomorphism and φ^g is an open map, we get that $\pi|_{\mathring{M}}(\varphi^g((-3\varepsilon/4, -\varepsilon/4) \times S))$ is an open subset of $\mathcal{M}$. Consequently, the set

$$\mathcal{U} := \phi_{\varepsilon/2}(\pi|_{\mathring{M}}(\varphi^g((-3\varepsilon/4, -\varepsilon/4) \times S))) \subset \mathcal{M}$$

is open in $\mathcal{M}$ because $\phi_{\varepsilon/2}$ is an open map. Moreover, using (13) and Lemma 2.4 *v)*, we see that $\phi_{\varepsilon/2} \circ \pi|_{\mathring{M}} \circ \varphi^g|_{(-3\varepsilon/4,-\varepsilon/4)\times S}$ is a diffeomorphism from $(-3\varepsilon/4, -\varepsilon/4) \times S$ onto $\mathcal{U}$.

However, thanks to (21), (13), and the flow property of φ we have

$$\mathcal{U} = (\pi \circ \varphi)((-\varepsilon/4, \varepsilon/4) \times S), \qquad \phi_{\varepsilon/2} \circ \pi|_{\mathring{M}} \circ \varphi^g|_{(-3\varepsilon/4,-\varepsilon/4)\times S} = \pi \circ \varphi|_{(-\varepsilon/4,\varepsilon/4)\times S},$$

which shows that $\mathcal{G} \subset \mathcal{U}$ and that $\pi \circ \varphi|_{(-\varepsilon/4,\varepsilon/4)\times S} : (-\varepsilon/4, \varepsilon/4) \times S \to \mathcal{U}$ is a diffeomorphism mapping $\{0\} \times S$ onto $\mathcal{U} \cap \mathcal{G} =: \mathcal{S}$. In particular, the identity $\pi|_S = \phi_{\varepsilon/2} \circ \pi|_{\mathring{M}} \circ \varphi^g_{-\varepsilon/2}|_S$ shows that $\pi|_S : S \to \mathcal{S}$ is a diffeomorphism. Applying (21) again we find that $\phi|_{(-\varepsilon/4,\varepsilon/4)\times\mathcal{S}} : (-\varepsilon/4, \varepsilon/4) \times \mathcal{S} \to \mathcal{U}$ is a diffeomorphism. This shows that ϕ is transversal to $\mathcal{G}$ at each point in $\mathcal{S}$.

Since $(x, v) \in \partial_{\mathrm{in}} M$ was arbitrary and we know that $\pi(\partial_{\mathrm{in}} M) = \mathcal{G}$, we have proved that $\mathcal{G}$ is a smooth submanifold of $\mathcal{M}$ of the same dimension as $\partial_{\mathrm{in}} M$, i.e., of codimension 1, that $\pi|_{\partial_{\mathrm{in}} M} : \partial_{\mathrm{in}} M \to \mathcal{G}$ is a local diffeomorphism, and that ϕ is transversal to $\mathcal{G}$.

To prove that $\pi|_{\partial_{\mathrm{in}} M}$ is injective it suffices to observe that given $(x_1, v_1), (x_2, v_2) \in \partial_{\mathrm{in}} M$ we can repeat the above argument with an $S \subset \partial_{\mathrm{in}} M$ containing both (x_1, v_1) and (x_2, v_2) and some small enough $\varepsilon > 0$ depending on (x_1, v_1) and (x_2, v_2); then the same trick of writing $\pi|_S = \phi_{\varepsilon/2} \circ \pi|_{\mathring{M}} \circ \varphi^g_{-\varepsilon/2}|_S$ shows that the assumption $\pi(x_1, v_1) = \pi(x_2, v_2)$ implies $(x_1, v_1) = (x_2, v_2)$ by injectivity of $\phi_{\varepsilon/2}$, $\pi|_{\mathring{M}}$, and $\varphi^g_{-\varepsilon/2}$.

The restriction $\pi|_{\partial_{\mathrm{out}} M}$ is treated analogously, finishing the proof that the maps $\pi|_{\partial_{\mathrm{in/out}} M} : \partial_{\mathrm{in/out}} M \to \mathcal{G}$ are diffeomorphisms.

Finally, that π is proper follows from the continuity of π and the observation that by the above the inverse image $\pi^{-1}(p)$ of any point $p \in \mathcal{M}$ contains at most 2 points. □

We are now in a position to prove Proposition 3.3:

Proof of Proposition 3.3. Using Lemma A.1, we define $F : \mathcal{M} \to \mathcal{M}'$ by

$$F(p) := \begin{cases} (\pi' \circ \pi|^{-1}_{\mathring{M}})(p), & p \in \pi(\mathring{M}), \\ (\pi' \circ \pi|^{-1}_{\partial_{\mathrm{in}} M})(p), & p \in \pi(\partial_{\mathrm{in}} M) = \mathcal{G}. \end{cases}$$

Then F satisfies by construction the relation $F \circ \pi = \pi'$ and F is bijective with inverse

$$F^{-1}(p') = \begin{cases} (\pi \circ \pi'|^{-1}_{\mathring{M}})(p'), & p' \in \pi'(\mathring{M}), \\ (\pi \circ \pi'|^{-1}_{\partial_{\mathrm{in}} M})(p'), & p' \in \pi'(\partial_{\mathrm{in}} M) = \mathcal{G}'. \end{cases}$$

From (21) and the relations $\mathcal{D} = (\mathrm{id}_{\mathbb{R}} \times \pi)(D)$, $\mathcal{D}' = (\mathrm{id}_{\mathbb{R}} \times \pi')(D)$ we get $(\mathrm{id}_{\mathbb{R}} \times F)(\mathcal{D}) = \mathcal{D}'$ and $F \circ \phi = \phi' \circ (\mathrm{id}_{\mathbb{R}} \times F)|_{\mathcal{D}}$.

It remains to prove that F and F^{-1} are smooth. By Definition 3.1 and Lemma A.1 the maps $F : \pi(\mathring{M}) \to \pi'(\mathring{M})$ and $F : \mathcal{G} \to \mathcal{G}'$ are diffeomorphisms, in particular F and F^{-1} are smooth on the open sets $\pi(\mathring{M}) \subset \mathcal{M}$ and $\pi'(\mathring{M}) \subset \mathcal{M}'$, respectively. To prove smoothness of F and F^{-1} near $\mathcal{G}$ and $\mathcal{G}'$, we note that since $\mathcal{D}$ and $\mathcal{D}'$ are open and ϕ, ϕ' are flows transversal to $\mathcal{G}$ and $\mathcal{G}'$, respectively by Lemma A.1, the inverse function theorem implies that there is an open set $U \subset \mathcal{M}$ containing $\mathcal{G}$, an open set $V \subset (\mathbb{R} \times \mathcal{G}) \cap \mathcal{D}$ containing $\{0\} \times \mathcal{G}$, an open set $U' \subset \mathcal{M}'$ containing $\mathcal{G}'$, and an open set $V' \subset (\mathbb{R} \times \mathcal{G}') \cap \mathcal{D}'$ containing $\{0\} \times \mathcal{G}'$ such that

$$\phi : V \to U, \qquad \phi' : V' \to U'$$

are smooth local coordinate charts on their respective domains. In fact, since $F \circ \phi = \phi' \circ (\mathrm{id}_{\mathbb{R}} \times F)|_{\mathcal{D}}$, we can achieve

$$V' = (\mathrm{id}_{\mathbb{R}} \times F|_{\mathcal{G}})(V)$$

by shrinking V or V'. To show that F is smooth on U and F^{-1} is smooth on U' it now suffices to prove that

$$(\mathrm{id}_{\mathbb{R}} \times F|_{\mathcal{G}}^{-1}) \circ \phi'|_{V'}^{-1} \circ F \circ \phi : V \to V, \qquad (\mathrm{id}_{\mathbb{R}} \times F|_{\mathcal{G}}) \circ \phi|_{V}^{-1} \circ F^{-1} \circ \phi' : V' \to V'$$

are smooth maps. However, the latter are nothing but the identity maps as one sees by employing again the relation $F \circ \phi = \phi' \circ (\mathrm{id}_{\mathbb{R}} \times F)|_{\mathcal{D}}$.

Finally, the uniqueness of F follows from the fact that by Lemma A.1 the complement $\mathcal{M} \setminus \mathcal{G}$ is dense in $\mathcal{M}$ and F is uniquely determined by π and π' on $\mathcal{M} \setminus \mathcal{G}$. □

A.4. **Proof of Proposition 4.5.** Consider the gluing regions $\mathcal{G}_g = \pi_g(\partial M \setminus \partial_{\mathrm{g}} M) \subset \mathcal{M}_g$ and $\mathcal{G}_{g'} = \pi_{g'}(\partial M \setminus \partial_{\mathrm{g}} M) \subset \mathcal{M}_{g'}$, respectively. Then by the fact that $\pi_g|_{\mathring{M}}$ and $\pi_{g'}|_{\mathring{M}}$ are diffeomorphisms onto $\mathcal{M}_g \setminus \mathcal{G}_g$ and $\mathcal{M}_{g'} \setminus \mathcal{G}_{g'}$, respectively, we immediately get the built-in diffeomorphism

$$\pi_{g'}|_{\mathring{M}} \circ \pi_g|_{\mathring{M}}^{-1} : \mathcal{M}_g \setminus \mathcal{G}_g \xrightarrow{\cong} \mathcal{M}_{g'} \setminus \mathcal{G}_{g'} \tag{49}$$

that makes the analogue of the diagram (34), with $M \setminus \partial_{\mathrm{g}} M$ replaced by $\mathring{M}$, commute. Moreover, we see that any diffeomorphism $\mathcal{M}_g \cong \mathcal{M}_{g'}$ making (34) commute coincides with (49) on the dense set $\mathcal{M}_g \setminus \mathcal{G}_g$, so that it is uniquely determined by this property.

In order to extend (49) to a (necessarily unique) diffeomorphism $\mathcal{M}_g \cong \mathcal{M}_{g'}$, let $N_g, N_{g'} \subset \mathbb{R} \times (\partial M \setminus \partial_{\mathrm{g}} M)$ be two sets as in Lemma 2.4, applied separately for g and g', respectively, and consider the intersection $N_{\mathrm{in}} \coloneqq (N_g)_{\mathrm{in}} \cap (N_{g'})_{\mathrm{in}} = N \cap (\mathbb{R} \times \partial_{\mathrm{in}} M)$, where $N \coloneqq N_g \cap N_{g'}$. Then the set $O \coloneqq \varphi_g(N_{\mathrm{in}}) \cap \varphi_{g'}(N_{\mathrm{in}})$ is an open neighborhood of $\partial M \setminus \partial_{\mathrm{g}} M$ in $M \setminus \partial_{\mathrm{g}} M$ by Lemma 2.4. In particular, $O \cap (\partial M \setminus \partial_{\mathrm{g}} M) = \partial M \setminus \partial_{\mathrm{g}} M$ is invariant under tangential reflection with respect to g and g'. Thus, by Lemma 2.7 (also applied separately for g and g'), the sets

$$N_{g,g'} \coloneqq \varphi_g^{-1}(O) \cap N_{\mathrm{in}}, \qquad N_{g',g} \coloneqq \varphi_{g'}^{-1}(O) \cap N_{\mathrm{in}}$$

are open in $\mathbb{R} \times \partial_{\mathrm{in}} M$, and by definition of the quotient topologies on $\mathcal{M}_g$ and $\mathcal{M}_{g'}$ the identity map $O \to O$ descends to a homeomorphism

$$\mathcal{O}_g \cong \mathcal{O}_{g'} \tag{50}$$

between the open neighborhood $\mathcal{O}_g \coloneqq \pi_g(O)$ of $\mathcal{G}_g$ in $\mathcal{M}_g$ and the open neighborhood $\mathcal{O}_{g'} \coloneqq \pi_{g'}(O)$ of $\mathcal{G}_{g'}$ in $\mathcal{M}_{g'}$. Moreover, by definition of the quotient maps π_g and $\pi_{g'}$, the diffeomorphism (49) and the homeomorphism (50) agree on $\mathcal{O}_g \cap (\mathcal{M}_g \setminus \mathcal{G}_g)$, so that they glue to a global homeomorphism $\mathcal{M}_g \cong \mathcal{M}_{g'}$. It remains to prove that the latter is a diffeomorphism, which reduces to proving that the map (50) and its inverse are smooth. By definition of the smooth structures on $\mathcal{M}$ and $\mathcal{M}_{g'}$, this reduces to checking that

$$\begin{aligned} &\varphi_g|_{N_{g,g'}}^{-1} \circ \varphi_{g'}|_{N_{g',g}} : N_{g',g} \to N_{g,g'}, \\ &\varphi_{g'}|_{N_{g',g}}^{-1} \circ \varphi_g|_{N_{g,g'}} : N_{g,g'} \to N_{g',g} \end{aligned} \tag{51}$$

are smooth maps. By (13) the maps (51) can be expressed in terms of the geodesic flows φ^g, $\varphi^{g'}$ and the reflection maps $R_g, R_{g'} : \mathbb{R} \times (\partial M \setminus \partial_{\mathrm{g}} M) \to \mathbb{R} \times (\partial M \setminus \partial_{\mathrm{g}} M)$, $(t,x,v) \mapsto (t,x,R_{g(x)}v)$, $(t,x,v) \mapsto (t,x,R_{g'(x)}v)$, by

$$(\varphi_g|_{N_{g,g'}}^{-1} \circ \varphi_{g'}|_{N_{g',g}})(t,x,v) = \begin{cases} (\varphi^g|_{N_{g,g'}}^{-1} \circ \varphi^{g'}|_{N_{g',g}})(t,x,v), & t \le 0, \\ (R_g \circ \varphi^g|_{R_g(N_{g,g'})}^{-1} \circ \varphi^{g'}|_{R_{g'}(N_{g',g})} \circ R_{g'})(t,x,v), & t > 0, \end{cases}$$

$$(\varphi_{g'}|_{N_{g',g}}^{-1} \circ \varphi_g|_{N_{g,g'}})(t,x,v) = \begin{cases} (\varphi^{g'}|_{N_{g',g}}^{-1} \circ \varphi^g|_{N_{g,g'}})(t,x,v), & t \le 0, \\ (R_{g'} \circ \varphi^{g'}|_{R_{g'}(N_{g',g})}^{-1} \circ \varphi^g|_{R_g(N_{g,g'})} \circ R_g)(t,x,v), & t > 0. \end{cases}$$

Since $\varphi^g|_{N_{g,g'}}$ and $\varphi^{g'}|_{N_{g',g}}$ are diffeomorphisms onto their images, the above maps are smooth iff their post-compositions with $\varphi^g|_{N_{g,g'}}$ and $\varphi^{g'}|_{N_{g',g}}$ are smooth, respectively. In view of the definitions of R_g and $\tilde{R}_g$, the proof is finished. □

Appendix B. Construction of smooth model bundles

Here we provide a concrete construction of smooth models in the vector-valued setting, i.e., of smooth model bundles. The reader who is not interested in the vector-valued case may safely skip this appendix. The construction follows ideas very similar to those employed in the above construction of smooth models for non-grazing billiard flows.

We begin by reminding the reader of some notation used in the main text: There we introduced the non-grazing billiard flow φ acting on the phase-space $M \setminus \partial_{\mathrm{g}} M$, defined on the domain $D \subset \mathbb{R} \times (M \setminus \partial_{\mathrm{g}} M)$ from (10) which is open by Lemma 2.7. For the analytic treatment of this dynamical system we constructed a model manifold $\mathcal{M}$ together with a smooth surjection $\pi : M \setminus \partial_{\mathrm{g}} M \to \mathcal{M}$ and a smooth model flow ϕ on $\mathcal{M}$, defined on the domain $\mathcal{D} \subset \mathbb{R} \times \mathcal{M}$, such that $\pi \circ \varphi_t = \phi_t \circ \pi$. This was necessary because φ is non-smooth (in fact non-continuous and not even a flow) due to the presence of the instantaneous boundary reflections $R : \partial M \setminus \partial_{\mathrm{g}} M \to \partial M \setminus \partial_{\mathrm{g}} M$, $(x, v) \mapsto (x, v')$.

For the remainder of this appendix we now assume a smooth $\mathbb{C}$-vector bundle

$$\pi_{\widetilde{\mathcal{E}}} : \widetilde{\mathcal{E}} \to M \setminus \partial_{\mathrm{g}} M$$

of rank r to be given, the fibers of which we denote by $\widetilde{\mathcal{E}}_{(x,v)} \coloneqq \pi_{\widetilde{\mathcal{E}}}^{-1}(\{(x, v)\})$.

Furthermore we require a first-order differential operator $\widetilde{\mathbb{X}}$ acting on smooth sections of $\widetilde{\mathcal{E}}$ and satisfying the following Leibniz rule:

$$\widetilde{\mathbb{X}}\big(\widetilde{f} \cdot \widetilde{\sigma}\big) = (\mathbf{P}\widetilde{f}) \cdot \widetilde{\sigma} + \widetilde{f} \cdot \widetilde{\mathbb{X}}\widetilde{\sigma}, \quad \forall \widetilde{f} \in \mathrm{C}^\infty_{\mathrm{Bill}}(M \setminus \partial_{\mathrm{g}} M),\, \widetilde{\sigma} \in \mathrm{C}^\infty(M \setminus \partial_{\mathrm{g}} M, \widetilde{\mathcal{E}}), \tag{52}$$

where $\mathbf{P}$ denotes the billiard generator defined in Section 2.4. An additional piece of data necessary for the construction of a smooth model for $\widetilde{\mathcal{E}}$ is a bundle isomorphism

$$\kappa : \widetilde{\mathcal{E}}\big|_{\partial_{\mathrm{in}} M} \longrightarrow \widetilde{\mathcal{E}}\big|_{\partial_{\mathrm{out}} M}$$

such that $\pi_{\widetilde{\mathcal{E}}} \circ \kappa = R \circ \pi_{\widetilde{\mathcal{E}}}\big|_{\pi_{\widetilde{\mathcal{E}}}^{-1}(\partial_{\mathrm{in}} M)}$ holds. For example, such an isomorphism exists if both $\widetilde{\mathcal{E}}\big|_{\partial_{\mathrm{in}} M}$ and $\widetilde{\mathcal{E}}\big|_{\partial_{\mathrm{out}} M}$ can be trivialized: Then we can simply define κ as the composition of the first trivialization, the map $R \times \mathrm{id}_{\mathbb{C}^r}$, and the inverse of the second trivialization.

Before proving our main theorem we first have to describe a dynamical quantity associated with the above data, namely the *billiard parallel transport*. Morally it is derived from the operator $\widetilde{\mathbb{X}}$ in the same intuitive manner as the billiard flow is derived from the geodesic flow:

Lemma B.1. *There exists a unique map $\widetilde{\alpha} : \widetilde{\mathcal{D}} \to \widetilde{\mathcal{E}}$ on the flow domain*

$$\widetilde{\mathcal{D}} \coloneqq \big\{(t, e) \,\big|\, \exists (x, v) \in M \setminus \partial_{\mathrm{g}} M :\, (t, x, v) \in D \text{ and } e \in \widetilde{\mathcal{E}}_{(x,v)}\big\}\ ,$$

called the billiard parallel transport*, with the following properties:*

(1) For each $(t, x, v) \in D$ the map

$$\widetilde{\alpha}_{(x,v),t} : \widetilde{\mathcal{E}}_{(x,v)} \longrightarrow \widetilde{\mathcal{E}}_{\varphi_t(x,v)}, \qquad e \mapsto \widetilde{\alpha}_{(x,v),t}(e) \coloneqq \widetilde{\alpha}(t, e), \tag{53}$$

is a well-defined linear isomorphism.

(2) $\widetilde{\alpha}$ is a flow up to composition with κ on boundary fibers. More precisely, one has

$$\widetilde{\alpha}_{(x,v),0} = \mathrm{id}_{\widetilde{\mathcal{E}}_{(x,v)}} \qquad \forall\, (x, v) \in M \setminus \partial_{\mathrm{g}} M \tag{54}$$

and if $(t,x,v)\in D$ and $t'\in\mathbb{R}$ are such that $(t',\varphi_t(x,v))\in D$, then the following generalization of (8) *holds:*

$$\widetilde{\alpha}_{\varphi_t(x,v),t'}\circ\widetilde{\alpha}_{(x,v),t}=\begin{cases}\widetilde{\alpha}_{(x,v),t+t'}, & t+t'\neq 0 \text{ or } \varphi_{t+t'}(x,v)\in\mathring{M} \text{ or}\\ & t<0,(x,v)\in\partial_{\mathrm{in}}M \text{ or } t>0,(x,v)\in\partial_{\mathrm{out}}M,\\ \kappa|_{\widetilde{\mathcal{E}}_{(x,v)}}, & t+t'=0 \text{ and } t>0,(x,v)\in\partial_{\mathrm{in}}M,\\ \kappa^{-1}|_{\widetilde{\mathcal{E}}_{(x,v)}}, & t+t'=0 \text{ and } t<0,(x,v)\in\partial_{\mathrm{out}}M.\end{cases}\tag{55}$$

(3) For each $\widetilde{\sigma}\in\mathrm{C}^\infty(M\setminus\partial_{\mathrm{g}}M,\widetilde{\mathcal{E}})$ the map

$$\varphi^{-1}(\mathring{M})\to\widetilde{\mathcal{E}},\qquad (t,x,v)\mapsto\widetilde{\alpha}_{(x,v),t}\big(\widetilde{\sigma}(x,v)\big),$$

is smooth.

(4) For each $(x,v)\in\mathring{M}$ and $\widetilde{\sigma}\in\mathrm{C}^\infty(M\setminus\partial_{\mathrm{g}}M,\widetilde{\mathcal{E}})$ one has

$$(\widetilde{\mathbb{X}}\widetilde{\sigma})(x,v)=\frac{d}{dt}\Big|_{t=0}\widetilde{\alpha}_{\varphi_t(x,v),-t}\widetilde{\sigma}(\varphi_t(x,v)).$$

Proof. As a preliminary step we embed a neighborhood of $M\setminus\partial_{\mathrm{g}}M$ in $S\Sigma$ into a closed manifold N and extend $\widetilde{\mathcal{E}}$ and $\widetilde{\mathbb{X}}$ arbitrarily to N such that near $M\setminus\partial_{\mathrm{g}}M$ they satisfy the Leibniz rule (52) with $\mathbf{P}$ replaced by the geodesic vector field X^g (recall from (20) that $\mathbf{P}$ agrees with X^g on billiard functions). We continue to denote these extensions by $\widetilde{\mathcal{E}},\widetilde{\mathbb{X}}$ and obtain a well-defined transfer operator $\exp(-t\widetilde{\mathbb{X}})$ acting on smooth sections of $\widetilde{\mathcal{E}}$.

Given $(t,x,v)\in D$ we begin by assuming that $t\geq 0$ is small enough such that $\varphi_s(x,v)$, $s\in[0,t]$, intersects $\partial M\setminus\partial_{\mathrm{g}}M$ only at its endpoint $\varphi_t(x,v)$, if at all. Then two cases must be distinguished:

(1) $(x,v)\in\mathring{M}$: Given $e\in\widetilde{\mathcal{E}}_{(x,v)}$ choose $\widetilde{\sigma}\in\mathrm{C}^\infty(N,\widetilde{\mathcal{E}})$ with $\widetilde{\sigma}(x,v)=e$ and supported in $\mathring{M}$. Then we define

$$\widetilde{\alpha}_{(x,v),t}(e)\coloneqq\big(\exp(-t\widetilde{\mathbb{X}})\widetilde{\sigma}\big)(\varphi_t(x,v)),$$

which is independent of the choice of $\widetilde{\sigma}$ by the Leibniz rule (52), which in turn applies by the support property of $\widetilde{\sigma}$ and where we use that any smooth function supported in $\mathring{M}$ is a billiard function.

(2) $(x,v)\in\partial M\setminus\partial_{\mathrm{g}}M$: If $(x,v)\in\partial_{\mathrm{out}}M$, given $e\in\widetilde{\mathcal{E}}_{(x,v)}$, choose $\widetilde{\sigma}\in\mathrm{C}^\infty(N,\widetilde{\mathcal{E}})$ with $\widetilde{\sigma}(x,v)=e$ by multiplying some local frame with cutoffs that restrict to billiard functions on $M\setminus\partial_{\mathrm{g}}M$. Again we define

$$\widetilde{\alpha}_{(x,v),t}(e)\coloneqq\big(\exp(-t\widetilde{\mathbb{X}})\widetilde{\sigma}\big)(\varphi_t(x,v)),$$

independently of the choice of $\widetilde{\sigma}$. If instead $(x,v)\in\partial_{\mathrm{in}}M$ we proceed in the same way but with $\kappa(e)$ instead of e.

This construction can analogously be transferred to sufficiently small $t<0$.

Now, without these smallness assumptions on t, we use that by definition of D and φ there exists a unique finite sequence $t_0,t_1,...,t_N$ with $t=t_0+\cdots+t_N$ such that $\varphi_t(x,v)$ can be written in terms of the geodesic flow φ^g as $\varphi_t(x,v)=\varphi^g_{t_N}\circ R\circ\cdots\circ R\circ\varphi^g_{t_0}(x,v)$. We then define the billiard parallel transport of $e\in\widetilde{\mathcal{E}}_{(x,v)}$ as

$$\widetilde{\alpha}_{(x,v),t}(e)\coloneqq\widetilde{\alpha}_{(x,v),t_N}\circ\cdots\circ\widetilde{\alpha}_{(x,v),t_0}(e).$$

The claimed Properties (1), (2) of $\widetilde{\alpha}$ are now satisfied by construction and Properties (3), (4) follow from the properties of $\exp(-t\widetilde{\mathbb{X}})$ since φ is smooth on $\varphi^{-1}(\mathring{M})$. Finally, Property (1), Eq. (54), and Property (4) determine $\widetilde{\alpha}$ uniquely on $\varphi^{-1}(\mathring{M})\times\widetilde{\mathcal{E}}$ and (55) then implies that the full map $\widetilde{\alpha}$ is unique because its values at points outside $\varphi^{-1}(\mathring{M})\times\widetilde{\mathcal{E}}$ are determined by κ and values at points inside $\varphi^{-1}(\mathring{M})\times\widetilde{\mathcal{E}}$. □

Definition B.2. *We call the operator*

$$\begin{aligned}\mathcal{L} : D \times \mathrm{C}^\infty(M \setminus \partial_{\mathrm{g}} M, \widetilde{\mathcal{E}}) &\longrightarrow \Gamma(M \setminus \partial_{\mathrm{g}} M, \widetilde{\mathcal{E}}) \\ ((t,x,v), \widetilde{\sigma}) &\longmapsto \widetilde{\alpha}_{\varphi_{-t}(x,v),t}(\widetilde{\sigma}(\varphi_{-t}(x,v))) =: (\mathcal{L}_t \widetilde{\sigma})(x,v)\end{aligned}$$

the billiard transfer operator *associated with* $\widetilde{\mathbb{X}}$. *Here* $\Gamma(M \setminus \partial_{\mathrm{g}} M, \widetilde{\mathcal{E}})$ *denotes the set of arbitrary sections of* $\widetilde{\mathcal{E}}$ *without any continuity or smoothness assumption.*

This terminology is of course motivated by Lemma B.1, which implies that for each $\widetilde{\sigma} \in \mathrm{C}^\infty(M \setminus \partial_{\mathrm{g}} M, \widetilde{\mathcal{E}})$ the map

$$\varphi^{-1}(\mathring{M}) \cap (\mathbb{R} \times \mathring{M}) \to \widetilde{\mathcal{E}}|_{\mathring{M}}, \qquad (t,x,v) \mapsto (\mathcal{L}_t \widetilde{\sigma})(x,v),$$

is smooth and one has

$$(\widetilde{\mathbb{X}}\widetilde{\sigma})(x,v) = -\frac{d}{dt}\Big|_{t=0} (\mathcal{L}_t \widetilde{\sigma})(x,v) \quad \forall\, (x,v) \in \mathring{M}. \tag{56}$$

We can now introduce the vector-valued equivalent of the billiard functions:

Definition B.3. *The set of* smooth billiard sections *of* $\widetilde{\mathcal{E}}$ *is*

$$\mathrm{C}^\infty_{\mathrm{Bill}}(M \setminus \partial_{\mathrm{g}} M, \widetilde{\mathcal{E}}) := \left\{ \widetilde{\sigma} \in \mathrm{C}^\infty(M \setminus \partial_{\mathrm{g}} M) \,\middle|\, \big((t,x,v) \mapsto (\mathcal{L}_t \widetilde{\sigma})(x,v)\big) \in \mathrm{C}^\infty(D, \widetilde{\mathcal{E}}) \right\}.$$

An elementary property of the smooth billiard sections is that they are stable with respect to multiplication by smooth billiard functions – in other words, $\mathrm{C}^\infty_{\mathrm{Bill}}(M \setminus \partial_{\mathrm{g}} M, \widetilde{\mathcal{E}})$ is a $\mathrm{C}^\infty_{\mathrm{Bill}}(M \setminus \partial_{\mathrm{g}} M)$-module. The main siginificance of the smooth billiard sections is that they are preserved by the operator $\widetilde{\mathbb{X}}$ and the latter acts on them by differentiation of the billiard transfer operator:

$$\widetilde{\mathbb{X}} : \mathrm{C}^\infty_{\mathrm{Bill}}(M \setminus \partial_{\mathrm{g}} M, \widetilde{\mathcal{E}}) \longrightarrow \mathrm{C}^\infty_{\mathrm{Bill}}(M \setminus \partial_{\mathrm{g}} M, \widetilde{\mathcal{E}}), \qquad (\widetilde{\mathbb{X}}\widetilde{\sigma})(x,v) = -\frac{d}{dt}\Big|_{t=0} (\mathcal{L}_t \widetilde{\sigma})(x,v).$$

This follows from (56). It provides the vector-valued generalization of the formula (19).

With this data as our point of departure we can now prove our main theorem in the vector-valued situation:

Theorem B.4 (Existence of smooth model bundles)**.** *There exists a smooth vector bundle* $\pi_{\mathcal{E}} : \mathcal{E} \to \mathcal{M}$ *and a smooth surjection* $\Pi : \widetilde{\mathcal{E}} \to \mathcal{E}$ *such that the diagram*

$$\begin{array}{ccc} \widetilde{\mathcal{E}} & \xrightarrow{\ \Pi\ } & \mathcal{E} \\ \big\downarrow{\scriptstyle \pi_{\widetilde{\mathcal{E}}}} & & \big\downarrow{\scriptstyle \pi_{\mathcal{E}}} \\ M \setminus \partial_{\mathrm{g}} M & \xrightarrow{\ \pi\ } & \mathcal{M} \end{array} \tag{57}$$

commutes, as well as a linear isomorphism

$$\Sigma_{\mathcal{E}} : \mathrm{C}^\infty_{\mathrm{Bill}}(M \setminus \partial_{\mathrm{g}} M, \widetilde{\mathcal{E}}) \longrightarrow \mathrm{C}^\infty(\mathcal{M}, \mathcal{E}) \tag{58}$$

that is uniquely characterized by the relation

$$\Sigma_{\mathcal{E}}(\widetilde{\sigma}) \circ \pi = \Pi \circ \widetilde{\sigma} \qquad \forall\, \widetilde{\sigma} \in \mathrm{C}^\infty_{\mathrm{Bill}}(M \setminus \partial_{\mathrm{g}} M, \widetilde{\mathcal{E}}).$$

Furthermore, introducing the first order differential operator

$$\mathbb{X} := \Sigma_{\mathcal{E}} \circ \widetilde{\mathbb{X}} \circ \Sigma_{\mathcal{E}}^{-1} : \mathrm{C}^\infty(\mathcal{M}, \mathcal{E}) \to \mathrm{C}^\infty(\mathcal{M}, \mathcal{E})$$

and for $(t,p) \in \mathcal{D}$ *the parallel transport*

$$\begin{aligned}\alpha_{p,t} : \mathcal{E}_p &\longrightarrow \mathcal{E}_{\phi_t(p)}, \\ e &\longmapsto \big(\exp(-t\mathbb{X})\sigma_e\big)(\phi_t(p)),\end{aligned} \tag{59}$$

where $\exp(-t\mathbb{X})$ *is the transfer operator of* $\mathbb{X}$ *and* σ_e *denotes any smooth section with* $\sigma_e(p) = e$, *then the trace of* $\alpha_{p,t}$ *on a periodic trajectory (i.e., when* $\phi_t(p) = p$*) coincides*

with the trace of the billiard parallel transport from Lemma B.1 on the corresponding periodic trajectory of the non-grazing billiard flow φ.

Proof. Our proof is constructive and uses the abstract vector bundle construction lemma well established in the differential geometry literature, see e.g. [Lee12, Lemma 10.6]. We start by specifying the total space of our new bundle:

$$\mathcal{E} \coloneqq \bigsqcup_{p\in\mathcal{M}\setminus\mathcal{G}} \widetilde{\mathcal{E}}_{\pi^{-1}(p)} \sqcup \bigsqcup_{(x,v)\in\partial_{\mathrm{in}}M} \widetilde{\mathcal{E}}_{(x,v)} \oplus \widetilde{\mathcal{E}}_{(x,v')} / \sim_\kappa, \tag{60}$$

where $\sim_\kappa$ means that we quotient out the linear subspace of $\widetilde{\mathcal{E}}_{(x,v)} \oplus \widetilde{\mathcal{E}}_{(x,v')}$ defined by the elements of the form $(e, -\kappa(e))$, which is possible by the relation $\pi_{\widetilde{\mathcal{E}}} \circ \kappa = R \circ \pi_{\widetilde{\mathcal{E}}}\big|_{\pi_{\widetilde{\mathcal{E}}}^{-1}(\partial_{\mathrm{in}}M)}$. Note that over each point $p = [x, v] \in \mathcal{G}$ the fiber $\mathcal{E}_p = \widetilde{\mathcal{E}}_{(x,v)} \oplus \widetilde{\mathcal{E}}_{(x,v')} / \sim_\kappa$ is canonically isomorphic to $\widetilde{\mathcal{E}}_{(x,v)}$ as well as $\widetilde{\mathcal{E}}_{(x,v')}$ via the maps $e \mapsto [e, 0]$ and $e \mapsto [0, e]$, respectively. Next we need to specify the trivializations of $\mathcal{E}$: In a neighborhood of any point of $\mathcal{M}\setminus\mathcal{G}$ we make the obvious choice and take trivializations of $\widetilde{\mathcal{E}}$ composed with (a suitable restriction of) $\pi \times \mathrm{id}_{\mathbb{C}^r}$. Around a point $p = [x, v] \in \mathcal{G}$, $(x, v) \in \partial_{\mathrm{in}}M$, we define *flow-trivializations* using the billiard parallel transport map: Take any trivialization t_{in} of $\widetilde{\mathcal{E}}\big|_{\partial_{\mathrm{in}}M}$ on an open set $U_{\mathrm{in}} \subset \partial_{\mathrm{in}}M$ around (x, v) and put

$$\begin{aligned} \mathbf{t} : \pi_{\mathcal{E}}^{-1}\left(\Phi(N_{\mathrm{in}} \cap \mathbb{R} \times U_{\mathrm{in}})\right) &\longrightarrow \Phi(N_{\mathrm{in}} \cap \mathbb{R} \times U_{\mathrm{in}}) \times \mathbb{C}^r, \\ \mathcal{E}_{\Phi(t,[y,w])} \ni e &\longmapsto \left((\phi_t \circ \pi) \times \mathrm{id}_{\mathbb{C}^r}\right) \circ t_{\mathrm{in}}\left(\widetilde{\alpha}_{\varphi_t(y,w),-t}(e)\right), \end{aligned}$$

where $\Phi : N_{\mathrm{in}} \to \mathcal{M}$ denotes the flow chart from Section 4.2, (y, w) is the unique lift of $[y, w]$ to $\partial_{\mathrm{in}}M$, and if $t = 0$ we identified $[e, 0]$ and e. This defines a trivialization $\mathbf{t}$ around p. Now, $\mathbf{t}$ transitions smoothly with any trivialization around points in $\mathcal{M} \setminus \mathcal{G}$ thanks to Lemma B.1 (1), and furthermore $\mathbf{t}$ transitions smoothly with any trivialization $\mathbf{t}'$ built analogously but from another trivialization t'_{in} since $t'_{\mathrm{in}} \circ t_{\mathrm{in}}^{-1}$ is smooth and the smooth structure of $\mathcal{M}$ near $\mathcal{G}$ has been defined using flow charts.

The desired surjection $\Pi : \widetilde{\mathcal{E}} \to \mathcal{E}$ is given by

$$\Pi(e) \coloneqq \begin{cases} e, & e \in \bigsqcup_{p\in\mathcal{M}\setminus\mathcal{G}} \widetilde{\mathcal{E}}_{\pi^{-1}(p)}, \\ [e, 0], & e \in \bigsqcup_{(x,v)\in\partial_{\mathrm{in}}M} \widetilde{\mathcal{E}}_{(x,v)}, \\ [0, e], & e \in \bigsqcup_{(x,v)\in\partial_{\mathrm{out}}M} \widetilde{\mathcal{E}}_{(x,v)}. \end{cases}$$

This map is continuous by definition of the topology on $\mathcal{E}$ and it is clearly smooth on $\bigsqcup_{p\in\mathcal{M}\setminus\mathcal{G}} \widetilde{\mathcal{E}}_{\pi^{-1}(p)}$. To check that Π is also smooth near $\bigsqcup_{(x,v)\in\partial_{\mathrm{in}}M} \widetilde{\mathcal{E}}_{(x,v)}$, we compose it with a trivializaton $\mathbf{t}$ as above. For $e \in \bigsqcup_{(x,v)\in\partial_{\mathrm{in}}M} \widetilde{\mathcal{E}}_{(x,v)}$ the point e has been identified with $[e, 0]$ in the definition of $\mathbf{t}$, so that by definition of the smooth structure on $\mathcal{E}$ the composition $\mathbf{t} \circ \Pi$ is smooth near e. On the other hand, for $e \in \bigsqcup_{(x,v)\in\partial_{\mathrm{out}}M} \widetilde{\mathcal{E}}_{(x,v)}$ the point $[0, e] = [\kappa^{-1}(e), 0]$ appearing in $\mathbf{t}$ at $t = 0$ is identified with $\kappa^{-1}(e)$. Using the relation $\pi_{\widetilde{\mathcal{E}}} \circ \kappa = R \circ \pi_{\widetilde{\mathcal{E}}}\big|_{\pi_{\widetilde{\mathcal{E}}}^{-1}(\partial_{\mathrm{in}}M)}$ and the definition of $\widetilde{\alpha}$ from the proof of Lemma B.1, we obtain

$$\widetilde{\alpha}_{\varphi_t(y,w),-t}\big(\kappa^{-1}(e)\big) = \widetilde{\alpha}_{\varphi_t(y,w),-t}(e)$$

and hence $\mathbf{t} \circ \Pi$ is again smooth near e.

Next we define for a smooth billiard section $\widetilde{\sigma}$ of $\widetilde{\mathcal{E}}$ the section $\Sigma_{\mathcal{E}}(\widetilde{\sigma}) \coloneqq \sigma$ as

$$\sigma([x, v]) \coloneqq \begin{cases} \widetilde{\sigma}(x, v), & [x, v] \notin \mathcal{G}, \\ [\widetilde{\sigma}(x, v), 0]_\kappa, & [x, v] \in \mathcal{G},\ (x, v) \in \partial_{\mathrm{in}}M \end{cases}$$

where $[\cdot, \cdot]_\kappa$ denotes the equivalence class with respect to $\sim_\kappa$. The map σ is well-defined (i.e., independently of the choice of the lift $(x, v) \in \partial_{\mathrm{in}}M$ of $[x, v]$) because $\widetilde{\sigma}$ being a billiard section implies that $\widetilde{\sigma}(x, v') = \kappa(\widetilde{\sigma}(x, v))$ for $(x, v) \in \partial_{\mathrm{in}}M$, and hence $[\widetilde{\sigma}(x, v), 0]_\kappa =$

$[0, \widetilde{\sigma}(x,v')]_\kappa$. Clearly, σ is a section and smooth at any point of $\mathcal{M} \setminus \mathcal{G}$. To test smoothness at any point of the gluing region $\mathcal{G}$ we have to compose with flow charts and flow trivializations to obtain a coordinate expression. Doing so yields

$$\begin{aligned} \mathbb{R} \times U_{\mathrm{in}} \cap N_{\mathrm{in}} &\longrightarrow (\mathbb{R} \times U_{\mathrm{in}} \cap N_{\mathrm{in}}) \times \mathbb{C}^r \\ (t,x,v) &\longmapsto t_{\mathrm{in}} \left(\widetilde{\alpha}_{\varphi_t(x,v),-t} \left(\widetilde{\sigma}(\varphi_t(x,v)) \right) \right). \end{aligned}$$

To prove the mapping properties claimed in (58) it therefore only remains to show that $\Sigma_{\mathcal{E}}$ is bijective on the given domains, but this follows easily from the observation that

$$\Sigma_{\mathcal{E}}^{-1}(\sigma)(x,v) = \begin{cases} \sigma([x,v]), & (x,v) \in \mathring{M}, \\ e, & (x,v) \in \partial_{\mathrm{in}} M,\ \sigma([x,v]) = [e,0]_\kappa, \\ e', & (x,v) \in \partial_{\mathrm{out}} M,\ \sigma([x,v]) = [0,e']_\kappa \end{cases}$$

is indeed the inverse of $\Sigma_{\mathcal{E}}$ and has its image in $\mathrm{C}^\infty_{\mathrm{Bill}}(M \setminus \partial_{\mathrm{g}} M, \widetilde{\mathcal{E}})$ due to a similar coordinate calculation.

The definition of α is independent of the chosen section σ_e by virtue of the Leibniz rule which trivially follows for $\mathbb{X}$ from the Leibniz rule for $\widetilde{\mathbb{X}}$. The claimed equality of traces follows immediately because the model bundle $\mathcal{E}$ was constructed in such a way that the boundary map κ present in the definition of $\widetilde{\alpha}$ acts trivially on it. □

Remark B.5. We refrain from stating and proving a vector-valued uniqueness result analogous to Proposition 3.3, as well as a vector-valued version of the resolvent study as in Corollary 5.5 for the sake of brevity.

References

[BDL18] Viviane Baladi, Mark F. Demers, and Carlangelo Liverani, *Exponential decay of correlations for finite horizon Sinai billiard flows*, Invent. Math. **211** (2018), no. 1, 39–177.

[BFW14] Sonja Barkhofen, Frédéric Faure, and Tobias Weich, *Resonance chains in open systems, generalized zeta functions and clustering of the length spectrum*, Nonlinearity **27** (2014), no. 8, 1829.

[WBK+14] Sonja Barkhofen, Ulrich Kuhl, Charles Poli, Henning Schomerus, and Tobias Weich, *Formation and interaction of resonance chains in the open three-disk system*, New Journal of Physics **16** (2014), no. 3, 033029.

[BWP+13] Sonja Barkhofen, Ulrich Kuhl, Alexander Potzuweit, H-J Stöckmann, Tobias Weich, and Maciej Zworski, *Experimental observation of the spectral gap in microwave n-disk systems*, Physical Review Letters **110** (2013), no. 16, 164102.

[PWB+12] ———, *Weyl asymptotics: from closed to open systems*, Physical Review E **86** (2012), no. 6, 066205.

[BSW22a] Sonja Barkhofen, Philipp Schütte, and Tobias Weich, *Meromorphic Continuation of Weighted Zeta Functions on Open Hyperbolic Systems*, Commun. Math. Phys. **398** (2022), no. 2, 655–678.

[BSW22b] ———, *Semiclassical formulae for Wigner distributions*, J. Phys. A: Math. Theor. **55** (2022), no. 24, 244007.

[BWS21] Yonah Borns-Weil and Shu Shen, *Dynamical zeta functions in the nonorientable case*, Nonlinearity **34** (2021), no. 10, 7322–7334.

[BFK02] D Burago, S Ferleger, and A Kononenko, *Collisions in semi-dispersing billiard on Riemannian manifold*, Topology and its Applications **122** (2002), no. 1-2, 87–103.

[BL07] Oliver Butterley and Carlangelo Liverani, *Smooth Anosov flows: Correlation spectra and stability*, J. Mod. Dyn. **1** (2007), no. 2, 301–322.

[Cha21] Yann Chaubet, *Closed geodesics with prescribed intersection numbers*, arXiv:2103.16301 (2021), to appear in Geometry & Topology.

[Cha22] ———, *Closed Billiards Trajectories with Prescribed Bounces*, Ann. Henri Poincaré **24** (2022), no. 3, 1051–1075.

[CP22] Yann Chaubet and Vesselin Petkov, *Dynamical zeta functions for billiards*, arXiv:2201.00683 (2022).

[CM06] Nikolaj Chernov and Roberto Markarian, *Chaotic billiards*, Mathematical surveys and monographs, Providence, R.I : American Mathematical Soc., 2006.

[CE71] Charles Conley and Robert Easton, *Isolated invariant sets and isolating blocks*, Transactions of the American Mathematical Society **158** (1971), no. 1, 35–61.

[CE89] Predrag Cvitanović and Bruno Eckhardt, *Periodic-orbit quantization of chaotic systems*, Physical Review Letters **63** (1989), no. 8, 823.

[Dal10] Françoise Dal'Bo, *Geodesic and horocyclic trajectories*, Springer Science & Business Media, 2010.

[DR19] Nguyen Viet Dang and Gabriel Rivière, *Spectral analysis of Morse-Smale gradient flows*, Ann. Sci. Éc. Norm. Supér. (4) **52** (2019), no. 6, 1403–1458.

[DR20a] ———, *Poincaré series and linking of legendrian knots*, arXiv:2005.13235 (2020), to appear in Duke Math. J.

[DR20b] ———, *Spectral analysis of Morse-Smale flows. II: Resonances and resonant states*, Am. J. Math. **142** (2020), no. 2, 547–593.

[Dol98] Dmitry Dolgopyat, *On decay of correlations in anosov flows*, Annals of Mathematics **147** (1998), no. 2, 357–390.

[Dya18] Semyon Dyatlov, *Notes on hyperbolic dynamics*, 2018.

[DG16] Semyon Dyatlov and Colin Guillarmou, *Pollicott–Ruelle Resonances for Open Systems*, Annales Henri Poincaré **17** (2016), no. 11, 3089–3146.

[DG18] ———, *Afterword: Dynamical zeta functions for axiom a flows*, Bull. Amer. Math. Soc. (2018), no. 55, 337–342.

[DZ16] Semyon Dyatlov and Maciej Zworski, *Dynamical Zeta Functions for Anosov Flows via Microlocal Analysis*, Annales Scientifiques de L'Ecole Normale Superieure **4** (2016), no. 49, 543–577.

[EFMW92] B Eckhardt, S Fishman, K Müller, and D Wintgen, *Semiclassical matrix elements from periodic orbits*, Physical Review A **45** (1992), no. 6, 3531.

[FS11] Frédéric Faure and Johannes Sjöstrand, *Upper bound on the density of Ruelle resonances for Anosov flows*, Commun. Math. Phys. **308** (2011), no. 2, 325–364.

[FL21] Anna Florio and Martin Leguil, *Smooth conjugacy classes of 3D Axiom A flows*, arXiv:2010.04120 (2021).

[Fri86] David Fried, *The zeta functions of Ruelle and Selberg. I*, Annales scientifiques de l'Ecole normale supérieure, vol. 19, 1986, pp. 491–517.

[GR89a] Pierre Gaspard and Stuart A Rice, *Exact quantization of the scattering from a classically chaotic repellor*, The Journal of chemical physics **90** (1989), no. 4, 2255–2262.

[GR89b] ———, *Scattering from a classically chaotic repellor*, The Journal of Chemical Physics **90** (1989), no. 4, 2225–2241.

[GR89c] ———, *Semiclassical quantization of the scattering from a classically chaotic repellor*, The Journal of chemical physics **90** (1989), no. 4, 2242–2254.

[Gé88] Christian Gérard, *Asymptotique des pôles de la matrice de scattering pour deux obstacles strictement convexes*, Mémoires de la Société Mathématique de France **31** (1988), 1–146 (French).

[GLP13] Paolo Giulietti, Carlangelo Liverani, and Mark Pollicott, *Anosov flows and dynamical zeta functions*, Ann. Math. (2) **178** (2013), no. 2, 687–773.

[GBGHW20] Yannick Guedes Bonthonneau, Colin Guillarmou, Joachim Hilgert, and Tobias Weich, *Ruelle-Taylor resonances of Anosov actions*, arXiv:2007.14275 (2020), to appear in J. Eur. Math. Soc. (JEMS).

[GBL23] Yannick Guedes Bonthonneau and Thibault Lefeuvre, *Local rigidity of manifolds with hyperbolic cusps I. Linear theory and microlocal tools*, Annales de l'Institut Fourier **73** (2023), no. 1, 335–421.

[GBW21] Yannick Guedes Bonthonneau and Tobias Weich, *Ruelle–Pollicott resonances for manifolds with hyperbolic cusps*, J. Eur. Math. Soc. **24** (2021), no. 3, 851–923.

[GHW18] Colin Guillarmou, Joachim Hilgert, and Tobias Weich, *Classical and quantum resonances for hyperbolic surfaces*, Math. Ann. **370** (2018), no. 3-4, 1231–1275.

[GMT21] Colin Guillarmou, Marco Mazzucchelli, and Leo Tzou, *Boundary and lens rigidity for non-convex manifolds*, American Journal of Mathematics **143** (2021), no. 2, 533–575.

[GL19] Colin Guillarmou and Thibault Lefeuvre, *The marked length spectrum of Anosov manifolds*, Ann. Math. (2) **190** (2019), no. 1, 321–344.

[Gui86] Laurent Guillopé, *Sur la distribution des longueurs des géodésiques fermées d'une surface compacte à bord totalement géodésique*, Duke Mathematical Journal **53** (1986), no. 3, 827–848.

[Gui92] ———, *Fonctions zêta de selberg et surfaces de géométrie finie*, Séminaire de théorie spectrale et géométrie **8** (1992), 89–94.

[Ika88] Mitsuru Ikawa, *Decay of solutions of the wave equation in the exterior of several convex bodies*, Annales de l'Institut Fourier **38** (1988), no. 2, 113–146.

[Lal89] Steven P Lalley, *Renewal theorems in symbolic dynamics, with applications to geodesic flows, noneuclidean tessellations and their fractal limits*, Acta Mathematica **163** (1989), no. 1, 1–55.

[Lee12] John M. Lee, *Introduction to Smooth Manifolds*, 2nd ed., Graduate Texts in Mathematics, vol. 218, Springer New York, New York, NY, 2012.

[Liv04] Carlangelo Liverani, *On contact Anosov flows*, Ann. of Math. (2) **159** (2004), no. 3, 1275–1312.

[LSZ03] WT Lu, Srinivas Sridhar, and Maciej Zworski, *Fractal weyl laws for chaotic open systems*, Physical Review Letters **91** (2003), no. 15, 154101.

[Med21] Antoine Meddane, *A Morse complex for Axiom A flows*, arXiv:2107.08875 (2021).

[Mor07] Takehiko Morita, *Meromorphic extensions of a class of zeta functions for two-dimensional billiards without eclipse*, Tohoku Mathematical Journal **59** (2007), no. 2, 167 – 202.

[NZ09] Stéphane Nonnenmacher and Maciej Zworski, *Quantum decay rates in chaotic scattering*, Acta Mathematica **203** (2009), no. 2, 149–233.

[PLS00] Kristi Pance, Wentao Lu, and S Sridhar, *Quantum fingerprints of classical Ruelle-Pollicott resonances*, Physical Review Letters **85** (2000), no. 13, 2737.

[Pat99] Gabriel P. Paternain, *Geodesic Flows*, 1st ed., Progress in Mathematics, vol. 180, Springer Science+Business Media, LLC, Boston, Mass., 1999.

[Pet08] Vesselin Petkov, *Dynamical zeta function for several strictly convex obstacles*, Can. Math. Bull. **51** (2008), no. 1, 100–113.

[Pol85] Mark Pollicott, *On the rate of mixing of Axiom A flows*, Invent. Math. **81** (1985), 413–426.

[Rob80] Clark Robinson, *Structural stability on manifolds with boundary*, Journal of Differential Equations **37** (1980), no. 1, 1–11.

[Rue76] David Ruelle, *Zeta-functions for expanding maps and Anosov flows*, Invent. Math. **34** (1976), 231–242.

[Wir99] Andreas Wirzba, *Quantum mechanics and semiclassics of hyperbolic n-disk scattering systems*, Physics Reports **309** (1999), no. 1-2, 1–116.

Email address: bdelarue@math.uni-paderborn.de

Email address: pschuet2@mail.uni-paderborn.de

Email address: weich@math.uni-paderborn.de

Institut für Mathematik, Universität Paderborn, Paderborn, Germany

C. Invariant Ruelle Distributions on Convex-Cocompact Hyperbolic Surfaces

This appendix contains the research paper *Invariant Ruelle Distributions on Convex-Cocompact Hyperbolic Surfaces – A Numerical Algorithm via Weighted Zeta Functions* [SW23] which was written and made available as an *arXiv* preprint with the co-author Tobias Weich during the author's PhD.

Both co-authors developed the research question and proof strategy. P.S. worked out the proofs and wrote the manuscript. This was accompanied by regular blackboard discussions between the co-authors.

The implementations were done by P.S. who also conducted the numerical experiments based on a mutually developed research plan. Both co-authors contributed equally to the proof reading of the manuscript.

INVARIANT RUELLE DISTRIBUTIONS ON CONVEX-COCOMPACT HYPERBOLIC SURFACES
–
A NUMERICAL ALGORITHM VIA WEIGHTED ZETA FUNCTIONS

PHILIPP SCHÜTTE AND TOBIAS WEICH

Abstract. We present a numerical algorithm for the computation of invariant Ruelle distributions on convex co-compact hyperbolic surfaces. This is achieved by exploiting the connection between invariant Ruelle distributions and residues of meromorphically continued weighted zeta functions established by the authors together with Barkhofen (2021). To make this applicable for numerics we express the weighted zeta as the logarithmic derivative of a suitable parameter dependent Fredholm determinant similar to Borthwick (2014). As an additional difficulty our transfer operator has to include a contracting direction which we account for with techniques developed by Rugh (1992). We achieve a further improvement in convergence speed for our algorithm in the case of surfaces with additional symmetries by proving and applying a symmetry reduction of weighted zeta functions.

Mathematical Subject Classification. 37D05, 37C30 (Primary), 58J50 (Secondary).

Introduction

An important notion that has significantly advanced the theory of chaotic, i.e. hyperbolic, dynamical systems over the last couple of decades is that of *Pollicott-Ruelle resonances* [Rue76, Pol85, BKL02, DZ19]. They constitute a discrete subset of the complex plane that provides a spectral invariant refining the ordinary L^2-spectrum of the generator of the dynamics. From a dynamical systems point of view the central relevance of Pollicott-Ruelle resonances is that they describe the mixing properties of the dynamical system. Roughly speaking, if there is a simple leading resonance and a spectral gap then the system is exponentially mixing and the gap quantifies the exponential decay rate of the correlation function. Furthermore if there is an asymptotic spectral gap the other resonances describe additional decay modes [Tsu10, NZ15].

Apart from their dynamical importance for mixing properties the distribution of Pollicott-Ruelle resonances as well as the multiplicities of certain Pollicott-Ruelle resonances have proven to be intimately linked to geometrical [CDDP22, FT23] and topological properties [DZ17, KW20, DGRS20] of the underlying manifolds, respectively. For sufficiently concrete hyperbolic flows such as geodesic flows on Schottky surfaces [Bor14, BW16, BPSW20] or 3-disc obstacle scattering [GR89, DSW21, SWB23, BSW22] there are even efficient numerical algorithms that allow to calculate the spectrum of Pollicott-Ruelle resonances numerically. These algorithms do not only enable testing of conjectures (see e.g. [Dya19]) but the numerical experiments regarding resonances also made possible the discovery of new and unexpected phenomena such as the alignment of resonance into chains subsequently leading to new mathematical theorems [Wei15, PV19].

Beyond Pollicott-Ruelle resonances themselves the spectral approach also allows to associate with each Pollicott-Ruelle resonance a flow invariant distribution which has been

Key words and phrases. Ruelle resonances, invariant Ruelle distributions, zeta functions, hyperbolic dynamics, Schottky surfaces, numerical zeta functions.

termed *invariant Ruelle distribution* [GHW21] (see Section 1 for a definition in our setting). The invariant Ruelle distribution associated with the leading resonance is always an invariant measure which coincides with the Sinai-Ruelle-Bowen (SRB) measure for Anosov flows on compact manifolds and with the Bowen-Margulis-Sullivan measure (following the terminology of Roblin [Rob03]) for geodesic flows on non-compact manifolds in negative curvature. This includes for example Schottky surfaces which will be studied in the present paper. In the case of compact surfaces of constant negative curvature or more generally compact rank-1 locally symmetric spaces it has been proven that the invariant Ruelle distributions coincide with quantum phase space distributions [GHW21]. These are the so-called Patterson-Sullivan distributions introduced by Anantharaman and Zelditch [AZ07]. Apart from these results the properties of invariant Ruelle distributions are widely unexplored territory. Nevertheless motivated by the above results it is very likely that these invariant distributions are closely connected to the finer spectral and dynamical properties of the underlying flow.

The purpose of the present article is to develop a numerical algorithm that allows to concretely calculate the invariant Ruelle distributions and to provide some first numerical experiments that support the claim that invariant Ruelle distributions are an interesting spectral invariant that deserves further investigation. As a concrete model we chose geodesic flows on Schottky surfaces which are a paradigmatic model for hyperbolic flows on non-compact manifolds. In practice our numerical approach can and has been applied to 3-disc scattering as well but the rigorous justification of its numerical convergence would require much more technical tools. We therefore restrict to the setting of Schottky surfaces in this article.

Statement of results. The primary concern of the present article are certain generalized densities $\mathcal{T}_{\lambda_0}$ called *invariant Ruelle distributions*. For a given convex-cocompact hyperbolic surface $\mathbf{X}_\Gamma = \Gamma\backslash\mathbb{H}$ these can be attached to any member $\lambda_0 \in \mathrm{res}(\mathbf{X}_\Gamma)$ of the discrete set of *Pollicott-Ruelle resonances* $\mathrm{res}(\mathbf{X}_\Gamma) \subset \mathbb{C}$ of the geodesic flow and they act on smooth test functions on the unit sphere bundle of the surface in a flow-invariant manner:

$$\mathcal{T}_{\lambda_0} : \ f \longmapsto \mathcal{T}_{\lambda_0}(f) \in \mathbb{C} \ , \qquad f \in \mathrm{C}^\infty(S\mathbf{X}_\Gamma) \ .$$

These distributions encode non-trivial information about resonant states and in the particular case of $\lambda_0 = \delta - 1$ with δ the Hausdorff dimension of the limit set of Γ being the first resonance they coincide with the Bowen-Margulis measures. For the precise definition of Pollicott-Ruelle resonances and $\mathcal{T}_{\lambda_0}$ refer to Section 1.1.

Our means of investigating $\mathcal{T}_{\lambda_0}$ is the *weighted zeta function* for $\mathbf{X}_\Gamma$

$$Z_f(\lambda) \coloneqq \sum_\gamma \frac{\mathrm{e}^{-\lambda T_\gamma}}{|\det(\mathrm{id} - \mathcal{P}_\gamma)|} \int_{\gamma^\#} f \ ,$$

where the sum extends over all closed geodesics γ of $\mathbf{X}_\Gamma$, T_γ denotes the length of γ, $\gamma^\#$ the primitive closed geodesic corresponding to γ, and $\mathcal{P}_\gamma$ is the associated linearized Poincaré map. It is known that $Z_f(\lambda)$ continues meromorphically to $\mathbb{C}$ and that this continuation is connected to the invariant Ruelle distributions via the residue formula

$$\operatorname*{Res}_{\lambda=\lambda_0} [Z_f(\lambda)] = \mathcal{T}_{\lambda_0}(f) \ ,$$

which is valid for any test function $f \in \mathrm{C}^\infty(S\mathbf{X}_\Gamma)$. An algorithm for the calculation of weighted zeta functions therefore translates directly to an algorithm for the invariant Ruelle distributions.

Our main results are exactly such concrete formulae for $Z_f(\lambda)$ feasible for numerical evaluation. To this end we introduce a *dynamical determinant* for the given surface $\mathbf{X}_\Gamma$

as defined in Definition 2.1:

$$d_f(\lambda, z, \beta) \coloneqq \exp\left(-\sum_{k=1}^{\infty} \sum_{\gamma^\#} \frac{z^{k\cdot n(\gamma^\#)}}{k} \frac{\mathrm{e}^{-k\lambda T_\gamma^\# - k\beta \int_{\gamma^\#} f}}{\left|\det\left(\mathrm{id} - \mathcal{P}_{\gamma^\#}^k\right)\right|} \right) ,$$

where now the sum extends over all primitive closed geodesics $\gamma^\#$ of $\mathbf{X}_\Gamma$ and the number $n(\gamma^\#) \in \mathbb{N}$ is the so-called word length of $\gamma^\#$.

A priori $d_f(\lambda, z, \beta)$ converges locally uniformly for any fixed $(z, \beta) \in \mathbb{C}^2$ and $\mathrm{Re}(\lambda)$ sufficiently large by the exponential growth of the number of closed geodesics as a function of their maximal length. This is considerably strengthened in Corollary 2.4: $d_f(\lambda, z, \beta)$ continuous holomorphically to $\mathbb{C}$ in all of its three variables. Furthermore d_f can be used to calculate Z_f due to Corollary 2.5

$$Z_f(\lambda) = \frac{\partial_\beta d_f(\lambda, 1, 0)}{d_f(\lambda, 1, 0)} ,$$

which provides an independent proof of the meromorphic continuation of the weighted zeta function.[1] This together with an everywhere absolutely convergent cycle expansion derived in Corollary 3.1

$$d_f(\lambda, z, \beta) \coloneqq 1 + \sum_{n=1}^{\infty} d_n(\lambda, \beta) z^n$$

almost puts us in a position to calculate concretely $Z_f(\lambda)$ for a given $\lambda \in \mathbb{C}$. The missing ingredient to obtain numerically feasible formulae for $d_n(\lambda, \beta)$ is a concrete expression for the *period integrals* $\int_{\gamma^\#} f$. We present two approaches which are both reasonably cheap to evaluate and at the same time possess a straightforward geometrical interpretation.

In practice it turns out to be very favorable to exploit the symmetries of the underlying geometry as much as possible: If $\mathbf{X}_\Gamma$ has an additional finite symmetry group $\mathbf{G}$ in a certain sense to be specified in Chapter 5 then we can prove that d_f factorizes which immediately implies a corresponding decomposition of Z_f:

$$d_f(\lambda, z, \beta) = \prod_{\chi \in \widehat{\mathbf{G}}} d_{f,\chi}(\lambda, z, \beta) . \qquad Z_f(\lambda) = \sum_{\chi \in \widehat{\mathbf{G}}} \frac{\partial d_{f,\chi}(\lambda, 1, 0)}{d_{f,\chi}(\lambda, 1, 0)} ,$$

with both the product and the sum spanning the finitely many equivalence classes of unitary, irreducible representations of $\mathbf{G}$. The individual terms $d_{f,\chi}$ exhibit far superior convergence properties compared to d_f which is demonstrated as part of the numerical experiments which round off this article.

Paper organization. The present paper is organized as follows: In the introductory Chapter 1 the central objects of interest are defined namely Pollicott-Ruelle resonances, the invariant Ruelle distribution associated to such a resonances, and the weighted zeta function $Z_f(\lambda)$ (Chapter 1.1). While these definitions can be stated quite generally for the class of open hyperbolic systems our application is to the concrete subclass of geodesic flows on convex-cocompact hyperbolic surfaces (Chapter 1.2).

As mentioned above the overall goal is the derivation of a numerical algorithm for the calculation of $Z_f(\lambda)$ on convex-cocompact surfaces. The means to do just this is the dynamical determinant $d_f(\lambda, z, \beta)$ defined in Chapter 2. Just as Z_f continues meromorphically to $\mathbb{C}$ so does d_f continue holomorphically to $\mathbb{C}$ in all three of its arguments (Chapter 2.1). Furthermore a suitable logarithmic derivative of d_f coincides with Z_f (Chapter 2.2) meaning that a numerical algorithm for the calculation of d_f immediately transfers to one for Z_f.

[1] Note that this does not recover the whole strength of the general continuation theorem for Z_f because it does not admit a straightforward interpretation of the poles as resonances and the residues as invariant Ruelle distributions.

Our numerical treatment of d_f follows a philosophy termed cycle expansion which circumvents the difficulty that the original definition of d_f in terms of an infinite sum does not converge in the domain where its zeros are located. This culminates in the derivation of concrete formulae in Chapter 3. The subsequent Chapter 4 lays out two approaches for the last missing ingredient namely the (geometrically meaningful) numerical approximation of the period integrals $\int_{\gamma^\#} f$ appearing both in d_f and Z_f.

While this completes a practically useful algorithm for the calculation of d_f often one can do better in terms of runtime resource requirements by exploiting the inherent symmetries of the underlying surface. Formalizing this symmetry reduction requires significant additional notation as well as effort and occupies the whole of Chapter 5.

The second-to-last Chapter 6 compiles a collection of example plots calculated with the machinery developed so far. In particular this includes a case study supporting the claim of enhanced convergence properties of the symmetry reduced variants $d_{f,\chi}$ of the dynamical determinant d_f. Finally Chapter 7 presents an outlook on open questions both in the realms of alternative numerical algorithms as well as of interesting numerical experiments to conduct in the future.

Acknowledgments. This work has received funding from the Deutsche Forschungsgemeinschaft (DFG) (Grant No. WE 6173/1–1 Emmy Noether group "Microlocal Methods for Hyperbolic Dynamics") as well as SFB-TRR 358/1 2023 — 491392403 (CRC "Integral Structures in Geometry and Representation Theory"). P.S. was supported by an individual grant from the Studienstiftung des Deutschen Volkes.

1. Analytical Preliminaries

We start this chapter off by giving a short introduction to the analytical theory of weighted zeta functions on open hyperbolic systems as presented in the companion paper [SWB23] (Section 1.1). Afterwards we describe the significantly more concrete dynamical setting which we will work in for the remainder of this article: Geodesic flows on Schottky surfaces (Section 1.2).

1.1. Weighted Zeta Functions and Invariant Ruelle Distributions.

Our presentation here follows closely a simplified version of [SWB23], see also [DG16]. Let a smooth, possibly non-compact, manifold $\mathcal{M}$ and a smooth, possibly non-complete, flow φ_t on $\mathcal{M}$ be given. We make the following dynamical assumptions on φ_t:

(1) The generator X of φ_t vanishes nowhere,
(2) The trapped set of φ_t defined by
$$K \coloneqq \left\{ x \in \mathcal{M} \,\middle|\, \varphi_t(x) \text{ exists } \forall t \in \mathbb{R} \text{ and } \overline{\varphi_{\mathbb{R}}(x)} \text{ compact} \right\}$$
is *compact*,
(3) φ_t is *hyperbolic on* K in the sense that for every $x \in K$ there exists a φ_t-invariant splitting of the tangent bundle
$$T_x\mathcal{M} = \mathbb{R} \cdot X(x) \oplus E_s(x) \oplus E_u(x)$$
such that E_s, E_u depend continuously on x and the differential $\mathrm{d}\varphi_t$ acts in a contracting manner on E_s and an expanding manner on E_u:
$$\begin{aligned} \|\mathrm{d}\varphi_t(x)v\|_{T_{\varphi_t(x)}\mathcal{M}} &\leq C\exp(-c|t|)\|v\|_{T_x\mathcal{M}}, \qquad t \geq 0,\ v \in E_s(x) \\ \|\mathrm{d}\varphi_t(x)v\|_{T_{\varphi_t(x)}\mathcal{M}} &\leq C\exp(-c|t|)\|v\|_{T_x\mathcal{M}}, \qquad t \leq 0,\ v \in E_u(x)\ . \end{aligned}$$

In this setting one can define a discrete subset $\mathrm{res}(X) \subseteq \mathbb{C}$ called *Pollicott-Ruelle resonances of* X as follows: Basic function analysis proves that the resolvent[2] $(X+\lambda)^{-1}$ yields

[2] Or rather its restriction to a suitable subset in a compact ambient manifold; we disregard this technical detail in the upcoming rather informal discussion.

a holomorphic family of bounded operators $\mathrm{L}^2 \to \mathrm{L}^2$ for sufficiently large $\mathrm{Re}(\lambda) \gg 0$. Through the usage of anisotropic Sobolev spaces one can show [DZ16, DG16] that restricting the domain and enlarging the codomain enables meromorphic continuation to $\mathbb{C}$ of $(X+\lambda)^{-1}$ but now as a family of operators $\mathrm{C}^\infty_\mathrm{c} \to \mathcal{D}'$. Our resonances are precisely the poles of this continuation.

Given a resonance $\lambda_0 \in \mathrm{res}(X)$ we can compute the residue Π_{λ_0} of $(X+\lambda)^{-1}$ at $\lambda = \lambda_0$. The meromorphic continuation outlined above uses the analytic Fredholm theorem as a central tool so the operator Π_{λ_0} turns out to be of finite rank. Furthermore, as a consequence of wavefront estimates for Π_{λ_0}, a certain generalization of the Hilbert space trace called a flat trace exists for the family of operators $\mathrm{Tr}^\flat\big(f\Pi_{\lambda_0}\big)$ where $f \in \mathrm{C}^\infty(\mathcal{M})$. One calls the generalized density

$$\mathcal{T}_{\lambda_0} : \mathrm{C}^\infty(\mathcal{M}) \ni f \longmapsto \mathrm{Tr}^\flat\big(f\Pi_{\lambda_0}\big) \in \mathbb{C}$$

the *invariant Ruelle distribution associated with* λ_0 [GHW21]. We remark here that $\mathcal{T}_{\lambda_0}$ is supported on the trapped set K, so in particular it is compactly supported: $\mathcal{T}_{\lambda_0} \in \mathcal{E}'(\mathcal{M})$.

In [SWB23] the authors introduced a weighted zeta function which allows for a significantly more concrete approach to invariant Ruelle distributions. They associated with the flow φ_t and a weight $f \in \mathrm{C}^\infty(\mathcal{M})$ the complex function

$$Z_f(\lambda) \coloneqq \sum_\gamma \frac{\mathrm{e}^{-\lambda T_\gamma}}{\big|\det\big(\mathrm{id} - \mathcal{P}_\gamma\big)\big|} \int_\gamma f \ , \tag{1}$$

with the sum extending over all closed trajectories of φ_t, T_γ denoting the period length of the trajectory γ, and $\mathcal{P}_\gamma$ being the linearized Poincaré map associated with γ. The latter is simply the differential of φ_t restricted to stable and unstable directions:

$$\mathcal{P}_{\gamma(t)} \coloneqq \mathrm{d}\varphi_{-t}(\gamma(t))\big|_{E_s(\gamma(t))\oplus E_u(\gamma(t))} \ ,$$

where the dependence on the base point can be omitted when taking the determinant. While Z_f converges absolutely only for $\mathrm{Re}(\lambda) \gg 0$ it continues meromorphically to the whole complex plane [SWB23, Theorem 1.1]. The circumstance that Z_f is a useful function to consider stems from the following residue formula relating Z_f to Ruelle distributions:

$$\mathcal{T}_{\lambda_0}(f) = \operatorname*{Res}_{\lambda=\lambda_0}\left[Z_f(\lambda)\right], \qquad f \in \mathrm{C}^\infty(\mathcal{M}) \ . \tag{2}$$

1.2. **Introduction to Schottky Surfaces.** In this section we provide a short introduction to Schottky, i.e. convex cocompact hyperbolic, surfaces. The material presented here is quite classic and can be found in e.g. [Bor16, Dal11].

Schottky groups are discrete subgroups of the group $G \coloneqq \mathrm{PSL}(2,\mathbb{R})$ of orientation preserving isometries of the *upper half plane*

$$\mathbb{H} \coloneqq \{z \in \mathbb{C} \,|\, \mathrm{Im}(z) > 0\} \ ,$$

equipped with the Riemannian metric

$$\mathrm{g}_\mathbb{H}(x+\mathrm{i}y) \coloneqq \frac{\mathrm{d}x^2 + \mathrm{d}y^2}{y^2} \ .$$

The geodesics of $(\mathbb{H}, \mathrm{g}_\mathbb{H})$ are given by semicircles centered on the real line and by straight lines parallel to the imaginary axis. We denote the associated geodesic flow on the unit tangent bundle $S\mathbb{H} = \mathbb{H} \times \{v \in \mathbb{C} \,|\, |v| = 1\}$ by φ_t.

We will introduce Schottky groups by their dynamics on $\mathbb{H}$ To this end let the reader be reminded that G acts on the whole Riemann sphere $\mathbb{C} \cup \{\infty\}$ and therefore on $\mathbb{H}$ via Moebius transformations

$$\begin{pmatrix} a & b \\ c & d \end{pmatrix} \cdot z \coloneqq \frac{az+b}{cz+d} \ .$$

This action extends to $S\mathbb{H}$ by acting on fiber coordinates via the derivative of a Moebius transformation. Now recall that non-trivial isometries can be classified according to the absolute value of the trace of their matrix representation which determines a certain dynamical and fixed point behavior on the compactification $\overline{\mathbb{H}} \coloneqq \mathbb{H} \cup \mathbb{R} \cup \{\infty\}$:

(1) $|\mathrm{tr}| > 2$: hyperbolic isometry, two distinct fixed points in $\mathbb{R} \cup \{\infty\}$
(2) $|\mathrm{tr}| = 2$: parabolic isometry, one unique fixed point on $\mathbb{R} \cup \{\infty\}$,
(3) $|\mathrm{tr}| < 2$: elliptic isometry, one unique fixed point in $\mathbb{H}$.

We summarize shortly the dynamical properties of hyperbolic isometries because those will be particularly important for us: Given a hyperbolic g there exists a unique hyperbolic geodesic $\gamma(t)$ such that its endpoints at infinity $\lim_{t\to\pm\infty}\gamma(t)$ are the attracting and repelling fixed points of g. One calls $\gamma(\mathbb{R}) \subseteq \mathbb{H}$ the axis of g and g acts on γ as a translation by a fixed hyperbolic distance $\ell(g) > 0$. This distance is called the *displacement length* of the isometry g.

With this in mind we can define *Schottky groups* as those discrete, free subgroups $\Gamma < \mathrm{PSL}(2,\mathbb{R})$ which are finitely generated by hyperbolic isometries. If $\{g_1, \dots, g_r\}$ is a generating set for Γ of minimal size then r is called the *rank* of Γ and by a classical result of Maskit [Mas67] there exists a collection of open Euclidean discs $D_1, \dots, D_{2r}$ with disjoint closures and centered on the real line such that

$$g_i(\partial D_i) = \partial D_{i+r}, \qquad g_i(D_i) = \mathbb{C} \setminus D_{i+r} \ . \tag{3}$$

We call these circles *fundamental circles* for the chosen generators and a fundamental domain for the action of Γ on $\mathbb{H}$ is given by their complement $\mathbb{H} \setminus \bigcup_{i=1}^{2r} D_i$. We will refer to this particular fundamental domain as the *canonical* one. For an illustration see Figure 1.

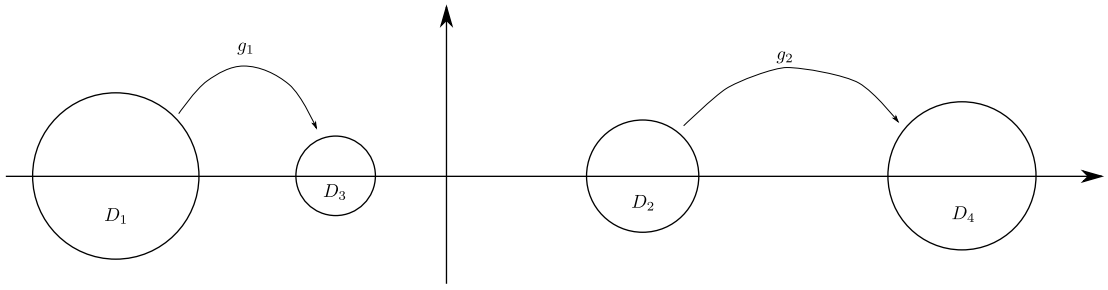

FIGURE 1. The fundamental circles and group element actions for a Schottky group of rank $r = 2$ (three-funnel surface, see Figure 2 below).

Conversely one can define a Schottky group of rank r by fixing open discs $D_1, \dots, D_{2r}$ with pairwise disjoint closures and centered on the real line and then taking the group generated by hyperbolic elements $g_1, \dots, g_r$ satisfying (3).

For convenience of notation one usually defines $g_{i+r} \coloneqq g_i^{-1}$ for $1 \le i \le r$ and subsequently extends the indexing of generators to arbitrary $i > 2r$ by defining $g_i \coloneqq g_{(i \bmod 2r)}$. Setting $D_i \coloneqq D_{(i \bmod 2r)}$ property (3) continues to hold for these extended definitions. We will also frequently use indices in the quotient ring $\mathbb{Z}/2r\mathbb{Z}$.

To every Schottky group Γ we associate a *Schottky surface* obtained as the quotient space $\mathbf{X}_\Gamma \coloneqq \Gamma \setminus \mathbb{H}$. By discreteness of Γ the set $\mathbf{X}_\Gamma$ can be equipped with a canonical smooth structure. Furthermore the metric $\mathrm{g}_{\mathbb{H}}$ is Γ-invariant and thus descends to $\mathbf{X}_\Gamma$ again making the quotient space a Riemannian manifold of constant negative curvature. It is non-compact, of infinite volume, and the geodesic flow on its unit tangent bundle fits into the framework of open hyperbolic systems as presented in Section 1.1, see [DG16, Section 6.3]. In particular we can speak about Ruelle resonances, weighted zeta functions, and invariant Ruelle distributions on Schottky surfaces.

At first glance the non-compactness of Schottky surfaces might make them seem quite difficult in terms of numerical treatment. Their suitability for our purposes follows from the particularly simply structure of free groups combined with the more general correspondence between group elements and closed geodesics [Bor16, Proposition 2.25]: The closed oriented geodesics of a Schottky surface $\mathbf{X}_\Gamma$ are in bijection to the conjugacy classes of the group Γ and the length of a geodesic T_γ coincides with the displacement length $\ell(g)$ for any element g in the associated conjugacy class. We denote by $\gamma(g)$ the image of the conjugacy class containing the group element $g \in \Gamma$ under this bijection record the important relation [Bor16, Eq. (15.3)]

$$g'(x_-) = \mathrm{e}^{-\ell(g)} = \mathrm{e}^{-T_{\gamma(g)}} \tag{4}$$

between displacement length and attracting fixed point x_+ of g.

Because Γ is finitely generated we can represent its elements as sequences $(i_1, \ldots, i_n) \in \mathcal{A}^*$ over the alphabet $\mathcal{A} \coloneqq (\mathbb{Z}/2r\mathbb{Z})$ by defining

$$g_{(i_1,\ldots,i_n)} \coloneqq g_{i_n} \cdots g_{i_1} \ .$$

Any such sequence $(i_1, \ldots, i_n)$ is called a *word*, the i_j its *letters*, and n its *(word) length*. From the fact that Γ is free it follows immediately that the map from words to group elements becomes a bijection if we restrict to *reduced words*, i.e. elements of $\{(i_1, \ldots, i_n) \in \mathcal{A}^* \,|\, i_j \neq i_{j+1} + r \,\forall\, 1 \leq j \leq n-1\}$.

Now the conjugacy classes of Γ can be represented by words of minimal length and such a representation is unique modulo cyclic shifts of its letters. We denote the set of all possible indices of such representatives of length n by $\mathcal{W}_n$, i.e.:

$$\mathcal{W}_n \coloneqq \left\{(i_1, \ldots, i_n) \in \mathcal{A}^n \,\middle|\, i_j \neq i_{j+1} + r \,\forall\, 1 \leq j \leq n-1 \text{ and } i_n \neq i_1 + r\right\} .$$

We will also call $\mathcal{W}_n$ the *set of closed words of length n*. If the geodesic $\gamma \subseteq \mathbf{X}_\Gamma$ is represented by $g_{(i_1,\ldots,i_n)}$ with $(i_1, \ldots, i_n) \in \mathcal{W}_n$ then we denote by $n(\gamma) \coloneqq n$ the length of its minimal representation and call this the *word length* of γ.

Finally, given a function $f : \bigcup_{i \neq j} D_i \times D_j \to \mathbb{C}$ we define its *iteration along the group element* $g = g_{i_n} \cdots g_{i_1}$ to be the product

$$f_g \coloneqq f_{(i_1,\ldots,i_n)} \coloneqq f(x_-, x_+) \cdot f(g_{i_1} x_-, g_{i_1} x_+) \cdot \ldots \cdot f(g_{i_{n-1}} \cdots g_{i_1} x_-, g_{i_{n-1}} \cdots g_{i_1} x_+) \ ,$$

where(x_-, x_+) are the repelling and attracting fixed points of g.

In our numerics we will mostly be dealing with Schottky surfaces of rank $r = 2$. From the topological standpoint there are only two possibilities for such surfaces corresponding to distinct combinatorics of their actions on the canonical fundamental domain. These are depicted in Figure 2.

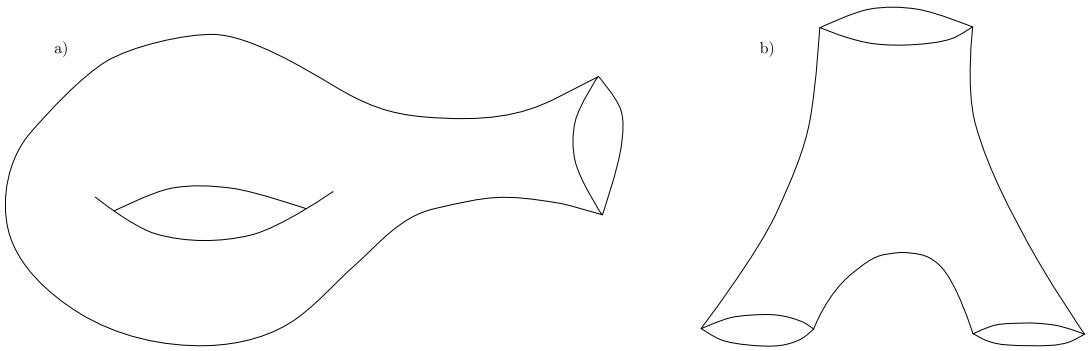

FIGURE 2. The two topological possibilities for Schottky surfaces of rank two: (a) Funneled torus. (b) Three-funnel surface.

2. Introducing Dynamical Determinants

In this section we introduce the central object from which our numerically feasible formula for weighted zeta functions Z_f will be derived: The dynamical determinant.

Definition 2.1. *Let $\mathbf{X}_\Gamma$ be a Schottky surface and $f \in \mathrm{C}^\infty(S\mathbf{X}_\Gamma)$. Then the associated* dynamical determinant *at $(\lambda, z, \beta) \in \mathbb{C}^3$ is formally defined as*

$$d_f(\lambda, z, \beta) \coloneqq \exp\left(-\sum_{k=1}^{\infty} \sum_{\gamma^\#} \frac{z^{k\cdot n(\gamma^\#)}}{k} \frac{\mathrm{e}^{-k\lambda T_\gamma^\# - k\beta \int_{\gamma^\#} f}}{\left|\det\left(\mathrm{id} - \mathcal{P}_{\gamma^\#}^k\right)\right|} \right) , \tag{5}$$

where the sum stretches over all primitive closed geodesics $\gamma^\#$.

A numerical implementation of the individual summands appearing in this dynamical determinant is straightforward. One simply uses the symbolic coding of closed geodesics and the fact that eigenvalues of the linearized Poincaré map are given by exponentials of lengths. The concrete calculation of periods integrals $f_{\gamma^\#}$ is slightly less obvious but can be done quite efficiently after certain simplifications. Two alternatives will be presented in Section 4. Calculation of d_f itself demands additional attention as the defining formula (2.1) does not converge on the whole complex plane but for sufficiently small $|z|$ only. How to overcome this difficulty is the main content of Section 3.

The question remains how we can exploit d_f for the calculation of Z_f, the latter being the actual object of interest for us. We will answer this question in two steps in the upcoming sections: First we prove that d_f is analytic in its variables in Section 2.1. Its logarithmic derivative $\partial_\beta \log d_f(\lambda, 1, 0)$ is thus meromorphic and Section 2.2 demonstrates that it coincides with $Z_f(\lambda)$.

2.1. Dynamical Determinants as Fredholm Determinants.

In this section we prove that the dynamical determinant of Definition 2.1 actually yields a well-defined holomorphic function of (λ, z, β). One possible way to do this would be applying microlocal techniques and anisotropic Sobolev spaces as for example presented in Baladi's book [Bal18]. While generally feasible for the problem at hand, the methods presented in [Bal18] are specifically geared towards the setting of low regularity: Applying it to Schottky surfaces would discard the additional information provided by the fact that Schottky groups are defined in terms of holomorphic functions.

We therefore turn towards the ideas developed by Rugh [Rug92, Rug96] in the analytic setting. Instead of inferring analyticity of d_f directly from [Rug96, Theorem 1] we provide a self-contained proof by adapting his techniques and notation to our concrete setting of Schottky surfaces. Besides being self-contained this will later on offer a convenient entry point for symmetry reduction (Section 5) and should come in handy for the development of alternative numerical algorithms (Section 7).

Before diving into the proof we give some definitions: Let $\mathcal{D} \subseteq \mathbb{C}$ be an open disc in the complex plane. Then we denote by

$$\mathcal{H}^2(\mathcal{D}) \coloneqq \{f \in \mathrm{L}^2(\mathcal{D}) \,|\, f \text{ is holomorphic}\}$$

the Bergman space of square-integrable, holomorphic functions on $\mathcal{D}$. Furthermore we denote its dual space by $\mathcal{H}^{-2}(\mathcal{D})$ and identify it with the Bergman space $\mathcal{H}^2(\mathbb{C} \setminus \mathcal{D})$ via the bilinear pairing

$$\langle u, v\rangle \coloneqq \int_{\partial\mathcal{D}} u(z)v(z)\frac{\mathrm{d}z}{2\pi\mathrm{i}} , \qquad u \in \mathcal{H}^2(\mathcal{D}),\, v \in \mathcal{H}^{-2}(\mathcal{D}) .$$

If $\mathcal{D}$ is the unit disc $\mathbb{D} = \{z \in \mathbb{C} \,|\, |z| < 1\}$ then $\psi_n(z) \coloneqq \sqrt{(n+1)/\pi}z^n$ defines an orthonormal basis for $\mathcal{H}^2(\mathcal{D})$ with dual basis given by $\psi_n^*(z) \coloneqq \sqrt{\pi/(n+1)}z^{-n-1}$, i.e.

$\langle \psi_n, \psi_m^* \rangle = \delta_{n,m}$. An arbitrary disc is easily reduced to this case by translation and scaling.

A last ingredient which will appear in the following proof is the so-called *Bergman kernel* $K_{\mathcal{D}}(z,w)$ of $\mathcal{D}$. This reproducing kernel satisfies the defining relation[3]

$$f(z) = \int_{\partial\mathcal{D}} K_{\mathcal{D}}(z,w) f(w) \mathrm{d}w \ ,$$

and can be expressed as a sum over an orthonormal basis. Below we will employ an explicit expression for the unit disc and again reduce the case of a general disc by translation and scaling.

With these prerequisites at hand the main theorem now reads as follows:

Theorem 2.2 ([Rug96], Thm. 1)**.** *Let Γ be a rank-r Schottky surface with generators $g_1, \dots, g_r$ and fundamental circles $D_1, \dots, D_{2r}$. Given a potential V which is analytic in a neighborhood of $\bigcup_{i\neq j} D_i \times D_j$, the associated* transfer operator *defined by the formula*

$$\begin{aligned} \mathrm{L}_V &: \bigoplus_{i\neq j} \mathcal{H}^{-2}(D_i) \otimes \mathcal{H}^2(D_j) \longrightarrow \bigoplus_{i\neq j} \mathcal{H}^{-2}(D_i) \otimes \mathcal{H}^2(D_j) \ , \\ \langle \mathrm{L}_V u(z_1,z_2), v(z_1) \rangle \Big|_{\substack{v\in\mathcal{H}^2(D_i) \\ z_2 \in D_j}} &:= \int_{\partial D_i} V(z_1,z_2) v(z_1) u(g_i z_1, g_i z_2) \frac{\mathrm{d}z_1}{2\pi \mathrm{i}} \ , \quad i \neq j \ , \end{aligned} \tag{6}$$

is a well-defined trace-class operator and its Fredholm determinant is an analytic function that satisfies the following identity for sufficiently small $|z|$:

$$\det\left(\mathrm{id} - z\mathrm{L}_V\right) = \exp\left(- \sum_{n=1}^{\infty} \frac{z^n}{n} \sum_{w\in\mathcal{W}_n} \frac{V_w}{(1-\mathrm{e}^{-T_{\gamma(gw)}})(\mathrm{e}^{T_{\gamma(gw)}}-1)} \right) \ . \tag{7}$$

Proof. As in [Bor16, Lemma 15.7] we may deduce the trace-class property of (6) from exponential bounds on the singular values $\mu_j(\mathrm{L}_V)$ of the transfer operator. To obtain such bounds it suffices to consider the norms of the images of an orthonormal basis of $\mathcal{H}^{-2}(D_i) \otimes \mathcal{H}^2(D_j)$ under the components of L_V by combining the additive Fan inequality [Bor16, A.25], c.f. Appendix A, with the basic estimate

$$\mu_j(A) \leq \sum_{i=j}^{\infty} \|A\phi_i\| \ ,$$

obtained via the min-max estimate [Bor16, A.23], see also Appendix A, and valid for any bounded operator $A : \mathcal{H} \to \mathcal{H}'$ between Hilbert spaces $\mathcal{H}, \mathcal{H}'$ and an orthonormal basis $\{\phi_i\}$ of $\mathcal{H}$.

Now the potential V is bounded on the closure of the poly-discs $D_i \times D_j$ and therefore acts as a bounded operator. As in [Bor16, Eq. (15.15)] are thus left with the task of estimating the pullback action

$$\|(\psi_n^{i,*} \circ g_i) \otimes (\psi_n^j \circ g_i)\|_{\mathrm{L}^2((\mathbb{C}\setminus D_i)\times D_j)} \ , \quad i \neq j \ ,$$

where the orthonormal basis elements ψ_n^i and $\psi_n^{i,*}$ are obtained from ψ_n and ψ_n^* by a suitable scaling and translating to D_i and $\mathbb{C}\setminus D_j$, respectively. Now we observe that g_i, $i \neq j$, acts in contracting fashion on D_j and in expanding fashion on D_i. It thus follows that for some constants $C, c > 0$ we have

$$\|(\psi_n^{i,*} \circ g_i) \otimes (\psi_n^j \circ g_i)\|_{\mathrm{L}^2((\mathbb{C}\setminus D_i)\times D_j)} \leq C\mathrm{e}^{-cn} \ , \quad i \neq j \ ,$$

[3] Classically one expresses this relation as an integral over $\mathcal{D}$ instead of $\partial\mathcal{D}$. In our proof below we will need to deal with integrals over $\partial\mathcal{D}$, though, so we use this slightly less common definition.

where the constants dependent on the rate of contraction/expansion and the derivative of g_i. Now this in turn implies the estimate

$$\mu_j(\mathrm{L}_V) \leq C' \sum_{n=j}^{\infty} \mathrm{e}^{-cn} = C' \frac{\mathrm{e}^{-cj}}{1-\mathrm{e}^{-c}} \ , \tag{8}$$

for some constant $C' > 0$ which additionally depends on the potential V and finally proving the trace-class claim.

To demonstrate the determinant formula (7) we proceed similarly to [Bor16, Theorem 15.10] by first rewriting

$$\det\left(\mathrm{id} - z\mathrm{L}_V\right) = \exp\left(\mathrm{Tr}\left(\log(\mathrm{id} - z\mathrm{L}_V)\right)\right) = \exp\left(-\sum_{n=1}^{\infty} \frac{z^n}{n} \mathrm{Tr}\left(\mathrm{L}_V^n\right)\right) \ . \tag{9}$$

for values of $|z|$ small enough that the logarithm converges. The traces of iterates L_V^n decompose further in terms of components of L_V, i.e. its restrictions in domain and codomain to the individual spaces $\mathcal{H}^{-2}(D_i) \otimes \mathcal{H}^2(D_j)$ for $i \neq j$. Multiplying out the defining formula (6) and collecting all resulting components we see that only the *diagonal entries* of the form

$$\mathrm{L}_V^{i_1,\dots,i_n} : \mathcal{H}^{-2}(D_{i_n+r}) \otimes \mathcal{H}^2(D_{i_1}) \longrightarrow \mathcal{H}^{-2}(D_{i_n+r}) \otimes \mathcal{H}^2(D_{i_1})$$

can contribute to the trace. As a result we obtain

$$\mathrm{Tr}\left(\mathrm{L}_V^n\right) = \sum_{i_1,\dots,i_n} \mathrm{Tr}\left(\mathrm{L}_V^{i_1,\dots,i_n}\right) \ ,$$

where $i_j + r \neq i_{j+1}$ for $1 \leq j \leq n-1$, $i_n + r \neq i_1$, and the diagonal components are explicitly given by

$$\begin{aligned} &\left\langle \mathrm{L}_V^{i_1,\dots,i_n} u(z_1,z_2), v(z_1) \right\rangle \Big|_{\substack{v \in \mathcal{H}^2(D_{i_n+r}) \\ z_2 \in D_{i_1}}} \\ &= \int_{\partial D_{i_n+r}} V_{g^{-1}_{(i_1,\dots,i_n)}}(z_1,z_2) v(z_1) u\big(g^{-1}_{(i_1,\dots,i_n)}(z_1), g^{-1}_{(i_1,\dots,i_n)}(z_2)\big) \frac{\mathrm{d}z_1}{2\pi\mathrm{i}} \ , \end{aligned} \tag{10}$$

for any element $u \in \mathcal{H}^{-2}(D_{i_n+r}) \otimes \mathcal{H}^2(D_{i_1})$ and using the shorthand notations $g_{i_1}^{-1} \cdots g_{i_n}^{-1} = g^{-1}_{(i_1,\dots,i_n)}$ as well as $V_{g^{-1}_{(i_1,\dots,i_n)}}$ as defined in (1.2). To see this observe that by (6) the group element to apply is determined by the tensor product's first factor which in this particular instance yields $g_{i_n+r} = g_{i_n}^{-1}$ as the first element. A similar remark holds for the subsequent generators.

Now the trace of an operator of the form given in (10) can be calculated as follows (with $g \coloneqq g^{-1}_{(i_1,\dots,i_n)}$ for convenience):

$$\begin{aligned} &\mathrm{Tr}\left(\mathrm{L}_V^{i_1,\dots,i_n}\right) \\ &= \sum_{k,l \geq 0} \left\langle \mathrm{L}_V^{i_1,\dots,i_n} \psi_k^{i_n+r,*} \otimes \psi_l^{i_1}, \psi_k^{i_n+r} \otimes \psi_l^{i_1,*} \right\rangle \\ &= \sum_{k,l \geq 0} \int_{\partial D_{i_n+r}} \int_{\partial D_{i_1}} V_g(z_1,z_2) \psi_k^{i_n+r,*}(g(z_1)) \psi_k^{i_n+r}(z_1) \psi_l^{i_1}(z_2) \psi_l^{i_1,*}(g(z_2)) \frac{\mathrm{d}z_2}{2\pi\mathrm{i}} \frac{\mathrm{d}z_1}{2\pi\mathrm{i}} \\ &= \int_{\partial D_{i_n+r}} \int_{\partial D_{i_1}} V_g(z_1,z_2) K_{i_n+r}(z_1, g(z_1)) K_{i_1}(g(z_2), z_2) \frac{\mathrm{d}z_2}{2\pi\mathrm{i}} \frac{\mathrm{d}z_1}{2\pi\mathrm{i}} \ , \end{aligned} \tag{11}$$

where K_{i_n+r} and K_{i_1} denote the Bergman kernels of the domains $\mathbb{C} \setminus D_{i_n+r}$ and D_{i_1}, respectively. After translation and scaling we may assume that both discs coincide with the

unit disc $\mathbb{D}$ such that $K_{i_n+r}(x,y) = K_{i_1}(x,y) = \sum_{k=0}^{\infty} \frac{x^k}{y^{k+1}} = \frac{1}{y-x}$. A simple application of the residue theorem then yields

$$\begin{aligned}
&\int_{\partial D_{i_n+r}} \int_{\partial D_{i_1}} V_g(z_1,z_2) K_{i_n+r}(z_1,g(z_1)) K_{i_1}(g(z_2),z_2) \frac{\mathrm{d}z_2}{2\pi\mathrm{i}} \frac{\mathrm{d}z_1}{2\pi\mathrm{i}} \\
&= \int_{\partial\mathbb{D}} \int_{\partial\mathbb{D}} \widetilde{V}_g(z_1,z_2) \frac{1}{\widetilde{g}(z_1)-z_1} \frac{1}{z_2-\widehat{g}(z_2)} \frac{\mathrm{d}z_2}{2\pi\mathrm{i}} \frac{\mathrm{d}z_1}{2\pi\mathrm{i}} \\
&= \frac{V_g(x_-,x_+)}{(g'(x_-)-1)(1-g'(x_+))} \,,
\end{aligned}$$

with a rescaled version $\widetilde{V}_g$ of V_g and two different rescalings $\widetilde{g}$ and $\widehat{g}$ of g. In the last line the repelling and attracting fixed points (x_-,x_+) of g appear because they are the unique solutions of $g(z)=z$ on D_{i_n+r} and D_{i_1}, respectively.

In summary we obtain for the trace of diagonal entries of n-fold iterates of the transfer operator the concrete formula

$$\mathrm{Tr}\left(\mathrm{L}_V^{i_1,\dots,i_n}\right) = \frac{V_g(x_-,x_+)}{(g'(x_-)-1)(1-g'(x_+))} = \frac{V_g(x_-,x_+)}{(\mathrm{e}^{\ell(g)}-1)(1-\mathrm{e}^{-\ell(g)})} \,, \tag{12}$$

where second equality follows immediately from (4). If we plug (12) into (9) we obtain (7) because the constraints on the finite sequence $(i_1,\dots,i_n)$ mentioned above guarantees that the sum runs exactly over the set of closed words $\mathcal{W}_n$. □

Theorem 2.2 immediately yields a representation of d_f as a Fredholm determinant by choosing an appropriate potential. It must obviously include period integrals $\int_\gamma f$ over geodesics $\gamma \subseteq S\mathbf{X}_\Gamma$ which we encode in a fashion similar to [AZ07]: Given a weight $f \in \mathrm{C}^\omega(S\mathbf{X}_\Gamma)$ we can consider its lift to $S\mathbb{H}$ which in turn can be expressed as a function on $\mathbb{R}\times(\partial\mathbb{H}^2\setminus\Delta)$, where Δ denotes the diagonal of $\partial\mathbb{H}^2$. In these so-called *Hopf coordinates* a point (t,x_1,x_2) maps to $\gamma_{(x_1,x_2)}(t)$ with $\gamma_{(x_1,x_2)}$ a geodesic with x_1 and x_2 as its endpoints at infinity and a suitably chosen starting point $\gamma_{(x_1,x_2)}(0)$.[4] Keeping in mind that closed geodesics of $\mathbf{X}_\Gamma$ possess endpoints at infinity in the intersections $I_i \coloneqq \overline{D_i} \cap \partial\mathbb{H}$, we define the following function which is real-analytic, c.f. [AZ07, Section 7.2]:

$$\bigcup_{i\neq j} I_i \times I_j \ni (x_1,x_2) \longmapsto f_{\gamma_{(x_1,x_2)}} \coloneqq \int_{t(x_1,x_2)}^{t(x_1,x_2)+\tau(x_1,x_2)} f(t,x_1,x_2)\mathrm{d}t \,, \tag{13}$$

where $\tau(x_1,x_2)$ denotes the length of the segment of $\gamma_{(x_1,x_2)}$ that intersects the canonical fundamental domain $\mathcal{F}$ of $\mathbf{X}_\Gamma$ and $\gamma_{x_1,x_2}(t(x_1,x_2))$ is the starting point of this intersecting arc. By analytic continuation it extends to a neighborhood of $\bigcup_{i\neq j} I_i \times I_j$ in $\mathbb{C}\times\mathbb{C}$ and we denote this extension by $f_{\gamma_{(z_1,z_2)}}$.

Remark 2.3. Note that the analytic function $f_{\gamma(z_1,z_2)}$ will in general not extend to the entire poly-discs $D_i \times D_j$. This does not pose a significant problem as one can simply re-do the proof of Theorem 2.2 with suitable smaller poly-discs on which $f_{\gamma_{(z_1,z_2)}}$ actually is analytic. The theorem then continues to hold for any potential V analytic on an open neighborhood of $\bigcup_{i\neq j} I_i \times I_j$.

Corollary 2.4. *Let an analytic weight $f \in \mathrm{C}^\omega(S\mathbf{X}_\Gamma)$ be given. The Fredholm determinant (of the scaling by z) of $\mathrm{L}^f_{\lambda,\beta} \coloneqq \mathrm{L}_{V_{\lambda,\beta}}$ for the parameter-dependent choice of potential*

$$V_{\lambda,\beta}(z_1,z_2) \coloneqq [g_i'(z_2)]^{-\lambda} \cdot \exp\left(-\beta \cdot f_{\gamma_{(z_1,z_2)}}\right) \,, \quad (z_1,z_2) \in D_i \times D_j,\, i \neq j \,,$$

[4] One advantage of these coordinates is the fact that the geodesic flow simply acts by translation in the first component. We will come back to these coordinates in Section 4 where we use them to derive approximations for period integrals practical for numerical implementation.

coincides with the dynamical determinant of weight f evaluated at (λ, z, β), i.e. for sufficiently small $|z| < C(\lambda, \beta)$ we have:

$$d_f(\lambda, z, \beta) = \det\left(\mathrm{id} - z\mathrm{L}^f_{\lambda,\beta}\right) \ .$$

In particular the dynamical determinant $d_f(\lambda, z, \beta)$ continues to a holomorphic function in all three variables.

Proof. We begin by observing that given an element g_w^m, $w \in \mathcal{W}_n$, with fixed points (x_-, x_+) we have

$$\left(V_{\lambda,\beta}\right)_{g_w^m}(x_-, x_+) = \left(V_{\lambda,\beta}\right)^m_{g_w}(x_-, x_+)$$

immediately by definition of $V_{\lambda,\beta}$ and the iterate along a group element. If we denote by $\mathcal{W}_n^{\mathrm{p}}$ the primitive elements of $\mathcal{W}_n$, i.e. words which cannot be written as non-trivial iterations of shorter words, we observe that members of $\mathcal{W}_n^{\mathrm{p}}$ correspond to primitive geodesics under the correspondence between geodesics and members of $\mathcal{W}_n$. Now we calculate using (7) for sufficiently small $|z|$ (with constant dependent on the particular λ and β) that

$$\begin{aligned}
\det\left(\mathrm{id} - z\mathrm{L}^f_{\lambda,\beta}\right) &= \exp\left(-\sum_{n=1}^{\infty}\sum_{m=1}^{\infty}\frac{z^{mn}}{mn}\sum_{w\in\mathcal{W}_n^{\mathrm{p}}}\frac{\exp\left(-m\lambda T_{\gamma(g_w)} - m\beta\int_{\gamma(g_w)} f\right)}{\left|\det\left(\mathrm{id} - \mathcal{P}^m_{\gamma(g_w)}\right)\right|}\right) \\
&= \exp\left(-\sum_{m=1}^{\infty}\sum_{n=1}^{\infty}\frac{z^{mn}}{mn}\sum_{\gamma^{\#}:\, n(\gamma^{\#})=n} n\cdot\frac{\exp\left(-m\lambda T_{\gamma^{\#}} - m\beta\int_{\gamma^{\#}} f\right)}{\left|\det\left(\mathrm{id} - \mathcal{P}^m_{\gamma^{\#}}\right)\right|}\right) \\
&= \exp\left(-\sum_{m=1}^{\infty}\sum_{\gamma^{\#}}\frac{z^{m\cdot n(\gamma^{\#})}}{m}\frac{\exp\left(-m\lambda T_{\gamma^{\#}} - m\beta\int_{\gamma^{\#}} f\right)}{\left|\det\left(\mathrm{id} - \mathcal{P}^m_{\gamma^{\#}}\right)\right|}\right) \\
&= d_f(\lambda, z, \beta) \ ,
\end{aligned}$$

where in the first equality we used the fact that the contracting and expanding eigenvalues of the linearized Poincaré map $\mathcal{P}_\gamma$ of the geodesic flow on $\mathbf{X}_\Gamma$ are $\exp(\pm T_\gamma)$. By analyticity of Fredholm determinants we obtain an analytic continuation of d_f in the z-variable and for fixed (λ, β) to the complex plane $\mathbb{C}$.

Lastly, we discuss regularity of d_f in its three variables. Analyticity with respect to z is standard in the theory of Fredholm determinants. For completeness we sketch the proof in Appendix A. Analyticity in λ and β can also be readily deduced from standard arguments in the theory of Fredholm determinants. For an explicit and self-contained proof we refer the reader to Corollary 3.1 which is independent of the calculations in the remainder of this section. □

2.2. **Dynamical Determinants and Weighted Zeta Functions.** We are finally in the position to prove the connection between the weighted zeta function Z_f and the dynamical (Fredholm) determinant d_f:

Corollary 2.5. *Given an analytic weight function $f \in \mathrm{C}^\omega(S\mathbf{X}_\gamma)$ the weighted zeta function at $\lambda \in \mathbb{C}$ coincides with the logarithmic derivative of the dynamical determinant w.r.t. β and evaluated at $(z, \beta) = (1, 0)$:*

$$Z_f(\lambda) = \frac{\partial_\beta d_f(\lambda, 1, 0)}{d_f(\lambda, 1, 0)} \ . \tag{14}$$

Proof. If we assume $\mathrm{Re}(\lambda) > 1$ and $|\beta|$ sufficiently small then plugging the potential defined in Corollary 2.4 into (7) yields an absolutely convergent expression for d_f at $z = 1$ and by

an application of Corollary 2.4 we may calculate:

$$\begin{aligned}\frac{\partial_\beta d_f(\lambda,1,0)}{d_f(\lambda,1,0)} &= \partial_\beta \log\left(d_f(\lambda,1,\beta)\right)\big|_{\beta=0} \\ &= \partial_\beta\left(-\sum_{m=1}^{\infty}\sum_{\gamma^\#}\frac{1}{m}\frac{\exp\left(-m\lambda T_{\gamma^\#}-m\beta\int_{\gamma^\#}f\right)}{|\det\left(\mathrm{id}-\mathcal{P}_{\gamma^\#}^m\right)|}\right)\Bigg|_{\beta=0} \\ &= \sum_{m=1}^{\infty}\sum_{\gamma^\#}\frac{\exp\left(-m\lambda T_{\gamma^\#}\right)}{|\det\left(\mathrm{id}-\mathcal{P}_{\gamma^\#}^m\right)|}\int_{\gamma^\#}f \\ &= \sum_{\gamma}\frac{\exp\left(-\lambda T_\gamma\right)}{|\det\left(\mathrm{id}-\mathcal{P}_\gamma\right)|}\int_{\gamma^\#}f\ .\end{aligned}$$

But then Z_f must coincide with the logarithmic derivative of d_f for all $\lambda\in\mathbb{C}$ by uniqueness of meromorphic continuation. □

Note that (the proof of) Corollary 2.5 can also be interpreted as given an alternative argument for meromorphic continuation of weighted zeta functions in the special case of Schottky surfaces and analytic weights: The proof shows equality between the logarithmic derivative and the defining formula for weighted zeta functions in the halfplane $\mathrm{Re}(\lambda)>0$ where the latter converges uniformly on compact subsets. But now the Fredholm determinant defines an analytic function in $\lambda\in\mathbb{C}$ making its logarithmic derivative meromorphic.

3. Cycle Expansion of Dynamical Determinants

Up to this point we actually only ever dealt with the λ- and β-variables of our dynamical determinant d_f. The former coincides with the parameter of the weighted zeta function Z_f while the latter was used in the central logarithmic derivative argument in Section 2.1. This section will now exploit the remaining z-variable introduced in d_f to derive formulae for d_f which provide convergent expressions everywhere and are much better suited for actual computation than (5). This is done by considering the Taylor expansion around $z=0$ before plugging in $z=1$. In the physics literature this procedure is known under the name *cycle expansion* and has previously been used to great effect in both the physical [CE89] as well as the mathematical [JP02, Bor14] communities.

Corollary 3.1. *Given an analytic weight f the dynamical determinant can be written as an absolutely convergent Taylor series*

$$d_f(\lambda,z,\beta)=1+\sum_{n=1}^{\infty}d_n(\lambda,\beta)z^n\ ,$$

where the coefficients are holomorphic in (λ,β) and explicitly given by the following recursive formula:

$$\begin{aligned}d_n(\lambda,\beta)&=\sum_{k=1}^{n}\frac{k}{n}d_{n-k}(\lambda,\beta)a_k(\lambda,\beta)\ ,\\ d_0(\lambda,\beta)\equiv 1,\quad a_k(\lambda,\beta)&=-\sum_{w\in\mathcal{W}_k}\frac{1}{k}\frac{\exp\left(-(\lambda-1)\ell(g_w)-\beta\int_{\gamma(g_w)}f\right)}{(\mathrm{e}^{\ell(g_w)}-1)^2}\ .\end{aligned}$$

Furthermore they satisfy the following super-exponential bounds for some positive constants $C,c_1,c_2,c_3>0$:

$$|d_n(\lambda,\beta)|\le C\cdot\mathrm{e}^{-c_1n^2+c_2n|\lambda|-c_3n|\beta|}\ .$$

Proof. First we derive the given recursion by starting from the following expression obtained by plugging the potential defined in Corollary 2.4 into (7) and valid for small $|z|$:

$$d_f(\lambda, z, \beta) = \exp\left(\sum_{n=1}^{\infty} a_n(\lambda,\beta) z^n\right), \quad a_n(\lambda,\beta) := -\frac{1}{n}\sum_{w\in\mathcal{W}_n} \frac{\exp\big(-\lambda\ell(g_w) - \beta\int_{\gamma(g_w)} f\big)}{(\mathrm{e}^{\ell(g_w)}-1)(1-\mathrm{e}^{-\ell(g_w)})} .$$

One now arrives at the claimed recursion by expanding the exponential function in terms of Cauchy products and collecting common powers of z. As $d_f(\lambda, z, \beta)$ is analytic in z on the whole complex plane the resulting power series must converge absolutely for any $z \in \mathbb{C}$.

As doing this expansion explicitly is a common combinatorial problem there exists a well-known solution given in terms of so-called (complete) Bell polynomials B_n (see e.g. [Com74, Section 3.3] or [Bor16, Section 16.1]). These are defined by

$$\exp\left(\sum_{n=1}^{\infty} \frac{a_n}{n!} z^n\right) = \sum_{n=0}^{\infty} \frac{B_n(a_1,\dots,a_n)}{n!} z^n$$

and can be shown to satisfy the recursion relation

$$B_{n+1}(a_1,\dots,a_{n+1}) = \sum_{i=0}^{n} \binom{n}{i} B_{n-i}(a_1,\dots,a_{n-i}) a_{i+1}, \quad B_0 = 1 .$$

For the straight-forward proof of this recursion we refer to the literature mentioned above. Using this relation it is elementary to calculate

$$\begin{aligned}
&d_n(\lambda,\beta)\\
&= \frac{1}{n!} B_n(1!a_1(\lambda,\beta),\dots,n!a_n(\lambda,\beta))\\
&= \frac{1}{n!}\sum_{i=0}^{n-1}(i+1)!\binom{n-1}{i} B_{n-1-i}(1!a_1(\lambda,\beta),\dots,(n-1-i)!a_{n-1-i}(\lambda,\beta)) a_{i+1}(\lambda,\beta)\\
&= \sum_{i=0}^{n-1}\frac{i+1}{n} d_{n-1-i}(\lambda,\beta) a_{i+1}(\lambda,\beta) = \sum_{k=1}^{n}\frac{k}{n} d_{n-k}(\lambda,\beta) a_k(\lambda,\beta) ,
\end{aligned}$$

and $d_0(\lambda,\beta) \equiv B_0 = 1$, proving the claimed formula.

To prove the estimates on the coefficients d_n we proceed in a similar fashion as in Corollary 2.4 but refine the arguments made there slightly, c.f. [Bor16, Lemma 16.1]: The Fredholm determinant can alternative be expressed as (see Appendix A)

$$\det\left(\mathrm{id} - \mathrm{L}^f_{\lambda,\beta}\right) = \sum_{n=0}^{\infty}(-1)^n \mathrm{Tr}\big(\bigwedge^n \mathrm{L}^f_{\lambda,\beta}\big) , \tag{15}$$

where $\bigwedge^n \mathrm{L}^f_{\lambda,\beta}$ denotes the n-fold exterior power of $\mathrm{L}^f_{\lambda,\beta}$ acting on the n-fold exterior power of its original domain. It immediately follows that we can re-write the coefficients $d_n(\lambda,\beta)$ as traces

$$d_n(\lambda,\beta) = (-1)^n \mathrm{Tr}\big(\bigwedge^n \mathrm{L}^f_{\lambda,\beta}\big) .$$

These traces can be estimates by the same technique employed in the proof of Theorem 2.2, but this time we explicitly keep the exponential dependency on the parameters λ and β

instead of bounding them on some compact subset:

$$\begin{aligned}\left|(-1)^n \mathrm{Tr}\left(\bigwedge^n \mathrm{L}^f_{\lambda,\beta}\right)\right| &\leq \sum_{j_1<\ldots<j_n} \mu_{j_1}\left(\mathrm{L}^f_{\lambda,\beta}\right)\cdots\mu_{j_n}\left(\mathrm{L}^f_{\lambda,\beta}\right)\\ &\leq C^n \mathrm{e}^{nc_2|\lambda|-nc_3|\beta|}\sum_{j_1<\ldots<j_n}\mathrm{e}^{-C(j_1+\ldots+j_n)}\\ &\leq C^n \mathrm{e}^{nc_2|\lambda|-nc_3|\beta|}\mathrm{e}^{-Cn^2}\ ,\end{aligned}$$

where the first inequality combines the standard estimate of the trace norm in terms of singular values with an explicit expression for singular values of tensor powers. Absorbing the polynomial factor into the exponential term proves the claim. □

Remark 3.2. The arguments made in the proof above could be refined further to obtain a result resembling [Bor16, Lemma 16.1] even more closely. We refrain from going into that much detail here as our concrete numerical calculations will rely on symmetry reduction (see Section 5) – with this reduction the empirical convergence rate is far better than the analytically obtained estimates. Thus we do not see a great benefit in optimizing the theoretical bounds.

Remark 3.3. From the appearance of the coefficients $a_k(\lambda,\beta)$ alone one immediately notices an invariance property under the action of $\mathbb{Z}$ generated by shifts of words

$$\mathcal{W}_n \ni (i_1,\ldots,i_n) \longmapsto (i_n,i_1,\ldots,i_{n-1})\ .$$

Furthermore, it is straight forward to reduce the sum over $\mathcal{W}_k$ appearing in $a_k(\lambda,\beta)$ to a sum over primitive words which reduces the number of words one has to calculate in practice even further.

We refrain from formalizing these simplifications here because they will be discussed in detail in Section 5 where they are combined with a reduction w.r.t. additional symmetries of the underlying Schottky surface. For numerical experiments one would resort to the symmetry reduced variant anyways.

4. The Numerical Algorithm

We are missing one further ingredient before we can really use a (cutoff version of) the formulae derived in Section 3 for numerics. This ingredient is a computationally feasible approach for the calculation of the period integrals $f_{\gamma\#}$ which figure prominently in the dynamical determinant d_f.

We begin with a short sketch of what is forthcoming in this section. To this end let the reader be reminded that being able to calculate the weighted zeta function Z_f via the dynamical determinant d_f was actually just a means for calculating invariant Ruelle distributions $\mathcal{T}_{\lambda_0}$ via the formula

$$\mathcal{T}_{\lambda_0}(f) = \operatorname*{Res}_{\lambda=\lambda_0}\left[Z_f(\lambda)\right]\ . \tag{16}$$

Now visualizing the *distribution* $\mathcal{T}_{\lambda_0}$ amounts to visualizing a suitable smooth approximation. The latter should come with a parameter that controls the accuracy of the approximation. We take the straightforward approach of choosing Gaussian test functions f_σ of width $\sigma>0$ and considering (roughly) the distributional convolution[5]

$$\mathrm{C}^\infty(S\mathbf{X}_\Gamma) \ni \mathrm{t}_\sigma \coloneqq \mathcal{T}_{\lambda_0} * f_\sigma \underset{\sigma\to 0}{\longrightarrow} \mathcal{T}_{\lambda_0} \in \mathcal{E}'(S\mathbf{X}_\Gamma)\ ,$$

[5] What we are actually using are smooth approximations inspired by but not identical to convolution because only $S\mathbb{H} \cong \mathrm{PSL}(2,\mathbb{R})$ and $S\mathbb{H} \cong \mathrm{PSL}(2,\mathbb{R})/\mathrm{PSO}(2)$ carry group structures but the quotients $\mathbf{X}_\Gamma \cong \Gamma\setminus\mathrm{PSL}(2,\mathbb{R})/\mathrm{PSO}(2)$ and $S\mathbf{X}_\Gamma \cong \Gamma\setminus\mathrm{PSL}(2,\mathbb{R})$ do not.

that converges to the original distribution $\mathcal{T}_{\lambda_0}$ in the limit $\sigma \to 0$. Details on these approximating families will be provided in the upcoming sections.

Having restricted the class of weights to the family f_σ we are still faced with the problem that t_σ is a function on the three-dimensional space $S\mathbf{X}_\Gamma$ and therefore still difficult to visualize. We remedy this situation by considering not $\mathcal{T}_{\lambda_0}$ itself but two reductions obtained by either pushforward (projection) to the base manifold $\mathbf{X}_\Gamma$ or pullback (restriction) to certain hypersurfaces $\Sigma \subseteq S\mathbf{X}_\Gamma$:

$$\begin{aligned} \mathrm{C}^\infty(\mathbf{X}_\Gamma) \ni \pi_*\big(\mathrm{t}_\sigma\big) &\longrightarrow \pi_*\mathcal{T}_{\lambda_0}, \qquad \pi : S\mathbf{X}_\Gamma \longrightarrow \mathbf{X}_\Gamma \ , \\ \mathrm{C}^\infty(\Sigma) \ni \iota_\Sigma^*\big(\mathrm{t}_\sigma\big) &\longrightarrow \iota_\Sigma^*\mathcal{T}_{\lambda_0}, \qquad \iota_\Sigma : \Sigma \hookrightarrow S\mathbf{X}_\Gamma \ . \end{aligned}$$

In the following two sections we will give precise operational prescriptions for both approaches. This encompasses suitable choices of parametrization for the respective domains, concrete test functions f_σ adapted to the specific application, and finally a numerically tractable approach to calculate the associated period integrals $\int_\gamma f_\sigma$. The last ingredient missing for an actual algorithm is a means of calculating the residue in (16). Different approaches to this problem are discussed in Remark 5.

4.1. **Ruelle Distributions on the Base Manifold.** The *pushforward* of the distribution $\mathcal{T}_{\lambda_0} \in \mathcal{E}'(S\mathbf{X}_\Gamma)$ under the projection $\pi : S\mathbf{X}_\Gamma \to \mathbf{X}_\Gamma$ is defined as a distribution on $\mathbf{X}_\Gamma$ by the following formula:

$$\big\langle \pi_*\big(\mathcal{T}_{\lambda_0}\big), f \big\rangle \coloneqq \langle \mathcal{T}_{\lambda_0}, f \circ \pi \rangle \, , \qquad f \in \mathrm{C}^\infty(\mathbf{X}_\Gamma) \ .$$

Intuitively this distribution encodes the dependency of $\mathcal{T}_{\lambda_0}$ on the base point and averages over the directions in $S\mathbf{X}_\Gamma$. It should therefore relate to those features of resonant states that are independent of direction.

As mentioned above we will use a variation of convolution as a means to obtain quantities that can actually be plotted. As test functions we take a family of (hyperbolic) Gaussians constructed as follows: Considering the transitive group action of G on $\mathbb{H}$ one calculates the stabilizer of $\mathrm{i} \in \mathbb{H}$ to be the subgroup of rotations $\mathrm{PSO}(2)$. This yields a diffeomorphism $G/K \cong \mathbb{H}$, $g \mapsto g \cdot \mathrm{i}$, and we may define a family of Gaussians f_σ, $\sigma > 0$, on the quotient G/K by the formula

$$\widetilde{f}_\sigma(gK) = \exp\left(- \frac{\mathrm{d}_{G/K}(gK, eK)^2}{\sigma^2} \right) , \tag{17}$$

where the G-invariant metric $\mathrm{d}_{G/K}$ is defined in terms of the hyperbolic distance $\mathrm{d}_\mathbb{H}$, derived from the metric $\mathrm{g}_\mathbb{H}$, by $\mathrm{d}_{G/K}(gK, g'K) \coloneqq \mathrm{d}_\mathbb{H}(g \cdot \mathrm{i}, g' \cdot \mathrm{i})$. We denoted the identity element by $e \in G$.

If $\mathcal{T}_{\lambda_0}$ were a distribution on G/K we could define the operation of convolution in a straight forward manner, well-known from harmonic analysis, by sampling our distribution against the family of shifted Gaussians $\widetilde{f}_{\sigma,gK}$ defined as $\widetilde{f}_{\sigma,gK}(g'K) \coloneqq \widetilde{f}_\sigma(g'^{-1}gK)$. It should be obvious that this is the correct notion of convolution by duality with respect to ordinary convolution of functions.

Even though the bi-quotient $\Gamma \setminus G/K$ no longer carries a group structure we can use the following family of smooth functions approximating $\pi_*\mathcal{T}_{\lambda_0}$ as a natural analogue of genuine convolution:[6]

[6] For notational convenience and because context removes any ambiguity we do not differentiate between the projections $S\mathbb{H} \to \mathbb{H}$ and $G \to G/K$. A similar comment applies to the projections $S\mathbf{X}_\Gamma \to \mathbf{X}_\Gamma$ and $\Gamma \setminus G \to \Gamma \setminus G/K$.

$$\begin{aligned} \mathrm{t}_{\lambda_0,\sigma}^{G/K}(gK) &\coloneqq \langle \mathcal{T}_{\lambda_0}, f_{\sigma,gK} \circ \pi \rangle \ , && gK \in G/K \\ f_{\sigma,gK}(g'K) &\coloneqq \frac{1}{\mathcal{N}_\sigma} \sum_{h\in\Gamma} \exp\left(- \frac{\mathrm{d}_{G/K}(hgK, g'K)^2}{\sigma^2} \right) , && g'K \in G/K \ . \end{aligned} \tag{18}$$

The normalization factor $\mathcal{N}_\sigma$ certifies the condition $\int_{\mathbf{X}_\Gamma} f_\sigma = 1$, and the sum over Γ converges absolutely for any $gK \in G/K$ by [Bor16, Eq. (2.22)]. Note that $f_{\sigma,gK}(g'K)$ is Γ-invariant both in gK and $g'K$.

We can make the previous paragraphs even more specific as follows: calculating our approximation $\mathrm{t}_{\lambda_0}^{G/K}(gK)$ basically amounts to evaluating (the residues of) the dynamical determinant $d_{f_{\sigma,gK}\circ\pi}$. This in turn boils down to an implementation of the following integrals over closed geodesics $\gamma \subseteq S\mathbf{X}_\Gamma$:

$$\int_{\pi\circ\gamma} f_{\sigma,gK} = \int_0^{T_\gamma} f_{\sigma,gK}(g_0^{-1} a_t K)\mathrm{d}t \ , \tag{19}$$

where $\{a_t\}_{t\in\mathbb{R}} \subseteq G$ is the standard geodesic through $\mathrm{i} \in \mathbb{H}$, i.e. $a_t \cdot \mathrm{i} = \mathrm{i}\mathrm{e}^t$, and the symmetry $g_0 \in G$ was chosen to satisfy $g_0^{-1}(0) = x_-$ as well as $g_0^{-1}(\infty) = x_+$ for the endpoints at infinity (x_-, x_+) of γ.

At this point we make a couple of simplifying assumptions to reach a computationally feasible expression. The error of our upcoming approximations will depend on σ in such a way that the difference between our final expression and (19) converges to 0 in the limit $\sigma \to 0$. This justifies using the former over the latter for numerical purposes. A graphical illustration of the upcoming discussion can be found in Figure 3.

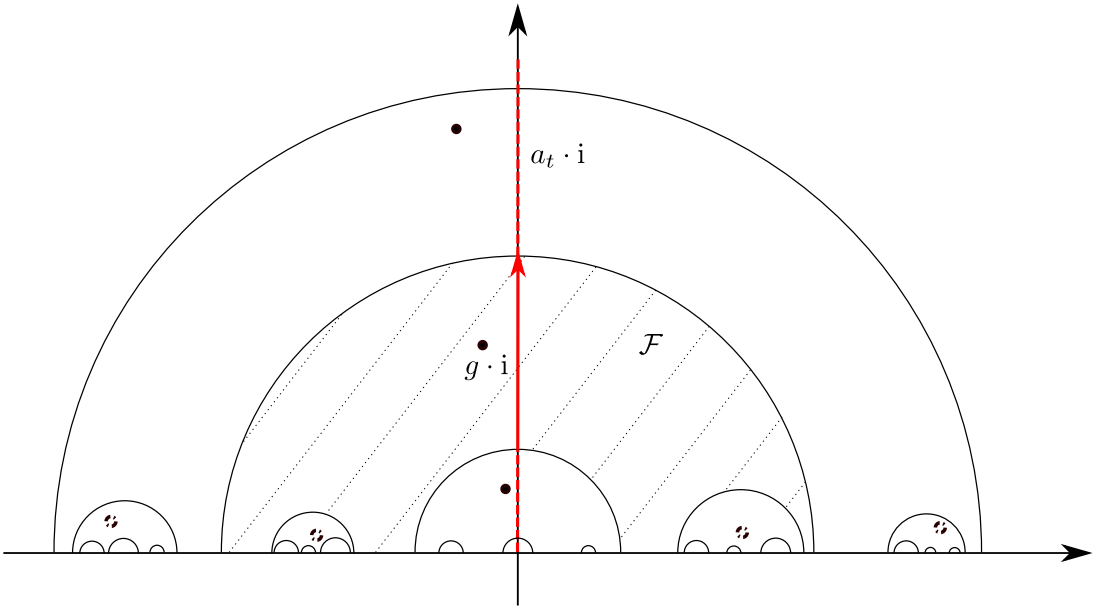

FIGURE 3. Illustration of the fundamental circles (in rank $r = 2$) and some of their translates as used in the approximation of Gaussian period integrals on the fundamental domain of a Schottky surface. The dashed points correspond to translates of $g \cdot \mathrm{i}$ along elements of Γ_0, with vanishing contribution in the limit $\sigma \to 0$, whereas the solid points correspond to translates along $\widetilde{\Gamma}$.

By the Γ-invariance of $f_{\sigma,gK}$ we may restrict attention to centers g inside the canonical fundamental domain, i.e. $g \cdot \mathrm{i} \in \mathcal{F}$. It is then practical to consider the following

decomposition of the group Γ into two disjoint subsets:

$$\Gamma = \Gamma_0 \sqcup \widetilde{\Gamma}\ , \qquad \Gamma_0 \coloneqq \left\{h \in \Gamma \,|\, h\mathcal{F} \cap (g_0^{-1} a_t \cdot \mathrm{i}) = \emptyset \,\forall t \in \mathbb{R}\right\}\ ,$$
$$\widetilde{\Gamma} \coloneqq \left\{h \in \Gamma \,|\, h\mathcal{F} \cap (g_0^{-1} a_t \cdot \mathrm{i}) \neq \emptyset \,\forall t \in \mathbb{R}\right\}\ .$$

The sum over Γ appearing in (18) splits accordingly. We begin our analysis with the sum over Γ_0 by noting that there exists a constant $c > 0$ such that every $h \in \Gamma_0$ satisfies

$$\mathrm{d}_{G/K}(g_0 h g K, a_t K) \geq c > 0 \quad \forall t \in \mathbb{R}\ .$$

Combining this estimate with the more general and well-known exponential growth bound [Bor16, Eq. (2.22)] we obtain

$$\#\left\{h \in \Gamma \,\middle|\, \inf_{t\in[0,T_\gamma]} \mathrm{d}_{G/K}(g_0 h g K, a_t K) \leq s\right\} = \mathcal{O}(\mathrm{e}^s)\ ,$$

which lets us conclude that

$$\mathcal{N}_\sigma^{-1} \sum_{h\in\Gamma_0} \int_0^{T_\gamma} \exp\left(-\frac{\mathrm{d}_{G/K}(g_0 h g K, a_t K)^2}{\sigma^2}\right) \mathrm{d}t$$
$$\leq C\mathcal{N}_\sigma^{-1} \sum_{n\in\mathbb{N}} \sum_{\substack{h\in\Gamma_0 \colon \forall t\in[0,T_\gamma] \\ \mathrm{d}_{G/K}(g_0 h g K, a_t K) \\ \leq c+1}} \mathrm{e}^{-\frac{c^2+n^2}{\sigma^2}}\ ,$$

i.e. the sum over Γ_0 is of the order $\mathcal{O}(\mathcal{N}_\sigma^{-1}\mathrm{e}^{-\frac{C}{\sigma^2}})$ as $\sigma \to 0$. Our discussion of the normalization factor below will reveal $\mathcal{N}_\sigma^{-1} = \mathcal{O}(\sigma^{-2})$ so this does indeed vanish in the limit $\sigma \to 0$.

The significant contribution to the total period integral is given by the second sum over $\widetilde{\Gamma}$. We treat this term by first fixing a group element g_w, $w = (i_1, ..., i_n) \in \mathcal{W}_n$, representing γ and observing that the action of g_w restricted to γ is simply translation. We may therefore absorb the cyclic subgroup generated by g_w into the integral and re-write

$$\sum_{h\in\widetilde{\Gamma}} \int_0^{T_\gamma} \exp\left(-\frac{\mathrm{d}_{G/K}(g_0 h g K, a_t K)^2}{\sigma^2}\right) \mathrm{d}t$$
$$= \sum_{j=1}^{n} \int_{-\infty}^{\infty} \exp\left(-\frac{\mathrm{d}_{G/K}(g_0 g_{i_j} \cdots g_{i_1} g K, a_t K)^2}{\sigma^2}\right) \mathrm{d}t\ .$$

As we approach our final expression we change perspective from the quotient G/K back to the upper half plane. To simplify the resulting Gaussian integral we make the following approximation

$$\mathrm{d}_{\mathbb{H}}(x + \mathrm{i}y, \mathrm{i}s)^2 = \mathrm{d}_{\mathbb{H}}(x + \mathrm{i}y, \mathrm{i}y)^2 + \mathrm{d}_{\mathbb{H}}(\mathrm{i}y, \mathrm{i}s)^2 + \mathcal{O}(x^4)\ ,$$

and substituting this into (19) we arrive at the following approximate expression for the period integrals:

$$\int_{\pi\circ\gamma} f_{\sigma,gK} \approx \mathcal{N}_\sigma^{-1} \sum_{j=1}^{n} \mathrm{e}^{-\frac{x_j^2}{\sigma^2 y_j^2}} \int_{-\infty}^{\infty} \mathrm{e}^{-\frac{(y_j-t)^2}{\sigma^2}}\, \mathrm{d}t = \mathcal{N}_\sigma^{-1}\sqrt{\pi}\sigma \sum_{j=1}^{n} \mathrm{e}^{-\frac{x_j^2}{\sigma^2 y_j^2}}\ ,$$

where we used the definition $x_j + \mathrm{i}y_j \coloneqq g_0 g_{i_j} \cdots g_{i_1} g \cdot \mathrm{i}$ for the complex coordinates of the points $g_0 g_{i_j} \cdots g_{i_1} g K \in G/K$.

Finally, we use the approximation $\cosh^{-1}(1+z)^2 = 2z + \mathcal{O}(z^3)$ to simplify hyperbolic distance. This lets us calculate the normalization factor $\mathcal{N}_\sigma$ in a straight forward manner:

$$\mathcal{N}_\sigma \approx \int_0^\infty \int_{-\infty}^{\infty} \exp\left(-\frac{x^2 + (y-1)^2}{\sigma^2 y}\right) \frac{\mathrm{d}x\mathrm{d}y}{y^2} = \sqrt{\pi}\sigma \int_0^\infty \exp\left(-\frac{(y-1)^2}{\sigma^2 y}\right) \frac{\mathrm{d}y}{y^{3/2}} = \pi\sigma^2\ ,$$

thus concluding our discussion on how to approximate $\pi_*\mathcal{T}_{\lambda_0}$ for practical implementation purposes with the final expression

$$\int_{\pi\circ\gamma} f_{\sigma,gK} \approx \frac{1}{\sqrt{\pi}\sigma}\sum_{j=1}^{n} \mathrm{e}^{-\frac{x_j^2}{\sigma^2 y_j^2}} \ . \tag{20}$$

For convenience we summarize the steps necessary for the calculation of $Z_{f_{\sigma,gK}\circ\pi}$ in the pseudo-code of the following Snippet 1. Taking the residue of this weighted zeta then yields the approximation $\mathrm{t}^{G/K}_{\lambda_0,\sigma}$. For remarks on how to calculate residues in practice we refer to Section 5.2.

Algorithm 1: Pseudo-code for the calculation of the weighted zeta function $Z_{f_{\sigma,gK}\circ\pi}$ used to approximate the distribution $\pi_*\mathcal{T}_{\lambda_0}$.

Input: width $\sigma > 0$, center $gK \in G/K$, resonance $\lambda_0 \in \mathbb{C}$, cut-off $N \in \mathbb{N}$
$d_f \leftarrow 1$;
$\partial_\beta d_f \leftarrow 0$;
$d[0] \leftarrow 1$;
$\partial_\beta d[0] \leftarrow 0$;
`/* calculate Bell recursion, for initial terms` $a[k]$ `see below */`
for $n := 1$ *to* N **do**
  $d[n] \leftarrow 0$;
  for $k := 1$ *to* n **do**
    $d[n] \leftarrow d[n] + \frac{k}{n} d[n-k]a[k]$;
    $\partial_\beta d[n] \leftarrow \partial_\beta d[n] + \partial_\beta d[n-k]a[k] + d[n-k]\partial_\beta a[k]$;
  end
  $d_f \leftarrow d_f + d[n]$;
  $\partial_\beta d_f \leftarrow \partial_\beta d_f + \partial_\beta d[n]$;
end
return $\frac{\partial_\beta d_f}{d_f}$;
`/* calculate initial terms` $a[k]$ `in Bell recursion */`
$a[k] \leftarrow 0$;
$\partial a[k] \leftarrow 0$;
for $w \in \mathcal{W}_k$ **do**
  $a[k] \leftarrow a[k] - \frac{1}{k}\frac{\exp(-(\lambda_0-1)\ell(g_w))}{(\mathrm{e}^{\ell(g_w)}-1)^2}$;
  $\partial_\beta a[k] \leftarrow \partial_\beta a[k] + \frac{\mathrm{calcInt}(w)}{k}\frac{\exp(-(\lambda_0-1)\ell(g_w))}{(\mathrm{e}^{\ell(g_w)}-1)^2}$; `/* calcInt implements (20) */`
end
Result: approximation of $Z_{f_{\sigma,gK}\circ\pi}(\lambda_0)$

4.2. **Restricted Ruelle Distributions.** As announced in the introduction we consider the pullback $\iota_\Sigma^*\mathcal{T}_{\lambda_0}$ along the inclusion $\iota_\Sigma : \Sigma \hookrightarrow S\mathbf{X}_\Gamma$ of a hypersurface Σ as a second approach of reducing the complexity of $\mathcal{T}_{\lambda_0}$ from the full three-dimensional space $S\mathbf{X}_\Gamma$ to a two-dimensional subspace. This distributional operation is well-defined by a classical theorem of Hörmander [Hö03, Thm. 8.2.4] as long as Σ is transversal to the geodesic flow [SWB23, Lemma 2.3]. If this is satisfied we call Σ a *Poincaré section* and the first part of the upcoming discussion applies to any such submanifold. Only once we require an implementation-level prescription for the calculation of period integrals will we introduce a specific choice of Σ. This Σ will be used throughout the numerical examples but could very well be replaced by a number of alternative choices (see Remark 4.2).

The operational meaning of the pullback is not provided by an explicit formula as was the case for the pushforward – instead it can only be defined as a limit in $\mathcal{D}'(\Sigma)$. Concretely if any family of smooth functions converges to $\mathcal{T}_{\lambda_0}$ in the space $\mathcal{D}'_{E_u^*\oplus E_s^*}(S\mathbf{X}_\Gamma)$ then their restrictions to Σ converge to the restriction of $\mathcal{T}_{\lambda_0}$. The latter space consists of distributions with wavefront set contained in $E_u^* \oplus E_s^*$:[7]

$$\lim_{\sigma\to 0} \mathrm{t}^\Sigma_{\lambda_0,\sigma} = \mathcal{T}_{\lambda_0} \text{ in } \mathcal{D}'(S\mathbf{X}_\Gamma) \quad \Longrightarrow \quad \iota_\Sigma^* \mathcal{T}_{\lambda_0} = \lim_{\sigma\to 0} \mathrm{t}^\Sigma_{\lambda_0,\sigma}\big|_\Sigma \text{ in } \mathcal{D}'(\Sigma) \ .$$

We construct the approximations $\mathrm{t}^\Sigma_{\lambda_0,\sigma}$ by a similar approach as the one that resulted in the functions $\mathrm{t}^{G/K}_{\lambda_0,\sigma}$ in the previous paragraph. Here we work on the whole group $G \cong S\mathbb{H}$ instead of G/K, though:

$$\begin{aligned} \mathrm{t}^\Sigma_{\lambda_0,\sigma}(g) &\coloneqq \langle \mathcal{T}_{\lambda_0}, f_{\sigma,g} \rangle \ , && g \in G \\ f_{\sigma,g}(g') &\coloneqq \frac{1}{\mathcal{M}_\sigma} \sum_{h\in\Gamma} \exp\left(- \frac{\mathrm{d}_G(g, hg')^2}{\sigma^2} \right) , && g' \in G \ , \end{aligned} \tag{21}$$

where $\mathcal{M}_\sigma$ again denotes an appropriate normalization factor and d_G is a smooth distance function on $G \times G$ to be specified later. By definition $f_{\sigma,g}(g')$ is left Γ-invariant in g' such that $\mathrm{t}^\Sigma_{\lambda_0,\sigma}$ is well-defined on $S\mathbf{X}_\Gamma$.

In terms of concrete calculation we need a way to evaluate integrals of $f_{\sigma,g}$ over closed geodesics for elements $g \in G$ such that $\Gamma g \cdot (\mathrm{i},\mathrm{i}) \in \Sigma$. To render these quantities as computationally inexpensive as possible we will proceed to specifying a suitable combination of surface Σ and adapted distance d_G.

As mentioned and exploited in Section 2.1 there exists a particular set of coordinates well adapted to the action of the geodesic flow called *Hopf coordinates* [Thi07, DG21]. Both Σ and d_G will be described in these coordinates but we start by giving a more structure theoretic definition: The following map is a G-equivariant[8] diffeomorphism

$$\begin{aligned} \mathcal{H} : G &\longrightarrow \mathbb{R} \times (G/P)_\Delta \\ g &\mapsto (\beta_{g_+}(g^{-1}\cdot o, o), g_+, g_-) \ , \end{aligned}$$

where g_+ and g_- are the fixed points on the boundary of hyperbolic space $G/P \coloneqq \mathrm{PSO}(2) \cong \partial\mathbb{H}$ of the isometry g and $\beta_{g_+}(g^{-1}\cdot o, o)$ denotes the hyperbolic distance between the point of intersection of $\gamma(g)$ with the horocycle[9] through $o \coloneqq (\mathrm{i},\mathrm{i})$ centered at g_+ and the point $g^{-1}\cdot o$. The subscript Δ indicates removal of the diagonal.

Geometrically, $\mathcal{H}$ describes a correspondence between the group $G \cong S\mathbb{H}$ and the space of parameterized geodesics of hyperbolic space. We note again that in these coordinates the geodesic flow acts as $(t, g_+, g_-) \mapsto (t+s, g_+, g_-)$.

Our surface $\Sigma \subseteq S\mathbf{X}_\Gamma$ is best described dynamically in terms of the geodesic flow: On the cover $\pi_\Gamma : S\mathbb{H} \to S\mathbf{X}_\Gamma$ its intersection $\widetilde{\Sigma} \coloneqq \pi_\Gamma^{-1}(\Sigma) \cap S\overline{\mathcal{F}}$ with the canonical fundamental domain consists of the points of intersection between the boundary ∂D_i of fundamental circles and geodesics γ with points at infinity $\gamma_\pm$ in distinct fundamental intervals I_i, I_k (see Figure 4 for an illustration):

$$\widetilde{\Sigma} = \left\{ (z,v) \in S\mathbb{H} \,\middle|\, \exists \,\text{geodesic}\, \gamma \subseteq \mathbb{H} : (\gamma_+,\gamma_-) \in \bigcup_{i\neq j} I_i \times I_j,\ (z,v) \in \gamma \cap S\big(\bigcup_i \partial D_i\big) \right\} .$$

[7] The direct sum $E_u^* \oplus E_s^* \subseteq T^*(S\mathbf{X}_\Gamma)$ is closely related to the hyperbolicity of the geodesic flow on $S\mathbf{X}_\Gamma$. The technical details can be found in [SWB23].

[8] We will not go into details about the G-action on the first component of the codomain of $\mathbb{H}$, c.f. [DG21, Proposition 2.9].

[9] In the upper halfplane model the horocycles centered at a boundary point $\xi \in \partial\mathbb{H}$ are the circles tangent to $\mathbb{R}$ at ξ if $\xi \in \mathbb{R}$ and the lines parallel to $\mathbb{R}$ if $\xi = \infty$.

With respect to Hopf coordinates we can describe $\widetilde{\Sigma}$ by means of a smooth function $t = t(g_+, g_-)$, where $(g_+, g_-) \in \bigcup_{i\neq j} I_i \times I_j \subseteq (G/P)_\Delta$, via its graph

$$\mathcal{H}(\widetilde{\Sigma}) = \left\{ (t(g_+, g_-), g_+, g_-) \,\middle|\, (g_+, g_-) \in \bigcup_{i\neq j} I_i \times I_j \right\},$$

i.e. $\widetilde{\Sigma}$ is essentially parameterized by pairs of boundary points in distinct fundamental intervals. Note that this definition determines a well-defined, unique hypersurface $\Sigma \subseteq S\mathbf{X}_\Gamma$ that satisfies the claimed relation $\widetilde{\Sigma} = \pi_\Gamma^{-1}(\Sigma) \cap S\overline{\mathcal{F}}$.

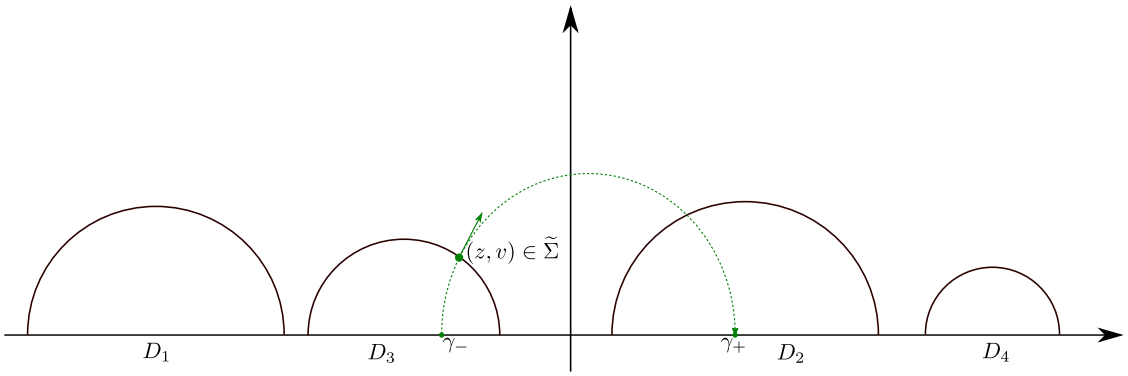

FIGURE 4. Sketch of a point (z, v) in the fundamental domain $\widetilde{\Sigma}$ for the preimage of the Poincaré section Σ together with its Hopf coordinates (γ_-, γ_+) in the coordinate space $\bigcup_{i\neq j} I_i \times I_j$.

To leverage the simplicity of the geodesic flow in Hopf coordinates we choose an adapted distance function d_G in the following fashion: Denoting by $\mathrm{d}_{G/P}$ some K-invariant metric on the boundary of hyperbolic space let

$$\mathrm{d}_G(g, g')^2 \coloneqq \mathrm{d}_{G/P}(g_+, g'_+)^2 + \mathrm{d}_{G/P}(g_-, g'_-)^2 + |t - t'|^2$$

in the respective Hopf coordinates of g and g'. In terms of dynamics the resulting Gaussian amounts to a product of Gaussians in the contracting, expanding, and neutral (flow-) directions.

Remark 4.1. Note that the resulting distance function is not analytic on the whole domain $\mathbb{R} \times (G/P)_\Delta$ if we make the obvious choice of angle coordinates on the unit circle $\mathrm{S}^1 \cong G/P$ such that $\mathrm{d}^2_{G/P}$ becomes absolute value square on $[0, 2\pi]$ with the endpoints identified. While this is certainly true we do not require this analyticity for an application of Corollary 2.4 but only the analyticity of the *resulting potential* as a function on the fundamental intervals I_i, c.f. the discussion surrounding (13). The final expression below will satisfy this analyticity making the theory of dynamical determinants developed above applicable here. From a theoretical standpoint the discussions involving the Poincaré section Σ should be viewed more as an interpretation of what the potential given below means geometrically.

Having made the choices above we can now calculate $\mathrm{t}^\Sigma_{\lambda_0,\sigma} \circ \mathcal{H}^{-1}|_{\mathcal{H}(\widetilde{\Sigma})}$ using dynamical determinants if we have suitable expressions for the following period integrals over closed geodesics $\gamma \subseteq S\mathbf{X}_\Gamma$:

$$\bigcup_{i\neq j} I_i \times I_j \ni (g_+, g_-) \mapsto \int_\gamma f_{\sigma, \mathcal{H}^{-1}(t(g_+,g_-),g_+,g_-)} \,.$$

First we may exploit Γ-invariance to re-write the integral as a sum over intersections with the fundamental domain. The argument here is quite similar to the previous Section 4.1.

If the geodesic γ is again represented by an isometry g_w, $w = (i_1, \dots, i_n) \in \mathcal{W}_n$ then these intersections are determined by fixed points (γ_+^i, γ_-^i) of cyclic permutations

$$g_{i_n} g_{i_{n-1}} \cdots g_{i_1},\ g_{i_1} g_{i_n} \cdots g_{i_2},\ g_{i_2} g_{i_1} g_{i_n} \cdots g_{i_3},\ \text{etc.}\ ,$$

and the period integrals become

$$\begin{aligned} &\int_\gamma f_{\sigma, \mathcal{H}^{-1}(t(g_+,g_-),g_+,g_-)} \\ &= \mathcal{M}_\sigma^{-1} \sum_{i=1}^{n} \mathrm{e}^{-\frac{\mathrm{d}_{G/P}(g_+,\gamma_+^i)^2 + \mathrm{d}_{G/P}(g_-,\gamma_-^i)^2}{\sigma^2}} \int_{-\infty}^{\infty} \mathrm{e}^{-\frac{|t(g_+,g_-)-t|^2}{\sigma^2}} \mathrm{d}t\ . \end{aligned}$$

Here the second integral comes from taking the t-entry of Hopf coordinates for the lift $\widetilde{\gamma}^i$ of γ with endpoints at infinity (γ_+^i, γ_-^i) and integrating its distance from $t(g_+, g_-)$ over the whole geodesic $\widetilde{\gamma}^i$ of γ. If we combine this with an evaluation of the constant $\mathcal{M}_\sigma$, which reduces to iterated Gaussian integrals, our period integrals becomes the rather handy expression

$$\int_\gamma f_{\sigma, \mathcal{H}^{-1}(t(g_+,g_-),g_+,g_-)} = \frac{1}{\pi\sigma^2} \sum_{i=1}^{n} \mathrm{e}^{-\frac{\mathrm{d}_{G/P}(g_+,\gamma_+^i)^2 + \mathrm{d}_{G/P}(g_+,\gamma_-^i)^2}{\sigma^2}}\ . \tag{22}$$

Again the approximation $\mathrm{t}^{\Sigma}_{\lambda_0,\sigma}$ restricted to Σ can be calculated via the residues of a weighted zeta function, concretely $Z_{f_{\sigma,\mathcal{H}^{-1}(t(g_+,g_-),g_+,g_-)}}$. The latter is straightforward to implement using Snippet 1 but substituting the routine `calcInt` with an implementation of (22). Furthermore if we take Equation (22) as a definition it does indeed yield an analytic potential which makes Corollary 2.4 immediately applicable.

Remark 4.2. Note that it is conceptually straight forward to replace the specific hypersurface Σ with another choice Σ'. One has to make sure that Σ' admits a family of test functions for which period integrals can be calculated efficiently. In most applications this should come down to finding an appropriate parametrization for Σ', adapting the test functions to this parametrization, and finally calculating the period integrals in this parametrization (using suitable approximations).

5. Symmetry Reduction of Weighted Zeta Functions

If we use the theoretical and practical tools developed up to this point it turns out that we require a large amount of closed geodesics and corresponding period integrals to compute the dynamical determinant with sufficient accuracy. In this section we will therefore develop a method that allows us to exploit inherent symmetries of different classes of Schottky surfaces to significantly reduce the required computational resources. Our approach to symmetry reduction essentially is an adaptation and generalization of similar work done by Borthwick and Weich [BW16] in the context of *iterated function schemes*. Even though these systems only incorporate an expanding direction it is quite straight forward to include the contracting direction present in the determinants constructed in Section 2.

Remark 5.1. It should be rather straight forward to formulate and prove a version of the upcoming symmetry reduced dynamical determinant in the full setting of [Rug92]. We refrain from explicitly treating this greater generality here to keep the discussion aligned with the previous sections, in particular Section 2. A practically important generalization will instead be included in the first author's PhD thesis, see also Section 6.

This section is organized as follows: In Section 5.1 we give some basic definitions and present the main theorem stating how our dynamical determinant d_f decomposes as a

product of symmetry reduced dynamical determinants with the product indexed by irreducible, unitary representations of some suitable symmetry group. While this theorem describes the theoretical situation completely it is not directly accessible to practical implementation. Section 5.2 remedies this by providing a detailed description how the symmetry reduction can be implemented. The final Section 5.3 contains a short comparison of the computational effort needed to calculate dynamical determinants with and without symmetry reduction.

5.1. **Main Theorem.** We begin by stating the fundamental definition of what the symmetry group of a particular representation of some Schottky surface should be [BW16, Theorem 3.1]:

Definition 5.2. *Let $\Gamma \subseteq \mathrm{SL}(2,\mathbb{R})$ be a rank-r Schottky group with generators $g_1,\dots,g_r$ and fundamental discs $D_1,\dots,D_{2r}$. Let $\mathbf{G}$ be a finite group acting on $\bigcup_i D_i$ by holomorphic functions extending continuously to the boundary and define a $\mathbf{G}$-action on $\{1,\dots,2r\}$ by the relation $\mathbf{g}(D_i) = D_{\mathbf{g}\cdot i}$.*

Then $\mathbf{G}$ is called a symmetry group of the generating set $\langle g_1,...,g_r\rangle = \Gamma$ *if for any $\mathbf{g} \in \mathbf{G}$ and $i \neq j \in \{1,\dots,2r\}$ there exists an index $k \in \{1,\dots,2r\}$ such that $k \neq \mathbf{g}\cdot i$ and*

$$\mathbf{g}\cdot(g_j z) = g_k(\mathbf{g}\cdot z), \qquad \forall z \in D_i \ ,$$

Because $\mathbf{g} \in \mathbf{G}$ acts on each disc as a biholomorphic map the image $\mathbf{g}(D_i)$ must again be some disc making $\mathbf{g}\cdot i$ well-defined. The index k in the relation $\mathbf{g}\cdot(g_j z) = g_k(\mathbf{g}\cdot z)$ is unique and we observe that $k = \mathbf{g}\cdot j$. Furthermore the group action of $\mathbf{G}$ on the elements of $\mathbb{Z}/2r\mathbb{Z}$ takes distinct pairs of indices $i \neq j$ to distinct pairs: $\mathbf{g}\cdot i \neq \mathbf{g}\cdot j$. The action of an element $\mathbf{g} \in \mathbf{G}$ can then be written concisely as

$$\mathbf{g}\cdot(g_j z) = g_{\mathbf{g}\cdot j}(\mathbf{g}\cdot z), \qquad \forall z \in D_i,\ j \neq i \ .$$

We extend this action to $(\mathbb{Z}/2r\mathbb{Z})^n$ (or $\mathcal{W}_n$) by acting on each element separately.

The desired composition of our dynamical (Fredholm) determinants now follows from the rather simple representation theory of finite groups by observing that $\mathbf{G}$ acts on the function spaces introduced in Section 2.1 via the *left-regular representation*:

$$\langle \mathbf{g}\cdot u(z_1,z_2), v(z_1)\rangle \coloneqq \big\langle u(\mathbf{g}^{-1}\cdot z_1, \mathbf{g}^{-1}\cdot z_2), v(z_1)\big\rangle\,, \qquad u \in \bigoplus_{i\neq j} \mathcal{H}^{-2}(D_i)\otimes\mathcal{H}^2(D_j)\ .$$

This representation will generally not be unitary because we defined the L^2-scalar product via Lebesgue measure. The standard trick of averaging the pushforward of Lebesgue measure over the finite group $\mathbf{G}$ guarantees unitary, though. This yields a modified Bergman space which contains the same functions but whose scalar product differs from the standard one used so far by some smooth density factor.

Well known representation theory of finite groups [FH04, Part I] now provides a direct sum decomposition of this modified Bergman space indexed by characters χ of (equivalence classes $\widehat{\mathbf{G}}$ of) irreducible, unitary representations of $\mathbf{G}$ with the projectors on the individual summands given by

$$\mathrm{P}_\chi \coloneqq \frac{d_\chi}{|\mathbf{G}|}\sum_{\mathbf{g}\in\mathbf{G}} \overline{\chi(\mathbf{g})}\mathbf{g}\ .$$

In this equation d_χ refers to the dimension of the representation with character χ and $|\mathbf{G}|$ denotes the cardinality of $\mathbf{G}$. As the projections do not involve the scalar product we immediately derive a corresponding non-orthogonal direct sum decomposition of our original Hilbert spaces:

$$\bigoplus_{i\neq j}\mathcal{H}^{-2}(D_i)\otimes\mathcal{H}^2(D_j) = \bigoplus_{\chi\in\widehat{\mathbf{G}}}\mathcal{H}_\chi, \qquad \mathcal{H}_\chi \coloneqq \mathrm{P}_\chi\Big(\bigoplus_{i\neq j}\mathcal{H}^{-2}(D_i)\otimes\mathcal{H}^2(D_j)\Big)\ .$$

The transfer operator L_V defined in Section 2.1 now commutes with the action of $\mathbf{G}$ if the potential V is $\mathbf{G}$-invariant, i.e. $V(\mathbf{g}^{-1}\cdot z_1, \mathbf{g}^{-1}\cdot z_2) = V(z_1,z_2)$:

$$\begin{aligned}
&\langle \mathrm{L}_V(\mathbf{g}\cdot u)(z_1,z_2), v(z_1)\rangle \Big|_{\substack{v\in\mathcal{H}^2(D_i)\\ z_2\in D_j}} \\
&= \int_{\partial D_i} u(\mathbf{g}^{-1}\cdot g_i(z_1), \mathbf{g}^{-1}\cdot g_i(z_2)) V(z_1,z_2) v(z_1)\frac{\mathrm{d}z_1}{2\pi\mathrm{i}} \\
&= \int_{\partial D_i} u(g_{\mathbf{g}^{-1}\cdot i}(\mathbf{g}^{-1}\cdot z_1), g_{\mathbf{g}^{-1}\cdot i}(\mathbf{g}^{-1}\cdot z_2)) V(\mathbf{g}^{-1}\cdot z_1, \mathbf{g}^{-1}\cdot z_2) v(z_1)\frac{\mathrm{d}z_1}{2\pi\mathrm{i}} \\
&= \big\langle \mathbf{g}\cdot\big(\mathrm{L}_V u\big)(z_1,z_2), v(z_1)\big\rangle \Big|_{\substack{v\in\mathcal{H}^2(D_i)\\ z_2\in D_j}} .
\end{aligned}$$

From this it is obvious that L_V commutes with the projections P_χ which makes the subspaces $\mathcal{H}_\chi$ invariant under L_V. This simple observation is already the key to the main factorization theorem of this section. Before we can state said theorem we need one additional definition: Given an element $\mathbf{g}\in\mathbf{G}$ we define a symmetry adapted version of $\mathcal{W}_n$ as follows

$$\mathcal{W}_n^{\mathbf{g}} := \big\{(i_1,\dots,i_n)\in(\mathbb{Z}/2r\mathbb{Z})^n \,\big|\, i_j \neq i_{j+1}+r \,\forall\, j\in\{1,\dots,n-1\},\, \mathbf{g}\cdot i_n \neq i_1 + r\big\} .$$

In unison with [BW16] we refer to elements of $\mathcal{W}_n^{\mathbf{g}}$ as $\mathbf{g}$-*closed words of length* n.

For the main theorem first note that $g_w\circ\mathbf{g}$ has a unique pair of repelling and attracting fixed points $x_-^{w,\mathbf{g}}\in D_{i_n+r}$ and $x_+^{w,\mathbf{g}}\in D_{\mathbf{g}^{-1}\cdot i_1}$ because $\mathbf{g}$ is biholomorphic and the same argument as in [BW16, Lemma 2.6] can be applied with domains D_{i_n+r} and $D_{\mathbf{g}^{-1}\cdot i_1}$. It can be stated as follows:

Theorem 5.3 ([BW16], Prop. 3.3 and Thm. 4.1)**.** *Let Γ be a Schottky group with symmetry group $\mathbf{G}$ and V a $\mathbf{G}$-invariant potential which is analytic in a neighborhood of the fundamental circles. Then the Fredholm determinant of the transfer operator L_V factorizes as*

$$\det(\mathrm{id} - z\mathrm{L}_V) = \prod_{\chi\in\widehat{\mathbf{G}}} d_{V,\chi}(z) ,$$

where for sufficiently small $|z|$ the symmetry reduced determinants *$d_{V,\chi}$ are explicitly given by the following expressions:*

$$d_{V,\chi}(z) = \exp\left(-\sum_{n=1}^{\infty}\frac{z^n}{n}\frac{d_\chi}{|\mathbf{G}|}\sum_{\mathbf{g}\in\mathbf{G}}\chi(\mathbf{g})\sum_{w\in\mathcal{W}_n^{\mathbf{g}}}\frac{V_w(\mathbf{g}\cdot x_-^{w,\mathbf{g}}, \mathbf{g}\cdot x_+^{w,\mathbf{g}})}{((g_w\circ\mathbf{g})'(x_-^{w,\mathbf{g}})-1)(1-(g_w\circ\mathbf{g})'(x_+^{w,\mathbf{g}}))}\right) .$$

Proof. By the previously discussed decomposition of the domain of L_V into the direct sum $\bigoplus_{\chi\in\widehat{\mathbf{G}}}\mathcal{H}_\chi$ it is clear that

$$\det(\mathrm{id} - z\mathrm{L}_V) = \prod_{\chi\in\widehat{\mathbf{G}}}\det\Big(\mathrm{id} - z\mathrm{L}_V\big|_{\mathcal{H}_\chi}\Big) .$$

We are therefore tasked with computing $d_{V,\chi}(z) := \det\big(\mathrm{id} - z\mathrm{L}_V\big|_{\mathcal{H}_\chi}\big)$. This Fredholm determinant can be expressed in terms of traces of n-fold iterates just as in (9). The key is therefore evaluating

$$\mathrm{Tr}\Big(\mathrm{L}_V^n\big|_{\mathcal{H}_\chi}\Big) = \mathrm{Tr}\big(\mathrm{P}_\chi\mathrm{L}_V^n\big) ,$$

where the equality immediately follows from the fact that L_V commutes with the projections P_χ and the trace-class property is inherited from L_V^n.

Now the (diagonal) components of n-fold iterates of L_V were already calculated in (10). A very similar calculation yields, after replacing the sum over $\mathbf{g}$ by with a sum over $\mathbf{g}^{-1}$, the following expression:

$$\mathrm{Tr}\Big(\mathrm{L}_V^n\big|_{\mathcal{H}_\chi}\Big) = \frac{d_\chi}{|\mathbf{G}|}\sum_{\mathbf{g}\in\mathbf{G}}\chi(\mathbf{g})\sum_{w\in\mathcal{W}_n^{\mathbf{g}}}\mathrm{Tr}\big(\mathrm{L}_{V,\mathbf{g}}^w\big)\ ,$$

where the modified diagonal components $\mathrm{L}_{V,\mathbf{g}}^w$, $w\in\mathcal{W}_n^{\mathbf{g}}$, are operators of the form

$$\big\langle \mathrm{L}_{V,\mathbf{g}}^w u(z_1,z_2), v(z_1)\big\rangle\Big|_{\substack{v\in\mathcal{H}^2(D_{i_n+r})\\ z_2\in D_{\mathbf{g}^{-1}i_1}}} = \int_{\partial D_{i_n+r}} V_g(\mathbf{g}\cdot z_1,\mathbf{g}\cdot z_2)u(g_w(\mathbf{g}\cdot z_1),g_w(\mathbf{g}\cdot z_2))v(z_1)\frac{\mathrm{d}z_1}{2\pi\mathrm{i}}\ .$$

Here the traces of these operators can be calculated in complete analogy to Theorem 2.2 but now the pair of fixed points $x_-^{w,\mathbf{g}}\in D_{i_n+r}$ and $x_+^{w,\mathbf{g}}\in D_{\mathbf{g}^{-1}\cdot i_1}$ of the holomorphic map $g_w\circ\mathbf{g}$ appears. We finally obtain

$$\mathrm{Tr}\left(\mathrm{L}_{V,\mathbf{g}}^w\right) = \frac{V_w(\mathbf{g}\cdot x_-^{w,\mathbf{g}},\mathbf{g}\cdot x_+^{w,\mathbf{g}})}{((g_w\circ\mathbf{g})'(x_-^{w,\mathbf{g}})-1)(1-(g_w\circ\mathbf{g})'(x_+^{w,\mathbf{g}}))}\ ,$$

which finishes the proof. □

5.2. **Implementation Details.** One of the key observations in [BW16] is a clever grouping of terms in $d_{V,\chi}$. On the one hand it provides convergence beyond small $|z|$ and on the other hand it speeds up the practical computation of symmetry reduced zeta functions tremendously. An adaptation of this work allows us to achieve both these benefits for our weighted zeta functions as well. The following presentation closely follows [BW16, Sections 4–5].

To meet our objective we first introduce some additional notation: Observing that elements $w\in\mathcal{W}_n^{\mathbf{g}}$ always occur together with their closing group element $\mathbf{g}$ in Theorem 5.3 it makes sense to define

$$\mathcal{W}^{\mathbf{G}} \coloneqq \left\{(w,\mathbf{g})\in\left(\bigcup_{n=1}^{\infty}\mathcal{W}_n\right)\times\mathbf{G}\ \middle|\ \mathbf{g}\cdot w_{n_w}\neq w_1+r\right\}\ ,$$

where n_w denotes the length of w, i.e. $w\in\mathcal{W}_{n_w}$, and we index words as $w=(w_1,\dots,w_{n_w})$. We will henceforth denote elements of $\mathcal{W}^{\mathbf{G}}$ by boldface letters and indicate their first and second components by the corresponding non-boldface letter and a suitable subscript: $\mathbf{w}=(w,\mathbf{g}_{\mathbf{w}})\in\mathcal{W}^{\mathbf{G}}$. This definition immediately allows us to shorten the notation for fixed points introduced in the previous section by setting $x_\pm^{\mathbf{w}}\coloneqq x_\pm^{w,\mathbf{g}_{\mathbf{w}}}$.

The actual regrouping of terms now happens due to a derived action of $\mathbf{G}\times\mathbb{Z}$ on $\mathcal{W}^{\mathbf{G}}$ which we will describe next. First of all an element $\mathbf{h}\in\mathbf{G}$ acts on $\mathcal{W}^{\mathbf{G}}$ via

$$\mathbf{h}\cdot\mathbf{w}=\mathbf{h}\cdot(w,\mathbf{g}_{\mathbf{w}})\coloneqq(\mathbf{h}\cdot w,\mathbf{h}\mathbf{g}_{\mathbf{w}}\mathbf{h}^{-1})\ .$$

This action is complemented by the $\mathbb{Z}$-action generated by the two (inverse) *shifts* acting in the first component as

$$\begin{aligned}\sigma_R\mathbf{w}&\coloneqq\big((\mathbf{g}_{\mathbf{w}}w_n,w_1,\dots,w_{n-1}),\mathbf{g}_{\mathbf{w}}\big)\ ,\\ \sigma_L\mathbf{w}&\coloneqq\big((w_2,\dots,w_n,\mathbf{g}_{\mathbf{w}}^{-1}w_1),\mathbf{g}_{\mathbf{w}}\big)\ .\end{aligned}$$

This $\mathbb{Z}$-action commutes with the action of $\mathbf{G}$. We can therefore consider the space $\big[\mathcal{W}^{\mathbf{G}}\big]\coloneqq(\mathbf{G}\times\mathbb{Z})\setminus\mathcal{W}^{\mathbf{G}}$ of orbits under the product of these actions and we denote the equivalence class containing $\mathbf{w}\in\mathcal{W}^{\mathbf{G}}$ by $[\mathbf{w}]$.

Before we can re-organize the sums appearing in Theorem 5.3 it remains to identify an appropriate notion of *composite* elements. To this end we define the *k-fold iteration* of $\mathbf{w}\in\mathcal{W}^{\mathbf{G}}$ by the formula

$$\mathbf{w}^k\coloneqq\big((\mathbf{g}_{\mathbf{w}}^{k-1}w_1,\dots,\mathbf{g}_{\mathbf{w}}^{k-1}w_n,\mathbf{g}_{\mathbf{w}}^{k-2}w_1,\dots,\mathbf{g}_{\mathbf{w}}w_1,\dots,\mathbf{g}_{\mathbf{w}}w_n,w_1,\dots w_n),\mathbf{g}_{\mathbf{w}}^k\big)\ ,$$

and we call an element of $\mathcal{W}^{\mathbf{G}}$ *prime* if it cannot be represented as such an iteration for $k > 1$. Otherwise we call the element composite.

Next we recall some features of the various notions just introduced. Complete proofs can be found in [BW16, Lemma 4.3, Prop. 4.4]. We continue to denote by $V(z_1, z_2)$ some $\mathbf{G}$-invariant potential.

(1) An orbit of the $\mathbf{G}\times\mathbb{Z}$-action consists either entirely of prime or entirely of composite elements making $\left[\mathcal{W}^{\mathbf{G}}_{\mathrm{p}}\right] := \{[\mathbf{w}] \,|\, w \text{ prime}\}$ well-defined;
(2) Given $\mathbf{v} \in [\mathbf{w}^k]$ one has the equalities $V_v(\mathbf{g}_{\mathbf{v}} x^{\mathbf{v}}_-, \mathbf{g}_{\mathbf{v}} x^{\mathbf{v}}_+) = V_w(\mathbf{g}_{\mathbf{w}} x^{\mathbf{w}}_-, \mathbf{g}_{\mathbf{w}} x^{\mathbf{w}}_+)^k$ and $(g_v \circ \mathbf{g}_{\mathbf{v}})'(x^{\mathbf{v}}_\pm) = (g_w \circ \mathbf{g}_{\mathbf{w}})'(x^{\mathbf{w}}_\pm)^k$;
(3) If $\mathbf{G}$ acts freely on $\mathcal{W}^{\mathbf{G}}$ then the number of elements in the equivalence class $[\mathbf{w}] \in \left[\mathcal{W}^{\mathbf{G}}_{\mathrm{p}}\right]$ can be calculated as $\#[\mathbf{w}] = |\mathbf{G}| \cdot n_{\mathbf{w}}$;
(4) If $m_{\mathbf{w}} := \mathrm{ord}(\mathbf{g})$ denotes the *order*[10] of $\mathbf{g} \in \mathbf{G}$ then the equalities $(g_w \circ \mathbf{g}_{\mathbf{w}})'(x^{\mathbf{w}}_\pm) = g'_{w^{m_{\mathbf{w}}}}(x^{w^{m_{\mathbf{w}}}}_\pm)^{1/m_{\mathbf{w}}}$ and $V_w(\mathbf{g}_{\mathbf{w}} \cdot x^{\mathbf{w}}_\pm) = V_{w^{m_{\mathbf{w}}}}(x^{w^{m_{\mathbf{w}}}}_\pm)^{1/m_{\mathbf{w}}}$ hold for any $[\mathbf{w}] \in \left[\mathcal{W}^{\mathbf{G}}_{\mathrm{p}}\right]$ and denoting by $x^v_\pm$ the fixed points of g_v.[11]

With this we can now reformulate Theorem 5.3 in a form which is very reminiscent of our definition of the dynamical determinant d_f in (5). From the preceding discussion combined with Theorem 5.3 and under the assumptions of $\mathbf{G}$-invariant potential and free $\mathbf{G}$-action on $\mathcal{W}^{\mathbf{G}}$ we immediately deduce the following for sufficiently small $|z|$

$$\begin{aligned} d_{V,\chi}(z) &= \exp\left(-d_\chi \sum_{[\mathbf{w}]\in\left[\mathcal{W}^{\mathbf{G}}\right]} \frac{\#[\mathbf{w}]\cdot z^{n_{\mathbf{w}}}}{n_{\mathbf{w}}\cdot|\mathbf{G}|} \frac{\chi(\mathbf{g}_{\mathbf{w}}) V_w(\mathbf{g}_{\mathbf{w}}\cdot x^{\mathbf{w}}_-, \mathbf{g}_{\mathbf{w}}\cdot x^{\mathbf{w}}_+)}{((g_w\circ\mathbf{g}_{\mathbf{w}})'(x^{\mathbf{w}}_-)-1)(1-(g_w\circ\mathbf{g}_{\mathbf{w}})'(x^{\mathbf{w}}_+))}\right) \\ &= \exp\left(-d_\chi \sum_{k=1}^{\infty} \sum_{[\mathbf{w}]\in\left[\mathcal{W}^{\mathbf{G}}_{\mathrm{p}}\right]} \frac{\#[\mathbf{w}^k] z^{kn_{\mathbf{w}}}}{kn_{\mathbf{w}}|\mathbf{G}|} \frac{\chi(\mathbf{g}^k_{\mathbf{w}})\cdot V_w(\mathbf{g}_{\mathbf{w}}\cdot x^{\mathbf{w}}_-, \mathbf{g}_{\mathbf{w}}\cdot x^{\mathbf{w}}_+)^k}{((g_w\circ\mathbf{g}_{\mathbf{w}})'(x^{\mathbf{w}}_-)^k-1)(1-(g_w\circ\mathbf{g}_{\mathbf{w}})'(x^{\mathbf{w}}_+)^k)}\right) \\ &= \exp\left(-d_\chi \sum_{k=1}^{\infty} \sum_{[\mathbf{w}]\in\left[\mathcal{W}^{\mathbf{G}}_{\mathrm{p}}\right]} \frac{z^{kn_{\mathbf{w}}}}{k} \frac{\chi(\mathbf{g}^k_{\mathbf{w}})\cdot V_{w^{m_{\mathbf{w}}}}(x^{w^{m_{\mathbf{w}}}}_-, x^{w^{m_{\mathbf{w}}}}_+)^{k/m_{\mathbf{w}}}}{\left(\mathrm{e}^{kT_{\gamma(g_{w^{m_{\mathbf{w}}}})}/m_{\mathbf{w}}}-1\right)\left(1-\mathrm{e}^{-kT_{\gamma(g_{w^{m_{\mathbf{w}}}})}/m_{\mathbf{w}}}\right)}\right) . \end{aligned} \tag{23}$$

From here we can proceed by applying the cycle expansion philosophy introduced in Section 3. This results in the following Proposition which generalizes Corollaries 2.5 as well as 3.1 and serves as our primary tool for practical implementation. We require a final definition before presenting the actual statement: Given a weight function $f \in \mathrm{C}^\omega(S\mathbf{X}_\Gamma)$ we say that it has $\mathbf{G}$-*invariant period integrals* if its integrals over closed geodesics satisfy

$$\int_{\gamma(g_w)} f = \int_{\gamma(g_{\mathbf{g}\cdot w})} f \ , \qquad \forall \mathbf{g} \in \mathbf{G},\, \forall w \in \mathcal{W}_n \ .$$

The main example for this is given by the case where $\mathbf{G}$ even acts on the whole unit sphere bundle $S\mathbf{H}$. It then acts on Γ-invariant elements of $\mathrm{C}^\infty(S\mathbb{H})$ by translation and if f is invariant under this $\mathbf{G}$-action then it also has $\mathbf{G}$-invariant period integrals because $\gamma(g_{\mathbf{g}\cdot w}) = \mathbf{g}\cdot\gamma(g_w)$ in this setting.

The central proposition now reads as follows:

Proposition 5.4. *Let Γ be a Schottky group with symmetry group $\mathbf{G}$ acting freely on $\mathcal{W}^{\mathbf{G}}$ and $f \in \mathrm{C}^\omega(S\mathbf{X}_\Gamma)$ an analytic weight with $\mathbf{G}$-invariant period integrals. Then the following hold:*

[10] I.e. the smallest integer $k > 0$ such that $\mathbf{g}^k = \mathrm{id}_{\mathbf{G}}$.

[11] And if the respective right-hand sides are real-valued, which is always the case for our particular potentials.

(1) *The dynamical determinant decomposes as a product*

$$d_f(\lambda, z, \beta) = \prod_{\chi \in \widehat{\mathbf{G}}} d_{f,\chi}(\lambda, z, \beta)$$

of symmetry reduced dynamical determinants $d_{f,\chi}$.

(2) *The* $d_{f,\chi}$ *are given by an everywhere convergent power series expansion*

$$d_{f,\chi}(\lambda, z, \beta) = 1 + \sum_{n=1}^{\infty} d_n^{\chi}(\lambda, \beta) z^n \ ,$$

with coefficients in this expansion being holomorphic functions in (λ, β) *and explicitly given by the recursion*

$$d_n^{\chi}(\lambda, \beta) = \sum_{m=1}^{n} \frac{m}{n} d_{n-m}^{\chi}(\lambda, \beta) a_m^{\chi}(\lambda, \beta) \ , \qquad d_0^{\chi}(\lambda, \beta) \equiv 1 \ ,$$

$$a_m^{\chi}(\lambda, \beta) = -d_{\chi} \sum_{\substack{([\mathbf{w}], k) \in \left[\mathcal{W}_{\mathrm{p}}^{\mathbf{G}}\right] \times \mathbb{N}_{>0} \\ n_{\mathbf{w}} \cdot k = m}} \frac{\chi(\mathbf{g}_{\mathbf{w}}^k)}{k} \frac{\exp\left(- \frac{k(\lambda-1)}{m_{\mathbf{w}}} T_{\gamma(g_w m_{\mathbf{w}})} - \frac{k\beta}{m_{\mathbf{w}}} \int_{\gamma(g_w m_{\mathbf{w}})} f \right)}{\left(\mathrm{e}^{k T_{\gamma(g_w m_{\mathbf{w}})}/m_{\mathbf{w}}} - 1 \right)^2} \ .$$

The coefficients $d_n^{\chi}(\lambda, \beta)$ *satisfies super-exponential bounds of the same kind as in Corollary 3.1.*

(3) *The weighted zeta function* Z_f *decomposes as a sum of meromorphic functions given by logarithmic derivatives of the* $d_{f,\chi}$*:*

$$Z_f(\lambda) = \sum_{\chi \in \widehat{\mathbf{G}}} \frac{\partial_\beta d_{f,\chi}(\lambda, 1, 0)}{d_{f,\chi}(\lambda, 1, 0)} \ .$$

Proof. The idea of proof is very much aligned with the material presented in Sections 2 and 3: To derive (1) we would like to plug the concrete potential of Corollary 2.4 into the product decomposition of Theorem 5.3.

A slight difficulty with this strategy is the fact that the potential $V_{\lambda,\beta}$ of Corollary 2.4 is not $\mathbf{G}$-invariant due to the presence of the derivative term. This can be remedied by substituting it with a $\mathbf{G}$-averaged version possessing built-in $\mathbf{G}$-invariant, c.f. [BW16, Lemma 5.6]:

$$V_{\lambda,\beta}^{\mathbf{G}} \coloneqq \prod_{\mathbf{g} \in \mathbf{G}} V_{\lambda,\beta}(\mathbf{g} \cdot z_1, \mathbf{g} \cdot z_2)^{1/|\mathbf{G}|} \ .$$

By (7) we only need to verify $(V_{\lambda,\beta})_w = (V_{\lambda,\beta}^{\mathbf{G}})_w$ for any closed word $w \in \mathcal{W}_n$ to prove that the transfer operators associated with these potentials give rise to the same Fredholm determinant. Using the $\mathbf{G}$-invariance of the period integrals of f and the proof of [BW16, Lemma 5.6] (which is essentially an application of the ordinary chain rule) we can now calculate

$$\begin{aligned} \left(V_{\lambda,\beta}^{\mathbf{G}}\right)_w &= \exp\left(-\frac{\beta}{|\mathbf{G}|} \sum_{\mathbf{g} \in \mathbf{G}} \int_{\gamma(g_{\mathbf{g}\cdot w})} f \right) \cdot \mathrm{e}^{-\lambda T_{\gamma(g_w)}} \\ &= \exp\left(-\lambda T_{\gamma(g_w)} - \beta \int_{\gamma(g_w)} f \right) = \left(V_{\lambda,\beta}\right)_w \ . \end{aligned}$$

This proves (1) if we define $d_{f,\chi}(\lambda, z, \beta) \coloneqq d_{V_{\lambda,\beta}^{\mathbf{G}},\chi}(z)$.

To obtain the expression for $d_{f,\chi}(\lambda, z, \beta)$ claimed in (2), we start with the following formula derived for a general potential in (23) above and valid for sufficiently small $|z|$

$$\begin{aligned} d_{f,\chi}(\lambda, z, \beta) &= \exp\left(-d_\chi \sum_{k=1}^{\infty} \sum_{[\mathbf{w}] \in \left[\mathcal{W}_{\mathrm{p}}^{\mathbf{G}}\right]} \frac{z^{k n_{\mathbf{w}}}}{k} \frac{\chi(\mathbf{g}_{\mathbf{w}}^k) \cdot \exp\big(-\frac{k\lambda}{m_{\mathbf{w}}} T_{\gamma(g_{w^{m_{\mathbf{w}}}})} - \frac{k\beta}{m_{\mathbf{w}}} \int_{\gamma(g_{w^{m_{\mathbf{w}}}})} f\big)}{\big(\mathrm{e}^{k T_{\gamma(g_{w^{m_{\mathbf{w}}}})}/m_{\mathbf{w}}} - 1\big)\big(1 - \mathrm{e}^{-k T_{\gamma(g_{w^{m_{\mathbf{w}}}})}/m_{\mathbf{w}}}\big)} \right) \\ &= \exp\left(\sum_{n=1}^{\infty} a_n^\chi(\lambda, \beta) z^n \right) , \end{aligned}$$

with the definition

$$a_n^\chi(\lambda, \beta) \coloneqq -d_\chi \sum_{\substack{([\mathbf{w}], k) \in \left[\mathcal{W}_{\mathrm{p}}^{\mathbf{G}}\right] \times \mathbb{N}_{>0} \\ n_{\mathbf{w}} \cdot k = n}} \frac{\chi(\mathbf{g}_{\mathbf{w}}^k)}{k} \frac{\exp\big(-\frac{k\lambda}{m_{\mathbf{w}}} T_{\gamma(g_{w^{m_{\mathbf{w}}}})} - \frac{k\beta}{m_{\mathbf{w}}} \int_{\gamma(g_{w^{m_{\mathbf{w}}}})} f\big)}{\big(\mathrm{e}^{k T_{\gamma(g_{w^{m_{\mathbf{w}}}})}/m_{\mathbf{w}}} - 1\big)\big(1 - \mathrm{e}^{-k T_{\gamma(g_{w^{m_{\mathbf{w}}}})}/m_{\mathbf{w}}}\big)} .$$

The theory of Bell polynomials already used in the proof of Corollary 3.1 now yields the claimed recursive relation.

The super-exponential bounds can be derived in the same manner as in Corollary 3.1 by simply observing that the singular values of the restrictions satisfy $\mu_i(\mathrm{P}_\chi \mathrm{L}_V) \leq \|\mathrm{P}_\chi\| \mu_i(\mathrm{L}_V)$. We can therefore recycle our previous calculations and arrive at the same bounds with possibly different constants.

Lastly we derive (3) in the following straightforward manner: Exchanging the logarithm of the product over $\widehat{\mathbf{G}}$ with a sum over logarithms in Corollary 2.5 lets us calculate

$$\begin{aligned} Z_f(\lambda) &= \partial_\beta \log\Big(\det\big(\mathrm{id} - z \mathrm{L}_{\lambda,\beta}^f\big)\Big) \Big|_{z=1,\beta=0} \\ &= \partial_\beta \log\Big(\det\big(\mathrm{id} - z \mathrm{L}_{V_{\lambda,\beta}^{\mathbf{G}}}\big)\Big) \Big|_{z=1,\beta=0} \\ &= \sum_{\chi \in \widehat{\mathbf{G}}} \partial_\beta \log\left(d_{f,\chi}(\lambda, z, \beta)\right) \Big|_{z=1,\beta=0} , \end{aligned}$$

finishing our proof. □

For practical purposes the following form for the coefficients occurring in the base of the recursion is more suitable:

$$a_m^\chi(\lambda, \beta) = -\frac{d_\chi}{m} \sum_{\substack{[\mathbf{w}] \in \left[\mathcal{W}_{\mathrm{p}}^{\mathbf{G}}\right] \\ n_{\mathbf{w}} || m}} n_{\mathbf{w}} \cdot \chi(\mathbf{g}_{\mathbf{w}}^{m/n_{\mathbf{w}}}) \frac{\exp\big(-\frac{m(\lambda-1)}{n_{\mathbf{w}} m_{\mathbf{w}}} T_{\gamma(g_{w^{m_{\mathbf{w}}}})} - \frac{m\beta}{n_{\mathbf{w}} m_{\mathbf{w}}} \int_{\gamma(g_{w^{m_{\mathbf{w}}}})} f\big)}{\big(\mathrm{e}^{m T_{\gamma(g_{w^{m_{\mathbf{w}}}})}/(n_{\mathbf{w}} m_{\mathbf{w}})} - 1\big)^2} ,$$

where $n || m$ for $n, m \in \mathbb{N}$ indicates that n divides m. Rescaling both lengths and period integrals by $1/(n_{\mathbf{w}} m_{\mathbf{w}})$ like this yields a rather convenient way for vectorized evaluation of the coefficients a_m^χ.

Remark 5.5. The proposition does not reveal if and why any improvement in terms of convergence should be expected from the coefficients d_n^χ compared with their non-symmetry reduced counterparts d_n. The practical calculations below will reveal a significant improvement, though. For a theoretical discussion of this phenomenon we refer to [BW16, Appendix B].

Remark 5.6. If we want to apply Proposition 5.4 we have to adjust the families of test functions presented in Section 4 to satisfy $\mathbf{G}$-invariance of their period integrals. But this is fairly straightforward: We simply replace the expressions derived in (20) and (22) by similar sums but over points $x_j + \mathrm{i}y_j$ or (γ_-^i, γ_+^i), respectively, derived not only from the

original word w but from all words $\mathbf{g} \cdot w$ for $\mathbf{g} \in \mathbf{G}$. A subsequent normalization by $|\mathbf{G}|$ then yields a suitable prescription.

Algorithm 2: Pseudo-code for the calculation of symmetry reduced determinants d_χ for a given character χ. Iterating this procedure over all characters $\chi \in \widehat{\mathbf{G}}$ and combining it with the first block of Snippet 1 yields a means for the symmetry reduced calculation of approximations to invariant Ruelle distributions.

Input: width $\sigma > 0$, center $gK \in G/K$, resonance $\lambda_0 \in \mathbb{C}$, character $\chi \in \widehat{\mathbf{G}}$, cut-off $N \in \mathbb{N}$

`/* calculate Bell recursion as in Snippet 1, but with` $a[]$ `replaced by modified initial terms` $a^\chi[]$ `*/`

`/* calculate modified initial terms` $a^\chi[k]$ `in Bell recursion */`

$a^\chi[k] \leftarrow 0$;

$\partial a^\chi[k] \leftarrow 0$;

for $[\mathbf{w}] \in \left[\mathcal{W}_p^{\mathbf{G}}\right]$ where $n_{\mathbf{w}} || k$ **do**

$a^\chi[k] \leftarrow a^\chi[k] - n_{\mathbf{w}} \chi(\mathbf{g}_{\mathbf{w}}^{k/n_{\mathbf{w}}}) \frac{\exp(-(\lambda_0 - 1) k \ell(g_w)/(n_{\mathbf{w}} m_{\mathbf{w}}))}{(\mathrm{e}^{k\ell(g_w)/(n_{\mathbf{w}} m_{\mathbf{w}})} - 1)^2}$;

$\partial_\beta a[k] \leftarrow \partial_\beta a[k] + n_{\mathbf{w}} \chi(\mathbf{g}_{\mathbf{w}}^{k/n_{\mathbf{w}}}) k \frac{\exp(-(\lambda_0 - 1) k \ell(g_w))/(n_{\mathbf{w}} m_{\mathbf{w}})}{(\mathrm{e}^{k\ell(g_w)/(n_{\mathbf{w}} m_{\mathbf{w}})} - 1)^2} \cdot \mathrm{calcInt}(w)$;

; `/* calcInt implements (20) */`

$a^\chi[k] \leftarrow \frac{d_\chi}{k} a^\chi[k]$;

$\partial_\beta a[k] \leftarrow \frac{d_\chi}{k} \partial_\beta a[k]$;

end

Result: approximation of one summand in the symmetry decomposition of $Z_{f_{\sigma,gK} \circ \pi}(\lambda_0)$ according to Proposition 5.4

5.3. **Example Surfaces.** In order to make use of Proposition 5.4 in practice one requires example surfaces with sufficiently rich symmetry groups. To meet this requirement we provide two classes of such examples covering both topological possibilities for Schottky surfaces of rank $r = 2$: The three-funneled surfaces and the funneled tori.

5.3.1. *Three-funneled surface.* The family of three-funneled surfaces constitutes the main class of examples in the original paper of Borthwick [Bor14] and many subsequent papers on the numerical calculation of resonances [BW16, BPSW20]. Due to this prevalence will we refrain from giving too many details and simply state their generators:

$$g_1 \coloneqq \begin{pmatrix} \cosh(\ell_1/2) & \sinh(\ell_1/2) \\ \sinh(\ell_1/2) & \cosh(\ell_1/2) \end{pmatrix}, \qquad g_2 \coloneqq \begin{pmatrix} \cosh(\ell_2/2) & a \sinh(\ell_2/2) \\ a^{-1} \sinh(\ell_2/2) & \cosh(\ell_2/2) \end{pmatrix}$$

The three numbers $\ell_1, \ell_2, \ell_3 > 0$ parameterize the family and can be interpreted geometrically as the lengths of the closed geodesics winding around the funnels. The parameter a is not free but must be chosen such that the condition $\mathrm{tr}(g_1 g_2^{-1}) = -2\cosh(\ell_3/2)$ is fulfilled. We follow the notation introduced in [Bor14] and denote the generated surface by $X(\ell_1, \ell_2, \ell_3)$.

The following realization $\mathbf{G} = \{\mathrm{e}, \sigma_1, \sigma_2, \sigma_1\sigma_2\}$ of Klein's four-group is a symmetry group of the generators given above provided that $\ell_1 = \ell_2$:[12]

$$\sigma_1 = \begin{pmatrix} -1 & 0 \\ 0 & 1 \end{pmatrix}, \qquad \sigma_2 = \begin{pmatrix} 0 & \sqrt{a} \\ 1/\sqrt{a} & 0 \end{pmatrix},$$

[12] For an elementary proof see [BW16, Example 3.2].

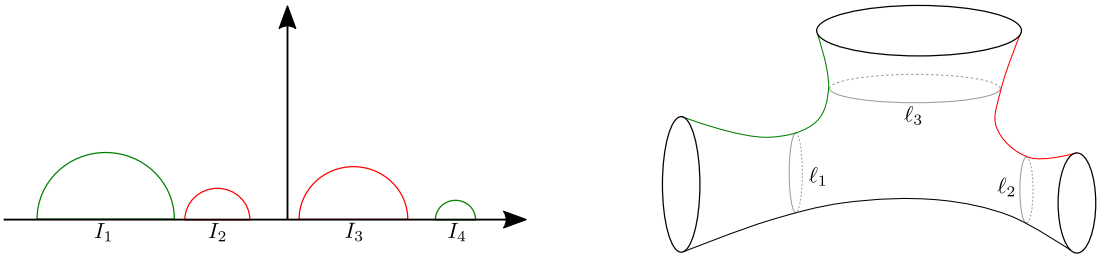

FIGURE 5. The right-hand side illustrates the three-funneled surface with boundary lengths ℓ_1, ℓ_2, ℓ_3 embedded (non-isometrically) into three-dimensional Euclidean space. Highlighted in red and green is the Poincaré section (projected onto the surface) corresponding to the fundamental domain on the left.

where both matrices act on $\mathbb{H}$ via Möbius transformations. The action on the letters is then given by

$$\begin{aligned} &\sigma_1(1) = 3,\ \sigma_1(2) = 4,\ \sigma_1(3) = 1,\ \sigma_1(4) = 2 \\ &\sigma_2(1) = 2,\ \sigma_2(2) = 1,\ \sigma_2(3) = 4,\ \sigma_2(4) = 3\ . \end{aligned} \tag{24}$$

The final ingredient for the calculation of symmetry reduced zeta functions is the character table of $\mathbf{G}$. This well-known data is given in Table 1.

TABLE 1. Character table for the symmetry group of three-funneled surfaces.

	e	σ_1	σ_2	$\sigma_1\sigma_2$
A	1	1	1	1
B	1	−1	1	−1
C	1	1	−1	−1
D	1	−1	−1	1

In the less symmetric case $\ell_1 \neq \ell_2$ the generators lose their symmetry with respect to σ_2 but retain $\{\mathrm{e}, \sigma_1\}$ as their symmetry group. This smaller group has only two irreducible representations, namely the trivial one and one that equals -1 on σ_1. Both are one-dimensional.

5.3.2. *Funneled torus.* Our second family of surfaces is also well-known in the literature. Generators are given by

$$\begin{aligned} g_1 &:= \begin{pmatrix} \exp(\ell_1/2) & 0 \\ 0 & \exp(-\ell_1/2) \end{pmatrix}\ , \\ g_2 &:= \begin{pmatrix} \cosh(\ell_2/2) - \cos(\varphi)\sinh(\ell_2/2) & \sin^2(\varphi)\sinh(\ell_2/2) \\ \sinh(\ell_2/2) & \cosh(\ell_2/2) + \cos(\varphi)\sinh(\ell_2/2) \end{pmatrix}\ , \end{aligned}$$

where again three parameters ℓ_1, ℓ_2, and φ are needed to specify a concrete member. Geometrically they describe the lengths of two closed geodesics on the surface and the angle between them. Obviously the generator g_1 contains the boundary point ∞ in its fundamental interval which makes it inaccessible for our algorithm because we use the fundamental intervals directly as coordinates of the Poincaré section. Conjugating the generators by a simple rotation yields a new pair $\widetilde{g}_1$ and $\widetilde{g}_2$ of generators which do not suffer from this problem. It turns out that $\pi/8$ is a particularly handy value in the maximally symmetric case $\ell_1 = \ell_2$ and $\varphi = \pi/2$ as it leads to a very symmetric arrangement of fundamental circles (see also [BPSW20, Section 5.3] where the boundary point ∞ must be

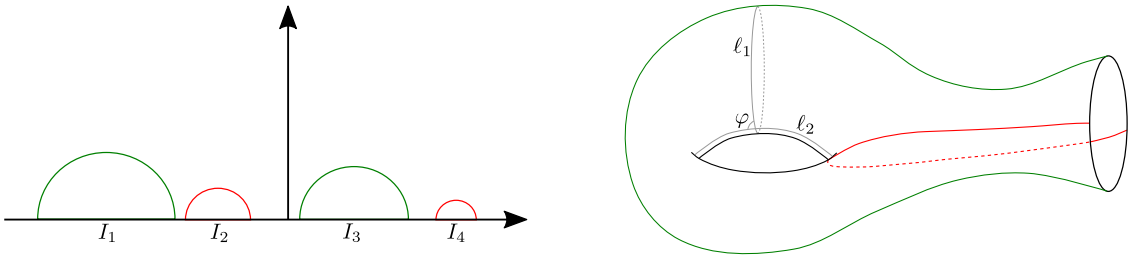

FIGURE 6. Here the right-hand side illustrates the funneled torus with parameters ℓ_1, ℓ_2, ϕ embedded (non-isometrically) into three-dimensional Euclidean space. Highlighted in red and green is the Poincaré section (projected onto the surface) corresponding to the fundamental domain on the left.

rotated outside of the fundamental intervals for somewhat similar reasons). In this case the conjugated generators are of the explicit form

$$\widetilde{g}_1 := \begin{pmatrix} \cosh(\ell/2) + \sinh(\ell/2)/\sqrt{2} & \sinh(\ell/2)/\sqrt{2} \\ \sinh(\ell/2)/\sqrt{2} & \cosh(\ell/2) - \sinh(\ell/2)/\sqrt{2} \end{pmatrix}$$
$$\widetilde{g}_2 := \begin{pmatrix} \cosh(\ell/2) - \sinh(\ell/2)/\sqrt{2} & \sinh(\ell/2)/\sqrt{2} \\ \sinh(\ell/2)/\sqrt{2} & \cosh(\ell/2) + \sinh(\ell/2)/\sqrt{2} \end{pmatrix} .$$

Again we adopt the same notation as in [Bor14] and denote the funneled tori generated by $\widetilde{g}_1$ and $\widetilde{g}_2$ by $Y(\ell_1, \ell_2, \varphi)$.

The generators $\widetilde{g}_1$ and $\widetilde{g}_2$ again admit a realization of Klein's four-group as their symmetry group. Concrete symmetries are given by the Möbius transformations induced via

$$\sigma_1 = \begin{pmatrix} 0 & 1 \\ 1 & 0 \end{pmatrix}, \qquad \sigma_2 = \begin{pmatrix} 0 & 1 \\ -1 & 0 \end{pmatrix} ,$$

with their action on the symbols being the same as in (24). One can easily verify these relations by elementary matrix calculations of the type $\sigma_1 \widetilde{g}_1 \sigma_1^{-1} = \widetilde{g}_2$. The character table thus coincides with the one given above in Table 1.

6. Numerical Results

This final section finishes the present paper by presenting some numerical calculations which were obtained with the tools developed up to this point. We begin with a comparison of convergence rates of invariant Ruelle distributions depending on the particular symmetry group used for a given surface.

Remark 6.1. To do this we still require a practically feasible approach for the calculation of residues of $Z_f(\lambda)$. If one can calculate the function $Z_f(\lambda)$ efficiently[13] for a large number of support points $\lambda \in \mathbb{C}$, i.e. on large arrays, then it would be possible to calculate its residue at λ_0 very generically via the classical integral formula

$$\operatorname*{Res}_{\lambda=\lambda_0} [Z_f(\lambda)] = \frac{1}{2\pi \mathrm{i}} \int_C Z_f(\lambda) \, \mathrm{d}\lambda ,$$

where a convenient choice for the contour C could e.g. be a sufficiently small rectangle with λ_0 at its center. This integral can then be evaluated using numerical quadrature methods.

[13] E.g. by vectorization or via a distributed computational scheme.

If a large number of function evaluations is too computationally expensive then the following well-known formula offers an alternative:

$$\operatorname*{Res}_{\lambda=\lambda_0}[Z_f(\lambda)] = \frac{1}{(N-1)!}\lim_{\lambda\to\lambda_0}\left(\frac{\mathrm{d}}{\mathrm{d}\lambda}\right)^{N-1}\left[(\lambda-\lambda_0)^N Z_f(\lambda)\right] \ ,$$

where N denotes the order of the pole λ_0. If $N = 1$, i.e. λ_0 is a simple pole, then this general formula takes a particularly simple shape and plugging in the logarithmic derivative of the dynamical determinant d_f yields for the simple case

$$\operatorname*{Res}_{\lambda=\lambda_0}[Z_f(\lambda)] = \frac{\partial_\beta d_f(\lambda_0,1,0)}{\partial_\lambda d_f(\lambda_0,1,0)} \ . \tag{25}$$

This expression can be evaluated directly because calculation of $\partial_\lambda d_f$ requires only a straightforward modification of our algorithm for d_f and $\partial_\beta d_f$. The numerics presented below feature only simple poles so we used (25) throughout our implementations.[14]

Funneled Torus Experiments. The first system we consider is the funneled torus for the two cases of its full 4-element Kleinian symmetry group as described in Section 5.3.2 and without any symmetry reduction. The quantum resonance spectrum for the concrete example $Y\left(10,10,\frac{\pi}{2}\right)$ was already obtained numerically by Borthwick [Bor14, Figure 11] by means of Selberg's zeta function. In Figure 7 we recover this spectrum but now using the dynamical determinant d_f with constant weight function f. This yields the Pollicott-Ruelle resonances of $Y\left(10,10,\frac{\pi}{2}\right)$ which by [GHW18] coincide with the quantum spectrum after a shift by -1. Compared with previous calculations of quantum resonances in the literature our numerics therefore illustrate this theorem about the relationship between classical and quantum resonances.

We begin by investigating in more detail the first resonance of $Y(10,10,\pi/2)$ which is located at $\delta - 1 \approx -0.8847$ with δ the Hausdorff dimension of the limit set. The result of numerically calculating $t^{\Sigma}_{\lambda_0,\sigma}$ is shown in Figure 9 as plots of three different quantities: The left-most plot shows the real part of the distribution which gets complemented by the imaginary part in the middle. The invariant Ruelle distribution associated with the first resonance coincides with the Bowen-Margulis measure so it should be expected that the numerical approximation is real-valued and positive which is exactly the case in the shown plot. The right-most coordinate square features a combination of real and imaginary parts: There the complex argument is indicated through the color of the peaks and the absolute value of $t^{\Sigma}_{\lambda_0,\sigma}$ was encoded as the lightness of the particular color. The mapping of colors to complex arguments is simply given by the angle on the standard color wheel in the HSB/HSL encoding of RGB shifted by π, i.e. light blue corresponds to an argument of 0 while red corresponds to π (see Figure 8). From this illustration it is immediately clear that the distribution is remarkably homogeneous within each square $I_i \times I_j$ of the coordinate domain parameterizing the Poincaré section.

Next we consider additional resonances from Figure 7 under the aspect of how well the associated distributions converge in practice. It is reasonable to expect that the outer edges of the square $[-1,\delta-1]+[0,1000]\mathrm{i}$ of the complex plane where resonances were calculated should correspond to the best respectively worst rates of convergence. To increase the resolution of the distribution the plots were additionally restricted to coordinates within strictly smaller intervals

$$(\widetilde{I}_2 \cup \widetilde{I}_3 \cup \widetilde{I}_3) \times (\widetilde{I}_1 \cup \widetilde{I}_2) \ , \qquad \widetilde{I}_i \subset I_i \ ,$$

where the location of the new intervals within the original fundamental domain is illustrated in Figure 10. This very basic *domain refinement* already reduces the amount of

[14] Our resonance calculations were obtained with a root finding algorithm that combines the argument principle from complex analysis with the classical Newton iteration. In particular our procedure always yields pairs of resonances and corresponding orders.

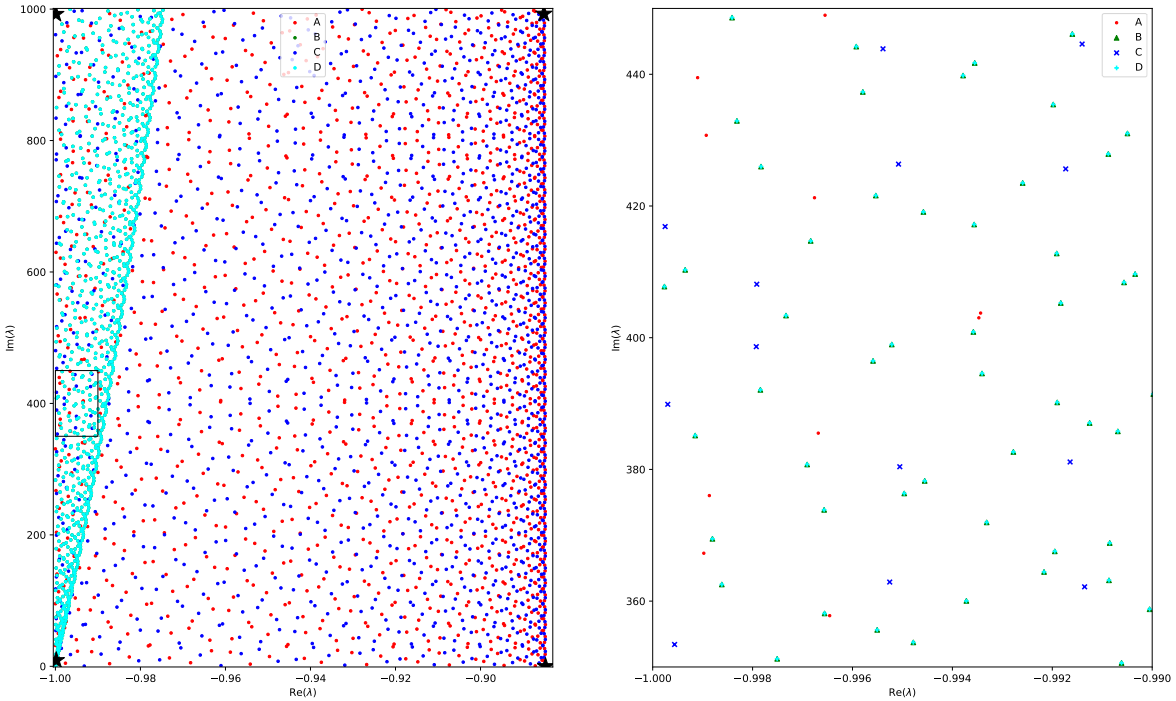

FIGURE 7. Resonances of the funneled torus $Y\left(10, 10, \frac{\pi}{2}\right)$ calculated in the symmetry reduction by the Klein four-group. The right-hand side shows a zoom into a small region of the left-hand side plot. Notice how the representations labeled B and D split resonances of multiplicity two into pairs of resonances of multiplicity one. In particular this simplifies the formula for the calculation of invariant Ruelle distributions via residues as described above. The four resonances marked by black stars in the left plot were used for investigations of Ruelle distributions below.

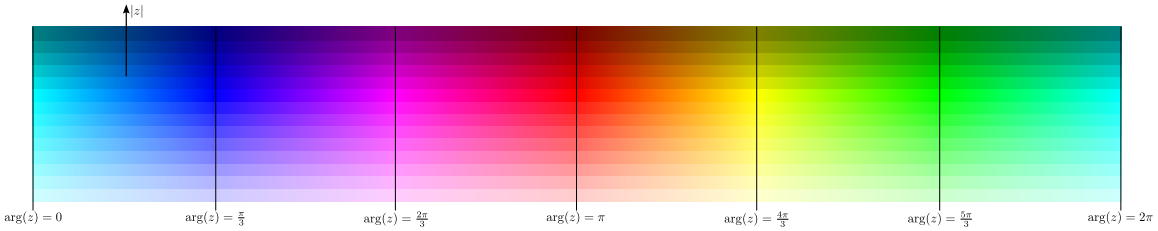

FIGURE 8. Sketch of how complex arguments $\arg(z)$ map to different colors in the phase plots above. The absolute value $|z|$ maps to the lightness of the color as a second dimension with darker colors corresponding to higher values of $|z|$.

redundancy in the resulting plots significantly by excluding large areas where the distributions vanish and exploiting the internal symmetries of the distributions as prominently visible in Figure 9.

The resulting plots for a collection of four resonances are depicted in Figure 11: Here the columns correspond to the same resonance whereas the rows share a common cutoff order $n_{\max}$, i.e. the number of summands used in the cycle expansion. From this figure

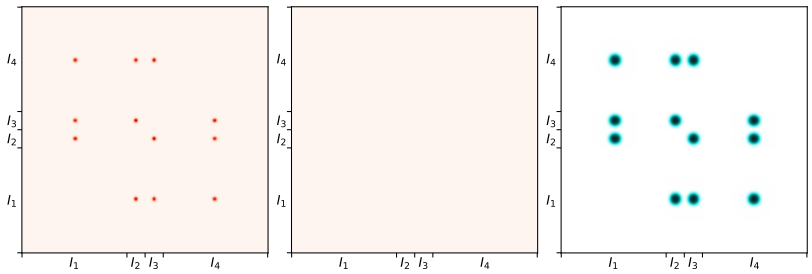

FIGURE 9. Invariant Ruelle distribution $t^{\Sigma}_{\lambda_0,\sigma}$ on the canonical Poincaré section Σ of the funneled torus $Y(10, 10, \pi/2)$ associated with the first resonance $\lambda_0 \approx -0.8847$. This figure uses the width $\sigma = 10^{-3}$ and $n_{\max} = 5$ summands in the cycle expansion of the dynamical determinant d_f. The fundamental intervals I_i which parameterize the section are ordered as qualitatively shown in Figure 6 The left and middle columns show the real and imaginary parts of the distribution. The right column encodes both real and imaginary parts by using the complex argument to determine the color (as an angle on the color wheel) and the absolute value to provide the lightness.

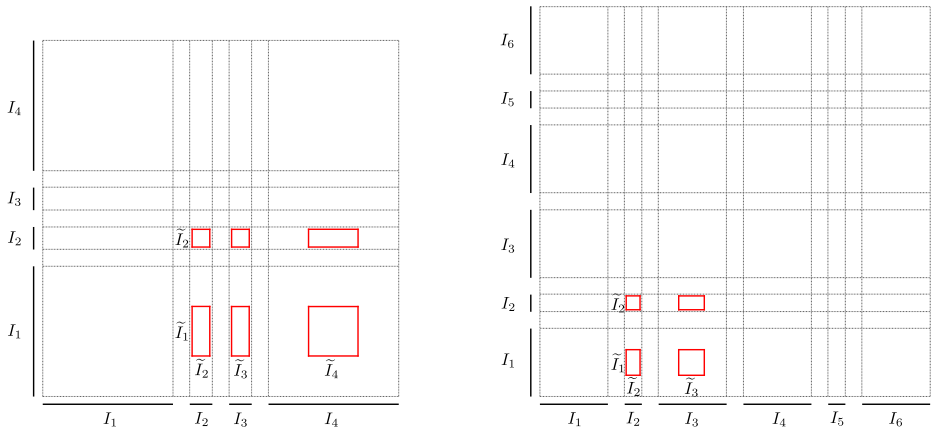

FIGURE 10. Location and relative size of the refined coordinate domains $\widetilde{I}_i \subset I_i$ compared to the original fundamental intervals of the funneled torus $X(10, 10, \pi/2)$ (left) and the three-funneled surface $X(12, 12, 12)$ (right).

we see that even the distribution associated with the resonance $\lambda_0 \approx -0.9999 + 992.4\mathrm{i}$ in the upper left of the considered resonance domain converges nicely already at $n_{\max} = 3$.

One particularly noteworthy feature of these plots is the large degree of similarity between the first and second columns both with respect to the absolute value as well as the complex argument. An explanation for this qualitative agreement might be the fact that both associated resonances are located near the global spectral gap at

$$\mathrm{Re}(\lambda) = \delta - 1$$

and a first conjecture could be that recurrence to this gap which was observed in previous investigations of quantum resonances on convex-cocompact hyperbolic surfaces is related to properties of resonant states.

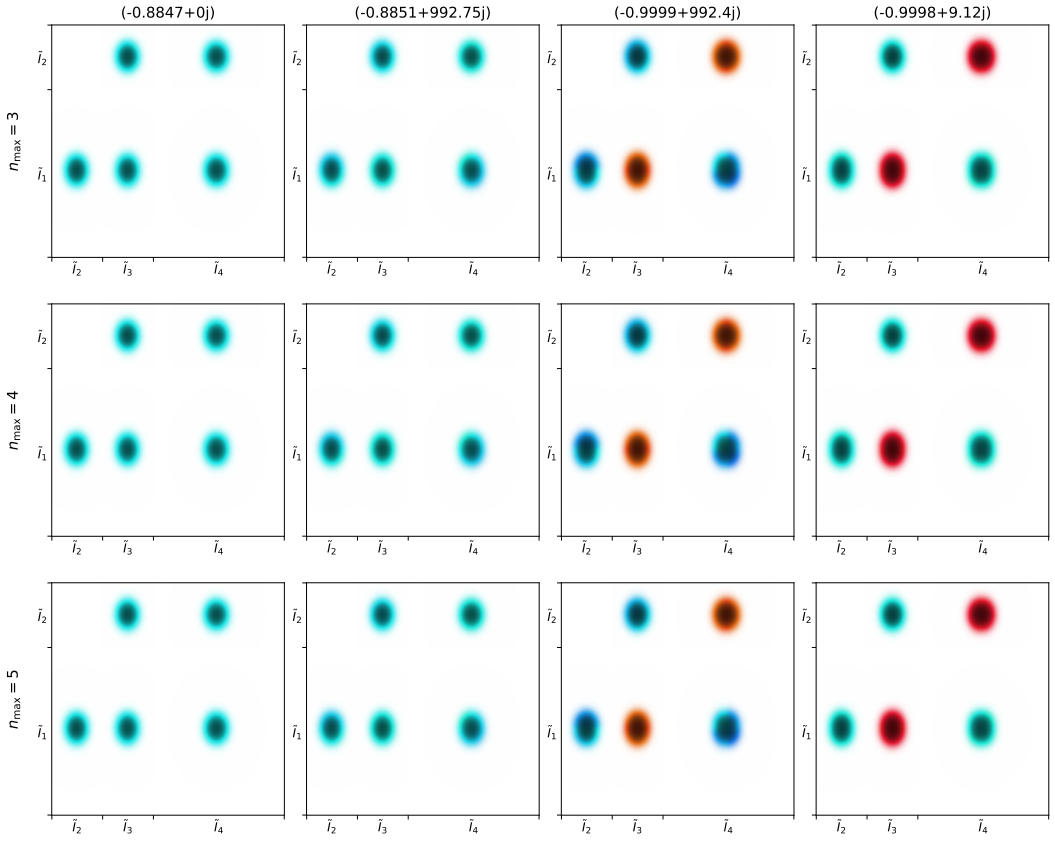

FIGURE 11. Fully symmetry reduced invariant Ruelle distributions $t^{\Sigma}_{\lambda_0,\sigma}$ on the canonical Poincaré section Σ of the funneled torus $Y(10, 10, \pi/2)$ evaluated at four different choices of resonance λ_0 (marked in Figure 7) with $\sigma = 10^{-3}$. The three different rows show the numerical results of using (from top to bottom) $n_{\max} \in \{3, 4, 5\}$ summands in the cycle expansion. Following along any of the four columns shows that the presented plots have converged rather well already at $n_{\max} = 3$. Due to symmetries in the distributions as visible in Figure 9 it suffices to consider as the coordinate domain the refined subset $(\widetilde{I}_2 \cup \widetilde{I}_3 \cup \widetilde{I}_4) \times (\widetilde{I}_1 \cup \widetilde{I}_2)$ of Figure 10.

By analogy with the application of cycle expansion to resonances it is straightforward to conjecture that symmetry reduction should improve the rate of convergence of invariant Ruelle distributions even for the (rather small) Klein four-group used with $Y(10, 10, \pi/2)$. To support this claim the experiment above was repeated with the trivial one-element symmetry group $\{e\}$.[15] Once converged our numerical results should be independent from the symmetry group used: While the approximation $t^{\Sigma}_{\lambda_0,\sigma}$ does contain a symmetric version of the Gaussian test functions this should not matter due to the global invariant Ruelle distribution also being invariant with respect to the full symmetry group of the surface.

The resulting plots in Figure 12 do indeed coincide with those of Figure 11 while at the same time exhibiting worse convergence properties: The distribution at $\lambda_0 \approx -0.9999 +$

[15] The $\mathbb{Z}$-symmetry was still factored out, though, which in itself reduces the computational cost of dynamical determinant evaluation by quite a margin.

992.4i has not converged until $n_{\max} = 7$. While not visible in the figure itself this worsened convergence rate also shows up for the other three resonances as can be seen by considering the relative errors of order N

$$\frac{\left|d_N^\chi(\lambda_0, 0)\right|}{\left|1 + \sum_{n=1}^N d_n^\chi(\lambda_0, 0)\right|} .$$

Note that these quantities are still functions of the coordinates (x_-, x_+) due to their dependence on the particular weight function used.[16] Two straightforward ways to obtain scalar measures of convergence quality are given by either averaging with respect to (x_-, x_+) over the whole coordinate domain of the Poincaré section or to take the maximum norm. We consistently tracked both variants for all our experiments and it turned out that in all cases they differed at most by one order of magnitude.

As an example we observed for the resonance $\lambda_0 \approx -0.9998 + 9.12\mathrm{i}$ errors of $3.38 \cdot 10^{-8}$ and $1.94 \cdot 10^{-8}$ after $n = 4$ iterations with symmetry reduction but $3.2 \cdot 10^{-4}$ as well as $9.82 \cdot 10^{-5}$ after $n_{\max} = 6$ iterations without reduction. This discrepancy becomes slightly smaller near the first resonances as $\lambda_0 = \delta - 1$ universally shows the best convergence behavior.

Three-funneled Surface Experiments. Next we conduct the analogous experiments for the three-funneled surface $X(12, 12, 12)$. The symmetry group of the standard set of generators was identified as the Klein four-group in Section 5.3.1 but this is actually not the full group of symmetries: In [BW16] it was demonstrated how a *flow-adapted* representation of $X(\ell, \ell, \ell)$ yields a strictly larger symmetry group thereby unlocking the full power of symmetry reduction for this class of surfaces. Without going into the details we state that this technique can be adapted to the dynamical determinants considered here so we may calculate with straightforward adaptations of the techniques described above invariant Ruelle distributions for the flow-adapted three-funnel surfaces. For a comprehensive description of the theoretical background refer to the first author's PhD thesis [Sch23].

Remark 6.2. Geometrically the flow-adapted representation is defined by gluing two copies of hyperbolic space with three disjoint halfplanes removed, see Figure 13. This corresponds to a canonical Poincaré section which is far more symmetric compared to the Schottky representation of three-funneled surfaces.

As a first step we again use the dynamical determinant to calculate the Pollicott-Ruelle resonances of this Schottky surface, see Figure 14. As expected from the quantum-classical correspondence this recovers the (shifted) quantum mechanical resonances already calculated in [Bor14, Figure 6] as well as the symmetry behavior of individual resonances as determined in [BW16, Figure 8]. Note that the full symmetry group of the flow-adapted three-funneled surfaces exhibits six irreducible unitary representations resulting in six different classes of resonances. One also prominently observes the same resonant chains already studied in [BW16].

With these first resonances available to us we can proceed very similarly to the funneled torus case. Again we compute the smoothed invariant Ruelle distribution $t^\Sigma_{\lambda_0,\sigma}$ on the canonical Poincaré section of the flow-adapted system associated with the first resonance $\lambda_0 = \delta - 1 \approx -0.8845$. The resulting plot is shown in Figure 15. Again the plot possesses the theoretically known properties of being real-valued and positive, as well as showing a clear symmetry with respect to the finite symmetry group of the underlying function system.

[16] At this point it is slightly inconvenient that in our notation for the individual summands d_n^χ of $d_{f,\chi}$ the weight f is only implicit. Nevertheless we chose this notation to keep the formulae in Section 5 as legible as possible and because the practically used d_n^χ always depend on Gaussian test functions anyways.

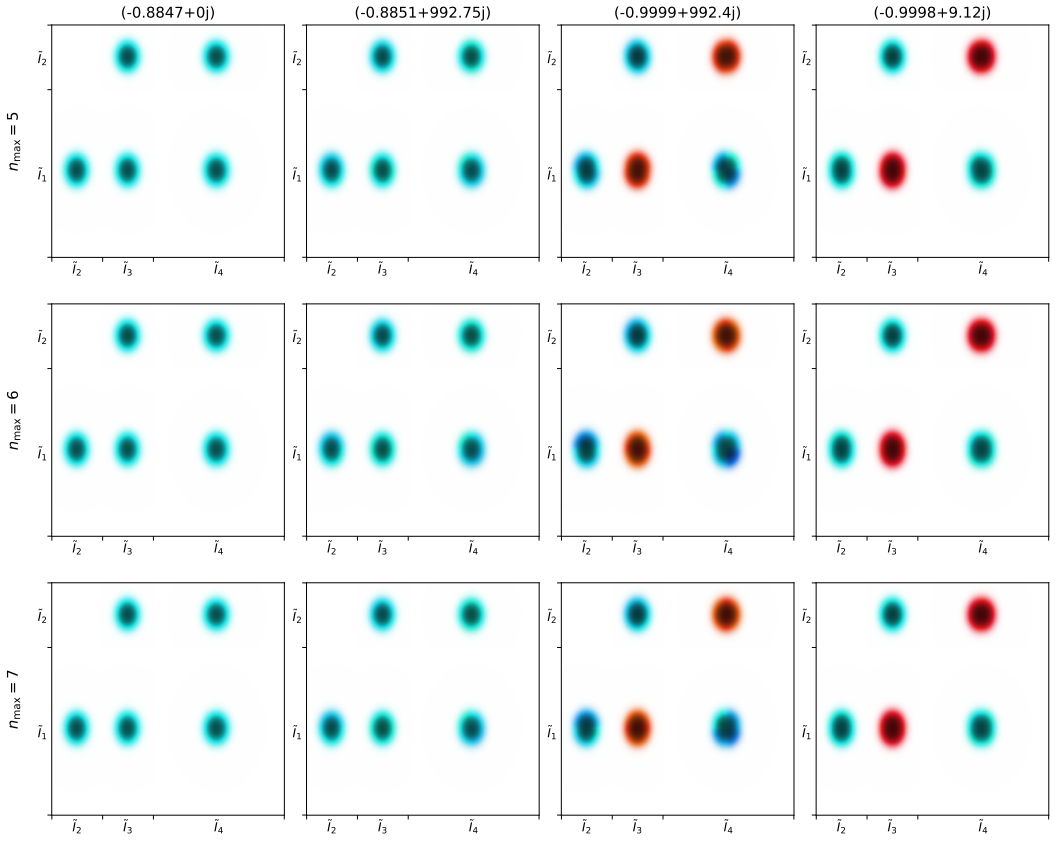

FIGURE 12. Analogous plots of $t^{\Sigma}_{\lambda_0,\sigma}$ for Σ the canonical Poincaré section of the funneled torus $Y(10, 10, \pi/2)$ and $\sigma = 10^{-3}$ as in Figure 11 but now symmetry reduced by the trivial (one-element) group $\{e\}$. The invariant Ruelle distribution is itself invariant under the finite symmetry group of the surface so these plots should (and do) coincide with those of Figure 11 apart from the significantly higher cutoff $n_{\max} = 7$ required for convergence of the cycle expansion (especially in the third column).

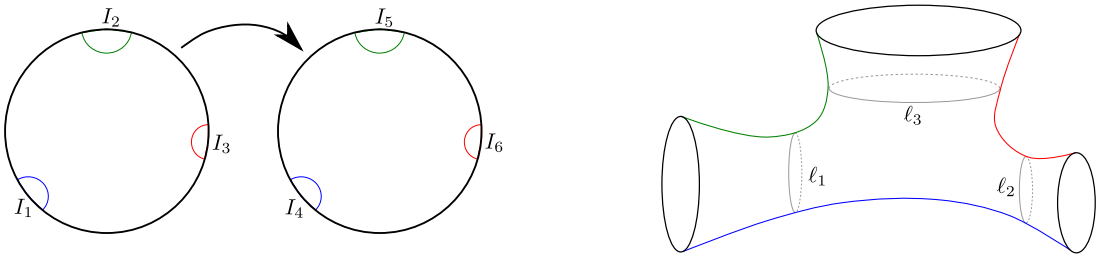

FIGURE 13. Illustration of the gluing of two copies of the Poincaré disc $\mathbb{D}$ (left) along the colored circles resulting in a three-funnel surface (right). The Poincaré section resulting from this gluing treats the three seams along the funnels equally.

As a next step we support the observations made above for the funneled torus with analogous experiments for $X(12, 12, 12)$: Figure 16 contains plots of invariant Ruelle distributions for a set of four different resonances located roughly on the corners of the resonance plot calculated in full symmetry reduction and the comparison with Figure 17 which

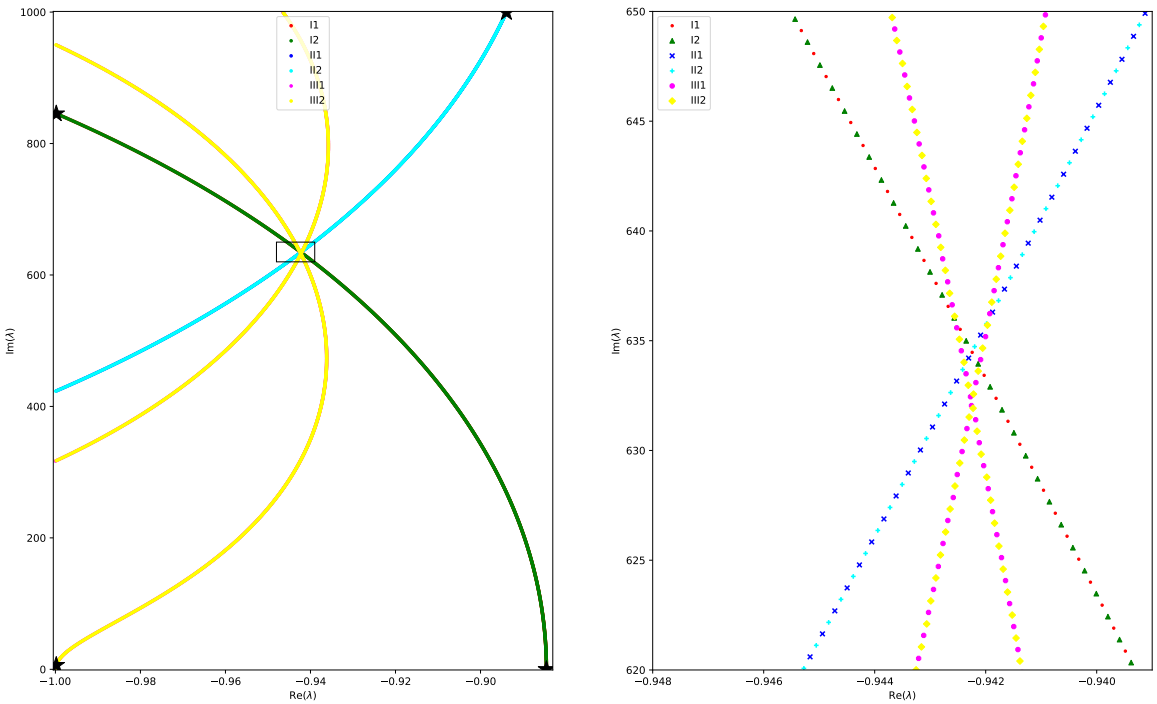

FIGURE 14. Resonances of the three-funnel surface $X(12, 12, 12)$ calculated in the full symmetry reduction of its flow-adapted representation. Due to the high degree of symmetry of the surface four very distinct resonance chains are visible. The right-hand side displays a zoom into the region where all four chains cross. It clearly shows how every chain belongs to a pair of representations which appear along the chain in alternating fashion. Again the four resonances considered below were marked with black stars.

uses the trivial symmetry group $\{e\}$ shows again the great benefit of symmetry reduction when it comes to the practical rate of convergence, i.e. the required number of summands in the cycle expansion. Comparing the funneled torus with the three-funneled surfaces also reveals that the former requires the determination of more geodesic lengths and orbit integrals to achieve the same relative errors as the latter even though this difference is not quite as significant as the difference between reduced and non-reduced calculations.

We note that the first and third columns of Figure 16 which correspond to the first resonance and the next resonance which is closest to the global spectral gap show far less similarity than observed for the funneled torus in the first and second columns of Figure 11. But this is simply due to the fact that we can follow the resonance chain corresponding to the representations II1/II2 further to the right and the resonance on this chain which is closest to the global gap actually turns out to be located quite a bit higher at $\lambda_0 \approx -0.8845 + 1269.2\mathrm{i}$.[17] In Figure 18 both this resonance chain as well as the invariant Ruelle distribution corresponding to the chain maximum were plotted. The distribution clearly supports the hypothesis developed for the funneled torus namely that

[17] Resonances were calculated with an accuracy of 10^{-4} in the real part which is apparently not sufficient to resolve the fact that the real part of the chain maximum should be *strictly* smaller than the real part of the first resonance.

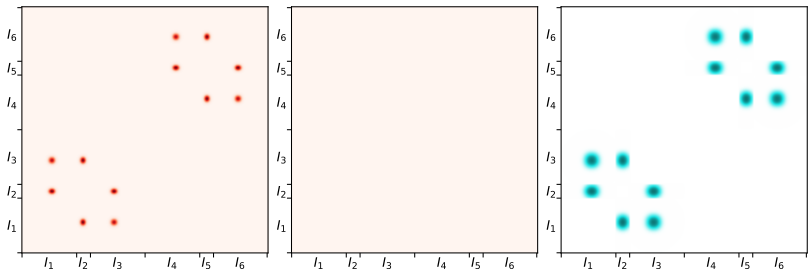

FIGURE 15. Invariant Ruelle distribution $t^{\Sigma}_{\lambda_0,\sigma}$ on the canonical Poincaré section Σ of the three-funnel surface $X(12, 12, 12)$ associated with the first resonance $\lambda_0 \approx 0.8845$. This figure uses the width $\sigma = 10^{-2}$ and $n_{\max} = 5$ summands in the cycle expansion of the dynamical determinant d_f. Notice how the finite symmetry group of the function system and the surface itself still shows up in the distribution. The plots show (from left to right) real part, imaginary part, and argument/absolute value encoding of the distribution similar to Figure 9.

Ruelle distributions associated with resonances near the global spectral gap should show high qualitative agreement with the one attached to the first resonance.

The experiment in Figure 18 also supports another trend with respect to convergence rates: The practical rates are much more sensitive to the real than the imaginary parts of the associated resonance. Even at the rather high imaginary part of ≈ 1269.2 the distributions convergence rapidly in full symmetry reduction with relative errors of magnitude $\approx 10^{-6}$ after only $n_{\max} = 4$ iterations. This behavior is rather promising for future experiments involving resonance chains near the global spectral gap!

The preceding examples should clearly justify the statements made in Section 5 – symmetry reduction does indeed improve the convergence properties of invariant Ruelle distributions drastically. Furthermore the example of three-funneled surfaces shows that one should use the largest available symmetry group for a given Schottky surface whenever possible to take maximal advantage of the symmetries of the surface. Finally refinement of the coordinate domain parameterizing the Poincaré section is vital if we want to be able to distinguish the relevant features of the calculated distributions with sufficient resolution. For systematic experiments in a regime where the fractal limit set is resolved beyond the first level our ad-hoc procedure can easily be augmented: After an application of group elements corresponding to a certain word length the initial fundamental intervals have multiplied according to the given word length but the resulting intervals are also contracted. One can now choose a subset of these contracted intervals which are representative for the distribution with respect to the symmetry group of the surface. This effectively increases the resolution of the numerical approximations without requiring a larger grid of support points on the coordinate domains.

Additional Three-funneled Surface Plots. Even though already restricted to two-dimensional quantities our approximations $t^{\Sigma}_{\lambda_0,\sigma}$ of invariant Ruelle distributions are still complex-valued functions on a two-dimensional domain effectively making them four-dimensional quantities. Any visualization will necessarily have to emphasize certain aspects of these distributions over others. The particular kind of phase-lightness plots used for illustration above showed nicely the qualitative behavior in terms of phase but the variations in absolute value are not as distinct. The following plots in Figure 19 therefore

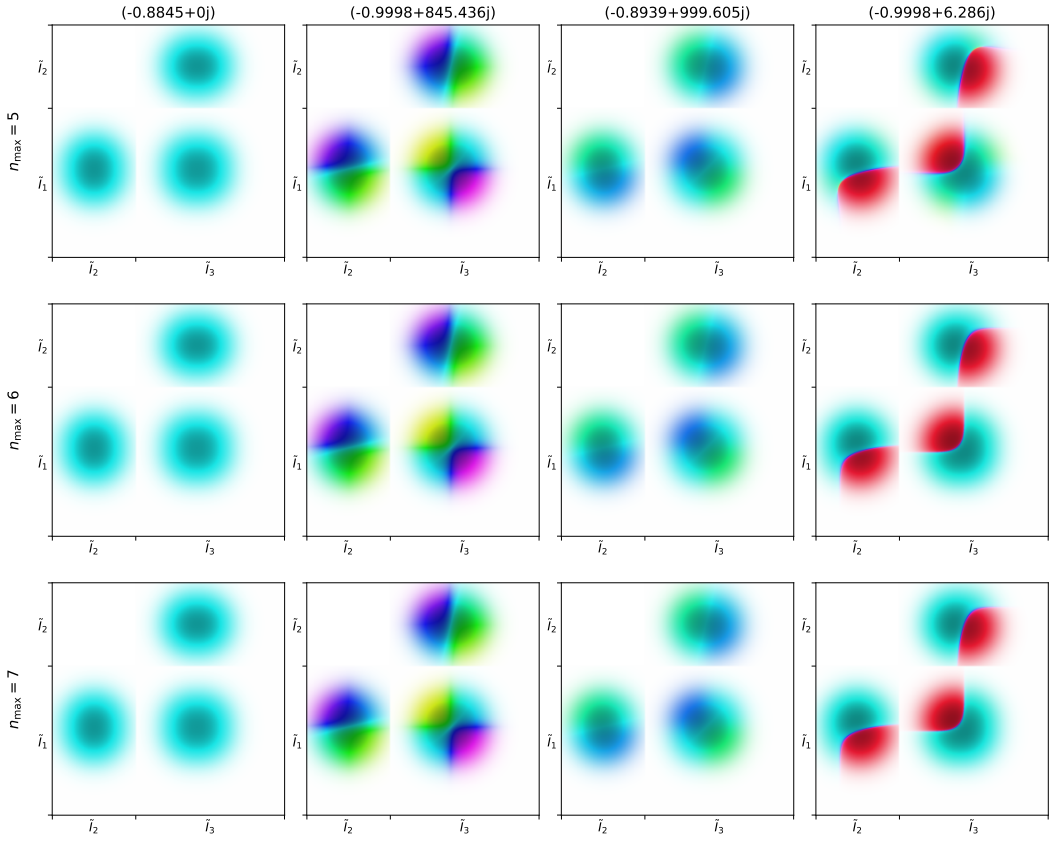

FIGURE 16. Fully symmetry reduced invariant Ruelle distributions $t^{\Sigma}_{\lambda_0,\sigma}$ on the canonical Poincaré section Σ of the flow-adapted three-funnel surface $X(12, 12, 12)$ evaluated at four different choices of resonance λ_0 with $\sigma = 10^{-2}$ and plotted as phase-lightness. The three different rows show the numerical results of using (from top to bottom) $n_{\max} \in \{5, 6, 7\}$ summands in the cycle expansion. Following along any of the four columns shows that the presented plots have converged rather well already at $n_{\max} = 5$. Due to symmetries in the distributions as shown in Figure 15 it again suffices to consider as the coordinate domain refined subsets $(\widetilde{I}_2 \cup \widetilde{I}_3) \times (\widetilde{I}_1 \cup \widetilde{I}_2)$ which are shown in Figure 10.

emphasize this latter aspect by showing the analogue of Figure 16 but as a plot of the absolute value alone.

As second important facet not yet discussed is the dependence of the qualitative features as well as the convergence behavior of $t^{\Sigma}_{\lambda_0,\sigma}$ on the Gaussian width σ. We therefore plotted the distributions using $\sigma = 10^{-2}$ in Figure 19 again for different values of $n_{\max}$ to compare them with the results for $\sigma = 7 \cdot 10^{-3}$ in the subsequent Figure 20.

The comparison shows how decreasing the width σ brings out additional features in the distributions in particular the convergence of their supports towards the fractal limit set of the underlying surface. This comes at the expense of decreased convergence speed, though, as illustrated by the fourth column in Figure 20. The benefits of symmetry reduction should therefore be even more pronounced when combined with experiments of

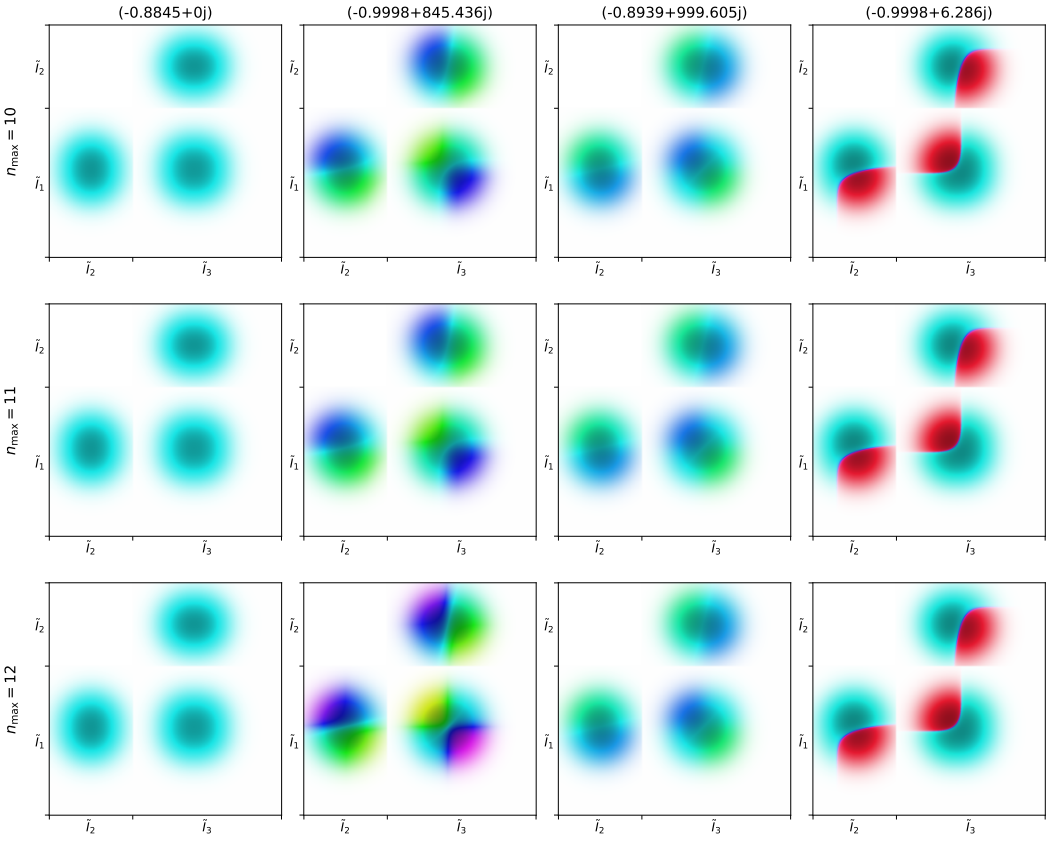

FIGURE 17. Analogous plots of $t^{\Sigma}_{\lambda_0,\sigma}$ for Σ the canonical Poincaré section of the flow-adapted representation of $X(12, 12, 12)$ and $\sigma = 10^{-2}$ as in Figure 16 but here the trivial symmetry group $\{e\}$ was used. Again the distributions are in close qualitative agreement with those in Figure 16 but convergence required significantly more terms in the cycle expansion as illustrated by the obvious lack of convergence in the second column.

the regime $\sigma \to 0$ for distributions associated with resonances far from the global spectral gap.

We finish this first numerical tour of invariant Ruelle distributions by considering a third technique to illustrate these that combines the phase-focused and absolute-valued focused approaches taken so far: By increasing the dimension of the plots themselves we can map the absolute value to the height of a surface in three-dimensional space and simultaneously color this surface according to the phase (argument) of the complex values. The resulting plot for the first resonance of $X(12, 12, 12)$ is shown in Figure 21. While visually more complex due to its three-dimensional nature it does illustrate the distribution in quite an intuitive manner and the high homogeneity present in the first invariant Ruelle distribution is immediately apparent.

The plots contained in Figures 22 and 23 show the three-dimensional representation of a different resonance already considered in Figures 19 and 20 for the widths $\sigma = 10^{-2}$ and $\sigma = 7 \cdot 10^{-3}$. The splitting of larger peaks into sub-peaks supported on a neighborhood of the limit set is brought out very clearly as well as the very distinct phases corresponding to

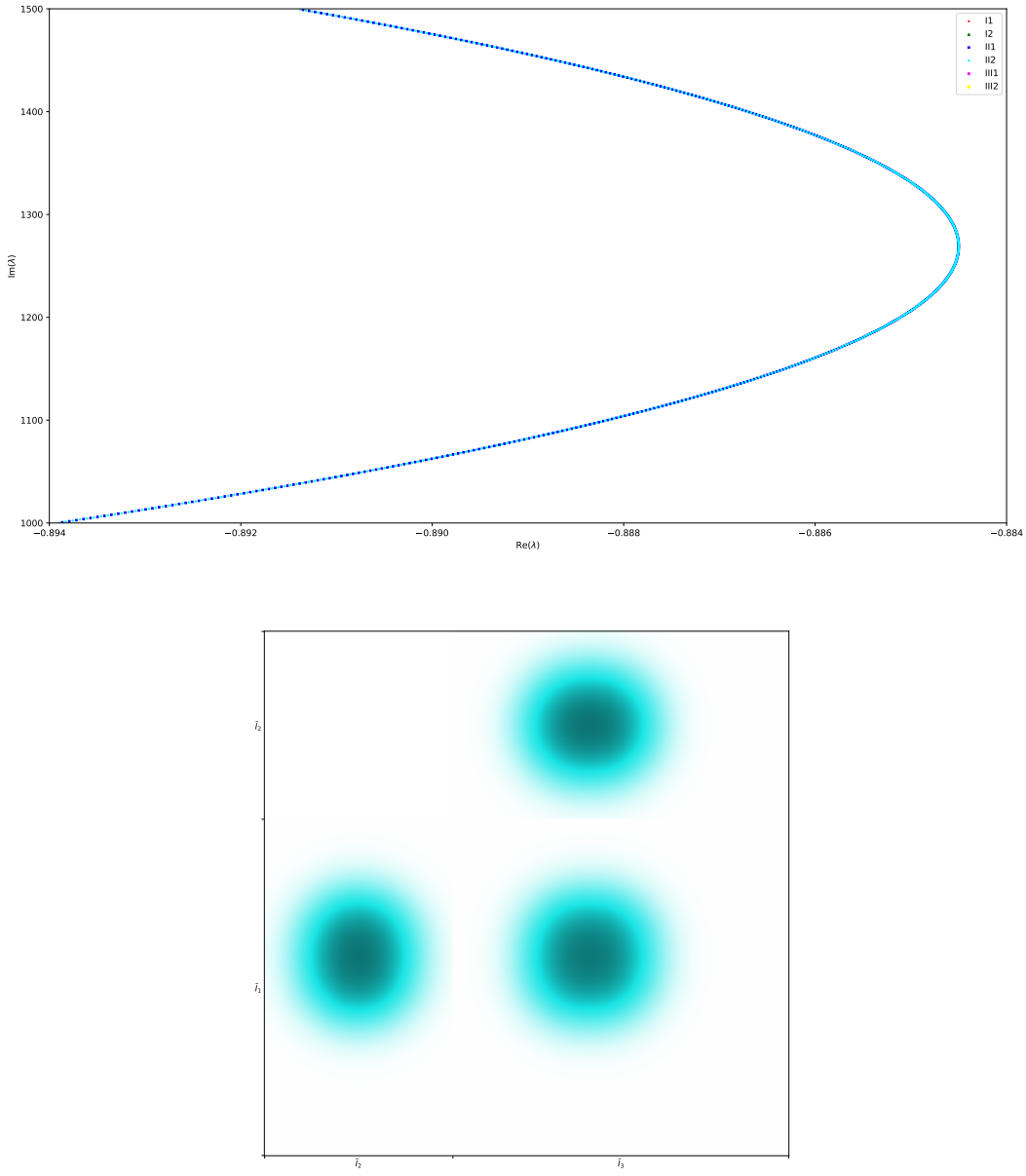

FIGURE 18. Additional resonances along the chain of II1/II2 resonances already starting in Figure 14 (top plot) together with the invariant Ruelle distribution at the chain resonance $\lambda_0 \approx -0.8845 + 1269.20\mathrm{i}$ closest to the global spectral gap $\mathrm{Re}(\lambda) = \delta - 1 \approx -0.8845$ (bottom plot). The comparison with the first column in Figure 16 which uses the same width $\sigma = 10^{-2}$ shows near perfect qualitative agreement supporting the analogous observation made for the funneled torus above.

different sub-peaks. Decreasing σ emphasizes these features further but is less necessary than for the absolute value plots considered previously.

Finally the same experiment was repeated in Figures 24 and 25 with a second resonance of $X(12, 12, 12)$ where one of the major peaks even splits into four sub-peaks already at $\sigma = 10^{-2}$ and more clearly at $\sigma = 7 \cdot 10^{-3}$.

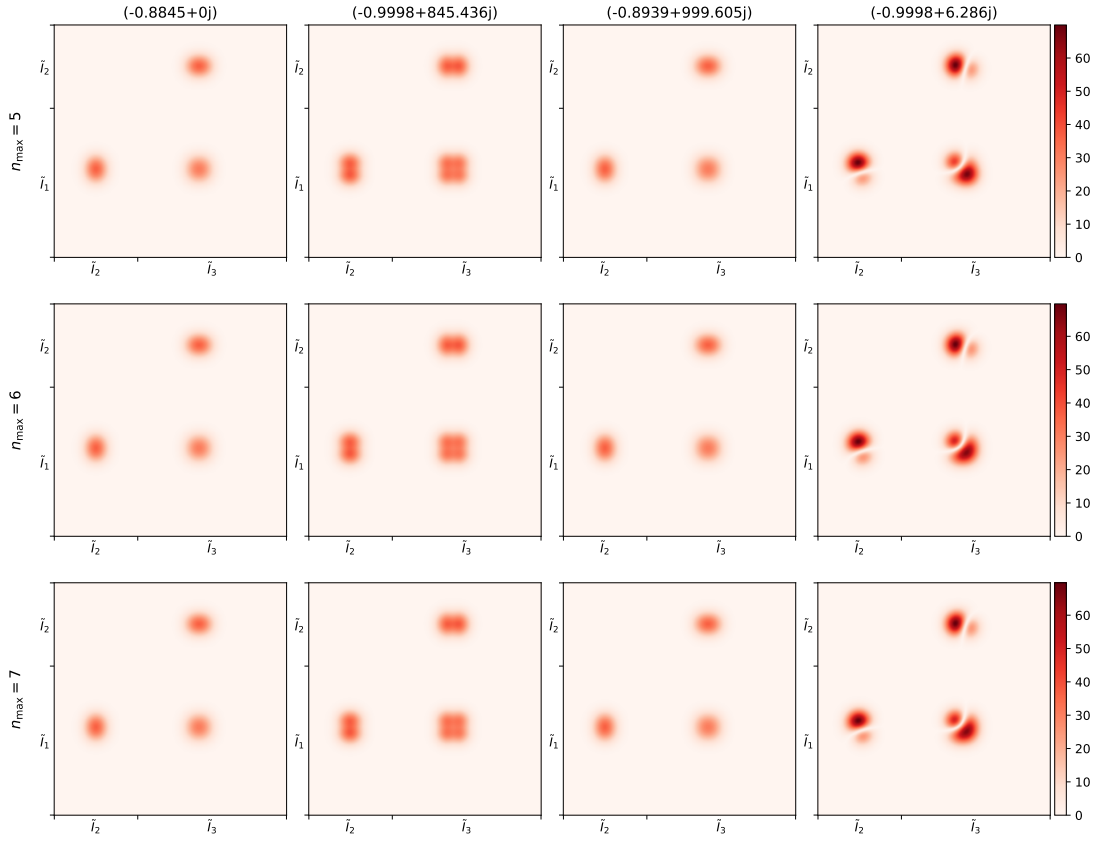

FIGURE 19. Absolute values of fully symmetry reduced invariant Ruelle distributions $t^{\Sigma}_{\lambda_0,\sigma}$ on the canonical Poincaré section Σ of the flow-adapted three-funnel surface $X(12,12,12)$ evaluated at four different choices of resonance λ_0 with $\sigma = 10^{-2}$. Again the different rows show the numerical results of using (from top to bottom) $n_{\max} \in \{5,6,7\}$ summands in the cycle expansion. Following along any of the four columns shows that the presented plots have converged rather well already at $n_{\max} = 5$. To increase resolution the coordinates (x_-, x_+) were again restricted to the refined rectangles $(\widetilde{I}_2 \cup \widetilde{I}_3) \times (\widetilde{I}_1 \cup \widetilde{I}_2)$ of Figure 10.

In summary we observe that the expected limiting behavior where for $\sigma \to 0$ the numerically calculated distributions should converge to quantities supported on the (fractal) limit set can indeed be found in our concrete experiments. We also observed that there are practical limits to the lower bound on σ mostly dictated by an inverse relationship between the value of σ and the required maximal number of summands $n_{\max}$ in the cycle expansion of the dynamical determinant. Here symmetry reduction begins to show its large potential despite the fact that only a few first experiments were conducted. But even with decently sized values of σ the three-dimensional representations of $t^{\Sigma}_{\lambda_0,\sigma}$ exhibit a number of interesting features that should provide further insights into the structure of invariant Ruelle distributions, resonant states, and their associated resonances.

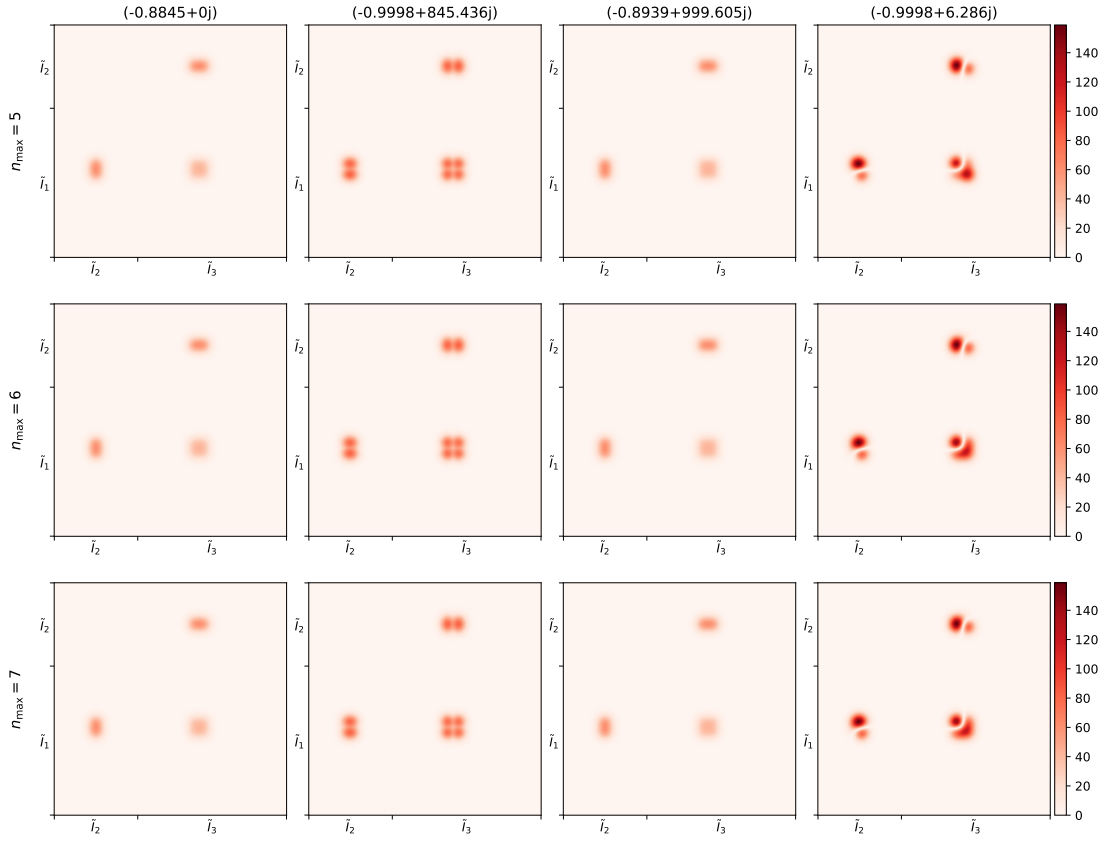

FIGURE 20. Similar to Figure 19 but now with $\sigma = 7 \cdot 10^{-3}$. Due to the smaller value of σ the resolution of the trapped set has become significantly better especially in columns two and four but at the expense of the rate of convergence: Now the right-most column changes noticeably between $n_{\max} = 5$ and $n_{\max} = 6$.

Remark 6.3. Additional numerical experiments including in particular animations are being prepared and will be included in future versions of this article as well as the first author's PhD thesis [Sch23].

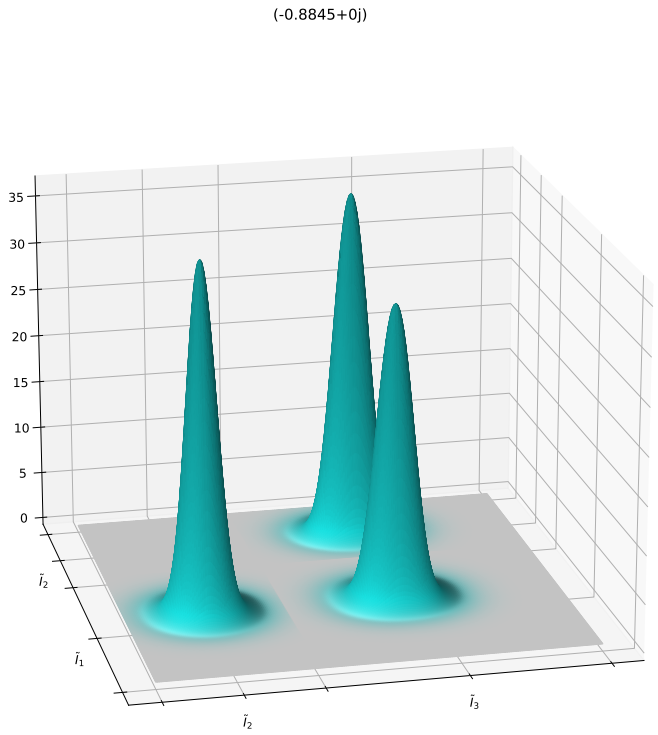

FIGURE 21. Three-dimensional representation of the invariant Ruelle distribution for the three-funneled surface $X(12, 12, 12)$ on the canonical Poincaré section of the flow-adapted system and with Gaussian width $\sigma = 10^{-2}$ associated to the first resonance $\lambda_0 \approx -0.8845$. The absolute value of the distribution determines the height of the surface whereas the colors indicate the position of the complex argument on the unit circle. This effectively combines the presentation in Figures 16 and 19 emphasizing nicely the homogeneity of the first invariant Ruelle distribution.

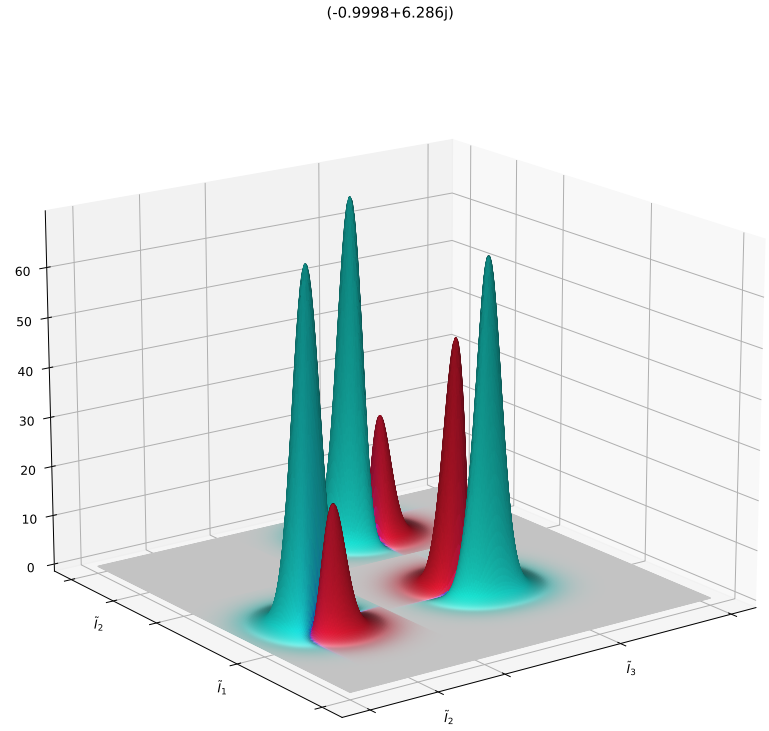

FIGURE 22. Analogous plot as in Figure 21 but for the resonance $\lambda_0 \approx -0.9998 + 6.286\mathrm{i}$ and again the same Gaussian width $\sigma = 10^{-2}$. The three-dimensional plot brings out the splitting of each peak into two sub-peaks of distinctly different phases better than the corresponding absolute value plot in the fourth column of Figure 19.

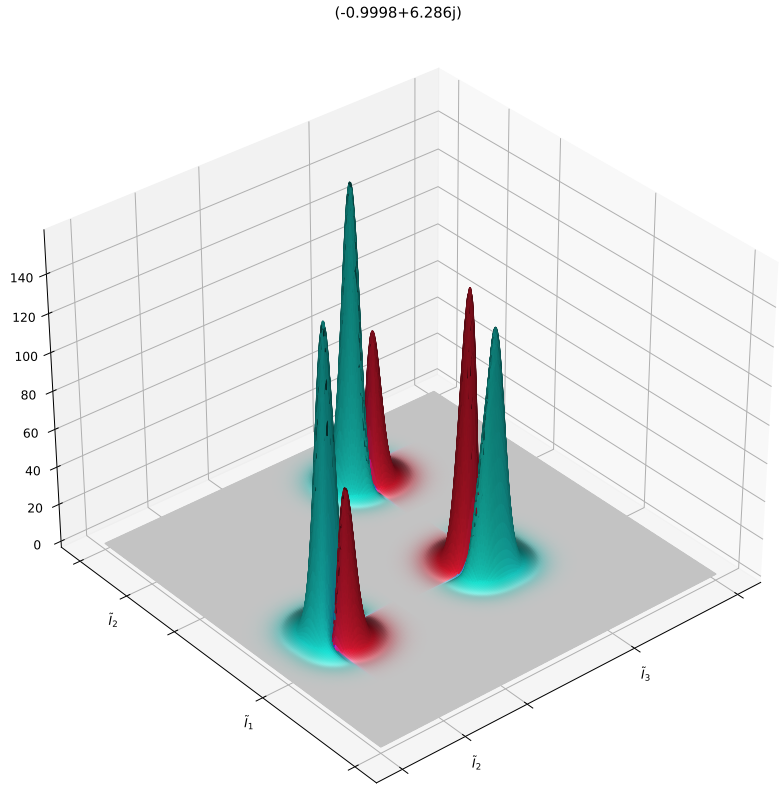

FIGURE 23. Analogous plot as in Figure 22 for the same resonance $\lambda_0 \approx -0.9998 + 6.286\mathrm{i}$ but a refined Gaussian width of $\sigma = 7 \cdot 10^{-3}$. Even this slight decrease in σ already increases the resolution of distinct sub-peaks with rather prominent differences in phase by quite a margin.

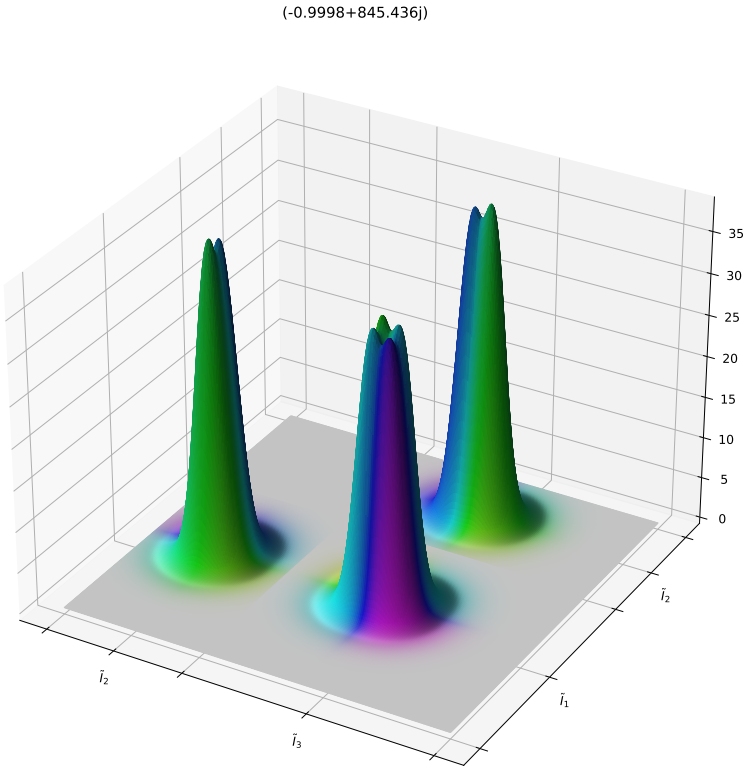

FIGURE 24. Analogous plot as in Figure 21 but for the resonance $\lambda_0 \approx -0.9998 + 845.436\mathrm{i}$ and again width $\sigma = 10^{-2}$. The splitting into pairs and quadruples of sub-peaks is significantly easier to distinguish than in the corresponding absolute value plot shown in the second column of Figure 19.

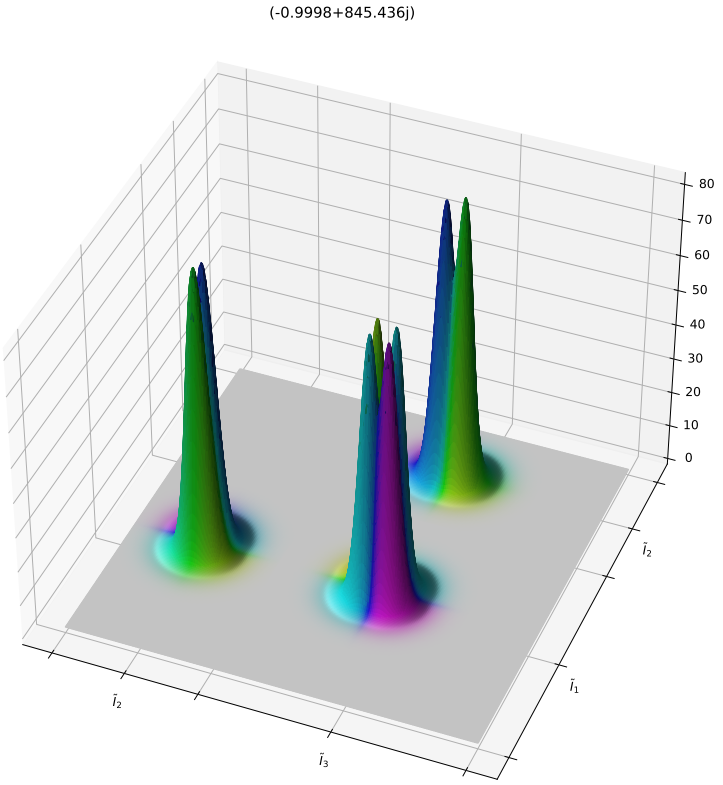

FIGURE 25. Analogous plot as in Figure 24 associated with the same resonance $\lambda_0 \approx -0.9998 + 845.436\mathrm{i}$ but for a refined Gaussian width of $\sigma = 7 \cdot 10^{-3}$. Note how both the pairs and the quadruple of peaks are visually more distinct due to the (slight) decrease in σ.

7. Outlook

In the present article we derived and implemented an algorithm for the practical numerical computation of invariant Ruelle distributions. This opens the possibility to perform a large number of different numerical experiments on which an outlook was already given in the final Section 6. More systematic investigations will be conducted in the future to fully leverage the tools developed here.

Besides such experiments another interesting perspective would be to transfer the methods of [BPSW20] for the numerical calculation of Fredholm determinants to our (weighted) dynamical determinants d_f. These techniques showed very promising improvements over the computational cost and convergence of cycle expansions in the resonance case and it is expected that similar improvements are possible with minor adaptations in the case of invariant Ruelle distributions.

Appendix A. Fredholm Determinants

In this appendix we summarize some facts regarding functional analysis in general and Fredholm determinants in particular. We include this appendix to make the present paper and specifically our proofs more self-contained. All of the following material is quite standard and the proofs can be found in e.g. [Bor16, Appendix A.4] or the monograph [Sim05, Chap. 1 & 3].

Definition A.1. *Let $T : \mathcal{H}_1 \to \mathcal{H}_2$ be a compact operator between the Hilbert spaces $\mathcal{H}_1$ and $\mathcal{H}_2$. The square roots of the eigenvalues of the self-adjoint operator TT^* are called* singular values *of T and denoted by*[18]

$$\mu_1(T) \geq \mu_2(T) \geq \ldots \longrightarrow 0 \ .$$

If $\mathcal{H}_1 = \mathcal{H}_2$ then T is called trace-class *in case $\sum_{i=1}^{\infty} \mu_i(T) < \infty$ holds.*

For the next definition we denote, analogously to the singular values, the sequence of eigenvalues of T ordered w.r.t. decreasing absolute value and repeated according to their multiplicity by $\lambda_1(T), \lambda_2(T), \ldots$.

Definition A.2. *Let $T : \mathcal{H} \to \mathcal{H}$ be a trace-class operator on the Hilbert space $\mathcal{H}$. Then the* Fredholm determinant *of T is defined as*

$$\det\left(\mathrm{id} - zT\right) \coloneqq \prod_{i=1}^{\infty} \left(1 + z\lambda_i(T)\right) \ , \tag{26}$$

and converges for any $z \in \mathbb{C}$.

Theorem A.3. *Let $T : \mathcal{H} \to \mathcal{H}$ be a compact operator on the Hilbert space $\mathcal{H}$ and denote by $\bigwedge^i T$ the i-th exterior power of T. Then the Fredholm determinant can be calculated via*

$$\det\left(\mathrm{id} - zT\right) = \sum_{i=0}^{\infty} z^i \cdot \mathrm{Tr}\left(\bigwedge^i T\right) \ ,$$

where the trace *of T may be defined as $\mathrm{Tr}(T) \coloneqq \sum_{i=1}^{\infty} \lambda_j(T)$.*

Combining this theorem with the inequality

$$\sum_{j=1}^{\infty} |\lambda_j(T)| \leq \sum_{j=1}^{\infty} \mu_j(T)$$

[18] Where in this decreasing enumeration multiple eigenvalues are repeated according to their multiplicity.

one can now prove the analyticity of the Fredholm determinant in the z-variable: The trace which is its i-th coefficient in the Taylor expansion about $z = 0$ can be bounded by

$$\sum_{j_1<\ldots<j_i} \mu_{j_1}(T) \cdot \ldots \cdot \mu_{j_i}(T) \leq \frac{1}{k!} \left(\sum_{j=1}^{\infty} \mu_j(T) \right)^i ,$$

because $\left(\bigwedge^i T\right)\left(\bigwedge^i T\right)^* = \bigwedge^i (TT^*)$. But this already finishes the proof due to T being trace-class.

We end this appendix by stating two well-known estimates regarding singular values:

Theorem A.4 (Min-Max-Theorem)**.** *Let $T : \mathcal{H} \to \mathcal{H}$ be a compact operator on the Hilbert space $\mathcal{H}$. Then the n-th singular value of T satisfies*

$$\mu_n(T) = \min_{\substack{V \subseteq \mathcal{H} \\ \dim(V)=n-1}} \max_{\varphi \in V^\perp} \frac{\|T\varphi\|}{\|\varphi\|} .$$

Theorem A.5 (Fan Inequality)**.** *Let compact operators $S, T : \mathcal{H} \to \mathcal{H}$ on the Hilbert space $\mathcal{H}$ be given. Then the singular values of $S + T$ satisfy*

$$\mu_{i+j-1}(S + T) \leq \mu_i(S) + \mu_j(T) .$$

References

[AZ07] N. Anantharaman and S. Zelditch, *Patterson–Sullivan distributions and quantum ergodicity*, Annales Henri Poincaré **8** (2007), no. 2, 361–426.

[Bal18] V. Baladi, *Dynamical Zeta Functions and Dynamical Determinants for Hyperbolic Maps*, 1st ed., Ergebnisse der Mathematik und ihrer Grenzgebiete. 3. Folge / A Series of Modern Surveys in Mathematics, Springer, 2018.

[BKL02] M. Blank, G. Keller, and C. Liverani, *Ruelle–Perron–Frobenius spectrum for Anosov maps*, Nonlinearity **15** (2002), no. 6, 1905–1973.

[Bor14] D. Borthwick, *Distribution of resonances for hyperbolic surfaces*, Experimental Mathematics **23** (2014), no. 1, 25–45.

[Bor16] ———, *Spectral Theory of Infinite-Area Hyperbolic Surfaces*, 2nd ed., Progress in Mathematics, Birkhäuser, 2016.

[BPSW20] O. F. Bandtlow, A. Pohl, T. Schick, and A. Weiße, *Numerical resonances for Schottky surfaces via Lagrange–Chebyshev approximation*, Stochastics and Dynamics (2020), 2140005.

[BSW22] S. Barkhofen, P. Schütte, and T. Weich, *Semiclassical formulae for Wigner distributions*, Journal of Physics A: Mathematical and Theoretical **55** (2022), no. 24, 20.

[BW16] D. Borthwick and T. Weich, *Symmetry reduction of holomorphic iterated function schemes and factorization of Selberg zeta functions*, Journal of Spectral Theory **6** (2016), no. 2, 267–329.

[CDDP22] Mihajlo Cekić, Benjamin Delarue, Semyon Dyatlov, and Gabriel P. Paternain, *The Ruelle zeta function at zero for nearly hyperbolic 3-manifolds*, Invent. Math. **229** (2022), no. 1, 303–394 (English).

[CE89] P. Cvitanović and B. Eckhardt, *Periodic-orbit quantization of chaotic systems*, Physical review letters **63** (1989), no. 8, 823–826.

[Com74] L. Comtet, *Advanced Combinatorics*, 1st revised and enlarged ed., Springer Dordrecht, 1974.

[Dal11] F. Dal'Bo, *Geodesic and Horocyclic Trajectories*, 1st ed., Universitext, Springer London, 2011.

[DG16] S. Dyatlov and C. Guillarmou, *Pollicott–Ruelle Resonances for Open Systems*, Annales Henri Poincaré **17** (2016), no. 11, 3089–3146.

[DG21] Nguyen-Thi Dang and Olivier Glorieux, *Topological mixing of Weyl chamber flows*, Ergodic Theory and Dynamical Systems **41** (2021), no. 5, 1342–1368.

[DGRS20] Nguyen Viet Dang, Colin Guillarmou, Gabriel Rivière, and Shu Shen, *The Fried conjecture in small dimensions*, Invent. Math. **220** (2020), no. 2, 525–579 (English).

[DSW21] B. Delarue, P. Schütte, and T. Weich, *Resonances and Weighted Zeta Functions for Obstacle Scattering via Smooth Models*, arXiv:2109.05907 (2021).

[Dya19] Semyon Dyatlov, *Improved fractal Weyl bounds for hyperbolic manifolds (with an appendix by David Borthwick, Semyon Dyatlov and Tobias Weich)*, J. Eur. Math. Soc. (JEMS) **21** (2019), no. 6, 1595–1639 (English).

[DZ16] S. Dyatlov and M. Zworski, *Dynamical zeta functions for Anosov flows via microlocal analysis*, Annales de l'ENS **49** (2016), 543–577.

[DZ17] Semyon Dyatlov and Maciej Zworski, *Ruelle zeta function at zero for surfaces*, Invent. Math. **210** (2017), no. 1, 211–229 (English).

[DZ19] S. Dyatlov and M. Zworski, *Mathematical theory of scattering resonances*, 1st ed., Graduate Studies in Mathematics, vol. 200, American Mathematical Soc., 2019.

[FH04] W. Fulton and J. Harris, *Representation Theory – A First Course*, 1st ed., Graduate Texts in Mathematics, Springer New York, NY, 2004.

[FT23] Frédéric Faure and Masato Tsujii, *Fractal weyl law for the ruelle spectrum of anosov flows*, Annales Henri Lebesgue **6** (2023), 331–426.

[GHW18] Colin Guillarmou, Joachim Hilgert, and Tobias Weich, *Classical and quantum resonances for hyperbolic surfaces*, Math. Ann. **370** (2018), 1231–1275.

[GHW21] C. Guillarmou, J. Hilgert, and T. Weich, *High frequency limits for invariant Ruelle densities*, Annales Henri Lebesgue **4** (2021), 81–119.

[GR89] Pierre Gaspard and Stuart A Rice, *Scattering from a classically chaotic repellor*, The Journal of Chemical Physics **90** (1989), no. 4, 2225–2241.

[Hö03] L. Hörmander, *The Analysis of Linear Partial Differential Operators I*, 2nd ed., Classics in Mathematics, Springer Berlin, Heidelberg, 2003.

[JP02] O. Jenkinson and M. Pollicott, *Calculating Hausdorff dimension of Julia sets and Kleinian limit sets*, American Journal of Mathematics **124** (2002), no. 3, 495–545.

[KW20] Benjamin Küster and Tobias Weich, *Pollicott-Ruelle resonant states and Betti numbers*, Commun. Math. Phys. **378** (2020), no. 2, 917–941 (English).

[Mas67] Bernard Maskit, *A characterization of Schottky groups*, Journal d'Analyse Mathématique **19** (1967), 227–230.

[NZ15] S. Nonnenmacher and M. Zworski, *Decay of correlations for normally hyperbolic trapping*, Invent. math. **200** (2015), 345–438.

[Pol85] Mark Pollicott, *On the rate of mixing of Axiom A flows*, Invent. Math. **81** (1985), 413–426.

[PV19] Mark Pollicott and Polina Vytnova, *Zeros of the Selberg zeta function for symmetric infinite area hyperbolic surfaces*, Geom. Dedicata **201** (2019), 155–186 (English).

[Rob03] Thomas Roblin, *Ergodicity and equidistribution in negative curvature*, Mém. Soc. Math. Fr., Nouv. Sér. **95** (2003), 96 (French).

[Rue76] David Ruelle, *Zeta-functions for expanding maps and Anosov flows*, Invent. Math. **34** (1976), 231–242.

[Rug92] H. H. Rugh, *The correlation spectrum for hyperbolic analytic maps*, Nonlinearity **5** (1992), no. 6, 1237–1263.

[Rug96] ———, *Generalized Fredholm determinants and Selberg zeta functions for Axiom A dynamical systems*, Ergodic Theory and Dynamical Systems **16** (1996), no. 4, 805–819.

[Sch23] Philipp Schütte, *Invariant Ruelle Distributions on Open Hyperbolic Systems – An Analytical and Numerical Investigation*, PhD Thesis (2023).

[Sim05] Barry Simon, *Trace ideals and their applications*, 2nd ed., Mathematical surveys and monographs, American Mathematical Society, Providence, 2005.

[SWB23] Philipp Schütte, Tobias Weich, and Sonja Barkhofen, *Meromorphic Continuation of Weighted Zeta Functions on Open Hyperbolic Systems*, Commun. Math. Phys. **398** (2023), no. 2, 655–678.

[Thi07] Xavier Thirion, *Sous-groupes discrets de SL(d, R) et equidistribution dans les espaces symetriques*, PhD Thesis (2007).

[Tsu10] M. Tsujii, *Quasi-compactness of transfer operators for contact Anosov flows*, Nonlinearity **23** (2010), 1495–1545.

[Wei15] Tobias Weich, *Resonance chains and geometric limits on Schottky surfaces*, Commun. Math. Phys. **337** (2015), no. 2, 727–765 (English).

Email address: pschuet2@math.uni-paderborn.de

Institute of Mathematics, Paderborn University, Paderborn, Germany

Email address: weich@math.uni-paderborn.de

Institute of Mathematic, Paderborn University, Paderborn, Germany

Institute for Photonic Quantum Systems, Paderborn University, Paderborn, Germany

Bibliography

[AZ07] N. Anantharaman and S. Zelditch, *Patterson–Sullivan distributions and quantum ergodicity*, Annales Henri Poincaré **8** (2007), no. 2, 361–426.

[Bal18] V. Baladi, *Dynamical Zeta Functions and Dynamical Determinants for Hyperbolic Maps*, 1st ed., Ergebnisse der Mathematik und ihrer Grenzgebiete. 3. Folge / A Series of Modern Surveys in Mathematics, Springer, 2018.

[BDH14] Christian Brouder, Viet Dang, and Frederic Helein, *Boundedness and continuity of the fundamental operations on distributions having a specific wave front set.*, Studia Mathematica **232** (2014).

[BGW23] Yannick Guedes Bonthonneau, Colin Guillarmou, and Tobias Weich, *SRB measures for Anosov actions*, arXiv:2103.12127 (2023).

[BL07] Oliver Butterley and Carlangelo Liverani, *Smooth Anosov flows: Correlation spectra and stability*, J. Mod. Dyn. **1** (2007), no. 2, 301–322.

[Bor14] D. Borthwick, *Distribution of resonances for hyperbolic surfaces*, Experimental Mathematics **23** (2014), no. 1, 25–45.

[Bor16] ———, *Spectral Theory of Infinite-Area Hyperbolic Surfaces*, 2nd ed., Progress in Mathematics, Birkhäuser, 2016.

[BPSW20] O. F. Bandtlow, A. Pohl, T. Schick, and A. Weiße, *Numerical resonances for Schottky surfaces via Lagrange–Chebyshev approximation*, Stochastics and Dynamics (2020), 2140005.

[BS88] P. Buser and K.-D. Semmler, *The geometry and spectrum of the one holed torus*, Comment. Math. Helvetici **63** (1988), 259–274.

[BSW22] S. Barkhofen, P. Schütte, and T. Weich, *Semiclassical formulae for Wigner distributions*, Journal of Physics A: Mathematical and Theoretical **55** (2022), no. 24.

[Bus10] Peter Buser, *Geometry and Spectra of Compact Riemann Surfaces*, 1st ed., Modern Birkhäuser Classics, Birkhäuser, Boston, MA, 2010.

[BW16] D. Borthwick and T. Weich, *Symmetry reduction of holomorphic iterated function schemes and factorization of Selberg zeta functions*, Journal of Spectral Theory **6** (2016), no. 2, 267–329.

[CDDP22] Mihajlo Cekić, Benjamin Delarue, Semyon Dyatlov, and Gabriel P. Paternain, *The Ruelle zeta function at zero for nearly hyperbolic 3-manifolds*, Invent. Math. **229** (2022), no. 1, 303–394.

[Che22] Haotian Chen, *On locating the zeros and poles of a meromorphic function*, Journal of Computational and Applied Mathematics **402** (2022), 113796.

[CS14] Scott Chacon and Ben Straub, *Pro Git*, 2nd ed., Apress, Berkeley, CA, 2014.

[Dal11] Francoise Dal'Bo, *Geodesic and Horocyclic Trajectories*, 1st ed., Universitext, Springer London, London and Dordrecht and Heidelberg and NY, 2011.

[DFG15] Semyon Dyatlov, Frédéric Faure, and Colin Guillarmou, *Power spectrum of the geodesic flow on hyperbolic manifolds*, Anal. PDE **8** (2015), no. 4, 923–1000.

[DG16] S. Dyatlov and C. Guillarmou, *Pollicott–Ruelle Resonances for Open Systems*, Annales Henri Poincaré **17** (2016), no. 11, 3089–3146.

[DL67] L. M. Delves and J. N. Lyness, *A Numerical Method for Locating the Zeros of an Analytic Function*, Mathematics of Computation **21** (1967), no. 100, 543–60.

[DSW21] B. Delarue, P. Schütte, and T. Weich, *Resonances and Weighted Zeta Functions for Obstacle Scattering via Smooth Models*, arXiv:2109.05907 (2021).

[DZ16] S. Dyatlov and M. Zworski, *Dynamical zeta functions for Anosov flows via microlocal analysis*, Annales de l'ENS **49** (2016), 543–577.

[DZ17] Semyon Dyatlov and Maciej Zworski, *Ruelle zeta function at zero for surfaces*, Invent. Math. **210** (2017), no. 1, 211–229.

[ES14] Manfred Einsiedler and Klaus Schmidt, *Dynamische Systeme – Ergodentheorie und topologische Dynamik*, 1st ed., Mathematik Kompakt, Birkhäuser, Basel, 2014.

[FR03] Martin Fowler and David Rice, *Patterns of enterprise application architecture*, 1st ed., The Addison-Wesley signature series, Addison-Wesley, 2003.

[FS11] Frédéric Faure and Johannes Sjöstrand, *Upper bound on the density of Ruelle resonances for Anosov flows*, Commun. Math. Phys. **308** (2011), no. 2, 325–364.

[GHJV03] Erich Gamma, Richard Helm, Ralph Johnson, and John Vlissides, *Design Patterns. Elements of Reusable Object-Oriented Software*, 26. print. ed., Addison-Wesley professional computing series, Addison-Wesley, 2003.

[GHW18] Colin Guillarmou, Joachim Hilgert, and Tobias Weich, *Classical and quantum resonances for hyperbolic surfaces*, Math. Ann. **370** (2018), 1231–1275.

[GKOS01] Michael Grosser, Michael Kunzinger, Michael Oberguggenberg, and Roland Steinbauer, *Geometric Theory of Generalized Functions with Applications to General Relativity*, 1st ed., Mathematics and Its Applications, vol. 537, Springer-Science+Business Media, B.V., Dordrecht, 2001.

[GO20] Micha Gorelick and Ian Ozsvald, *High Performance Python*, 2nd ed., O'Reilly Media, Inc., 2020.

[GR89a] Pierre Gaspard and Stuart A Rice, *Exact quantization of the scattering from a classically chaotic repellor*, The Journal of chemical physics **90** (1989), no. 4, 2255–2262.

[GR89b] ———, *Scattering from a classically chaotic repellor*, The Journal of Chemical Physics **90** (1989), no. 4, 2225–2241.

[GR89c] ———, *Semiclassical quantization of the scattering from a classically chaotic repellor*, The Journal of chemical physics **90** (1989), no. 4, 2242–2254.

[GS94] Alain Grigis and Johannes Sjöstrand, *Microlocal Analysis for Differential Operators – An Introduction*, 1st ed., London Mathematical Society Lecture Note Series, no. 196, Cambridge University Press, 1994.

[Gui77] Victor Guillemin, *Lectures on spectral theory of elliptic operators*, Duke Math. J. **44** (1977), no. 3, 485–517.

[Hen88] Peter Henrici, *Applied and Computational Complex Analysis, Volume 1*, 1st ed., Wiley Classics Library, Wiley & Sons Ltd., 1988.

[Hör13] Lars Hörmander, *The Analysis of Linear Partial Differential Operators I: Distribution Theory and Fourier Analysis*, 2nd ed., Classics in Mathematics, Springer, Berlin, Heidelberg, 2013.

[KLM+97] Gregor Kiczales, John Lamping, Anurag Mendhekar, Chris Maeda, Cristina Lopes, Jean-Marc Loingtier, and John Irwin, *Aspect-oriented programming*, Lecture Notes in Computer Science (Berlin, Heidelberg) (M. Akşit and S. Matsuoka, eds.), vol. 1241, European Conference on Object-Oriented Programming, Springer, 1997, pp. 220–242.

[Knu74] Donald Ervin Knuth, *Structured Programming with go to Statements*, ACM Computing Surveys (CSUR) **6** (1974), no. 4, 261–301.

[KV99] Peter Kravanja and Marc Van Barel, *A derivative-free algorithm for computing zeros of analytic functions*, Computing **63** (1999), no. 1, 69–91.

[KV00] ———, *Computing the Zeros of Analytic Functions*, 1st ed., Lecture Notes in Mathematics, Springer Berlin, Heidelberg, 2000.

[KVH99] Peter Kravanja, Marc Van Barel, and Ann Haegemans, *On computing zeros and poles of meromorphic functions*, Computational Methods and Function Theory 1997 (1999), 359–369.

[KVR+00] P. Kravanja, M. Van Barel, O. Ragos, M.N. Vrahatis, and F.A. Zafiropoulos, *ZEAL: A mathematical software package for computing zeros of analytic functions*, Computer Physics Communications **124** (2000), no. 2, 212–232.

[KW20] Benjamin Küster and Tobias Weich, *Pollicott-Ruelle resonant states and Betti numbers*, Commun. Math. Phys. **378** (2020), no. 2, 917–941.

[LD67] J.N. Lyness and L.M. Delves, *On numerical contour integration round a closed contour*, Mathematics of Computation **21** (1967), no. 100, 561–577.

[Lee12] John M. Lee, *Introduction to Smooth Manifolds*, 2nd ed., Graduate Texts in Mathematics, vol. 218, Springer New York, New York, NY, 2012.

[LS21] Michael Levitin and Alexander Strohmaier, *Computations of eigenvalues and resonances on perturbed hyperbolic surfaces with cusps*, Int. Math. Res. Not. **2021** (2021), no. 6, 4003–4050.

[McC04] Steve McConnell, *Code complete: a practical handbook of software construction*, 2nd ed., Best practices, Microsoft Press, 2004.

[Nau05] Frédéric Naud, *Expanding maps on Cantor sets and analytic continuation of zeta functions*, Ann. Sci. Éc. Norm. Supér. (4) **38** (2005), no. 1, 116–153.

[NN98] Marjatta Näätänen and Toshihiro Nakanishi, *Weil-Petersson Areas of the Moduli Spaces of Tori*, Result. Math. **33** (1998), 120–133.

[NZ15] Stéphane Nonnenmacher and Maciej Zworski, *Decay of correlations for normally hyperbolic trapping*, Invent. Math. **200** (2015), no. 2, 345–438.

[Pol85] Mark Pollicott, *On the rate of mixing of Axiom A flows*, Invent. Math. **81** (1985), 413–426.

[Rob03] Thomas Roblin, *Ergodicity and equidistribution in negative curvature*, Mém. Soc. Math. Fr., Nouv. Sér. **95** (2003), 96 (French).

[RS02] Reinhold Remmert and Georg Schumacher, *Funktionentheorie 1*, 5th ed., Springer-Lehrbuch, Springer Berlin, Heidelberg, 2002.

[Rue76] David Ruelle, *Zeta-functions for expanding maps and Anosov flows*, Invent. Math. **34** (1976), 231–242.

[Rug92] H. H. Rugh, *The correlation spectrum for hyperbolic analytic maps*, Nonlinearity **5** (1992), no. 6, 1237–1263.

[Sil13] Richard E. Silverman, *Git Pocket Guide*, 1st ed., O'Reilly Media, Inc., 1005 Gravenstein Highway North, Sebastopol, CA 95472, 2013.

[Str17] Alexander Strohmaier, *Computation of eigenvalues, spectral zeta functions and zeta-determinants on hyperbolic surfaces*, Geometric and computational spectral theory. Lectures from the Séminaire de Mathématiques Supérieures, Centre de Recherches Mathématiques, Université de Montréal, Montréal, QC, Canada, June 15–26, 2015, Providence, RI: American Mathematical Society (AMS); Montreal: Centre de Recherches Mathématiques (CRM), 2017, pp. 177–205.

[Sv19] Mark Seeman and Steven van Deursen, *Dependency Injection: Principles, practices and patterns*, 1st ed., Manning, 2019.

[SW23] P. Schütte and T. Weich, *Invariant Ruelle Distributions on Convex-Cocompact Hyperbolic Surfaces – A Numerical Algorithm via Weighted Zeta Functions*, arXiv:2308.13463 (2023).

[SWB23] P. Schütte, T. Weich, and S. Barkhofen, *Meromorphic Continuation of Weighted Zeta Functions on Open Hyperbolic Systems*, Commun. Math. Phys. **398** (2023), 655–678.

[Tay11] Michael E. Taylor, *Partial Differential Equations I, Basic Theory*, 2nd ed., Applied Mathematical Sciences, vol. 115, Springer Science+Business Media, LLC, NY, Dordrecth, Heidelberg, London, 2011.

[Tre07] Francois Treves, *Topological Vector Spaces, Distributions, and Kernels*, 1st ed., Dover Books on Mathematics, Dover Publications Inc., 2007.

[YNK88] Xingren Ying and I Norman Katz, *A reliable argument principle algorithm to find the number of zeros of an analytic function in a bounded domain*, Numerische Mathematik **53** (1988), no. 1, 143–163.

List of Figures

Index